NATIONAL URANIUM TAILINGS PROGRAM

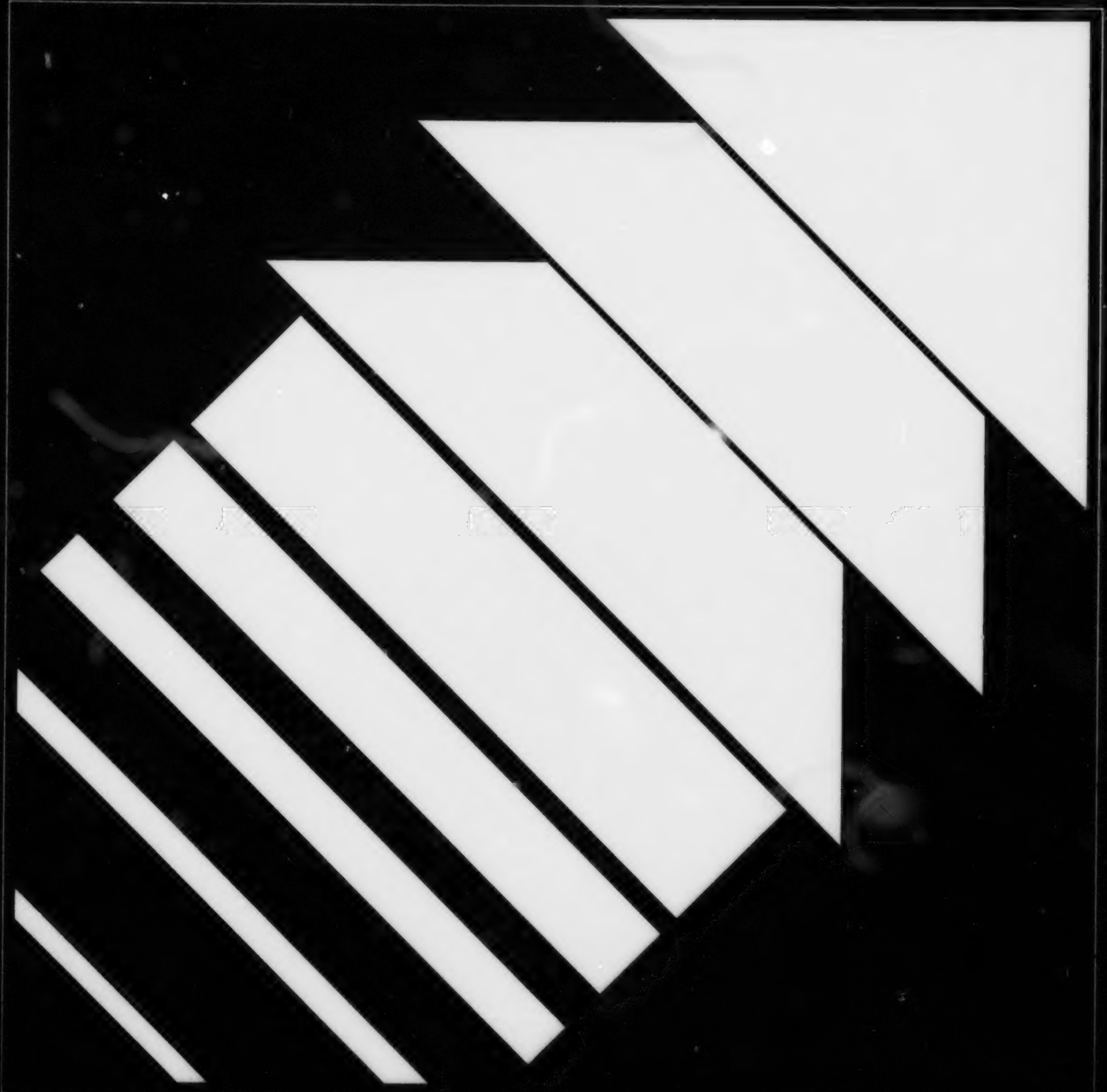

Energy, Mines and Énergie, Mines et
Resources Canada Ressources Canada

Canada

beak

DESCRIPTIVE ALGORITHM DEVELOPMENT FOR PHYSICAL, CHEMICAL AND BIOLOGICAL PROCESSES OPERATIONAL IN URANIUM MILL TAILINGS

Final Report

by:

William J. Snodgrass,
Ronald V. Nicholson
BEAK CONSULTANTS LIMITED
6870 Goreway Drive
Mississauga, Ontario L4V 1P1
BEAK Ref: 2250.1

and

Nava Garisto
Whiteshell Nuclear Research
Establishment (WNRE)
Atomic Energy of Canada Ltd.
Pinawa, Manitoba R0E 1L0

for:

The National Uranium Tailings Program
Canada Centre for Mineral and Energy Technology
Energy, Mines and Resources Canada
555 Booth Street
Ottawa, Ontario K1A 0G1
DSS Ref: 26SQ.23241-4-1677
Contract Serial No. 1SQ84-00048

Associated Personnel:

D.L. Lush and
P. McKee
Beak Consultants Limited

Robert Lemire and
Frank Garisto
WNRE, Atomic Energy of
Canada Ltd.

O.E. Hileman and
P. Groeneweg,
Consultants

454 pp

APR 23 1986
MICROMEDIA

September 1985

SUMMARY

This report presents a descriptive algorithm incorporating the physical, biological, chemical and geological factors that influence the geochemical evolution of uranium mill tailings. The descriptive algorithm is presented as a series of compartment diagrams in which the main geochemical states are defined and pathways between the geochemical states are presented. The pathways describe mineral-water transformations and transport pathways. Simplification of the data presented in this report and subsequent computer coding could lead to the development of a comprehensive source-term model that would quantitatively describe the geochemical evolution of uranium mill tailings and would predict the release of aqueous-phase, gaseous and particulate contaminants from the tailings.

Major elements, minerals and dissolved species of concern in both Ontario and Saskatchewan tailings have been identified. The major minerals in Elliot Lake-type tailings are quartz, sericite (mica), pyrite and gypsum*. Minor quantities of hydrous iron oxides*, aluminum hydroxides*, chlorapatite, monazite, calcite* and possibly barite* are also present. The major mineral components in the high-grade Saskatchewan-type tailings include quartz, gypsum*, clays, micas, iron oxides, graphite, metal arsenides, and possibly nickel oxides and metal arsenates. Minor quantities of metal sulphides, selenides or selenates are also present. The milling process results in the addition or formation of variable quantities of secondary minerals (indicated by an *) which significantly influence the geochemical evolution of the tailings, and the export of radiotoxic contaminants.

A suite of elements of concern was selected for further consideration in this project. These include Si, Al, Ca, Mg, K, Na, Fe, S, C, H (as H^+) as the major constituents, and Cu, Ni, As, Ba, Co, Mn, Pb, Ti, Se, Sr and Mo as the minor components. The radionuclides of concern include U-238, U-234, Th-230, Ra-226, Pb-210, Po-210, Th-232, Ra-228 and Th-228. Many of the minor or trace elements (and radionuclides) are of concern because of the potential for toxicity in the ecosystem and to humans. The major constituents are generally considered to be innocuous, but were selected because of their influence on the overall chemical processes that occur in the tailings system and their resulting control on the potential contaminants.

Mineral dissolution, recrystallization and transport (advection, diffusion) are the major processes affecting the flux of contaminants from tailings. The significance of

adsorption is not well defined. The principal driving force for chemical transformation is the progression toward lowering of free energy. This principle is quantitatively illustrated in this report, using examples such as the instability of pyrite in an oxidizing environment and the dissolution of minerals into undersaturated pore water.

A review of the literature and pertinent data was conducted to identify key chemical, mineralogical and biological factors in uranium tailings. Two modelling simulations were performed to illustrate the roles and relative importance of controlling processes such as thermodynamics, kinetics and mass transport in the tailings environment.

Dissolution and recrystallization can be either kinetically or thermodynamically controlled. The appropriate control is a function of the hydraulic residence time and the presence of other reactions. Methods, for estimating whether equilibrium (or possibly steady-state) will be attained, are illustrated. The key parameter, which is the chemical residence time, compares the kinetic parameters to the residence time of groundwater moving through the tailings. Even if kinetic data are sparse, however, it is still possible to evaluate the controlling factors using order-of-magnitude estimates. The relationships between chemical residence time and spatial scale and between thermodynamic and kinetic models are also illustrated.

Available kinetic data for dissolution (and recrystallization) of minerals of concern have been compiled and deficiencies critically analyzed. The data are sparse for most minerals (except for calcite, gypsum, feldspars and silica). Because the study of mineral kinetics is relatively new, much of the data have great uncertainties associated with them.

A partial compilation of free energy data was developed for minerals and dissolved species. The data were selected with preliminary, critical analysis to ensure that all data are internally consistent. Expansion of this compilation would allow one to use the relatively, simpler approach of assuming equilibrium conditions to model dissolution mathematically. It is critical, however, that the possibility of kinetic controls on dissolution be assessed before an equilibrium assumption is used in modelling. For uranium mill tailings, the literature is especially deficient in kinetic data for the dissolution of monazite, arsenides, arsenates and selenates —— minerals, which may provide important controls on contaminant concentrations.

The first modelling simulation was performed to evaluate the thermodynamic response of an assemblage of minerals and the affected solution to the stepwise oxidation of pyrite. Pyrite oxidation was simulated by the addition of calculated amounts of oxygen to the pyrite mineral assemblage, or addition of pyrite oxidation products only to a similar unit volume of solids. A reaction-path-code was used to simulate this titration and to equilibrate the system of initial minerals and solution at each step. The initial mineral assemblage included pyrite (FeS_2), gypsum ($CaSO_4 \cdot 2H_2O$), calcite ($CaCO_3$), goethite ($FeOOH$), and gibbsite ($Al(OH)_3$). Subsets of this assemblage were also considered. Other minerals that were calculated to form later in the mathematical simulations include siderite ($FeCO_3$), jarosite ($KFe_2(SO_4)_3(OH_6 \cdot 6H_2O)$ and mellanerite ($FeSO_4 \cdot 7H_2O$).

The calculations show that pH trends during pyrite oxidation are similar to those observed for neutralization of acidic solutions in the actual tailings. The calculated formation of siderite and jarosite also agree with field observations. However, the calculated redox conditions do not correspond with those observed in the field, suggesting that the assumption of equilibrium between pyrite and goethite is not appropriate. Despite these discrepancies, however, the reaction-code-path calculations provide useful insight into the behaviour of Elliot Lake-type (pyritic) tailings.

The second modelling exercise was performed to illustrate the role of oxygen transport from the atmosphere and into the tailings on the resulting acid generation behaviour. In this case, pyrite oxidation was kinetically controlled. Oxygen transport was diffusion-controlled and represented by a one-dimensional reactive-transport equation. Oxygen consumption with first-order kinetics was coupled with a shrinking particle approach to model pyrite depletion. Mass balance was accounted for over a finite-sized, mixing-cell.

Modelling was conducted as a sensitivity analysis to determine the relative importance of oxygen diffusion coefficients in the tailings and the reaction-rate coefficient for pyrite oxidation. Two levels of diffusion coefficients were used; one representing a value equivalent to diffusion through air (high) and the other an intermediate value between air and water (low). Two reaction-rate constants were also evaluated; one representing reaction at neutral pH (low) and the other representing rapid oxidation in a low pH microbial system (high).

Model calculations showed that the total consumption rate of oxygen and hence the rate of acid production decreases with time. The sensitivity analysis showed that the gaseous diffusion coefficient is much more important than the reaction rate constant for predicting the acid production rate over the long-term. As the zone of pyrite depletion moves downward in the tailings over time, the diffusion coefficient becomes the controlling factor for the rate of acid generation. This example illustrated the importance of identifying the dominant controls in a system in order to simplify the appropriate predictive model, as well as the critical data required to calibrate the model. The calculations suggest that future research priorities should stress the measurement of the gaseous oxygen diffusion coefficient, relative to measuring factors controlling the kinetics of pyrite oxidation.

The modelling exercises and the review and compilation of data have led to identification of major and minor gaps in the literature needed to develop a descriptive algorithm. They include the following:

- the time scales over which certain minerals are not at equilibrium with their environment require identification (e.g., monazite, pyrite, arsenide). Kinetic data and calculations of the chemical residence time are needed;
- a well-justified, internally-consistent compilation of free energy (solubility product, complexation constants) data requires development;
- the mineral form of certain metals in tailings (e.g., calcium arsenate) is not well defined;
- adsorption data available for different models (e.g., Langmuir, Freundlich, etc.) should be developed into the model form suitable for use in NUTP probabilistic assessment;
- the geochemical control upon the dissolution of radionuclides such as Ra-226 and Pb-210 requires fundamental evaluation;
- reaction-path-code calculations are required to establish conceptual ideas for the geochemical evolution of complex Saskatchewan-type tailings. Kinetic concepts for these tailings and Elliot Lake-type tailings should also be introduced; and
- a Monte Carlo study of a detailed source-term model should be conducted to evaluate possible simplifications for a probabilistic assessment.

TABLE OF CONTENTS

Page

SUMMARY

1.0 INTRODUCTION AND SCOPE OF WORK 1.1
- 1.1 Goal of Study 1.1
- 1.2 Contaminants of Concern to U-Tailings Management 1.1
- 1.3 Factors Influencing Contaminant Transport 1.2
- 1.4 Model Development 1.2
- 1.5 Solid and Solution Relationships 1.3
- 1.6 Summary Statements and Future Modelling Needs 1.4

2.0 DEFINITION OF DESCRIPTIVE ALGORITHM 2.1
- 2.1 General 2.1
- 2.2 Hierarchy of Source Term Models 2.3
- 2.3 Focus of this Report 2.4
- 2.4 Relationship of Descriptive Algorithm to Hierarchy of Source-Term Models 2.7
- 2.5 Recommendations for Reading this Report 2.8

3.0 ENVIRONMENTAL STABILITY OF TAILINGS 3.1
- 3.1 Introduction 3.1
- 3.2 Examples of Stability in Tailings Pile 3.2
- 3.3 Secondary Influences upon Stability 3.4
- 3.4 Assessment of Tailings Stability by the Reader 3.6

4.0 ELEMENTS AND MINERALS OF CONCERN 4.1
- 4.1 General 4.1
- 4.2 Elements and Minerals Found in Uranium Ores and Tailings 4.1
- 4.3 Radionuclides Found in Uranium Ores 4.4
- 4.4 Radionuclides Mobilized in Leaching Tanks 4.4
- 4.5 Elements Considered in this Project 4.4
- 4.6 Elements to be Considered in Future NUTP Projects 4.5

TABLE OF CONTENTS (cont'd)

Page

5.0 WEATHERING AND TRANSPORT PROCESSES IN TAILINGS PILES 5.1
- 5.1 Chemical Weathering and Relative Mineral Stability 5.1
- 5.2 Biological and Vegetative Reactions 5.3
- 5.3 Physical Processes 5.6

6.0 DESCRIPTIVE EXAMPLE OF DEVELOPING A SOURCE-TERM MODEL
- 6.1 Chemical System Considered in this Example 6.1
- 6.2 Model Development 6.3
- 6.3 Iterative Solution of Model 6.6
- 6.4 Model Calculations Over Time 6.13
- 6.5 Summary of Model's Calculations 6.17
- 6.6 Weaknesses of Calculations 6.17
- 6.7 Recommendations for Future Model Development 6.18

7.0 DECISIONS REQUIRED FOR FORMULATION OF A SOURCE TERM MODEL 7.1
- 7.1 Scope of This Chapter 7.1
- 7.2 Spatial Scale and Box Models 7.2
- 7.3 Time Scales 7.7
- 7.4 Equilibrium and Kinetic Controls on Mineral Dissolution 7.11
- 7.5 Model Calibration Procedures and Validation Tests 7.12
- 7.6 Method for Combining Equilibrium, Kinetic and Transport Processes Into a Probabilistic Framework 7.15
- 7.7 Evaluation of Time Scales for Computational Scheme of Source Model 7.22
- 7.8 Recommendations Related to Modelling Decisions 2.24

8.0 A QUANTITATIVE OVERVIEW OF CHEMICAL EQUILIBRIUM AND KINETICS 8.1
- 8.1 Equilibrium Viewed as Two Opposing Rates 8.2
- 8.2 Comparison of Rate Control and Steady State 8.3

TABLE OF CONTENTS (cont'd)

Page

8.3 Chemical Regimes Controlled by Kinetics 8.5
8.4 Overview of Precipitation and Dissolution Theory 8.8
8.5 Application of Precipitation and Dissolution Theory to Analysis of Uranium Tailings Piles 8.15

9.0 EQUILIBRIUM 9.1
9.1 Solid Phases 9.1
9.2 Soluble Complexes 9.2
9.3 Reaction Code Pathway Calculations 9.2
9.4 Recommendations to NUTP for Evaluation of Equilibrium Constants 9.2

10.0 SIMULATION OF EQUILIBRIUM MINERAL ASSEMBLAGES DURING ACIDIFICATION 10.1
10.1 Introduction 10.1
10.2 Reaction Pathway Calculations 10.2
10.3 Simulation of Acidification and Chemical Evolution 10.3
10.3.1 Solids Considered 10.3
10.3.2 Simulation of a Pyrite-Goethite System 10.4
10.3.3 Simulation of a Complex Suite of Solids Using Different Oxidants 10.5
10.3.4 Simulation of a Pyrite-Free System with an Acid Sulphate Titration 10.6
10.4 Comparison of Simulation Results with Field Observations 10.7
10.5 Conclusions Concerning Simulation Results 10.9

11.0 KINETICS OF INDIVIDUAL MINERALS 11.1
11.1 Overview of Kinetics 11.1
11.2 Kinetics of Major Calcium Solids 11.7
11.2.1 Calcium Oxide 11.7

TABLE OF CONTENTS (cont'd)

Page

11.2.2 Calcium Carbonate (Limestone) 11.8
11.2.3 Gypsum Kinetics 11.12
11.3 Kinetics of Major Iron Solids 11.15
11.3.1 Fe(II) to $Fe(OH)_3(s)$ (in the absence of bacteria) 11.15
11.3.2 Pyrite Oxidation Kinetics 11.16
11.3.3 Formation and Dissolution Kinetics of Jarosite 11.18
11.4 Kinetics of Silica 11.22
11.5 Kinetics of Feldspar and Related Minerals 11.25
11.6 Dissolution Kinetics of Clays and Micas 11.27
11.7 Dissolution Kinetics of Nickel Arsenide Minerals 11.29
11.8 Dissolution Kinetics of Chalcopyrite 11.29
11.9 Dissolution Kinetics of Zn, Mn, Co 11.30
11.10 Dissolution Kinetics of Radionuclides 11.30
11.11 Summary of Concentrations Predicted by Dissolution Kinetics 11.31
11.12 Recommendations for Further Work on Tailings Kinetics 11.31

12.0 DIFFUSION AND REACTION CONTROLS ON PYRITE OXIDATION 12.1
12.1 Oxidation Reaction 12.1
12.2 Kinetic Controls 12.1
12.3 Transport Control 12.4
12.4 Model Results 12.6
12.5 Conclusions 12.7

13.0 ADSORPTION AND CATION EXCHANGE PROCESSES 13.1
13.1 Factors Affecting Adsorption 13.1
13.2 Cation Exchange Capacity 13.7

TABLE OF CONTENTS (cont'd)

Page

13.3 Application of Adsorption and CEC Data to NUTP Modelling Efforts 13.10
13.4 Recommendations for Future Work on Adsorption Processes 13.12

14.0 THE DESCRIPTIVE ALGORITHM: PATHWAY DIAGRAMS FOR MODELLING MINERALS AND ELEMENTS OF CONCERN 14.1
14.1 Silica 14.1
14.2 Aluminum 14.2
14.3 Calcium 14.4
14.4 Iron 14.4
14.5 Sulphur 14.10
14.6 Carbon 14.12
14.7 pH 14.13
14.8 Nickel 14.18
14.9 Arsenic 14.20
14.10 Radionuclides in General 14.22
14.11 U-238 and U-234 14.23
14.12 Th-230, Th-232 and Th-228 14.24
14.13 Ra-226 and Ra-228 14.25
14.14 Pb-210 14.26
14.15 Po-210 14.26

15.0 SUMMARY, CONCLUSIONS AND KEY RECOMMENDATIONS 15.1
15.1 General 15.1
15.2 Synopsis of Principal Findings 15.2
15.3 Conclusions 15.2
15.4 Key Recommendations
15.4.1 Future Modelling Needs
15.4.2 Fundamental Information
15.4.3 Possible Approach to Improved Understanding

TABLE OF CONTENTS (cont'd)

Page

16.0 ACKNOWLEDGEMENTS 16.1

17.0 REFERENCES 17.1

APPENDIX A: PATHWAY DIAGRAMS FOR OTHER ELEMENTS AND RADIONUCLIDES

- A.1 Sodium, Potassium, Magnesium A.1
- A.2 Chloride A.2
- A.3 Cobalt A.3
- A.4 Manganese A.4
- A.5 Lead A.5
- A.6 Copper A.6
- A.7 Titanium A.7
- A.8 Barium A.8
- A.9 Selenium A.9

APPENDIX B: CHEMICAL MODELLING IN THE URANIUM TAILINGS SYSTEM: PYRITE DISSOLUTION

LIST OF TABLES

Chapter 1

Table 1.1: Elements and Radionuclides Selected for This Project

Chapter 2

No tables.

Chapter 3

No tables.

Chapter 4

Table 4.1: Elemental Analysis of Typical Ores in Elliot Lake Area
Table 4.2: Chemical Analyses of Key Lake Ore Components
Table 4.3: Elemental Analysis of Gunnar Solids
Table 4.4: Elemental Analysis of Lac Nor Tailings
Table 4.5: Portion of Element in Elliot Lake Ore Leached in Leaching Pachucas
Table 4.6: Extraction of Key Lake Ore Components Under Acid Leaching Conditions
Table 4.7: Major Minerals Found in Typical Elliot Lake Tailings
Table 4.8: Summary of Major Minerals Found in Typical Northern Saskatchewan Tailings
Table 4.9: Summary of Representative Data Describing the Degree of Mobilization in Leaching Pachucas of Elliot Lake Tails
Table 4.10: Elements and Radionuclides Selected for This Project
Table 4.11: Summary of Major Minerals Relevant to Uranium Tailings

Chapter 5

No tables.

LIST OF TABLES (cont'd)

Chapter 6

Table 6.1: Relevant Reactions for Consideration
Table 6.2: Overview of Simplified Model
Table 6.3: Summary of Modelling Calculations

Chapter 7

Table 7.1: Calculations of Retention Time of Contaminant in Tailings Pore Water

Chapter 8

No tables.

Chapter 9

Table 9.1: Equilibrium Solids
Table 9.2: Summary of Soluble Complexes of Potential Significance in U-Mill Tailings Solutions

Chapter 10

No tables.

Chapter 11

Table 11.1: Dissolution Rate-Controlling Mechanisms for Various Substances Arranged in Order of Solubilities in Pure Water
Table 11.2: Summary of Dissolution Kinetics
Table 11.3: pH Dependence of Mineral Dissolution Rates
Table 11.4: Activation Energies of Geochemical Reactions
Table 11.5: The Measured Mass Transfer Coefficients for Different Particles Sizes
Table 11.6: Half-Time to dissolve Calcite Solids as a Function of Particle Size and Solution pH

LIST OF TABLES (cont'd)

Table 11.7: Summary of Concentrations Predicted by Dissolution Kinetics

Chapter 12

Table 12.1: Summary of Parameter Values for the Oxidation/Diffusion Model Test Cases

Table 12.2: A 2 x 2 Table Showing Beta x 10^{-5}

Chapter 13

Table 13.1: Effect of L/S ratio and Ba^{2+} on Ra Adsorption by Sediments

Table 13.2: Al(III) Adsorption onto Quartz

Table 13.3: Typcial CEC Values for Clays

Table 13.4: Summary of CEC, Particle Size, and Surface Area Data

Table 13.5: Values for Sorption Coefficients from Various Environments

Chapter 14

Table 14.1: Major Solid Phases Composed of the Elements of Concern in Uranium Tailings in Canada

Chapter 15

No tables.

Chapter 16

No tables.

Chapter 17

No tables.

LIST OF FIGURES

Chapter 1

No figures.

Chapter 2

Figure 2.1: Computer Model Hierarchy
Figure 2.2: Hierarchy of Uses of Data and Models
Figure 2.3: Descriptive Algorithm (Transformation Diagram) for Calcium

Chapter 3

No figures.

Chapter 4

Figure 4.1: U-238 Decay Series Radionuclides
Figure 4.2: Th-232 Decay Series Radionuclides
Figure 4.3: U-235 Decay Series Radionuclides

Chapter 5

Figure 5.1: The Reaction Series

Chapter 6

Figure 6.1: Pathway Diagram Sketch of Reactions for Unsaturation Zones Compartments and Reaction Pathways in Unsaturated Zone for Descriptive Example

Chapter 7

Figure 7.1: Alternative Geometries of Tailings

LIST OF FIGURES (cont'd)

Figure 7.2: Time Scale of Observational Data
Figure 7.3a: Temporal Scales of Chemical, Biochemical and Geological Phenomena
Figure 7.3b: Half Life of Relevant Radionuclides of Concern to Uranium Mine-Mill Management
Figure 7.4: Diffusion Coefficients Characteristic of Aqueous and Solid Environments
Figure 7.5: Summary of Radiological and Physical Time Scales of Concern to a Probabilistic Assessment

Chapter 8

No Figures

Chapter 9

No Figures

Chapter 10

Figure 10.1: The Abundance of Solids as a Function of the Reaction Coordinate for Case 1A.1
Figure 10.2: H^+ Concentration as a Function of the Reaction Coordinate, for Case 1A.1
Figure 10.3: The Concentration of Fe^{2+} and Fe^{3+} as a Function of the Reaction Coordinate for Case 1A.1
Figure 10.4: The Abundance of Solids as a Function of the Reaction Coordinate for Cases 1A.1 and 4C.1
Figure 10.5: H^+ Concentration as a Function of the Reaction Coordinate for Cases 4A.1 and 4C.1
Figure 10.6: The Concentrations of Fe^{2+} and Fe^{3+} as a Function of the Reaction Coordinate for Cases A.1 and 4C.1

LIST OF FIGURES (cont'd)

Figure 10.7: The Abundance of Solids as a Function of the Reaction Coordinate for Case 4B.1

Figure 10.8: H^+ Concentrations as a Function of the Reaction Coordinate for Case 4B.1

Figure 10.9: The Concentration of Fe^{2+} and Fe^{3+} as a Function of the Reaction Coordinate for Case 4B.1

Figure 10.10a: pe-pH Plot for Iron Speciation in Groundwater

Figure 10.10b: pe-pH Plot for iron Species and Solid Phases for Groundwaters

Chapter 11

Figure 11.1: Rate Controlling Steps in Dissolution Processes

Figure 11.2: Calcite Dissolution Rate as a Function of pH

Figure 11.3: Electromicrographs Showing Effect of Sample Preparation

Figure 11.4: Dissolution Kinetics of Calcite as for Particle Size

Figure 11.5: Model Calculations Versus Observations for Calcite Dissolution

Figure 11.6: Oxidation Rate of Iron(II) as a Function of pH

Figure 11.7: Pathway Model of Pyrite Oxidation

Figure 11.8: Jarosite Formation Kinetics

Figure 11.9: Silica Dissolution Rate as a Function of Sample Preparation

Figure 11.10: Helgeson Calculations for Feldspar Dissolution

Figure 11.11: Dissolution Kinetics of Various Alumino Silicate Minerals as a Function of pH

Figure 11.12: Rate Controlling Step in Dissolution Processes

Chapter 12

Figure 12.1: Schematic Depth Profile Through a Pyritic Tailings Deposit

Figure 12.2: Oxygen Concentration Profiles for Different Values of K/D

Figure 12.3: Effective Depth of Active Oxidation Zone Versus the Ratio of D/K

Figure 12.4: Oxygen Concentration Profile With Time

Figure 12.5: Total Flux of Oxygen with Time

Figure 12.6: Time to Deplete Pyrite per Unit Depth Versus Depth

LIST OF FIGURES (cont'd)

Chapter 13

Figure 13.1: Interaction with Hydrous Oxides
Figure 13.2: F^- - α·FeOOH Adsorption
Figure 13.3: H_4SiO_4 Adsorption
Figure 13.4: Dependence of Adsorption on pH and Solution Variables
Figure 13.5: Adsorption of Al onto SiO_2
Figure 13.6: Al - Organic Carbon Relationships
Figure 13.7: K_d - DOC Relationships
Figure 13.8: Simplified Structure and Composition of the Principal Clay Minerals

Chapter 14:

Figure 14.1: Pathway Diagram for Silica
Figure 14.2a: Pathway Diagram for Aluminum
Figure 14.2b: Speciation Diagram for Aluminum
Figure 14.3: Pathway Diagram for Calcium
Figure 14.4a: Pathway Diagram for Iron
Figure 14.4b: Distribution of Hydrolysis Products (Fe(III))
Figure 14.4c: Distribution of Hydrolysis Products (Fe(II))
Figure 14.5: Pathway Diagram for Sulphur
Figure 14.6: Pathway Diagram for Carbon
Figure 14.7: Pathway Diagram for H
Figure 14.7a: Distribution of Solute Species in Aqueous Carbonate System
Figure 14.7b: Carbonate Titration Curve
Figure 14.7c: Experimental Acid Titration Curve for Tailings Solids (Elliot Lake)
Figure 14.8: Pathway Diagram for Nickel
Figure 14.9: Pathway Diagram for Arsenic
Figure 14.10: Pathway Diagram for U-238 Nuclides (Level 1)
Figure 14.11: Pathway Diagram for U-238 Nuclides (Level 2)
Figure 14.12: Pathway Diagram for Th-232 Nuclides

LIST OF FIGURES (cont'd)

Chapter 15

No figures.

Chapter 16

No figures.

Chapter 17

No figures.

Appendix

Figure A.1a: Pathway Diagram for Na
Figure A.1b: Pathway Diagram for Potassium
Figure A.1c: Pathway Diagram for Magnesium
Figure A.2: Pathway Diagram for Chloride
Figure A.3: Pathway Diagram for Cobalt
Figure A.4: Pathway Diagram for Manganese
Figure A.5: Pathway Diagram for Lead
Figure A.6: Pathway Diagram for Copper
Figure A.7: Pathway Diagram for Titanium
Figure A.8: Pathway Diagram for Barium
Figure A.9: Pathway Diagram for Selenium

1.0 INTRODUCTION AND SCOPE OF WORK

1.1 Goal of Study

Uranium mill tailings are of environmental concern from the perspective of both long-term exposure to low level radiation and the ongoing discharge of non-radioactive contaminants from these tailings. The future behaviour of these tailings is difficult to predict. Increased and possibly unacceptable discharges of contaminants may occur due to biological, chemical or physical processes, many of which are not well understood or defined. Thus, it has proven difficult for regulatory agencies and mine operators to know how to close out tailings areas in a manner which will be environmentally sound into the foreseeable future.

The National Uranium Tailings Program (NUTP) was formed to conduct research into long-term environmental behaviour of uranium mill tailings. The main objective of the NUTP is to provide a scientifically credible information base upon which decisions can be made, with a known degree of confidence, in establishing reasonable criteria for the protection of the environment and which can also be used to propose practical guidelines for uranium tailings management. The research program of the NUTP will provide the technical basis for the development of acceptable, uranium-mill close-out guidelines by regulatory authorities and to be used as codes of practice by industry. One part of the research of the NUTP is the development and demonstration of a probabilistic assessment methodology for the long-term effects of uranium mine tailings upon the environment and upon humans.

One key component of the probabilistic assessment is the development of a source-term model for predicting the release rate of contaminants from the tailings pile. The goal of this report is to present a strategy and rationale for development of an algorithm characterizing the physical, biological, chemical, and geological factors influencing and/or controlling the geochemical evolution of a U-mill tailings. Simplification of the data presented in this report and computer coding the algorithm would provide one with a basic source-term model for the probabilistic assessment.

Several tools are available for formulating the source-term model. Field and laboratory data, with component and research models, provide the basis for describing and interpreting the geochemical evolution of tailings. Thermodynamic and kinetic concepts describe relationships between the dissolution of solid phases and solution characteristics which are, in turn, influenced by mass transport. The mass balance equation integrates the thermodynamics, kinetics, and mass transport to allow one to calculate the flux of contaminants from the tailings. The integration of these components is presented in Chapter 2.

1.2 Contaminants of Concern to U-Tailings Management

Elements of concern in the management of uranium mill tailings are those:

(i) which pose a radiotoxic or chemical-toxic hazard to humans, and/or
(ii) which significantly influence the geochemical evolution of the tailings.

A discussion of the elements considered in this project and the reasons for selecting them appears in Chapter 4 and is summarized in Table 1.1. For any particular management application, a subset would probably be selected for analysis, to reflect site specific characteristics and/or economic resources available for analysing the problem.

1.3 Factors Influencing Contaminant Transport

Transport of contaminants (radionuclides, toxic elements) is influenced by the chemical stability of minerals in a weathering environment and by hydrological flow pathways through the tailings.

The chemical stability of tailings can be conceptually assessed by comparing the present environment of tailings to that from which they originated. For example, pyrite that formed under reducing conditions is unstable in the oxidizing environment of the unsaturated zone of tailings. Aluminosilicates formed under high temperatures are unstable at ambient environmental temperatures. The assessment of stability is, in part, based upon the principle that the more different the environments of formation and of disposal are, the more unstable the minerals are. Concepts for assessing stability are discussed in Chapter 3, while a summary of minerals and secondary precipitates of concern is presented in Chapter 4.

TABLE 1.1: ELEMENTS AND RADIONUCLIDES SELECTED FOR THIS PROJECT

Element	Reason	Radionuclide	Reason
Si	1	U-238	7
Al	1,2,3	U-234	7
Ca	1,2,4	Th-230	6,8
Mg	1	Ra-226	6,8
K	1	Rn-222	6
Na	1	Pb-210	6,8
Fe	1,2,5	Po-210	6
S	1,2	Th-232	7,8
C	1,2	Ra-228	7,8
H^+	2	Th-228	7
Cu	3		
Ni	3,4		
As	3,4		
Ba	5		
Co	3		
Mn	3		
Pb	3,5		
Ti	3		
Se	3,4		
Sr	5		

1. Major element
2. Potential controller of pH
3. Trace or heavy element. Found in sufficiently high concentrations in groundwater to be a potential health hazard.
4. Major element in some tailings.
5. Element of potential concern due to controlling radionuclide concentration.
6. Radionuclide of prime concern to man's health (based upon dose commitment calculations).
7. Radionuclide of potential concern to man's health
8. Radionuclide which has potential influence upon activity of daughters for time frame of 100-10,000 yrs.

Weathering is the major factor influencing dissolution of tailings. Weathering is influenced by acidity, hydrological transport, biological factors, temperature and frost effects. Hydrological transport is a function of permeability, the degree of porosity of the understructure (bedrock) and retaining structure (e.g., dam) and groundwater gradients. These factors are discussed in Chapter 5.

1.4 Model Development

Five aspects of model development are considered in this report. They are:

(i) An example of developing a model and solving the equations by hand calculator is given in Chapter 6 for the unsaturated zone. The example assumes that: (1) pyrite oxidation is kinetically controlled; (2) calcite dissolution results from acid production; and (3) gypsum precipitates and dissolves at equilibrium with pore water. The predicted pH and radium concentrations in pore water are given for 3 geochemically significant, time periods.

(ii) Modelling issues related to the selection of spatial scales (e.g., number of boxes) and temporal detail are considered in Chapter 7.

(iii) The evolution of an equilibrium assemblage of minerals undergoing increasingly oxidizing conditions is simulated as a closed system. The suite of pyrite, calcite, gypsum, goethite and amphorus aluminum hydroxide and subsets of these are used; the results of the simulation are described in Chapter 10 and Appendix B.

(iv) The relative importance of the gaseous diffusion coefficient of oxygen and the potential rate of pyrite oxidation in the unsaturated zone are simulated in Chapter 12.

(v) The descriptive algorithm for the different elements is presented in Chapter 14 and Appendix A.

1.5 Solid and Solution Relationships

Adsorption and precipitation are, theoretically, equilibrium processes which relate the amount of mass in a solid phase to solution concentrations. These equilibrium relationships can also be described in thermodynamic terms. A summary of minerals found in tailings, which could be at equilibrium with tailings pore water, is given in Chapter 9. A summary of adsorption models (Cation exchange capacity, selectivity coefficients, Langmuir and site-binding models, and K_d's) is given in Chapter 13.

However, not all minerals are at equilibrium with pore water, because their dissolution is kinetically controlled for a particular time scale. The dissolution of minerals which are far-from-equilibrium in the ambient environment is probably kinetically controlled. Mineral dissolution will be kinetically controlled for certain time scales (e.g., calcite for 1 day) and equilibrium controlled for others (e.g., calcite for time scales on the order of one year). A quantitative overview of the relationship between kinetics and equilibrium is given in Chapter 8, but must be referenced to the discussion of time scales given in Chapter 7.

A summary of the kinetics of dissolution of various minerals is given in Chapter 11; this data can be used for developing kinetic expressions for a source-term model, and in some cases, for deciding whether or not a mineral is at equilibrium with pore water for a particular time-scale.

1.6 Summary Statements and Future Modelling Needs

The work in this report allows one to make a few summary statements and to detail future modelling needs to meet the objectives of the NUTP. A detailed summary for each chapter is given in a concluding section of each chapter. A synposis of recommendations for further work is given in Chapter 15. The recommendations are summarized under the major headings of:

(i) Future Modelling Needs
(ii) Fundamental Information
(iii) Elemental and Mineralogical Characteristics of the Ore
(iv) Milling Modifications of Ores

(v) Initial Composition of Tailings

(vi) Effect of New Mill Technologies and Mill Management Options

(vii) Research and Component Models

- Stability Assessment
- Selection of Time and Space Scales
- Calibration and Validation Procedures
- Assessment of Kinetic vs. Equilibrium Controls
- Reaction Code Pathway Calculation
- Thermodynamic Data Base Development
- Kinetic Calculations
- Probabilistic Model of Tailings Processes
- Study of Hydrological Models
- Special Studies

(viii) Development of Source Term Model

2.0 DEFINITION OF DESCRIPTIVE ALGORITHM

2.1 General

One of the main approaches being used by the NUTP to fulfill their objectives is the development and demonstration of a probabilistic assessment methodology for the long-term effects of uranium mill tailings upon the environment and upon humans. Figure 2.1 presents, in schematic form, an overview of the different components. The probabilistic systems model is the organizational and computational tool for integrating the different submodels. It also contains the method for directing the probabilistic calculation.

The system submodels describe the biological, geochemical and physical controls upon the release of radiological and chemical contaminants to the environment (the source model), transport through the environment (groundwater, surface water, atmosphere models) and the resultant human exposure (exposure model). For radiological parameters, dose commitment concepts can be used for the 'exposure model'; for chemical parameters, water quality criteria can be used due to the paucity of accepted 'mathematical chemical toxicity models' for humans.

For such a modelling framework, the use of detailed component or research models in the system model is not feasible. But such models are often required to interpret field and laboratory data within a theoretical framework. Accordingly, field or laboratory data and the results of the component or research models are aggregated and simplified to the degree required by the system submodel. In some cases, the system submodel may be more complex than desired by the systems model, in order to provide sufficient information about a particular environment. Of all the system submodels described in Figure 2.1, the geochemical evolution of the tailings may be viewed as the most important submodel because it is a main control upon the temporal response of the receiving environments (groundwater, surface water, atmosphere). The temporal evolution of the tailings requires description in a mathematical or algebraic form to allow its incorporation into the probabilistic systems format.

Three timeframes are forseen as essential to this project: long term, short term and annual. The main time frame is long term: 100 years to 10,000 years after closeout of the tailings pile. The long term time frame is the main focus of the National Uranium

FIGURE 2.1: COMPUTER MODEL HIERARCHY

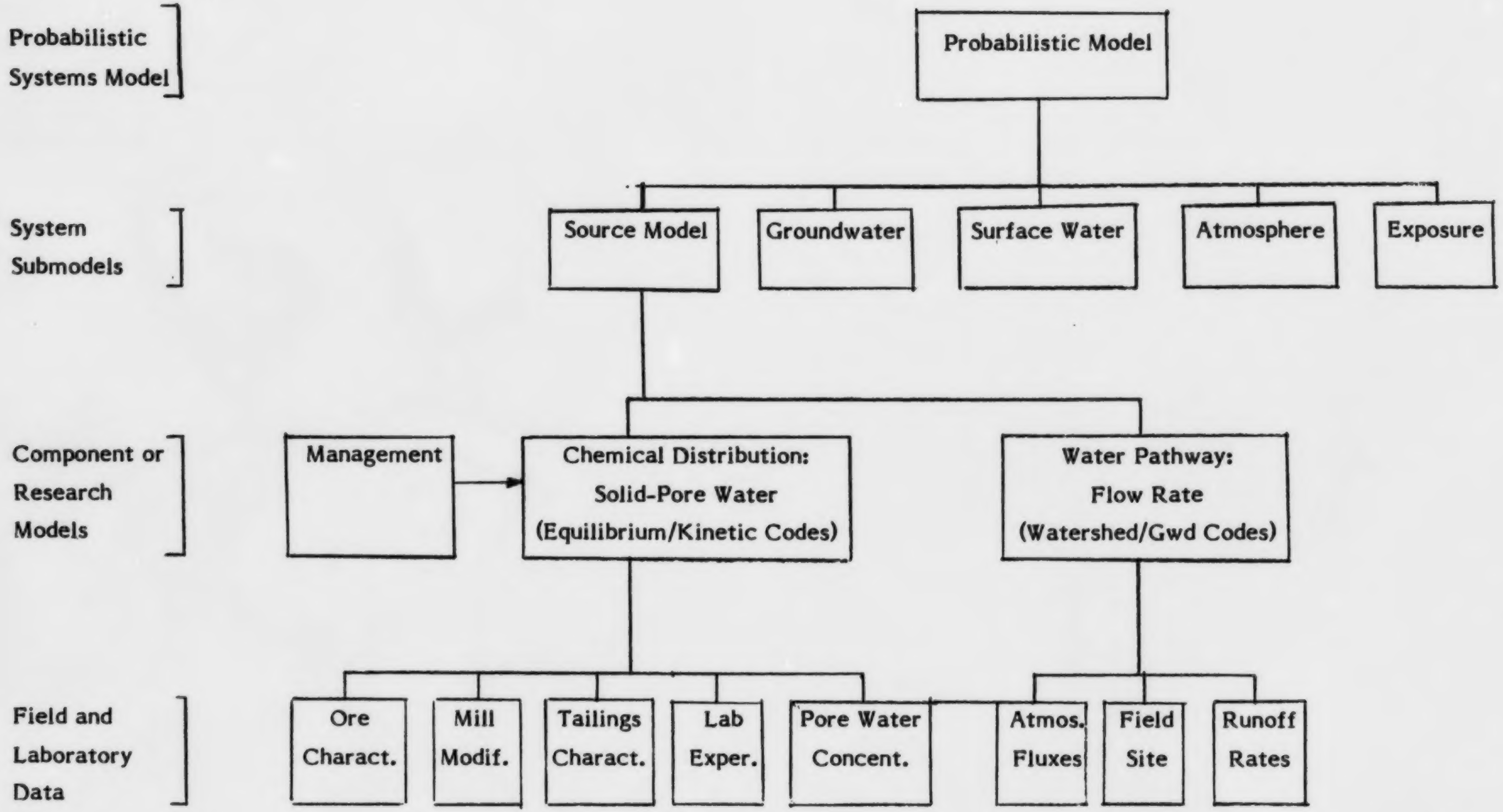
Probabilistic Systems Model
System Submodels
Component or Research Models
Field and Laboratory Data
Probabilistic Model
Source Model
Groundwater
Surface Water
Atmosphere
Exposure
Management
Chemical Distribution: Solid-Pore Water (Equilibrium/Kinetic Codes)
Water Pathway: Flow Rate (Watershed/Gwd Codes)
Ore Charact.
Mill Modif.
Tailings Charact.
Lab Exper.
Pore Water Concent.
Atmos. Fluxes
Field Site
Runoff Rates

Tailings Program. 100 years provides a useful definition of the beginning of a 'long term' time period. 10,000 years is chosen as the length of 'long term' for two reasons:

(i) previous studies have suggested that most of the geochemical evolution of concern and the export rate of radionuclides occurs well within 10,000 years, and

(ii) after 10,000 a, major climatological changes will likely be a more significant factor than the tailings management techniques originally employed.

The short-term time frame is defined as 1-100 years and the annual time frame is defined as ranging from minutes to a year. While not of major concern to the probabilistic assessment, these two time frames must be considered because data for calibrating and checking the predictions of any submodel are available for only these time periods. Existing field data characterizes approximately the first 20 years of the short term period, while laboratory and other data are usually available for the annual time frame.

2.2 Hierarchy of Source Term Models

Goal and Objectives of Source Term Models

The main goal of the source model will be to predict the release rate or flux of radionuclides and contaminants to aquatic pathways and the concentration of these substances near the surface of the tailings. When coupled with atmospheric boundary layer concepts, the flux of substances of concern to the atmosphere can be calculated.

The calculation of the fluxes of the following substances by the source models to aquatic pathways appears plausible. These contaminants include:

- radionuclides such as U-238, Th-230, Ra-226, Pb-210;
- metals such as aluminum, arsenic, selenium, copper, cobalt, and lead; and
- pH (hydrogen ion) and pH controlling parameters.

The calculation of the concentrations of the following substances in the surficial zones of tailings are plausible objectives for application to atmosphere pathways:

- radon (as a gas); and
- radionuclides (e.g., U-238, Th-230, Ra-226, Pb-210) in eroded particulate matter

It is also desirable to calculate the Eh (or pE) of the tailings for certain modelling applications.

Hierarchy of Models

Figure 2.2 presents a possible hierarchy of field/laboratory data, component and research models and system submodels which may be used in the probabilistic assessment process. The diagram emphasizes the following aspects:

- that mill, field and laboratory observations are used to feed component and research models;

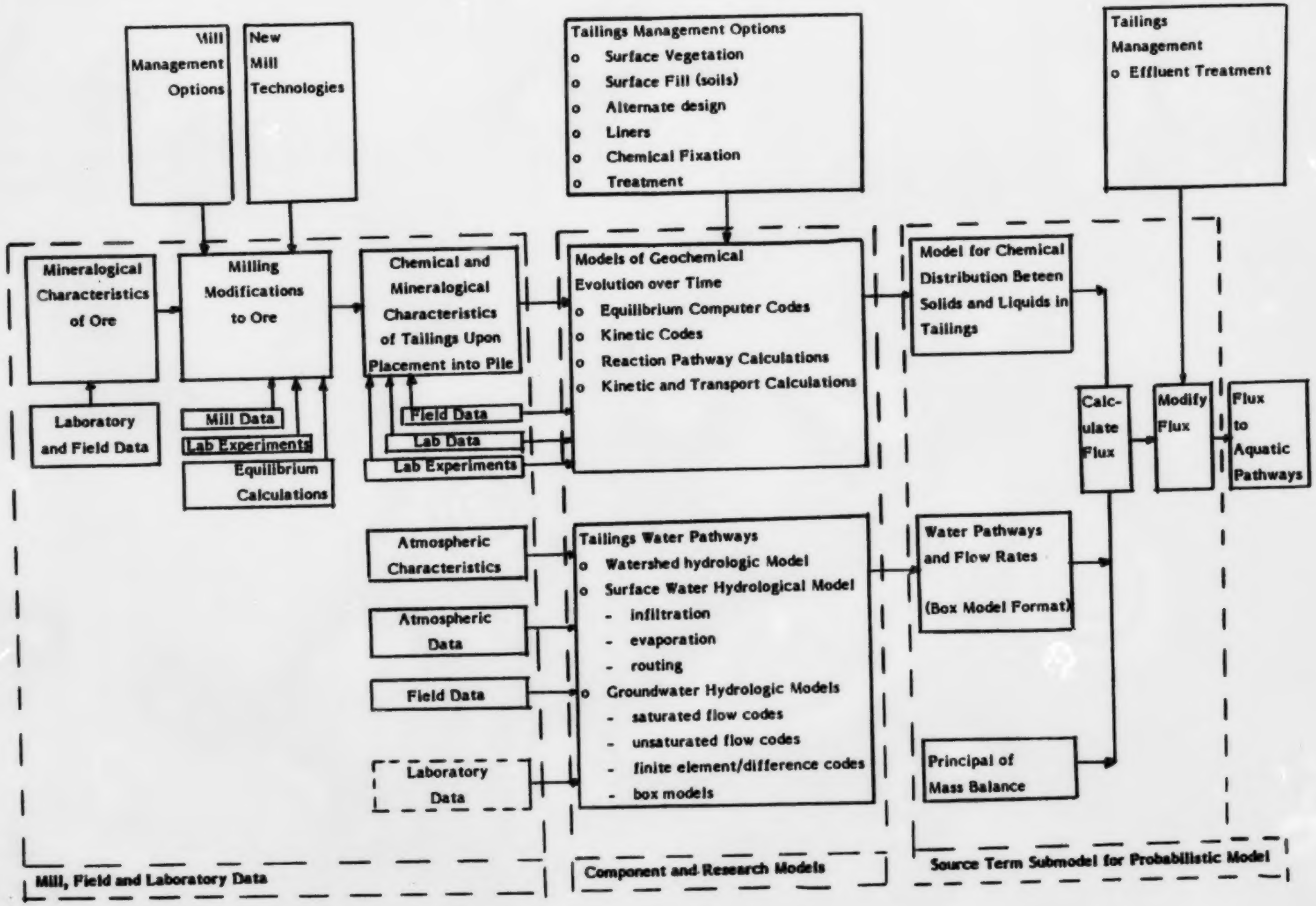
Mill Management Options
New Mill Technologies
Tailings Management Options
o Surface Vegetation
o Surface Fill (soils)
o Alternate design
o Liners
o Chemical Fixation
o Treatment
Tailings Management
o Effluent Treatment
Mineralogical Characteristics of Ore
Laboratory and Field Data
Milling Modifications to Ore
Mill Data
Lab Experiments
Equilibrium Calculations
Chemical and Mineralogical Characteristics of Tailings Upon Placement into Pile
Field Data
Lab Data
Lab Experiments
Models of Geochemical Evolution over Time
o Equilibrium Computer Codes
o Kinetic Codes
o Reaction Pathway Calculations
o Kinetic and Transport Calculations
Atmospheric Characteristics
Atmospheric Data
Field Data
Laboratory Data
Tailings Water Pathways
o Watershed hydrologic Model
o Surface Water Hydrological Model
- infiltration
- evaporation
- routing
o Groundwater Hydrologic Models
- saturated flow codes
- unsaturated flow codes
- finite element/difference codes
- box models
Model for Chemical Distribution Beteen Solids and Liquids in Tailings
Water Pathways and Flow Rates
(Box Model Format)
Principal of Mass Balance
Calc-ulate Flux
Modify Flux
Flux to Aquatic Pathways
Mill, Field and Laboratory Data
Component and Research Models
Source Term Submodel for Probabilistic Model

FIGURE 2.2: HIERARCHY OF USES OF DATA AND MODELS

- that various detailed computer codes for equilibrium and chemistry, groundwater transport, and kinetic concepts can be used (in simulation or diagnostic mode) to understand these observations;

- that the results from these detailed codes need to be simplified for incorporation into the source term submodel;

- that the original mineralogical and chemical characteristics of the ore and their modification in the mill are required to understand the initial chemical characteristics of several minerals and chemical precipitates in the tailings pile;

- that tailings disposal technology have an influence upon tailings characteristics and their geochemical evolution; and

- that tailings disposal technology should be considered in the design of a source term submodel for a probabilistic assessment.

2.3 Focus of This Report

This report presents a descriptive algorithm for describing how physical, biological, chemical and geological factors influence and/or control the geochemical evolution of a U-mill tailings pile. The algorithm is presented in the form of a transformation diagram which divides the elemental composition of the tailings into different chemical states and which describes the various biochemical, geochemical, and physical pathways for transfer of mass between chemical states.

Example of Descriptive Algorithm

An example of the descriptive algorithm is presented in Figure 2.3 for calcium for a particular ore and mill system. Physically, the tailings mass is divided into two boxes: the unsaturated zone and the saturated zone. Within each box, calcium is divided into five chemical forms (herein called compartments); four are solid and one is liquid. The trace Ca form (CaT) represents the mineral in the ore containing trace amounts of calcium; some of this calcium is lost from the mineral in the leaching pachucas. Gypsum

FIGURE 2.3: DESCRIPTIVE ALGORITHM (TRANSFORMATION DIAGRAM) FOR CALCIUM

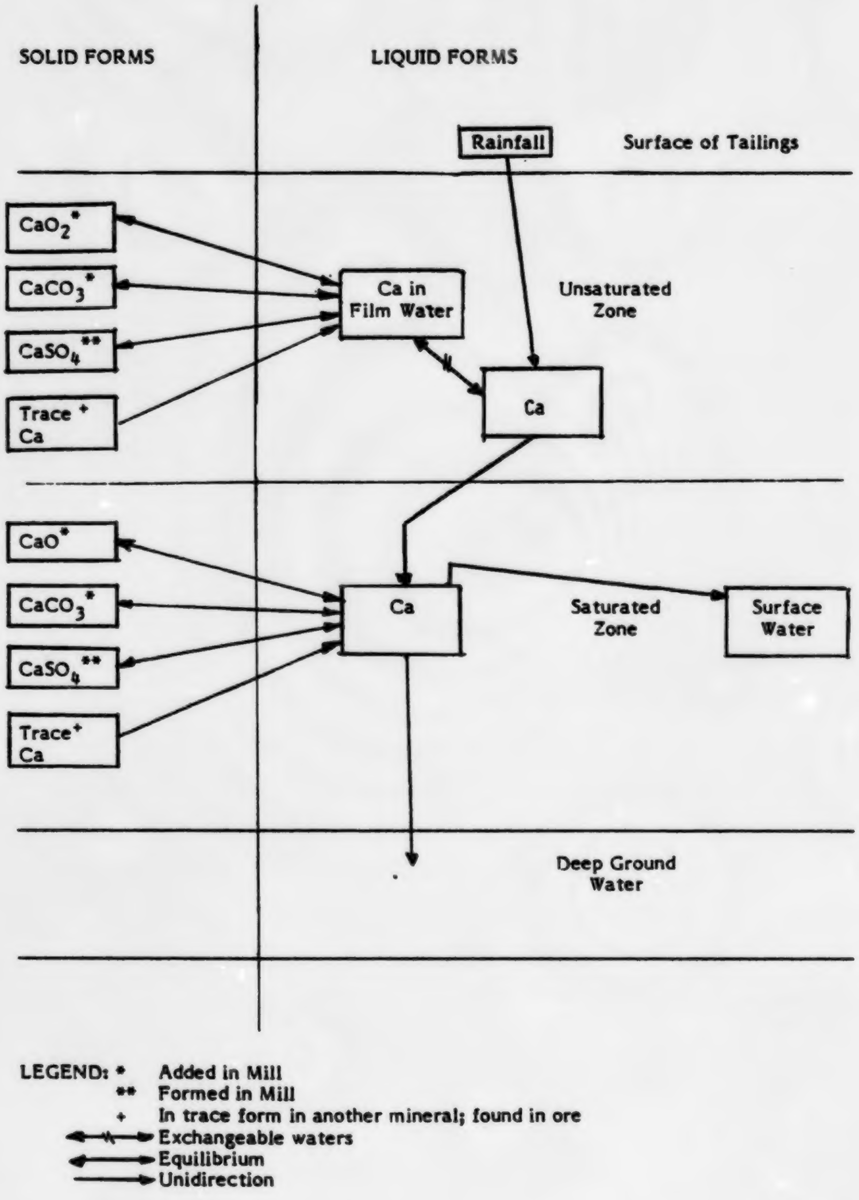
SOLID FORMS
LIQUID FORMS
Rainfall
Surface of Tailings
CaO_2*
$CaCO_3$*
$CaSO_4$**
Trace + Ca
Ca in Film Water
Ca
Unsaturated Zone
CaO*
$CaCO_3$*
$CaSO_4$**
Trace+ Ca
Ca
Saturated Zone
Surface Water
Deep Ground Water
LEGEND: * Added in Mill
** Formed in Mill
+ In trace form in another mineral; found in ore
Exchangeable waters
Equilibrium
Unidirection

is formed in the partial neutralization and final neutralization tanks due to the reaction of limestone ($CaCO_3$) and lime (CaO) with sulphate ion. The limestone and lime compartments represent residual amounts which did not dissolve in the mill; in many tailings CaO may not exist in significant amounts because of complete dissolution either in the final tanks or upon tailings placement.

The aqueous form of calcium is the only form assumed to be 'moveable'; its movement results from advective (convective) flow of groundwater. It moves downward with infiltrating rainwater to the groundwater table. After mixing in and transport from the saturated zone, it may flow directly to surface water (e.g., as in Lacnor) or percolate into deeper groundwater in a regional aquifer (e.g., as at Nordic). Figure 2.3 assumes that the movement of solids due to such physical mechanisms as erosion (land, water) and consolidation are insignificant compared to solution transport. Figure 2.3 also assumes that diffusion of calcium to deep groundwater is insignificant; in some situations diffusion may be a more significant transport mechanism than advection.

Figure 2.3 suggests that there are two significant dissolved forms of calcium in the unsaturated zone (film water, pore water) but only one form in the saturated zone. Between rainstorms, the voids of the unsaturated zone are occupied by air and soil moisture. Soil moisture takes the form of films around granular tailings and water trapped in narrow spaces (e.g., Freeze and Cherry, 1979). This film water may reach equilibrium with the solids present. During and after a rainfall or snow melt, infiltrating water will move downward through the unsaturated zone. The water may displace some film water, and partially exchange with other film waters, via diffusional processes. Accordingly, the infiltrating rain water reaching the saturated zone will have a composition different from that of the film waters. For the saturated zone, it is assumed that water movement is sufficiently slow that moving waters equilibrate with 'film waters'.

Principle of Mass Balance

Each compartment in Figure 2.3 is an entity about which a mass balance equation may be written. For example, for trace Ca in the unsaturated zone, the mass balance equation, in word form, is:

$$\begin{bmatrix}\text{The rate of} \\ \text{change of mass}\end{bmatrix} = - \begin{bmatrix}\text{Dissolution} \\ \text{Rate}\end{bmatrix} \times \begin{bmatrix}\text{Surface area of mineral} \\ \text{Per unit volume of tailings}\end{bmatrix} \quad (2.1)$$

In symbol form, the mass balance equation gives,

$$\frac{d}{dt} CS_{CaT} = - r_{CaT}\, S_{CaT} \cdot CS_{CaT}\, \rho_B \quad (2.2)$$

Here, CaT is the symbol for calcium as a trace constituent in a mineral

CS_{CaT} is the solid concentration of CaT (mol CaT/kg tailings)

ρ_B is the dry bulk density of tailings (kg tailings/m^3 of tailings)

r_{CaT} is the dissolution rate of CaT per unit area of mineral containing Ca (mol Ca/m^2/day)

S_{CaT} is the surface area of the mineral containing CaT (m^2 of surface/mol CaT)

t is time (day)

The value of CS_{CaT} is the concentration of Ca as a trace in a mineral upon placement of the tailings, less any loss due to dissolution. The value of r_{CaT} is a function of solution pH, other solution parameters and the ability of weathering processes to dissolve the mineral containing calcium.

Equation (2.2) contains many terms. The dissolution parameter, r_{CaT} is the mechanistic form commonly used to evaluate experimental data (e.g., see Chapter 10). But the surface area of specific minerals may not be known. In such a case, the equation could be simplified to,

$$\frac{d}{dt} CS_{CaT} = - k_{CaT}\, CS_{CaT} \quad (2.3)$$

where, $k_{CaT} = r_{CaT}\, S_{CaT}$
= dissolution coefficient (mol Ca/mol Ca/day)

Again, k_{CaT} is a function of solution parameters. If they vary over time, k_{CaT} will vary over time.

It is somewhat more difficult to see how to write mass balance equations for compartments of CaO, $CaCO_3$, $CaSO_4$ and aqueous Ca in Figure 2.3, using the concept of Equation 2.1, due to the existence of equilibrium between these compartments. Viewing dissolution and precipitation as two simultaneous processes which at equilibrium give a fixed relationship between the solid and solute concentration, the following word equation results for CaO.

$$\begin{bmatrix}\text{Rate of change}\\ \text{of Mass of CaO}\end{bmatrix} = - \begin{bmatrix}\text{Dissolution Rate}\\ \text{of CaO}\end{bmatrix} + \begin{bmatrix}\text{Precipitation}\\ \text{Rate of CaO}\end{bmatrix} \qquad (2.4)$$

Because the dissolution and precipitation rates are fast, one would probably choose not to use the resultant differential equation because it could be quite "stiff" relative to the time scale of the liquid phase (see Chapter 8). One would choose to use equilibrium to describe the relationship between the solid and solution composition and the principle of mass balance expressed in a form different from that of Equation 2.1 to describe the time evolution of CaO. For tailings which require evaluation of a stiff system of chemical kinetics differential equations, efficient numerical algorithms (e.g., FORSIM of AECL) are available to solve them.

2.4 Relationship of Descriptive Algorithm to Hierarchy of Source-Term Models

This report presents the descriptive algorithm for different radionuclides and elements in the form of the transformation diagram. This allows one to write a mass balance equation for each compartment in the transformation diagram (e.g., see Figure 2.3: CaO in the unsaturated zone; CaO in the saturated zone, etc.). By breaking each element up into chemical states (compartments) and writing a mass balance equation for each, one composes a 'bookkeeping' device - all mass initially present and its subsequent losses etc. are accounted for.

This descriptive algorithm centres upon the 'source term model' aspect of Figure 2.2. The water pathways and flow rates (Figure 2.2) describe the rainfall - groundwater discharge arrows (9, 10, 11, 12) of Figure 2.3. The 'model for chemical distribution' (Figure 2.2) would describe the distribution of calcium between solid and aqueous forms in Figure 2.3 (arrows 1 to 8). In other words, the 'model for chemical distribution' of Figure 2.2 considers such aspects as the biochemical kinetics and chemical equilibrium while the 'water pathways model' of Figure 2.2 considers the physical transport aspects. Coupling the 'chemical distribution model' and 'water transport model' using the principle of mass balance results in an overall equation which describes the flux of any calcium along a water pathway out of the tailings mass (e.g., arrows 11, 12 of Figure 2.3).

The descriptive algorithm presented herein considers more compartments than may be necessary for the long term time scale of the probabilistic assessment model. Future work should be directed towards assessing the degree of detail required for various probabilistic modelling objectives.

The compartments selected herein are judged to be significant for a variety of tailings areas. The compartments provide a framework for initiating reaction code pathway and other calculations (see "Models of Geochemical Evolution; Figure 2.2) and for examining laboratory and field data.

2.5 Recommendation for Reading This Report

As the reader examines this report, it is recommended that he continually ask the question:

> what level of detail of compartment selection is required for purposes of:
>
> a) incorporating mill, field or laboratory data into a source model or into research models,
> b) using component and research models, and
> c) examining the credibility of the source model.

3.0 ENVIRONMENTAL STABILITY OF TAILINGS

3.1 Introduction

An assessment of the environmental stability of tailings allows one to characterize their potential for mobilization and transport. A useful concept for considering their environmental stability is to compare the environment from which they originated to the environment in which they are deposited. If the environments are similar, then they will be relatively stable.

The present condition of tailings (fresh or 30 year old tails) is due to the following sequence:

(i) the initial mineral assemblage in the ore;
(ii) the modification to this assemblage in the mill;
(iii) the method of placement in the pile and resultant hydrological pathways; and
(iv) the geochemical evolution (if any) of the pile to the current time.

Tailings areas in Canada are generally less stable chemically than the original ore for the following reasons:

(i) change in redox conditions, temperature, etc.
(ii) change in pore water chemistry
(iii) change in elevation
(iv) milling processes

The first two reasons may be viewed as a change in thermodynamic stability. The third reason is physical in nature, changing the direction and nature of hydrological flow pathways. The fourth reason (milling) produces precipitates which may or may not be stable in the tailings environment.

A change in redox conditions or temperature from that under which minerals were formed will cause them to be thermodynamically unstable. Instability causes them to favour tranformation to another mineral or to dissolve. When these minerals are brought to the earth's surface, they are thermodynamically unstable under the oxidizing conditions of the surface.

The significant question is - how unstable are the minerals and how quickly will they transform (dissolve). Thermodynamics can be used to assess the degree of instability. Chemical kinetics (e.g., weathering) and biochemical kinetics (e.g., pyrite, oxidation) can be used to assess the rate of transformation.

3.2 Examples of Stabiity in Tailings Pile

Changes in Redox Condition

The following represent examples of minerals and chemical precipitates which undergo changes in redox conditions from the ore to the tailings pile.

(i) Residual uranium minerals: Many ores are formed under reducing conditions. For example, the formation of lead-zinc ore deposits in the Northwest Territories has been explained by the transport of lead and zinc in an oxidized state in groundwater from the Rocky mountains and its chemical precipitation at a redox boundary (Garvin and Freeze, 1984). The redox boundary may consist of organic matter and other substances. Similarly, for uranium, it will be transported in the U^{+6} state. A change of redox conditions causes U^{+6} to be reduced to U^{+4}; in this form uranium is relatively insoluble, precipitating as UO_2. For iron, aqueous elements such as Fe^{3+} and SO_4^{2-} are reduced, and precipitate as FeS and FeS_2 (pyrite) at a redox boundary. Subsequent sedimentary and other geological processes bury these minerals, completely encapsulating them within reducing conditions.

When the uranium is mined and milled, the oxidizing conditions of the leaching tanks oxidize and dissolve most of the uranium minerals. Residual uranium minerals not dissolved in the leaching tanks are placed in an oxidizing environment in the tailings pile. Dissolved uranium not extracted in the mill will be reprecipitated in the mill and be placed in the tailings pile in an oxidized state, possible as a gypsum coprecipitate.

With respect to redox conditions, the residual minerals will be relatively unstable in the pile while the reprecipitated uranium would be relatively stable.

(ii) Pyrite: When pyrite passes through the mill, it remains essentially unleached due to slow kinetics, despite its thermodynamic instability with respect to the oxidizing conditions. When placed in the oxic unsatuated zone, it readily dissolves due to catalysis by bacteria. When placed in the anoxic saturated zone, it is thermodynamically more stable, although it may not be as stable as in the original ore zone, because redox conditions in the tailings may not be as negative as in the original ore zone.

(iii) Nickel arsenide minerals: non-leached nickel arsenide minerals have reduced oxidation states. When placed in the unsaturated (oxidized) zone of tailings, they are relatively unstable.

(iv) Gypsum: Gypsum formed in the mill is stable under oxidizing conditions. When placed under reducing conditions in the saturated zone of tailings, it is relatively unstable because the oxidized form of sulfur (SO_4^{2-}) is thermodynamically unstable with respect to more reduced conditions. For sulphate reduction reactions mediated by "sulfate-reducing" bacteria, the kinetics will be rapid only if sufficient organic matter is present in the saturated zone.

(v) Metal arsenate: It is probable that metal arsenates such as calcium arsenate ($CaHAsO_4$; $Ca_3(AsO_4)_2.3H_2O$) and barium arsenate are formed after chemical neutralization of the liquor of northern Saskatchewan mills such as Key lake. These precipitates could be relatively unstable in the saturated zone if reducing conditions exist.

Changes in Temperature Conditions

With respect to temperature, many minerals are formed at high temperatures (70-2000°C) below the earth's surface. Subsequent geological processes transfer these minerals to cooler zones and even to the earth's surface. If these minerals are unstable, they will tend to transform to new phases or to dissolved to form new minerals. The instability with respect to temperature is one of the main thermodynamic criteria for weathering of minerals. The weathering of K feldspar in a tailings pile is one example of temperature induced instability.

Changes in pH Conditions

Aluminum hydroxide and iron hydroxide are two precipitates which may form in the final neutralization tanks. These precipitates are relatively more insoluble at neutral pH than at acidic pH. If placed in the unsaturated zone, these precipitates will become relatively less stable if the pH becomes acidic due to pyrite oxidation.

Changes due to Aging

Chemical precipitates such as amorphorus aluminum hydroxide and amorphorus iron (III) hydroxide may form in the mill due to rapid precipitation. These precipitates are not stable compared to more thermodynamically stable phases such as gibbsite and goethite (FeOOH) respectively. The transformation to a more thermodynamically stable phase is called aging.

Minerals, if thermodynamically unstable, will transform either by dissolving and reprecipitating into a more stable form (congruent dissolution) or by reordering molecular arrangements within the solid phase. If the solid phase rearrangement involves partial dissolution, it is termed incongruent dissolution. If the phase change involves dissolution, and if significant solution transport of dissolved elements occurs, reprecipitation may not occur because the solution is undersaturated with respect to the new phase.

3.3 Secondary Influences upon Stability

The hydrological flow rate past solid phases, and changes in other mineral phases are secondary factors which influence the stability of minerals in tailings.

Hydrological Flow in Tailings Pile

The design of tailings piles and their elevation influence the susceptability of minerals to dissolution and reprecipitation. Relative to the ore, minerals in tailings piles are more susceptible to dissolution because the composition of shall groundwater is generally more dilute than in deeper strata. The placement of tailings behind porous dams (e.g., valley dam as in Nordic tailings area) generally allows higher flow rates throughout the tailings than if they are placed in an old lake basin underlain by non-fractured bedrock (e.g., Stanleigh).

High rates of water movement make a mineral, more thermodynamically unstable than lower flow rates provided the solution is undersaturated and that kinetics control the rate of dissolution. This point is addressed in more detail in Chapters 4 and 8. In general terms it may be described as follows. For a mineral in contact with water, the degree of thermodynamic instability is a function of the difference between the solubility limit (the thermodynamic point of equilibrium) and the concentration of ions in solution. Higher flow rates dilute the mass of ions present in solution, resulting in a lower concentration. At a lower concentration, the mineral is more unstable.

Changes in Other Solid Phases in the Tailings Pile

Pyrite oxidation results in dissolution of pyrite and a decrease in pH. The lowering of pH may cause the solution phase to change from being supersaturated with respect to a solid phase to being undersaturated with respect to a solid phase. The lowering of pH changes conditions favorable to precipitation to thos favorable to dissolution. The stability of metal hydroxides ($Al(OH)_3(s)$, $Fe(OH)_3(s)$) are especially influenced by these changes.

Combined Influence of Primary and Secondary Factors upon Stability

The stability of aluminum hydroxide, iron (III) hydroxide, and calcium sulphate are examples of the combined influence of primary and secondary factors upon mineral stability in the tailings.

(i) Aluminum Hydroxide: Aluminum does not participate significantly in redox reactions. Its major transformations will involve conversion from amorphorus to more thermodynamically stable crystalline forms (e.g., gibbsite, bayerite, mixed alumino-silicates). Whether this recrystallization occurs via dissolution and reprecipitation or via solid-solid transformation is not clear.

The stability of $Al(OH)_3(s)$ in the tailings is mainly a function of water flow rate and pH conditions. Because low pH conditions are caused by the oxidation of pyrite, aluminum stability is indirectly related to redox conditions. Hence, aluminum hydroxide will be relatively unstable in the unsaturated zone if pyrite oxidation occurs, but relatively stable in the saturated zone if subsequent neutralization has occurred.

(ii) Iron Hydroxide: Iron hydroxide (III), will be unstable in the unsaturated zone if pyrite oxidation induces a decrease in pH. In the saturated zone iron hydroxide would be relatively stable, from a pH point of view, assuming that no pyrite oxidation occurs. But because iron (III) transformation to iron (II) is thermodynamically favoured under sufficiently reducing conditions, iron (III) hydroxide would tend to transform to another phase. Accordingly, iron (III) hydroxide is potentially unstable, throughout the tailings pile.

But, the reaction simulation of Chapter 10 shows that pyrite and iron (III) hydroxide can coexist and be at equilibrium. This seemingly surprising result is explained in Chapter 10 and points out the need for detailed calculations, to obtain a firm estimate of environmental stability of tailings.

(iii) Calcium Sulphate: Sulphur and oxygen are the main elements of gypsum which undergo significant redox reactions. Gypsum will dissolve, if waterflow keeps the water unsaturated with respect to calcium and sulphur. Accordingly, gypsum will be unstable (i) in the unsaturated zone where infiltrating rainfall passes through and (ii) possibly in the saturated zone where groundwater flow is significant. From a redox point of view, gypsum is thermodynamically stable in the unsaturated zone, relative to the anoxic satuated zone where sulphur (VI) may become unstable. Hence, overall, gypsum is potentially unstable throughout the tailings pile.

3.4 Assessment of Tailings Stability by the Reader

It is recommended that two approaches be adopted to assess the stability of solid phases in a uranium-mill tailings pile: a conceptual approach and a quantitative approach.

For the conceptual approach, the present environmental state (oxidizing conditions) should be referenced to the biogeochemical conditions under which the solid phase was formed. The divisions of:

(i) change in redox conditions
(ii) change in temperature conditions

(iii) change in pH conditions
(iv) mineral aging

provide a useful framework for analysing the spectrum of solids present.

For a quantitative approach, the degree of saturation (saturation index) of pore water with respect to mineral phases or the solubility product of different phases of the same chemical elements (e.g., amorphorus aluminum hydroxide, gibbsite, microcrystalline bayerite, bayerite) can be used to assess the potential degree of stability. The saturation index is especially useful because it incorporates the effects of groundwater flow and other primary factors (e.g., redox conditions, temperature, pH) into one expression.

For either approach, reference to where the minerals were formed (ore, mill, tailings pile) and to the age of the tailings (old or fresh) will aid the assessment.

In this report, aspects of stability are developed in the following chapters. In Chapter 4, an elemental analyses of ores and of tailings and a major mineralogical analyses is presented; this allows inferences about what mineral may be stable in the ore. Also, estimates of the mass of chemical precipitates formed in the mill are given in Chapter 4. Factors influencing weathering of these solid phases are described in qualitative terms in Chapter 5.

A quantitative description of solid phase stability with respect to pore water characteristics, and factors influencing stability is given in Chapter 8. This includes a quantitative summary of factors influencing dissolution and precipitation of solid phases (Chapter 11) and a summary of major phases present in U-mill tailings in Chapter 9. The potential influence of particular elements upon the stability of others are simulated for subsets of tailings solid phases in Chapter 10. These data form the basis for the descriptive algorithm presented in Chapter 14.

For future work of the NUTP, it is suggested that:

(i) A qualitative conceptual analysis of the stability of different minerals be developed for all minerals/precipitates (hereafter called solids) of concern to the NUTP for the sequence of ore-milling-tailings pile.

(ii) The indirect effects of stability upon others (e.g., effect of pyrite oxidation upon stability of aluminum hydroxide) could also be conceptually assessed. But due to the myriad of possible sequences of mineral succession, it is advantageous to use computer simulation with reaction code calculations. An example of this simulation is presented in Chapter 10.

4.0 ELEMENTS AND MINERALS OF CONCERN

4.1 General

The elements and minerals of concern to this project are those in uranium mill tailings which are mobilized in sufficient quantities to pose radiological or chemical toxicological hazards to biological organisms in the natural environment or to human beings. The radiological hazard may be expressed either in the form of water quality criteria or in the form of dose commitment calculations. The toxicological hazard is expected to be expressed in terms of concentration units for aquatic and atmospheric environments, because an equivalent methodology to dose commitment calculations is not available for quantifying chemical toxicity. For aquatic systems, the concentration units are expected to be expressed in the form of water quality criteria. Mutagenic, carcinogenic (e.g., AIMS) and other toxicological testing procedures may have been used as an aid for establishing the water quality criteria, but the tests, in general, are not sufficiently well advanced to allow rational quantification of the risk to human health.

4.2 Elements and Minerals Found in Uranium Ores and Tailings

To develop mathematical models of the geochemical evolution of uranium mill tailings, one writes a mass balance equation for each element (e.g., Si, Al) to describe their chemical states (e.g., silicon in SiO_2, Si in groundwater) and their transformations (e.g., SiO_2 dissolution to aqueous Si).

To describe the transformations of elements mathematically, knowledge of the mineralogy of ores (i.e., the minerals in the ore) and the elemental composition of each mineral is required. The minerals (and chemical precipitates formed in the leaching tanks) and their dissolution rates are among the prime controls on the resultant concentrations of radionuclides and chemical species in groundwater.

Elements Found

A summary of elements typically found in the Elliot Lake area and northern Saskatchewan ores and/or tailings is presented in Tables 4.1 - 4.6.

TABLE 4.1: ELEMENTAL ANALYSIS OF TYPICAL ORES IN ELLIOT LAKE AREA (The statistics are for 3 heads and 2 tails for 3 different mines, unless otherwise noted)

Element	Mean (%)	Standard Deviation (%)
SiO_2	78.4	2.4
Ca*	.10	.008
Mg	.12	.044
Na	.0992	.058
K	1.94	.40
Al	3.50	.39
Fe***	3.40	.75
Be	-	-
Mo	LT .001	-
V	LT .001	-
Ba	.023	.0051
Sr	-	-
Zn	.0054	.0015
Cd	LT .001	-
Mn	.004	0
Co	.0046	.0005
Cu	.0067	.0005
Ag	LT .002	-
Pb	0.035	.0088
Cr	LT .001	-
Ni	.003	.005
Ti	.067	.014
Bi	LT .001	-
Sb	LT .001	-
Sn	LT .001	-
B	.0004	0
As	LT .005	-
F	.02	-
PO_4^{3-}	.12	.043
CO_2*	.21	.009
Cl, Br, I	.005	.002
S*+	2.80	.78
L.O.I.	2.98	.69
Th	.028	.012
U_3O_8*	.079	.013
Ra (pCi/g)	251	38
Total**	90.94	

* Based upon values of Heads (Tails not included)

** Total of all means. 90.04% is due to SiO_2, Al, Fe, K and S. The remaining 9% is presumed due to oxides of Al and K.

*** Fe:S ratio in heads of 3 mines are respectively 1:1.5, 1:1.25; 1:1.4; Avg. is 1:1.4.

TABLE 4.2a: CHEMICAL ANALYSIS OF KEY LAKE ORE COMPONENTS

(The test results are for various ore samples from the two Key Lake orebodies (Table I-2; Sherritt, 1980). A ratio of sandstone:basement material of 20:80 was used to make up typical ore blends for Gaertner ore given in Table 4.6)

Element or Compound	Gaertner Ore													Deilmann Ore								
	Sandstone			Basement								High Arsenic 9	Graphite Ore	Sandstone			Basement					
	A1+A1[1]	B1	2+3	A4	A4[1]	B4	5	6	7	8				S1	S2	S3	B1	B2	B3	B4	B4*
U_3O_8	0.267	0.548	2.09	0.118	0.090	0.427	2.46	6.41	12.3	23.4		4.74	0.038	0.45	2.36	13.3	0.48	3.18	9.60	21.8	52.9
As	0.454	0.759	1.14	0.272	0.455	0.911	2.12	4.60	6.61	7.59		9.10	0.11	0.250	0.624	0.876	0.264	1.57	2.61	4.47	0.094
Ni	0.805	1.13	1.38	0.535	0.923	1.72	3.85	7.82	11.0	11.9		10.3	0.14	0.282	0.732	0.935	0.158	1.63	2.43	3.76	0.064
Fe	1.75	2.34	3.12	1.81	2.51	4.14	8.18	7.96	5.68	3.45		3.90	1.15	2.10	3.05	5.57	1.87	4.36	5.68	4.62	1.73
S_T	0.50	0.66	0.89	0.19	0.46	0.86	1.16	2.16	3.13	4.24		3.78	0.16	1.54	1.25	1.33	0.30	1.43	1.40	2.08	0.36
$S(SO_4)$	0.041	0.041	0.053	0.022	0.035	0.048	0.105	0.17	0.21	0.18		0.15									
SiO_2	80.3	78.9	71.1	54.7	50.1	47.3	39.2	29.9	22.7	22.5		30.7	63.6	72.6	64.6	44.4	48.2	35.4	31.6	23.2	14.7
Al	3.21	3.43	3.47	10.3	11.0	10.2	9.23	7.81	7.06	5.23		7.30	7.85	2.59	2.47	3.38	9.73	10.6	10.7	7.35	4.71
Mg	0.95	1.07	0.62	4.54	4.91	3.57	2.18	1.01	0.74	0.47		1.70	1.26	0.41	0.55	0.65	2.89	2.44	1.70	1.18	0.97
Ca	0.38	0.39	0.25	0.31	0.30	0.43	0.51	0.44	0.53	0.65		0.315	0.233	0.057	1.34	1.06	0.35	0.23	0.56	1.19	0.96
C_T	0.32	0.27	0.25	1.99	1.28	0.79	0.52	0.23	0.21	0.19		0.27	8.5								
CO_2	1.23	1.31	0.91	0.64	1.04	1.45	1.83	0.99	0.88	0.39		0.63	<0.1								
Co	0.029	0.035	0.039	0.017	0.029	0.069	0.121	0.169	0.177	0.197		0.237	0.0039								
Zn	0.087	0.090	0.058	0.046	0.066	0.154	0.235	0.194	0.188	0.110		0.194	0.175								
P_2O_5	0.140	0.083	0.093	0.140	0.256	0.162	0.163	0.163	0.180	0.180		0.246	0.28								
Cu (ppm)	280	380	690	150	410	960	760	700	980	850		550	130								
Mo (ppm)	31	26	130	21	25	38	62	170	210	300		220	25	98	70	87	130	360	550	818	3560
Approximate Amount (kg)	327	242	145	612	743	382	294	199	318	318		237	~100	27.2	2.0	2.3	345	114	36.3	37.2	3.4

Analyses in weight percent except as indicated.

TABLE 4.2b: CHEMICAL ANALYSIS OF KEY LAKE LAYERED TAILINGS
(The test results are for three core samples from Site A labelled A3, A7, A8 and three from Site B labelled B1, B2, B3)

Analysis	Units	A3	A7	A8	B1	B2	B3	Average
Al	%	3.3	2.8	3.0	2.3	2.7	2.4	2.8
As	%	1.3	1.3	1.2	1.3	0.3	1.2	1.1
Ca	%	9.5	8.0	9.2	6.0	6.6	4.0	7.2
Co	%	0.049	0.054	0.052	0.073	0.072	0.069	0.062
Fe	%	2.8	2.3	2.4	1.9	2.1	1.8	2.2
Mg	%	0.97	0.95	0.92	0.69	0.75	0.66	0.82
SO_4	%	18.6	16.7	17.3	12.8	15.9	10.3	15.3
CO_3	%	5.4	4.3	5.3	3.6	2.1	1.5	3.0
Ni	%	1.6	1.7	1.6	2.0	2.0	1.8	1.8
Si	%	18.9	20.3	23.9	26.7	23.9	30.2	24.0
Mo	ug/g	20	12	12	12	12	10	13
U	ug/g	473	403	471	626	543	530	508
Th-230	Bq/g	320	280	260	250	270	180	260
Ra-226	Bq/g	340	320	300	250	310	260	300
Pb-210	Bq/g	380	360	340	240	220	260	300
Po-210	Bq/g	260	290	230	200	250	230	250
Tertiary Amine	%	0.01	0.017	0.015	0.0072	0.0080	0.0051	0.1
Isodecanol	ug/g	L 10	L 10	L 10	L 10	L 10	L 10	L 10
Kerosene	ug/g	750	1,080	2,160	290	600	750	940
C.E.C.	meq/100 g	2.2	5.4	-	-	-	-	

C.E.C. - Caton Exchange Capacity

Note: Analyses for A3 and A7 were carried out after third leach.
Analyses for A8, B1, B2 and B3 were carried out after a brief initial wash.

TABLE 4.3: TYPICAL ELEMENTAL ANALYSIS OF GUNNAR SOLIDS

Parameter	Depth 3-3.5 m	Depth 6.5-7 m	Depth 9.5-10 m
Anions (ug/g)			
Bromide	-	-	-
Chloride	-	-	-
Fluoride	-	-	-
O-Phosphate	-	-	-
Sulphate	-	-	-
Nitrate	-	-	-
Major Cations (ug/g)			
Magnesium	13,900	15,700	13,800
Calcium	7,800	9,600	8,400
Iron	19,700	24,200	20,800
Manganese	246	286	288
Silica	581,000	591,000	611,000
Aluminum			
Sodium			
Potassium			
Trace Cations (ug/g)			
Strontium			
Lead	240	2246	188
Cobalt	6.5	14.6	6.4
Nickel	8.4	19.5	5.7
Zinc	32.3	32	30.3
Chromium	24	38	25
Copper	25	29	18.6
Cadmium	5.2	6.0	5.3
Barium	-	-	-
Vanadium	-	-	-
Titanium	-	-	-
Arsenic	-	-	-
Selenium	-	-	-
Molybdenum	-	-	-
Beryllium	-	-	-
Total Sulphur (%)	-	-	-
Radionuclides			
Uranium (ug/g)	58	74	
Thorium-230 (Bq/g)	3.0	4.5	
Radium-226 (Bq/g)	8.0	9.5	
Lead-210 (Bq/g)	8.0	9.5	
Polonium-210 (Bq/g)	5.5	7.5	
Radium-228 (Bq/g)	0.11	0.25	
LOI %	1.0	1.3	1.3

TABLE 4.4: ELEMENTAL ANALYSIS OF LACNOR TAILINGS*

Parameter	Concentration
Anions	
Br, Cl, F, P, S, N	data not available
P (ug/g)	110
Major Cations (mg/g)	
Magnesium	0.66
Calcium	2.66
Iron	31.7
Manganese	0.017
Silica	-
Aluminum	23.8
Sodium	1.5
Potassium	18.7
Trace Cations (ug/g)	
Strontium	18.7
Lead	145
Cobalt	41
Nickel	25
Zinc	27
Chromium	10
Copper	45.7
Cadmium	LT 1
Barium	-
Vanadium	17.6
Titanium	688
Arsenic	-
Selenium	-
Molybdenum	LT 20
Beryllium	0.52
Silver	LT 0.5
Thorium	60
Zirconium	73
Other Parameters (mg/g)	
Total C	LT 0.2
Organic C	LT 0.2
Total S	32.6
Sulphide	3.6
Radionuclides	
Uranium (ug/g)	44.7
Thorium-230 (Bq/g)	2.6
Radium-226 (Bq/g)	2.35
Lead-210 (Bq/g)	3.45
Polonium-210 (Bq/g)	-
Thorium-232 (Bq/g)	0.2
Radium-228 (Bq/g)	-
Thorium-228 (Bq/g)	0.2

* 16-18' depth section of core from Lacnor IA-7 (see Golder, 1985 for core description).

TABLE 4.5: PORTION OF ELEMENT IN ELLIOT LAKE (RIO) ORE DISSOLVED IN LEACHING TANK

	Portion of Element* in:		
Element	Leaching Liquor: Skaeff Survey** (%)	Leaching Liquor: NUTP Project*** (%)	Surface Solid**** (%)
Si	-	2.7	0.02
Ca	23	10	5
Mg	11	10	0.8
Na	1.8	7.9	-
K	1.8	2.2	0.07
Al	3.3	2.6	0.003
Fe	5.5	6.1	0.5
Be	-	-	-
Mo	-	GT 1$^+$	GT 4$^+$
V	-	GT 20$^+$	GT 0.6
Ba	1.2	.14	30
Sr	-	-	-
Zn	12	22	0.9
Cd	-	GT 5$^+$	++
Mn	31	41	0.15
Co	4	33	1
Cu	11	17	1
Ag	-	GT 5$^+$	-
Pb	20	72	100^{+++}
Cr	-	GT 40$^+$	++
Ni	10	24	3

* Composition of ore is given in Table 4.1. Portion of element mobilized is based upon difference in concentration between pachuca input and pachuca output.

** Skaeff survey data, provided by Rio Algom, is for "pachuca input and pachuca outflow".

*** NUTP project is for 04 December sampling of inflow to all pachucas and #12 leaching tank (outflow). Chemical concentrations were measured by IEC BAS.

**** Surface solid estimate is based upon three samples from EDTA solution. The solids were sampled, immediately filtered, washed with weak sulphuric acid and then ten volumes of distilled water at Rio's lab. The solids were treated with EDTA back at the lab.

+ Chemical data for solids are based upon assuming that the analytical detection limit is the concentration in the solids.

++ Estimate not possible because of analytical detection limit of leaching solution and solids.

+++ Actual solids data are required to provide a better estimate.

TABLE 4.6: EXTRACTION OF KEY LAKE ORE COMPONENTS UNDER ACID LEACHING CONDITIONS

(The test results are for lab testing results (Table I-13; Sherritt, 1980) on two ore blends anticipated in 1980 to be typcial of Key Lake: Gaertner and Deilmann. Actual full scale leaching conditions were anticipated to be 4 to 5 times more concentrated. The solution concentrations are pregnant solutions (product feed to solvent extraction) analyses.)

Leach Conditions: Combined single and two stage leach results
Maximum leach temperature 70°C
Extractions based on 99% uranium extraction

Component	Gaertner Ore			Deilmann Ore		
	Ore Analysis (%)	Solution (g/L)	Extraction (%)	Ore Analysis (%)	Solution (g/L)	Extraction (%)
U_3O_8	2.0	5.0	99.0	2.86	5.0	99.0
As	1.5	2.3-3.0	60-80	1.13	1.3-1.5	65-75
Ni	2.5	3.4-4.1	55-65	1.05	1.1-1.3	60-70
S	1.0		~50 *	0.77		*
Fe	3.5	3.1-3.9	35-45	3.04	1.9-2.1	35-40
Ca	0.35	0.5-0.6	57-69**	0.37		
CO_2	1.0	-	~100	0.82	-	~100
Al	9.0	1.0-2.0	4.4-8.8	10.3	1.1-1.8	6-10
Mg	3.0	0.8-1.8	11-24	2.9	0.9-1.3	17-25
SiO_2	50	0.2-0.6	0.2-0.5	50	0.7	0.8
Na	0.7	0.03	1.7	0.9	0.054	3.4
K	0.6	0.04	2.7	1.5	0.10	3.8
Co	0.076	0.050	26	0.081	0.055	39
Cu	0.029	0.023-0.046	32-63	0.087	0.044	29
Mo	0.006	0.0060	40	0.028	0.024-0.030	49-61
P_2O_5	0.16	0.17-0.20	43-50	0.15		
Ti	0.40	0.003-0.013	0.3-1.3	0.62	0.0083	0.8
V	0.08	0.040-0.058	20-29	0.092	0.035	22
Zn	0.08	0.078-0.163	39-82	0.033	0.022	38
Cl	0.05	0.020	16			
F	0.05	0.020-0.035	16-28			

* Sulphur extractions difficult to estimate because of high $S(SO_4)$ in leach residues.

** Net Ca extraction in two stage leach will be ~0 because solutions are gypsum saturated.

N.B. The leach solution analyses correspond to feeds to uranium recovery; full strength leach liquors are 4 to 5 times more concentrated (except for Ca).

The elemental analyses for Elliot Lake ores (Table 4.1) represent the mean values of data for 3 heads and 2 tails from 3 different mining-mill complexes of Rio Algom (A. Vivyurka, personal communication). The chemical analyses of "Key Lake" ores (Table 4.2) represent data from ore components (Table 4.2a) used in designing and evaluating the Key Lake Uranium milling process (Sherritt, Gordon Mines, 1980), and from an NUTP monitoring study (Table 4.2b) on a layered tailings system (Knight-Piesold, 1985). The chemical analyses for Gunnar and Lacnor Tailings represent data obtained from ongoing NUTP field programs.

For the Elliot Lake ores, the dominant elements are respectively silicon, aluminum, iron, sulphur (as sulphide) and potassium. These elements total 91% of the mass of the total given in Table 4.1 when silicon is represented as silica (SiO_2).

The elemental analyses of various samples from the Key Lake (northern Saskatchewan) ore components (Table 4.2a) were used to develop ore blends for laboratory pilot scale testing programs, for KLMC's design of the milling process (Sherritt, 1980). Silica is the dominant component in the sandstone and in most of the basement samples. In both the ore components and layer tailings (Table 4.2b), aluminum, iron, sulphur, arsenic, nickel, calcium, magnesium, uranium (U_3O_8) and carbonate have varying degrees of importance after silica.

The elemental analyses of various samples from Gunnar on Lake Athabasca (northern Saskatchewan) and Lacnor (Elliot Lake area) are given in Table 4.3 and 4.4 respectively.

These tailings are the two reference sites which the NUTP plan to use to demonstrate the probabilistic modelling methodology. The Gunnar and Lacnor tailings are both dominated by silica, aluminum and iron.

Elements in Leaching Tanks

Any element can be a potential source of aquatic contamination if it can be dissolved. The portion of elements mobilized in the leaching tanks provides one piece of information to determine their potential for dissolving in the tailings.

Estimates of the portion of different elements mobilized in the leaching tanks of Rio Algom (Elliot Lake) and in the acid leaching pilot trials of Key Lake are given in Table 4.5 and 4.6 respectively. The estimates for Rio Algom are based upon two different surveys (grab samples of inflow water to the first pachuca and the final pachuca effluent). Generally, less than 10% of the elemental composition of the ore is found in the leaching solutions. For a few elements (e.g., Zn, Mn, Pb, Ni), the data suggest that more than 10% is found in the leaching solution.

There is generally good agreement between the two sets of estimates (Table 4.5) based upon 1977 (Skaeff) and 1984 (NUTP) surveys. For three elements, the difference between the two surveys appears too large to probably be real (Pb, Ba, Co). The differences of estimates for four other elements (Ca, Zn, Mn, and Ni) are sufficiently large to suggest the need to refine the data. While the difference between two surveys could be real, the consistency of the percent mobilized for the several other elements (Al, Fe, Mg, etc.) suggests the need for further measurements.

For the Key Lake data, a much larger fraction of elements is in the leaching solutions than in the Rio Algom ores. The lab data suggests that between 40% and 99% of elements such as As, Ni, sulphide, iron, calcium, carbonate, copper, Mo, phosphorus and zinc are dissolved. Between 5 and 30% of aluminum, magnesium, cobalt, vanadium, chloride, and fluoride are mobilized while 3% and less of SiO_2, sodium, potassium, and titanium are dissolved.

The leaching tank data, however, may underestimate the amount of each element dissolved into solution during the leaching period. For example, in another NUTP study (BEAK, 1985), the solids separated from the leaching liquor by filtration (glass fiber filter) were treated with various washing agents (KCl, $CaCl_2$, $FeCl_3$, $BaCl_2$, EDTA). Other elements were dissolved with these agents. Thermodynamic analysis of the resultant washing solution concentrations suggest that the ionic strength of the salts through its affect upon activity coefficients can explain the chemical concentrations in the washing solutions. This suggests that the material dissolved in the washing solutions is a secondary precipitate formed in the leaching tanks on the surface of the ore. For this interpretation, the fourth column in Table 4.5 gives an estimate of the amount of an element dissolved and reprecipitated to form a secondary precipitate.

Minerals Found

A summary of the major minerals identified in Elliot Lake and northern Saskatchewan ores and tailings are given in Tables 4.7 and 4.8 respectively. A quantitative estimate of the mineral constituents of the Elliot Lake and Key Lake tailings are given in Table 4.7b and 4.8b. The estimates for Key Lake are from Knight-Piezold (1985), while those for Elliot Lake reflect the data of Table 4.1 supplemented by data for mill addition of chemicals such as calcium.

The total elemental composition of the ore of Rio Algom (Table 4.1) is 90.9%. The molecular ratio of K:Al in the ore is 1:2.6. Assuming that potassium is contained mainly in sericite (e.g., muscovite $K\,Al_2(AlSi_3O_{10})(OH)_{10}$), the expected K:Al ratio is 1.3. Hence all of K and Al cannot be contained in sericite. Assuming that aluminum is sericite and that the remaining potassium is an impurity, the major element composition becomes,

SiO_2	70.6%
Sericite	23.1%
Total (including other elements from Table 4.1)	100%

With this information, essentially all of the ore is accounted for.

The Elliot Lake tailings are dominated by silica and alumino-silicate minerals (e.g., sericite). Pyrite and gypsum are present in lesser amounts. All other minerals are present in trace quantities in a relative sense. The estimates of Table 4.7b are based upon the assumptions documented above, not on quantitative mineralogy. Hence, the reader should be cautioned against using the estimates as definitive, but rather as an approach for estimating the quantities of primary minerals and secondary precipitates present in tailings.

The estimated mineralogy for Key Lake tailings are based upon a combination of identification (XRD, microscopic methods) and inferences from chemical balances in the mill. The major phases identified are quartz, gypsum, ettringite, graphite and clay

TABLE 4.7a: SUMMARY OF MAJOR MINERALS FOUND IN TYPICAL ELLIOT LAKE TAILINGS

Original Ore	
Quartz	SiO_2
Pyrite	FeS_2
Brannerite	$(U, Ca, Ce)(Ti, Fe)_2O_6$
Uraninite	UO_2
Monazite	$(Ce, La, Y, Th)(PO_4)$
Sericite + Feldspars + Clays + Trace Minerals	
Tailings	
Quartz	SiO_2
Calcite	$CaCO_3$
Pyrite	FeS_2
Barite	$BaSO_4$
Gypsum	$CaSO_4 \cdot 2H_2O$
Jarosite	$KFe_3(SO_4)_2(OH)_6$
Chlorapatite	$Ca_5(PO_4)_3Cl$
Iron Oxides	e.g., α-Fe_2O_3
Monazite	$(Ce, La, Y, Th)(PO_4)$
Sericite + Feldspars + Clays + Trace Minerals	

TABLE 4.7b: ESTIMATE OF TYPICAL COMPOSITION OF ELLIOT LAKE ORES

Primary Constituents	Composition (mol/tonne)	Secondary Constituents (Formed in Mill)	Composition (mol/tonne)
SiO_2	10,900	$Fe(OH)_3(s)$	25
Sericite	400	$Al(OH)_3(s)$	29
Fe (as sulphide)	530	K (in pore water)	11
S (with Fe)	780	Gypsum	460
K_2O	24	$CaCO_3(s)$	18
Ba	1.6	$SiO_2(am)$	6
Pb	1.5	$SrSO_4$	0.014
Sr	-	$PbSO_4$	0.07
		$BaSO_4$	0.0005

Assumptions:

1. Based upon Rio Algom ores.

2. Solid:liquid ratio in leaching pachucas is 2.62 g solid/g liquid ~1:1, vol/vol.

3. Concentrations of cations in leaching liquor in pachucas are assumed to define the magnitude of secondary minerals formed. The leaching liquor concentrations from BEAK (1985) are: Fe: 4,100 mg/L (±480; n = 14); Al: 2,300 mg/L (±840, n = 14); Ba: 0.2 mg/L; K: 1,250 mg/L (±395, n = 14); Pb: 45 mg/L (±4.4, n = 14); SiO_2: 1,030 mg/L (±121, n = 12); Sr: 3.4 mg/L (±0.25, n = 13). Gypsum concentration is based upon sulphate concentration and mill mass balance (BEAK, 1982) and is 500 mol/tonne ore.

4. Composition of primary constituents is based upon ore composition minus the portion leached into solution in the leaching pachucas. Addition of gypsum and calcite increase ore mass by 8.7%. It is assumed that leaching processes act on the ore conservatively (i.e., that uranium extraction has a minimal effect upon the ore mass and that the material leached from the original ore mass becomes secondary precipitates in the tailings). The mass added as iron balls is assumed negligible. Accordingly, ore composition, gypsum and calcite are adjusted by 1.087 to account for the additional mass.

5. These data differ from data used in other sections of the report. The values in Chapter 6 (FeS_2: 415 mol/tonne; gypsum: 500 mol/tonne; calcite: 110 mol/tonne) are based on 5% pyrite (rather than 6.4% FeS) and a design addition of calcite. The values of Chapter 10 (FeS_2: 416 mol/t; $Fe(OH)_3(am)$: 305 mol/t; gibbsite: 204 mol/t; gypsum: 555 mol/t; and calcite: 20 mol/t) are based upon:

   - assumed mill concentrations of Fe_T = 10,200 mg/L, Al_T = 3,900 mg/L, total sulphate = 32,000 mg/L and a S:L ratio of 6:10, and
   - assumed tailings concentration of FeS_2 (5%) and $CaCO_3$ (0.2%).

TABLE 4.8a: SUMMARY OF MAJOR MINERALS FOUND IN TYPICAL NORTHERN SASKATCHEWAN TAILINGS

Original Ore	
Quartz	SiO_2
Feldspars	$NaAlSi_3O_8$
Micas	$KAl_2(AlSi_3O_{10})(OH)_{10}$
Clays	$MgAl_2Si_3O_{10}(OH)_2$
Arsenides	NiAs
Selenides	PbSe
Hematite	Fe_2O_3
Carbonates	$MgCa(CO_3)_2$
Trace Minerals	
Tailings	
Quartz	SiO_2
Feldspars	$NaAlSi_3O_8$
Micas	$KAl_2(AlSi_3O_{10})(OH)_{10}$
Clays	$MgAl_2Si_3O_{10}(OH)_2$
Arsenides	NiAs
Metal Oxides (Fe, Ni, Mg, Al)	$Fe(OH)_3$, $Ni(OH)_2$ etc.
Gypsum	$CaSO_4 \cdot 2H_2O$
Arsenates	$CaHAsO_4$
Selenates	$FeSeO_4$

TABLE 4.8b: ESTIMATE OF MAJOR MINERALS FOUND IN KEY LAKE LAYERED URANIUM TAILINGS (from Knight and Piesold, 1985)

Mineral/Compound	Formula	Weight (%)
Major Constituents		
Quartz	SiO_2	48
Gypsum	$CaSO_4.2H_2O(2CaSO_4.H_2O)$	26
Graphite*	C	2
Illite, Trichlorite	(K, Al, Mg, Si, Ti, O, OH, Al, Mg, Si, O, OH)	7.4
Ettringite	$Ca_6Al_2(SO_4)_3(OH)_{12}.26H_2O$	3.7
Calcium Arsenate*	$Ca_3(AsO_4)_2.3H_2O$	2.0
Calcite*	$CaCO_3$	5.0
Gersdorffite	NiAsS	0.8
Nickel Compounds	NiS, $Ni(OH)_2$ Ni,FeS_2	2.0
Iron Compounds	Fe_2O_3,FeS_2,$Fe(OH)_3$	3.2
Minor Constituents		
Cobalt Compounds*	CoS,$Co(OH)_2$	0.1
Uranium Compounds	U(adsorbed), hydrated oxides	< 0.1
Zinc Compounds	ZnS, ZnFeS, $Zn(OH)_2$	< 0.1
Lead Compounds	PbS, $Pb(OH)_2$	< 0.1
Copper Compounds	CuS, $Cu(OH)_2$	< 0.1
TOTAL		100.2%

* Assumed, no measurements available.

minerals. The heavy metals identified are gersdorffite; millerite and some bravoite for Ni; hematite, sphalerite, chalcopyrite, pyrite and some geothite for Fe; and linnaeite. Trace minerals identified included were salena, covelite and rutile. Calcium orthoarsenate, calcite, nickel hydroxide, hydrated oxides and hydroxides of iron and uranium were hypothesized to occur, but not identified.

The Key Lake and Elliot Lake estimates are based upon a combination of mineralogical identification (XRD, microscope, scanning electron microscope - x-ray emission) and chemical balance data from the mill. These approaches reinforced with other techniques, such as washing studies, illustrate the methods required to define the mineralogical state of the source term. When not used jointly, however, they do leave unanswered questions. For example, Knight-Piezold (1985) based their estimate for calcium arsenate upon:

- the Sheritt-Gordon (1979) estimate that 70% of the arsenic would dissolve and reprecipitate as a secondary arsenate;
- the arsenic content of 1.1% in the tailings; and
- an inspection of thermodynamic data describing arsenate compounds.

They hypothesize that calcium arsenate is transformed to hardingerite ($(CaO_2)_2 \cdot As_2O_5 \cdot 3H_2O(s)$) to explain the low arsenic concentration in the pore water as the pH decreases from basic (pH 10) to neutral. Mineralogical studies did not specifically identify either phase.

Their approach for estimating the quantity of calcium arsenate is sound, reflecting a fundamental premise that milling dissolves arsenic, alters its oxidation state and causes it to reprecipitate. More work is required, however, to confirm the secondary precipitate formed. Identification techniques, such as SEM-XRE in addition to XRD and comprehensive analysis of mill process waters, would be useful in this regard.

4.3 Radionuclides Found in Uranium Ores

The main radionuclides found in uranium ores are the parent and daughters in the U-238, Th-232, and U-235 series. The amount of U-235 present, compared to the amount of U-238 is sufficiently small that it may typically be ignored (Kilborn, 1979).

The main radionuclides in the decay series are given in Figures 4.1, 4.2 and 4.3. Very short-lived radionuclides are not included. The main radionuclides of radiological concern in the U-238 decay series are U-238, U-234, Th-230, Ra-226, Pb-210 and Po-210. In the Th-232 decay series, the main radionuclides are Th-232, Ra-228 and Th-228. U-238 decay series radionuclides are found in all ores. Th-232 decay series radionuclides are found in substantial quantities in Elliot Lake ores, particularly as monazite (Tables 4.1, 4.4), but not in the Gunnar tailings. The other ore deposits in northern Saskatchewan have negligible to minor quantities of thorium.

4.4 Radionuclides Mobilized in Leaching Tanks

Data describing radionuclide mobilization in leaching tanks is somewhat sparse. Most attention has centred upon uranium. Leaching mobilizes 93-97% of U. Some attention has centred upon Ra-226. The data of Skaeff (1977) suggest that 0.2% of Ra-226 is found in the leach tank. (This calculation is based on a value of 1,500 pCi/L measured in the leach tank (Skaeff, 1977), for a solids activity of 300 pCi/g and an assumed solids concentration of 74% on a weight basis.)

For a 1981 modelling study, CANMET and AECB personnel (E. Joe, K. Bragg, personal communication) suggested an assumption that 95% of U-238 minerals and 50% of Th-232 minerals were dissolved in the leaching tanks of Elliot Lake ores was justified by available evidence. Under the assumption of secular equilibrium within the minerals, one would expect that a similar proportion of daughters was also dissolved. This is not true for Ra-226, but it may be explainable by reprecipitation of Ra-226 as a coprecipitate upon the surface of the solids. For the other radionuclides, a more comprehensive data set is required to validate this assumption.

A summary of a few pieces of data describing radionuclide dissolution is given in Table 4.9.

4.5 Elements Considered in This Project

Of the various elements given in Tables 4.1 to 4.7, several have been selected for consideration in this project. A summary of these elements with the major reason for considering them is given in Table 4.10.

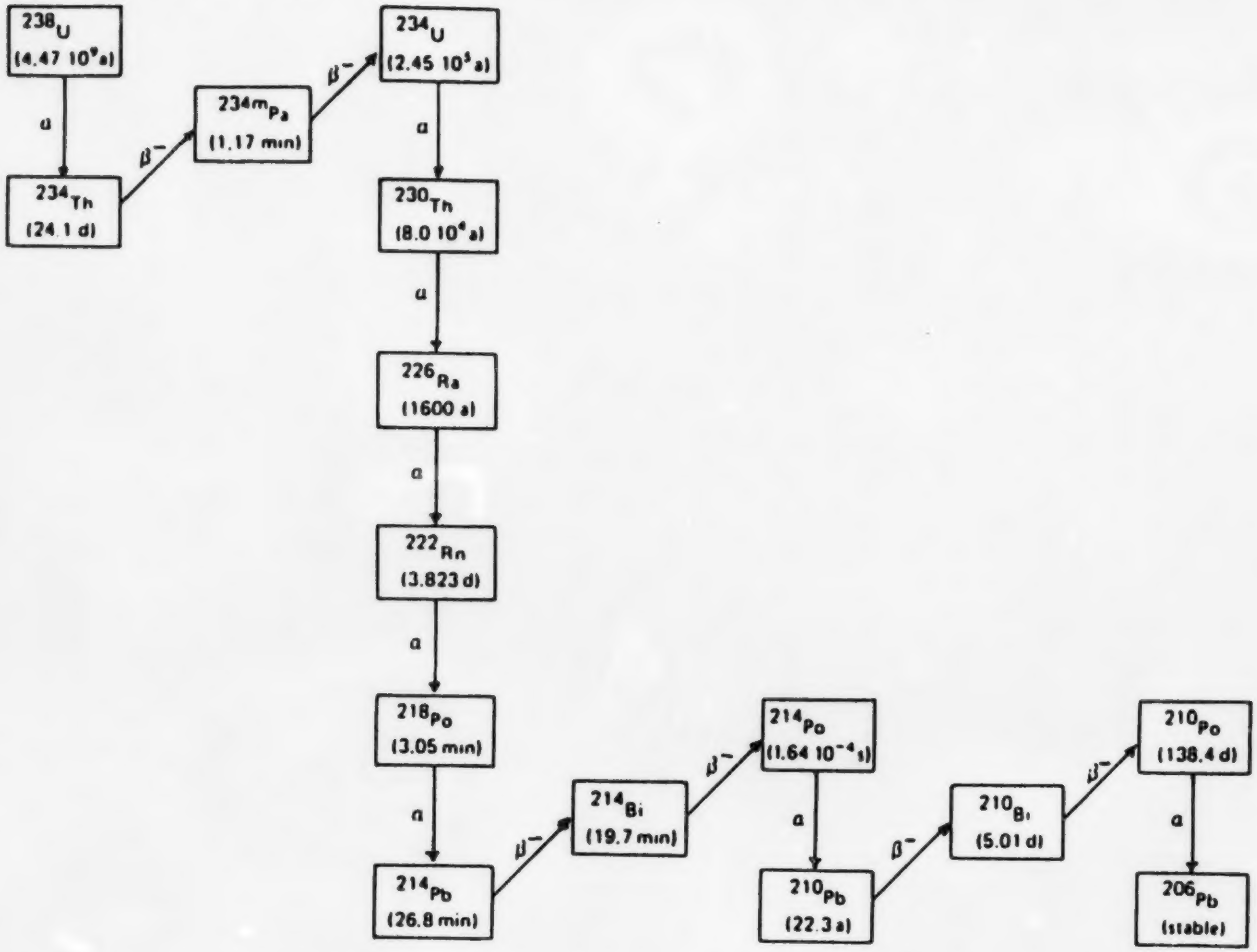
^{238}U (4.47 10^{9} a)
α
^{234}Th (24.1 d)
β^{-}
^{234m}Pa (1.17 min)
β^{-}
^{234}U (2.45 10^{5} a)
α
^{230}Th (8.0 10^{4} a)
α
^{226}Ra (1600 a)
α
^{222}Rn (3.823 d)
α
^{218}Po (3.05 min)
α
^{214}Pb (26.8 min)
β^{-}
^{214}Bi (19.7 min)
β^{-}
^{214}Po (1.64 10^{-4} s)
α
^{210}Pb (22.3 a)
β^{-}
^{210}Bi (5.01 d)
β^{-}
^{210}Po (138.4 d)
α
^{206}Pb (stable)

FIGURE 4.1 Uranium-238 decay series. Radionuclides produced in less than one percent of the transformations of the parent nuclide are not shown. (from Unscear 1982)

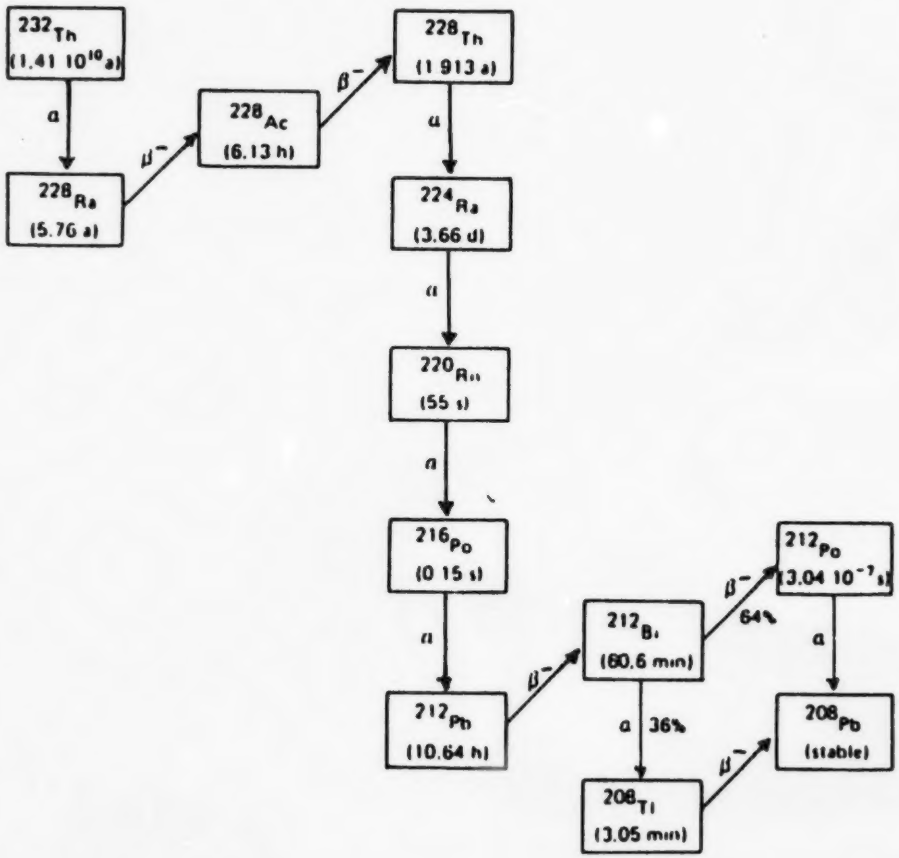
232Th (1.41 10^10 a)
a
228Ra (5.76 a)
β⁻
228Ac (6.13 h)
β⁻
228Th (1.913 a)
a
224Ra (3.66 d)
a
220Rn (55 s)
a
216Po (0.15 s)
a
212Pb (10.64 h)
β⁻
212Bi (60.6 min)
β⁻ 64%
212Po (3.04 10^-7 s)
a 36%
208Tl (3.05 min)
a
β⁻
208Pb (stable)

FIGURE 4.2 Thorium-232 Decay Series (from Unscear 1982)

FIGURE 4.3 U-235 Decay Series

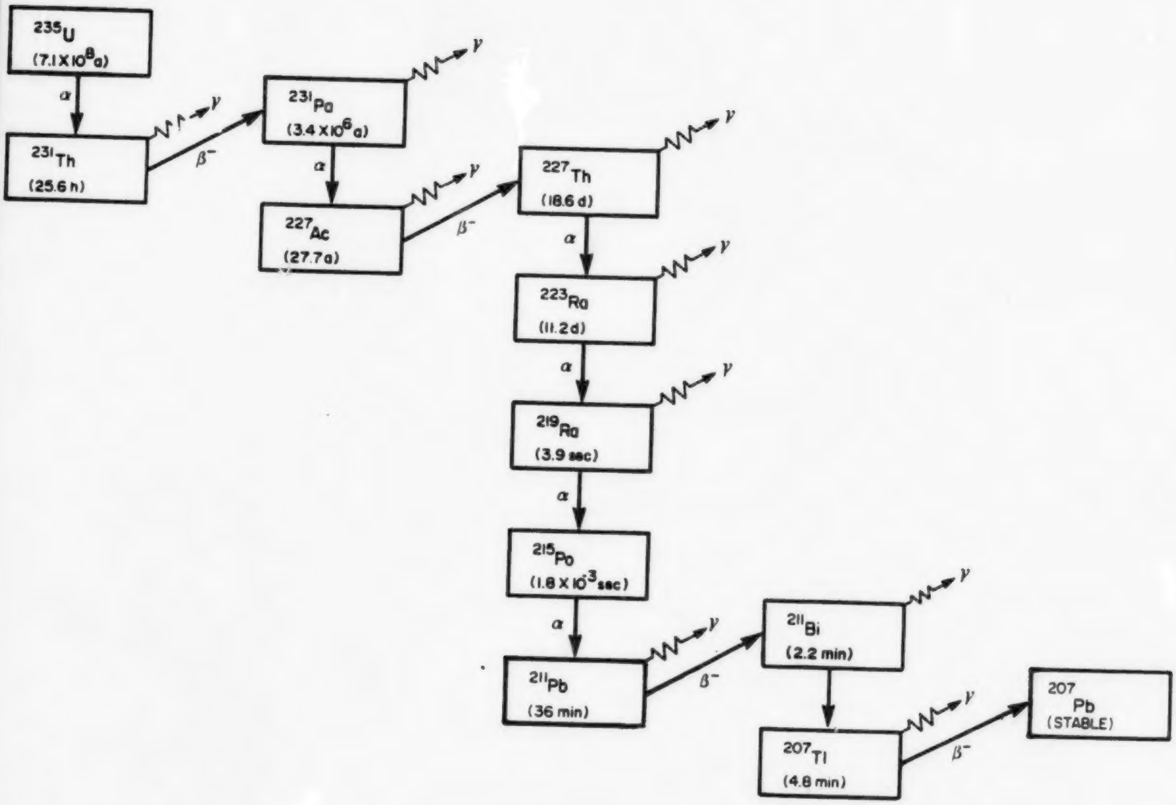

235U
(7.1 X 10^8 a)
α
231Th
(25.6 h)
β−
γ
231Pa
(3.4 X 10^6 a)
α
227Ac
(27.7 a)
β−
γ
227Th
(18.6 d)
α
223Ra
(11.2 d)
α
219Rn
(3.9 sec)
α
215Po
(1.8 X 10^-3 sec)
α
211Pb
(36 min)
β−
γ
211Bi
(2.2 min)
207Tl
(4.8 min)
β−
γ
207 Pb
(STABLE)

TABLE 4.9: TYPICAL CONCENTRATIONS OF VARIOUS CONSTITUENTS IN TAILING SEEPAGE ENVIRONMENTS

	Tailings Influent	Tailings Runoff Effluent	Porewater	Seepage	Leaching Tests		Saskatchewan Authorized avg. monthly concentrations
					Batch Agitated (SRC 1985)	Column Studies (Sherritt Gordon 1979)	
As	.763-2.2	-	.26-2.2	.062-.076	1.6-2.6	1.8-6.7	0.5
Cr	.008-.024	.011-.022	< .005	.004-.014	< .005-.024	< .01-0.1	-
Mo	0.11-2.1	.58-1.3	.43-1.2	.48-.85	0.28-1.0	0.2-3.3	0.5**
Ni	.01-95	.005-.011	.016-.087	.041-.094	.026-.26	< .1-1.6	0.5
Pb	< .005-.28	< .005-.02	< .02-.04	< .005-.02	< .02-.04	< .1-.7(6.5*)	0.2
Si	0.2-0.6	-	1.8-4.1	1.3	1.7-3.4	5.1-48.4	-
U	.0035-.1	.0032-.013	.0014-.005	.042-.132	-	0.5-3.7	1.0
Zn	.002-.29	.001	.02-.032	.062-.21	.004-.05	< .01-4.0	0.5
W	.01-1.1	.45-.89	.23-.25	.06-.31	.25-.44	-	-
Ra-226 (Bq/L)	25-420	270	9.5-55	10-45	30-55	35-41	0.37
Pb-210 (Bq/L)	0.4-25	3	0.13-0.7	.45	-	-	1.85
Th-230 (Bq/L)	0.5-4.0	2	.08-1.6	0.2	.35-1.0	-	1.85
Po-210 (Bq/L)	0.5	.15	-	.09	-	-	-
pH	6.41-12.1	11.3-11.5	9.33-11.14	7.1-7.43	6.68-9.19	5.6-9.9	5-9.5
Ca	520-1050	655-780	582-627	374-550	610-660	364-840	-
SO_4	1310-3450	1590-1720	1340-1650	1150-1470	1420-1620	1500-1950	-

* likely an erroneous measurement

** level may be revised upward

TABLE 4.10: ELEMENTS AND RADIONUCLIDES SELECTED FOR THIS PROJECT

Element	Reason	Radionuclide	Reason
Si	1	U-238	7
Al	1,2,3	U-234	7
Ca	1,2,4	Th-230	6,8
Mg	1	Ra-226	6,8
K	1	Rn-222	6
Na	1	Pb-210	6,8
Fe	1,2,5	Po-210	6
S	1,2	Th-232	7,8
C	1,2	Ra-228	7,8
H^+	2	Th-228	7
Cu	3		
Ni	3,4		
As	3,4		
Ba	5		
Co	3		
Mn	3		
Pb	3,5		
Ti	3		
Se	3,4		
Sr	5		

1. Major element
2. Potential controller of pH
3. Trace or heavy element. Found in sufficiently high concentrations in groundwater to be a potential health hazard.
4. Major element in some tailings.
5. Element of potential concern due to controlling radionuclide concentration.
6. Radionuclide of prime concern to man's health (based upon dose commitment calculations).
7. Radionuclide of potential concern to man's health
8. Radionuclide which has potential influence upon activity of daughters for time frame of 100-10,000 yrs.

For trace metals, the major reasons for their selection are that they may have a significant influence upon human health. Several major elements are included because they may have a significant influence upon the geochemical evolution of minerals which control elements related to pH or because they pose potential human health hazards.

All of the radionuclides given in Table 4.10 have some potential radiological hazard to humans. Ra-226, Rn-222, Pb-210 and possibly Th-230 and Po-210 are labelled as of particular concern, based upon dose commitment calculations for aquatic and atmospheric pathways (e.g., IEC BEAK, 1982).

4.6 Elements to be Considered in Future NUTP Projects

It is possible that future NUTP projects will require consideration of a lesser number of elements. Elimination of certain elements could be made using the following rationale:

(i) the elements are small in quantity in certain ores (e.g., Ni and As) are of concern in northern Saskatchewan ores, but not in Elliot Lake ores),

(ii) the elements do not have a substantial effect upon the geochemical evolution of the tailings pile (e.g., Mg, Na in certain regions),

(iii) the elements control only particular radionuclides (e.g., Ca, Fe, Ba, Pb and Sr sulphates are potential candidates as controllers upon the mobilization behaviour of Ra-226; BEAK, 1985),

(iv) certain radionuclides are present in small quantities or do not make a major contribution to human dose (e.g., U-238, U-234, Th-232, Ra-228 and Th-228), and

(v) certain radionuclides are in secular equilibrium with their parents for time scales of concern (e.g., Po-210 in equilibrium with Pb-210). For such nuclides, their dose can be attributed to the parent, provided that there is not extensive chemical segregation between parent and daughter in the tailings.

4.7 Minerals Requiring Thermodynamic Data

A summary of the solid phases of concern in Canadian uranium mill tailings is given in Table 4.11. For purposes of equilibrium code pathway calculations (see Chapters 9 and 10), it is expected that these would constitute most of the solid phases for which thermodynamic data are required for Canadian uranium tailings. For particular uranium tailings, subsets of this set of solid phases would be used in the calcualtions.

This set of solid phases will be expanded over time as more data become available. For example, it does not include anglesite ($PbSO_4$) which may control the dissolution behaviour of Ra-226 (BEAK, 1985).

TABLE 4.11:

SOLID PHASES

Mineral		Formula
Quartz		SiO_2
K-Feldspar		$KAlSi_3O_8$
Plagioclase	- abilite	$Na(AlSi_3O_8)$
	- amorthite	$Ca(Al_2Si_2O_8)$
Pyroxenes		$(Ca,Mg,Fe)_2Si_2O_6$
Amphiboles		$(Ca,Mg,Fe)_7Si_8O_{22}(OH)_2$
Biotite		$K(Mg,Fe)_3(AlSi_3O_{10})(OH)_2$
Muscovite		$KAl_2(AlSi_3O_{10})(OH)_{10}$
Chlorite		$Mg_3(Si_4O_{10})(OH)_2 \cdot Mg_3(OH)_6$
Serpentine		$Mg_6(Si_4O_{10})(OH)_8$
Talc		$Mg_3Si_4O_{10})(OH)_2$
Zircon		$ZrSiO_4$
Tourmaline		$Na(Fe,Mg,Li_2,Al)_3Al_6(BO_3)_3(Si_6O_{18})(OH)_4$
Hisingerite		$Fe_2Si_2O_5(OH)_4 \cdot 2H_2O$
Kaolinte		$Al_2Si_2O_5(OH)_4$
Chlorite		$Mg_5Al_2Si_3O_{10}(OH)_8$
Ca-Montmorillonite		$Ca_{0.17}Al_{2.33}Si_{3.67}O_{10}(OH)_2$
Illite		$K_{0.6}Mg_{0.25}Al_{2.3}Si_{3.5}O_{10}(OH)_2$
Pyrite		FeS_2
Pyrrhotite		$Fe_{1-x}S$
Galena		PbS
Chalcopyrite		$CuFeS_2$
Bornite		Cu_5FeS_4
Covellite		CuS
Chalcocite		Cu_2S
Sphalerite		ZnS
Arsenopyrite		$FeAsS$
Carrollite		$Cu(Co,Ni)_2S_4$
Niccolite		$NiAs$
Skutterudite		$(Co,Fe,Ni)As_3$
Pararammelsbergite		$NiAs_2$
Gersdorffite		$NiAsS$

TABLE 4.11: SOLID PHASES (cont'd)

Mineral	Formula
Berzelianite	Cu_2Se
Umangite	Cu_3Se_2
Clausthalite	$PbSe$
Dolomite	$CaMg(CO_3)_2$
Calcite	$CaCO_3$
Siderite	$FeCO_3$
Gypsum	$CaSO_4 \cdot 2H_2O$
Ettringite	$Ca_6Al_2(SO_4)_3(OH)_{12} \cdot 26H_2O$
Bassinite	$CaSO_4 \cdot 1/2H_2O$
Barite	$BaSO_4$
Alunite	$KAl_3(SO_4)_2(OH)_6$
Basaluminite	$Al_4SO_4(OH)_{10} \cdot 5H_2O$
K-Jarosite	$KFe_3(SO_4)_2(OH)_6$
Graphite	C
Apatite	$Ca_5(F,Cl,OH)\ (PO_4)_3$
Monazite	$(Ce,La,Y,Th)\ PO_4$
Ferric hydroxide (am)	$Fe(OH)_3$
Geothite	$FeOOH$
Hematite	Fe_2O_3
Magnetite	Fe_3O_4
Ilmenite	$FeTiO_3$
Rutile	TiO_2
Al hydroxide (am)	$Al(OH)_3$
Gibbsite	$Al(OH)_3$
Pitchblende	UO_2
Urananite	UO_2
Coffinite	$USiO_4$
Brannerite	$(U,Ca,Fe,Th,Y)Ti_2O_6$
Thucolite	$(U,Th)\ CH_2O$ (?)

5.0 WEATHERING AND TRANSPORT PROCESSES IN TAILINGS

The chemical, biological and physical processes discussed here apply to the breakdown and removal of constituents from a tailings pile. These transformations generally affect weathering processes, but also include transport processes. They are now examined descriptively in the context of a tailings environment.

5.1 Chemical Weathering and Relative Mineral Stability

Dissolution

The dominant process in most weathering environments involves dissolution and transport of dissolved constituents with infiltrating rainwater. The rate of release of chemical constituents is generally limited by the solubility of the original minerals and secondary products, as well as by constraints on the rate of dissolution of particular mineral phases.

pH as a Master Variable

The solubilities of many minerals are affected by pH values of the infiltrating water. Lower pH values usually correlate with greater solubility. In natural environments, in which soil development occurs, carbon dioxide generation by microbial activity plays a key role in pH control. In some tailings deposits, however, pH controls will likely be dominated by sulphide-mineral oxidation at low pH values (2-3) and by limestone dissolution at upper pH levels (7). Although the concentrations of many chemical species will remain high under low pH conditions, subsequent neutralization can result in precipitation of these species as oxides or hydroxides.

Relative Mineral Stability

The relative stability of minerals was recognized through observations of their persistence at the earth's surface. Goldich (1938) classified minerals according to their order of increasing stability. The similarity was noted between the weathering sequence and Bowen's reaction series that describes the formation of groups of minerals from silicate melts that cool and crystalize (Figure 5.1). Just as lower energy environments are more stable, minerals that form at lower temperatures and pressures are less prone

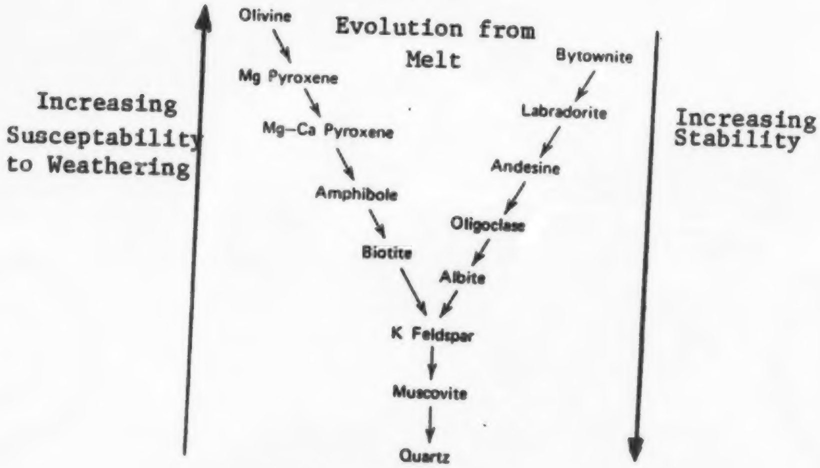
Increasing
Susceptability
to Weathering
Evolution from
Melt
Olivine
Mg Pyroxene
Mg–Ca Pyroxene
Amphibole
Biotite
Bytownite
Labradorite
Andesine
Oligoclase
Albite
K Feldspar
Muscovite
Quartz
Increasing
Stability

FIG. 5.1 The reaction series.

(from Hurlburt, 1971)

to chemical weathering. However, most mineral phases that were formed primarily in melts will be unstable or only metastable at the earth's surface, hence weathering is almost certain.

There are some minerals, however, that form during weathering and persist to a greater extent than most primary solids. Among these secondary phases are iron oxides, aluminum oxides and some clays. Because of the unusual concentrations and pH values within some uranium tailings deposits, other secondary minerals can be important. These metastable phases could include aluminum and iron hydroxides, ferric sulphate, gypsum and siderite. It should be noted that such solids are relatively soluble when pH values occur in the more neutral range or when sulphate concentrations in solution are lowered by dilution or other processes. In any case, it should be recognized that weathering not only consists of dissolution and removal of mass, but also involves transformations between certain solid phases.

Sorption Reactions

In addition to precipitation and dissolution reactions, ion exchange and surface adsorption can strongly influence the mobility of many ionic species. These processes are normally considered to be reversible. Although cations are affected to a greater extent by exchange processes, anion exchange on hydrous metal oxide surfaces can also be important.

In many situations, sorption reactions result in an irreversible adsorption or kinetically hindered release of the solute that has been previously taken up on solid surfaces. In many irreversible sorption reactions, it may not be possible to differentiate between simple surface adsorption and coprecipitation of a solute into the crystal structure at the surface.

The net effect of sorption reactions is to retard the movement of dissolved constituents relative to the movement of water through the tailings.

Aqueous Chemical Complexation

Complexing and chelation are additional processes that can affect the relative removal rates of dissolved components. Many dissolved ions do not remain in solution as simple cations or anions but are present as complexes and ion pairs. This may result in the formation of neutral or less-charged dissolved species that are not as susceptible to surface exchange reactions, and that tend to increase the relative mobility of a particular constituent. In addition, chelation of metals and other cationic species with organic molecules tends to increase relative mobility of those components.

The net effect of chemical complexation is to increase the transport of soluble constituents by reducing or preventing their participation in surface reactions.

5.2 Biological and Vegetative Reactions

Major biological components include bacterial and plant processes in a tailings system. Although insect and animal behaviour may contribute to erosion, particularly by burrowing, this process is likely of limited chemical significance.

Microbial Organisms as a Catalyst for Chemical Reactions

Bacteria can contribute to weathering processes in a number of ways. The main example is that of bacterially-catalysed oxidation of pyrite that causes low pH conditions within particular environments. The low pH water results in further weathering of other solids. Aerobic heterotrophic bacteria also contribute to dissolution of solids, particularly carbonates, when CO_2 gas is produced during metabolism. Bacteria may also affect the fate of constituents such as organic compounds that are used for anabolic or metabolic processes or those such as metals that are preferentially taken-up by the organisms and thereby affect mobility in the subsurface.

Role of Vegetation

Vegetation may also affect the transport or release of constituents by way of metabolic processes. Carbon dioxide gas is released by roots thereby increasing acid production in the root zone. Vegetation also transports dissolved constituents from the root zone to other portions of the plant, usually above ground level. Some constituents such as radon gas may be transported to the atmosphere during respiration. At the end of the life-cycle the plant material will decompose thereby contributing dissolved organic material to the infiltrating water. If the organic matter develops into a soil material, it may substantially mediate the transport of metals.

Role of Energy Source and Final Electron Acceptors in Bacterial Metabolism

The role of an energy source is that it influences the type of bacteria which can be present. For example, organic matter is an energy source for the growth of heterotrophes while pyrite and ferrous iron are energy sources for the growth of certain chemoautotrophic bacteria. Electron acceptors also determine which type of bacteria will be present. For example, heterotrophes and pyrite-oxidizing bacteria both use oxygen as a final electron acceptor.

From a perspective of freshwater through salt water systems, at least 6 aqueous chemical species may be the final electron acceptors for microbial metabolism: oxygen, nitrate, manganese (Mn IV), iron (FeIII), sulphate and organic matter.

Equilibrium chemistry provides a reference point for considering the possible sequence of reactions in sediments. In a system containing finite amounts of (i) organic matter, (ii) O_2, (iii) NO_3^-, (iv) SO_4^{2-}, (v) HCO_3^-, and (vi) oxides of iron (e.g., FeOOH(s)) and manganese (e.g., MnO_2(s)), oxidation of organic matter should first occur by reduction of O_2 (Stumm and Morgan, 1981). This would be followed by reduction of nitrate (denitrification or nitrate reduction), MnO_2, and FeOOH(s), fermentation of organic matter, and reduction of SO_4^{2-} and CO_2. The reduction of nitrate and MnO_2 would occur at about the same place in the sequence, as would the group of organic matter, SO_4^{2-} and CO_2. The sequence of these reactions may occur with depth of tailings as the redox potential becomes increasingly negative or locally in a horizontal fashion into local zones of lower redox potential.

Not all reactions will be significant in a tailings deposit. When Elliot Lake tailings are initially deposited, for instance, there is generally very little organic carbon present. Thus inorganic energy sources (pyrite for the iron- and sulphur- oxidizing bacteria in the unsaturated zone) can be expected to dominate. Only in tailings where large amounts of organic matter are initially deposited, where groundwater infiltration transports dissolved organic carbon (DOC), or in surficical zones where organic matter is produced by vegetative decay will organic energy sources be significant (e.g., sulphate reducing bacteria, which require organic carbon as the energy source). For example, GUNNAR data indicates that relatively high quantities of organic carbon matter and corresponding DOC are present.

In this work, it is assumed that pyrite and other sulphide minerals are the major energy sources for oxidation reactions and that organic matter has a secondary role. It is assumed that oxygen, sulphate, iron (III), manganese (IV) and to a lesser extent, organic matter are the main electron acceptors. For oceanic applications, Berner (1978) has had considerable success describing decomposition by considering only sulphate and oxygen. Other aspects of oceanic sediment diagenesis have been addressed by Berner and Raiswell (1983), Grundmanis and Murray (1982), Berner (1984), Reimers et al. (1984), Kaul and Froelich (1984), and Aller (1984). Such work would have particular applications to tailings rich in sulphate if significant organic matter is found or is generated.

Stoichiometry of Decay Reactions

Where organic matter is available, the following stoichiometric reactions can be used to identify the major electron acceptors. The formula $C_{106}H_{263}O_{110}N_{16}P$ represents a typical formula for unicellular plants. Other stoichiometry would be required for plant roots, etc.

For Aerobic Decay

Particulate Organic:

(i) If nitrification is not considered

$$C_{106}H_{263}O_{110}N_{16}P + 106O_2 \longrightarrow 106CO_2 + 106H_2O + 16NH_3 + H_3PO_4 \qquad (5.1)$$

(ii) If nitrification is included

$$C_{106}H_{263}O_{110}N_{16}P + 138O_2 \longrightarrow 106CO_2 + 12H_2O + 16HNO_3 + H_3PO_4 \qquad (5.2)$$

For Anoxic Decay

Particulate Organics:

$$C_{106}H_{263}O_{110}N_{16}P + 84.8\ NO_3^- \longrightarrow 106CO_2 + 84.8\ OH^- + 42.4\ N_2 \qquad (5.3)$$

For Anaerobic Decay

Particulate Organics (Methane Fermentation):

$$C_{106}H_{263}O_{110}N_{16}P \longrightarrow 53CO_2 + 16NH_3 + H_3PO_4 + 53\ CH_4 + H_2O \qquad (5.4)$$

Particulate Organics (Sulphate Reduction):

$$C_{106}H_{263}O_{110}N_{16}P + 53\ SO_4^{2-} + 106\ H^+ \longrightarrow 106\ CO_2 + 16\ NH_3 + H_3PO_4 + 53\ H_2S + 106\ H_2O \qquad (5.5)$$

5.3 Physical Processes

General

Physical processes interact with tailings in many ways. For example, physical parameters influence chemical and biological processes. Transport of dissolved constituents by subsurface and surface waters is also a physical process. Purely physical processes such as erosion by wind and water contribute to mass removal, while the outflux of radon gas through a tailings surface is controlled by physical conditions.

Temperature Effects

Temperature has an important influence on microbial and chemical kinetics. In general, the effect of temperature on the weathering rate constant k has been expressed by the empirical Arrhenius relationship.

$$k = A^{*}\exp^{-\ E/RT} \qquad (5.6)$$

where, k is substrate removal constant
A^* is pre-exponential, frequency factor
E is the activation energy (cal/g-mol)
R is the universal gas constant (= 1.98 cal/°K/mol)
T is the absolute temperature.

In reparameterized form, the relationship is changed to

$$k = A \exp^- E(1/T - 1/T_o)/R \qquad A = A^* \exp^- E/RT_o \tag{5.7}$$

where, T_o is reference temperature (°K)
A is the substrate removal constant at temperature T_o

Temperature also affects diffusion. According to Li and Gregory (1979), the relationship between diffusion and temperature in fluids is given by:

$$D_1 = D_2 \times \frac{n_2}{n_1} \times \frac{T_2}{T_1} \tag{5.8}$$

The relative change of diffusion coefficient with temperature (T) and the values for viscosity (n) can be obtained from the Handbook of Chemistry and Physics.

Frost and Snow Effects

Cold temperatures transform moisture contained in cracks and fissures into ice. The ice expands, causing the size of the cracks to increase or even breaking a solid into two parts. This action increases the surface area subjected to weathering reactions and the resultant dissolution rates per unit volume of tailings.

Wind Effects

Wind affects tailings by eroding mineral grains, increasing oxygen transport into the unsaturated zone and increasing radon exhalation from the tailings pile. The transport of radon and dust containing radionuclides are significant concerns in the management of U-mill tailings. In some environments, transported dust bombards a geological feature, causing erosion of the feature; however, such abrasive action is probably not significant to the objectives of the NUTP. In some dry environments, wind-induced erosion may transport more material from the pile than water transport (solution, suspended solids, bedload). This is not expected to be the case for Canadian tailings in general but wind-borne transport may be significant for specific sites.

Advective (Convective) Transport

Advective transport involves the bulk movement of surface water and groundwater from one point to another. It is the transport process which is generally most significant for moving dissolved chemical constituents.

Diffusive Transport

Diffusive transport involves the transport of mass due to chemical gradients and random fluid processes. At molecular scales, the random processes are caused by Brownian motion. At larger scales, the random processes involve turbulence, (if the flow regime is non-laminar) and dispersivity (due to bulk advective flow about mineral grains). Turbulence is expected to be significant only in surface waters associated with tailings environments.

Modelling Physical Transport

The principles for modelling physical transport are outlined in succeeding chapters for aqueous pathways and for atmospheric diffusion of gases within the unsaturated zone because these processes directly affect the bio-geochemical evolution of the tailings pile. Transport processes external to the pile such as wind-driven erosion are considered to be boundary conditions and hence not of direct concern to the scope of this project.

6.0 DESCRIPTIVE EXAMPLE OF DEVELOPING A SOURCE TERM MODEL

This section presents an example of a simplified model to predict the concentration of iron, calcium, sulphate, Ra-226 and the pH in pore water, leaving the unsaturated zone. It treats the unsaturated zone as a one box system with a physical scale of 2 m. It assumes that only pyrite, limestone ($CaCO_3(s)$) and gypsum containing radium, are the solids which react with the pore water to any measureable extent.

The example developed and calculations involved might appear to be somewhat circuitous to the reader. This results from solving the equations by hand calculator which requires an iterative, trial-and-error procedure. However, the approach provides chemical insight into assumptions of the model which is not as readily obtained if a computer code is used.

The example is incomplete for several reasons. Other solid-phase buffering systems significantly influence pH. These other systems are considered later in Chapter 10, using a reaction code pathway simulation. Also, as inspection of the calculations will show, the Ra-226 content in gypsum is quite low, being only 0.2% of the total Ra-226 in the tailings. Other solids control the remainder of the radium.

6.1 Chemical System Considered in this Example

The solid phases and the reaction pathways are given in Figure 6.1. The possible individual reactions are given in Table 6.1. Pyrite oxidation is assumed to be kinetically controlled with a zero order oxidation rate. Because diffusion of oxygen in the void spaces of the unsaturated zone can be low, oxygen limits the actual pyrite oxidation rate to a lower value than its maximum value, at an atmospheric partial pressure of 0.2atm. The combination of kinetic rate and oxygen limitation is assumed to give an average pyrite oxidation rate of 2 mol pyrite oxidized/m^3/yr. Pyrite oxidation delivers 2 mol sulphate and 4 mol H^+ per mole of pyrite oxidized to the pore water (see Equation 1, Table 6.1).

The other solid phases, (calcite, gypsum) are assumed to be at equilibrium with the pore water, as is the adsorbed phase. These are represented by two-directional arrows in Figure 6.1.

FIGURE 6.1: PATHWAY DIAGRAM SKETCH OF REACTIONS FOR UNSATURATION ZONE COMPARTMENTS AND REACTION PATHWAYS IN UNSATURATED ZONE FOR DESCRIPTIVE EXAMPLE

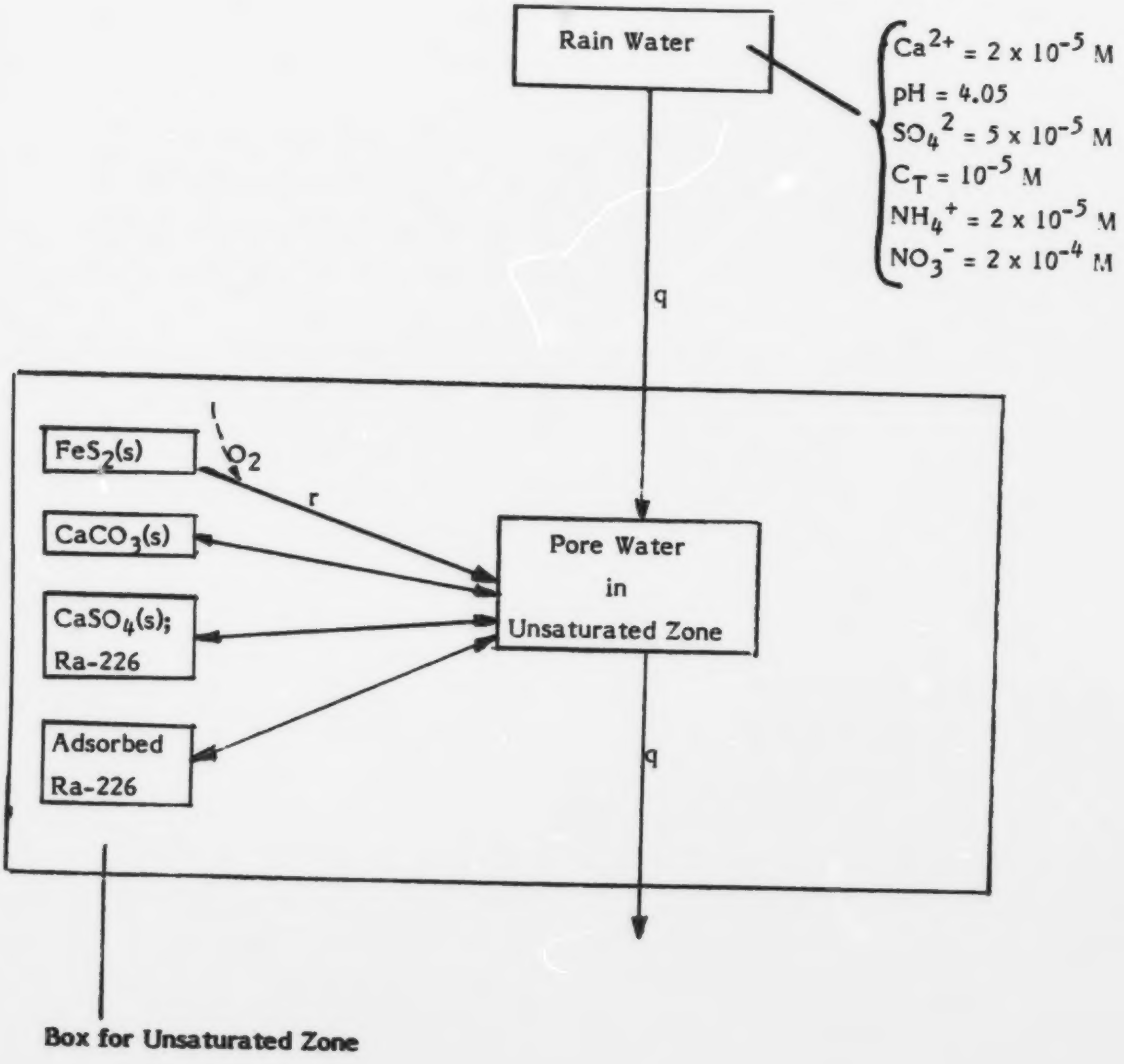
Rain Water
$Ca^{2+} = 2 \times 10^{-5}$ M
pH = 4.05
$SO_4^{2} = 5 \times 10^{-5}$ M
$C_T = 10^{-5}$ M
$NH_4^+ = 2 \times 10^{-5}$ M
$NO_3^- = 2 \times 10^{-4}$ M
q
$FeS_2(s)$
O_2
r
$CaCO_3(s)$
$CaSO_4(s)$;
Ra-226
Adsorbed
Ra-226
Pore Water
in
Unsaturated Zone
q
Box for Unsaturated Zone

TABLE 6.1: RELEVANT REACTIONS FOR CONSIDERATION

Iron Reactions

$FeS_2(s) + 15/4\ O_2 + 7/2\ H_2O \longrightarrow 2SO_4^{2-} + Fe(OH)_3(s) + 4H^+$ (6.1)

- o pyrite oxidation reaction (kinetically controlled)

$Fe(OH)_3(s) = Fe^{3+} + 3OH^-$ (6.2)

- o amorphorus iron hydroxide equilibria

$Fe^{3+} + H_2O = FeOH^+ + H^+$ (6.3)

- o reaction dominates at and below pH 5.5

$FeOH^{++} + H_2O = Fe(OH)_2^+ + H^+$ (6.4)

- o reaction important between pH 5 and 7

$Fe(OH)_2^+ + H_2O = Fe(OH)_3^o + H^*$ (6.5)

- o reaction important between pH 5 and 8

$Fe(OH)_3^o + H_2O = Fe(OH)_4^- + H^+$ (6.6)

- o reaction important between pH 7 and greater

$2\ FeOH^{++} = Fe_2(OH)_2^{4+}$ (6.7)

- o reaction important between pH 5 and 8

Carbon Reactions

$H_2CO_3^* = H^+ + HCO_3^-$ (6.8)

- o reaction important below pH 8.3

$HCO_3^- = H^+ + CO_3^{2-}$ (6.9)

- o reaction important above pH 8.3

Sulphate Reactions

$SO_4^{2-} + H^+ = HSO_4^-$ (6.10)

- reaction important below pH 3

Calcium Reactions

$CaCO_3(s) = Ca^{2+} + CO_3^{2-}$ (6.11)

- reaction important above pH 8.3

$CaCO_3(s) + H_2O = Ca^{2+} + HCO_3^- + OH^-$ (6.12)

- reaction important below pH 8.3

$CaSO_4(s) = Ca^{2+} + SO_4^{2-}$ (6.13)

$CaSO_4^o = Ca^{2+} + SO_4^{2-}$ (6.14)

Iron-Sulphate Equilbrium

$Fe^{3+} + SO_4^{2-} = FeSO_4^+$ (6.15)

$FeSO_4^+ + SO_4^{2-} = Fe(SO_4)_2^-$ (6.16)

$K^+ + 3Fe^{3+} + 2\,SO_4^{2-} + 12\,H_2O = KFe_3(SO_4)_2(OH)_6.6\,H_2O(s) + 6H^+$ (6.17)

K-jarosite

$Fe^{3+} + SO_4^{2-} + 12\,H_2O = HFe_3(SO_4)_2(OH)_6.6H_2O(s) + 5H^+$ (6.18)

Hydronium-jarosite

Rainwater containing small quantities of sulphate and calcium and having a pH of 4.5 enters the unsaturated zone (see Figure 6.1). These conditions are characteristic of acidic precipitation. The rainwater enters the tailings, mixes with pore water, and discharges below to the saturated zone.

It is assumed that the unsaturated zone is 2 m deep, has a porosity of 40% and a solids density of 2.0 g/cc. The proportions of pyrite (5%), mill-formed gypsum and residual limestone result in quantities for pyrite of 500 mol/m^3; for gypsum of 600 mol/m^3; and for limestone of 132 mol/m^3 as calcite. The adsorption coefficient for Ra-226 is assumed to be 5 mL/g. The quantity of limestone (calcite) assumes that limestone is added to the tailings in excess of normal practice to provide acid neutralization capacity. This may or may not be done depending on the system. These solids characteristics and mineral quantities were derived in a previous study (Snodgrass et al., 1983) which evaluated alternate management practices. They differ somewhat from those derived for Chapters 4 and 10 (see Table 4.7b).

With respect to iron reactions (Table 6.1), the pyrite oxidation reaction assumes that oxidation is complete and that amphorus iron hydroxide ($Fe(OH)_3(s)$) forms. Alternative chemical solids which could form are: goethite (FeOOH) or hematite (Fe_2O_3). They are, in fact, equivalent to $Fe(OH)_3$, but represent less hydrated forms of the solid phase (i.e., a solid phase containing fewer water molecules in the unit cell). These forms will be mainly stable over the neutral pH range; if the pore water is quite acidic, incomplete oxidation of Fe^{3+} will result. If the pH is low enough, sulphate minerals of iron (e.g., K-jarosite: Equation 6.16, Table 6.1; hydronium-jarosite: Equation 6.17, Table 6.1) become stable, particularly in the pH range of 0 to 2.

Equations 6.2 to 6.7 of Table 6.1 represents solid-solution reactions and hydrolysis reactions in solution. The Fe^{3+}, $FeOH^{2+}$ and $Fe(OH)^+$ species are particularly important at low pH while the $Fe(OH)_4^-$ specie is important at high pH (see Stumm and Morgan, 1980). The zero charged complex ($Fe(OH)_3^0$) and the dimer ($Fe_2(OH)_2^{4+}$) have been demonstrated to exist (Baes and Messmer, 1976), unlike the situation for aluminum in which the zero charged complex has been hypothesized to exist (Baes and Mesmer) but not chemically observed. Two other iron complexes involving sulphate ion are given in Equation 6.14 and 6.15 in Table 6.1; these are particularly important at low pH.

Reactions involving carbon, sulphate and calcium are given in Equation 6.8 to 6.13. The two reactions for carbon (Equations 6.8, 6.9) are the ones which are important in most surface waters (lakes, oceans) and many groundwaters because of the high concentration of inorganic carbon and its ability to react with H^+. These are the reactions which provide the major buffering system controlling pH in these waters. As is asserted below, other minerals will be most important over the long-term in tailings because the tailings generally have very little carbonate in the solid phase and hence very little total inorganic carbon in the pore water.

The four reactions involving calcium represent only three equilibria, because equations Equations 6.11 and 6.12 describe the same reaction - dissolution of calcite. The only difference is the way that the reaction is written. In Equation 6.11, the reaction is written in terms of the complex which dominates at pH greater than 10.3 (CO_3^{2-}) while Equation 6.12 is written in terms of the complex that dominates at pH 6.3 and 10.3.

6.2 Model Development

Chemical Model

The mechamisms considered for this example are given in Table 6.2(a). They represent a simplification of the large number of reactions given in Table 6.1. Assuming that the pore water pH is neutral, the aqueous concentrations of iron species (Equation 6.3-6.7, 6.14, 6.15 of Table 6.1) are negligible, because iron in the form of solid $Fe(OH)_3(s)$ dominates. Similarly, because of the neutral pH, evaluation of the other reactions of Table 6.1 show that the reactions given in Table 6.2 for H_2CO_3*, $CaCO_3$ and $CaSO_4$ are the main ones involving carbon and calcium.

For the four equilibrium reactions (Equation 6.20 to 6.22; Table 6.2), there are four mass law reactions (Equation 6.23 to 6.26) which result.

There are four mass balance relationships. Equation 6.27 states that the concentration of sulphate in the infiltrating rain water equals the amount from pyrite oxidation and a gain or loss respectively from gypsum dissolution or gypsum precipitation. Equation 6.28 (Table 6.2) states that the total calcium concentration in infiltrating rainwater is due to dissolution of calcite and a gain or loss respectively from gypsum dissolution or

TABLE 6.2: OVERVIEW OF SIMPLIFIED MODEL

6.2(a): Reactions Selected for Model

$$FeS_2 + 15/4\, O_2 + 7/2\, H_2O \longrightarrow 2\, SO_4^{2-} + Fe(OH)_3(s) + 4H^+ \qquad (6.19)$$

o kinetically controlled

$$H_2CO_3^* = H^+ + HCO_3^- \qquad (6.20)$$

$$CaCO_3(s) + H^+ = Ca^{2+} + HCO_3^- \qquad (6.21)$$

$$CaSO_4(s) = Ca^{2+} + SO_4^{2-} \qquad (6.22a)$$

$$CaSO_4^o = Ca^{2+} + SO_4^{2-} \qquad (6.22b)$$

6.2(b): Mass Law Equations for Above Reactions

$$\frac{(Ca^{2+})\ (HCO_3^-)}{(H^+)\ (CaCO_3(s) = 1)} = K_C \qquad (6.23)$$

$$\frac{(Ca^{2+})\ (SO_4^{2-})}{(CaSO_4(s) = 1)} = K_S \qquad (6.24)$$

$$\frac{(HCO_3^-)\ (H^+)}{(H_2CO_3^*)} = K_1 \qquad (6.25)$$

$$\frac{CaSO_4^o}{(Ca^{2+})\ (SO_4^{2-})} = 210 \qquad (6.26)$$

6.2(c): Mass Balance

$$(\text{Total Sulphate}) = 2\,\frac{rz}{q} \begin{cases} + & (\text{Gyp Diss}) \\ - & (\text{Gyp Precip}) \end{cases} \qquad (6.27)$$

$$(\text{Total Calcium}) = (\text{Ca Diss}) \begin{cases} + & (\text{Gyp Diss}) \\ - & (\text{Gyp Precip}) \end{cases} \qquad (6.28)$$

TABLE 6.2: OVERVIEW OF SIMPLIFIED MODEL (cont'd)

$$(\text{Total H}) = \frac{4\,rz}{q} = (H^+) + (HCO_3^-) \qquad (6.29)$$

$$(\text{Total } C_T) = (HCO_3^-) = (\text{Ca Diss}) \qquad (6.30)$$

6.2(d): Electroneutrality

$$2\,(Ca^{2+}) + (H^+) = (HCO_3^-) + 2\,(SO_4^{2-}) \qquad (6.31)$$

Symbols

r = pyrite oxidation rate ($M/m^3/yr$)
z = depth of unsaturated zone (m)
q = rainfall infiltration rate (m/yr)
(Gyp Diss) = Concentration of gypsum which dissolves (M/m^3)
(Gyp Precip) = Concentration of gypsum which precipitates (M/m^3)
(Ca Diss) = Concentration of calcite which dissolves (M/m^3)

precipitation. The total hydrogen ion concentration in solution (TOT H; Equation 6.29) is produced by pyrite oxidation; it is distributed between free hydrogen ion and HCO_3^- (Equation 6.21), because ($H_2CO_3^*$) is negligible, relative to (HCO_3^-) at neutral or alkaline pH. Finally, total C_T, (dissolved inorganic carbon), equals (HCO_3^-) and equals the concentration determined by calcite dissolution.

There is one electroneutrality equation (Equation 6.31) giving a relationship between the two main positive ions and two main negative ions.

Inspection of Table 6.2 shows that there are several non-linear equations which will make solution of even this simplified model difficult. Substituting Equation 6.23 into 6.24 for factoring out (Ca) gives:

$$\frac{K_S}{(SO_4^{2-})} \quad \frac{(HCO_3^-)}{H^+} = K_C \tag{6.32}$$

Substituting Equation 6.3 (Table 6.2) into the electroneutrality equation for (Ca^{2+}) and merging with equation (6.30) gives:

$$2 \; \frac{K_C\,(H^+)}{(HCO_3^-)} + (H^+) = (HCO_3^-) + \frac{2\,K_S\,(HCO_3^-)}{K_C\,(H^+)} \tag{6.33}$$

Substituting the equation for TOT H (Equation 6.29) into (6.33) gives:

$$\frac{2 \; K_C\,(H^+)}{(TOT\ H - (H^+)} + (H^+) = TOT\ H - (H^+) + \frac{2\,K_S\,(TOT\ H - (H^+))}{K_C\,(H^+)} \tag{6.34}$$

This rather formidable looking equation is actually a third order polyonomial which requires numerical methods to obtain a solution. This suggests that further model simplifications would be useful for this descriptive example.

Assuming that the pH is between 5 and 9 and that calcium and sulphate concentrations are in the millimolar range means that (H^+) is small relative to (Ca^{2+}) in the electroneutrality equation. Furthermore, (TOTH) approximately equals (HCO_3^-).

Accordingly, the electroneutrality equation with substitutions becomes:

$$2\,(Ca^{2+}) = (TOT\ H) + 2(SO_4{}^{2-}) \qquad (6.35)$$

The calcium concentration results from calcite and gypsum dissolution while the sulphate concentration results from gypsum dissolution and pyrite oxidation. Using these two mass balance conditions (Equation 6.27, 6.28) gives:

$$2((CA\ dis + Gyp\ Diss)) = (TOT\ H) + 2((Gyp\ Diss + Pyr)) \qquad (6.36)$$

where Pyr = 2rz/q (Equation 6.27) is the amount of sulphate which dissolves per mole of pyrite oxidized. Using Equation 6.30 gives:

$$2\,((TOT\ H + Gyp\ Diss)) = (TOT\ H) + 2((Gyp\ Diss + Pyr)) \qquad (6.37)$$

Its simplification gives:

$$(TOT\ H) = 2\,(Pyr) \qquad (6.38)$$

which is the mass balance represented by Equation 6.19 for pyrite oxidation. This shows that the assumptions are consistent but that a few of the above equations are redundant.

Accordingly, the model is now developed by considering the mass balances and mass laws excluding gypsum precipitation and then allowing gypsum precipitation. The equations are solved by making an initial assumption, solving the remaining equations and then checking the residual error.

Several iterations are required to obtain the true solution, even for a simplified model. This demonstrates the value of using equilibrium computer codes, reaction pathways codes and other numerical techniques to more readily solve this and similar models.

Hydrological Model

Two approaches could be used to develop the hydrological model: assume a fluctuating, or a constant, volume of water in the unsaturated zone. Consider, with reference to Figure 6.1, the mass balance equation for any constituent in percolating water:

$$\frac{dVC}{dt} = q_i(t)\,C_rA - q_o\,(t)\,CA + SV \qquad (6.39)$$

where	C	is the concentration of any constituent in the percolating water (mol/m^3)
	C_r	is its concentration in rainfall (mol/m^3)
	$q_i(t)$	is the infiltrating rainfall rate (m/year)
	$q_o(t)$	is the percolating water rate from the tailings (m/yr)
	A	is the horizontal area (m^2)
	S	is the net source of the constituent (mol/m^3/yr)
	V	is the volume of water in the unsaturated zone (m^3)
and	t	is time (yr)

The corresponding hydrological model is

$$\frac{dV}{dt} = q_i(t) - q_o(t) - q_e(t) \qquad (6.40)$$

where $q_e(t)$ is the loss of water through evapotranspiration.

These equations show that the volume of pore water in the unsatuated zone is a dynamic quantity which changes over time in response to rainfall. The moisture content will vary from a small portion of void volume (e.g., 10%) during a dry period to fully saturated (100% of void volume) during a sustained rainfall.

For this chapter (and for purposes of probabilistic modelling), it appears justified to assume that the average pore content over time (e.g., 20% of void volume) rapidly equilibriates with infiltrating rainwater, and that considerations of mineral kinetics and mineral equilibrium are expressed relative to the void volume being completely saturated for a period of time during and after rainfall. Accordingly, the mass balance equation simplifies to the quasi steady-state equation:

$$0 = q(t)\,C_rA - q(t)CA + SV^1 \qquad (6.41)$$

where $q(t) = q_o(t)$
V^1 = void volume of tailings in the unsaturated zone.

6.3 Iterative Solution of Model

The mathematical problem to solve is a combined kinetic-equilibrium problem. Our assessment of the literature (see Chapter 8 to 10), suggests that pyrite oxidation will continue irrespective of solution composition over a reasonable range of solution conditions. Therefore, the rate of pyrite production "forces" 4 mol sulphate/m^3 tailings/year into solution. For the rainfall infiltration rate of 0.25 m/yr, the average annual concentration is:

$$\frac{4 \text{ mol } (SO_4^{2})}{m^3 \text{ tailings.yr}} \quad * \quad \frac{2 \text{ m depth tailings}}{0.25 \text{ water/yr}} \quad \text{or} \quad 32 \text{ mol/m}^3$$

or 0.032 mol/L of total sulphate (S_T). Secondly, it forces 8 mol H^+/m^3 tailings/yr into solution; this results in a water concentration of 0.064 mol/L of total hydrogen (TOT H).

The equilibrium problem is to allow these aqueous constituents (0.032 mol/L S_T; 0.064 mol/L TOT H) to redistribute themselves so that the water is at equilibrium with calcite (limestone) and gypsum, provided that equilibrium is attained with both solid phases. The kinetic data in Chapter 11 show that calcite can dissolve at a rate of approximately 2.8×10^{-10} mol/cm^2 surface/sec at pH 6.3. Assuming 1 cm^3 particles of calcite, the calcite dissolution rate is 2.1/year. For the calcite concentration in the solid phase of 110 mol/tonne (132 mol/m^3), the resultant maximum calcite ($CaCO_3$) concentration in the infiltrating water is 0.61 mol/L. If the pH is lower, the rate and associated concentration are higher. But equilibrium considerations show that the maximum aqueous $CaCO_3$ concentration at pH 6.3 is lower than 0.61 mol/L. Accordingly, calcite may be considered to be at equilibrium for an annual time scale.

A similar analysis, (see Chapter 11) of field data and of the rate-controlling step during dissolution, suggests that gypsum equilibrium will be maintained for these time scales as well.

Buffering System for Hydrogen Ion

The key to the iterative approach adopted herein for mathematically solving the model is to assess the form of hydrogen ions in solution. For the solution pH expected in this problem, inspection of Table 6.1 and 6.2 shows that hydrogen in a free form and complexation of hydrogen with SO_4^{2-}, CO_3^{2-} and/or HCO_3^- are the dominant forms. Accordingly, the model is solved by assuming the dominant form of H^+ and then solving the remaining equations.

TOT H Complexed with SO_4^{2-}

If no carbon dissolves, the hydrogen ion activity is given from Equation 6.10 (Table 6.1) by:

$$\frac{(H^+)\,(SO_4^{2-})}{HSO_4^-} = 10^{-1.9} \qquad (6.42)$$

For TOT H = .064 M and S_T = 0.032 M, and using Equation 6.42, one can calculate that the pH is 1.4. This means that, of the .064 M of TOT H, 62% is free as H^+ (0.040 M) and 38% is complexed as HSO_4^- (.024 M).

Assuming that sufficient calcium carbonate dissolves, the pH will be greater than 2. Hence, HSO_4^- will be mainly dissociated. Accordingly, TOT H will be complexed mainly with $H_2CO_3^*$ or HCO_3^- when limestone dissolves and Reaction 6.10 (Table 6.1) has a negligible effect.

TOT H Complexed as Bicarbonate (HCO_3^-)

This approach assumes that the pH is greater than 6.3 and hence that HCO_3^- contains all TOT H. Thus (HCO_3^-) = 0.064 M. It implies that the reaction:

$$CaCO_3(s) + H^+ \longrightarrow HCO_3^- + Ca^{2+} \qquad (6.21)$$

goes to completion. Hence, the total dissolved calcium concentration is (Ca_T) = 0.064 M.

The next set of calculations assume that calcium equilibrium exists but that gypsum does not dissolve. Use of the complexation reaction

$$\frac{(CaSO_4^{\,o})}{(Ca^{2+})\,(SO_4^{\,2-})} \quad = \quad 210 \qquad (6.26)$$

and the mass balances

$$(CaSO_4^{\,o}) + (Ca^{2+}) = .064 \qquad (6.43)$$

$$(CaSO_4^{\,o}) + (SO_4^{\,2-}) = .032$$

gives the following values assuming no gypsum precipitation:

$(Ca^{2+}) = .0357$ M
$(SO_4^{\,2-}) = .0037$ M
$(CaSO_4^{\,o}) = .0283$ M

The resultant pH derived from the calcite equilibrium reaction is 4.6:

But gypsum will precipitate. Allowing gypsum precipitation gives the following values for a water also at equilibrium with calcite;

$(Ca^{2+}) = .0328$ M
$(SO_4^{\,2-}) = .00077$ M
$(CaSO_4^{\,o}) = .0053$ M

pH = 4.7

For this calculation, the mass law used for gypsum is:

$$(Ca_T)\,(S_T) = 2.34 \times 10^{-4} \qquad (6.44)$$

It is based upon the data of Christopherson and Christopherson (1976). The equilibrium constant (2.34×10^{-4}) is not a true solubility product because the equation (6.44) completely incorporates the existance of the $CaSO_4^{\,o}$ complex into its formulation. Accordingly, the values given above are viewed as an approximations of the true numerical values.

These calculations show that the initial assumption is violated in a significant fashion. The approximation of HCO_3^- being the dominant form of carbon is erroneous because the calculated pH is 4.7. The dominant form of carbon must be $H_2CO_3^*$. This approximation is used in the next section.

TOT H Complexed as Carbonic Acid ($H_2CO_3^*$)

This approach assumes that the pH is less than 6.3 and that $H_2CO_3^*$ contains all TOT H. This gives $(H_2CO_3^*) = 1/2\ (.064) = 0.032$ M. It implies that the reaction:

$$CaCO_3(s) + 2H^+ \longrightarrow H_2CO_3^* + Ca^{2+} \qquad (6.45)$$

goes to completion. This means that the total dissolved calcium concentration without gypsum precipitation is 0.032 M.

Excluding gypsum precipitation, the following concentrations in the infiltrating water are calculated:

Ca^{2+} = 0.0102 M
SO_4^{2-} = 0.0102 M
$CaSO_4^o$ = 0.0218 M

pH = 5.89

Furthermore, the actual (HCO_3^-) is 0.0124 M meaning that the electroneutrality balance is in error by 50%.

Including gypsum precipitation, the following concentrations in the infiltrating pore water are calculated:

Ca^{2+} = 0.0065 M
SO_4^{2+} = 0.0065 M
$CaSO_4^o$ = 0.0088 M

pH = 5.99

(HCO_3^-) = 0.0157 M

This results in an electroneutrality error of 110%.

This approximation (TOT H = $(H_2CO_3^*)$ shows that the pH is less than 6.3, but that $H_2CO_3^*$ and HCO_3^- must be considered.

TOT H Complexed as Carbonic Acid $(H_2CO_3^*)$ and Bicarbonate (HCO_3^-)

This approach assumes that $(HCO_3^-) = 1/2\ (H_2CO_3^*)$. Accordingly, dissolution of $CaCO_3(s)$ results in $(HCO_3^-) = .0128$ M and $(H_2CO_3^*) = .0256$ M with $C_T = .0384$ M and $Ca_T = .0384$ M.

Excluding gypsum precipitation and using reaction (6.43) as the appropriate equilibrium reaction to calculate pH, the concentrations in infiltrating water are:

(Ca^{2+}) = 0.0144 M

(SO_4^{2-}) = 0.008 M

$(CaSO_4^o)$ = 0.024 M

pH = 5.87

(HCO_3^-) = 0.010 M

The resulting electroneutrality error is 10%

Including gypsum precipitation, the concentrations in infiltrating rainwater leaving the unsaturated zone are:

(Ca^{2+}) = 0.0102 M

$(CaSO_4^o)$ = 0.0084 M

(SO_4^{2-}) = 0.004 M

pH = 5.94

(HCO_3^-) = 0.0112

The electroneutrality error is 6%

Overview of Above Calculations

A series of iterative calculations and approximations are required to solve this problem. It could be solved numerically by solving Equation 6.34 or by using an equilibrium computation program (REDEQU, Morel and Morgan, 1972; GEOCHEM; PHREEQE, Parkhurst et al., 1982) or a reaction pathway computer code (PHREEQE; EQ3/EQ6). Such codes give fast, accurate calculations, and should be the method of choice for any complex equilibrium problem.

Using REDEQL (Morel and Morgan, 1972), the predicted pore water concentrations are:

$(Ca^{2+}) = 0.0104$ M
$(CaSO_4^{o}) = 0.0040$ M
$(CaHCO_3) = 0.0022$ M
$(SO_4^{2-}) = 0.00596$ M
pH = 5.82
$(HCO_3^{-}) = 0.0105$ M
$(H_2CO_3^{*}) = 0.0257$ M

when $(Ca_T) = 0.0380$ M, $C_T = 0.0380$ M, $S_T = 0.032$ M and TOT H = 0.064 M. In this case, gypsum precipitates, but the system is not at equilibrium with calcite.

For a water at equilibrium with both calcite and gypsum, $S_T = 0.032$ M and TOT H = 0.064, the following concentrations are calculated:

$(Ca^{2+}) = 0.0112$ M
$(CaSO_4^{o}) = 0.0040$ M
$(CaHCO_3) = 0.0022$ M
$(SO_4^{2-}) = 0.00548$ M
pH = 5.96
$(HCO_3^{-}) = 0.0138$ M
$(H_2CO_3^{*}) = 0.0240$ M

Inspection of these results shows that the concentrations of calcium, bicarbonate, carbonic acid and pH calculated by hand are in excellent agreement with the more exact calculations (REDEQL2) in which all equations are used simultaneously. The substantive difference relates to the proportion of sulphate as SO_4^{2-} and as $CaSO_4^o$; in the computer code calculations, $CaSO_4^o$ concentrations are less than those calculated by hand; as well, SO_4^{2-} is somewhat lower. The major difference for $CaSO_4^o$ results from considering the $CaHCO_3$ complex in the REDEQL2 calculcations - a large proportion of Ca is calculated for the $CaHCO_3$ complex. The different value for SO_4^{2-} results from considering both gypsum and $CaSO_4^o$ and their respective equilibrium constants.

One might also question whether ignoring the equilibrium with iron hydroxide has any effect upon calculation of pH. By reformulating the pyrite oxidation reaction to:

$$FeS_2 + 15/4O_2 + 7/2\,H_2O \longrightarrow 2SO_4^{2-} + Fe^{3+} + 3H_2O + H^+ \qquad (6.19b)$$

one can investigate the equilibrium pH. This equation results in the following concentrations: Fe_T = 0.0160 M, TOT H = 0.0160 M, S_T = 0.032 M available for participating in reactions. Most of the Fe_T forms $Fe(OH)_3(s)$. For water in equilibrium with $Fe(OH)_3(s)$, calcite, and gypsum, and initially containing these concentrations (Fe_T, TOT H, S_T) before precipitation occurs, the calculated values are:

(Ca^{2+}) = 0.0112 M
(SO_4^{2-}) = 0.00548 M
pH = 5.98
(HCO_3^-) = 0.0138 M
$(H_2CO_3^*)$ = 0.0240 M
$Fe(OH)_2^+$ = 9×10^{-9} M

This shows that the earlier calculations remain essentially unchanged.

The calculations by hand for the model can take of the order of one to two days; much of the time is spent in thinking through the model and its implications. Once the system is thought through, it takes approximately 15 minutes to run the calculations with the computer code. While the relative time factors (2 days for calculations by hand; fifteen minutes by computer) are not quite correct due to time spent in thinking through the example, they do point out the significant time advantage to using an equilibrium computer code for solving the model.

6.4 Model Calculations Over Time

The model gives three distinct geochemical periods of time:

PHASE 1: CALCITE AND GYPSUM PRESENT

The pore water concentrations over time are:

$(Ca^{2+}) = 0.0102\ M$
$(CaSO_4^{o}) = 0.0084\ M$
$(SO_4^{2-}) = 0.004\ M$
$(H_2CO_3^{*}) = 0.0256\ M$
$(HCO_3^{-}) = 0.0112\ M$
$pH = 6$

During time period 1, while pyrite is oxidizing, calcite is dissolving (by proton attack), and gypsum is precipitating. Hence, assuming that Ra-226 is only in gypsum, and that gypsum is not dissolving, the radiological activity of Ra-226 in the infiltrating rainwater is 0.

This time period will be limited by the time required to dissolve all the calcite. This is:

$$\frac{\dfrac{132\ \text{mol calcite}}{m^3} \ * \ 2m}{\dfrac{.0384\ \text{mol calcite}}{L} \ * \ \dfrac{10^3 L}{m^3} \ * \ 0.25\ \dfrac{m\ \text{rainwater}}{yr}}$$

or 28 yrs. Of the calcite which dissolves, 52% reprecipitates as gypsum. Hence, 68 mol gypsum/m^3 is precipitated during this phase.

PHASE 2: GYPSUM PRESENT, PYRITE OXIDATION OCCURRING

During Phase 2, pyrite oxidation continues and gypsum dissolution is initiated. No more calcite is present. The calcium concentration results from the amount of gypsum which dissolves and can be calculated from the following combined mass balance - mass law equation:

$$(\text{Ca from gyp})\ ((.032\ \text{M})\ +\ (\text{SO}_4\ \text{from gyp}))\ =\ 2.3 \times 10^{-4} \qquad (6.46)$$

In Equation 6.46 the value of .032 M for sulphate results from pyrite oxidation. From considering the stoichiometry of gypsum dissolution, (Ca from gyp) = (SO_4 from gyp). The solution of Equation 6.46 gives (Ca_T) = 0.00614 M and (S_T) = 0.0381 M.

The calculation of pH is made from the mass balance that 0.064 M TOT H is in solution. This will be complexed with sulphate and carbon, and will be in free form (H^+).

The carbon concentration which originates in rainfall, and is typically $C_T = 10^{-5}$ M. Hence, the maximum of TOT H complexed with carbon is 2×10^{-5} M, a negligible amount relative to the magnitude of TOT H. Most of the TOT H will be free or complexed with SO_4^{2-}.

Of the sulphate in solution, part will be free and part will complex with H^+ and Ca^{2+}. A useful approximation is that 90% of Ca_T is complexed with SO_4 giving $CaSO_4^o$ = (0.9) (0.00614) = 0.0055 M. Thus, the SO_4 available for complexing with H^+ is 0.0326 M.

For the system S_T = 0.0326 M and TOT H = 0.064 M, the resultant pH is approximately 1.4. This calculation is not exact because one needs simultaneously to consider sulphate complexation with Ca^{2+} and H^+; but the pH calculated is reasonably close to the actual situation for the model's assumptions. Comments on the veracity of this pH value are given below.

With respect to Ra-226 concentrations, one of two possibilities could control its concentration. The gypsum precipitated in Phase 1 dissolves first, followed by the gypsum dissolved in the mill. Alternatively, gypsum precipitated in Phase 1 is deposited at fresh nucleation sites, allowing old gypsum to remain exposed to infiltrating rainwater. The latter is the most probable situation. Accordingly, the radium concentration in infiltrating rainwater will result from dissolution of the mill-formed gypsum and from the 68 mol gypsum/m^3 deposited during the first time period. The value of the radium concentration in the mill-formed gypsum is 1000 pCi/mol gypsum. This is based upon the initial assumption of 4600 tonne of solid per 1616 tonne of liquid in the milling circuit and that the radium concentration in the leaching tanks (1500 pCi/L) is precipitated by gypsum (500 M/tonne) formed in the partial and final neutralization tanks. Accordingly, the average radium concentration in gypsum during the second time period is 950 pCi Ra-226/mol gypsum.

Gypsum dissolution gives a pore water concentration of 0.00614 M Gypsum; the equivalent Ra-226 concentration is 6 pCi/L in the percolating water leaving the unsaturated zone. This Ra-226 will be in the aqueous phase and partially adsorbed. For pH 1-2, adsorption data are extremely sparse. A reasonable assumption would be a linear distribution coefficient (K_D) of 5. For this value, the Ra-226 concentration in the migrating fluid is approximately 0.4 pCi/L.

The time to dissolve all the gypsum is:

$$\frac{668 \text{ mol/m}^3 * 2\text{m}}{(6.14 \text{ mol/m}^3) * 0.25 \text{ m/yr}} = 870 \text{ yr}$$

in the 2 m unsaturated zone, if pyrite oxidation continues at a constant rate.

For 5% pyrite in the tailings, the composition is equivalent to 416 mol pyrite/tonne of tailings (500 mol pyrite/m^3). For a pyrite oxidation rate of 2 mol/m^3/yr, 250 yr are required to completely oxidize the pyrite. Accordingly, gypsum dissolution will continue at the above rate for (250 - 28) = 222 years after which it accelerates to maintain chemical saturation. During 222 years, 170 mol gypsum dissolves, leaving 498 mol gypsum at the end of Phase 2.

PHASE 3: GYPSUM DISSOLVING

The only solid phase in this time frame (T GT 250 yr) is gypsum. Gypsum solubility gives:

Ca_T = .0153 M

$(SO_4)_T$ = .0153 M

The pH of the infiltrating water will remain that of rainwater (Equation 6.45) except for adjustments which occur because of the change in ionic strength induced by gypsum dissolution. These adjustments are not calculated here.

The time to dissolve all this gypsum is:

$$\frac{498 \text{ mol/m}^3 * 2 \text{ m}}{(15.3 \text{ mol/m}^3)(0.25 \text{ m/yr})} = 260 \text{ yr}$$

The Ra-226 concentration neglecting adsorption is 15 pCi/L. Including adsorption, the Ra-226 concentration is 1 pCi/L.

6.5 Summary of Model's Calculations

The calculations of the model for infiltrating rainwater leaving the unsaturated zone are summarized in Table 6.3. They assume that the unsaturated zone can be described as one box.

6.6 Weaknesses of Calculations

There are several weaknesses to the calculations, including:

1. The calculations do not consider all equilibrium simultaneously. Accordingly many of the values given are imprecise. For example the simultaneous effects of $Ca\text{-}SO_4$ complexation and precipitation are not calculated.

2. The One-Box assumption may or may not, describe reality in sufficient detail for the unsaturated zone. This zone has substantial one-dimensional variations. For example, pyrite will oxidize mainly at one depth (i.e., at a front), rather than uniformly over the unsaturated zone (see Chapter 12). This means that gypsum will be dissolving above the front and reprecipitating below the front.

TABLE 6.3: SUMMARY OF MODELLING CALCULATIONS

Period	1	2	3
Length of Time	28 yr	232 yr	260 yr
Time Period	0-28 yr	28-250 yr	250-510 yr
$(Ca)_T$	.018 M	.0061 M	.015 M
$(SO_4)_T$	.0088 M	.038 M	.015 M
$(H_2CO_3^*)$	.0256 M	10^{-5} M	10^{-5} M
(HCO_3^-)	.0112 M	-	10^{-7} M
pH	6	1.4	4.5
(Ra-226)	0 pCi/L	0.4 pCi/L	1 pCi/L
Major Solid Phases	Pyrite Calcite Gypsum	Pyrite Gypsum	Gypsum
Major Chemical Reactions	Pyrite Oxidation Calcite Dissolution Gypsum Reprecipitation	Pyrite Oxidation Gypsum Dissolution	Gypsum Dissolution

3. Ion activity coefficients have not been used in the above calculations. They will change the equilibrium concentrations.

4. The radium levels would appear to be too low. The values given are approximately correct for the assumption used: that Ra-226 in gypsum originates only from leaching tank liquors. This means that another mechanism (another solid form) is needed to explain higher Ra-226 levels and/or that adsorption does not occur significantly.

5. The calculated pH trend is similar to that observed, but it does not agree in the absolute sense. The normal sequence is that the pH in coarse tailings of the unsaturated zone is 8 for several months or years and then rapidly decreasing to 2-3. For such field observations, smaller amounts of residual limestone maintains the pH until exhaused after which pyrite oxidation reactions dominate.

   In the above example (pH = 6) would represent reality if the tailings had 120 mol/m^3 calcite added after lime neutralization.

The pH calculated for the second phase is not usually observed in tailings because:

(i) pyrite oxidation is less complete at low pH than indicated by Equation 6.19. Hence, the pyrite reaction given in Table 6.2 (Equation 6.19) is not applicable.

(ii) other buffering systems become important at low pH, where higher iron concentrations are thermodynamically stable in solution. As well, iron-sulphate complexation becomes important (Equation 6.15, 6.16; Table 6.1). These act to counteract the predicted pH depression.

During Phase 3, other buffering systems would also become important. They include solids involving aluminum ($Al(OH)_3(s)$, K-feldspar, clays).

6.7 Recommendations for Future Model Development

Although these calculations provide considerable insight, they show the impossibility of constructing and calculating a comprehensive model by hand. They suggest that the following procedure should be adopted:

(i) Select simple systems (e.g., calcite, pyrite, gypsum) and more complex systems (e.g., calcite, pyrite, gypsum, $Fe(OH)_3(s)$, $Al(OH)_3(s)$).

(ii) Use equilibrium computer codes to calculate equilibrium conditions. Use reaction pathway codes to calculate how these conditions change over time as successive minerals are dissolved.

(iii) Modify these computer codes or use these codes in conjunction with kinetic considerations (e.g., as demonstrated above in which TOT H and S_T from pyrite oxidation are known) to examine how conditions change as successive minerals dissolve or precipitate.

(iv) Aggregate the results from these model systems into a format suitable for determining the appropriate level of complexity required for a source term model.

If comprehensive calculations (e.g., reaction path calculations) are carried out first, one can use the results to construct a simple, analytical model. This modelling approach has been used with considerable success by AECL in deriving an analytical expression for UO_2 solubility in the source term of the probabilistic assessment of the High Level Nuclear Waste program.

These recommendations do not preclude the types of calculations given in this chapter. In fact the calculations given in this chapter are necessary tools for checking the calculations given by reaction pathway codes and for estimating the major time frames involved during a succession of minerals being dissolved.

In the remainder of this report, a few aspects of these recommendations and weaknesses identified above are examined in detail. In particular a review of kinetic data for some minerals is presented (Chapter 11), a few reaction pathway calculations are presented (Chapter 10) and the one-dimensional nature of pyrite oxidation in the unsaturated zone is examined (Chapter 12).

7.0 DECISIONS REQUIRED FOR FORMULATION OF A SOURCE TERM MODEL

7.1 Scope of This Chapter

Of various physical abstractions which are possible, the descriptive example presented in Chapter 6 has used a two box format: unsaturated zone and saturated zone. Chemically, it assumes (i) that pyrite oxidation continues at a constant rate independent of other factors, (ii) that calcite is dissolved at the stoichiometric rate that hydrogen ions are produced and (iii) that calcite and gypsum equilibria are maintained. Hence, the example assumes that pyrite dissolution is controlled by kinetics, and that gypsum dissolution/reprecipitation and calcite dissolution are controlled by equilibrium conditions between pore water and the solid phase. Both calcite and gypsum dissolution are indirectly controlled by kinetics - the kinetics of pyrite oxidation. Whether equilibrium or kinetics controls a particular reaction depends, in part, on the time scale and spatial scale of concern. Hence, one needs to define the time scale and space scale applicable in any model development.

For these three solids, three coefficients in the model require values; the dissolution (oxidation) rate of pyrite and the solubility constants for calcite and gypsum. Selecting these coefficients is usually termed "calibration"; comparison of the model's predictions with observations from a data set which has not been previously used in model formulation or calibration is termed "validation". Procedures for calibrating a model and for conducting validation tests should be specified before the modelling begins. The confidence that one has in the model's prediction will be a function of the length of time that data is available for conducting validation tests.

This chapter addresses five areas which require decisions before model formulation and descriptive algorithm development can begin:

- (i) spatial scale adopted for model;
- (ii) time scale adopted for model;
- (iii) equilibrium or kinetic concepts applicable to various minerals;
- (iv) calibration procedures and validation tests of the model; and
- (v) methods for combining equilibrium, kinetic and transport processes into a probabilistic framework.

7.2 Spatial Scale and Box Models

Complexity of Tailings

Tailings are physically a heterogeneous mass containing fines overlain by coarse solids or intermixed. The fines may be sufficiently cemented with slimes (gypsum and other solids formed in the final neutralization tank) to give them an effective permeability approaching that of clay.

During a rainfall, water will collect in depressions and infiltrate into the ground, unless the rainfall rate exceeds the infiltration capacity in which case it will run off across the surface. The infiltration capacity for fines will be significantly less than that for coarse surface tailings. Infiltrating rainfall replenishes soil moisture, evaporates and percolates downward to the water table. In the saturated zone, the groundwater will move horizontally to surface streams and/or downward to deep groundwater. The actual direction of groundwater movement will partially depend upon the slope of heterogeneous fines, their location and whether the tailings are underlain by gravels, silt-clays or bedrock.

Definition of Discretization of Tailings

Discretization is the conceptual process in which the tailings are broken up into discrete physcial boxes, each box being relatively homogeneous. A "box" is the physical entity about which a mass balance equation can be written. For each box, the chemical elements are subdivided into individual geochemical states; for example, for the description of calcium in Chapter 2 (see Figure 2.3) calcium in each box is subdivided into five geochemical states: CaO, $CaCO_3$(s), $CaSO_4$(s), CaT, and soluble Ca.

The two extremes of discretizing the tailings are:

(i) one box (the saturated and unsaturated zone combined); and
(ii) several hundred boxes to describe all zones observed.

Several intermediate degrees of discretization could be chosen, including:

- (i) two boxes (saturated zone, unsatuated zone);
- (ii) three boxes (unsaturated zone, top of saturated zone, bottom zone of saturated zone); and
- (iii) multi boxes. Different combinations of "multi boxes" include:
  - (a) one box for the saturated zone; several vertical boxes below each other for the unsaturated zones,
  - (b) several boxes horizontally for each of the saturated and unsaturated zones,
  - (c) four boxes consisting of two boxes for the unsaturated zone (unsaturated zone; vadose zone) and two boxes for the saturated zone (upper mixing zone; deep, relatively inactive zone);
- (iv) finite difference discretization for saturated zone;
- (v) finite element discretization for saturated zone; and
- (vi) finite difference/element discretization for saturated - unsaturated zones.

Several of these different combinations of boxes are described below.

In the limit, a multibox discretization approaches the characteristics of a finite difference discretization, because as the number of boxes becomes quite large, the spatial scale of a box becomes quite small and of the same physical size as the finite difference discretization. Finite element and finite difference discretization are normally used as the basis for modeling water transport when small-scale effects are important.

Surface Water and Groundwater Hydrology Models

The hydrology of tailings is commonly viewed by the groundwater hydrologist as being a "sub-surface" problem. This approach has been used with considerable success when one is concerned with:

- (i) the tailings as the "source of contaminants", and
- (ii) subsurface groundwater hydrology.

In this approach, net infiltration is treated as a boundary condition for a groundwater model. That is, atmospheric - land interactions are treated to some degree in a "black box" fashion.

Another view is that of the surface water hydrologist. Here, much emphasis is placed upon rainfall patterns, surface interception, infiltration, depression storage, channel routing, snow accumulation and snow melt, groundwater interflow, etc., to allow accurate predictions of streamwater runoff.

To the surface water hydrologist, the tailings area is treated as one or two subcatchments of the whole watershed. Groundwater flow pathways are considered by surface water models, but the model parameters are generally more empirical than those of a groundwater model.

Hence, two types of hydrology models are available to describe transport: surface hydrology models and groundwater models. Surface water models are particularly appropriate for short time scales (e.g., flood flow), but they are weak at describing subsurface phenomena. Groundwater models are appropriate for long time scales (e.g., seepage and base flow conditions), but they are weak in describing factors affecting surface water hydrology.

For the NUTP program, it is anticipated that the groundwater view of tailings will be most appropriate for modelling time scales of the order of one year. However, if only one year of atmospheric, hydrological and chemical runoff data is available for model calibration, monthly or shorter time scales should be used to test the models. For these shorter time scales, surface hydrology models will be one of the important component models used for assembling data and aggregating up to the source term model (see "Tailing Water Pathways" to "Water Pathway" arrow in Figure 2.2).

Description of Discretization for Sub-Surface Modelling

The following discretizations of tailings are described in this section:

(i) Two-box model
(ii) Three-box model
(iii) Multi-boxes horizontally
(iv) Multi-boxes-vertically
(v) Finite element and finite difference models

(i) Two Box Model

A two box model (saturated zone, unsaturated zone) would be used to describe several essential features of tailings. These include:

(i) the unsaturated zone is generally aerobic and is the zone from which dust blows and radon exhalation occurs and in which most pyrite oxidation occurs, and

(ii) the saturated zone is constantly filled with water on an annual average basis and is mainly anoxic or anaerobic.

Due to hydrological variations, the surface of the saturated zone is not constant from month to month. Hence, a two box model adopts a time scale which is sufficiently long (e.g., a year; a decade) that groundwater variations can be neglected; it assumes that groundwater level variations do not significantly affect rates of processes.

The two box format is that chosen for this report for presentation of the descriptive algorithm. It may be particularly useful for a valley dam in which infiltrating rainwater circulates fairly well throughout the saturated zone (see Figure 7.1(a))

(ii) Three Box Model

A three box model could divide the unsaturated zone into two boxes (unsaturated and vadose zones) or the saturated zone into two boxes (surface mixing, deep groundwater) while retaining the other box of the two box format.

Selection of three boxes consisting of a mixing zone and deep groundwater would be most useful for NUTP purposes where the "mixing zone" has substantially different chemistry than that of deep groundwater (e.g., the iron sulphate front from the unsaturated zone) and where most of the infiltrating rain water flows horizontally through the mixing zone. Figure 7.1(b) presents such an example. Hence, the basement material, of low permeability, precludes substantial infiltration below the mixing zone.

FIGURE 7.1

Alternative Geometries of Tailings

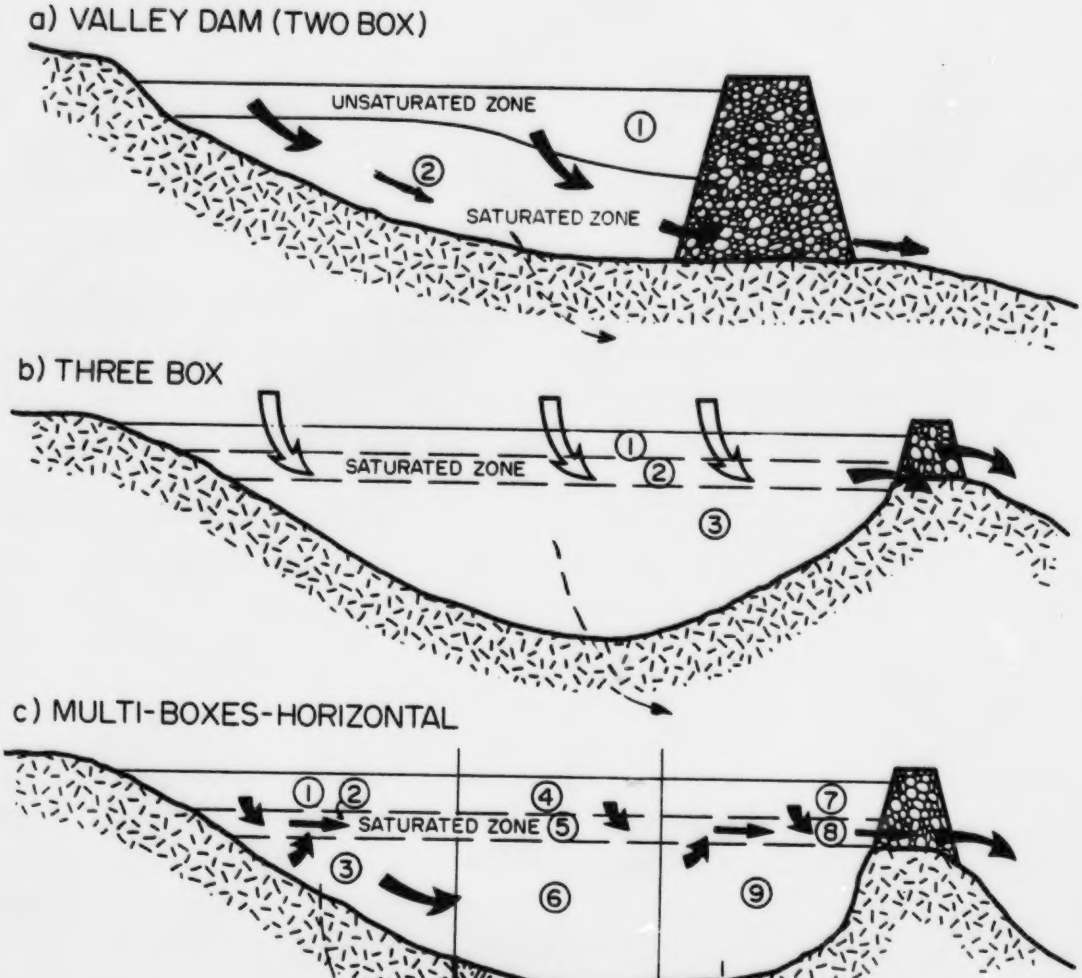
a) VALLEY DAM (TWO BOX)
UNSATURATED ZONE
①
②
SATURATED ZONE
b) THREE BOX
①
SATURATED ZONE
②
③
c) MULTI-BOXES-HORIZONTAL
① ②
④
⑦
SATURATED ZONE ⑤
⑧
③
⑥
⑨
d) MULTI-BOXES-VERTICAL
LEACHED ZONE
REPRECIPITATED CHEMICAL
ORIGINAL TAILINGS CONCENTRATION

(iii) Multi-Boxes - Horizontally

Figure 7.1(c) presents the vertical three box model format, further subdivided into three horizontal sections. This illustrates the possibility that one section of the tailings (left section) is underlain by fractured bedrock and that one section (far right) is composed of fines while the other two (left and middle) sections are composed of relatively coarser material.

This level of detail would be quite site specific. It might be used to consider transport of contaminants from particular zones in the tailings area. It's selection would probably be for a specific research or component modelling application, as opposed to a source term modelling application (see Figure 2.2).

(iv) Multi-Boxes - Vertically

Figure 7.1(d) presents several vertical boxes. This discretization may be used for thickened and layered tailings in which alternate layers of coarse and fine tailings are deposited. This discretization may be used to describe the vertical evolution of the porous zone for mechanisms such as pyrite oxidation, gypsum or calcite dissolution or radium-226 dissolution in specific layers. Such detail is particularly useful for describing how Ra-226 migration controls the flux of Rn-222 because dissolution of Ra-226 in the upper layers, downward migration and reprecipitation of Ra-226 in the deeper layers means that the Rn-222 flux reaching the surface will have decreased.

The sketch in Figure 7.1(d) shows a vertical profile for gypsum in which the upper zone is leached. It is partially reprecipitated in the middle zone and has remained essentially unaltered from the original tailings composition in the bottom zone. This sketch as a controller upon Ra-226 redistribution, is relevant for any metal sulfate, if Ra-226 migration is controlled by its coprecipitation with that metal sulfate.

(v) Finite Element and Finite Difference Models

These models provide much more hydraulic detail than is usually feasible for use with chemical modelling (Garvin and Freeze, 1984). However, this level of detail is often needed by requirements of the computational algorithm. For purposes of the NUTP, it is probable that such models would only be used as research or component tools (see Figure 2.2). They might be used to simulate the hydrology of a particular tailings area in detail or to check the approximations of a box model. Their geometry would be substantially simplified (e.g., to a two box or three box model format) and the hydrological flow results aggregated for use in a source term model.

7.3 Time Scales

General Comments on Time Scales

There will be two different time scales of concern for formulating a tailings source term model:

(i) the time scale of concern to the probabilistic source term model (e.g., greater than one year), and
(ii) the time scale of data available for model calibration (e.g., minutes to months).

These scales are diagrammed in Figure 7.2 to 7.4 in two forms. Figure 7.2 shows the relationship of time scales to observational data. Figure 7.3 shows time scales of various chemical, biological and geological phenomena. Figure 7.4 presents data which are useful for relating physical scales to time scales.

Figure 7.3 presents several time scales observed on earth. The Figure is not comprehensive but points out several essential features. The Figure is composed from 3 main sources. Most of the biological information (Harris, 1980) describes aspects of phytoplankton ecology (10^1 - 10^{10}s). Decay rates of organic matter have typical rates ranging from 0.1 - 0.01 day^{-1} (Metcalfe and Eddy, 1979). Higher rates are noted for simple sugars while slower rates are observed for very complex organics (e.g., ocean sediments, Berner, 1979). Although not noted, present-day knowledge about biochemical decay rates for persistent, synthetic organics is sparse. General statements suggest that they are non-biodegradable, implying that $k \rightarrow 0$ as $t_{1/2} \rightarrow \infty$.

The information at long time scales (10^8 - 10^{17}s) describes epochs and eras of the earth over geological time. The information at short time scales (10^{-10} - 10^0s) describes water-exchange rates for aqua ions (Cotton and Wilkinson, 1980). The exchange rates

FIGURE 7.2: TIME SCALE OF OBSERVATIONAL DATA

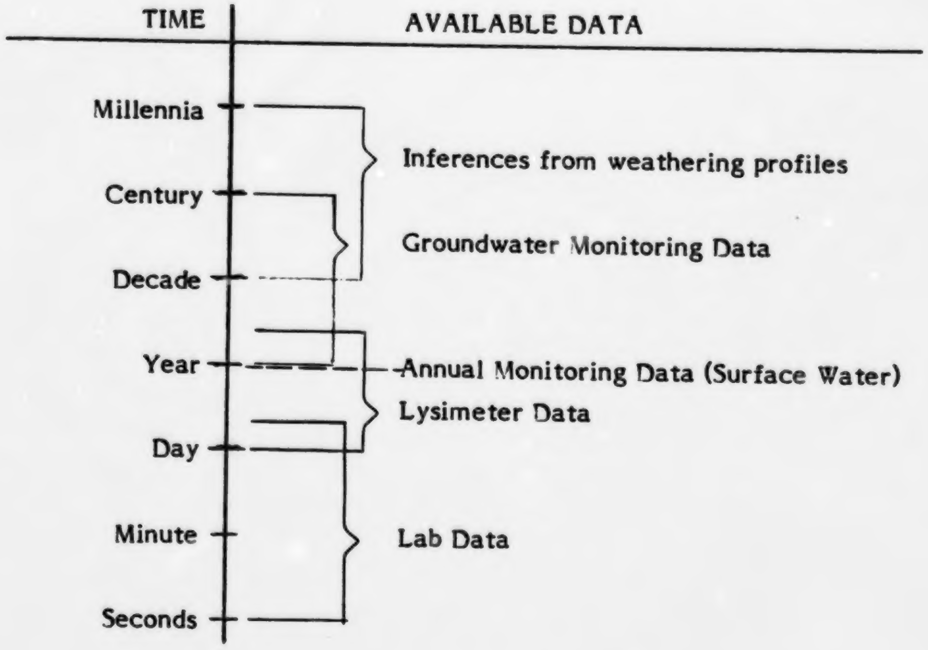
TIME
AVAILABLE DATA
Millennia
Century
Decade
Year
Day
Minute
Seconds
Inferences from weathering profiles
Groundwater Monitoring Data
Annual Monitoring Data (Surface Water)
Lysimeter Data
Lab Data

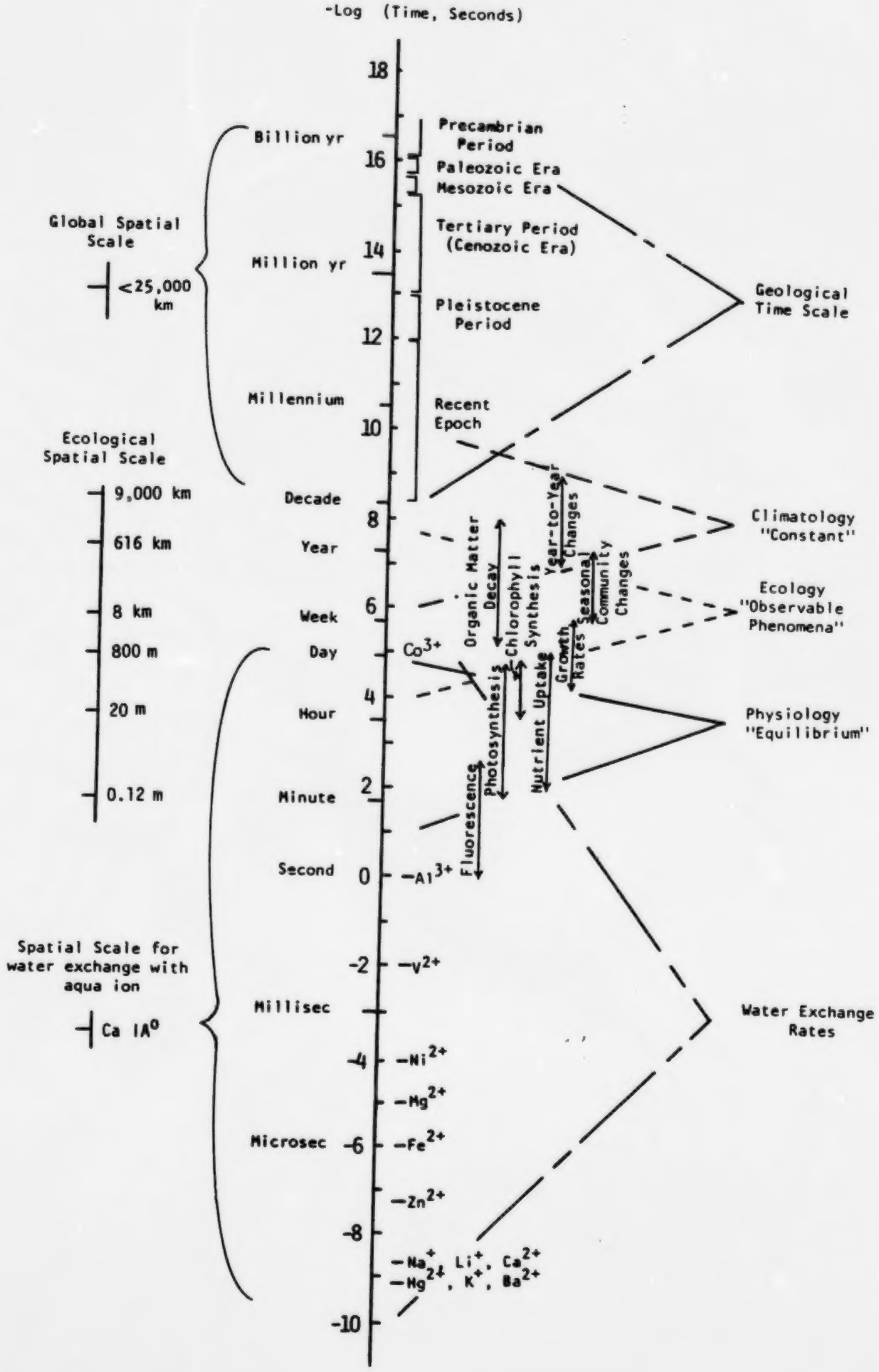
-Log (Time, Seconds)
18
16
14
12
10
8
6
4
2
0
-2
-4
-6
-8
-10
Billion yr
Million yr
Millennium
Decade
Year
Week
Day
Hour
Minute
Second
Millisec
Microsec
Global Spatial Scale
<25,000 km
Ecological Spatial Scale
9,000 km
616 km
8 km
800 m
20 m
0.12 m
Spatial Scale for water exchange with aqua ion
Ca 1A°
Precambrian Period
Paleozoic Era
Mesozoic Era
Tertiary Period (Cenozoic Era)
Pleistocene Period
Recent Epoch
Geological Time Scale
Climatology "Constant"
Ecology "Observable Phenomena"
Physiology "Equilibrium"
Water Exchange Rates
Organic Matter Decay
Chlorophyll Synthesis
Year-to-Year Changes
Seasonal Community Changes
Growth Rates
Nutrient Uptake
Photosynthesis
Fluorescence
Co3+
Al3+
V2+
Ni2+
Mg2+
Fe2+
Zn2+
Na+, Li+, Ca2+
Hg2+, K+, Ba2+

FIGURE 7.3a: **TEMPORAL SCALES FOR VARIOUS CHEMICAL, BIOCHEMICAL AND GEOLOGICAL PHENOMENA** (from Snodgrass, 1983; constructed from Cotton and Wilkinson, 1980; Harris, 1980; and standard geological textbooks)

FIGURE 7.3b: HALF LIVES OF RELEVANT RADIONUCLIDES OF CONCERN TO URANIUM MINE-MILL MANAGEMENT

TIME SCALE	RADIONUCLIDE (ACTUAL HALF LIFE)
	Th-230 (1.4 x 10^{10} yr)
	U-238 (1.6 x 10^{9} yr)
Million	
	U-234 (2.5 x 10^{5} yr)
	Th-230 (8.1 x 10^{4} yr)
Millenia	
	Ra-226 (1,620 yr)
Century	
	Pb-210 (25 yr)
Decade	
	Ra-228 (6.5 yr)
	Th-228 (1.9 yr)
Annual	
	Po-210 (138 d)
	Th-234* (24.1 d)
Week	
	Rn-222 (3.8 d)
Day	
	Pb-214* (26.8 min)
	Bi-214* (19.7 min)
Minutes	

(* Not normally of concern radiologically, measurement is useful for understanding transport)

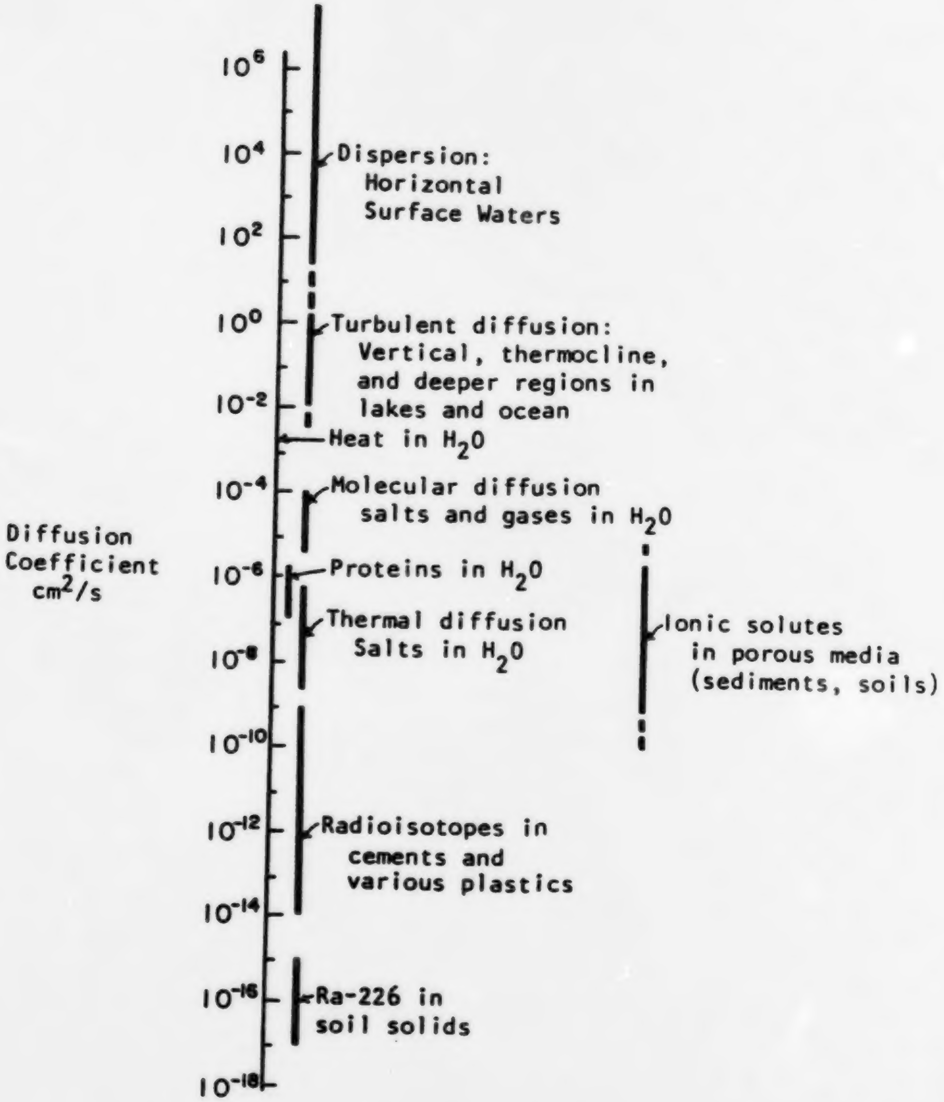

FIGURE 7.4: **DIFFUSIVITY COEFFICIENTS CHARACTERISTIC OF AQUEOUS AND SOLID ENVIRONMENTS** (from Snodgrass, 1983; adapted from Lerman, 1971; Nathwani and Philips, 1978, 1979; and Godbee et al., 1980)

describe the time required for innersphere H_2O molecules, coordinated with the central aqua ion, to substitute with solvent water. Except for a few ions such as Cr $(H_2O)_6^{3+}$, the time scales are all rapid (i.e., less than 1 sec) although they span a range of over 10 orders of magnitude.

Time scales of many other substances could have been included in Figure 7.3a. For example, radioisotope decay reactions span the range from short times (e.g., 10s for Pb-214) to long times (e.g., 10^{13}s for U-238). Relevant half times of decay for radionuclides of concern to this project are given in Figure 7.3(b).

Figure 7.3a also shows an ecological spatial-scale plot (9,000 km to 0.12 m) which corresponds to the time-scale plot (1 decade to 1 min). It is based upon a link between the growth rate of algae and the coefficient of horizontal diffusion. A theoretical explanation (the Kiss Model; Harris, 1980) calculates the critical patch size of algae below which diffusion destroys any growth effects. It predicts that any patch of algae less than 100 m in size will be rapidly destroyed by horizontal diffusion because the algae cannot grow as rapidly as nutrients can be transported to them by horizontal diffusion. Diffusion studies and the acceptance of a maximum division rate of algae give 1 km as equivalent to approximately one day.

Figure 7.3 describes 3 time "zones" whch are conceptually useful for describing biological processes, including cellular functions and community response. But the spatial scale suggested by the graph may be inappropriate for certain cellular functions, because different environments have different rates of diffusivity, and because there are practical limits on the scale being considered. Geological time scales which span ca 9 orders of magnitude of temporal scales may be viewed as occurring mainly at one scale (the global scale), while water exchange rates which may span ca 15 orders of magnitude of temporal scales may also be viewed to occur at one spatial scale (1A°).

Spatial scales of interest (1A° - the globe) are practically governed by the diffusivity coefficient of a substance in its parent material. Figure 7.4 gives an overview of the range of values. They vary from substantial values in open water bodies to quite small values for the diffusion of metals through solids. If one is interested in the time scale of 1 day - 1 year, physical limits are those suggested by the ecological spatial scale of Figure 7.3. Only if one is interested in long time scales does the diffusion of ions through solids become significantly greater than several centimetres.

Relating Physical Scales to Time Scales in Tailings

For biological processes, growth rates (e.g., of bacteria or algae) and physical scales (e.g., coefficient of horizontal diffusion) can be linked by considering the ratio of growth rate to transport rate (the Kiss Model). Similarly, chemical processes can be linked to physical scales. In this section, one method for linking time scales to length scale is illustrated for dissolution processes. In subsequent sections, aspects of kinetic and equilibrium concepts are related to physical scales (Section 7.6; Chapter 8; Chapter 12).

For dissolution, the transport rate from the surface of a mineral into the bulk of solution often controls the dissolution rate. This may be viewed as a dissolution process which is controlled by transport across a fluid zone in contact with the mineral. The fluid zone is only a few microns thick.

Consider a deep groundwater system containing groundwater and minerals and to which external transport due to advection or dispersion is negligible. This system may be modelled physically as a batch reactor (one box) with no inflow or outflow. If the volume of water (V) surrounding the mineral surface area A_s initially has a concentration of 0 (C=0), the concentration over time 't' is given by,

$$V \frac{dC}{dt} = - \frac{D \ A_s}{\text{del } Z} (C_s - C) \tag{7.1}$$

which gives a mathematical solution of

$$C = C_s \ (1 - \exp (- D \ A_s \ t/V \ \text{del } Z)) \tag{7.2}$$

Here D is the diffusion coefficient, del Z is the distance over which a linear approximation of the concentration gradient is valid and C_s is the saturation concentration. D/del Z is a mass transfer coefficient. By estimating the diffusional length (del Z), one can use Equation 7.1 to estimate the time scale required for the volume of water to reach equilibrium. Such calculations are presented in Chapter 11 (gypsum dissolution).

Analysis of Equation 7.2 shows that the timing constant of response of the pore water consists of the coefficients multiplying time in the exponential. By analogy to radiological decay concepts, the "effective decay constant", Beta, of the pore water is:

$$\text{"Beta"} = \frac{D\ A_s}{V \text{ del } Z} \tag{7.3}$$

and the half-time of response is

$$t1/2 = 0.693/\text{Beta} \tag{7.4}$$

Inspection of Equation 7.3 shows that A_s/V is a mean length - the length over which diffusion must occur whereas Beta is the system time constant. Accordingly, the length scale, A_s/V, is related to the time scale, Beta, by the mass transfer coefficient, D/del Z.

This definition of time scale is conditional upon the kinetics used for dissolution (Equation 7.1). Other kinetic expressions for dissolution and/or consideration of crystallization as per Rimsted and Barnes (1980) will result in different definitions of time scale.

Time and Spatial Scales of Concern in Tailings

Unlike the time and spatial scales considered in Figure 7.3a, the time scale and spatial scales of the tailings mass are much more constrained. A summary of relevant radiological and physical time scales is given in Figure 7.5. Chemical time scale data are described in Chapters 8 and 11.

The upper limits of a spatial scale are constrained by the size of the tailings mass (10 - 100 ha). The lower size limit is of the order of one micron (the film thickness of water around tailings grains; the size of bacteria such as T. ferrooxidans). A smaller size scale (less than one micron) might be needed to interpret particular data describing precipitation and dissolution kinetics.

FIGURE 7.5: SUMMARY OF RADIOLOGICAL AND PHYSICAL TIME SCALES OF CONCERN TO A PROBABILISTIC ASSESSMENT

Time Scale	Phenomena	
?	Glaciation Age	
10,000 yr	Hydraulic detention time - old groundwater	
1,620 yr	**Ra-226 half time**	
50 yr	Hydraulic dention time - impermeable bottom	
25 yr	**Pb-210 half time**	
6.5 yr	**Ra-228 half time**	
3 yr	Hydraulic detention time - leaky dam	
1.9 yr	**Th-228 half time**	
180 d	length of snow cover in N. Saskatchewan	
138 d	**Po-138 half time**	
30-60 d	length of summer	
1 wk		
3.8 d	**Rn-222 half time**	) time for infiltrating) rain water to reach) saturated zone in) granular tailings
1 d		
1 hour		

The time scales of concern to probabilistic models are expected to be of the order of 1 year to 10,000 years. The length of 1 year may be the basic time step used in the model's computations. Shorter time scales will also be of concern, but these are expected to be related more to observational data and to time scales useful for modelling transport along atmospheric and aquatic pathways.

For the two box format (adopted in this report) the spatial scale of interest is the "whole" saturated zone or the "whole" unsaturated zone. For these boxes, there are different residence times which could be adopted: biological, chemical, and physical.

The snow residence time for the frozen ground surface is of the order of one month to 6 months (dependent upon thaws). The hydraulic residence time of the unsaturated zone is of the order of days to months while the hydraulic residence time of the saturated zone will generally vary from one year to one century - time scales which are similar to those of lakes.

For NUTP purposes, it is suggested that the time scale should be defined relative to the hydraulic residence time of the appropriate water mass because advective flow is the fundamental variable controlling the movement of chemical contaminants.

7.4 Equilibrium and Kinetic Controls on Mineral Dissolution

Whether equilibrium or kinetic factors control the quantity of a mineral in solution affects how a model is computationally algorithmed. If all minerals are controlled by equilibrium, a reaction code (e.g., EQ3/EQ6) in combination with transport considerations can be used to simulate the system. If all minerals are controlled by kinetics, a different kind of algorithm is required. If some minerals are controlled by kinetics and others by equilibria, a combined equilibria-kinetic algorithm would be used.

As developed in Chapter 8, equilibrium can be modelled as consisting of two kinetic reactions: a formation reaction and a dissolution reaction. Hence, a mixed system in which some minerals are controlled by equilibrium and others are controlled by kinetics can be viewed as simply a system in which kinetics can be used to describe relationships between all minerals and the solution. But in this mixed system, the rate constants describing formation and disolution of minerals close to equilibrium are much faster than the rate constants for minerals not at equilibrium. This presents computation difficulties because extremely small time steps are required to integrate numerically the differential equations and maintain convergence of the integration scheme.

Use of an algorithm based upon chemical knowledge of the system allows larger time steps in the numerical integration of differential equations by properly describing those minerals at equilibrium and minerals whose formation or precipitation is kinetically controlled.

Hence in developing a source term model, the reader should specify the time scale of the computational step and then determine whether the relationship between all minerals and the constituents of pore water is controlled by equilibrium, kinetics or a mixture before selecting a computational methodology and algorithm.

7.5 Model Calibration Procedures and Validation Tests

General

In any model formulation exercise, there is always some information not known about particular processes. This information is usually defined in terms of model coefficients. Examples include the dispersion coefficient in water, the pyrite oxidation rate and the solubility product. Due to the constancy of certain processes, coefficients such as the radioactive decay constant are usually assumed to be true and hence to have the validity of a physical law.

From the point of view of thermodynamics, solubility products may also be viewed as following a physical law (e.g., in order to maintain the consistency of definitions used in thermodynamics). But because the laboratory measurement of solubility products is fraught with errors and uncertainties, they are often viewed as model coefficients.

Definition of Model Calibration and Model Validation

Selection of coefficient values for a model is generally termed model calibration, while comparison of a calibrated-model's predictions with observations is often termed model validation. Calibration of a model may be made by using literature data or by choosing coefficient values which cause the model's predictions to show agreement with a set of observations. Selection of coefficient values may be made by eye, by judgement or by using some statistical routine based upon maximum likelihood or minimization of error principles (e.g., Marguardt, 1983). An example of such statistical procedures is linear least squares. An alternative approach for model calibration is to represent the coefficients as distribution functions (taking variability and uncertainty into account) rather than using best-fit values. The parameter distribution function is particularly useful in probabilistic assessments.

Approaches to Model Evaluation

The utility of a model depends upon the objectives of the investigator. Different objectives include:

(i) the application of a "validated" model to make predictions of absolute concentration of a contaminant in tailings pore water;

(ii) the application of a "calibrated" model to evaluate the sensitivity of concentrations of a contaminant to alternative management schemes by comparing the relative magnitude of model predictions; and

(iii) the aggregation of known facts, processes, and/or mass balances to allow evaluation of the relative importance of different geochemical processes for prioritizing research efforts.

To validate models for making predictions, different tests can be used. They include:

(i) To compare the model structure (compartments and intercompartmental mass flows) with known processes to ascertain that the functional formulation is reasonable and that all major factors are included.

(ii) To compare model prediction with observations for:

    (a) one tailings area and one time period;
    (b) one tailings area and several time periods;

(c) several tailings areas; and

(d) several tailings areas and several time periods.

The evaluation of model structure represents a credibility test: if processes thought to be significant are not included in the model, it may be arbitrarily rejected by an investigator as inadequate. This is a first level of testing. The second and ultimate level of testing is to compare model predictions with observations. Use of long time periods and several tailings piles for model testing will severely stress the model and hence provide more confidence in its application.

The method for determining the adequacy of agreement between model predictions and observations has been a matter of considerable debate. The methods devolve into using qualitative or quantitative criteria. Qualitative methods are judgemental and by eye; in these methods the trend predicted, and the magnitude of concentration predicted are used as decision points. Quantitative criteria use appropriate statistics and lack-of-fit tests (Reckhow, 1979; Thomann, 1982; Reynolds et al., 1981). The use of appropriate parametric and non-parametric statistical tests has recently been demonstrated for algal biomass models (Thomann, 1982) and for renewable resource problems (forestry; Reynolds et al., 1981). The use of qualitatve criteria before use of quantitative criteria should continue because there is a possibility that a model may give an equally good fit to data showing repetitive behaviour over time, as it would to the same data randomly distributed with time (Remington and Schork, 1970).

Terminology of Other Fields

With respect to terminology, different fields appear to use the words "verification" and "validation" for opposite components of modelling. The field of eutrophication and water quality modelling (e.g., Thomann, 1982; Snodgrass, 1979) uses the term "verification" to describe a comparison of model predictions with observations. The field of "renewable resource modelling" (e.g., Reynolds et al., 1981) appears to use the term "verification" to describe checking a computer code and the term "validation" to compare model predictions with observations. This divergence of terminology is unfortunate. For this report, the definition for "validation" used by the "renewable resources" field is used because this appears to be the terminology being advanced by the fields of systems analysis and computer science.

Procedures Suggested for Use by National Uranium Tailings Program

Within a probabilistic framework, the problem being examined by the NUTP is to take knowledge of tailings biogeochemical processes and project it for up to 10,000 years in the future with a set of constraints such as assuming constant human behaviour for certain periods of time. The modelling projection will be based essentially upon data with a time scale of less than 20 years (the length of time over which tailings have existed). Some time scale information for conducting validation tests may be obtained from natural sites where dissolution of U-ore bodies has been occurring for several centuries to several millenia.

Due to the large uncertainties asociated with many processes and coefficient values, the probabilistic framework has been chosen to aid assessment of the future effects. This can be carried out by using model calibration procedures outlined above.

But wherever possible, model validation procedures should be conducted. This is particularly important because the tailings problem is mathematically an initial value governed problem. Validation procedures could involve, for example, taking literature data to calibrate a model and using data from the monitoring program to validate its predictions. But if the modelling problem is viewed from a one-year time step perspective, the testing, will not take advantage of all features of the available data. A monthly time step should be used to take full advantage of the data.

A second procedure is to apply a tailings source model to two or more tailings areas of different hydrological and chemical character. Successful prediction of observed groundwater chemistry and outflow chemistry will provide significant validation of that model.

7.6 Method for Combining Equilibrium, Kinetic and Transport Processes Into a Probabilistic Framework

Combining Equilibrium, Kinetic and Transport Processes with The Mass Balance Equation

As described in section 7.3 and in Chapter 8, one can use equilibrium and kinetics to relate solid characteristics to solution characteristics. The mass balance equation represents the method for relating solid-solution relationships to physical transport (advection, diffusion).

In this section, examples are presented which define a spatial scale and then which use transport, kinetics or equilibrium, and the mass balance equation to define a temporal scale. Consider three examples, one involving inflow, outflow and decay; a second involving advective transport, decay and adsorption; and a third involving diffusion and reaction.

(i) Transport and Reaction

Consider a mass balance upon a groundwater body treated as one box with an advective inflow and outflow. The mass balance gives:

$$V\frac{dC}{dt} = QC_{IN} - QC - kCV \qquad (7.5)$$

$$C = C_{IN}\,(1-\exp(-\,\text{Beta}\ t)) \qquad (7.6)$$

$$\text{Beta} = \frac{1}{\tau_w} + k \qquad (7.7)$$

$$\tau_{1/2} = 0.693/\text{Beta} \qquad (7.8)$$

This assumes that $C=0$ at $t=0$ and that a step function input C_{IN} occurs at $t=0$.

Here: V is the volume of the water
Q is the advective inflow and outflow rate
k is the radioactive decay constant
τ_w is the hydraulic detention time = V/Q
$\tau_{1/2}$ is a half time

For the spatial scale of the box, the half-time of response is inversely related to Beta and equal to $0.693\,\tau_w/(1 + k\tau_w)$.

(ii) Transport, Reaction and Adsorption

A second example can consider adsorption, in addition to advection and decay. Adsorption is first considered as a kinetically controlled process and then as an equilibrium process. For a batch system (one box; no inflow or outflow) the derivation of the Langmuir isotherm gives:

$$A \frac{dT}{dt} = k_1 (T_m - T) AC - k_2 TA \qquad (7.9)$$

This assumes that the rate of adsorption is proportional to the product of the solution concentration and the number of unfilled sites (T_m-T) on the surface; and that the rate of desorption is proportional to the surface concentration (T). Here, k_1 is the kinetic constant for adsorption, k_2 is the kinetic constant for desorption, and A is the surface area.

For adsorption onto solids in groundwater, the mass balance for the groundwater body which has inflow, outflow and decay is;

$$V \frac{dC}{dt} = QC_{IN} - (Q+kV)C + k_2 TA - k_1 T_m AC \qquad (7.10)$$

and for the surface is;

$$A \frac{dT}{dt} = k_1 T_m AC - k_2 TA - k\ TA \qquad (7.11)$$

This simplifies Equation 7.9 by assuming that T_m is much greater than T (i.e., a linear isotherm results) and that decay of sorbed material is proportional to the mass on the surface. This latter assumption is valid for radioactive substances but its authenticity for biological decay awaits further work.

A similar equation to Equation 7.11 results when precipitation-dissolution processes dominate solid-solution transfer.

These equations for adsorption and precipitation-dissolution often present computational problems. If the values of the kinetic coefficient describing sorption-desorption are much faster than those describing transport, "stiff" differential equations result. Such equations require very short time steps to solve them because of the fast rate coefficients describing adsorption-desorption.

If the kinetics of adsorption and desorption are rapid relative to other mechanisms,

$\frac{dT}{dt}$ approximately equals 0, and

$$V \frac{dC}{dt} = QC_{IN} - (Q + kV)C - kBT_mAC \qquad (7.12)$$

where $T = BT_m$ and B is the Bindings constant. Thus

$$\text{Beta} = \frac{1}{t_w} + k\left(1 + \frac{BT_mA}{V}\right) \qquad (7.13)$$

$$t_{1/2} = 1/\text{Beta} \qquad (7.14)$$

Analysis of this expression for half-time (Equation 7.14) shows that decay of the sorbed phase decreases the response time of the water body. If reversible adsorption occurs but decay does not occur in a system, the half-time is exactly the same as that of a conservative substance. This occurs because equilibrium is continually maintained between the water phase and the sorbed phase during the response of the groundwater body to a change in inputs. That is the kinetics of adsorption-desorption do not affect the response characteristics of the ground water body, due to the assumption of adsorption being an equilibrium process.

(iii) Diffusion and Reaction

Combining reaction and transport makes possible an analytical solution for estimating a flux across an interface. For example, consider oxygen transport from the tailings unsaturated zone into the saturated groundwater zone. If the oxygen partial pressure is known, one can calculate an equivalent saturated water concentration. Then knowing the the oxygen consumption rate in the water, one can calculate flux of oxygen across the sediment-water interface as a function of the diffusion coefficient in the water.

Similarly, one can calculate the oxygen flux from the atmosphere into the unsaturated zone. Here, the oxygen consumption rate is stoichiometrically equal to the pyrite oxidation rate. The the flux can be calculated as a function of the diffusion coefficient for oxygen in the unsaturated zone. This flux then controls the flux of sulphate and hydrogen ions produced by oxidation.

The calculations are based upon the following mathematical development. Assuming that diffusion is the only significant transport process (as opposed to advection), the one-dimensional mass transport equation for any soluble substance is:

$$\frac{dC}{dt} - D \frac{d^2C}{dZ^2} = S \qquad (7.15)$$

where: C is Concentration of any substance (e.g., g/m^3)
t is Time (e.g., day)
D is Diffusion coefficient of the substance (e.g., m^3/d)
Z is Vertical Distance from interface (e.g., m)
S is Net source or sink of substance (e.g., $g/m^3/d$)

This equation assumes that $Z = 0$ at the atmosphere-tailings interface and that the effect of tortuosity is incorporated into D. The equation represents the diffusive transport through a large number of boxes lying vertically on top of each other, and each of thickness dZ. It provides the basis for biofilm kinetic concepts.

Equation (7.15) has been solved by several investigators, depending upon the assumptions for the decay kinetics (S) and the availability of suitable boundary conditions. The kinetics for biofilms are typically described by zero-order, first-order or Monod kinetics. Investigators who use the different kinetic formulations (Riemer, 1977) include:

(i) First-order kinetics, e.g., Levenspiel (1972).
(ii) Zero-order kinetics, e.g., Wuhrmann (1964), LaMotta (1974), Harremoes and Riemer (1975), Harremoes (1976).
(iii) Monod kinetics, e.g., Williamson and McCarty (1976A and B), Atkinson and Fowler (1974), Harremoes (1976).
(iv) General 17th order removal kinetics, e.g., Satterfield (1970).

Riemer (1977) gives a solution for diffusion into the reaction zone and one of three possible reactions in the reaction zone: zero-order, first-order and Monod-kinetics. He concludes that first-order reaction in the reaction zone causes a first-order reaction with respect to concentration at the interface (Z=0). With zero-order reaction in the reaction zone, he distinguishes two cases. In the first case, the reaction zone is sufficiently thin that at the extreme depth of the reaction zone, there is oxygen left; in this case, the reaction is also zero-order with respect to concentrations at interface. In the second case, with a thick reaction zone and diffusion limiting the thickness of the reactive zone, the reaction is half-order with respect to concentration at the interface.

Example: Oxygen Transport Model

For oxygen, zero order reaction kinetics in the tailings can be assumed (i.e., S = ROX). This is a valid approximation because oxygen does not limit bacterial respiration unless concentrations are less than 0.5 mg/L (Zobell and Anderson, 1936). Steady-state conditions, give expressions (Bouldin, 1968) for the flux of oxygen across the interface (OD) as

$$OD = 2\,COX_0 \cdot ROX \cdot DOX \qquad (7.16)$$

and for the thickness of the aerobic zone (ZOX),

$$ZOX = \frac{2 \cdot DOX \cdot COX_0}{ROX'} \qquad (7.17)$$

Here, COX_0 is the oxygen concentration of the interface and DOX is the diffusion coefficient of oxygen. Application of Equation (7.15) assumes that the oxygen gradient is only vertical.

Incorporation of the Mass Balance Equation of a Source Model into Probabilistic Framework

In other applications of the probabilistic framework, such as the nuclear fuel waste management program, much attention has focussed upon evaluating transport through several barriers, through geological materials (bedrock; soils; groundwater) and in the biosphere. For such applications, the source term has been treated as a boundary condition - a leaching rate of uranium and other radionuclides which is essentially constant for a period of time. For certain radionuclides, three different leaching rates have been identified: a sudden release (impulse type) at t=0, a rapid rate (during the next time period), and a slower rate (during the last time period). The different rates are keyed to leaching from particular types of crystals and gas spaces in the waste fuel rods.

To estimate a leaching rate for each period, the mean values of laboratory data for each period are used. The statistical distribution of the leaching rate is estimated using variability in the lab data. Effects of different solution complexes are also incorporated into the statistical distribution.

For uranium mill tailings, the development of a leaching rate and an associated distribution would greatly simplify the probabilistic framework. But for tailings, it is our judgement that use of different leaching rates as a boundary condition for pathway analysis is inappropriate because one cannot be sure how "predictive" the values for leaching rate will be over time. Furthermore, the statistical distribution may be so wide that it swamps the whole probabilistic assessment, resulting in the predicted distribution for dose or chemical toxicity being the same as that of the leaching rate.

It is our assertion that the different geochemical processes in the tailings must be modelled using the mass balance equation for the different minerals and elements of concern and that the coefficients in the mass balance equation must be used in the probabilistic assessment.

Accordingly, unlike the nuclear fuel waste program, the source model and its coefficients are part of the probabilistic assessment problem, rather than being a boundary condition to it.

It is suggested that the NUTP develop a miniaturized probabilistic assessment of the geochemical evolution of tailings by using a detailed source term model. If this analysis proves appropriate, it may be feasible to simplify the source model to being a boundary condition to an environmental transfer model. It is more probable that this miniaturized assessment will show it feasible to simplify the source model, but not to the point of being a boundary condition.

7.7 Evaluation of Time Scales for Computational Scheme of Source Model

The time scale of concern for developing the computational scheme of a source model is the time scale of chemical substances in the pore water. It is not the half-time of mineral dissolution (see Figure 1.1), for example, nor is it the hydraulic detention time of groundwater. It is influenced by these two phenomena (mineral dissolution half-time, detention time) and by other phenomena (e.g., recrystallization rate, diffusion coefficients).

It is perhaps natural to think of the modelling time scale as being equivalent to the mineral dissolution half-time. A summary of half-times for various minerals, composed from the kinetic data of Chapter II, is given in Figure 1.1. These time scales vary from seconds to millions of years. These time scales present a perspective defining the length of time that one would need to model a tailings mass. But they do not provide an absolute answer because of the influence of physical transport and recrystallization reactions.

Consider a model describing the concentration of a contaminant involving dissolution, recrystallization and flow in a tailings box. Using the kinetic formulations of Rimsted and Barnes (1982) for dissolution and recrystallization, the mass balance equation gives:

$$V \frac{dC}{dt} = r_d V - kCV - QC \qquad (7.18)$$

where: V is the volume of the pore water in the box,

C is the pore water concentration,

r_d is a zero order dissolution rate,

k is the recrystallization rate, and

Q is the outflow rate.

At steady-state:

$$C = \frac{r_d}{k + q/z} \qquad (7.19)$$

where: q is the hydraulic loading ($q = Q/A$; A = surface area), and
z is the mean depth of the box.

The term q/z is the inverse of the hydraulic detention time (t_w) of the box.

Two time scales can be defined: the retention time of C in the pore water ($\bar{t}_c$) and the half-time of C ($t_{1/2}$). The retention time is the time to replace the mass present in the pore water. It is defined as:

$$\bar{t}_c = \frac{\text{Mass Present}}{\text{Dissolution Rate}} = \frac{1}{k + t_w^{-1}} \qquad (7.20)$$

The retention time of mass is directly analogous to the hydraulic detention time. The half-time is the time required to attain one-half of the new steady-state concentration if the dissolution rate changes. Evaluation of the mass balance equation (7.18) gives:

$$t_{1/2} = \frac{0.693}{k + t_w^{-1}} \qquad (7.21)$$

Inspection of the two formulae show that the two time scales are similar, with $t_{1/2}$ being approximately 70% of t_c.

Calculated values of the retention time are given in Table 7.1 for different characteristics of an unsaturated and saturated tailings box. The retention time is calculated for two cases: where chemical recrystallization does not occur ($K = 0$), and where recrystallization does occur. The chemical retention time exactly equals the hydraulic detention time when crystallization does not occur ($k = 0$). When recrystallization occurs, the retention time is essentially unaffected by crystallization in the unsaturated zone and in the saturated zone unless the hydraulic detention time is 50 years or greater. At long hydraulic detention times, the chemical retention time approaches 85 years, a value established by the crystallization rate constant.

The values for retention time of Table 7.1 are specific for the values given and for the kinetic formulations of Equation 7.18. Hence, cnsiderable care must be taken in extrapolating them to specific sites. But they illustrate the following points:

TABLE 7.1: CALCULATIONS OF RETENTION TIME OF CONTAMINANT IN TAILINGS PORE WATER

Case	Considering Only Hydrology ($K = 0$)	Considering Hydrology and Crystallization ($K = 0.012\ yr^{-1}$)
Unsaturated Zone (2 m thick)	8 yr	7.3 yr
Saturated Zone (8 m thick):		
t_w = 2.5 yr	2.5 yr	2.4 yr
t_w = 50 yr	50 yr	31 yr
t_w = 500 yr	500 yr	78 yr
$t_w = \infty$	-	85 yr

(i) that the chemical retention time of the pore water is a function of both hydrology and chemical reaction;

(ii) that the hydraulic retention time of a particular groundwater body is one key to defining the chemical retention time;

(iii) that long hydraulic detention times do not define the chemical retention time, but rather chemical rate constants do; and

(iv) that the chemical retention time of the pore water may be substantially shorter than the dissolution half-time of minerals such as silica and feldspars.

7.8 Recommendations Related to Modelling Decisions

There are two time scales of concern for developing a source term model for a probabilistic assessment: the computation time scale and the length of time that one must model. The computational time scale is a function of the chemical retention time of an element in the pore water which is a function of the hydraulic detention time. The total length of time is a function of the mass initially in the tailings and the rate of export from the tailings.

It is recommended that the computational time step of the source term model be established. For this time step, certain reactions can be described using equilibirum concepts while others need to be described using kinetic concepts. An analysis of relevant literature is given in Chapter 11. Then the mass balance equation for each element of concern can be formulated using the appropriate concept for different minerals. Using this mass balance equation, the time constant of various combinations of reaction and transport can then be determined.

For the probabilistic assessment, it is anticipated that possibly two or more different time steps may be used for different tailings time frames. For example, BEAK (1982) used a five-year time step for computations of a maximum time period of 500 years, and a 200 year time step for computations of a maximum time period of 10,000 years. For these alternative time steps, dissolution of certain minerals may be kinetically controlled for the shorter time step, but equilibrium controlled for the longer time step.

This presents a computation problem which is difficult to solve in a completely general manner. This report does not advocate any particular approach to this problem. It may be sufficient for most minerals to be able to define them as either/or (kinetic-thermodynamic) with only a few minerals requiring dual consideration.

The different degrees of complexity that a source term model may attain should be determined initially. Then a miniaturized probabilistic assessment of these source term models should be undertaken to determine how much simplification may be possible and yet give sufficient predictive capability for a probabilistic assessment.

8.0 A QUANTITATIVE OVERVIEW OF CHEMICAL EQUILIBRIUM AND KINETICS

Many types of reactions occur in the tailings pore-water system. Of these, reactions between the solid and solution phases are the most significant. The dissolution and precipitation of solids are controlled by a number of processes that are driven by a common directive, that of lowering the free energy of the system. It is usually possible through simple calculations, (e.g., thermodynamics) to determine whether a reaction (i.e., dissolution or precipitation) is favoured or not. Many systems behave such that actual concentrations of solid components in aqueous solution can be predicted from free energy data.

But this information is not sufficient to know whether the reaction will in fact occur on a time scale that is of interest. This unpredictable aspect of chemical behaviour occurs because factors other than thermodynamic properties influence the progress of favourable reactions. For example, in an oxidizing environment, pyrite is thermodynamically very unstable. This would suggest that in the oxidized environment of leaching pachucas, all pyrite would dissolve. But this does not occur because the kinetic rate is rather slow and the detention time in the tanks is short (ca 1-2 days). Only when significant quantities of bacteria develop, and at longer detention times, are the large quantities of pyrite dissolved. Hence, it is often necessary to determine empirically (lab kinetic data; field evidence) whether a particular system will behave in a thermodynamic fashion or whether kinetic controls will prevail.

To analyze whether chemical equilibrium or kinetics controls a system, one needs to define a physical scale and an associated time. For this report, the physical scale is defined at the macroscopic scale of a few cubic centimeters - a scale sufficient to contain several mineral grains and groundwater in contact with each other, but a scale small enough to contain the width of a weathering front. The time scale of concern is of the order of 1 month to 10,000 years. The time scale of concern will vary, depending upon whether research (component) models or a source term model for a probabilistic assessment are being applied.

8.1 Equilibrium Viewed as Two Opposing Rates

Although classical thermodynamics treats equilibrium as a relationship between two chemical states of a system, an alternative approach is possible. For an elementary reaction;

$$aA + bB \underset{k_b}{\overset{k_f}{\rightleftharpoons}} cC + dD \tag{8.1}$$

the rate laws for the forward(f) and backward(b) reaction are:

$$r_f = k_f \quad (A)^a \quad (B)^b \tag{8.2}$$

and

$$r_b = k_b \quad (C)^c \quad (D)^d \tag{8.3}$$

respectively. In this case, r represents the rate, k is a rate constant and the brackets denote chemical activity. At equilibrium the rates must be equal and hence:

$$k_f \quad (A)^a \ (B)^b = k_b \quad (C)^c \ (D)^d \tag{8.4}$$

After rearranging terms this relationship can be expressed as:

$$k_f/k_b = \quad ((C)^c \ (D)^d) \ / \ ((A)^a \ (B)^b) \tag{8.5}$$

The right-hand term is actually the definition of the equilibrium constant (K_{so}) for the overall reaction. Therefore, for an elementary reaction:

$$K_{so} = k_f/k_b \tag{8.6}$$

When k_f is much greater than k_b, K_{so} is much greater than 1 and the formation of the products C and D is favoured.

This relationship suggests that when a mineral remains in equilibrium with the surrounding porewater, during significant perturbations in the system, it is because both forward and backward rate constants are relatively large.

However, the dependence of equilibrium on a reaction rate also implies that any system will be out of equilibrium at the instant it is perturbed (i.e., addition of one reactant or instant change in temperature etc.). In addition, if the system is continually disturbed, such as would occur when a fresh non-equilibrated solution passes in contact with a mineral phase (e.g., calcite),the system may never attain thermodynamic equilibrium. It is also possible that while one mineral phase is dissolving to attain equilibrium, one dissolved component of that solid would be precipitating to form a different solid. The incongruent dissolution of certain minerals may be the factor that is responsible for controlling the chemical composition of water in some subsurface environments. (Congruent dissolution is defined as the complete dissolution of a mineral, while incongruent dissolution is partial or complete loss of one element from the mineral and transformation of the old mineral to a new mineral.) Although rate controls can result in disequilibrium in a particular system, combinations of controls on a particular component may result in relatively steady-state concentrations of that species.

8.2 Comparison of Rate Control and Steady State

For conceptual purposes, chemical kinetics related to dissolution and precipitation of mineral phases can be viewed as being either:

1. near equilibrium, or
2. far from equilibrium processes.

As a generalized example, the reaction may be described by a simple first order equation such as;

$$\frac{1}{A}\frac{dC_i}{dt} = R_i = k_{ij}\,(Cs_{ij}-C_i) \qquad (8.7)$$

in which A is the surface area of mineral, C is the concentration of component i, t is time, R_i is the rate, k_{ij} is the rate constant for component i in solid j, that is usually determined empirically and Cs_{ij} is the equilibrium concentration of component i in solid j. In a system in which one component can occur in more than one solid (i.e., Ca in $CaCO_3$, $CaSO_4 \cdot 2H_2O$, $CaAl_2Si_2O_8$) the net rate of appearance (or disappearance) of the component can be expressed as;

$$\sum_{j=1}^{n} R_i = \sum_{j=1}^{n} k_{ij}(Cs_{ij} - C_i) \qquad (8.8)$$

Because one mineral can be dissolving while another is precipitating and because the rates of reaction change with the relative differences from equilibrium, it is possible to obtain a constant concentration of component i. In this case, the net rate becomes zero and the steady-state concentration C_i* is:

$$C_i* = (1/\sum_{j=1}^{n} k_{ij}) \; (\sum_{j=1}^{n} k_{ij} Cs_{ij}) \qquad (8.9)$$

This relationship shows that for any rate constant k_m where k_m $k_{j \neq m}$, the "steady-state" concentration $C_i^* = Cs_{im}$. In other words, the concentration would be in equilibrium with the mineral whose reaction rate constant has an absolute value which is much greater than any other. If rates are of the same order-of-magnitude and have opposing counterparts (i.e., incongruent dissolution), the concentration of component i would be intermediate between the values expected from equilibrium with the solid exhibiting the largest positive rate and that exhibiting the largest absolute value of the negative rate.

An example of intermediate steady-state concentrations has been obtained experimentally and evaluated mathematically (Lasaga, 1981) for aqueous Al derived from nepheline ($NaAlSiO_4$) dissolution. In this case, gibbsite ($Al(OH)_3$) precipitation was occurring concurrently with nepheline dissolution at pH = 3.1. The resultant steady-state concentration of Al was intermediate between those expected for equilibrium with each mineral phase.

Even in more complex systems in which transient behaviour occurs, the concentrations of soluble components can attain a quasi-steady-state condition. An example of the predicted weathering progress in a nepheline, syenite system is simulated mathematically by Lasaga (1984). During the first year, solution transport, dissolution of the primary nepheline, and formation of kaolinite and gibbsite resulted in time dependent behaviour. But after approximately one year, the weathering system had attained relatively steady-state conditions with respect to mineral assemblages and solute concentrations. Some lateral movements of mineral boundaries occurred with time after one year, but this was quite slow in comparison to solution transport rates.

Many dissolution reactions in geologic media represent far-from-equilibrium systems. In such systems, the concentration of the products need not be considered. This is shown for feldspar dissolution by Helgeson et al. (1984) who concluded that the reaction depended mainly on surface area and to a lesser extent, pH. Therefore, the rate could be expressed in terms of the increase of the concentration of the dissolved constituents as;

$$\frac{dC_i}{dt} = k^* (T, H^+, A) \qquad (8.10)$$

in which k^* is the rate constant that is dependent on temperature (T), pH (or H^+) and surface area (A).

Steady-state concentrations in solution can be obtained if one of the components precipitates, or if the advective flow rate is steady. In the latter case, the steady-state concentration of a component can be expressed as;

$$C_i^* = R_{ij}/J \qquad (8.11)$$

in which R_i is a rate of dissolution (mol/yr) and J is the advective flow rate (e.g., m^3/yr).

8.3 Chemical Regimes Controlled by Kinetics

The precipitation of a mineral involves transfer of mass from the solution phase to the solid phase via the following steps:

(i) transport of an element from the fluid to the mineral surface;
(ii) movement of the element along the mineral surface to a site where the precipitate is forming; and
(iii) arrangement of the element into the crystal lattice.

Dissolution involves the opposite sequence of steps. If the movement of the element along the mineral surface or arrangement to form the crystal lattice is the rate controlling step, the formation or dissolution process is termed "surface reaction" controlled (i.e., at the surface of the mineral) or within a "kinetic regime". If the transport of the element through the fluid is the rate controlling step, the precipitation or dissolution process is termed "diffusion" or "transport" controlled (i.e., within a "transport regime").

Rates of reaction are controlled by factors such as the chemical activity of reactants and products; the rate of transport (e.g., by diffusion) of reactants and/or products in the fluid; the temperature; and the surface area of participating solids. One can determine whether specific reactions are within kinetic (i.e., reaction only) or transport controlled regimes. In general, fast reactions are transport controlled whereas slower reactions are not inhibited by the transfer of components. There is also a strong correlation between solubility constants (K_{so}) for minerals and their respective kinetic regimes. Berner (1978a, 1981) shows that dissolution rates for minerals with low K_{so} values are surface (reaction) controlled while those with high values are generally controlled by transport processes.

Microscopic Scale

Transport control can be attributed to a number of mechanisms. At the microscopic level (1-10 um), the transfer of reactants and/or products can be retarded by the relatively stagnant film of water that adheres to solid surfaces or by the resistance to movement through a solid coating that may form on parent minerals during dissolution.

The net rate of reaction of spherical particles has been shown to be additive for processes involving the 3 sequential processes of reaction, film transport and reaction layer transport (Levenspiel, 1972). The net reaction rate is given by:

$$R = C_i/(1/k_f + r/2De + 3/k_s) \qquad (8.12)$$

Here, k_f is the mass transfer coefficient through the thin liquid film resulting from diffusion, r is the original radius of the particle, De is the effective diffusion coefficient through the reaction coating and k_s is the surface-controlled rate constant. This expression has, as indicated above, a physical scale of a few microns to a few centimeters.

It can be seen in this equation that the liquid film resistance is important only when k_s is on the same order or greater than k_f. Because water films are generally quite thin, the k_f term is relatively large in most cases in geologic settings, meaning that film resistance is insignificant. The value of De in solids is relatively small; hence resistance through a reaction coating would be significant if such a coating were to form during dissolution of a mineral phase. Although reaction coatings are not commonly observed, they may be important under certain conditions. For example, in a study of pyrite oxidation in dilute carbonate-buffered solution, Nicholson and Gillham (in prep.) found that oxide coatings, formed during pyrite oxidation, significantly affected the predicted rates of reaction in a continuous flow system that was monitored over a one-year period.

Factors influencing these two regimes (kinetic regime; transport regime) and a description of which minerals in uranium mill tailings are controlled by "surface-reaction" or "transport control" are considered in more detail in Chapter 11.

Macroscopic Scale

On a more macroscopic scale (e.g., 1-2 m) certain rates of reactions are affected by transport of reactants through the geologic medium, when one component, not readily available within the tailings, must be transferred there from another location. An example of potential transport-controlling-conditions is pyrite oxidation in a tailings pile where oxygen transfer from the atmosphere may be the rate-determining step (see Chapter 12).

Modelling of a particular system, in terms of kinetically controlled reactions is made simpler if one process (i.e., surface reaction versus transport) determines the net rate of reactions involved. It is, therefore, useful to compare the magnitude of individual kinetic components to determine whether one is dominant. In this manner the prediction of rates may be simplified to reflect the appropriate kinetic regimes.

Fluid Scale

In the above descriptions of microscopic scale and macroscopic scale, two different fluid scales are used. The microscopic scale is of the order of 1-10 um. The macroscopic scale is of the order of a meter.

In analyses of the literature, the terminology used occasionally makes it difficult to determine the scale involved.

For reaction kinetics which differentiate "surface reaction" from "transport controlled reaction", the microscopic scale is normally the scale under consideration. For modelling a tailings area using a one or several box model, the macroscopic scale is probably the scale under consideration.

8.4 Overview of Precipitation and Dissolution Theory

An overview of precipitation and dissolution theory is useful for assessing the kinetics used for different temporal and spatial scales by various investigators. Because most theory applies to experimental scales in the laboratory, this is the scale used in this report. Precipitation theory has been developed for such systems as, condensation of water vapour ("rainfall = precipitation") and formation of solids of sparingly soluble salts (e.g., AgCl; $BaSO_4$). The formation of minerals has been treated thermodynamically (e.g., free energy of the solid) by geologists and others for decades, but only recently have attempts been made to apply precipitation and dissolution kinetic theory rigorously to the study of mineral formation and dissolution (e.g., Lasaga, 1984).

Precipitation Theory

The formation of a precipitate has been viewed classically, as involving several steps, including:

(i) the formation of a cluster (embryo)
(ii) the formation of a nucleus
(iii) the formation of a crystal
(iv) the formation of aggregates of crystals and nuclei

A cluster is composed of several to many atoms of the ultimate crystal, but is thermodynamically unstable. A nucleus is the minimum-sized cluster which is thermodynamically stable and upon which crystal growth is initiated. The nucleus may range from several angstroms to a micron in size while the size of the crystal may range from submicron to several centimeters in size. Aggregates form by different sized particles colliding with each other.

The rate of formation of a nucleus (rate of nucleation) or the rate of crystal growth may limit the overall rate of precipitation. The rate of nucleation depends upon whether homogeneous nucleation, heterogeneous nucleation or secondary nucleation is the main mechanism for producing nuclei for crystal growth. Homogeneous nucleation is the formation of nuclei in pure solution. Heterogeneous nucleation is the formation of a nucleus on a foreign object (i.e., condensation of water vapour onto a dust particle). Secondary nucleation is the break-off of small fragments from a large crystal; these fragments become the nucleus for new crystal growth.

In a complex solution such as groundwater, it is doubtful that homogeneous nucleation would explain nucleation. Heterogeneous nucleation and possibly secondary nucleation are the most probable mechanisms. Whether nucleation or crystal growth limits the overall rate of precipitation is unclear. Because of the large amount of foreign matter present, it is possible that crystal growth will be rate limiting in most cases of practical significance.

Crystal growth involves transfer of mass:

(a) from the bulk solution to the solution just outside the crystal;
(b) from the solution into an adsorption layer;
(c) from the adsorption layer or solution to a growth step (surface nucleus or spiral);
(d) from the solution, adsorption layer or growth step to the growth site on the step (Nielsen, 1981).

The growth process is often visualized as involving addition of a unit sized, rectangular block to a step; the step increases in size to become a layer by forming a set of rectangular steps or spirals.

The following kinetic expressions are observed for each of the flow processes involved in growth:

(a) transport controlled growth (movement from bulk solution) is proportional to $C\text{-}C_s$ and is a function of crystal size and shape;

(b) movement into the adsorption layer is surface controlled growth and is proportional to $C-C_s$;

(c) movement to the growth step is approximately proportional to $(C-C_s) \ln (C/C_s)$;

(d) movement to the growth site on the step is proportional to $(C-C_s)(C/C_s)^{1/2} \ln (C/C_s)$.

Here, C is the solution concentration and C_s is the saturation concentration. The first two processes are linearly dependent upon $C-C_s$ while the last two processes are parabolic rate laws - when C/C_s is close to 1 the rate is proportional to $(C-C_s)^2$.

Hence, at high supersaturation, the rate law will be linear. But after substantial crystal growth, a transition occurs to a parabolic rate law at low supersaturation.

At non-equivalent concentrations, the rate of growth of sparingly soluble crystals is proportional to $(IAP^{i/v} - K_{so}{}^{i/v})^2$ where IAP is the ion activity product, K_{so} is the solubility product and $v=a+b$ for the electrolyte A_aB_b. Nielsen (1981) explores this functional form by assuming that ions are adsorbed in electroneutral amounts on the crystal surface by displacing one or more water molecules.

Dissolution Theory

Mineral dissolution involves similar steps to those involved in crystal growth but in reverse order. Dissolution is particularly dependent upon solution pH.

The dissolution process involves proton transfer and specific adsorption of cations and anions at the solution - solid interface of a metal oxide, for example. The surface is viewed as consisting of $\}\!-OH_2{}^+$, $\}\!-OH$, AND $\}\!-O^-$ groups in contact with solution with the relative abundance of the different groups being determined by the pK of sets of two (e.g., $\}\!-OH_2^+ = \}\!-OH + H^+$) and solution pH. Adsorption and desorption of hydrogen ion, cations and anions are involved in the dissolution process.

The resultant rate law derived for metal oxides (Grauer and Stumm, 1982) is

$$R = k\,(H^+)\,\phi_A$$

where R is the dissolution rate and ϕ_A is the relative surface coverage with an anionic surface complex.

The coordination model has been used to interpret the catalytical effect of chloride upon dissolution of goethite and the inhibitory effect of phosphate upon the dissolution of calcite.

Overview of Both Processes

A complete overview of both processes is not possible for many minerals, as experimental, conceptual, or mechanistic information is usually missing. However, the above ideas can be sketched into an overview of all processes involved.

Consider aluminum as a system. In solution, the following major ions may be present:

$Al(H_2O)_6^{3+}$	$Al(H_2O)_6SO_4^{+}$
$Al(OH)(H_2O)_5^{2+}$	$Al(H_2O)_6(SO_4)_2^{-}$
$Al(OH)_2(H_2O)_4^{+}$	$Al_2(OH)_2(H_2O)_{10}^{4+}$
$Al(OH)_3(H_2O)_3^{0}$	
$Al(OH)_4^{-}$	

The following solids may be present:

$Al(OH)_3(H_2O)_3(s)$ - amorphorus aluminum hydroxide
$Al(OH)_3(s)$ - gibbsite, bayerite, or microcrystalline gibbsite.

The processes of nucleation and crystal growth are a continuum which can be represented by:

$$A + A \longrightarrow 2A$$
$$A + 2A \longrightarrow 3A$$
$$\bullet \bullet \bullet \bullet \bullet \bullet \bullet$$
$$A + (n-1)A \longrightarrow nA$$
$$\bullet \bullet \bullet \bullet \bullet \bullet \bullet$$

$$\begin{aligned} &A+\text{cryst}\,▨ \dashrightarrow \text{cryst}\,▨A \\ &A+\text{cryst}\,▨\text{-}A \dashrightarrow \text{cryst}\,▨\begin{smallmatrix}-A\\-A\end{smallmatrix} \end{aligned} \qquad (8.13)$$

Here, A is represented as the basic building block in classical theory;

2A,3A, 4A, are clusters;

nA is a nucleus;

cryst▨ is a crystal which has grown upon the nucleus;

cryst ▨-A is the addition of one unit of A to the crystal. A may be thought of as the addition of a rectangular block to a plane surface;

cryst $▨\begin{smallmatrix}-A\\-A\end{smallmatrix}$ is the addition of a second unit of A to the crystal. This may be the second block added to form a new layer or to be the start of a spiral.

From the point of view of solution chemistry, the definition of A is not always clear. For 1:1 electrolytes, it may be defined as $BaSO_4$ for barium sulphate and $CaSO_4$ for gypsum. Only recently has consideration been given to the possibility that both Ba^{2+} and SO_4^{2-} ions for the 1:1 electrolyte, or both $Al(H_2O)_6^{3+}$ and H^+ for the aluminum system arrive at the surface at different locations but still constitute a proportion of the basic building block. Such a possibility has been considered empirically by describing one part of the precipitation process as being the surface diffusion of an anion or cation adsorbed to the surface to the site where crystal growth is occurring. It is being considered in another way (e.g., Nielsen, 1981) by the developing concepts of surface complexes by analogy to the complexes which exist in solution (e.g., a surface complex of Al▨$\text{-}OH_2\text{-}SO_4^{2-}$ in analogy to the $Al(H_2O)_6SO_4^+$ complex in solution).

For the crystal growth of aluminum hydroxide, classical theory might represent the process as:

$$\begin{aligned} &Al▨\text{-}OH + Al(H_2O)_6^{3+} \dashrightarrow (Al▨\text{-}OH)(Al(H_2O)_6^{3+})* \\ &Al▨\text{-}OH)(Al(H_2O)_6^{3+})* \dashrightarrow Al▨\text{-}Al(OH)_3(H_2O) + 4H_2O + 2H^+ \end{aligned}$$

(8.14)

where the starred quantity is an activated complex. The breakup of the activated complex would involve several steps whose precise details await further analyses, and which include surface adsorption, formation of surface complexes and release of protons.

Crystal growth could also involve the other monomeric species of aluminum given above (e.g., the hydroxo and sulfate complexes). Development of the theory for these complexes awaits further work.

With respect to solids which can form, two possibilities are the amorphorus form and the crystalline form. The amorphorus form is generally a more hydrated form. A high degree of supersaturation promotes rapid kinetics resulting in formation of the amorphorus form. This may be viewed as occurring, because the water molecules which are strongly coordinated to the aluminum cation do not have time to leave the central atom before the atom is incorporated into the solid. Relevant time scales for the loss of water molecules are described in Chapter 7. Over longer time frames, (or lower degrees of supersaturation), more orderly development of a crystal occurs because water molecules can be lost from the central atoms. This results in the formation of a crystalline solid.

Dissolution can also be illustrated considering surface coordination chemistry. For aluminum, the problem may be viewed as the breaking of several bonds to allow release of an aluminum atom. For example, dissolution of gibbsite may be viewed as requiring the breaking of three bonds. For one bond the process might be:

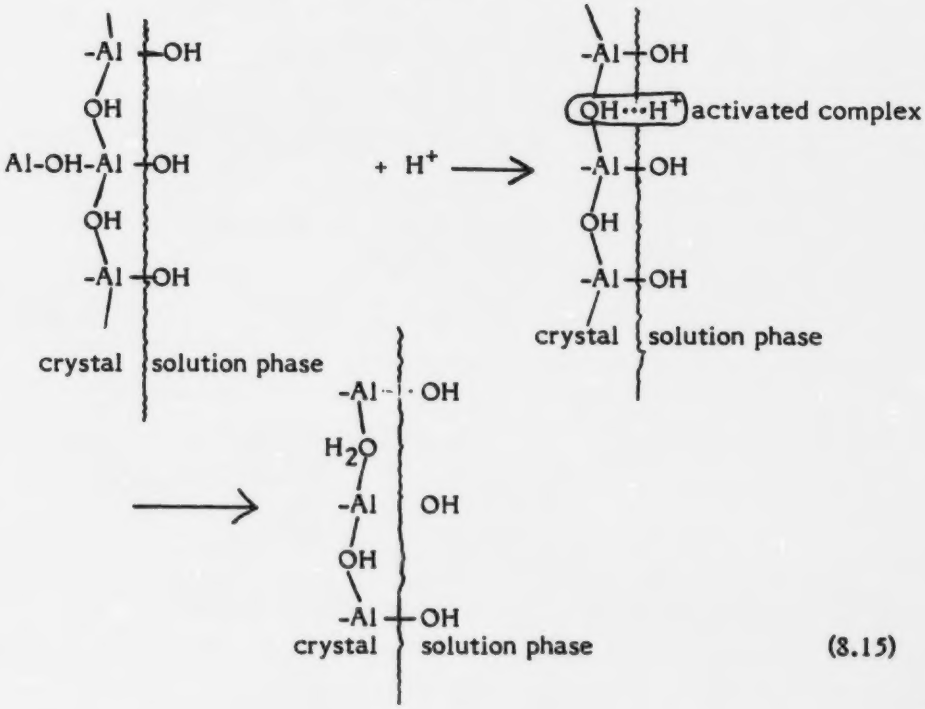
-Al
OH
OH
Al-OH-Al
OH
OH
-Al
OH
crystal
solution phase
+ H⁺
-Al
OH
OH···H⁺
activated complex
-Al
OH
OH
-Al
OH
crystal
solution phase
-Al
OH
H₂O
-Al
OH
OH
-Al
OH
crystal
solution phase

(8.15)

The overall process gives:

$$Al_n(OH)_{3n} + 3H^+ + 3H_2O \longrightarrow Al_{n-1}(OH)_{3(n-1)} + Al^{3+}(H_2O)_6 \qquad (8.16)$$

Consideration of the above shows that the overall rate expression for dissolution might be reduced to terms involving a rate constant, hydrogen ion concentration, and the number of sites that hydrogen ion will attack. Such an approach is the basis for the expression given above.

Thermodynamics of Precipitation and Dissolution

The application of thermodynamics to solid-solution relationships assumes that "an equilibrium" exists between the solid and solution. This may be expressed as a solubility constant or as free energy. For the aluminum hydroxide system, the relationship is:

$$Al(OH)_3(s) + 3H^+ + 3H_2O = Al(H_2O)_6^{3+} \qquad K_{so} = 10^{8.5}$$

or

$$Al(OH)_3(amorph) + 3H^+ + 3H_2O = Al(H_2O)_6^{3+} \qquad K_{so} = 10^{10.8}$$

Here the solubility product K_{so} is defined as:

$$K_{so} = \frac{Al(H_2O)^{3+}}{(H^+)^3(H_2O)^3(Al(OH)_3(s))} = \frac{Al(H_2O)_6{}^{3+}}{(H^+)^3} \qquad (8.17)$$

because the water molecule and solid phase are assigned a chemical activity of unity.

The solubility constant is related to the standard Gibbs free energy of the reaction (ΔG^o) by:

$$K_{so} = \exp\left\{-\frac{\Delta G^o}{RT}\right\} \qquad (8.18)$$

where R is the universal gas constant and T is absolute temperature. Also,

$$\Delta G^o = \Delta H^o - T\Delta S^o \qquad (8.19)$$

Solid formation is favoured (i.e., the solution is supersaturated:IAP $>$ K_{so}) if the net free energy is lowered. Hence, the formation of gibbsite is favoured over amorphorus aluminum hydroxide and calcite formation is favoured over aragonite formation under earth-surface conditions.

For systems in which the less favoured solids form, kinetic factors are involved in the formation. Such systems can be analysed by imposing the solid upon the system.

8.5 Application of Precipitation and Dissolution Theory to Analyses of Uranium Tailings Piles

The reference point for any analyses is the mineral assemblage present in the ore, and secondary precipitates formed in the mill and tailings pile and their mineralogical state. An analysis of candidate minerals and possible solution complexes of concern to the management of uranium mine tailings is given next in Chapter 9. Thermodynamic data are only briefly summarized because critical analyses are required to develop a self consistent data base.

In Chapter 10 (and the Appendix), a partial, self-consistent thermodynamic data base is developed and used to simulate the geochemical evolution of an equilibrium assemblage of minerals. The assemblage considered is pyrite-calcite-goethite-gypsum-jarosite-aluminum hydroxide and subsets. To the extent that the equilibrium assumption is valid, one would calculate the contaminant flux from such an assemblage by combining the reaction code with a transport model. The mass flow of aluminum leaving the tailings for example would be equal to:

$$(Al_T)Q \qquad (8.20)$$

where (Al_T) is the soluble concentration and Q is the outflow rate.

However, many of the minerals present in the tailings are far from equilibrium (for example, pyrite because of its presence in an oxidizing environment and alumino-silicate minerals formed at higher temperatures). A conceptual analysis of aspects of environmental stability is given earlier in Chapter 3. For such minerals, kinetics control their dissolution.

Hence, in Chapter 11, an analysis of the kinetics controlling the dissolution of particular minerals is given. Also kinetics of formation of particular minerals are analysed. The precipitation kinetics are mainly applicable to mill formed precipitates, although they are also used to comment upon the possible formation of jarosite in the tailings pile. Then in Chapter 12, dissolution kinetics of pyrite and transport of atmospheric oxygen are used to analyse the probable geochemical controls on the production of acidity.

9.0 EQUILIBRIUM

9.1 Solid Phases

In a weathering environment, there is a strong trend toward chemical degradation of all primary mineral phases. With the continual leaching by rain water and snow melt, minerals at the earth's surface are usually far from equilibrium and consequently their dissolution is kinetically controlled.

There are some minerals, however, that are metastable at the earth's surface. These are typically referred to as secondary phases. Although these too will dissolve when subjected to continuous leaching by dilute solution, the solution composition attains equilibrium relatively quickly in the subsurface pore water. Examples of such minerals include hydrous oxides of ferric iron and manganese, aluminum hydroxide, some clays and, in certain environments, calcite and gypsum. The formation of other secondary minerals is also possible. Probably the most detailed information has been generated for supergene enriched ore bodies. In that environment, primary sulphide ores have transformed at the surface to oxides, carbonates and sulphates of the various metals.

Field evidence is available to indicate the probable condition of equilibrium for certain mineral phases. This evidence is usually indirect and is based upon a comparison between measured concentrations in subsurface water and those expected from equilibrium conditions defined by thermodynamic data. The comparative parameter is sometimes referred to as the saturation index (SI) where:

$$SI = \log (IAP/K_{so}) \qquad (9.1)$$

in which IAP is the ion activity product (quotient) calculated for ions in solution which make up the solid phase and K_{so} is the solubility product. Negative values of SI indicate undersaturation (or a tendency for further dissolution), positive values represent oversaturation (or favourable conditions for precipitation), and an SI value of zero indicates the presence of an equilibrium condition.

Evidence from various subsurface environments suggests that certain minerals attain equilibrium. Examples of landfill-contaminated groundwater indicate equilibrium conditions (within probable error) for calcite, ferric hydroxides (amorphous), siderite and others (Nicholson et al., 1983; Buzka et al., 1983). In the Elliot Lake tailings and associated environments, mineral stability was observed for solids such as ferric hydroxide, gypsum, calcite, siderite, aluminum hydroxide, jarosite and amorphous silica (Dubrovsky et al., 1984; Morin et al., 1984).

In Table 9.1, solids which are of potential concern to NUTP objectives are listed. Minerals with a high probability of attaining equilibrium in tailings pore water are summarized in Table 14.1.

9.2 Soluble Complexes

Most cations, anions and radionculides form complexes with each other. The reaction rates of a water molecule replacing another water molecule coordinated to a metal ion have been summarized in Figure 7.3. With the exception of a few complexes, the reaction rates are sufficiently quick (half-times of less than a minute) that the complexes are at equilibrium with each other.

Complexes of the different anions and cations which should be considered for reaction code, and other calculations are given in Table 9.2. The listing in Table 9.2 may be incomplete for certain elements and should be reviewed and updated for any further NUTP projects.

9.3 Reaction Code Pathway Calculations

In Chapter 10, the evolution of various minerals and soluble complexes along several pathways is simulated. For a more comprehensive set of calculations, other minerals and complexes will need to be included.

9.4 Recommendations to NUTP for Evaluation of Equilibrium Constants

Constants for complexation reactions and solid formation are available in standard compilations (Sellen and Martel, 1964, 1971; IUPAC, 1982; Ringbom, 1963) and in the data bases of various computer codes (GEOCHEM, REDEQU, PHREEQE, WATEQF, EQ3). The constants are given either as solubility (complexation) constants or as free energies.

TABLE 9.1: EQUILIBRIUM SOLIDS

Name	Reaction	Possible Value of pK_{so}
Silica (amorph)	$SiO_2(s) = H_4SiO_4^o$	2.71
Calcite	$CaCO_3(s) = Ca^{2+} + CO_3^{2-}$	8.475
Siderite	$FeCO_3(s) = Fe^{2+} + CO_3^{2-}$	10.55
Gypsum	$CaSO_4 \cdot 2H_2O(s) = Ca^{2+} + SO_4^{2-} + 2H_2O^3$	4.848
Alunite	$KAl_3(SO_4)_2(OH)_6(s) + 6H^+ = K^+ + 3Al^{3+} + 2SO_4^{2-} + 6H_2O$	3.33
Basaluminite	$Al_4SO_4(OH)_{10}(s) + 10H^+ = 4Al^{3+} + SO_4^{2-} + 10H_2O$	-22.7
K-Jarosite	$KFe_3(SO_4)_2(OH)_6(s) + 6H^+ = K^+ + 3Fe^{3+} + 2SO_4^{2-} + 6H_2O$	14.8
Ferric-hydroxide	$Fe(OH)_3(s) + 3H^+ = Fe^{3+} + 3H_2O$	-4.89
Al-hydroxide	$Al(OH)_3(s) + 3H^+ = Al^{3+} + 3H_2O$	-10.39
Barite	$BaSO_4(s) = Ba^{2+} + SO_4^{2-}$	9.976
$CuCO_3$	$CuCO_3(s) = Cu^{2+} + CO_3^{2-}$	9.63
Malachite	$Cu_2(OH)_2(CO_3)_2(s) + 4H^+ = 2Cu^{2+} + 2HCO_3^- + 2H_2O$	-5.15
Smithsonite	$ZnCO_3(s) = Zn^{2+} + CO_3^{2-}$	10.00
$ZnCO_3 \cdot H_2O$	$ZnCO_3 \cdot H_2O(s) = Zn^{2+} + CO_3^{2-} + H_2O$	10.26
Melanerite	$FeSO_4 \cdot 7H_2O(s) = Fe^{2+} + SO_4^{2-} + 7H_2O$	2.47
Cerrusite	$PbCO_3(s) = Pb^{2+} + CO_3^{2-}$	13.13
$PbHPO_4$	$PbHPO_4(s) = Pb^{2+} + HPO_4^{2-}$	11.46

TABLE 9.1: EQUILIBRIUM SOLIDS (cont'd)

Name	Reaction	Possible Values for pK_{so}
$NiCO_3$	$NiCO_3(s) = Ni^{2+} + CO_3^{2-}$	6.84
$Fe_3(OH)_8$	$Fe_3(OH)_8(s) + 9H^+ = 2Fe^{3+} + Fe^{2+} + 9H_2O$	-20.22
$AlAsO_4 \cdot 2H_2O$	$AlAsO_4 \cdot 2H_2O(s) = Al^{3+} + AsO_4^{3-} + 2H_2O$	15.84
$Ca_3(AsO_4)_2 \cdot 4H_2O$	$Ca_3(AsO_4)_2 \cdot 4H_2O(s) = 3Ca^{2+} + 2AsO_4^{3-} + 4H_2O$	18.90
$FeAsO_4 \cdot 2H_2O$	$FeAsO_4 \cdot 2H_2O(s) = Fe^{3+} + AsO_4^{3-} + 2H_2O$	20.25
Claudetite	$As_4O_6(s) + 6H_2O = 4H_3AsO_3^o$	3.06
Kaolinite	$Al_2Si_2O_5(OH)_4(s) + 6H^+ = 2Al^{3+} + 2H_4SiO_4^o + H_2O$	-7.18
Chlorite	$Mg_5Al_2Si_3O_{10}(OH)_8(s) + 16H^+ = 5\,Mg^{2+} + 3H_4SiO_4 + 6H_2O$	-134.44
Ca-Montmorillonite	$Ca_{0.17}Al_{2.33}Si_{3.67}O_{10}(OH)_2(s) + 7.32H^+ + 2.68\,H_2O = 0.17\,Ca^{2+} + 2.33\,Al^{3+} + 3.67\,H_4SiO_4$	-85.45
Illite	$K_{0.6}Mg_{0.25}Al_{2.3}Si_{3.5}O_{10}(OH)_2 + 8H^+ + 2H_2O = 0.6K^+ + 0.25\,Mg^{2+} + 2.3Al^{3+} + 3.5H_4SiO_4^o$	-88.43

TABLE 9.2: SUMMARY OF SOLUBLE COMPLEXES OF POTENTIAL SIGNIFICANCE IN URANIUM MILL TAILINGS SOLUTIONS

	Soluble Complex	Dissociation Constant (pK)	Percent of Total* at pH		
			1-2	3-4	6-7
Ca:	$CaOH^+$	1.40	L	L	L
	$CaHCO_3^+$	1.02	L	L	L
	$CaCO_3^o$	3.15	L	L	L
	$CaSO_4^o$	2.31	42	42	38
	CaF^{+1}	0.94	NA	NA	NA
	$CaPO_4^-$	6.46	NA	NA	NA
	$CaHPO_4^o$	2.74	NA	NA	NA
	$CaH_2PO_4^+$	1.41	NA	NA	NA
Al:	$AlOH^{2+}$	-4.97	L	L	NA
	$Al(OH)_2^+$	-9.3	L	L	NA
	$Al(OH)_4^-$	-23.0	L	L	NA
	AlF^{2+}	7.01	NA	NA	NA
	AlF_2^+	12.75	NA	NA	NA
	AlF_3^o	17.02	NA	NA	NA
	AlF_4^-	19.72	NA	NA	NA
	$AlSO_4^+$	3.02	31	38	NA
	$Al(SO_4)_2^-$	4.92	42	31	NA
	$Al(OH)_3^o$	-15.00	L	L	NA
Fe(III):	$FeSO_4^+$	3.92	62	19	L
	$FeCl^{2+}$	1.41	L	L	L
	$FeCl_2^-$	2.09	L	L	L
	$FeOH^{2+}$	-2.19	L	20	L
	$FeCl_3^o$	1.09	L	L	L
	$Fe(OH)_2^+$	-5.67	L	54	94

TABLE 9.2: SUMMARY OF SOLUBLE COMPLEXES OF POTENTIAL SIGNIFICANCE IN URANIUM MILL TAILINGS SOLUTIONS (cont'd)

	Soluble Complex	Dissociation Constant (pK)	Percent of Total* at pH		
			1-2	3-4	6-7
	$Fe(OH)_3^o$	-13.60	L	L	5
	$Fe(OH)_4^-$	-21.60	L	L	L
	$FeH_2PO_4^{2+}$		NA	NA	NA
	$FeHPO_4^+$	5.40	NA	NA	NA
	FeF^{2+}	6.2	NA	NA	NA
	FeF_2^+	10.8	NA	NA	NA
	FeF_3^o	14.0	NA	NA	NA
	$Fe(SO_4)_2^-$	3.91	33	6	L
Fe(II):	$Fe(OH)^+$	-9.50	L	L	L
	$Fe(OH)_2^o$	20.57	L	L	L
	$Fe(OH)_3^-$	-31.00	L	L	L
	$FeH_2PO_4^+$	2.70	NA	NA	NA
	$FeHPO_4^o$	3.60	NA	NA	NA
	$FeSO_4^o$	2.25	43	35	32
Mg:	$MgOH^+$	2.21	L	L	L
	$MgCO_3^o$	2.98	L	L	L
	$MgHCO_3^+$	1.07	L	L	1
	$MgSO_4^o$	2.25	40	36	31
	$MgPO_4^-$	6.59	NA	NA	NA
	$MgHPO_4^o$	2.87	NA	NA	NA
	$MgH_2PO_4^+$	1.51	NA	NA	NA
K:	KSO_4^-	0.85	9	6	4
	$KHPO_4^-$	0.29	NA	NA	NA

TABLE 9.2: SUMMARY OF SOLUBLE COMPLEXES OF POTENTIAL SIGNIFICANCE IN URANIUM MILL TAILINGS SOLUTIONS (cont'd)

	Soluble Complex	Dissociation Constant (pK)	Percent of Total at pH 1-2	Percent of Total at pH 3-4	Percent of Total at pH 6-7
Na:	$NaCO_3^-$	1.27	L	L	L
	$NaHCO_3^o$	-0.25	L	L	L
	$NaSO_4^-$	0.70	7	5	4
Ni:	NiF	1.30		NA	NA
	$NiOH^+$	-9.86		L	L
	$Ni(OH)_2^o$	-19.0		L	L
	$Ni(OH)_3^-$	-30.0		L	L
	$NiSO_4^o$	2.29		49	15
	$NiCO_3^o$	6.87		L	49
	$NiHCO_3^+$	2.14		L	5
Pb:	$PbCl^+$	1.60		L	1
	$PbCl_2^o$	1.80		L	L
	$PbCl_3^-$	1.43		L	L
	$PbCl_4^{2-}$	1.38		L	L
	$Pb(OH)^+$	-7.71		L	L
	$Pb(OH)_2^o$	-17.12		L	L
	$Pb(OH)_3^-$	-28.06		L	L
	Pb_2OH^{3+}	-6.36		L	L
	$PbSO_4^o$	2.62		78	18
	$Pb_3(OH)_4^{2+}$	-23.88		L	L
	$HPbO_2^-$	-28.09		L	L
	$Pb(OH)_4^{2-}$	-39.70		L	L
	$Pb(SO_4)_2^{2-}$	3.47		22	3
	$PbHCO_3^+$	2.90		L	13
	$Pb(CO_3)^{2-}$	10.64		L	L

TABLE 9.2: SUMMARY OF SOLUBLE COMPLEXES OF POTENTIAL SIGNIFICANCE IN URANIUM MILL TAILINGS SOLUTIONS (cont'd)

	Soluble Complex	Dissociation Constant (pK)
Ba:	$BaOH^+$	0.64
	$BaSO_4^o$	
Ra:	$RaOH^+$	
	$RaSO_4^o$	
U(VI):	UO_2^{2+}	
	$UO_2CO_3^o$	
	$UO_2(CO_3)^{2-}$	
	$UO_2(CO_3)_3^{4-}$	
	UO_2F^+	
	$UO_2F_2^o$	
	$UO_2SO_4^o$	
	$UO_2(HPO_4)^{2-}$	
	$UO_2HPO_4^o$	
U(V):	UO_2^+	
U(IV):	UOH^{3+}	
	$U(OH)^{2+}$	
	$U(OH)^{2+}{}_3$	
	$U(OH)_4^o$	
	$U(OH)_5^-$	
	UF_2^{2+}	
	UF_3^+	
	UF_4^o	

TABLE 9.2: SUMMARY OF SOLUBLE COMPLEXES OF POTENTIAL SIGNIFICANCE IN URANIUM MILL TAILINGS SOLUTIONS (cont'd)

	Soluble Complex	Dissociation Constant (pK)
Th:	Th^{4+}	-
	$Th(OH)^{3+}$	10.8
	$Th(OH)_2^{2+}$	21.07
	$Th(OH)_3^{+}$	30.3
	$Th(OH)_4^{o}$	40.1
	ThF^{3+}	8.03
	ThF_2^{2+}	14.25
	ThF_3^{+}	18.93
	ThF_4^{o}	22.31
	$ThCl^{3+}$	1.09
	$ThCl_2^{2+}$	0.80
	$ThCl_3^{+}$	1.65
	$ThCl_4^{o}$	1.26
	$ThSO_4^{2+}$	5.45
	$Th(SO_4)_2^{o}$	9.73
	$Th(SO_4)_3^{2-}$	10.50
	$Th(SO_4)_4^{4-}$	8.48
	$ThH_3PO_4^{4+}$	1.91
	$ThH_2PO_4^{3+}$	4.52
	$Th(H_2PO_4)_2^{2+}$	8.88
	$ThHPO_4^{2+}$	10.8
	$Th(HPO_4)_2^{o}$	22.8
	$Th(HPO_4)_3^{2-}$	31.3
	$ThC_2O_4^{2+}$	9.30
	$Th(C_2O_4)_2^{o}$	18.54
	$Th(C_2O_3)_3^{2-}$	25.73

TABLE 9.2: SUMMARY OF SOLUBLE COMPLEXES OF POTENTIAL SIGNIFICANCE IN URANIUM MILL TAILINGS SOLUTIONS (cont'd)

Soluble Complex	Dissociation Constant (pK)
$ThNO_3^{3+}$	0.94
$Th(NO_3)_2^{2+}$	1.97

* Example of the percent of complex at the given pH for high sulphate solutions. Calculations from WATEQ2 (provided by N.M. Dubrovsky, 1985)

L = low, negligible

NA = one or more components not analysed

Some of these constants have been compiled but not critically evaluated here. A few have been evaluated for use in the reaction pathway calculations of Chapter 14.

For the long-term, it is recommended that all constants for complexes and solids of concern to the NUTP be evaluated and developed into a thermodynamic data base. The source of the data, and reasons for selecting it in preference to some other value should be systematically documented.

10.0 SIMULATION OF EQUILIBRIUM MINERAL ASSEMBLAGES DURING ACIDIFICATION

10.1 Introduction

The objective of a source term model is to calculate (predict) the time history of concentrations of various chemical and radioactive elements in seepage from a tailings pile. These concentrations are a function of (i) the seepage rate, (ii) whether chemical equilibrium is maintained between the pore water and each mineral in the tailings pile or whether kinetics controls solid-solution relationships and (iii) the minerals and secondary precipitates present. To obtain a quantitative estimate, one can use hand calculations as was done in Chapter 6, but such calculations are labor intensive, imprecise and subject to severe limitations due to simplifying assumptions made.

An alternative approach is to combine an equilibrium computer code, a reaction pathway code or a kinetic computer code with a transport code to calculate contaminant transport. In the case of a simpler system (e.g., the system considered in Chapter 6), one can program an algorithm for kinetic reactions, equilibrium reactions, and transport into one overall computer code. But it is difficult to combine existing equilibrium or reaction codes with existing transport codes directly because they have been formulated with different objectives in mind. One can combine the results of two codes (equilibrium, transport) externally to interpret the geochemical evolution of the problem of concern (e.g., Garvin and Freeze, 1984a,b, for formation of lead-zinc bodies). External combination of code results may be advantageous over a simplier system if it considers too few minerals and elements, for example.

In this chapter, an equilibrium speciation code is used to calculate the geochemical evolution of minerals along "reaction pathways". The reaction pathway is defined as the addition or removal of a certain amount of a particular element at each step. The chemical system is a closed system, except for the addition or removal of a particular element. Hence, the reaction code simulates the expected sequence of minerals along the reaction pathway considered but does not change the mass of each element present in the system except for the element involved in the reaction pathway.

Thus, the reaction code calculations may deviate somewhat from the real system because hydrological transport and diffusional processes would add or remove several solution elements from a defined volume of tailings rather than just one element. Simultaneous addition or removal of solution elements can be accomplished by external specification of the elements involved and the amount removed. Such calculations are presented below for addition of iron, sulphate and hydrogen ions.

The utility of the reaction code calculations is that it provides conceptual information about the expected geochemical sequence of minerals. This is particularly important where many sequences of minerals are possible. When applied to minerals at equilibrium with the pore water and interpreted using various reaction pathways, it provides a powerful component modelling tool in the process of developing a source term model.

10.2 Reaction Pathway Calculations

Under an assumption of equilibrium conditions, one can calculate the expected concentrations of all soluble species, complexes and ion pairs and solids present for a specific chemical system. When solid species are considered, the dissolved species associated with each solid are fixed by solubility limits. If the system is perturbed so that there is an increase in the concentration of one soluble species, this may result in the precipitation of more solid, for instance, to maintain equilibrium conditions.

Models to perform such computations are time intensive and therefore computer programs are used. The computer code CHEMP (CHEMical reaction Path) is one such model that is capable of dealing both with solution chemistry and solids dissolution and precipitation to predict equilibrium conditions. This code was used here to simulate the sequence of minerals in equilibrium during acidification of a tailings pile containing pyrite. A detailed description of the code and of the reaction pathway calculations is given in Appendix B. A summary of pertinent calculations is presented in this Chapter.

The simulation was performed by adding an oxidant (oxygen or Fe(III)) to solids containing pyrite in a stepwise fashion and determining the equilibrium assemblage of minerals and soluble species at each step. In some cases, a titrant containing a stoichiometric equivalence of pyrite oxidation products ($Fe(III) + Fe(II) + 2SO_4^{2} + H^+$) was added to the system to simulate conditions in which pyrite does not attain equilibrium with the other components. The latter approach was used because fairly high concentrations of Fe(III) are observed in pore water of active oxidation zones of Elliot Lake tailings (Dubrovsky et al., 1985), but these concentrations are not thermodynamically stable. In other words, kinetics may hinder the thermodynamically favourable reactions with pyrite. The value of the ratio of Fe(III)/Fe(II) was set at 10^4 to simulate a highly oxidizing environment with some Fe(II) available. To some extent this corresponds to real systems in which rapid oxidation of pyrite is occurring.

The cases in this study were chosen to simulate an active oxidation zone and the evolution of the tailings chemistry with ongoing pyrite oxidation and subsequent acidification. It should be noted that simulation of neutralization reactions such as those reported by Morin et al. (1985), can also be performed with CHEMP. In Morin's study an acidic solution would be titrated with the appropriate solids in a stepwise fashion with computation of equilibrium conditions at each step. Conceptually, this would be similar to reversing the simulation made herein, because increases in pH values and the formation of solids in reverse would occur.

A number of representative simulation cases have been chosen to illustrate the important aspects of the predicted evolution sequence. These calculations are then compared with observations from the field. Finally, the limitations of the equilibrium model approach are discussed.

10.3 Simulation of Acidification and Chemical Evolution

10.3.1 Solids Considered

A mineral assemblage containing iron, calcium, aluminum, sulphur, carbon, oxygen and water was selected for simulation. The initial assemblage involved pyrite and secondary precipitates formed in the mill (amorphorus aluminum hydroxide and iron hydroxide, gypsum, lime or calcite). The objective was to simulate acid formation due to pyrite oxidation and to examine the predicted pH and solid buffering systems which result.

The following solids occurred in the simulation. They were either initially present or precipitated (marked by an *) in the most comprehensive simulation runs.

- Pyrite (FeS_2)
- Goethite (alpha - FeOOH)
- Ferric Hydroxide (amorp - $Fe(OH)_3$)
- Gibbsite ($Al(OH)_3$)
- Gypsum ($CaSO_4.2H_2O$)
- Calcite ($CaCO_3$)
- Mellanerite ($FeSO_4.7H_2O$) *
- Siderite ($FeCO_3$) *
- Jarosite ($KFe_3(SO_4)_2(OH)_6$) *

Other solids were considered for potential formation (see Appendix B), but did not exert any influence on the system chemistry.

The initial quantities of solids present were chosen to reflect the mass of minerals and secondary precipitates present in fresh tailings from Elliot Lake.

The simulation approach was to use several subsets of the initial minerals present in cases of increasing complexity. These subsets and the full suite of minerals were titrated with the different oxidants.

10.3.2 Simulation of a Pyrite-Goethite System (see Case 1A.1, Appendix B)

In one run, oxygen was used to titrate a system containing FeS_2, FeOOH and $CaSO_4.2H_2O$. During oxidation, aqueous H^+, SO_4^{2-} and Fe^{2+} and Fe^{3+} are produced. Pyrite (FeS_2) is dissolved, FeOOH is initially dissolved and then reforms, and both jarosite and $FeSO_4.7H_2O$ form. $FeSO_4.7H_2O$ later redissolves (see Figure 10.1).

The response of solution pH is important because of the role it has in controlling toxic metal and certain radionuclide concentrations. In simulation of the pyrite-goethite system, the pH remains relatively constant at a value of about 5 ($(H^+) = 10^{-5}$) until the FeOOH is initially dissolved, despite the fact that H^+ is continuously being added, from pyrite oxidation (Figure 10.2). The pH buffer in this case results from an overall reaction between two solid phases as given by;

$$FeS_2(s) + 14FeOOH(s) + 26H^+ = 15Fe^{2+} + 2SO_4^{2-} + 20H_2O \qquad (10.1)$$

FIGURE 10.1 THE ABUNDANCES OF SOLIDS AS A FUNCTION OF THE REACTION COORDINATE, FOR CASE 1A.1

○ — $CaSO_4 \cdot 2H_2O$, ◇ — FeS_2 (pyrite),
△ — FeOOH(α), ⋈ — $FeSO_4 \cdot 7H_2O$,
* — jarosite.

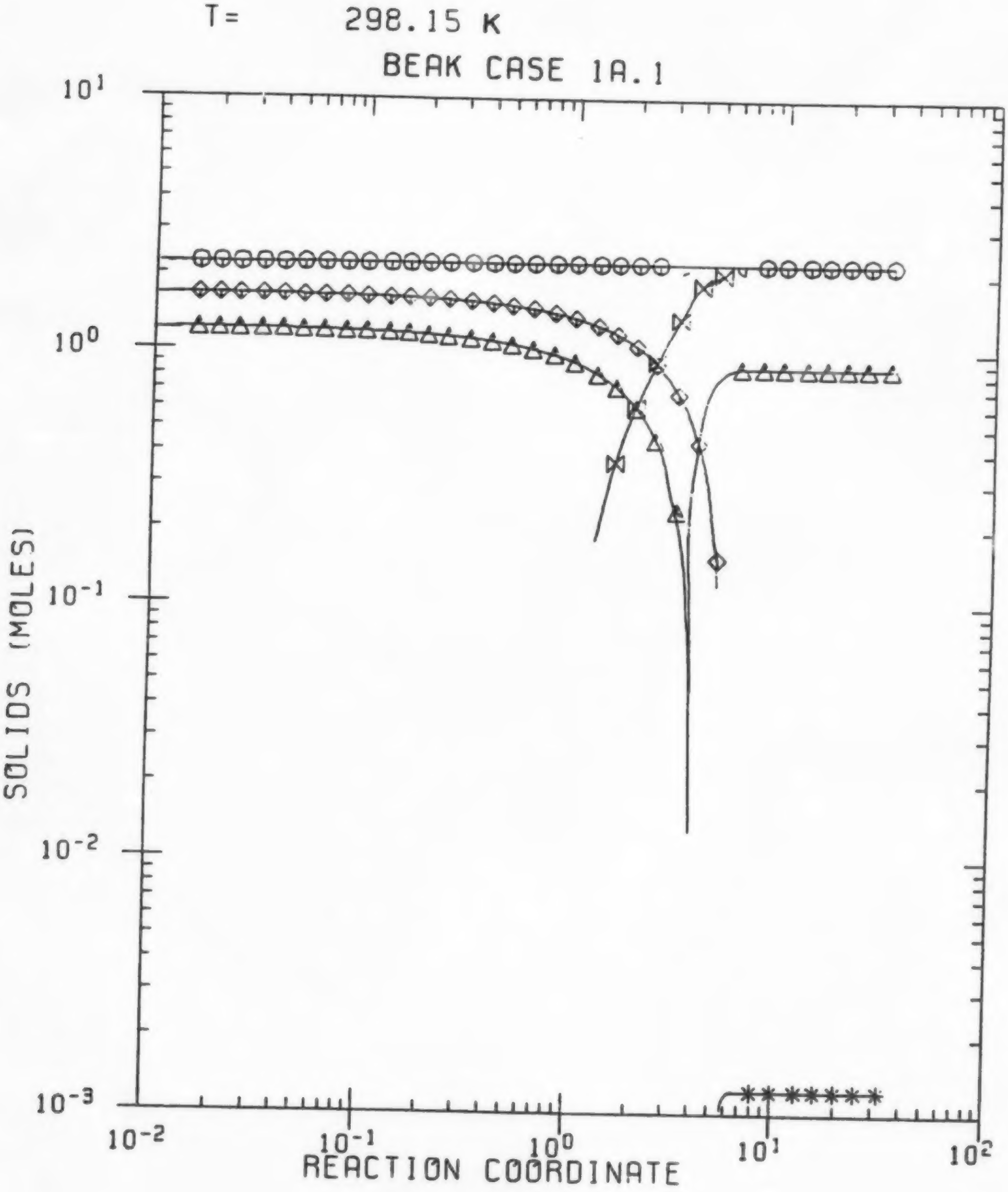

(number of moles of oxygen consummed per kilogram of water)

Figure 10.2 H^+ concentration as a function of the reaction coordinate, for case 1A.1.

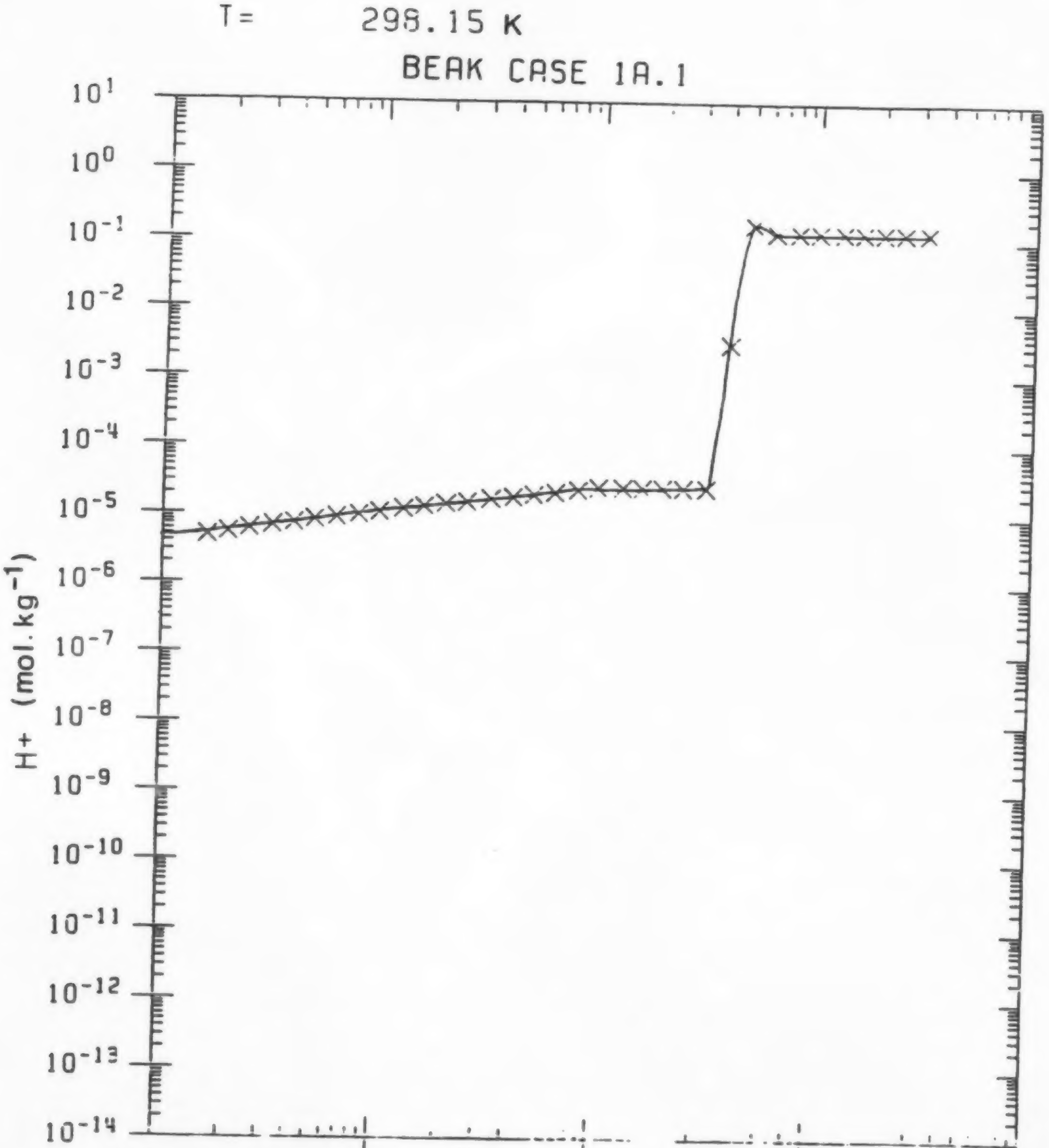

Because both concentrations of Fe^{2+} and ${SO_4}^{2-}$ and concentrations of their complexes are controlled by these solid phases at relatively stable levels, the pH (or H^+ concentration) is also relatively stable. The pH can be calculated from Equation 10.1 as follows:

$$pH = 1/26 (\log K_{so} - 15 \log Fe^{2+} - 2 \log {SO_4}^{2-}) \qquad (10.2)$$

in which the equilibrium constant ($\log K_{so}$) has a value of 98.46. In this case, when the $\log Fe^{2+} = -2$ and $\log {SO_4}^{2-}=1$ the resulting pH is about 5. The former values for Fe^{2+} and SO_4^{2-} are close to those predicted and also are reasonable in terms of observations in pyrite oxidation systems. When the mass of FeOOH is dissolved, the buffer no longer exists and the pH decreases in response to added H^+. The pH plateau at a value of about 0.7 (Figure 10.2) in this simulation occurs because pyrite has been depleted at that stage and addition of oxygen no longer results in the addition of H^+.

The redox potential of the system is also controlled by equilibrium reactions in this simulation. When pyrite is present, the redox potential exhibits a low value as indicated by the high Fe^{2+}/Fe^{3+} ratios (Figure 10.3). When pyrite is depleted, the addition of excess oxygen induces higher redox potentials reflected by the low Fe^{2+}/Fe^{3+} ratios. This point is discussed further in Section 10.4 where these calculations are compared to field observations.

10.3.3 Simulation of a Complete Suite of Solids Using Different Oxidants (see Case 4A.1,4C.1, Appendix B)

Two simulations were performed using all solid phases but different oxidants. In the first example (Case 4A.1), oxygen was used to titrate the system. In the second example the acid-sulphate solution containing $Fe^{3+} + Fe^{2+}$ was used (Case 4C.1). The overall effects with regard to solid-phase and pH behaviour are similar.

Calcite ($CaCO_3$) dissolves early in the titration resulting in formation of siderite ($FeCO_3$). Later in the titration, siderite dissolves in both cases (see the oxygen titrant in Figure 10.4a and the Fe^{3+} and Fe^{2+} titrant in Figure 10.4b). Gibbsite ($Al(OH)_3$) and pyrite, both initially present, are also depleted in both cases. In the first case, however,

Figure 10.3 The concentration of Fe^{2+} (—o—) and Fe^{3+} (—◇—) as a function of the reaction coordinate, for case 1A.1.

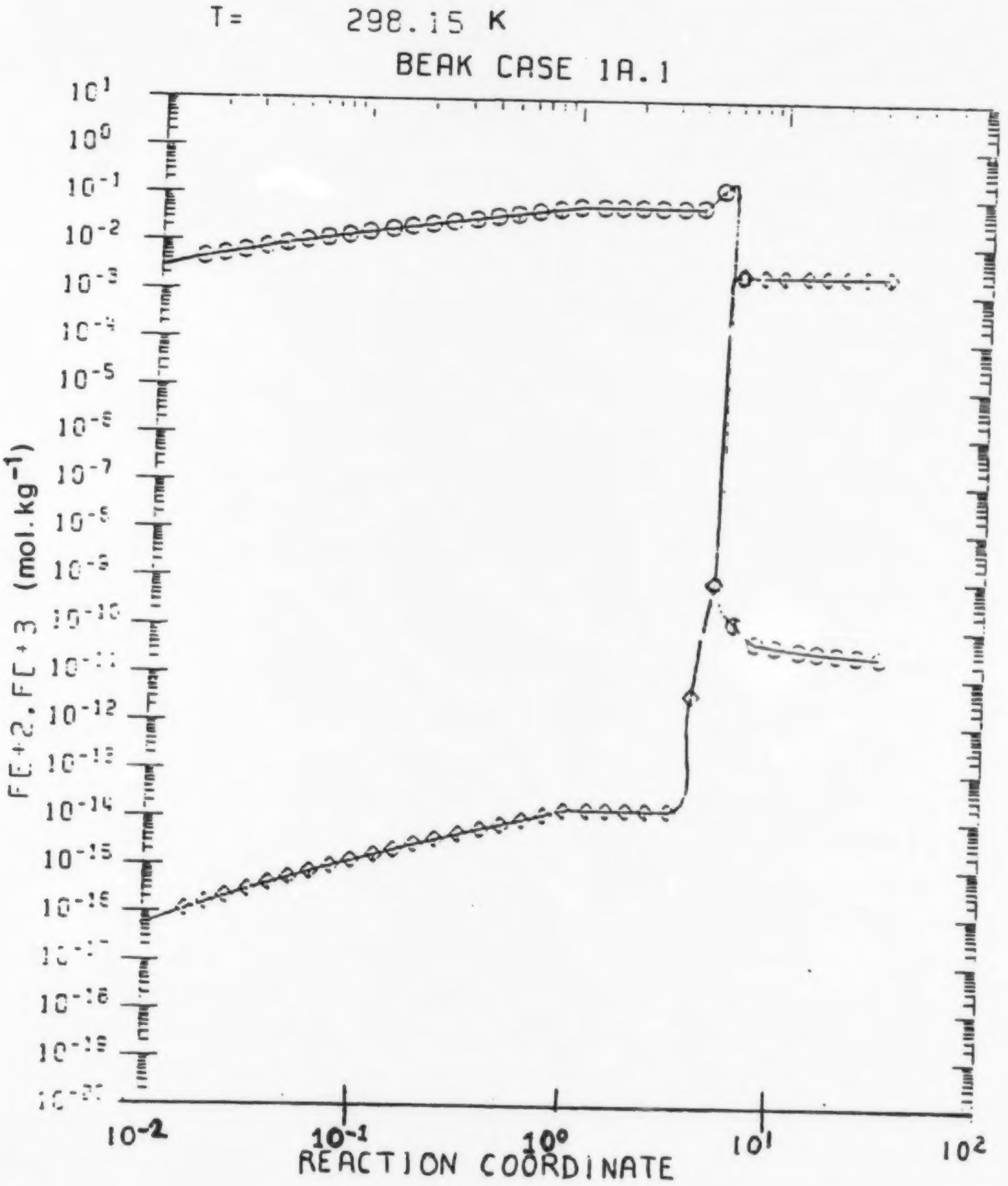

Figure 10.4a The abundances of solids as a function of the reaction coordinate, for case 4A.1.
○ — $CaSO_4 \cdot 2H_2O$, ◇ — FeS_2 (pyrite),
x — FeOOH(α), ⋈ — $Al(OH)_3$ (gibbsite),
Δ — $FeSO_4 \cdot 7H_2O$, ⧖ — $FeCO_3$ (s),
* — $CaCO_3$ (s) .

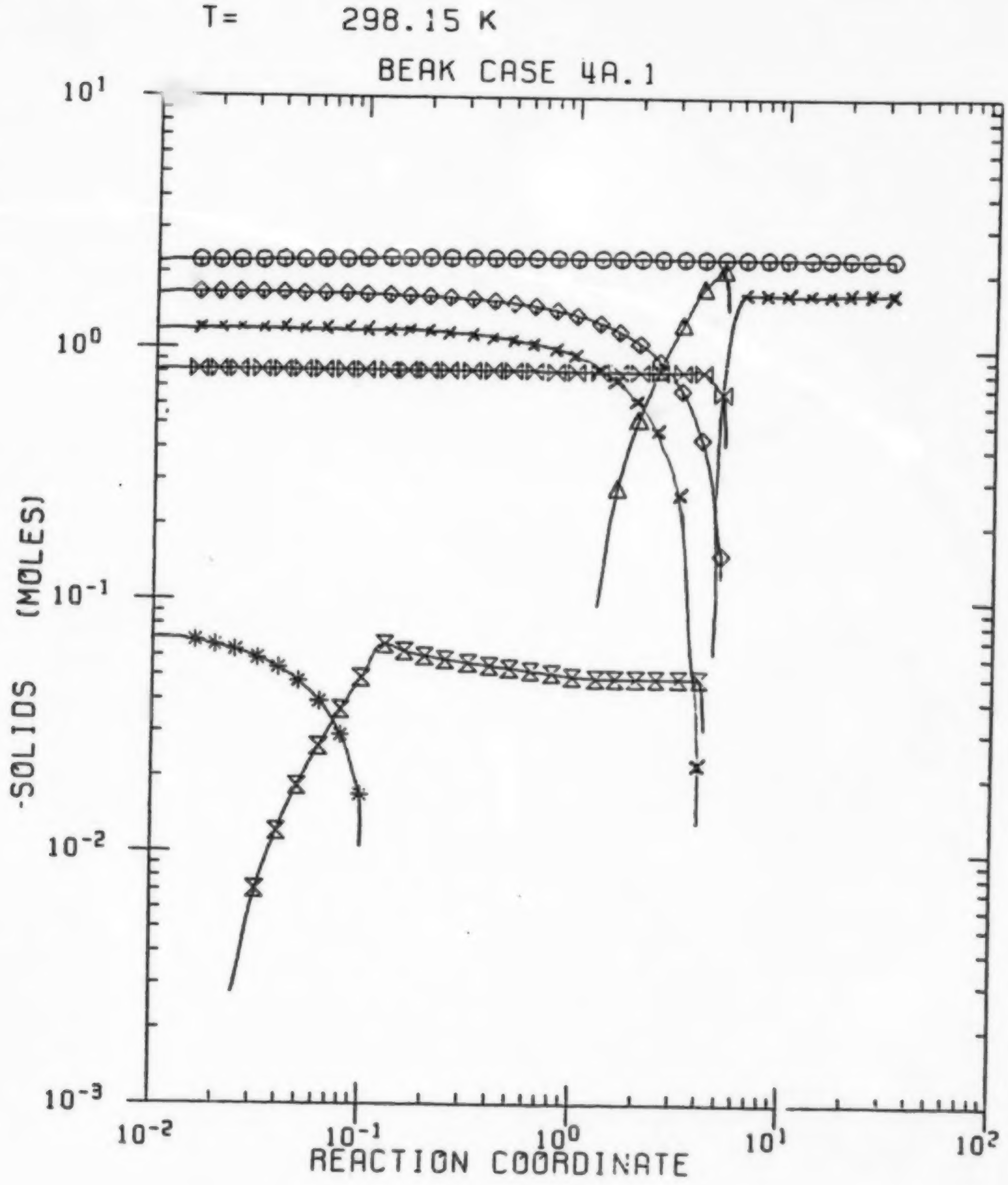

Figure 10.4b The abundances of solids as a function of the reaction coordinate, for case 4C.1.

○ — $CaSO_4 \cdot 2H_2O$, Δ — FeOOH(α)

◇ — FeS_2 (pyrite), ⋈ — $FeSO_4 \cdot 7H_2O$,

* —— jarosite, ● — $Al(OH)_3$ (gibbsite),

⧖ — $CaCO_3$ (s), ◆ — $FeCO_3$ (s).

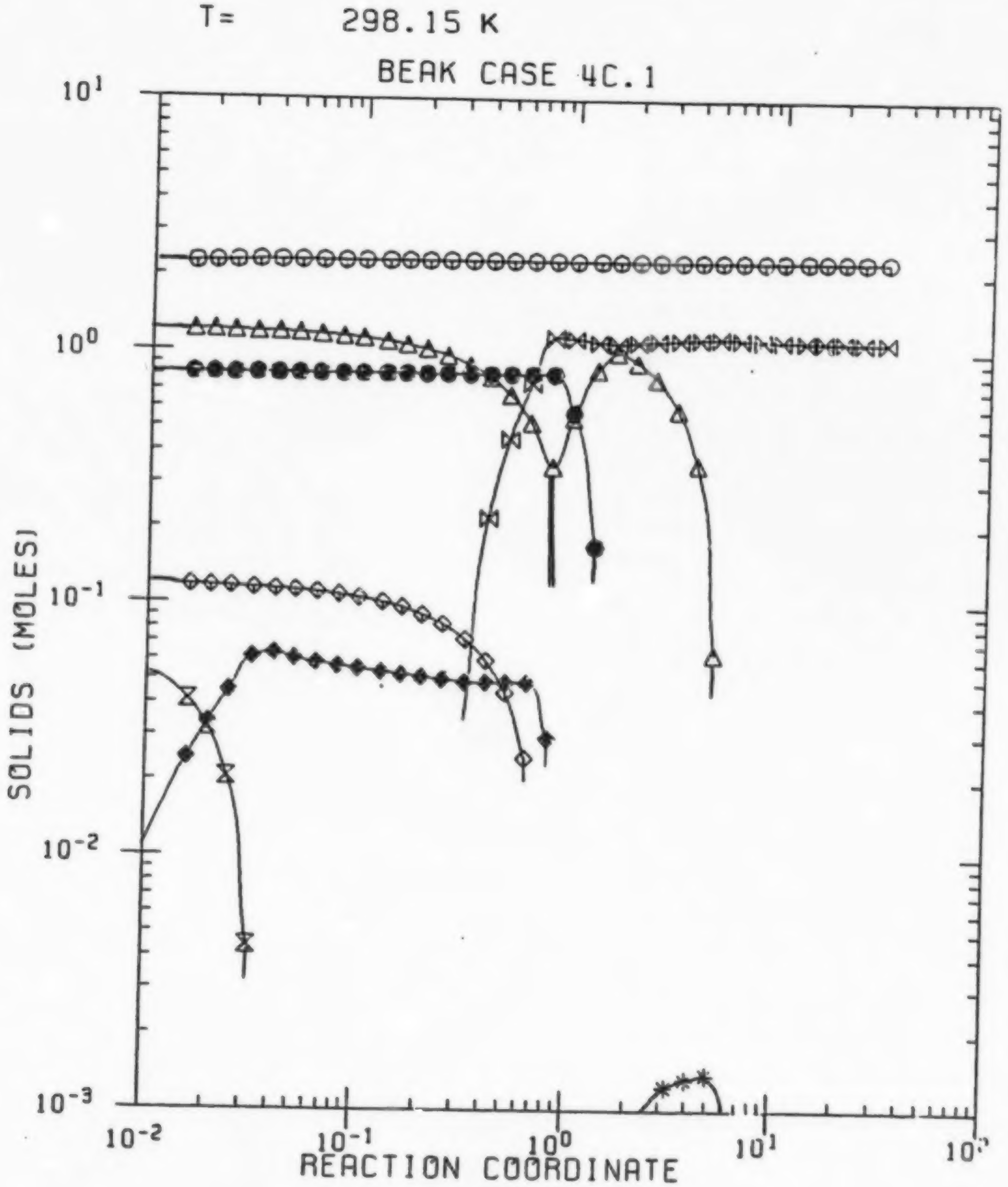

$FeSO_4.7H_2O$ is formed and then dissolved in response to oxidation by oxygen; its dissolution results in formation of goethite. In contrast, $FeSO_4.7H_2O$ is formed and remains in the second case whereas the secondary goethite forms and redissolves; this stability of $FeSO_4.7\ H_2O$ is maintained by the addition of Fe^{2+} while the dissolution of goethite results from the low pH.

The pH responses to the titration are almost identical (Figures 10.5 a and 10.5b). First, calcite dissolves and buffers the pH at a value of about 6.3. The reaction corresponds to,

$$CaCO_3(s) + H^+ \Longleftrightarrow Ca^{2+} + HCO_3^- \qquad (10.3)$$

After calcite is depleted, pH decreases in response to H^+ addition until the FeS_2 - FeOOH buffer (shown previously) is initiated at a pH value of about 5. The pH again decreases after FeOOH is depleted and a slight buffering effect is observed at a pH of about 3.4. This buffering is due to the dissolution of gibbsite and may be represented;

$$Al(OH)_3(s) + H^+ \Longleftrightarrow Al(OH)_2^+ + H_2O \qquad (10.4)$$

Further reduction in pH occurs in the oxygen titration until pyrite is depleted, at which point the pH remains stable. In the case with titration by the acid-sulphate solution, further buffering occurs at a pH of about 1 by dissolution of goethite. This buffering is due to the reaction;

$$FeOOH(s) + 3H^+ \Longleftrightarrow Fe^{3+} + 2H_2O \qquad (10.5)$$

After the goethite is depleted, the pH again decreases in response to further addition of H^+ in the titrating solution.

The redox responses for the two cases exhibit the most significant differences but only after the pyrite is depleted in the oxygen titration (Figures 10.6a and 10.6b). In the oxygen titration the redox potential increases abruptly in response to addition of excess oxygen and subsequent oxidation of Fe^{2+}. In contrast, the addition of Fe^{3+} as the sole oxidant for the acid-sulphate titration does not result in as significant a change in the Fe^{2+}/Fe^{3+} ratios.

Figure 10.5a H^+ concentration as a function of the reaction coordinate, for case 4A.1.

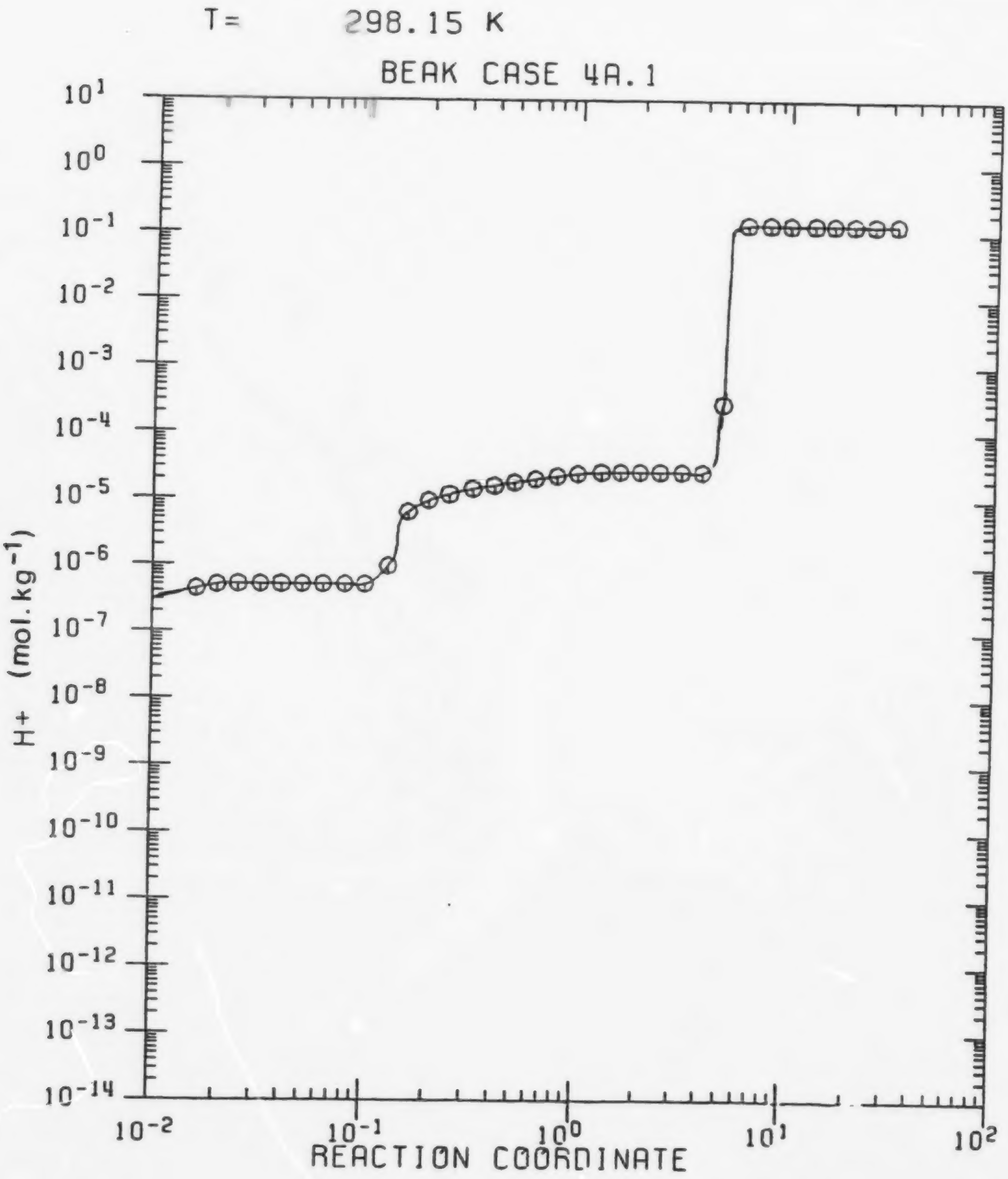

Figure 10.5b H^+ concentration as a function of the reaction coordinate, for case 4C.1.

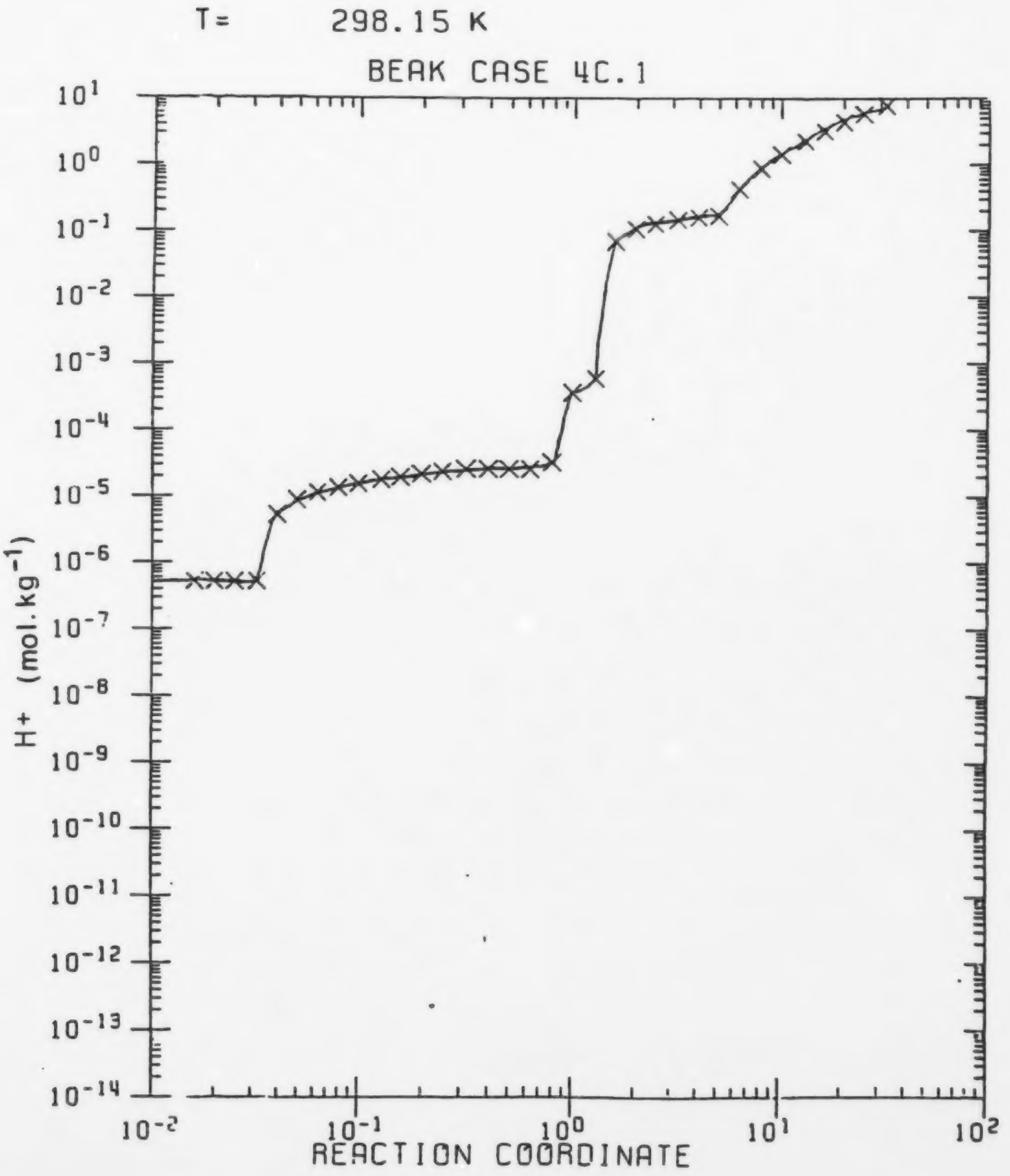

Figure 10.6a : The concentrations of Fe^{2+} (○ –) and Fe^{3+} (◇ –) as a function of the reaction coordinate, for case 4A.1.

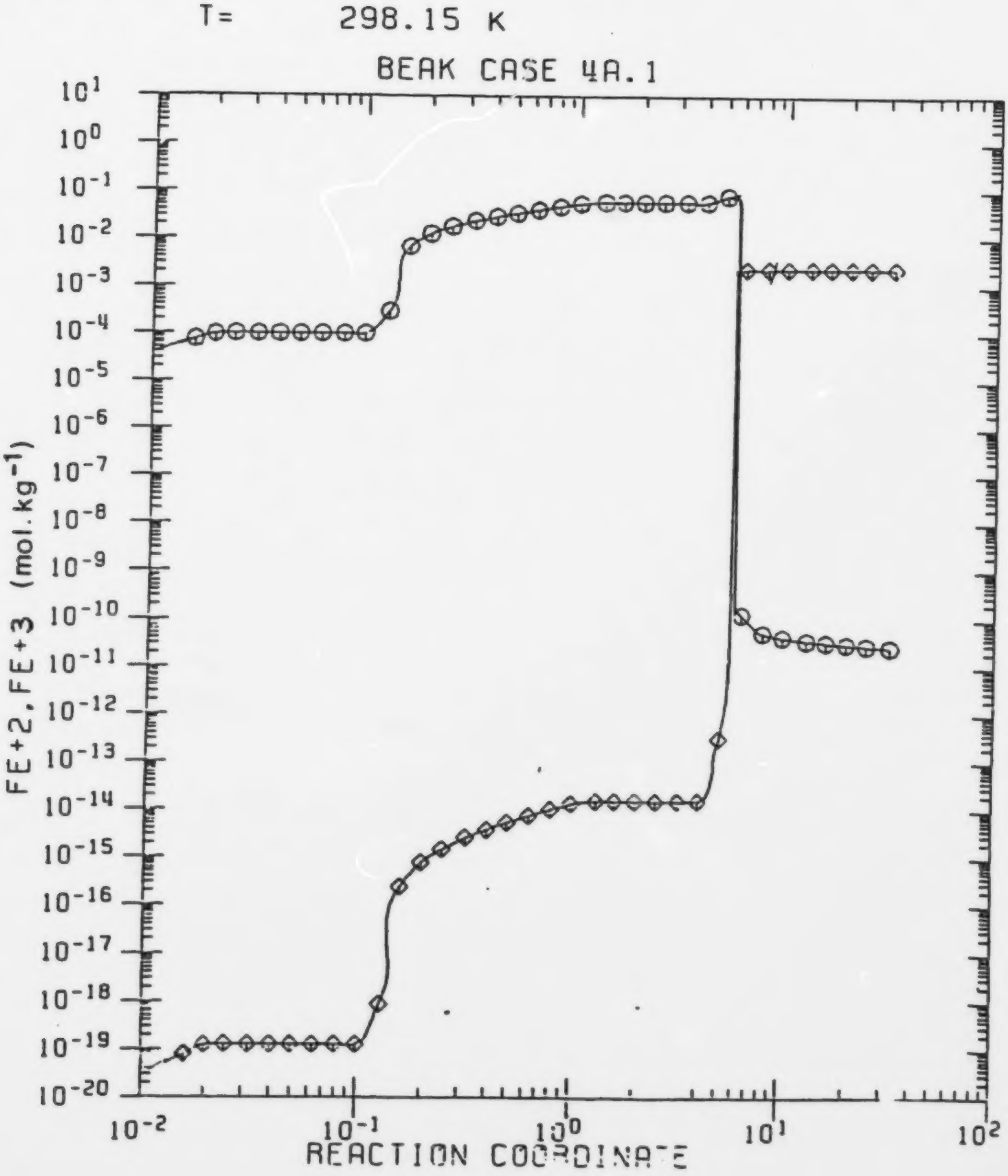

Figure 10.6b :The concentrations of Fe^{2+} (O –) and Fe^{3+} (◇ –) as a function of the reaction coordinate, for case 4C.1.

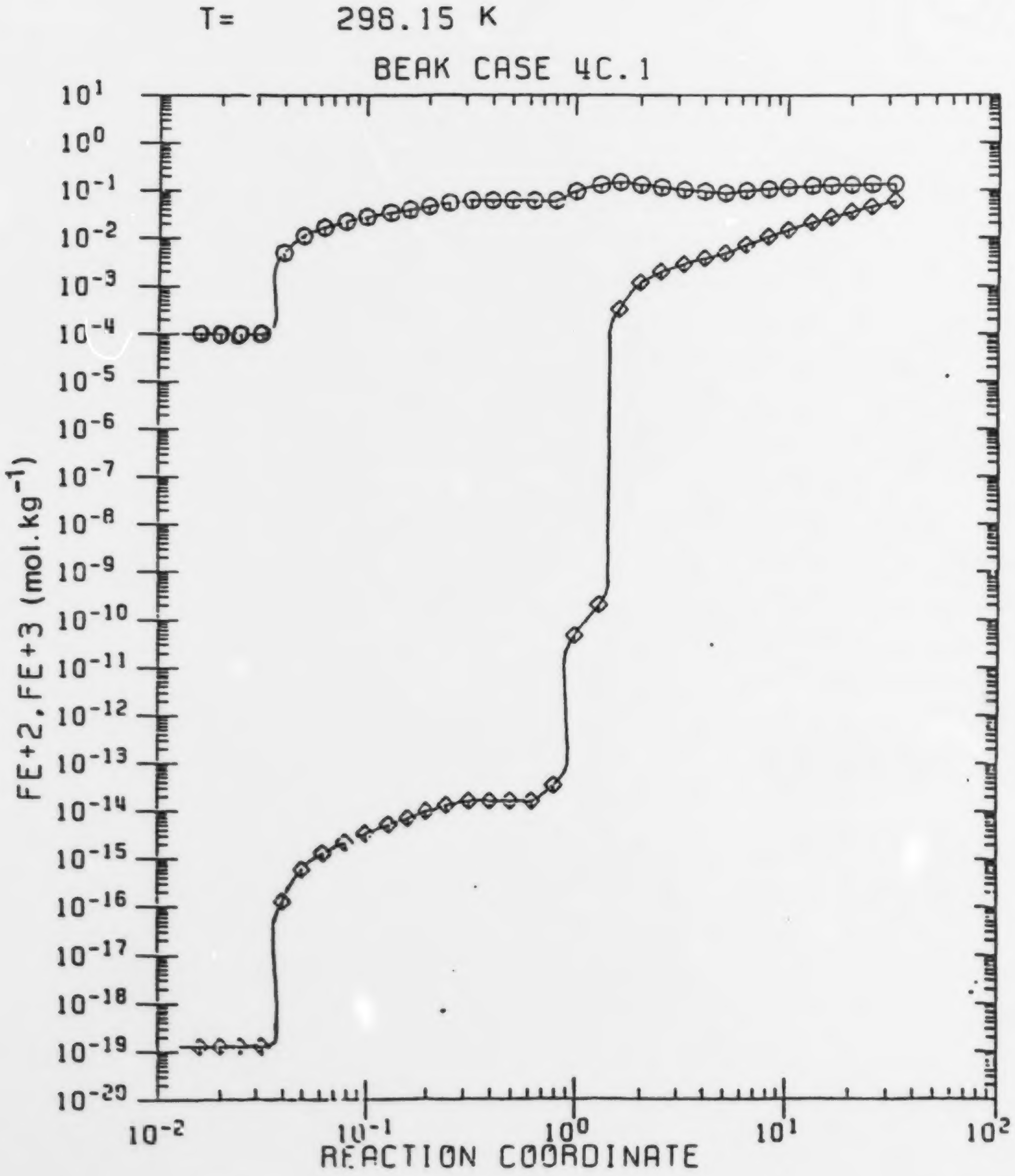

10.3.4 Simulation of Pyrite-Free System With a Acid-Sulphate Titration (see Case 4B.1, Appendix B)

One simulation was performed to examine chemical evolution in an acid generating system in which pyrite does not attain equilibrium with other components in the system (Case 4B.1). The non-equilibrium condition was simulated by titrating oxidation products into a set of solids devoid of pyrite. A number of notable differences exist between this case and the previous two cases.

Although calcite, gibbsite and goethite all dissolve, and jarosite forms and redissolves along the reaction pathway as in the previous two cases, the absence of siderite formation and goethite reappearance is evident (Figure 10.7). The pH response is also different in that no buffer exists at pH=5; instead the pH is buffered at pH=3.4 by gibbsite (Figure 10.8). In this case, the FeS_2 - FeOOH buffer has not masked the effect of the aluminum buffer allowing the latter to become significant. Also because no significant redox reactions occur in the system, the redox potential remains relatively constant as exhibited by the relatively stable $Fe^{2+}/Fe3^{+}$ ratios (Figure 10.9). The changes in ratio that do occur are due to solubility constraints on Fe^{3+} as well as the stability of Fe(III) and Fe(II) complexes.

10.4 Comparison of Simulation Results with Field Observations

The most comprehensive studies of the solution and solids chemistry of the active oxidation zone in pyritic uranium tailings have been reported by Smyth (1981) and Dubrovsky et al. (1985). Profiles of solution chemistry with depth are given. Many of the general trends noted in the simulation model results agree well with those reported in the studies cited above.

Field observations suggest that pH buffering occurs at values of about 6 and also at about 3.5. These pH values agree fairly well with those of calcite and gibbsite shown previously. In addition, the formation of siderite in zones containing residual calcite and the formation of jarosite in active oxidation zones has been postulated from field evidence. This agrees with the model predictions.

Figure 10.7 : The abundances of solids as a function of the reaction coordinate, for case 4B.1.

O — $CaSO_4 \cdot 2H_2O$, ◇ — FeOOH(α), * — $CaCO_3$ (s)

Δ —— jarosite, ⋈ — $Al(OH)_3$ (gibbsite)

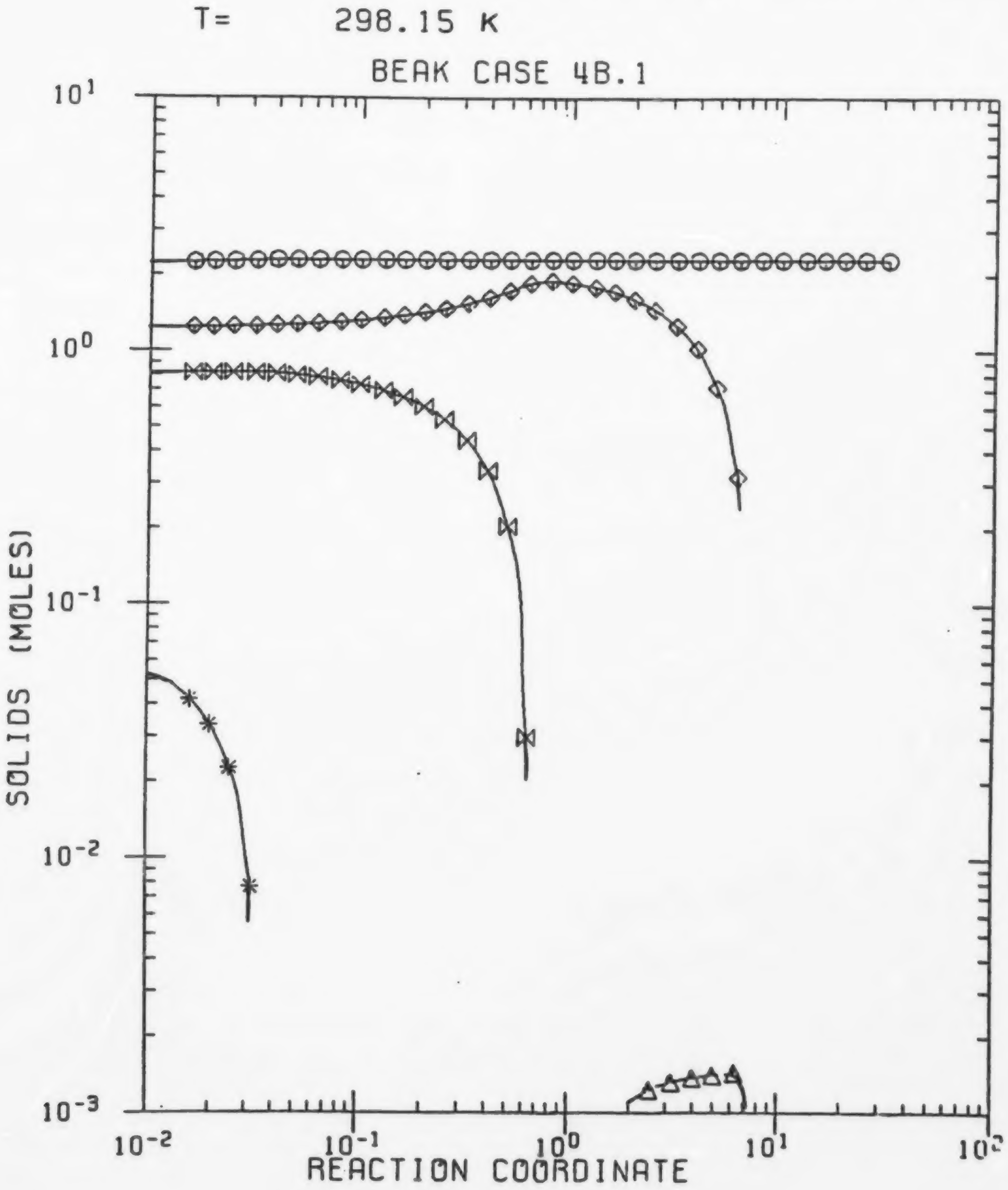

Figure 10.8 H^+ concentration as a function of the reaction coordinate, for case 4B.1.

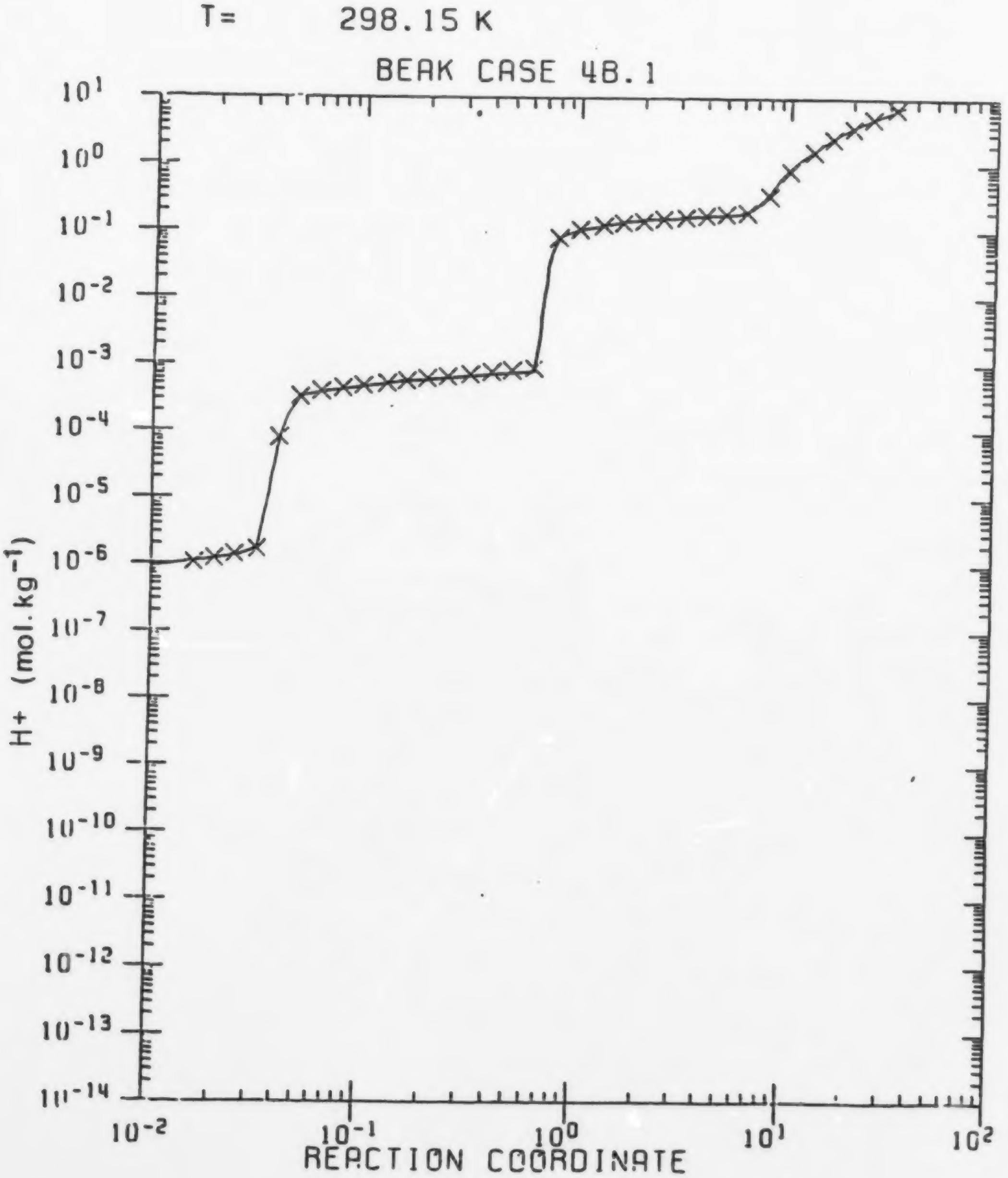

Figure 10.9 The concentrations of Fe^{2+} (o –) and Fe^{3+} (◇ –) as a function of the reaction coordinate, for case 4B.1.

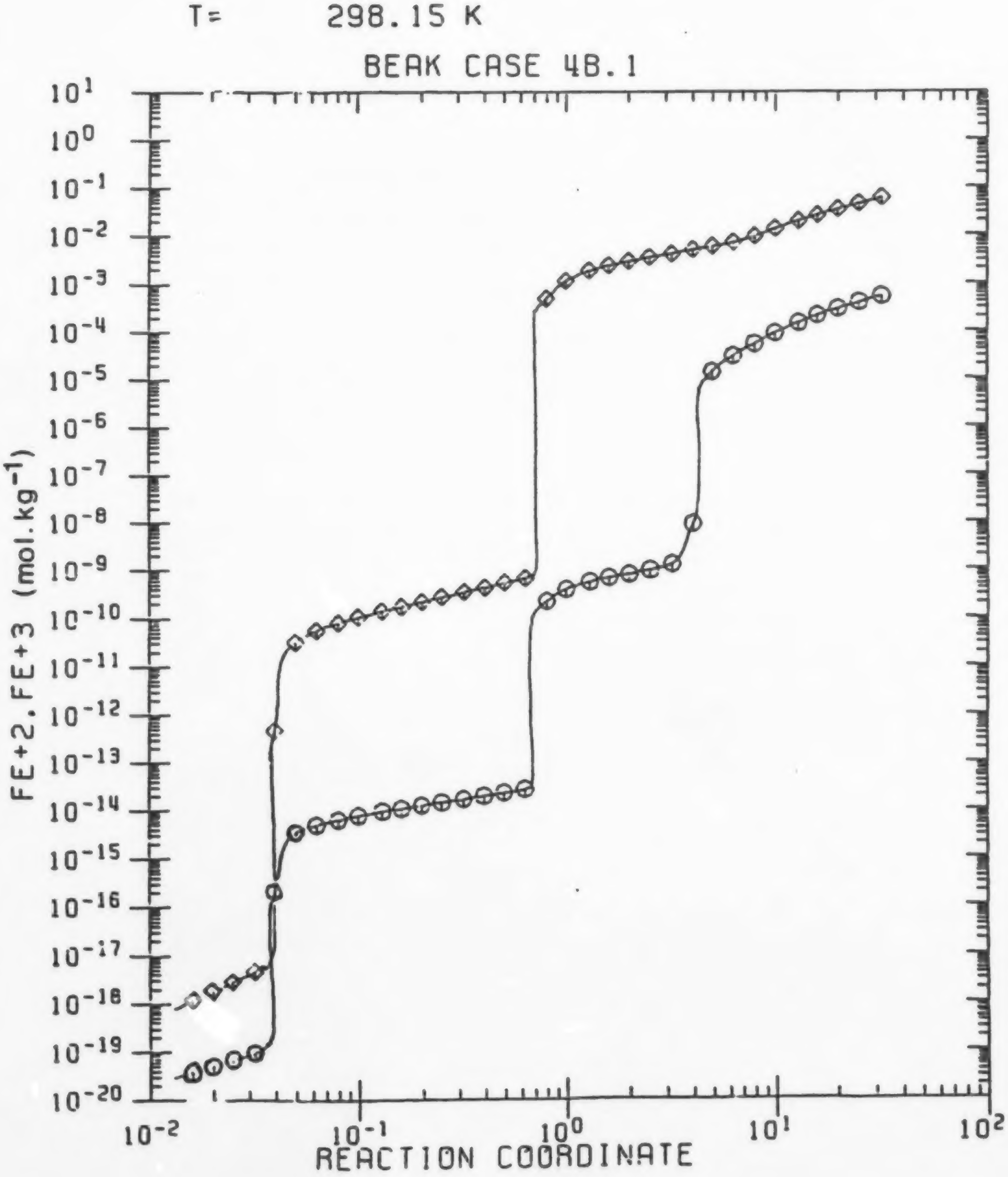

Some disagreement or at least uncertainty exists in other areas. For instance, there does not appear to be a buffering mechanism at pH=5 in the field as is calculated in the simulations. This apparent disagreement may arise for two reasons. First, equilibrium may not actually exist between the pyrite and the goethite phases. Secondly, equilibrium may exist but the thermodynamic characteristics of the ferric hydroxide phase may be different than those specified by the solubility product used in the simulations, because the ferric hydroxide phase present as a solid and its associated solubility product vary significantly in nature. If the active ferric solid is less stable than goethite, the buffered pH would be higher than predicted by the simulation model. Reaction of pyrite with an amorphous ferric hyroxide rather than goethite could result in such a condition.

One area that exhibits a more significant disagreement is that of redox conditions. Field data describing concentrations of Fe^{2+} and Fe^{3+} and the trend of pe ($pe = -\log e^-$ and is a measure of electron activity or redox potential) suggest control of Fe^{3+} concentrations is by its solubility relationship with amorphous $Fe(OH)_3$ (Figure 10.10), and that there is no apparent control on Fe^{2+} concentrations by amorphorus iron (III) hydroxide. In contrast, the model calculations (shown as X 's in Figure 10.10) exhibiting equilibrium between pyrite and goethite displays a different trend for the redox potential.

Existence of equilibrium between an "oxidized" phase (FeOOH) and a "reduced" phase (FeS_2) may not intuitively make sense. But it is explained by an equilibrium between

(i) solution (Fe^{2+}) and pyrite,
(ii) solution (Fe^{3+}) and goethite, and
(iii) solution (Fe^{2+}) and solution (Fe^{3+}) via the redox reaction.

At neutral and near-neutral pH, the solution concentration of Fe^{3+} is so low that Fe^{2+} and Fe^{3+} equilibria are maintained, hence allowing goethite and pyrite to coexist at equilibrium. Goethite and pyrite can coexist at equilibrium as long as the amount of oxidant is limited. Hence, all of the oxidized phases would be reduced at the start of the simulation only if lower redox conditions were initially imposed upon the system (i.e., more electrons donated to the system).

The disagreement between field evidence and the simulations suggests that an overall equilibrium does not occur between pyrite and goethite because observed Fe^{2+}

FIGURES 10.10a and 10.10b

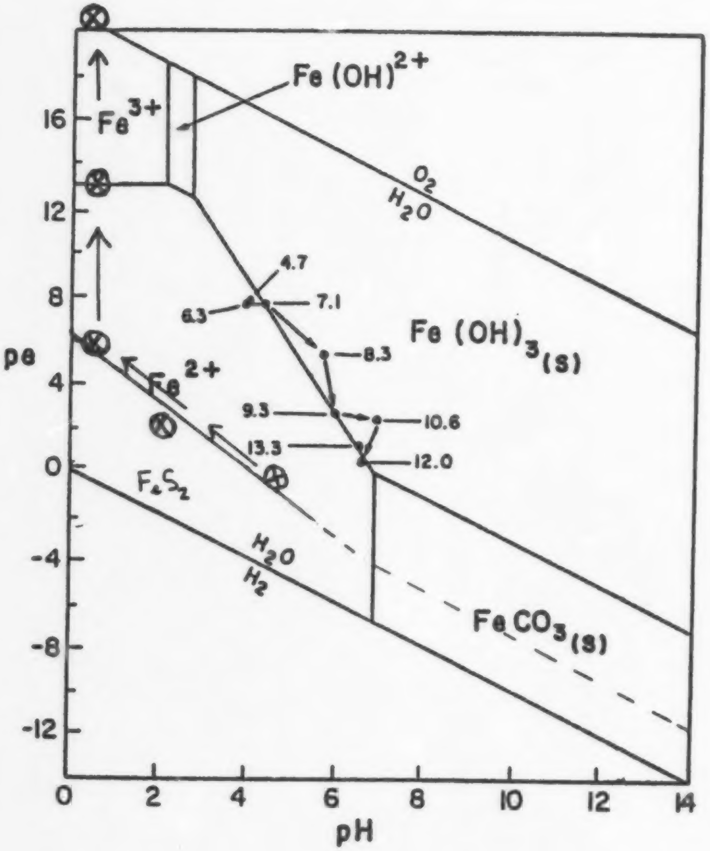

FIG. 10.10a: pe-pH plot for iron speciation in groundwater from piezometer nest T6, drawn for (Fe) - $10^{-4.05}$ iron, PCO_2 of 10^{-2}, pK of $Fe(OH)_3$=38.5. Upward arrows indicate evolution in model simulation (as X). Downward arrows indicate direction of pore water movement in field. Depth of piezometer noted next to the data points (as dots).

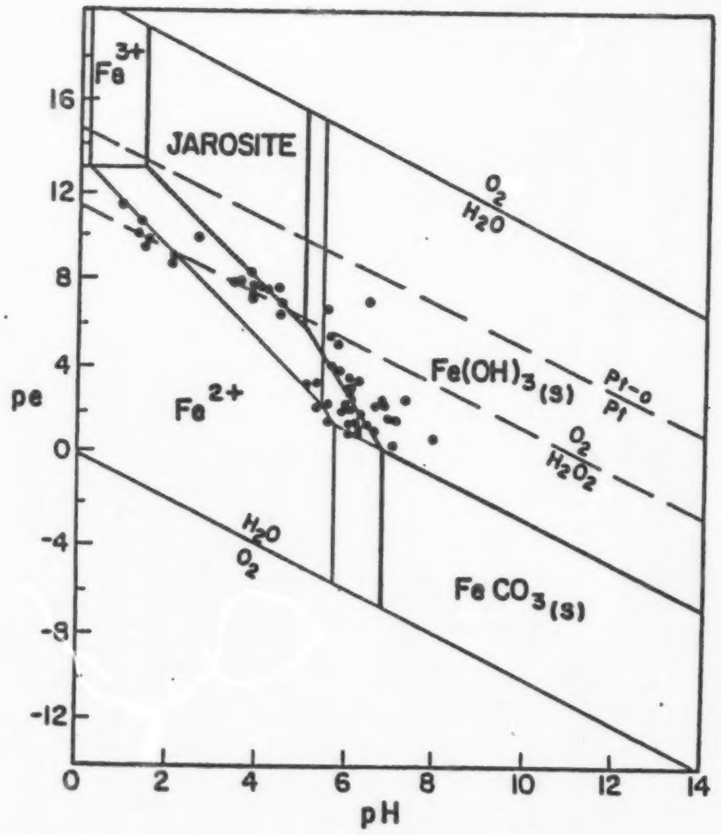

pe-pH plot for iron species and solid phases for groundwaters from the Nordic Main, Nordic West Arm and Lacnor tailings. Heavy line defines fields drawn for (Fe) = $10^{-4.05}$, (K) = 10^{-3}, (SO_4^{2-}) = 10^{-2}, pK of $Fe(OH)_3$ = 38; thin line (Fe) = $10^{-1.79}$, (K) = $10^{-2.53}$, (SO_4) = $10^{-1.8}$, of $pFe(OH)_3$ = 38

(from Dubrovsky et al., 1985)

concentrations and measured values of pe are not at equilibrium with pyrite (Dubrovsky et al., 1985). The actual control on Fe^{2+} concentrations is not clear, hence precluding a definitive statement concerning whether equilbrium with pseudo-stable phases or kinetics controls the Fe^{2+} concentrations. It does, however, represent one limitation of using reaction code calculations when pyrite is present.

10.5 Conclusions Concerning Simulation Results

Equilibrium modelling of an acidifying system involving pyrite oxidation highlights the role of pH as a master variable. The titration of a suite of solids containing pyrite with oxygen or ferric iron results in the progressive acidification of the resident solution. Equilibrium reactions between certain solids (e.g., pyrite-goethite), and dissolution of other solids (e.g., gibbsite, calcite) act to maintain pH at specific levels until the solids are depleted. Rapid decreases in pH occur where no solid buffers are present.

In general, the model results agree fairly well with field observations, in terms of pH buffering. The models also predict the formation of siderite and jarosite under certain conditions; minerals which have also been postulated to occur in pyritic tailings environments.

Differences between the model results and field observations exist for certain sets of solids. Whereas the model indicates redox control by equilibrium between the two solids pyrite and goethite, field data suggests control by amorphous ferric hydroxide solubility and ferrous iron concentrations. However, whether other solid phases, kinetics, or transport control these ferrous iron concentrations is not clear.

It should also be noted that many minerals that actually occur in uranium tailings from Elliot Lake were not included in these simulations. One reason for the omissions was to reduce the complexity and subsequent modelling effort. A second reason, however, is that the dissolution of many minerals is controlled by kinetic processes. If feldspars were included in the suite of solids, for instance, the equilibrium simulation would maintain concentrations of the individual components (i.e., K^+, Al^{3+}, H_4SiO_4) in equilibrium with the system. However, it is known that this rarely occurs in nature because the dissolution of feldspars is kinetically hindered (see Chapter 11) and hence the solution almost always contains less than the equilibrium concentrations of the respective elements.

It is, therefore, concluded that equilibrium modelling can play a significant role in simulating the chemical evolution of a pyritic tailings system, but kinetic controls also need to be considered. The kinetics of dissolution and precipitation of various minerals and secondary precipitates are considered next in Chapter 11.

11.0 KINETICS OF INDIVIDUAL MINERALS

This section presents a summary of data available to us concerning kinetics of dissolution and/or precipitation of different precipitates and solids. Where available, field and/or lab data are presented as a check upon the theory. The theory is most precise for calcite and most imprecise for radionuclides such as thorium.

11.1 Overview of Kinetics

Scope

This section presents an overview of geochemical kinetics. Six particular aspects are examined:

- congruent versus incongruent dissolution,
- concentrations predicted by kinetics for porewater leaving the unsaturated zone
- relationship of kinetics to steady-state
- kinetic versus transport control,
- rate constants of different minerals, and
- activation energies.

Congruent and Incongruent Dissolution

Congruent dissolution is the stoichiometric dissolution of a mineral into water. Incongruent dissolution is the stoichiometric dissolution of the mineral involving formation of a new solid phase and release of some elements into water.

The congruent dissolution of K feldspar can be represented by the reaction:

$$\mathrm{K\,AlSi_3O_8(s)} + 4\mathrm{H}^+ + 4\mathrm{H_2O} = \mathrm{Al}^{3+} + 3\mathrm{H_4SiO_4^o} + \mathrm{K}^+ \qquad (11.1)$$

The incongruent dissolution of K feldspar to amorphorus aluminum hydroxide can be represented by the reaction:

$$K\,Al\,Si_3O_8(s) + H^+ + 7H_2O = Al(OH)_3(s) + 3H_4SiO_4^o + K^+ \qquad (11.2)$$

Incongruent dissolution can occur by one of two methods:

- migration of an ion out of the parent crystal lattice and reformation of the parent lattice with a new lattice; and
- congruent dissolution and formation of a new phase composed of some of the elements in the dissolved solid.

In the case of incongruent dissolution of feldspars, the second method is most probable. The two reactions involved are:

$$K\,Al\,Si_3O_8(s) + 4H^+ + 4H_2O = Al^{3+} + 4H_4SiO_4^o + K^+ \qquad (11.3)$$

$$Al^{3+} + 3OH^- = Al(OH)_3(s) \qquad (11.4)$$

Relationship of Kinetics and Equilibrium Constants to Steady-State

In the system in which K-feldspar dissolves and gibbsite precipitates, the reactions involved can be summarized (Lasaga, 1981) as:

$$KAlSi_3O_8 + 4H^+ + 4H_2O \underset{k_{-1}}{\overset{k1}{\rightleftharpoons}} Al^{3+} + 3H_4SiO_4^o + K^+ \qquad (11.5)$$

K-feldspar

$$Al^{3+} + 3OH^- \underset{k_{-2}}{\overset{k2}{\rightleftharpoons}} Al(OH)_3(s) \qquad (11.6)$$

$$H^+ + OH \underset{k_{-3}}{\overset{k3}{\rightleftharpoons}} H_2O \qquad (11.7)$$

The mass balance equation for aluminum (Al^{3+}) is:

$$\frac{d}{dt}(Al^{3+}) = k_1f_1 + k_{-2}f_{-2} - k_{-1}f_{-1} - k_2f_2 - q(Al^{3+}) \qquad (11.8)$$

Here k_1, k_2 and k_3, and k_{-1}, k_{-2} and k_{-3} respectively represent forward and backward rate constants of Equations 11.5 to 11.7; f represents heterogeneous reaction functions and q represents the effect of outflow upon the concentration of Al^{3+}. For the heterogeneous reaction, for example, the kinetic expression for dissolution of feldspar is:

$$f_1 = \frac{A_{feldspar}(H^+)}{V} \tag{11.9}$$

where, $A_{feldspar}$ is the area of feldspar minerals, V is the volume of water, and (H^+) is the hydrogen ion activity in solution.

Equation 11.5 is the generalized equation describing the concentration of aluminum in solution. Due to the rapidity of the reaction involving H^+ and OH^- (high values of k_3 and k_{-3}), reaction 11.5 is at equilibrium giving:

$$(H^+)(OH^-) = K_w \tag{11.10}$$

This "fixes" the relationship between the activity of H^+ and the activity of OH^-.

If steady-state is attained, $d(Al^{3+})/dt = 0$. Hence, Equation 11.8 becomes:

$$0 = k_1 f_1 + k_{-2} f_{-2} - f_{-1} k_{-1} - k_2 f_2 - q(Al^{3+}) \tag{11.11}$$

That is, a constant concentration of (Al^{3+}) is obtained at a value other than equilibrium. If Al^{3+} is in equilibrium with $Al(OH)_3(s)$, then the net rate of precipitation of gibbsite ($k_2 f_2$; $k_{-2} f_{-2}$) is much faster than the rate of dissolution of feldspar diluted by washout (q). At equilibrium:

$$(Al^{3+}) = K_{so}/(OH)^3 \tag{11.12}$$

where, K_{so} is the $Al(OH)_3(s)$ solubility product. In this case, (Al^{3+}) is independent of time and $k_2 f_2 = k_{-2} f_{-2}$. Then:

$$0 = k_1 f - k_{-1} f_{-1} - q(Al^{3+}) \tag{11.13}$$

That is, the net dissolution rate of feldspar ($k_1 f_1 - k_{-2} f_{-1}$) is balanced by washout (q).

If feldspar is far from equilibrium, then $k_1 f_1$ is much greater than $k_{-1} f_{-1}$ and Equation 11.13 reduces to:

$$0 = k_1 f - q(Al^{3+}) \qquad (11.14)$$

Hence, knowing (Al^{3+}) and the washout rate, the 'laboratory' dissolution rate of feldspar ($k_1 f_1$) can be calculated.

In summary, Equation 11.11 represents the relationship between kinetics and steady-state, while Equations 11.12 and 11.13 represent the relationship between equilibrium and steady-state.

Controlling Step of Mineral Dissolution

(i) Surface Reaction Versus Diffusional (Transport) Control of Dissolution Kinetics

Ignoring the formation of a surface coating on a mineral, dissolution of the mineral can be viewed as involving two steps: mobilzation of an element from the solid to the fluid at the solid-liquid interface (surface reaction) and diffusion of the element from the solid-liquid interface into the fluid bulk through a water film attached to the mineral. the slowest of these two processes (surface reaction, diffusion) will be the rate-controlling step in dissolution kinetics. This has been demonstrated above in Chapter 8, in a mathematical fashion.

Figure 11.1 shows concentration profiles away from the solid-liquid interface expected for diffusion and surface reaction control of dissolution kinetics. C_{eq} is the equilibrium concentration if transport was zero, whereas C_{oo} is the bulk solution concentration. In the case of diffusion control (Figure 11.1a), transport from the surface is slower than surface reaction, allowing an equilibrium concentration to exist at the surface. In the case of reaction control, surface release of molecules is so slow that diffusion can essentially transport all molecules released away from the surface to give a uniform profile.

FIGURE 11.1: RATE CONTROLLING STEPS IN DISSOLUTION PROCESSES

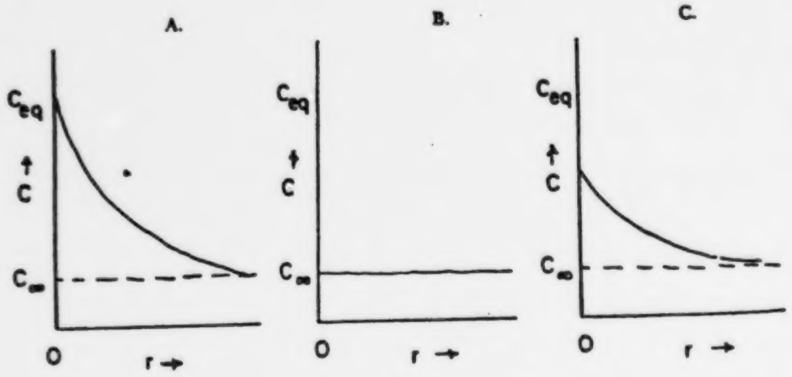

Concentration C versus distance r from a crystal surface for three rate controlling processes C_{eq} = saturation concentration: C_∞ = concentration out in solution.

(A) Transport-control; (B) surface reaction-control; (C) mixed transport and surface reaction-control.

In certain cases, the surface release rate will be of the same order as transport diffusion. This results in the concentration at the surface being intermediate between C_{eq} and C_{bulk} (Figure11.1c).

(ii) Evaluation of Transport Versus Reaction Control as Rate Controlling

There are four possible methods for distinguishing the rate controlling step:

- order of reaction,
- effect of stirring in experiments,
- activation energy, and
- morphology of the surface.

Inspection of the reaction order provides information more about the rate limiting step of precipitation than the rate limiting step of dissolution. Diffusional transport can be represented as a first order reaction:

$$r = k(C_s - C) \tag{11.15}$$

where, k is the mass transfer coefficient. Surface reaction control of precipitation may also be described by Equation 11.15 but also may have a reaction order, n, given by:

$$r = k\,C^n \tag{11.16}$$

varying from 1 to 4.

With respect to stirring, the observed dissolution rate will increase with increase in rate of stirring if dissolution is controlled by diffusion. This results from a decrease in film thickness through which diffusional transport is significant.

With respect to activation energy, diffusional control will have an activation energy of 3 to 5 kcal/mol in water. Surface control will have an activation energy greater than 8 kcal/mol.

With respect to surface morphology, diffusional control will result in a general attack on the surface with consequent rounding. In surface controlled dissolution, dissolution occurs via characteristic, crystallographically-controlled etch pits on the mineral surface. The etch pits indicate selective attack of surfaces at points of excess (thermodynamic) energy such as dissolution outcrops (Lasaga, 1981; Berner, 1981).

(iii) Rate Controlling Dissolution Step for Different Minerals

Minerals described in this chapter generally have surface reactions as the rate controlling step. For some minerals of interest, the mechanism of dissolution during weathering has not been determined. But, as Berner (1981) notes, some predictions of the dissolution rate can be made based upon correlations between solubility product and rate controlling mechanism.

A summary of Berner's data is given in Table 11.1. The less soluble minerals all dissolve by surface reaction. AgCl is an exception to this rule, although some experimental artifacts may explain its relative position in the 'rate controlling' column. From this table, Berner (1981) argues that most minerals involved in weathering may be viewed as being surface-reaction controlled because of low solubilities.

The probable rate controlling step for different minerals of concern to this project are summarized on Table 11.2.

(iv) Relationship of Rate Controlling Dissolution Step to Bulk Transport

In Sections 11.2 (for calcite) and 11.3 (for gypsum) it is suggested that for NUTP modelling purposes and time steps of the order of one year, groundwater may be viewed as being at equilibrium with calcite and gypsum if these two minerals are present as solid phases. This would infer, by way of analogy to the above, that transport is not rate controlling. But the data of Berner suggest that gypsum dissolution is transport controlled and calcite is surface reaction controlled.

Care must be used in interpreting "transport control". In the theory of dissolution kinetics, "transport control" is referenced to diffusion and to a small spatial scale (less than 10 um). In evaluation of calcite and gypsum data given below in Sections 11.2 and

TABLE 11.1: DISSOLUTION RATE-CONTROLLING MECHANISM FOR VARIOUS SUBSTANCES ARRANGED IN ORDER OF SOLUBILITIES IN PURE WATER (Mass of mineral which will dissolve to equilibrium.) (After Berner, 1978a; 1980)

Substance	Solubility mole per liter	Dissolution rate control
$Ca_5(PO_4)_3OH$	2×10^{-8}	Surface-reaction
$KAlSi_3O_8$	3×10^{-7}	Surface-reaction
$NaAlSi_3O_8$	6×10^{-7}	Surface-reaction
$BaSO_4$	1×10^{-5}	Surface-reaction
$AgCl$	1×10^{-5}	Transport
$SrCO_3$	3×10^{-5}	Surface-reaction
$CaCO_3$	6×10^{-5}	Surface-reaction
Ag_2CrO_4	1×10^{-4}	Surface-reaction
$PbSO_4$	1×10^{-4}	Mixed
$Ba(IO_3)_2$	8×10^{-4}	Transport
$SrSO_4$	9×10^{-4}	Surface-reaction
Opaline SiO_2	2×10^{-3}	Surface-reaction
$CaSO_4 \cdot 2H_2O$	5×10^{-3}	Transport
$Na_2SO_4 \cdot 10H_2O$	2×10^{-1}	Transport
$MgSO_4 \cdot 7H_2O$	3×10^{0}	Transport
$Na_2CO_3 \cdot 10H_2O$	3×10^{0}	Transport
KCl	4×10^{0}	Transport
$NaCl$	5×10^{0}	Transport
$MgCl_2 \cdot 6H_2O$	5×10^{0}	Transport

TABLE 11.2: SUMMARY OF DISSOLUTION KINETICS

Mineral	Reaction	Equilibrium Constant	Kinetic Expression	k	E	Surface or Diffusion Control	Other Comments
K-Feldspar $KAlSi_3O_8$	$KAlSi_3O_8 + 7H_2O + H^+ \longrightarrow$ $K^+ + Al(OH)_3^0 + 3H_4SiO_4$	3×10^{-9} mol/L	$\frac{d}{dt} C_{H_4SiO_4} = 3 \frac{A}{V} a_{H^+} k_+$ for pH<7 or 5	$k_+ = 1.67 \times 10^{-12}$ molSiO_2/m^2/s at 25°C and pH = 3		Surface	
Silica (SiO_2)				$k_+ = 4.1 \times 10^{-14}$ molSiO_2/m^2/s at 25°C and pH = 5		Surface	
	$H_4SiO_4 \longrightarrow SiO_2(s) + 2H_2O$			$\log k_- = 0.707 + \frac{2598}{T}$	11.9 kcal/mol (0-300°C)		
	$SiO_2(qtz) + 2H_2O \longrightarrow H_4SiO_4$		$\frac{d}{dt}C_{H_4SiO_4} = \frac{A}{M}\gamma_{H_4SiO_4}(k_+ a_{SiO_2} a^2_{H_2O} - k_- a_{H_4SiO_4})$ Dissolution Precipitation	$\log k_+ = 1.174 - 2.028 \times 10^{-3}T - 4158/T$	16-18 kal/mol (0-300°C)		
	$SiO_2(am) + 2H_2O \longrightarrow H_4SiO_4$			independent of a_{H^+} for pH< 7 $\log k_+ = 0.369 - 7.89 \times 10^{-4}T - 3438/T$ Units: k_+ = l/sec/M^2 k_- = l/sec	14.5 - 15.5 (0-300°C)		
Barium Sulphate	$BaSO_4 \longrightarrow Ba^{2+} + SO_4^{2+}$	1×10^{-5} M	$\frac{dm}{dt} = k_d S (m_0 - m)^2$	k_d = 13-50 l^2/mol/m^2/min at 25°C	?	Surface	Precipitation is surface controlled at lower supersaturation and diffusion controlled at high supersaturation
AgCl	$AgCl \longrightarrow Ag^+ + Cl^-$	1×10^{-5} M					
Pyrite	see Chapter 11 and 12		Not simplified; see Chapter 11 and 12				
Calcite	$CaCO_3 \rightleftharpoons Ca^{2+} + CO_3^{2+}$	6×10^{-5} M	$\frac{dc}{dt} = k_1 a_{H^+} + k_2 a_{H_2CO_3^*} + k_3 a_{H_2O} - k_4 a_{Ca^{2+}} a_{HCO_3^-}$ Dissolution Crystallization		8.4 kcal/mol (5-60°C)	Surface	
$PbSO_4$		1×10^{-4} M				Mixed	
Opaline SiO_2		2×10^{-3} M				Surface Rxn	
Gypsum	$CaSO_4 \cdot 2H_2O \longrightarrow Ca^{2+} + SO_4^{2-} + H_2O$	5×10^{-3} M ($K_{sp} = 2.58 \times 10^{-5}$ M^2)	$\frac{d}{dt} C_{Ca} = 4 D (C_s - C) \frac{\sum Nr}{V}$	$D = 4 \times 10^{-6}$ cm^2/s at 25°C		Transport Transport	
KCl		4×10^{0} M				Transport	
NaCl		3×10^{0} M					

11.3 "transport control" is referenced to a much larger spatial scale (1 m to 1000 m) and to the advective transport rate.

pH Dependency of Dissolution

pH is a master variable of concern in tailings because of its extremes (1 to 2 in acidic tailings, 0.5 to 1 in leaching tanks; 7 to 8 in fresh treated tailings; 4 to 5 in older tailings (buffered by iron and aluminum oxides).

The dependency of dissolution of various minerals is given in Table 11.3. The dependency is given in Table 11.2 for minerals of concern to this project. Of note is the pH independence of quartz dissolution and of K feldspar dissolution over the range of 3 to 7.

Activation Energy of Dissolution

The activation energy of dissolution can be used to evaluate the rate controlling step and to make inferences about whether bond breaking or other chemical phenomena are involved in dissolution. A summary of various activation energies is given in Table 11.4. Those for minerals of relevance to the NUTP are summarized also in Table 11.2.

11.2 Kinetics of Major Calcium Solids

The major calcium solids of concern, added in the mill, are calcium oxide (lime, CaO or $Ca(OH)_2$) and calcium carbonate (limestone), although not all mills use lime addition. The formation of gypsum in the mill makes it a third solid of concern.

11.2.1 Calcium Oxide

CaO is added as a slurry to partial neutralization and to final neutralization tanks (MacLarens, 1977). It dissolves rapidly in slaking systems. Some residual CaO may remain in the process stream as a solid after slaking, but this should dissolve after several hours.

Accordingly, the dissolution kinetics of CaO are judged to be sufficiently rapid that it may be considered to be a solid at equilibrium with ground and surface water for time scales of concern to tailings management.

TABLE 11.3: pH DEPENDENCE OF MINERAL DISSOLUTION RATES
(Generally at 25°C)

Mineral	pH Dependency	pH Range	Reference
K-feldspar	$(H^+)^{1.0}$	2.5 pH	Helgeson et al., 1984
Albite	$(H^+)^0$	$2.5<pH<8$	Helgeson et al., 1984
Microcline	$(H)^{-0.4}$	$pH>8$	Helgeson et al., 1984
Nepheline	$(H^+)^{-0.2}$	pH 7	Lasaga, 1983
Diopside	$(H^+)^{0.7}$	$2<pH<6$	Schott et al., 1981; Lasaga, 1983
Enstatite	$(H^+)^{0.8}$	$2<pH<6$	Schott et al., 1981; Lasaga, 1983
Forsterite	$(H^+)^{1.0}$	$3<pH<5$	Grandstaff, 1980; Lasaga, 1983
Anorthite	$(H^+)^{0.54}$	$2<pH<5.6$	Fleer, 1982; Lasaga, 1983
Sr-feldspar	$(H^+)^{1.0}$	pH 4	Fleer, 1982; Lasaga, 1983
	$(H^+)^{-0.28}$	pH 6	Fleer, 1982; Lasaga, 1983
Quartz	$(H^+)^{0.0}$	slightly acidic	Rimstidt and Barnes, 1980)
-Cristobalite		to pH 7	
-Cristobalite			
Amorphorus Silica	$(H^+)^{0.0}$		
Calcite	$(H^+)^{1.0}$		
Slaked Lime	$(H^+)^0$	2 to 7	Sverdrup and Bjerle, 1982
Calcite	$(H^+)^{1.0}$	2 to 7	Sverdrup and Bjerle, 1982
Dolomite	$(H^+)^{0.5}$	2 to 7	Sverdrup and Bjerle, 1982
Olivine	$(H^+)^{1.0}$	2 to 7	Sverdrup and Bjerle, 1982

TABLE 11.4: ACTIVATION ENERGIES OF GEOCHEMICAL REACTIONS (k cal/mol)

Rxn	E (k cal/mol)	Comments	Reference
$Fe^{2+} + Fe^{3+} \rightarrow Fe^{3+} + Fe^{2+}$	16.8	-	Berner, 1981
Calcite + $Mg^{2+} \rightarrow$ Dolomite + Ca^{2+}	49	252-295°C	Berner, 1981
$H_4SiO_4 \rightarrow SiO_2$ (qtz) + $2H_2O$	11.9	0-300°C	Rimstidt and Barnes, 1980
SiO_2(qtz) + $2H_2O \rightarrow H_4SiO_4$	16-18	0-300°C	Rimstidt and Barnes, 1980
SiO_2(am) + $2H_2O \rightarrow H_4SiO_4$	14.5-15.5	0-300°C	Rimstidt and Barnes, 1980
Calcite $\rightarrow Ca^{2+} + CO_3^{2-}$	8.4	5-50°C	Lasaga, 1983
K-feldspar	20	25-200°C for pH dependent region	Helgeson et al., 1984
	9	25-650°C for pH dependent region	Helgeson et al., 1984
Monazite (Th)	?		
Bannerite (U)	Coming from Rio	50-70°C @ pH = 1	

11.2.2 Calcium Carbonate (Limestone)

Calcium carbonate limestone is added to neutralize leaching pachuca effluent in the partial neutralization tanks. Most of the limestone added is dissolved within 2 hours, the detention time of the partial neutralization tanks, because very little limestone appears in solids leaving the neutralization tanks or is found in fresh tailings. This infers that, over the range of pH 0.5 to 2, the dissolution kinetics have a half time much less than 2 hours.

i) Kinetics of Calcite

The kinetics of calcite formation (crystallization) and dissolution appear to have received the most attention of all solids of concern to tailings management. This results partly from the wide spread application of limestone and related compounds to industrial processes and the role of calcite formation and dissolution in hard water lakes and the world's oceans. Work upon dissolution kinetics has concentrated upon industrial processes and the use of dissolution kinetics as a tool for understanding growth kinetics.

Nancollas, Reddy and House and co-workers have extensively studied crystallization kinetics. Nancollas and co-workers (Kazmierczak et al., 1981, 1982; Nancollas et al., 1981; Tomson and Nancollas, 1978) have developed laboratory techniques to study formation kinetics in a reproducible manner. This has allowed them to study the influence of various factors upon formation kinetics of calcite including the presence of magnesium, strontium, sulphate, oxalates, phosphate, ammonia, the solid/solution ratio and the presence of inhibitory ions (Nancollas and Reddy, 1974, 1976; Reddy and Gaillard, 1981; Reddy and Wang, 1980; Nancollas, 1979; Nancollas and Sawada, 1982; Kagawa et al., 1981; Nancollas, 1983; Nancollas et al., 1983). House and co-workers (House, 1981a, b; House and Tutton, 1982; Cassford et al., 1983) have examined nucleation aspects and concentrated upon the role of carbon dioxide and bicarbonate in crystal growth. Overall, this work has elucidated the role of particular ions in growth or inhibition of growth. The role of phosphate ion as a growth inhibitor has been conceptually and qualitatively explained by Stumm and co-workers (e.g., Sigg and Stumm, 1980; Graucr and Stumm, 1982) using the competitive site-binding model (see Chapter 8 and 13 for explanation of the site-binding model).

Significant advances in understanding dissolution kinetics of calcite are represented by the work of Berner and Morse (1974), Plummer et al. (1974) and Plummer et al. (1978). The advances are based upon considering the types of surface complexes which may exist at the calcite-water interface. The Plummer et al. (1978) work is the basis for the application of limestone dissolution kinetics (i) to deriving requirements for liming acid lakes (Sjoberg, 1979; Sverdrup and Bjerle, 1982; Sverdrup et al., 1981, 1983; Chan and Rochelle, 1982; Bjerle et al., 1982; Meserole et al., 1981); (ii) development of technology for SO_2 removal in scrubbers (Toprac and Rochelle, 1982; Change et al., 1982; Rochelle, 1981); and (iii) for understanding calcite formation kinetics (Reddy et al., 1981). In addition, the lake liming analysis has used mass transfer concepts, developed in chemical engineering (Crank, 1979; Sherwood et al., 1975), to describe transport both from the particle surface to the sediment pore water; and from sediment pore water to the overlying water column.

The adequacy of the kinetics for describing actual systems has also been of concern to many of these workers. Dreybrodt, in a series of papers (1980, 1981a, b, c) has evaluated the kinetics for both dissolution and precipitation from thin films to explain karstification processes. Rochelle and co-workers (Chan and Rochelle, 1982; Chan et al., 1982) have spent some time studying how well the dissolution behaviour of laboratory-formed calcite compares to that of natural limestone.

From this work, it appears that the appropriate kinetic expression for explaining precipitation-dissolution behaviour of calcite is:

$$R = \underbrace{k_1 a_{H^+} + k_2 a_{H_2CO_3^*} + k_3 a_{H_2O}}_{\text{Dissolution Component}} - \underbrace{k_4 a_{Ca}{}^{2+} + a_{HCO_3^-}}_{\text{Crystallization Component}} \qquad (11.17)$$

where: R is the net dissolution rate

a_i denotes the chemical activity of the ith ion

k_1, k_2, k_3 and k_4 are reaction rate constants.

This is the expression derived by Plummer et al. (1978) for pH ranges of 2 to 7, for P_{CO2} from 0.0003 to 0.97 atm and for temperature from 5 to 60°C. The dissolution component is based upon three proposed reactions occurring at the calcite surface. They are:

$$\dashv CaCO_3 + H^+ = Ca^{2+} + HCO_3^- + \dashv \qquad (11.18)$$

$$\dashv CaCO_3 + H_2CO_3^o = Ca^{2+} + 2HCO_3^- + \dashv \qquad (11.19)$$

$$\dashv CaCO_3 + H_2O = Ca^{2+} + HCO_3^- + OH^- + \dashv \qquad (11.20)$$

Here, $\dashv CaCO_3$ represents a surface $CaCO_3$ complex attached to the calcite surface.

Figure 11.2 gives typical experimental data for laboratory and natural samples (slaked lime, calcite, dolomite, olivine and sodium carbonate) obtained by Sverdrup and Bjerle. It demonstrates the strong pH dependence of the dissolution mechanism. This is explained by the interpretation that the H^+ reaction with calcite (Equation 11.18) dominants over the other two mechanisms. The other two reactions are significant only at lower pH or at high CO_2 partial pressures (e.g., soils, Equation 11.19).

Four other factors have important effects upon the dissolution kinetics: surface area, the effects of mass transfer (diffusion through solution to the solid liquid interface), protonation reactions of $H_2CO_3^*$, and precipitation of other solids.

a) Surface Area: In several experimental studies, apparent artifacts are observed in rate data (plot of cumulative concentration in solution versus time) suggesting a non-linear or biphasic mechanism (see below, discussion of feldspars). Such artifacts probably result from small particles cemented to the surface of larger particles. Figure 11.3 (a, b) show that a large number of small particles exist on the surface of the 90 to 100 um size fraction after dry sieving but that they are removed by wet sieving.

b) Mass Transfer: Of the two steps controlling dissolution (chemical reaction on the surface, and transport to the bulk of the liquid), the mass transfer step is rate-liming for calcite in the pH range of 2 to 7. Diffusion and the thickness of the fluid boundary layer around the solid surface control the mass trasfer rate. The thickness of this boundary layer depends on the hydrodynamic conditions of the fluid.

Typical data gathered to evaluate calcite dissolution kinetics are given in Figure 11.4 and in Table 11.5. The kinetic data for laboratory solutions are given in terms of the mass transfer coefficient which is the diffusion

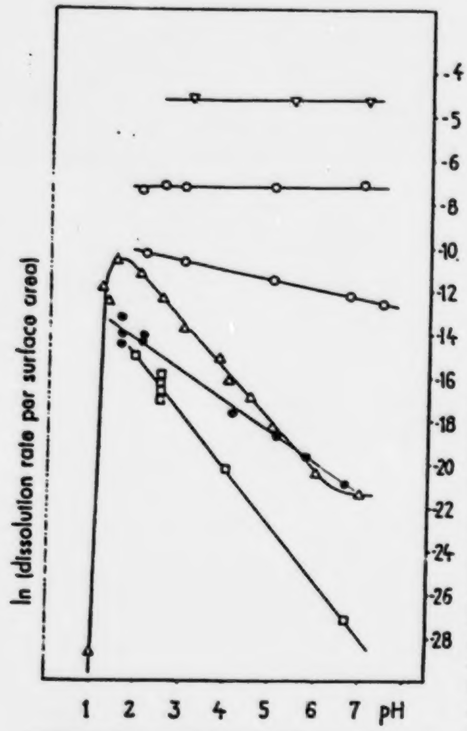

FIGURE 11.2:

The diagram shows the dissolution rate per particle surface area versus pH. The open rings represent slaked lime. The upper line is for dissolution in dilute hydrocloric acid, the lower for sulfric acid. The uniform-size particles of slaked lime were produced by wet sieving with organic liquids in which the slaked lime is insoluble. The triangles marke the line for calcite, the black dots the line for dolomite and the squares the line for olivine. The sharp decline in dissolution rate at pH-values lower than 2 is caused by precipitation of gypsum on the calcite surface. The inverted triangles show the dissolution rate for sodium carbonate. The dimensions for the two upper lines are Kg/m^2s, and for the other $Kmol/m^2s$.

(from Sverdrup and Bjerle, 1982)

FIGURES 11.3a and 11.3b: The photographs were made with a scanning electron microscope and show a fraction obtained as 90 - 100 microns after sieving in dry condition. The magnification is 600 x and 200 x. It can clearly be seen that the obtained fraction contains a large amount of smaller particles which adheres to the surface of larger particles. The fraction should rather be named 0 - 100 microns. (from Sverdrup and Bjerle, 1982)

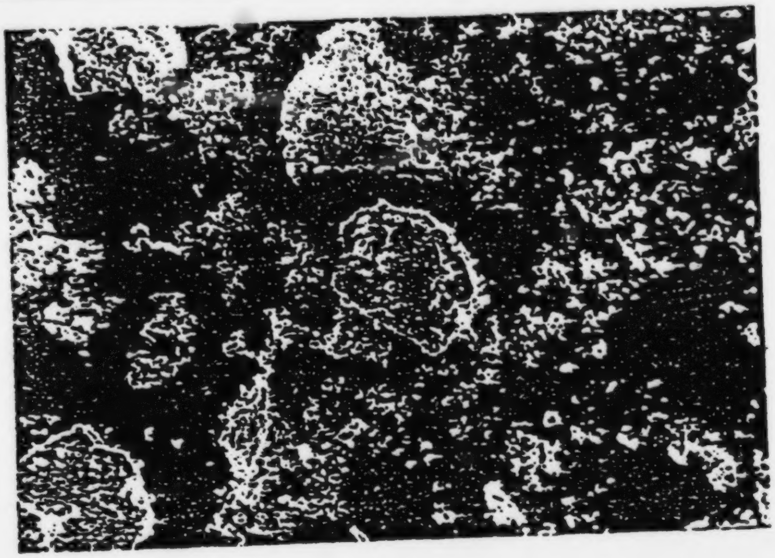

FIGURE 11.3a

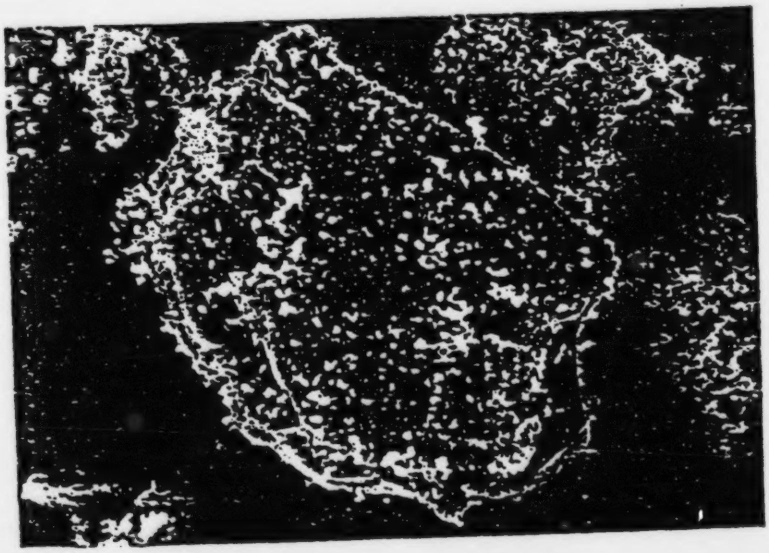

FIGURE 11.3b

FIGURES 11.3c and 11.3d: These are photographs as FIGURES 11.2a and 11.2b but made of a fraction obtained as 90 - 100 microns after wet sieving. They are of relatively equal size and have an average size of about 90 - 100 microns. No smaller particles can be detected. (Figure 3 and 4 from Sverdrup and Bjerle, 1982)

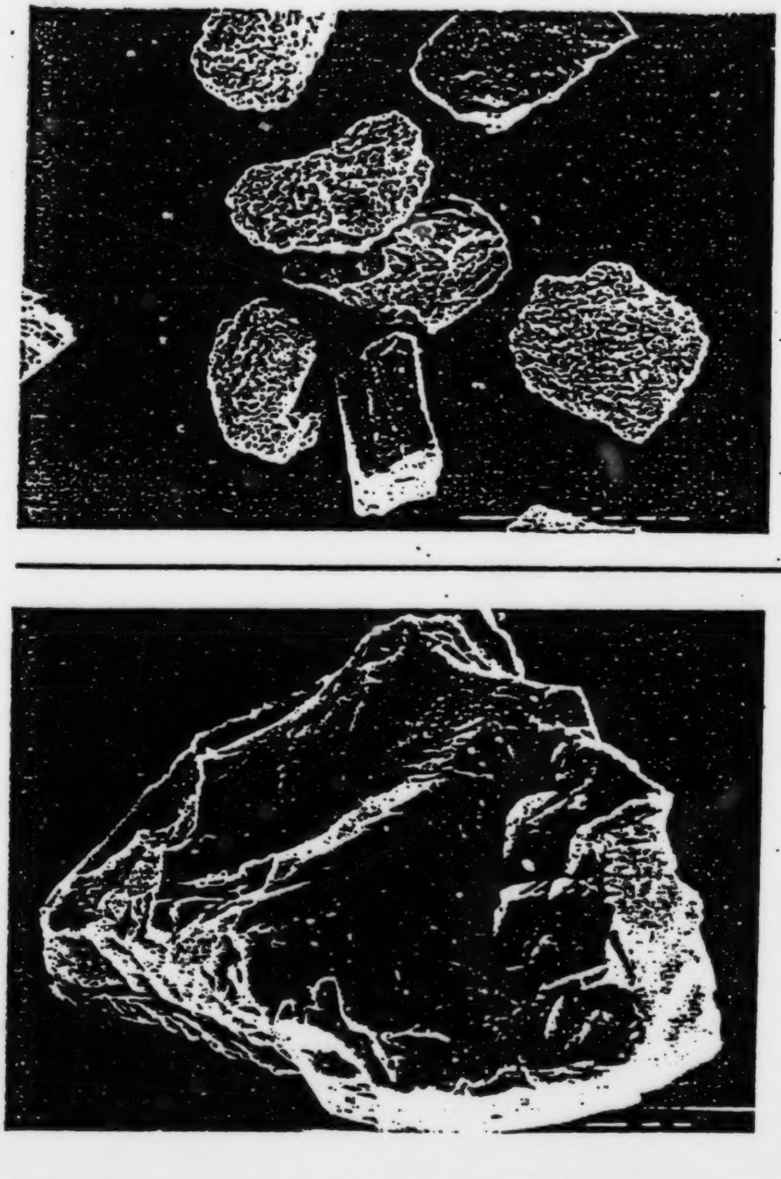

COMMENT: It is quite obvious that if the two fractions, the dry method fraction and the wet method fraction, are used in experiments they would give quite different results and conclusions, if they both were to be consdiered as only 90 - 100 micron particles.

FIGURES 11.4 and 11.5:

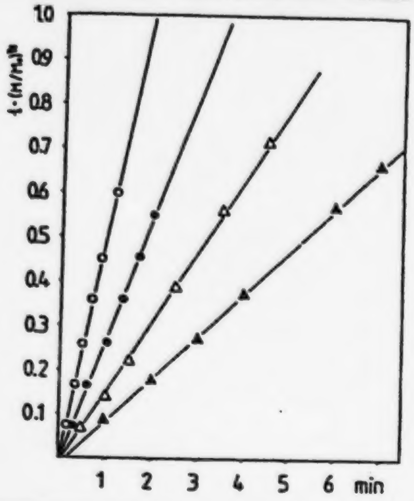

FIGURE 11.4:
Fig. *The kinetics of dissolution for some of the particle fractions used in the experiments.* $1-(M/M_0)^{1/3}$ versus time is plotted here. The open circles represent the fraction 11—15 microns, the black dots 15—23 microns, the open triangles 23—33 microns and the black triangles 33—43 microns.

(from Figure 7, Sverdrup and Bjerle, 1983)

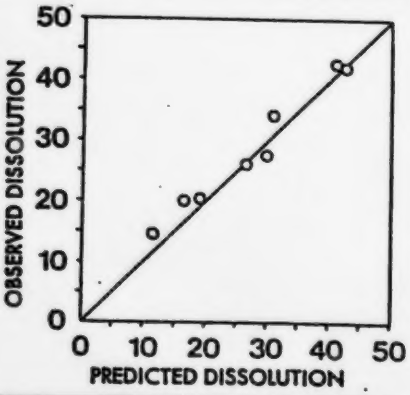

FIGURE 11.5:
Fig. . *The observed instant dissolution plotted versus the theoretical prediction for the limings in this study.* The observations are confirming the theoretical predictions to within ±13 %.

(from Figure 3, Sverdrup and Bjerle, 1983)

Table 11.5 *The measured mass transfer coefficients for different particle sizes.* C is the correlation between the experimental points and the straight line represents the theory. K_M is the mass transfer coefficient measured. The very small particles did not give the same accuracy due to their having been produced by sedimentation in very small amounts. The values of K_M is therefore approximate and may vary ±40 %.

Particle size	Correlation	Mass transfer coefficient
11.2—14.9 μm	0.9990	$(1.04 \pm 0.16) \cdot 10^{-3}$ ms^{-1}
14.9—22.7 μm	0.9992	$(0.75 \pm 0.16) \cdot 10^{-3}$ ms^{-1}
22.7—32.5 μm	0.9995	$(0.65 \pm 0.12) \cdot 10^{-3}$ ms^{-1}
32.5—43.1 μm	0.9996	$(0.55 \pm 0.08) \cdot 10^{-3}$ ms^{-1}
18— 25 μm	0.98	$(0.76 \pm 0.12) \cdot 10^{-3}$ ms^{-1}
25— 30 μm	0.994	$(0.93 \pm 0.09) \cdot 10^{-3}$ ms^{-1}
46— 50 μm	0.9996	$(0.94 \pm 0.04) \cdot 10^{-3}$ ms^{-1}
64— 90 μm	0.998	$(1.00 \pm 0.17) \cdot 10^{-3}$ ms^{-1}
90—100 μm	0.995	$(0.87 \pm 0.05) \cdot 10^{-3}$ ms^{-1}
100—104 μm	0.9996	$(0.84 \pm 0.02) \cdot 10^{-3}$ ms^{-1}
100—125 μm	0.9995	$(0.91 \pm 0.10) \cdot 10^{-3}$ ms^{-1}
125—147 μm	0.9992	$(0.81 \pm 0.08) \cdot 10^{-3}$ ms^{-1}
177—200 μm	0.9992	$(0.79 \pm 0.05) \cdot 10^{-3}$ ms^{-1}
354—400 μm	0.9995	$(0.81 \pm 0.05) \cdot 10^{-3}$ ms^{-1}
0.15—0.25 μm		0.09 ms^{-1}
0.11—0.15 μm		0.08 ms^{-1}
0.40—0.60 μm		0.029 ms^{-1}
0.90—1.1 μm		0.009 ms^{-1}

From Sverdrup and Bjerle, 1982

coefficient divided by the thickness of the fluid boundary layer. The data demonstrate that the laboratory rate data are correctly interpreted in terms of the mass transfer concept (Figure 11.4) and that the rate is independent of surface area once the dissolution rate is corrected for this parameter (see Figure 11.4 and Table 11.5).

Accordingly, for the time scales of concern for modelling tailings, it is expected that fluid processes rather than surface reaction kinetics will control dissolution behaviour of calcite. This means that thermodynamic concepts can be used to model limestone dissolution in tailings.

c) Protonation Reactions: The dissolution of calcite is increased by high concentrations of carbonic acid (H_2CO_3*). In laboratory systems in which CO_2 is injected into the liquid by aeration, dissolved CO_2 has to react with water to form H_2CO_3 before carbonic acid will react with calcite. The hydrolysis reaction is relatively slow. In some cases, the hydrolysis reaction rate in solution may be the rate limiting step rather than mass transfer, but this is not expected to be important for time scales of concern in tailings management.

d) Precipitation of Other Solids: This factor is significant for interpretation of laboratory data. Figure 11.2 shows that below pH 2, the "observed" dissolution rate of calcite decreases. This "observed" drop is interpreted to be due to surface precipitation of gypsum on the calcite solid (Sverdrup and Bjerle, 1982). The authors do not state the acid used, but this implies that sulphuric acid was used in their experiments, a likely possibility since they are trying to emulate lake acidification.

ii) Comparison of Theory to Uranium Mill Data: The theory predicts that at pH 2, the dissolution half time will vary from 5 sec to 1 hour (Table 11.6) for up to a 1 cm^3 particle. The hydraulic detention time of the neutralization tank in the mill is approximately 2 hours. Hence, the dissolution kinetics would predict that most of the limestone should dissolve in the neutralization tanks, a prediction that is typically observed.

TABLE 11.6: HALF-TIME TO DISSOLVE CALCITE SOLIDS AS A FUNCTION OF PARTICLE SIZE AND SOLUTION pH

	Particle Size	
pH	1 cm^3	1 um^3
2	1.3 hr	5 sec
7	1.2 yr	1 hr

iii) Comparison of Theory to Observed Release Rates in Lakes: Figure 11.5 shows the observed degree of dissolution of limestone in lakes reported by Sverdrup and Bjerle (1983) compared to that predicted by the theory (Equation 11.18 to 11.20). The limestone had a size range of 0 to 0.5 mm. The limestone particles settled through lake depths ranging from 1 m to 15 m, in lakes whose pH ranged from 4.5 to 5.2. The degree of agreement is quite good (± 13%), presenting some validation of the kinetics and calculations given above.

The theory also predicts that at pH 7, calcite dissolution is approximately 1,000 times slower than at pH 2. This is validated by the operational history of uranium mills which found that calcite dissolution (to pH 8) as a final neutralization technique is impractical because the slow rate of dissolution does not achieve the desired effluent quality (pH 7) during the detention time of the final neutralization tanks.

iv) Application of Theory to Tailings Management: Calculations of the time to dissolve particles using the above theory and laboratory data are given in Table 11.6. Even at neutral pH's, the half-time is of the order of one year for a 1 cm^3 particle. This suggests that for time scales of concern to the NUTP (greater than a decade), residual calcite can be considered to be at equilibrium with groundwater.

v) Comparison of Theory to Field Observations on Tailings

Blair et al (1980) have observed acidic groundwater flowing from a tailings area into an aquifer containing up to 1% calcite in the Nordic Main tailings area. Groundwater velocities are of the order of 300 m/year near the dam. The observed solution chemistry infers that calcite is being dissolved and siderite ($FeCO_3$) precipitated (Morin et al, 1982; Dubrovsky et al., 1985). The rate of retardation of movement of the iron is consistent with calcite equilibrium being maintained with groundwater; that is, slow calcite dissolution kinetics do not appear to control the reaction. Hence, equilibrium processes appear to describe calcite dissolution for time scales of the order of a year.

11.2.3 Gypsum Kinetics

Relative to calcite, a mathematical description for gypsum precipitation and dissolution kinetics is not as well worked out, although substantial amounts of research have investigated these two processes.

Early work centered upon describing nucleation kinetics and nucleation controlled surface growth. Some of this classical work has been well summarized by Nielsen (1964). Many measurements of solubility constants for gypsum were also made during the 1960's (e.g., Schaefer and Hunger, 1969; Ostrovski et al., 1969) and 1970's (e.g., Lui and Nancollas, 1971; Christoffersen and Christoffersen, 1976) to aid the interpretation of crystal growth data, particularly at low degrees of supersaturation. These studies have been aimed at understanding scale formation (e.g., Kazmierczak et al., 1981) and adapted for considering the formation of anhydride from gypsum precursors under arid conditions (e.g., Cody and Hull, 1980; Cody, 1975, 1981).

The experimental studies show that kinetics of growth can be described (Christottersen et al., 1982; Gill and Nancollas, 1980) by:

$$r_g = k\ S\,(C-C_s)^{2.0\pm0.2} \qquad (11.21)$$

where: r_g is the rate of removal of gypsum from solution
k is the kinetic constant
S is a function of the number of active growth sites
C is the stoichiometric concentration of gypsum in supersaturated solution
C_s is the equivalent of C in saturated solution

At low degrees of supersaturation ($1.03 \leqq C/Cs \leqq 1.15$), Christoffersen et al. (1982) found that crystal growth is controlled mainly by severe dislocation growth but that several other types of growth are required to explain the complete range (growth of grain boundary, spirals, partial outgrowth of concave parts of crystals).

The experimental studies show that dissolution kinetics can be described (Christoffersen and Christoffersen, 1976) by an expression of the form:

$$r_d = k\,A\,(C-C_s) \qquad (11.22)$$

where, k is the kinetic constant and A the surface area of the crystal. A first order rate expression is a prerequisite for diffusion control.

Analysis of the kinetic data for Equations 11.21 and 11.22 shows that growth is controlled by surface growth whereas dissolution is controlled by transport (diffusion) of calcium sulphate from the gypsum solid to the solution bulk. The associated diffusion coefficient for dissolution is of the order of 4×10^{-6} cm^2/s and independent of surface area. The time scales of dissolution experiments are not directly given, but appear to be of the order of hours.

Application of Gypsum Kinetics to Tailings Management

Calcium in the form of limestone (partial neutralization tanks) and lime (partial and final neutralization tanks) is added in the mill to neutralize sulphuric acid solutions. SEM-XRE analysis and thermodynamic analyses of leaching solutions shows that the leaching solutions are approximately at equilibrium with respect to gypsum. This suggests that precipitation reactions are complete within the time frame of the neutralization processes (1 to 4 hours). It is difficult to directly compare this data with the kinetic data given above because heteorgeneous and secondary nucleation must be considered in addition to crystal growth. But these time scales appear to be comparable to those for crystal growth in the literature.

For dissolution, the experimental data suggest that the dissolution rate is transport-controlled; that is, for time scales of the order of hours, fluid diffusion controls. One can consider diffusion over longer length scales. Viewing the diffusion process as a diffusion coefficient divided by a length scale, one can formulate a model which describes the rate of increase in concentration in pore water starting from zero concentration (see Chapter 7). It is:

$$\frac{VdC}{dt} = \frac{A_s D(C_s - C)}{\text{del } Z} \qquad (11.23)$$

where, V is the volume of the pore water, A_s is the mineral interfacial area and del Z is the diffusion length. Defining del Z as equal to V/A_s, one can calculate that the time for C to attain one-half the value of C_s is two days if del Z is 1 cm and 200 days if del Z is 10 cm.

Hence, for time scales of one year and greater, one can essentially assume that equilibrium controls gypsum dissolution provided that the diffusional length scale is not greater than 10 cm.

Validation of Gypsum Kinetics

Leachate from fresh tailings obtained from Rio Algom and mounted in a lysimeter showed sulphate concentrations and TDS concentrations which are consistent with gypsum saturation. The nominal flushing time is of the order of a day to a week suggesting that near equilibrium conditions are readily established.

Field evidence (Dubrovsky et al., 1985) is also consistent with "equilibrium controls" on dissolution because all pore water samples exhibit saturation with respect to gypsum in Elliot Lake tailings areas, provided that gypsum solid phases are still present.

11.3 Kinetics of Major Iron Solids

11.3.1 Fe (II) to Fe $(OH)_3(s)$ (in the Absence of Sulphate and Bacteria)

The oxidation of Fe (II) and the mathematical description of its kinetics represents one of the classic pieces of work in the field of geochemistry and environmental science. In a pure solution, Stumm and Lee (1961) and Singer and Stumm (1970) found that the rate of loss of Fe (II) from aqueous solution under abiotic conditions was described by:

$$\frac{d}{dt}(\mathrm{Fe\,(II)}) = k\,(\mathrm{Fe\,(II)})\,(\mathrm{OH^-})^2\,P_{O_2} \qquad (11.24)$$

or

$$\frac{d}{dt}(\mathrm{Fe\,(II)}) = k_H\,\frac{(O_2\,(aq))}{(H^+)^2}\,(\mathrm{Fe\,(II)}) \qquad (11.25)$$

where (OH^-) = hydroxide ion concentration
(H^+) = hydrogen ion concentration
$(\mathrm{Fe\,(II)})$ = iron (II) concentration
P_{O_2} = partial pressure of oxygen (atm)
$(O_2(aq))$ = oxygen concentration in water

$K = 8.0\ (\pm 2.5) \times 10^{13}\ \mathrm{min}^{-1}\ \mathrm{atm}^{-1}\ \mathrm{mol}^{-1}\ L^{2}$ at 20°C
$k_H = 3\mathrm{x}10^{-12}\ \mathrm{min}^{-1}\ \mathrm{mol}^{-1}\ L^{-1}$ at 20°C

Typical results are plotted in Figure 11.6 (Figure 7.15 from Stumm and Morgan). Oxidation of Fe (II) is fairly slow below pH = 6 and quite rapid above pH 6.

The results also show that the model does not fit the data well below pH 3. In fact, the oxidation rate of Singer and Stumm (1970) is independent of pH below pH = 2. This lack of fit is not widely discussed in the literature. Also, recent evidence (Stumm and Morgan, 1981) indicate that the kinetic rates are 100 times slower in sea water than in fresh water. This may be explainable by the effects of high ionic strength and anions (Cl^-, SO_4^{2}) in slowing the reaction (Sung and Morgan, 1981).

11.3.2 Pyrite Oxidation Kinetics

Various workers have developed an overview of the steps involved in the oxidation of pyrite. This work has been ably summarized by Senes (1984), Nicholson (1984), Lowson (1982), and Nordstrom (1982). A summary of the steps involved is presented here. To our knowledge, a detailed kinetic expression for each step has not been developed. For our purposes, an overview of the kinetics and an empirical formulation as a function of solution conditions and oxygen concentration are developed in Chapter 12 and used to examine the relative importance of reaction rate coefficients and oxygen diffusion coefficients in air upon the overall rate of pyrite oxidation. The mathematical formalization for combining reaction rate and diffusion is developed in Chapter 7 (combining reaction and transport processes).

Qualitative Description of Bacterial Oxidation of Pyrite

As Stumm and Morgan (1981) note, the reactions given in Figure 11.7 for pyrite oxidation are "schematic" and do not represent the exact mechanistic steps. The model is similar to and carries with it the same overall consequences as that suggested by Temple and Delchamps (1953). The rate-determining step is a reactive step in the specific oxidation of ferrous iron (reaction b). As Figure 11.7 shows, the rate of oxidation of ferrous iron under chemical conditions analogous to those found in tailings waters is very slow, indeed considerably slower than the oxidation of iron pyrite by ferric iron (reaction c). At pH 3,

FIGURE 11.6: OXIDATION RATE OF IRON(II) AS A FUNCTION OF pH
(from Singer and Stumm, 1970)

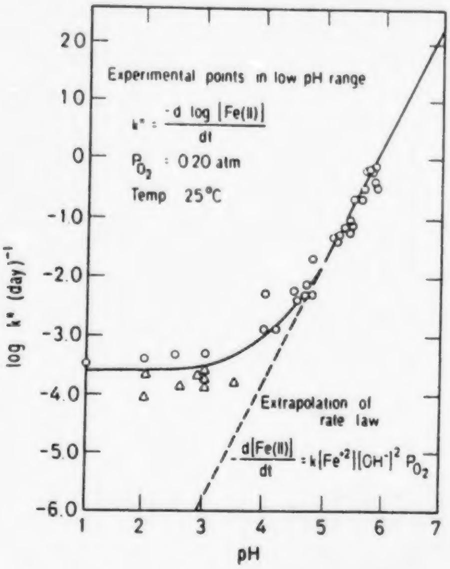

FIGURE 11.7: MODEL FOR THE OXIDATION OF PYRITE
(from Stumm and Morgan, 1981)

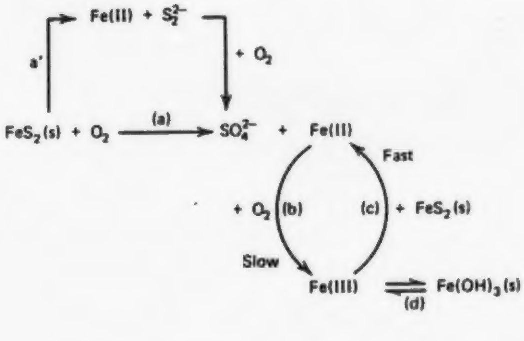
Fe(II) + S_2^{2-}
a'
+ O_2
$FeS_2(s) + O_2$
(a)
SO_4^{2-} + Fe(II)
Fast
+ O_2 (b)
(c) + $FeS_2(s)$
Slow
Fe(III)
(d)
$Fe(OH)_3(s)$

half-times for the oxidation of Fe(II) are on the order of 1,000 days, while in the case of oxidation of pyrite by Fe(III), half-times on the order of 20 to 1,000 min were observed. Similar rates have been observed for this latter reaction by Garrels and Thompson (1960).

To indicate the sequence, pyrite is oxidized directly by oxygen (a) or is dissolved and then oxidized (a^1). The ferrous iron formed is oxygenated extremely slowly (b) and the resultant ferric iron is rapidly reduced by pyrite (c), releasing additional acidity and new Fe(II) to enter the cycle via reaction b. Once the sequence has been started, oxygen is involved only indirectly in the reoxidation of Fe(II) (b), the oxygenation of FeS_2 (a) being no longer of significance.

Precipitated ferric hydroxide deposited in the mine and the streams serves as a reservoir for soluble Fe(III) (d). If the regeneration of Fe(III) by reaction b is halted so that the concentration of soluble Fe(III) decreases, it will be replenished by dissolution of the solid $Fe(OH)_3$ and will be free to act again should it come in contact with additional FeS_2.

The following pertinent consequences of this model need to be emphasized:

1. Ferric iron cannot exist in prolonged contact with pyritic agglomerates because Fe(III) is rapidly reduced by pyrite. The exclusion of oxygen halts the regeneration of Fe(III) via oxidation of Fe(II).

2. The overall rate of dissolution of pyrite should be independent of its surface structure and its surface area concentration in bacterial systems.

3. Microorganisms influence the overall rate of reaction by mediating the oxidation of ferrous iron, since it appears to be the rate-determining step (Silverman and Lundgren, 1959; Stumm-Zollinger, 1972). Microbial catalysis, such as by the autotrophic iron bacteria, Thiobacillus ferrooxidans, seems to be ecologically significant as evidenced by the few field investigations conducted.

The same cycle is probably responsible for the dissolution and leaching of other mineral sulphides found in copper and uranium mines. Microbial leaching of these other minerals has always been demonstrated in the presence of iron, pyrite being the most abundant and widespread of all sulphide minerals.

Qualitative Description of Abiotic and Near Abiotic Oxidation of Pyrite

Much of the early work in the field of pyrite oxidation and acid production has assumed that pyrite oxidation occurred at significant rates only in the presence of bacteria. However, Nicholson (1984) has recently shown that under seemingly abiotic, neutral pH conditions, pyrite oxidation occurs at rates that can be significant in systems containing little or no buffer capacity. This oxidation is attributed to strictly chemical processes and is a function of surface area, partial pressure of oxygen, temperature and porewater pH. These factors are described in more detail in Chapter 12.

11.3.3 Formation and Dissolution Kinetics of Jarosite

Precise observations upon formation and dissolution kinetics of jarosite have not been obtained. However, the following observations permit us to develop some estimates of the rates involved.

Jarosite Formation

Jarosite is important to tailings management because of the association of Ra-226 with jarosite observed by Kaiman (1977). (80,000 pCi Ra-226/g of jarosite). How widespread this association is awaits further work.

We have used Mossbauer spectroscopy to attempt to identify jarosite in the leaching pachucas and tailings (Constable and Snodgrass, 1984). Mossbauer spectroscopy allows one to identify separate minerals with Fe^{2+} and Fe^{3+} oxidation states. The difficulty with tailings samples is that both jarosite (Fe^{3+}) and pyrite (Fe^{2+}) have a doublet on the spectrum at about the same location making their identification difficult. The Mossbauer analysis by Bancroft of the University of Western Ontario found no jarosite detectable in either leaching pachuca solids or in the CCIW lysimeter solids (old Nordic tailings leached for an additional five years), despite thermodynamic calculations that suggest that K-jarosite should be stable in both situations (Constable and Snodgrass, 1984).

Recently, we have used ESCA (S. McIntyre, UWO) and Mossbauer again to analyze the same sample. ESCA results were negative, but the Mossbauer analysis (J. Capobianco, University of Geneva, private communication) indicates that jarosite is found in the old tailings but not in the leaching pachuca solids. Also, re-examination of SEM micrographs of solids that were removed ultrasonically from the CCIW tailings, show 1 um near-cubic rhombs whose morphology is consistent with jarosite rhombs identified in acid soils (Wagner et al., 1982). This suggests that jarosite does exist in the tailings.

Most of the relevant laboratory scale work on jarosite has been aimed at understanding jarosite formation in 'acid soils'. In particular, the work of Ivarson and colleagues is particularly helpful (Ross et al., 1982; Ivarson et al., 1978, 1979, 1980, 1981, 1982; Ross and Ivarson, 1980). They examined the formation rate of jarosite in laboratory solutions of ferrous iron and other cations and in solutions containing pyrite and other minerals (e.g., micas, feldspars, clays, etc.). The data give the following relevant observations:

- in solutions of ferrous iron, various cations and T. ferrooxidans, jarosite is completely formed in three to four weeks while 80% of ammoniojarosite ($NH_4 Fe_3 (SO_4) (OH)_6$) and 60% of natrojarosite ($NaFe_3(SO_4)_2(OH)_6$) are formed after 42 weeks. They note that these observations agree with available field data.

- in solutions containing pyrite and other minerals and T. ferrooxidans, the rate of formation of jarosite-type minerals depended upon the "weatherability" (dissolution rate) of the other minerals.

These data suggest that the kinetics make jarosite formation feasible if the solution conditions are appropriate. For example, the potassium concentration in the solution was, 1.4 mM (.025% K_2HPO_4; 112 mg K/L), the iron concentration was 0.16 M (4.4% $FeSO_4.7H_2O$; 8.8 gm Fe/L) and the sulphate concentration was 0.16 M (15 g SO_4/L). This compares to leaching pachuca concentrations for potassium of 0.025 M (1,000 mg/L), iron of 0.095 M (5.3 g/L), and sulphate of 0.73 M (70 g/L). This compares to concentrations in leachate water from the lysimeter solids where jarosite has been identified of 2.5×10^{-6} M (0.1 mg/L) of K, 1.8×10^{-5} M (1 mg/L) of Fe_T and 4.2×10^{-5} (4 mg/L) sulphate. Both the leaching pachucas and lysimeter waters are supersaturated with respect to jarosite. Thus, these solutions appear to have sufficient concentrations of K, Fe and SO_4 and the appropriate time scale to favour jarosite formation in both the leaching pachucas and lysimeters.

It is suggested that if future experimental evidence does not find jarosite in the leaching pachuca, the lack of jarosite formation must result from slow formation kinetics relative to the detention time of the pachucas, to temperature effects, or to the lack of a sufficient number of bacteria. It is our hypothesis that jarosite formation is slow chemically, but that in the presence of bacteria (T. ferrooxidans), the kinetics are much faster. This results from bacterial oxidation of Fe^{2+} and possibly from bacteria acting as nucleation sites.

The effect of temperature in the leaching pachucas (50 to 60°C) should be to increase the chemical rate of jarosite formation. But at this temperature, bacterial growth may be inhibited or the bacteria may even lyse because the optimum temperature for the growth of T. ferrooxidans appears to be in the order of 15 to 25°C. The effect of temperature can be assessed by examining the literature for Q_{10} or del E values for T. ferrooxidans between 25 to 60°C.

It is possible that even with bacteria present, the formation kinetics of jarosite are longer than 36 hours. We have not found precise data on this point, but one data set of Ivarson et al. (1979) given as Figure 11.8 herein provides us a basis for estimating the kinetics. The data can only be used to estimate the kinetics for K-jarosite because Ivarson et al. only sampled every few days. Inspection of their Figures 5 and 6 for an experiment on $FeSO_4.7H_2O$ at 25°C (Figure 11.8, herein) suggests that 30 to 40% of the potassium had been removed from solution when the first sample was taken at ten days after initiation of the experiment. The next sample (at approximately 14 d) shows that 100% of potassium had been removed from solution. This suggests an induction time (before measureable crystals are observed) of four to five days after which crystal growth occurs over a few days. In other work (Ivarson, 1973; Ivarson et al., 1978), formation of jarosite was observed after five to ten days. This suggests that the induction time is longer than the detention time of the leaching tanks (36 hr).

The above interpretation would suggest a half-time for jarosite formation in the leaching pachucas of greater than 15 days assuming that 0.1% of jarosite would form within 1.5 days in the leaching pachucas and that the formation follows first order kinetics.

FIGURE 11.8a and 11.8b: KINETICS OF JAROSITE FORMATION IN LABORATORY SYSTEMS (from Ivarson et al., 1979)

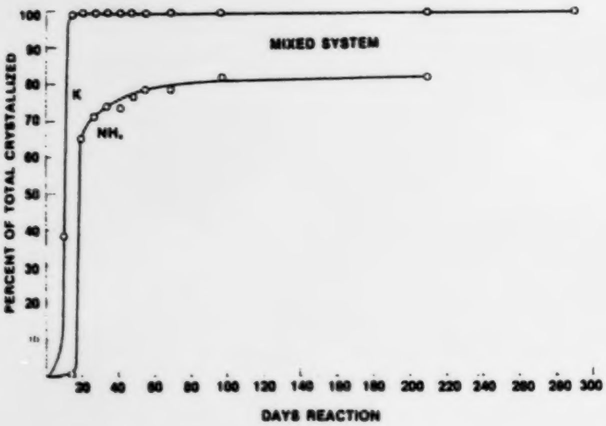

Fig. 8a Cumulative formation of K and NH_4 jarosite in an incubated system containing K^+ and NH_4^+. Calculated from amount of cations remaining in solution.

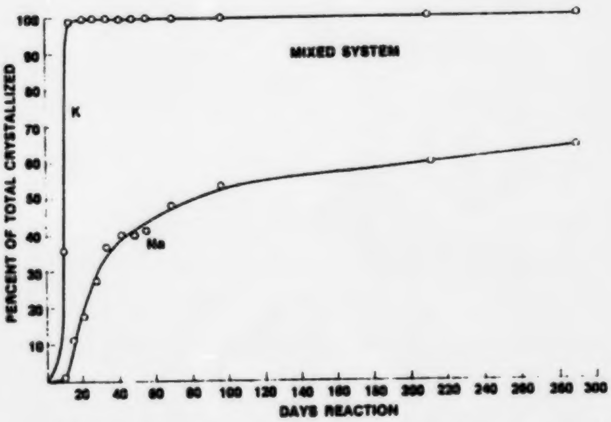

Fig. 8b Cumulative formation of K and Na jarosite in an incubated system containing K^+ and Na^+. Calculated from amount of cations remaining in solution.

Jarosite Dissolution

We have not found literature which gives a kinetic expression for the dissolution rate of jarosite. Evidence for its stability in weathering profiles underlying acid soils and laboratory evidence for its dissolution present seemingly conflicting estimates of dissolution rates.

Wagner et al. (1982) found jarosite in sub-soils and deeply weathered strata well below the zone of active jarosite formation. These soil strata are "quite old" (precise dates are not given). The presence of jarosite, at pH 4 where the authors suggest that it is not thermodynamically stable, is attributed to low rate of transformation kinetics to goethite or ferric oxide. Such slow kinetics make jarosite an important geological 'marker' of soils which have gone through acid sulphate weathering (oxidation of soils having low concentrations of pyrite). A numerical estimate of the kinetics of transformation is not possible from Wagner's data.

A somewhat different view of jarosite dissolution kinetics is presented by the laboratory work of Miller (1979). In this work, jarosite formed in a pyritic column experiment under oxidizing conditions. When oxygen was restricted, K-jarosite dissolved and $Fe(OH)_3$ precipitated to buffer the pH of the effluent. No rate data are given, but the effluent concentrations suggest maintenance of equilibrium conditions, implying that the jarosite dissolution kinetics are rapid.

The apparently slow dissolution rates observed in the field can possibly be rationalized as follows. Our thermodynamic calculations suggest that jarosite could be at equilibrium with an amorphous ferric hydroxide solid, even when the solution pH is relatively high (pH = 5) and the solution concentrations of SO_4^{2-} and K^+ are moderate-to-low. This would explain the apparent stability of jarosite in old soils. The choice of an amorphous or unstable ferric hydroxide can be rationalized from evidence by Langmuir and Whittmore (1971) who conclude that this type of solid phase would be more favourable when $Fe(OH)_3(am)$ precipitation is occurring than when $Fe(OH)_3(am)$ dissolution is occurring. This suggests an alternate hypothesis to that of Wagner et al. (1982): It appears possible to maintain equilibrium conditions over long periods of time for these two low-solubility minerals.

11.4 Kinetics of Silica

The definitive work on silica-water reactions is that of Rimstedt and Barnes (1980). They developed reaction kinetics to be consistent with the thermodynamic approach of geochemistry. The rate equations are based upon transition state theory (Eyring, 1935; Lasaga, 1984) in terms of chemical activities of the reacting substances. Thus, the rate constants have standard states which are consistent with the equilibrium constants for the reactions. The use of kinetics as opposed to equilibrium is particularly important for silica-water reactions at ambient environmental temperatures, because equilibrium conditions between silica and water are generally not maintained.

The reaction rate, r, as a function of the precipitation and dissolution rate is:

$$r = \frac{d}{dt}\, a(H_4SiO_4)/_{P,T,M}, = \frac{A}{M}.G\,(H_4SiO_4)\,(k_-a(SiO_2)a(H_2O)^2 - k_+\,a(H_4SiO_4)) \qquad (11.26)$$

where: $a(H_4SiO_4)$ denotes chemical activity of H_4SiO_4
$G\,(H_4SiO_4)$ denotes activity coefficient of H_4SiO_4
k_- is the dissolution rate constant (sec^{-1})
k_+ is the precipitation rate constant (sec^{-1})
A is the relative interfacial area between solid and aqueous phases (area/area)
M is the relative mass of water in the system (mass/mass)

For precipitation, an empirical relationship was obtained relating k_+ to temperature (T). It is:

$$\log k_+ = -0.707 - 2598/T \qquad (11.27)$$

with an activation energy (del E) of 49.8 k J/mol. For dissolution, the empirical relationship is:

$$\log k_- = a + bT + c/T \qquad (11.28)$$

The dissolution coefficients of Equation 11.28 have different values for different solid phases. They are:

Phase	a	b	c	del E (k J/mol)
Quartz	1.174	-.002028	-4158	67.4-76.6
-Cristobalite	-0.739	0	-3586	68.7
-Christobalite	-0.936	0	-3392	65.0
Amorphorus silica	-0.369	-7.894×10^{-4}	-3438	60.9-64.9

But the precipitation rate constant (k^+) is the same for all solid phases.

Application to U-Mill Tailings

The rate expression for precipitation and dissolution and the associated rate constants were derived for the temperature range of 0 to 300°C. The range of interest to this project is the "low" temperature end of this band.

The expression is relatively simple for several reasons including:

- extensive solubility data in the literature permit reliable temperature functions for equilibrium constants;
- there is no solid solution in the silica phases; and
- silica dissolves congruently to H_4SiO_4(aq)

The expression has some limitations due to the range of experiments used in determining the coefficients:

- The effect of pH over a broad range is not known; the expression is valid over the slightly acidic-to-neutral range. A modification to this expression to include pH effects for the pH 2 to 4 range in tailings may be needed.

- The effect of salts on reaction rate was not evaluated. Some effect is included through the effect of ionic strength upon the activity of water (a_{H_2O}) and hence upon silica solubility.

- The expression is limited to 1 um and larger particles because very small particles have higher solubilities than microscopic grains. For particles smaller than 0.1 um, the equilibrium constant should be corrected for surface free energy.

- The expression was demonstrated to be valid for $(A/M) < 10^4$.

Considering that only dissolution occurs, these rate constants give order-of-magnitude values of the dissolution rate for quartz of 1.3×10^{-6} mol/m^2/hr and for amorphorus silica of 2.3×10^{-5} mol/m^2/yr. For the net infiltration rate of 0.25 m/yr used in Chapter 6, the silica concentration in water migrating from the unsaturated zone is approximately 0.9 mg Si/L if the tailings solids are quartz, and 18 mg/L if the tailings solids are amorphorus silica. This calculation ignores ionic strength effects. This calculation assumes that the solids are 0.1 mm spheres of density 2.65. The equilibrium silica concentration in pore water is approximately 6 mg/L for quartz and 60 mg/L for amorphorus silica. This means that the net dissolution rate is essentially the same as the absolute dissolution rate, because the rate of precipitation is quite small. But the precipitation mechanism (k_+) will become an important influence upon the net dissolution rate (-r) at higher aqueous concentrations of silica (lower flow rates).

Since uranium tailings contain mainly quartz, the pore water value of 0.9 mg/L for silica best describes the expected value in migrating pore water over the long-term.

In fresh tailings in which some amphorus silica may have formed in the leaching pachucas, 18 mg Si/L would be a plausible value for the concentration of silica in infiltrating water. This value would be limited to the period of time required to dissolve all amorphorus silica. Consideration of these kinetics for quartz at 60°C, and those for feldspar and clay given below at 60°C (the temperature of the leaching pachucas) will allow one to estimate the amount of silica which may be formed as amorphorus silica in the leaching tank.

11.5 Kinetics of Feldspar and Related Minerals

Kinetics of Aluminosilicates

The kinetics of dissolution of various aluminosilicates has been the subject of various investigators including Aagaard and Helgelson (1982), Berner (1978), Berner and Morse (1974), Berner and Holdren (1979), Berner et al. (1980a, b), Busenberg and Clemency (1976), Flevi (1982), Grandstaff (1980), Helgeson et al. (1984), Lasaga (1981, 1984), Lin and Clemency (1981), Nesbitt and Young (1984), and Schott et al. (1981). Early work centred upon determining whether the release kinetics of silica from the alumino-silicate minerals was linear or non-linear with time. These parabolic-type (non-linear) kinetics were hypothesized by early investigators to be due to the formation of a new mineral on the surface of the aluminosilicate which acted as a surface coating to minimize the diffusion of silica into solution.

But the work of the Berner group has demonstrated that most of the curvatuve is due to sample preparation procedures. SEM analysis of aluminosilicates demonstrated the presence of ultrafine aluminosilicate particles on the surface of the large aluminosilicate solids. Etching with HF removed these particles and reduced the parabolic dissolution curve to a linear curve with time (see Figure 11.9 for albite, feldspar and enstatite).

The contribution of these ultrafine particles to the overall dissolution rate has been considered by Helgeson et al. (1983) by accounting for their surface area relative to that of large minerals and by assuming a uniform rate of dissolution per unit area. Their model calculations given in Figure 11.10 show good agreement with the data of Holdren and Berner (1979). This provides one additional piece of information that the parabolic character results from sample preparation procedures.

Three definitive pieces of work relating aluminosilicate dissolution kinetics to weathering are those of Lasaga (1983), Nesbitt and Young (1984) and Helgeson et al. (1984).

The rates of dissolution of various aluminosilicates as a function of temperature and pH calculated from the experimental data of others by Helgeson et al. (1984) are given in Figure 11.11. At 25°C, the apparent rate of hydrolysis depends on pH only below 2.9

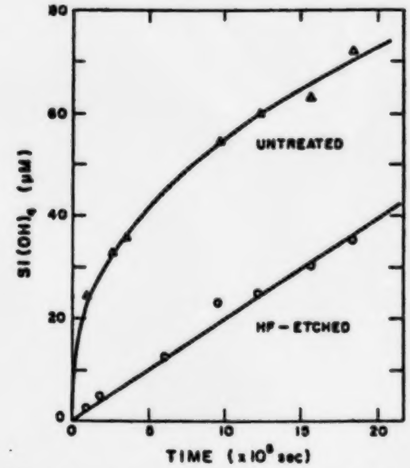

Fig. 11.9a Effect of sample preparation on the dissolution behavior of albite feldspar [from *Holdren and Berner*, 1979].

Silica dissolution rate from alumino silicates as a function of sample preparation techniques

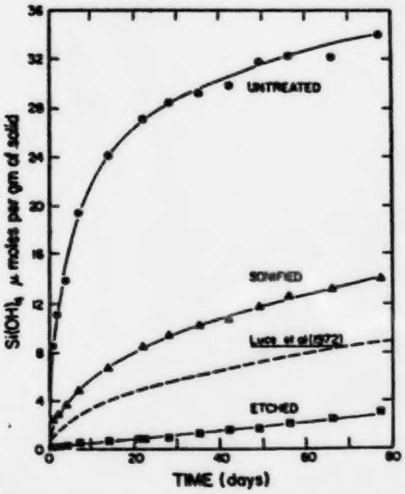

Fig. 11.9b Silica release during the dissolution of untreated, sonified, and etched enstatite in buffer solution at pH = 6, T = 20°C. The curve labelled Luce *et al.* (1972) refers to washed, but otherwise untreated, material from the same location.

(from Schott et al., 1981)

FIGURE 11.10: CALCULATIONS BY HELGESON ET AL. (1984) OF FELDSPAR DISSOLUTION RATE USING K 24.2 x 10^{-16} mol/cm^2/s. SIZE OF FINE PARTICLES WAS ESTIMATED FROM SEM PHOTOGRAPHS

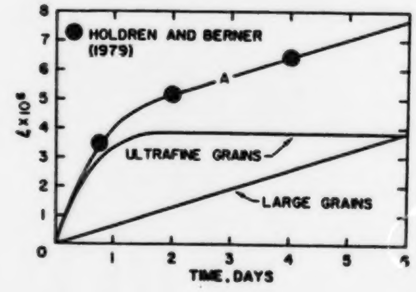

FIGURE 11.11: KINETICS OF DISSOLUTION OF VARIOUS ALUMNIO SILICATE MINERALS AS A FUNCTION OF pH (FROM HELGESON ET AL., 1984)

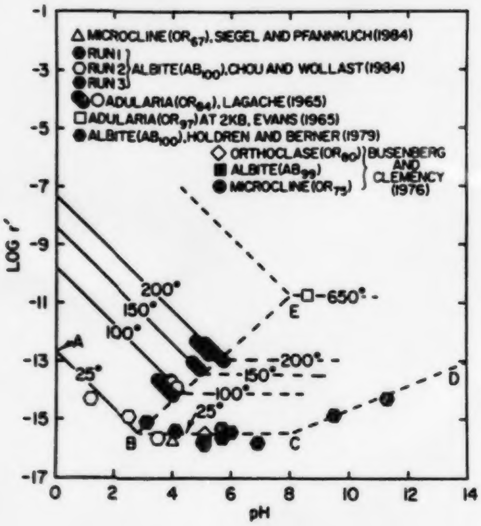

whereas at higher temperatures, the rate of hydrolysis (dissolution) depends on pH over a different range (e.g., at 200°C, the hydrolysis rate is pH-dependent below pH 5.5). The dissolution rates of microcline, albite and adularia (all feldspars) are essentially the same between pH 2.9 and 8.

The mechanism of dissolution of these aluminosilicates has also been of concern. Berner et al. (1979) conclude that dissolution occurs mainly at parallel, lens-shaped etch pits which develop at dislocation outcrops. In general, weathering takes place by selective etching and not by general attack of the surface which is implied by theories of bulk diffusional-type weathering.

Kinetics of Feldspars

The data of Helgeson et al. (1984) suggest that the feldspar hydrolysis rate constant (k_-) is:

$$k_- = 1.0\times10^{-4}\ \text{mol/m}^2\text{/yr for } 2.9 \leq \text{pH} \leq 8 \qquad (11.29)$$

and $$\log k_- = -1.5 - \text{pH for } 0 \leq \text{pH} \leq 2.9 \qquad (11.30)$$

and $$\log k_- = -7.1 + 0.4\ \text{pH for } 8 \leq \text{pH} \leq 14 \qquad (11.31)$$

at 25°C. Here k_- has units of mol/m^2/yr which differ from those of Figure 11.11 which are in mol/cm^2/sec.

At pH 5, the data of Busenberg and Clemency (1976) give a value for the rate of silica release of 0.53×10^{-4} mol/m^2/yr (Lasaga, 1983). This is somewhat less than the rate developed by Helgeson et al. (1984).

Mass balance measurements upon a watershed permit one to check these laboratory-measured rate constants. The data of Paces (1983) suggest that feldspar dissolution is approximately an order-of-magnitude lower. But this could result from incongruent dissolution and a mixture of minerals in the watershed. Hence, field and laboratory data appear to show good qualitative agreement.

Application of Kinetics to NUTP Data

Stoichiometric analysis in Chapter 4 of the solid phase mill feed suggest that sericite constitutes at least 13.7% of uranium mill ore. Part of this material (less than 10% in Elliot Lake ores) is dissolved in the leaching pachucas. Assuming that the remainder constitutes 12% of the ore, the above dissolution rates for feldspar can be used to estimate concentrations in the pore water assuming that feldspar data is a reasonable model for sericite dissolution. These data give an aqueous concentration of 13 mg K/L, 9 mg Al/L and 9 mg Si/L in infiltrating rain water leaving the unsaturated tailings if the pH were 3 and above. The concentrations in the infiltrating rain water would be 130 mg K/L, 90 mg Al/L and 90 mg Si/L if the pH were 2 and if no chemical precipitation occurred. Since the solubility limit for amorphorus Si is approximately 60 mg/L (neglecting ionic strength corrections), the concentration in infiltrating rainwater would be less than 90 mg Si/L.

In the leaching tanks, the pH is approximately 0.4. The data in Figure 11.11 suggest a feldspar dissolution rate of 10^{-13} mol/cm^2/s. Assuming the solid/liquid ratio in the leaching pachucas of 4,600 kg solids/1,616 kg water and 100 um sericite particles constituting 13.7% of the ore results in 3.4×10^7 feldspar particles per litre. For a 36-hour leaching time, the calculated leaching water concentrations are 130 mg/L K, 90 mg/L Al and 90 mg/L Si at 25°C and 2,600 mg/L K, 1,800 mg/L Al and 1,800 mg/L Si at 55°C. Again, the silica concentration should be limited by the solubility limit of amorphorus silica provided that nucleation kinetics of amorphorus silica are sufficiently fast.

In the leaching puchacas of Elliot Lake mills, the observed concentrations of these three elements are of the order of 1,000 mg/L K, 3,000 mg/L Al and 60 mg/L Si. The calculations from the kinetics suggest that all of the observed potassium can be explained by dissolution of sericite. But, only a portion of the observed aluminum is explained by dissolution of sericite.

11.6 Dissolution Kinetics of Clays and Micas

General

The dissolution kinetics of clays have been studied by Osthaus (1955), Miller (1965, 1968), Coleman and Craig (1961) and Cabrera and Talibudeer (1978). This work has been used by

Bouti (1983) in a study of H^+ adsorption onto clays and the breakup of clays due to acidic rainfall.

Osthaus (1955) determined that the dissolution of octahedral Al, Mg and Fe in several montmorillonites followed first order kinetics at the same rate for each element while dissolution of tetrahedral Fe and Al followed first order kinetics at a different rate.

Miller (1965) studied the rates of release of aluminum from montmorillonite and kaolinite clays by acid dissolution at 105°C. The following reaction was assumed to take place:

$$\text{Lattice-Al} + \text{H (from solution)} \Longleftrightarrow \text{lattice-H} + \text{Al (in solution)} \qquad (11.32)$$

Miller found that the release of Al from montmorillonite followed pseudo first-order kinetics ($d\,Al/dt = -K(Al)$) where $K = K^1\,(H)$. The same rate constant was obtained for both 1 um and 2 um particles. The release of Al followed pseudo zero order kinetics for kaolinite ($d\,Al/dt = -K$) where $K = K^1\,(H)$. The rate was found to depend on particle size. He proposed an all-surfaces (edges and planar) attack for montmorillonites and a diffusion controlled edge attack for kaolinite. Miller (1968) verified the edge attack on kaolinite but was unable to verify that all surfaces are attacked on montmorillonite.

Coleman and Craig (1961) found that spontaneous alteration of H- bentonite followed first-order kinetics. Measurements at 30, 50 and 70°C showed that the rate constant K approximately doubled for each 10° rise in temperature.

The rates of release of Al by NH_4NO_3 leaching of "Al-saturated" minerals at pH 3 were studied by Cabrera and Talibudeen (1978). Their work suggests that Al ions migrated from both the surface layers and the matrix cores of kaolinite, montmorillonite, illite and biotite, but only from the matrix core of muscovite. For 0.25 to 0.5 um kaolinite and montmorillonite, a rapid exchange reaction occurred in less than one hour; this accounted for approximately 80% of the surface aluminum. The rest is lost by first-order kinetics.

Other more recent work on clay dissolution has been undertaken by AECL. Much of this work is at high temperatures, a range not relevant to ambient environmental conditions.

Application to Tailings Management

These rates for clay dissolution have not been used to calculate concentrations in leaching pachucas and tailings. But the general order of kinetics can be used to estimate the gross behaviour of different clays. In general, it is expected that expandable clays such as montmorillonite will be broken up in the leaching tanks whereas clays such as kaolinite and chlorite $(Mg, Fe, Mn)_6 (AlSi_3)O_{10}(OH)_8)$ will remain relatively more stable. These latter clays would be expected to remain after milling and to furnish adsorption sites, etc. in the tailings. The clays which break up are expected to furnish some of the cations found in the leaching pachucas.

11.7 Dissolution Kinetics of Nickel Arsenide Minerals

Data describing dissolution kinetics of nickel arsenides are sparse. Mill operating data have not been obtained. Data from laboratory scale studies (Sherritt, 1980) suggest leaching of 60 to 80% of As and 55 to 70% of Ni after 2 hr at 70°C.

Data for leaching of these minerals from tailings (e.g., as a function of pH) has not been made available. The initial mineralogical composition of tailings is required to assess such data. The laboratory data (Sherritt, 1980) suggest that 60 to 80% of arsenic may be present as calcium arsenate and 40 to 20% as a residual arsenide mineral, while monitoring data (Knight, 1985) suggest that calcium arsenate constitute 70% of arsenic.

11.8 Dissolution Kinetics of Chalcopyrite

Data describing dissolution kinetics of chalcopyrite are sparse. Laboratory design data (Sherritt, 1980) suggest that 30 to 60% of copper is leached in 2 hr at 70°C; whether this Cu is in chalcopyrite is unclear.

A plausible hypothesis for modelling chalcopyrite is to consider it as a pyrite mineral because the iron sulphide part of $CuFeS_2$ would provide energy for the growth of T. ferrooxidans. That is, one would use similar rate constants for chalcopyrite oxidation as for pyrite oxidation. This may provide an under-estimate of chalcopyrite oxidation rate because heap leaching studies show that chalcopyrite oxidizes more rapidly than pyrite. What role that the copper ion has in modifying this rate (as a bacterial inhibitor, or as having different energy involved in its oxidation) is unclear.

11.9 Dissolution Kinetics of Zn, Mn, Co

Certain elements such as Zn, Mn and Co are found as trace quantities in pyrite minerals. Recently, stoichiometric relationships have been found between these metals and iron and sulphate concentrations in Elliot Lake tailings' pore water (N.M. Dubrovsky, pers. comm., 1985).

It is our hypothesis that one can usefully model the dissolution kinetics of such metals by using the dissolution rate of pyrite and the stoichometry of each metal to iron or sulphur in the pyrite.

11.10 Dissolution Kinetics of Radionuclides

In comparison to the work on calcite, gypsum, feldspar and quartz, models of dissolution and the associated kinetic data are quite sparse. In particular, kinetic data for residual minerals represent a substantial gap in the literature examined.

For NUTP purposes, kinetic data are required for the following minerals:

- U-minerals in the ore,
- residual U-minerals in the tailings,
- Th-232 minerals in the ore,
- residual Th-232 minerals in the tailings,
- thorium hydroxide (Th-232 with a small mass of Th-230),
- Ra-226 and Ra-228 in gypsum,
- Ra-226 and Ra-228 in barite and anglesite,
- Pb-210 in gypsum, and
- Po-210 in gypsum.

An order-of-magnitude estimate of dissolution rates for U-minerals and Th-232 minerals in the ore can be established by evaluating leaching tank data. For example, Rio Algom's rule of thumb for their ores is that approximately 50% of U (and hence Th-230, Ra-226, Pb-210 and Po-210) are leached in the first tank (detention time 3 hr) and that 93 to 97% is leached after 36 hours at 55 to 60°C. With respect to Th-232 minerals, CANMET has suggested a rule of thumb that 50% of Th-232 minerals are leached in the leaching tanks of Elliot Lake ores (E. Joe, pers. comm.). This assumption was used in a previous modelling study (BEAK, 1982). It suggests that 50% of Th-232 minerals (and hence Th-232, Ra-228, Th-228) are leached in 36 hours at 55 to 60°C.

Kinetic data for residual U-238 and Th-232 minerals have not been found. But some available data could be analyzed to infer rough values for these kinetics. The old Nordic tailings used in the CCIW lysimeters for five years have been characterized for Th-230, Th-232 and Th-228 and H^+ leaching rates and residual activity of these thorium radionuclides in the solids. It is improbable, at pH 1 to 3, that any residual thorium hydroxide formed in the mill would be found in these tailings at the start of their leaching period. Accordingly, these leaching rates can be used to estimate dissolution rate of residual U-238 and Th-232 minerals and their daughters (U-234, Th-230, Ra-226, Pb-210, Po-210, Th-232, Ra-228, Th-228). The size of the minerals and mineral identification would be required; SEM could be useful here. The recent models of Riese (1983) should be used to check for possible thorium adsorption at pH 2.

Kinetic data for thorium hydroxide dissolution has not been found. Analysis of its effective solubility product as a function of pH and reaction control concepts (see Section 11.1 above) would allow inferences about its kinetics.

Kinetics for Ra-226, Ra-228, Pb-210 and Po-210 will depend upon the kinetics of the parent solid. Kinetics of gypsum suggest that solubility may be assumed for time scales of one year. The kinetics of dissolution of barium sulphate and of a mixed (Ba, Ca) sulphate await future evaluation.

11.11 Summary of Concentrations Predicted by Dissolution Kinetics

A summary of concentrations predicted by dissolution kinetics for quartz and sericite are given in Table 11.7. The concentrations have been calculated in Sections 11.4 and 11.5. They are for infiltrating rain water leaving the two m deep unsaturated zone.

11.12 Recommendations for Further Work on Tailings Kinetics

The above work on kinetics suggest the following perspective:

TABLE 11.7: SUMMARY OF CONCENTRATIONS PREDICTED BY DISSOLUTION KINETICS

Mineral	Concentration (mg/L) Si	K	Al	Conditions
Quartz	0.9	-	-	25°C; tailings
Amorphorus Silica	15	-	-	25°C; all tailings are covered by armor silica
Feldspar	9	13	9	25°C; tailings; pH = 3
	90*	130	90	25°C; tailings; pH = 2
	90*	130	90	25°C; leaching pachucas; pH = 0.4
	2,800*	2,600	1,800	55°C; leaching pachucas; pH = 0.4

*Solubility limit of amorphorus silica would limit this value.

1. For certain minerals, the kinetics are sufficiently well known that their dissolution may be viewed as controlled by solubility concepts for one year time frames. Examples include calcite.

2. For certain minerals, field and laboratory observations suggest that they may be considered as at equilibrium. An example is gypsum. However, for such minerals, laboratory work on mechanistic kinetics would be useful to confirm the exact time scales involved.

3. For certain minerals (e.g., feldspar, quartz), the dissolution kinetics are sufficiently known to infer useful expressions for modelling purposes. Further calibration work in sulphuric acid solutions would be useful to confirm the exact magnitude of rates. The literature data permits useful ± estimates for setting distributions on the kinetic parameters for feldspar and other similar alumino silicates.

4. For certain minerals (e.g., clays) some dissolution work has been done. This dissolution work needs to be amplified by a more in-depth analysis of the literature. Also, knowledge of formation of other minerals in other environments and reaction-code pathway calculations need to be undertaken to confirm the probable transformation pathways before these kinetics are analysed in more depth.

5. For minerals containing radionuclides, more in-depth analyses of the kinetics of U-238 and Th-232 minerals in the ore and as residual minerals in the tailings are required. This can be initiated by obtaining more mill operating data and analysing data from lysimeters. Some laboratory work would also appear to be necessary.

12.0 DIFFUSION AND REACTION CONTROLS ON PYRITE OXIDATION

The rate of pyrite oxidation in the uranium tailings is a critical geochemical process. It generates acid which indirectly controls the solubility of many tailings constituents. Because the reaction is favourable at the earth's surface and because the oxidation process is governed by kinetics, it is important to understand the controlling mechanisms involved. In this chapter a brief overview of the controlling factors involved in the oxidation process is presented. A simplistic model is also presented to show the effects of limiting oxygen transport when pyrite depletion occurs from the surface downward into a tailings mass.

12.1 Oxidation Reaction

Pyrite is a ferrous sulphide mineral in which both elements are subject to oxidation. The complete oxidation of one pyrite formula (FeS_2) involves the transfer of 15 electrons. The overall reaction consists of several intermediate steps. There is some question as to whether "complete" oxidation occurs in all environments but because there is not much evidence for the persistence of reaction intermediates, such as elemental sulphur in most environments, it is probable that complete oxidation is the most significant process. When this occurs, the reaction can be represented by;

$$FeS_2(s) + 7/2O_2 + 1/2H_2O \dashrightarrow Fe^{3+} + 2SO_4^{2-} + H^+ \qquad (12.1)$$

At pH values of about 4 or greater, significant precipitation of ferric hydroxide will occur and result in further generation of acid as indicated by;

$$Fe^{3+} + 3H_2O \dashrightarrow Fe(OH)_3(s) + 3H^+ \qquad (12.2)$$

This last reaction is reversible. When the pH decreases, the solubility of the ferric hydroxide increases and hence the extent of reaction (12.2) decreases, precluding it from contributing significantly to acidification under those conditions.

12.2 Kinetic Controls

Of all naturally-occurring minerals, the weathering of pyrite and mechanisms involved have probably been the most closely studied. Much is known about the macroscopic factors controlling the rate of oxidation, but because of the complex nature of the reaction, little is understood with regard to the microscopic or mechanistic details. Recent reviews of oxidation kinetics are given by Lowson (1982) and Nordstrom (1982). Some theories on surface related mechanisms are provided by Tributch and Bennett (1981a, 1981b) and by Goldhaber (1982). A brief summary of the known controls is given below. The major controlling factors include: (1) surface area; (2) oxygen; (3) temperature; (4) pH; (5) ferric iron; and (6) bacteria.

Chemical Oxidation

As with many mineral dissolution reactions, surface area plays a key role. The chemical rate of reaction is first-order with respect to surface area in the initial stages of the reaction. This order of reaction rate appears to change with time but this may be due to reaction coatings which form on the pyrite surface, altering the observed oxidation rates (Cherry et al., 1984).

The concentration of oxygen appears to control chemical oxidation rates according to a Langmuir-type adsorption isotherm (rate of oxidation vs. partial pressure of oxygen, P_{O_2}). This behaviour implies that at low concentrations of oxygen, the rate is proportional to P_{O_2} levels (first-order) while at high concentrations, the rate is independent of oxygen levels (zero-order) implying that the surface is completely saturated (Nicholson, 1984).

The chemical reaction rate is affected by temperature. Using the Arrhenius concept the activation energy has been determined under various conditions to be on the order of 80 to 90 kJ mol^{-1} for conditions in the natural environment. This represents an approximate tripling of reaction rate for every 10^oC rise in temperature.

The solution pH can also control the chemical rate of oxidation. Although, this has not been related to an actual mechanism (Nicholson, 1984) it has been observed that the rate is a function of pH to a fractional power with the exponent in the range of zero to one. The observed trends indicate that the chemical rate of oxidation decreases with decreasing pH. This is consistent with what is known about the kinetics of ferrous iron oxidation in solution and it would be expected that pyrite would be more stable, chemically, in acidic solution (i.e., in the absence of bacteria).

The concentration of ferric iron in solution also contributes to the oxidation reaction. Ferric iron reacts with the pyrite surface to form sulphate and ferrous iron. This reaction is relatively rapid and depends on the concentration of Fe^{3+}, as well as available surface area of pyrite. In most environments, Fe^{3+} concentrations will be limited to low values by the solubility of $Fe(OH)_3$ and therefore will not represent an important source of oxidant. Under acidic conditions, however, Fe^{3+} concentration levels can be high and may provide a significant contribution to reaction with the pyrite surface. Furthermore, in microbially active systems, relatively large quantities of Fe^{3+} are rapidly generated, thereby providing a greater source of oxidant. It should be noted that this Fe^{3+} is depleted rapidly during its reaction with the pyrite surface. Observation of significant (FeIII/FeII) ratios (greater than 0.01) in tailings leachate suggests that microbial activity is a significant factor.

Biochemical Oxidation

The role of acidophilic bacteria in the catalysis of pyrite oxidation has been well documented (SENES, 1984; Lungden and Silver, 1980). While the role of various factors has been shown above with respect to chemical oxidation rates, the rate of oxidation resulting from bacterial action does not necessarily parallel this behaviour. Thiobacillus ferrooxidans is the organism responsible for catalysing the oxidation of Fe^{2+} to Fe^{3+}; the production of Fe^{3+} catalyzes the reaction at the pyrite surface.

When bacteria are the dominant control on reaction rates, the surface area of pyrite appears to play a similar role to that for chemical oxidation. The effect of oxygen concentration may not be of significance, however, until levels below about 1% of the saturated value. The dependence on oxygen concentration below these levels appear to be linear. Because bacterial metabolism is involved, the temperature range has an optimal level (approx. 30°C) with declining rates on either side of this value. Similar behaviour is observed for variations in pH with optimal values in the range of 2.5. Most evidence suggests that bacterial catalysis of the oxidation reaction is insignificant at pH values above about 4.0 (Arkesteyn, 1980). This implies that the acidification of pore water associated with pyritic material is initiated through strictly chemical processes from the pH range of neutral to about 4.0.

It is important to note that, although a number of factors affect the rate of oxidation, the role of oxygen is the most critical. Without oxygen, there would be no reaction at all. And even though Fe^{3+} may act as an alternative oxidant, this species would not be regenerated if not for the presence of O_2. Hence, in this chapter, it is hypothesized that a key to quantifying the extent of pyrite oxidation is the concentration of oxygen and the control on its availability.

12.3 Transport Control

Oxygen movement into a porous material below ground level can be a slow process. When pyrite oxidation can consume oxygen faster than it is being transported to the reaction sites, then transport controls the overall oxidation rate. Because some oxidation will occur immediately below the tailings surface where oxygen is readily available and also at depth if oxygen penetrates into the unsaturated zone of the deposit, it is expected that actual rates will reflect a control that is intermediate between the kinetic and transport extremes. A more quantitative approach to evaluating the resulting oxidation rates can be made by modelling the movement and uptake of oxygen in a generic unsaturated zone.

A schematic of the physical setting, moisture content, oxygen concentrations and pH values is given in Figure 12.1. The profiles show the potential evolution from a fully water-saturated deposit with little oxygen and neutral pH in the early active stages of the deposit to a better-drained medium containing more oxygen and lower pH pore water. This schematic is now abstracted and a mathematical model developed to examine the relative importance of transport and diffusion upon pyrite oxidation rates.

Air Diffusion - Pore Water Oxidation Model

Oxygen movement in a subsurface unsaturated porous medium is controlled by diffusion. Although there will be some deviation from expected diffusive transport at shallow depths (about 20 cm or less) the movement of oxygen will be dominated by diffusional processes below this level and therefore can be modelled with the appropriate differential equations.

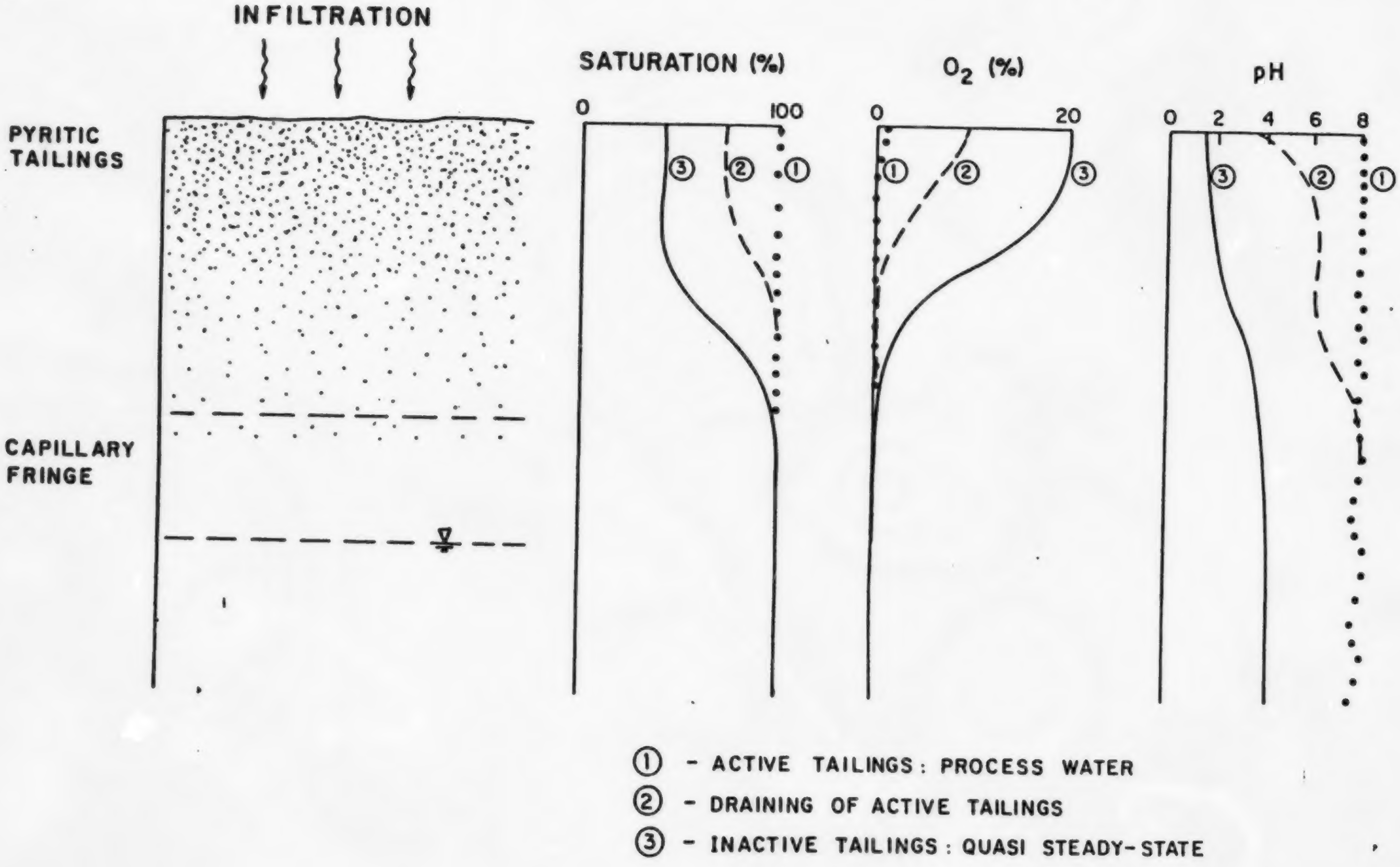

FIGURE 12.1: SCHEMATIC DEPTH PROFILE THROUGH A PYRITIC TAILINGS DEPOSIT SHOWING THE PHYSICAL SETTING, WATER SATURATION, OXYGEN AND PORE WATER pH

With reference to Figure 12.1, vertical diffusional transport and removal of oxygen is described by the equation;

$$D_e \frac{\partial^2 C}{\partial x^2} - KC = \frac{\partial C}{\partial t} \tag{12.3}$$

in which D_e is the effective diffusion coefficient for gaseous oxygen in the medium (L^2/T), C is the concentration of oxygen (M/L^3), K is the composite first-order rate constant (T^{-1}), x is depth (L) and t is time (T).

The value of De in this equation can vary over four-orders-of-magnitude with the upper value representing diffusion through air-filled pores only and the lower value representing diffusion through completely water-filled pores. The range of values of K could be equally as large. The specific value of the rate constant depends on the physicochemical conditions and whether or not microbial catalysis is significant. Low values of K represent conditions of near neutral pH values with low values of available surface area. A high value, perhaps six orders-of-magnitude greater than the lower limit, would be found in active microbial systems under near-ideal conditions. Because of the large variability of parameters and the uncertainties in determining their appropriate values for a particular environment, it is useful to examine scenarios that bracket probable behaviour. In this manner, trends can be identified and a better understanding of controlling factors gained.

In addition to simple oxygen transport and consumption, another constraint on the system is the mass law that pyrite mass will be consumed with time. Near complete pyrite depletion in the uppermost zone will cause a downward movement of the oxidation front over extended periods.

In an attempt to simulate such behaviour, a model was developed based on Equation 12.3 that would account for:

- diffusive transport and consumption of oxygen,
- shrinking size of pyrite particles, and
- depletion of pyrite in the appropriate zones.

The model also calculates the flux of oxygen to allow comparison of predicted mass transport as well as predicted concentrations of oxygen.

Some simplifications (steady-state, spherical particles) have been made for computational purposes. The analytical solution for Equation (12.3) shows that steady-state is approached rapidly in most cases (Nicholson, 1984). It was therefore, decided to use the steady-state solution (dC/dt=0) to Equation 12.3. The loss in particle mass and subsequent shrinkage was calculated by assuming that spherical particles of a uniform radius are present throughout the medium (Levenspiel, 1972) at time=0.

The loss of pyrite mass was calculated for finite cells that represent a unit cross-sectional area and whose length is sufficiently small to maintain definition of gradients with depth. In this manner, the continuous steady-state solution to oxygen transport/consumption was incorprorated into a reaction cell model that simulates time-step progression of pyrite oxidation. The computational errors associated with this approach are small (Thomann, 1972).

Values for parameters were chosen to represent realistic limits. The low reaction-rate-constant represents oxidation at near - neutral pH (Nicholson, 1984) while the upper limit represents a potential value that could be representative of microbial activty. The high diffusion coefficient represents an approximate value for diffusion of oxygen through air. The lower value for this parameter represents an intermediate one between diffusion in air and that in water. This implies that the cases tested reflect conditions in an unsaturated zone, with significant air-filled porosity. A summary of the parameters used in the model is given in Table 12.1.

12.4 Model Results

The oxidation rate model calculates an exponential decrease of oxygen with depth over most oxygen concentrations but shows asymptotic behaviour near zero oxygen concentration with depth (see Figure 12.2). The depth of oxygen penetration varies with the values of K and D. In general, the higher the ratio of K/D the shallower is the depth of penetration of oxygen. In the cases studied here, the width of the effective oxidation zone (defined as the zone having oxygen concentrations greater than 1% of surface concentrations) varies over four orders-of-magnitude (Figure 12.3).

TABLE 12.1: SUMMARY OF PARAMETER VALUES FOR THE OXIDATION/DIFFUSION MODEL TEST CASES

Global Parameters	Value	Units
Bulk density	1600	$kg\ m^{-3}$
Moisture content	0.20	$m^3\ m^{-3}$
Pyrite content	0.05	$kg\ kg^{-1}$
Initial particle diameter	70	$10^{-6}\ m$

Case	D ($m^2\ h^{-1}$)	K_p ($m\ h^{-1}$)	Cell depth (m)
I	5×10^{-2}	5×10^{-6}	0.2
II	5×10^{-4}	5×10^{-6}	0.02
III	5×10^{-2}	5×10^{-2}	0.0025
IV	5×10^{-4}	5×10^{-2}	0.000125

FIGURE 12.2

Oxygen Concentration Profiles for Different Values of K/D

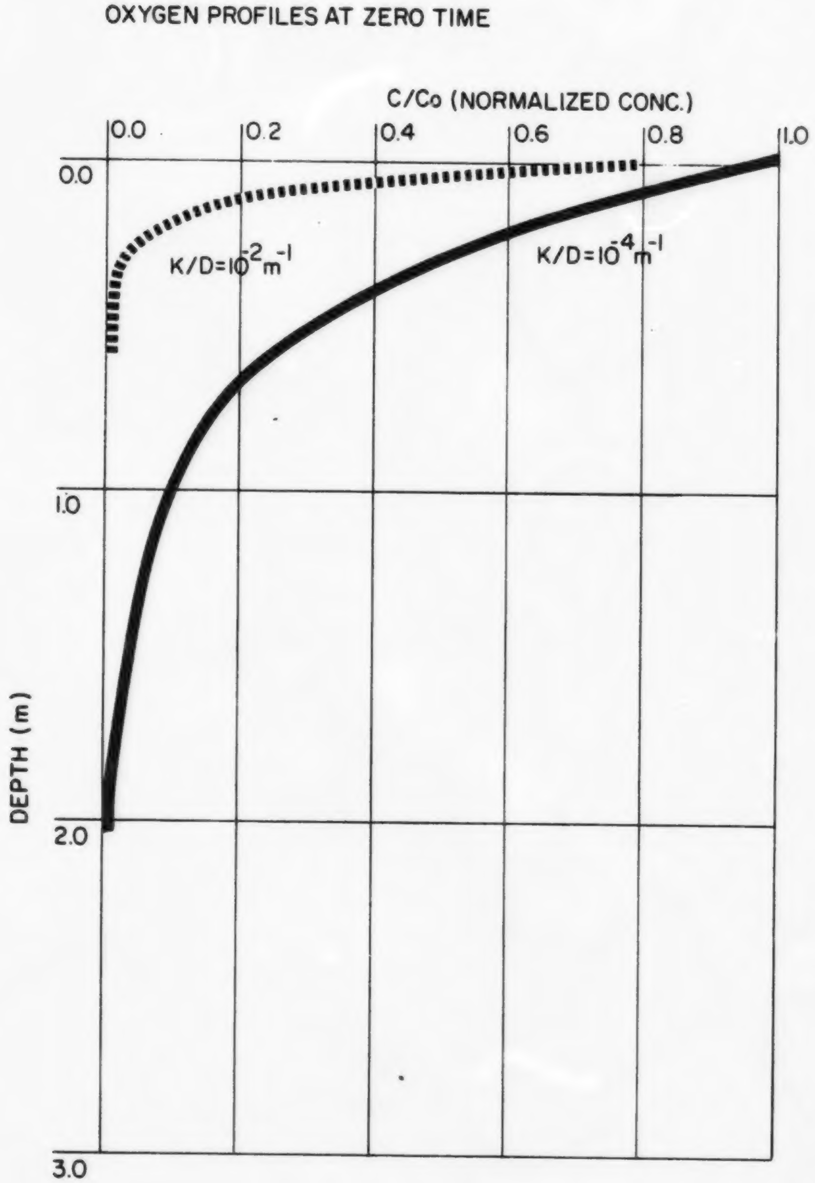

FIGURE 12.3

Effective Depth of Active Oxidation Zone Versus the Ratio of D/K

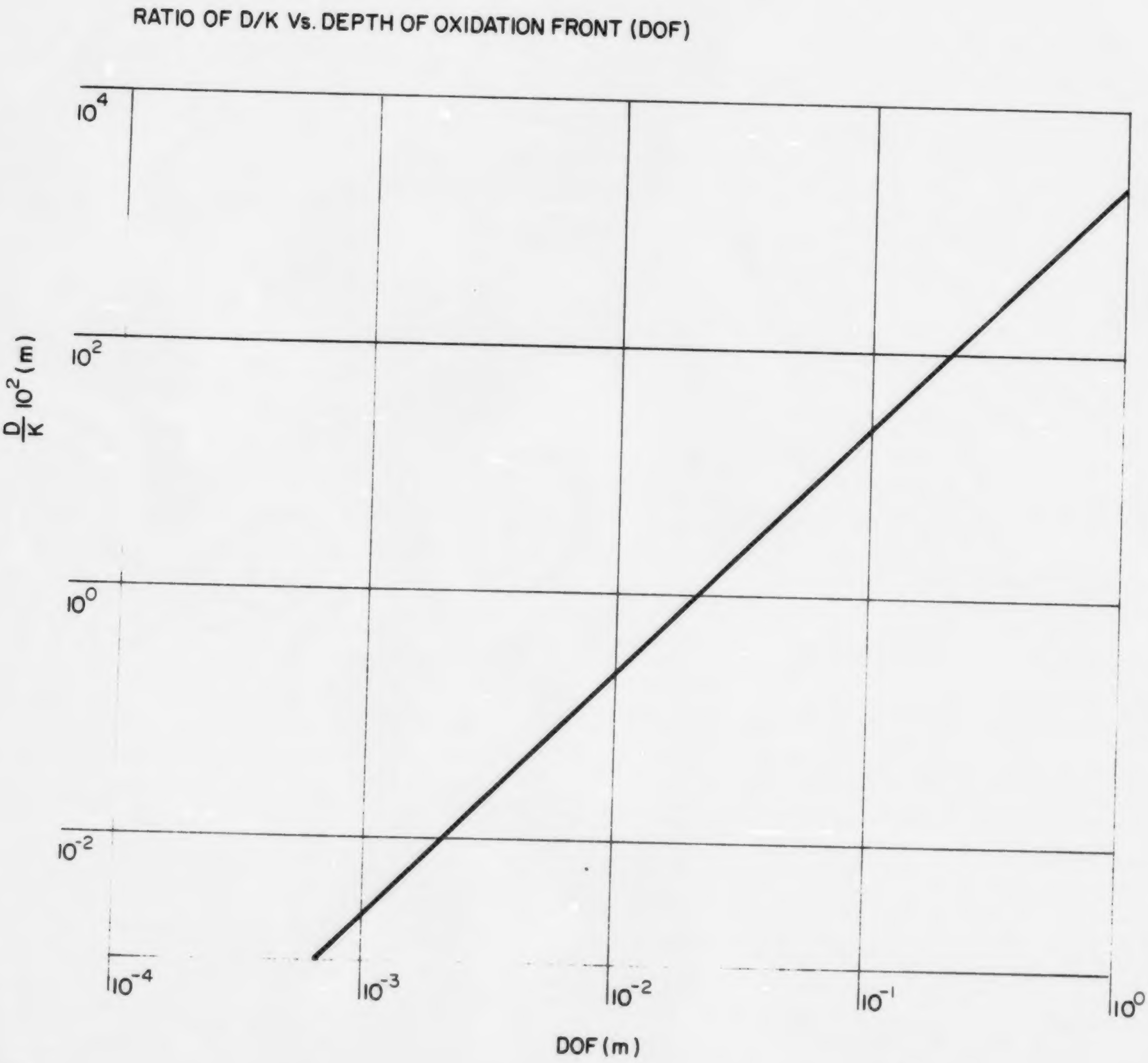

The penetration of oxygen into the pyritic deposit is shown to change with time. Profiles of oxygen concentration with depth for different times are shown in Figure 12.4. In early stages, the profile reflects the expected exponential decrease with depth. At later stages, however, the oxygen concentrations are calculated to decrease linearly over the topmost region but to vary exponentially in deeper zones. The linear region is the zone in which pyrite has been depleted.

The flux of oxygen and hence the net rate of acid generation depends on the product of K and D; the flux is proportional to $(KD)^{1/2}$. As the pyrite depletion zone moves downward with time, the flux decreases as shown in Figure 12.5. This implies that the depth to the top of the active oxidation zone has a significant effect on the net generation of acid in the pyritic zone. It also suggests that the diffusivity of the tailings itself may be the overall controlling factor of pyrite oxidation after the initial phase of pyrite depletion at the surface, and that the rate constant for oxidation may not be a critical parameter at these later stages.

The effect of changing fluxes with time is also illustrated by a plot of the time required to deplete the pyrite in one cell (normalized for the thickness of that cell) versus the depth of the cell within the profile (see Figure 12.6a to d). The longer times needed to remove the pyrite in cells at greater depth indicate that there are lower fluxes of oxygen into the active oxidation zone. The inverse slopes of these plots represent the relative change in time for pyrite depletion with depth, the values of which are different for the four cases of K/D used here. A high value for this parameter suggests a more significant relative decrease in oxidation rates with time. A summary of these values for both the high and low values of both K and D (Table 12.2) shows that the main effect is due to the value of D and not to K. Although there is some effect of K on the decreased fluxes for the low D cases, it is relatively small compared with the overall difference between the high and low D scenarios.

12.5 Conclusions

The overall conclusions from the simulations are as follows:

- over the long-term, pyrite oxidation rates and therefore, fluxes of acid into the tailings pore water will decrease with time;

FIGURE 12.4

Oxygen Concentration Profile With Time

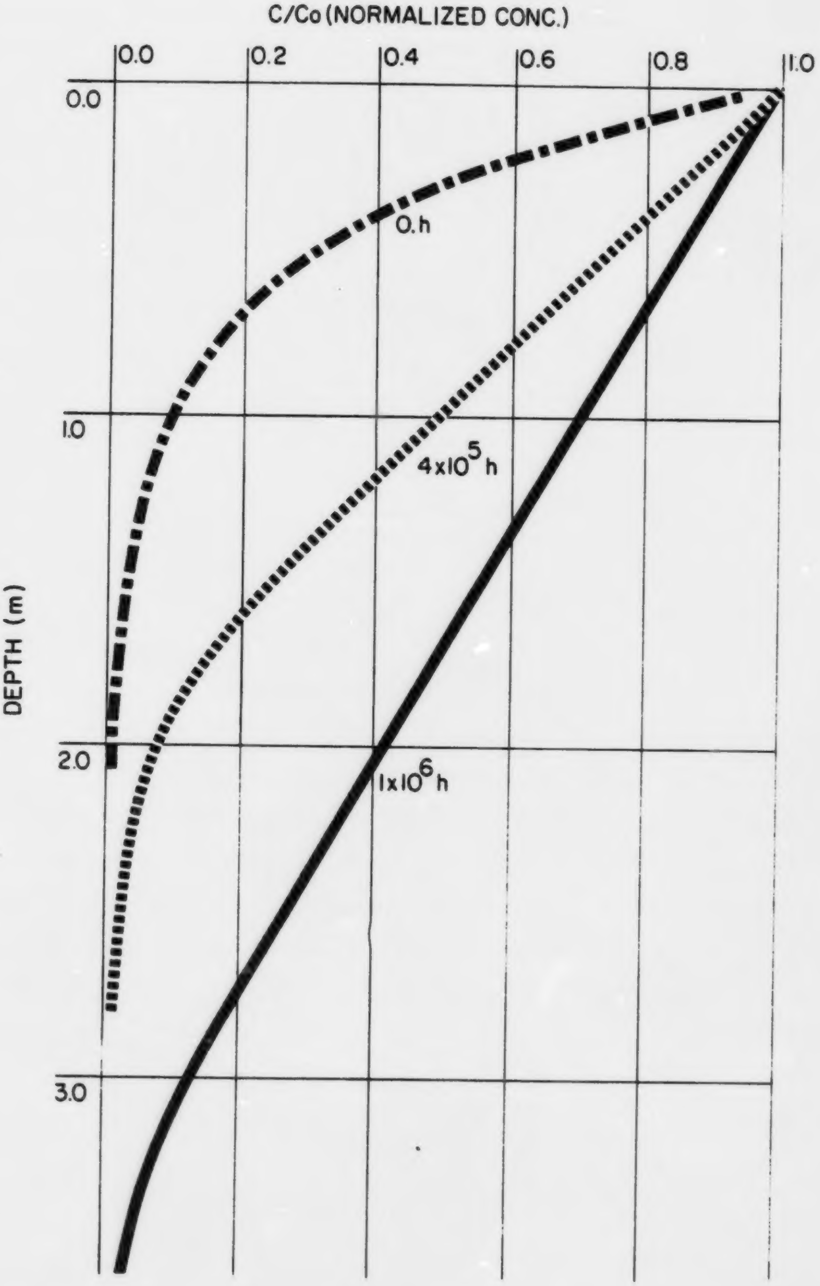

FIGURE 12.5: Oxygen flux as a function of time

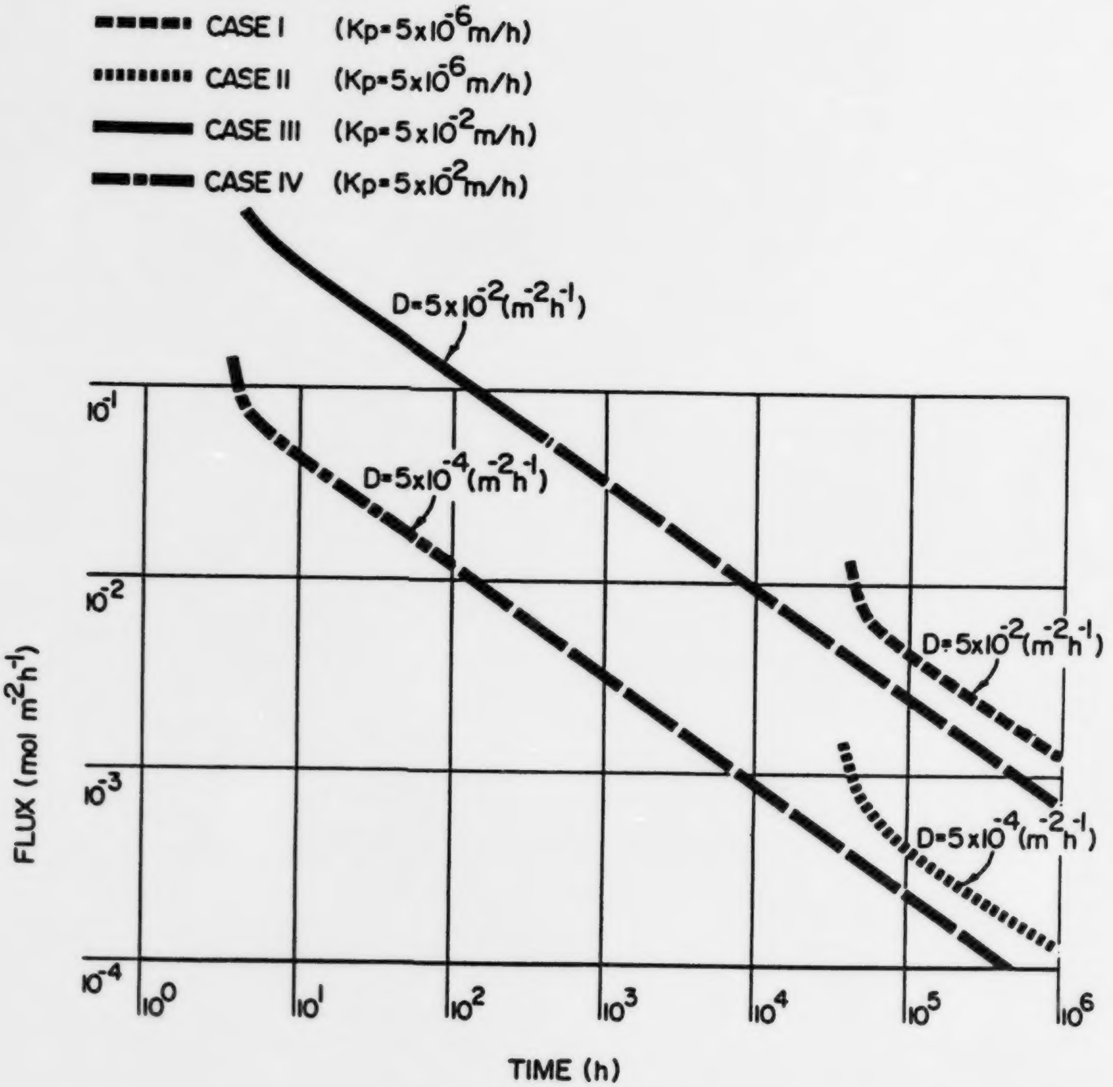

FIGURE 12.6a

Time to Deplete Pyrite per Unit Depth Versus Depth;– Case I

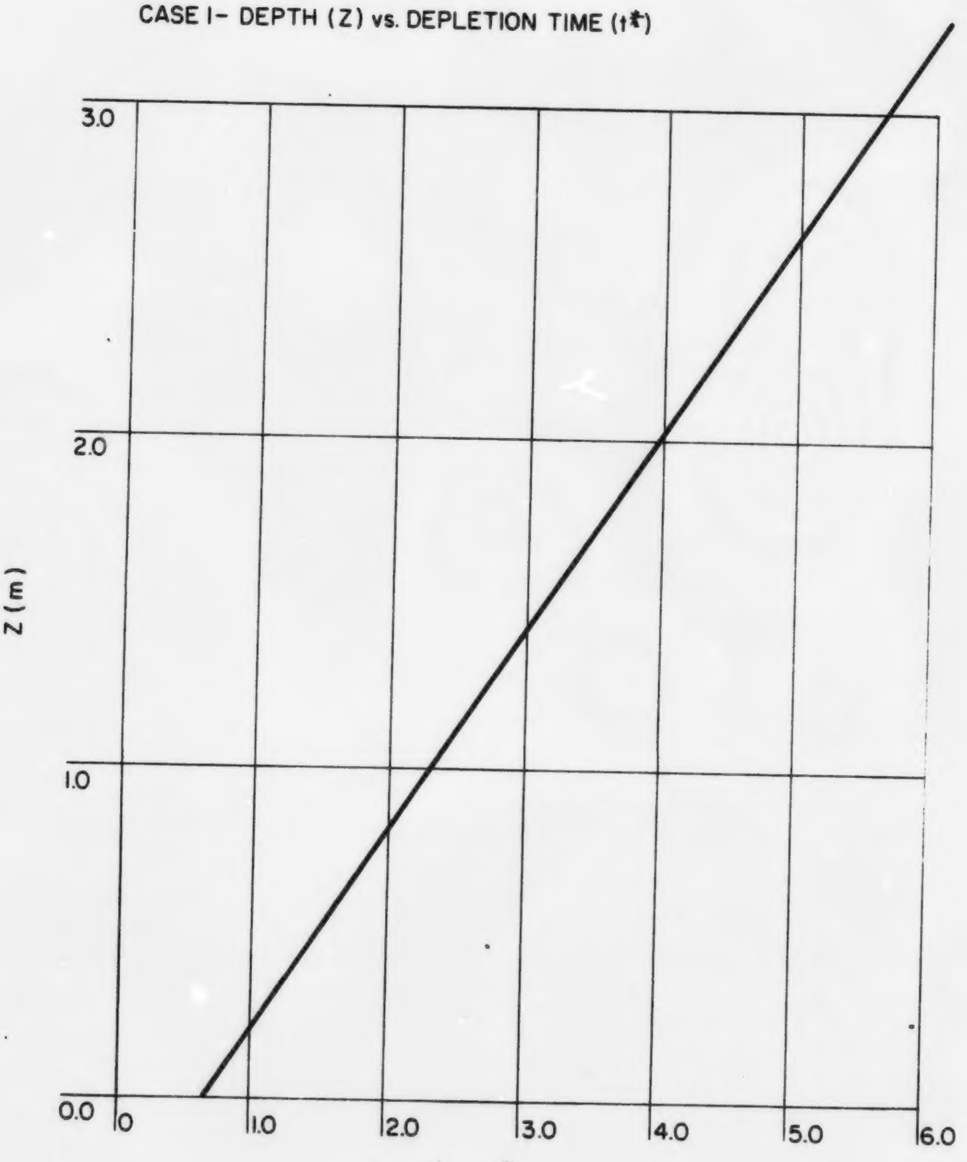

FIGURE 12.6b.

Time to Deplete Pyrite per Unit Depth Versus Depth–Case II

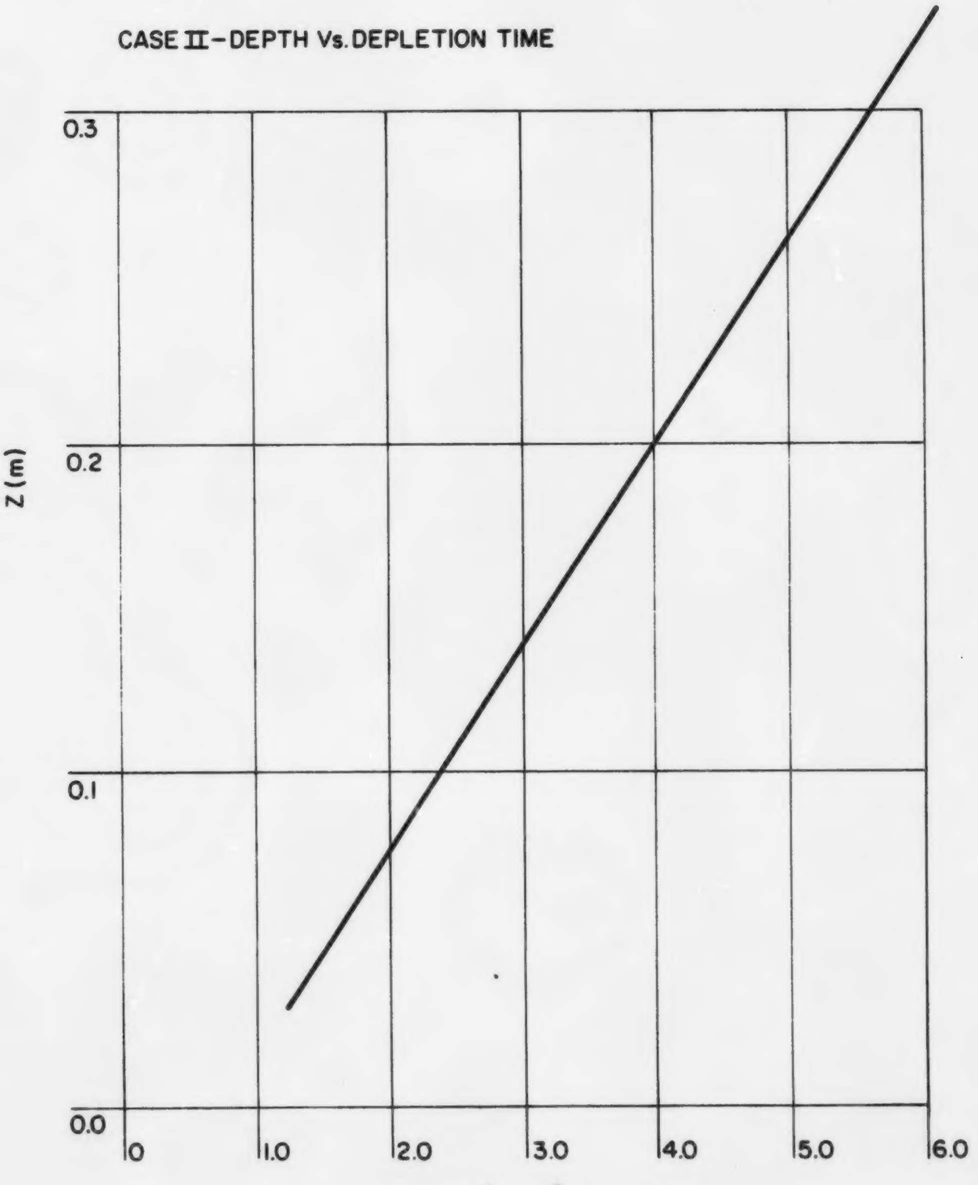

FIGURE 12.6c

Time to Deplete Pyrite per Unit Depth Versus Depth–Case III

CASE III DEPTH Vs. DEPLETION TIME (t*)

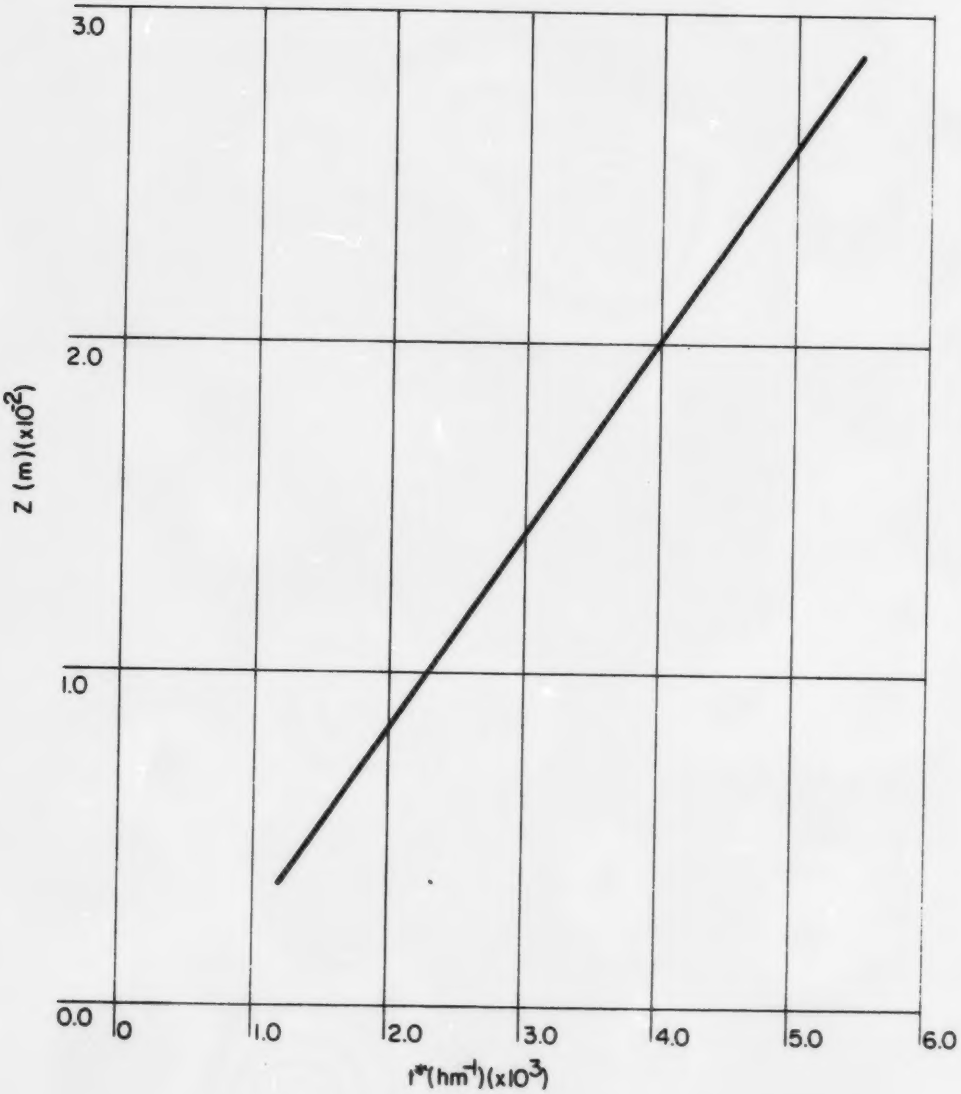

FIGURE 12.6d

Time to Deplete Pyrite per Unit Depth Versus Depth-Case IV

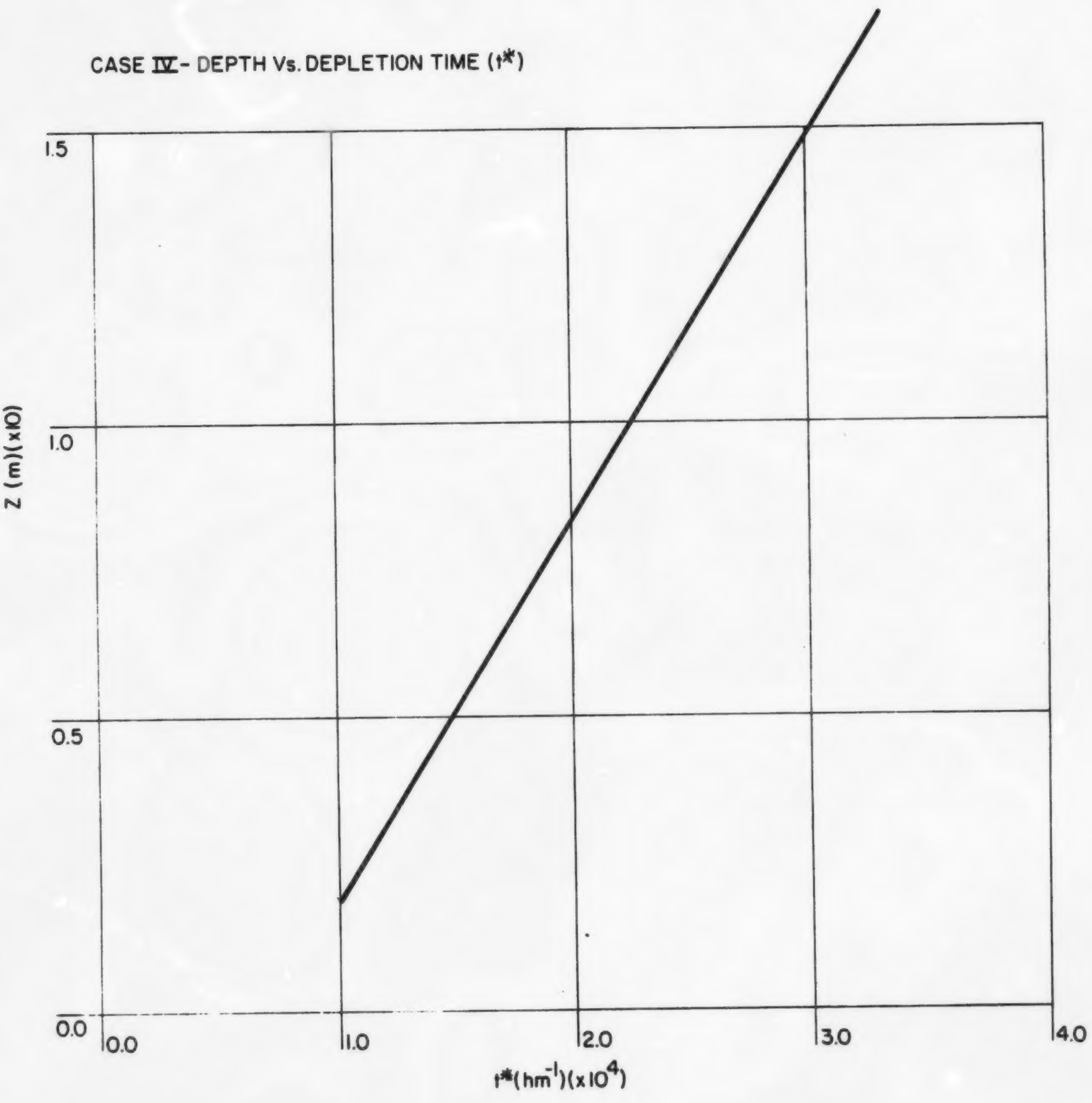

TABLE 12.2: A 2 X 2 TABLE SHOWING BETA X 10^{-5}

Note: higher beta indicates increased time for depletion with depth - (i.e., more signficant decreases in H^+ etc., flux with depth and time.

		K	
		Low	High
D	Low	163 (case II)	154 (case (IV)
	High	1.7 (case I)	1.7 (case III)

- an effective means of decreasing fluxes and acid generation is to maintain low diffusivities in the pyritic deposit; and

- the diffusivity of the deposit is more significant in controlling the effective acid production rates over the long term than the rate controls on pyrite oxidation (i.e., bacteria, etc.).

13.0 ADSORPTION AND CATION EXCHANGE PROCESSES

The interaction between species in solution and solid surfaces is complex and in general is not well defined. In many instances, the dissolved component adsorbs to surfaces in an irreversible manner or may adsorb rapidly with kinetically controlled desorption. In some cases, especially with trace quantities of radionuclides, the adsorption behaviour is specific to the geologic materials used. Cation exchange, however, is one process that is relatively well defined.

Adsorption and cation exchange conceptually represent the same process. Cation exchange is a sorption type process which involves identifiable displacement of one ion by another ion. Adsorption of elements present in trace quantities may or may not involve a displacement. For example, Ra-226 may adsorb to a negative site or it may adsorb by displacing a hydrogen ion from the surface. The latter example (H^+ displacement) is, in fact, an "ion exchange" but the change in H^+ concentration in solution will be so miniscule that it cannot be measured.

This chapter assumes that the linear distribution coefficient (K_d) will be the method used to describe adsorption phenomena for most metals in any probabilistic modelling effort. K_d is the ratio of the amount adsorbed to amount in solution. But to interpret laboratory and other data, it becomes essential to properly model the overall adsorption process using such models as the site-binding model (Riese, personal communication). Application of such a model has recently been demonstrated for Ra-226 and Thorium (Riese, 1983) onto quartz and kaolinite. For other metals adsorbed to surfaces such as clay, cation exchange models are assumed to form the basis for developing a model.

13.1 Factors Affecting Adsorption

The factors affecting adsorption include:

(i) type of surface (quartz, kaolinite, feldspar)
(ii) surface area and number of adsorption sites
(iii) ions in solution
(iv) amount of surface covered by other ions
(v) solution pH

(vi) solution ionic strength
(vii) degree of solution undersaturation or oversaturation
(viii) presence of organic matter
(ix) amount of fluid in contact with surface (i.e., m^2 surface area per m^3 solution)

Typically, laboratory and other efforts have examined the effects of pH, solution composition, and liquid-to-solid ratios.

Laboratory adsorption data for Ra-226 are presented in Table 13.1. They show that K_d varies as a function of barium concentration and the liquid-to-solid ratio. Other data (e.g., Rancon, 1974) shows that K_d for Thorium increases from 1 to 10^5 for a pH varying from 1 to5 and from 10^6 to 5 mL/g for a pH varying from 7.6 to 14. Some differences are also observed between laboratory and field K_d data.

Summary of Present Theory

At present, adsorption theory, as advanced by Stumm and co-workers and Davis and co-workers (see references), uses a surface complexation model to explain adsorption, competitive adsorption and pH effects upon adsorption. The surface is viewed as composed of three types of OH based groups as shown on Figure 13.1.The effects of pH are represented as follows:

$$SOH_2^+ \rightleftharpoons SOH + H^+ \qquad K_{a_1}{}^s = \frac{(SOH)\,(H^+)}{(SOH_2^+)} \qquad (13.1)$$

$$SOH \rightleftharpoons SO^- + H^+ \qquad K_{a_2}{}^s = \frac{(SO^-)\,(H^+)}{(SOH)} \qquad (13.2)$$

where S means the surface and $SOH_2{}^+$, SOH and SO^- are positive, neutral and negative groups associated with the hydroxyl group.

The constants $K_{a_1}{}^s$ and $K_{a_2}{}^s$ are called microscopic acidity constants.

TABLE 13.1 EFFECT OF THE LIQUID/SOLID RATIO AND BARIUM IONS ON RADIUM ADSORPTION BY SEDIMENTS (48) From

(AFTER BENES, 1982)

V/m ($cm^3 \cdot g^{-1}$)	$c_{Ba^{2+}}$ (molar)	Adsorption (%)	K_D ($cm^3 \cdot g^{-1}$)
10	10^{-5}	93.7	149
50	10^{-5}	81.9	225
500	10^{-5}	42.8	374
10	10^{-4}	91.1	103
50	10^{-4}	70.3	118
500	10^{-4}	42.2	365
10	10^{-3}	77.7	35
50	10^{-3}	48.4	47
500	10^{-3}	12.8	73

[a] Little-contaminated river bed sediment, particle size < 2 mm, solution for adsorption prepared from distilled water, original concentration of ^{226}Ra in the solution 740 $Bq \cdot ltr^{-1}$.

Table 13.2 ADSORPTION OF Al (111) ONTO QUARTZ
(From Hahn, 1969)

pH	Al Dosage (mol/L)	Concentration of Particles (g/L)	Γ_m (mol/m^2)	β $(mol/L)^{-1}$
4.5	(2.5-3) E-5	3-34	2.7 E-7	7.7 E04
4.75	(4.2-4.3) E-5	2-33	9.9 E-7	4.1 E04
5.0	(4.4-4.9) E-5	1-18	5.5 E-6	6.2 E04
5.25	(1.2-1.8) E-5	1-7	2.4 E-5	0.9 E04

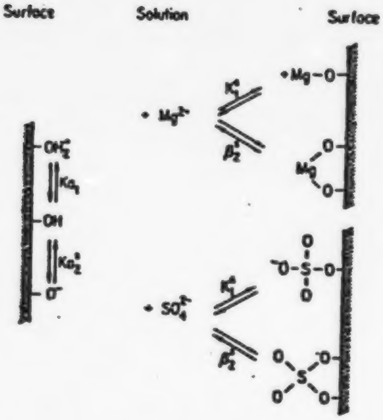
Surface
Solution
Surface
$-OH_2^+$
$K^s_{a_1}$
$-OH$
$K^s_{a_2}$
$-O^-$
$+ Mg^{2+}$
K_1^s
β_2^s
$^+Mg-O-$
Mg
$+ SO_4^{2-}$
$^-O-S-O-$
O
S

FIGURE 13.1 Interaction of Hydrous Oxides with Acid and Base and with Cations and Anions, exemplified for the specific adsorption of Mg^{2+} and SO_4^{2-}, is interpreted in terms of surface complex formation and ligand exchange equilibria. The surface coordination equilibria are given in Eqs. (1—6).

(from Sigg and Stumm, 1980)

For the reaction between a metal and a negatively charged site, one might represent it as

$$SO^- + M_e^+ \rightleftharpoons SOM_e \qquad K_1^s \tag{13.3}$$

and between a positively charge site and a negative ligand as

$$SOH_2^+ + L^- \rightleftharpoons SOH_2L \qquad K_2^s \tag{13.4}$$

Any reaction like reaction (13.3) or (13.4) is the basis for the Langmuir isotherm which is described as

$$T = Tm \frac{C}{\mathbf{Beta} + C} \tag{13.5}$$

where T is the amount adsorbed (mass/m^2) (SOM_e)

T_m is the maximum amount adsorbed (mass/m^2) = maximum number of sites to which the metal can adsorb ((SO^-) + (SOM_e))

C is the concentration of metal in solution

Beta is the concentration at which $T = 0.5\ T_m$ (also called the half saturation constant)

In reality

$$1/\mathbf{Beta} = K_1^s = \frac{(SOM_e)}{(SO^-)(M_e^+)} \tag{13.6}$$

Hence, **Beta** is sometimes called a function of the binding constant which describes how much metal can be "bound" to the surface.

Because the number of sites (SO^-) available for metal adsorption is a function of pH, T_m will be a function of pH. Furthermore, the model for surface complexation shows that K_1^s is a weak function of the amount of metal adsorbed.

Hence, one can say qualitatively that the Langmuir isotherm can be used to model adsorption, but that T_m and **Beta** will vary in a predictable way as a function of pH.

Modelling Efforts in the Literature

Using these ideas, various workers have had some success at modelling adsorption. Adsorption of fluoride into goethite (Figure 13.2) of orthosilicic acid (H_4SiO_4) onto goethite (Figure 13.3) and of iron, lead, copper and cadmium onto silica (Figure 13.4) have been successfully modelled. Of particular interest is the demonstrated ability to predict over an order of magnitude change in adsorption characteristics as a function of pH shift for some ions (e.g., fluoride adsorption, Figure 13.2) while others only show a small increase with change in pH (e.g., H_4SiO_4 adsorption, Figure 13.3).

Adsorption and Surface Precipitation

In addition to adsorption, surface precipitation may occur. Figure 13.5 shows data for the adsorption of Al^{3+} onto silica (Hahn, 1969). Data from the first part of the adsorption curve of Figure 13.5a was used to derive the Langmuir fits of Figure 13.5b and the values given in Table 13.2.

Table 13.2 shows that both the maximum adsorption density (T_m) and the binding constant (Beta) change with pH. T_m (i.e., the number of sites to which Al can adsorb) changes by over 2 orders of magnitude from pH 4.5 to pH 5.25, while Beta is relatively constant until the pH exceeds 5.0. Preliminary modelling efforts suggest that only part of the change in T_m can be explained by the effects of pH upon ionization of surface groups.

It is probable that formation of a surface precipitate (($Al(OH)_3$) occurs upon the silica solids, particularly at pH 5.25. This is supported by two pieces of evidence. First, at pH 5.25, the solution is supersaturated with respect to amorphorus $Al(OH)_{3(s)}$ while it is not supersaturated at pH 4.5. Secondly, Hahn (1969) argues that precipitation occurs in the experiments when the concentrations become high enough; this is indicated by the steep increase in "amount absorbed" after a plateau region in Figure 13.5a (i.e. (Al) 3×10^{-5} M).

This phenomenon occurs because the surface presents an opportunity in which less energy is required to initiate precipitation on the surface than nucleation and formation of a new precipitate in solution.

FIGURE 13.2 : Extent of specific adsorption of F^- on a αFeOOH. Curves were calculated from the experimentally determined equilibrium constant. Points are experimental (from Sigg and Stumm, 1980)

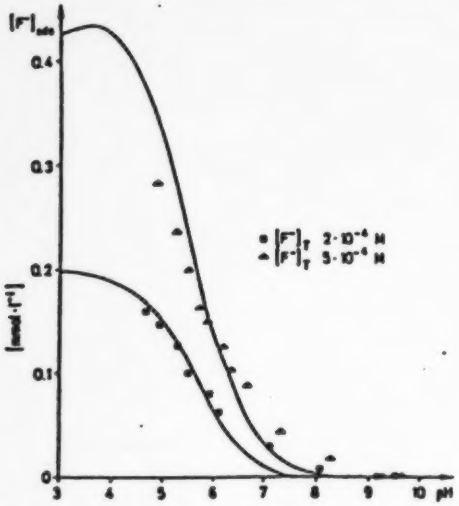

FIGURE 13.3 : H_4SiO_4 is adsorbed specifically over a wide pH range because two surface species $\equiv FeH_3SiO_4$ and $\equiv FeH_2SiO_4^-$ are formed. (Lines calculated with equilibrium constants) Points are experimental. (from Sigg and Stumm, 1980)

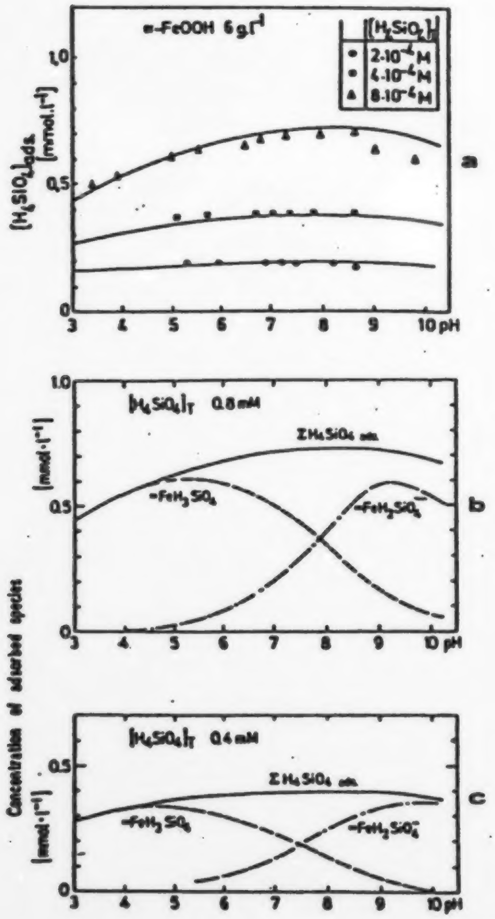

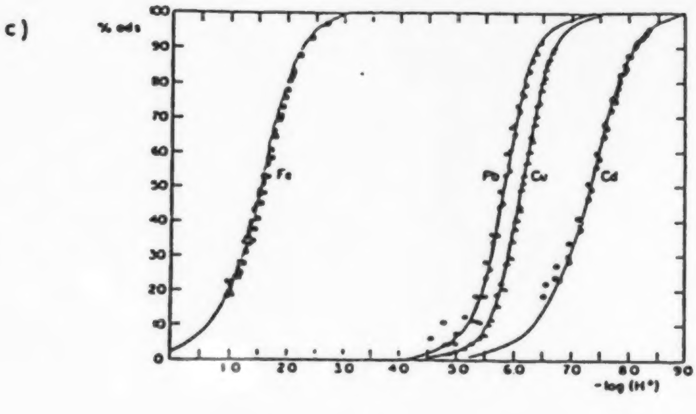

FIGURE 13.4 Dependence of adsorption on pH and solution variables.
% adsorption is plotted as a function of pH.
c) of metal ions on silica

(from Stumm, 1982)

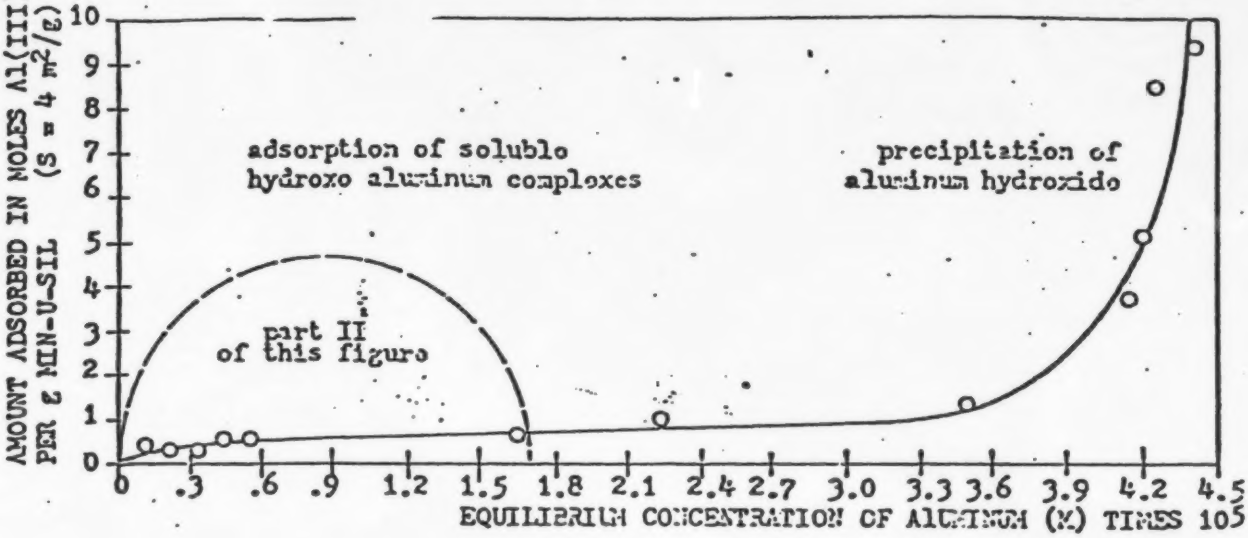

FIGURE 13.5a Raw adsorption data from Hahn's experiments.

(after Fig.III-4a Hahn, 1969)

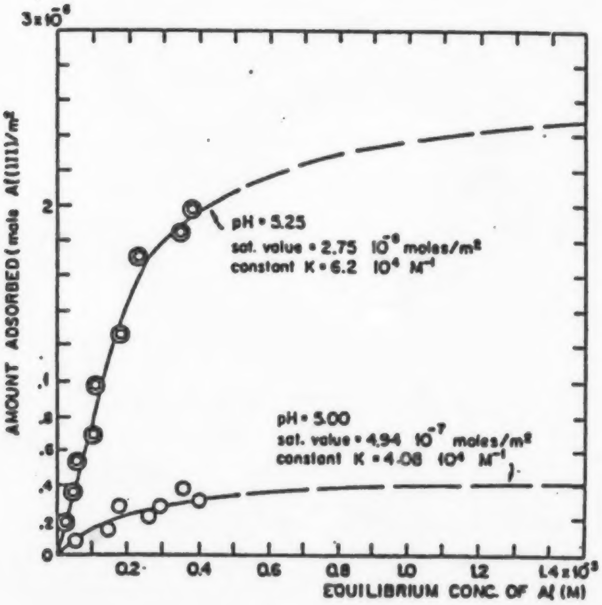

FIGURE 13.5b Adsorption of hydrolyzed Al(III) on colloidal silica

Curves are computed from Langmuir isotherms that have been fitted to the observed adsorption data

(after Hahn and Stumm, 1970)

The effects of (Ba^{2+}) on Ra-226 adsorption (Table 13.1) can be explained by the surface complexation model - for a given number of sites, both Ra-226 and Ba^{2+} can compete; when the concentration of Ba^{2+} in solution is increased, it competes more successfully for sites, decreasing the ability of Ra-226 to adsorb.

For radionuclides such as Thorium where a few orders of magnitude change in adsorption parameters are observed as a function of pH, it is possible that first adsorption and then surface precipitation are occurring.

Effects of Organic Matter on Metals

Organic matter can affect both the amount of radionuclide which is in a dissolved form and the adsorption coefficient. Figure 13.6 shows data from New Hampshire streams and lakes for dissolved organic forms of aluminum vs. TOC. It shows roughly a linear relationship. The relationship can be explained by a reaction involving incorporation of the metal into the dissolved organic matter. This probably involves reaction with humic and/or fulvic acid, the two dominant forms of TOC in natural waters.

The literature suggests that it is a reasonable hypothesis to expect that radionuclides such as thorium and radium will react with organic matter in similar fashion to other metals. They will react in differing amounts. Organic matter can remain in solution or adsorb to solid phases. The extent of reaction of the radionuclides (RN) with organic matter (OM) and of adsorption of the RN-OM complex onto a solid phase will influence the amount of solid form of the radionuclide which will settle from solution. It may explain differences in K_d between field and laboratory data.

Other more recent data suggest that K_d for certain radionuclides may be a function of organic carbon concentration (e.g., thorium as a function of DOC - see Figure 13.7 from Wahlgren, 1982). Such relationships imply that much of the "dissolved metal" is complexed with dissolved organic matter and effectively unavailable for adsorption onto particles; consideration of such a concept might make the actual value for K_d independent of organic matter concentration.

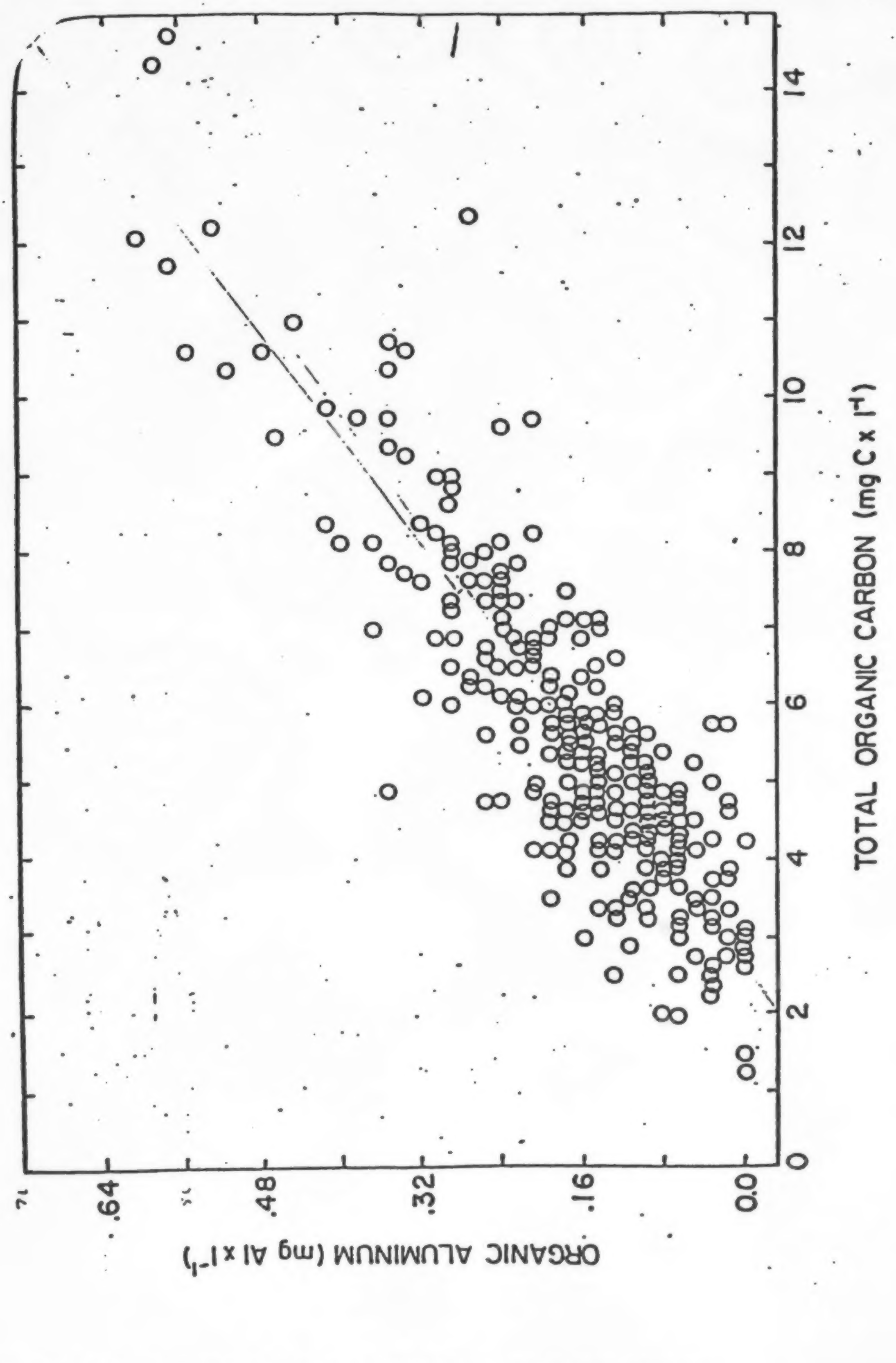

FIGURE 13.6 Organic Aluminum vs TOC in New Hampshire streams.

(after Driscoll et al, 1982)

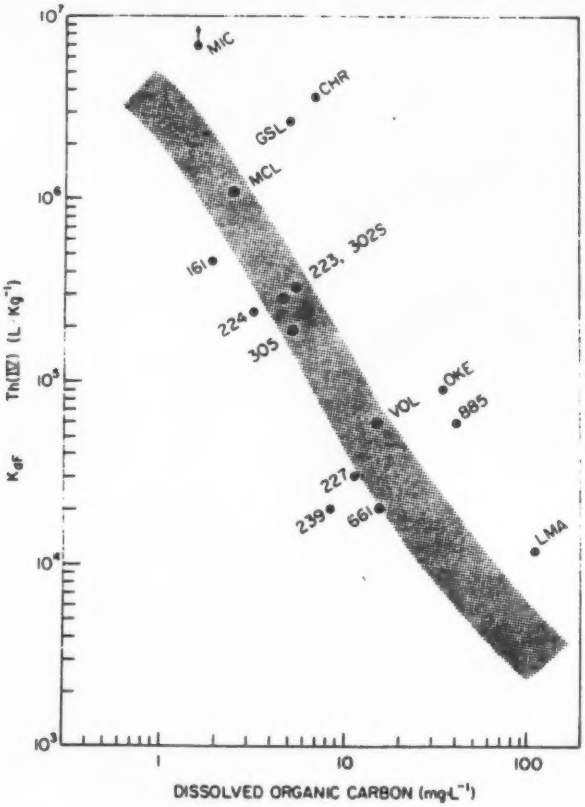

FIGURE 13.7 *Relationship of the K_{df} for Th(IV) to the concentration of dissolved organic carbon.*

(from Wahlgren and Orlandini, 1982)

Relationships of K_d to Suspended Solids Concentration in Surface Waters

There is an increasing amount of credible evidence showing that K_d is a function of solution solids concentration at constant pH. Typically, K_d increases approximately 0.5 to 1.0 order of magnitude for each order of magnitude decrease in suspended solids concentration. This relationship was first observed by O'Connor and Connelly (1980); it has been observed for the adsorption of metals and organics (e.g., PCB's) onto clean surfaces (e.g., clays, sands) as well as organic sediments.

Theoretically, such a relationship should not exist. There are several plausible explanations, but none has been able to explain satisfactorily the observations to date.

Surface Area Effects

Adsorption is described as the mass adsorbed per unit surface area. Measurements typically give values as mass adsorbed per unit mass of parent solids. Where the particle size distribution is narrow and unimodal, the surface area per unit mass of solids is roughly constant. But where the size distribution varies over several orders of magnitude, different adsorption densities result, even though the surface coverage is constant. For example, for 5 adsorption sites/nm^2, the value of T_m varies from 2×10^{-4} g Ra-226 per g solids for 10 um solids to 2×10^{-6} g per g solids for 1 mm solids.

Effects of Other Ions and Liquid/Solid Ratio on Adsorption

Literature data indicates that K_d varies with concentrations of other ions and the L/S ratio.

From the Langmuir isotherm, one obtains

$$T = \frac{Tm\ C}{Beta} \qquad (13.6)$$

or

$$T = K_d C \qquad (13.7)$$

if Beta$\gg$ C. If Beta is not much larger than C, then the number of surface sites becomes limiting to adsorption and K_d is a function of C. Analyses of the data of Table 13.1 indicates that such is occurring (Benes, 1982). That is, where K_d varies with L/S ratio, a probable cause is that T_m is limiting adsorption and the approximation of Beta$\gg$C breaks down.

13.2 Cation Exchange Capacity

Cation exchange can be viewed as a process that involves the electrostatic attraction of cations to the negatively charged sites on a mineral surface. The cation exchange capacity (CEC) is usually defined in terms of the potential number of equivalents of cations that can be accommodated to balance surface charges per unit weight of solids. Different materials are characterized by different values of CEC. In general, clays have high CEC values, while more primary silicates, are characterized by smaller values. In part this results from the higher surface areas of clays (see Figure 13.8). Typical CEC values for different materials are listed in Table 13.3.

Freeze and Cherry (1979) note that:

> Cation exchange capacity (CEC) of a colloidal material is defined by van Olphen (1963) as the excess of counter ions in the zone adjacent to the charged surface or layer which can be exchanged for other cations. The cation exchange capacity of geological materials is normally expressed as the number of milliequivalents of cations that can be exchanged in a sample with a dry mass of 100 g. The standard test for determining the CEC of these materials involves (1) saturation of the exchange sites with NH_4^+ by mixing the soil sample with a solution of ammonium acetate, (2) adjustment of the pore water pH to 7.0, (3) removal of the adsorbed NH_4^+ by leaching with a strong solution of NaCl (Na^+ replaces NH_4^+ on the exchange sites), and (4) determination of the Na^+ content of the leaching solution after equilbrium has been attained. CEC values obtained from standard laboratory tests are a measure of the exchange capacity under the specified conditions of the test. For minerals that owe their exchange capacity to chemical dissociation reactions on their surfaces, the actual exchange capacity can be strongly dependent on pH.

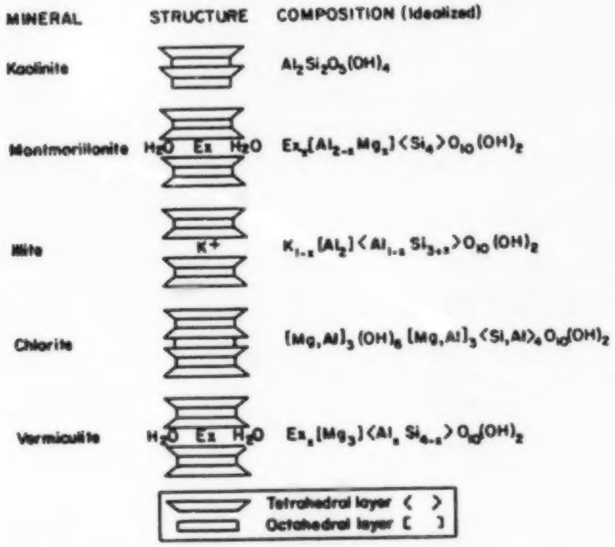
MINERAL
STRUCTURE
COMPOSITION (Idealized)
Kaolinite
$Al_2Si_2O_5(OH)_4$
Montmorillonite
H_2O Ex H_2O
$Ex_x[Al_{2-x}Mg_x]\langle Si_4\rangle O_{10}(OH)_2$
Illite
K^+
$K_{1-x}[Al_2]\langle Al_{1-x}Si_{3+x}\rangle O_{10}(OH)_2$
Chlorite
$[Mg,Al]_3(OH)_6[Mg,Al]_3\langle Si,Al\rangle_4O_{10}(OH)_2$
Vermiculite
H_2O Ex H_2O
$Ex_x[Mg_3]\langle Al_xSi_{4-x}\rangle O_{10}(OH)_2$
Tetrahedral layer ⟨ ⟩
Octahedral layer [ ]

Figure13.8 Simplified structure and composition of the principal clay minerals (after Berner, 1971).

TABLE 13.3: Cation exchange capacity (CEC), surface area, and surface charge density values for soil minerals

(1) Variation and range of values between different minerals and between members of each type (compiled from Brown *et al.*, Greenland and Mott, Farmer, in the companion volume (1978), and data from the author's laboratory)

Mineral type	Surface area ($m^2 g^{-1}$)	CEC ($\mu eq\ g^{-1}$)	Surface charge density ($\mu eq\ m^{-2}$)
Allophanes	500–700	500–1000	0.71–2.0
Hydrous oxides of Fe and Al (pH ~ 8.0)	25–42	5–10	0.12–0.4
Kaolinites	10–20	20–60	1–6
Clay micas (Illites)	90–130	200–400	1.5–4.4
Fithian illite	93	260	2.8
Smectites	750–800	600–1200	0.75–1.6
Wyoming bentonite	750	1000	1.33
Vermiculites	750–800	1200–2000	1.5–2.7
Kenya vermiculite	780	1240	1.6
Llano vermiculite	780	2070	2.7

The chemical potential for exchange results from the elemental substitution of one lattice ion for another. For example, for montmorillonite in which 0.67 mol Mg substitute for Al, in the clay lattice, the CEC can be calculated to be 91.5 meq/100 g.

Cation exchange can generally be described as an equilibrium process in which various cations exchange with solids and yet maintain the total number of cations on the surface. The exchange equation can be represented by:

$$aA^{b+} + bBX \rightleftharpoons bB^{a+} + aAX \tag{13.7}$$

in which A and B are dissolved species and AX and BX are sorbed species. In this case, the selectivity coefficient is given as:

$$K_s = \frac{(B)^a (AX)^b}{(A)^b (BX)^a}$$

where the brackets denote activities. Therefore, it is seen that exchange coefficients are needed for all possible pairs of cations in solution. Some difficulties arise, however, because the CEC is actually affected by pH and, to some extent, by solution composition. Therefore, selectivity coefficients measured under specific conditions may not be applicable under others. In any case, abundant data are available for a variety of conditions and many cation pairs. A survey of experimental results has been reported by Bruggenwert and Kamphorst (1979) and includes a compilation of vast quantities of data.

Anion exchange can also occur, especially on surfaces of hydrous metal oxides, but less experimental data for anion exchange are available. This topic is discussed by Davis et al. (1978a,b) and by Davis and Leckie (1978) and an example of sulphate adsorption is given by Wood (1978).

Early indications that CEC was constant when measured below pH 5 led Schofield (1949) to distinguish between "permanent" (structural substitution) charge and variable "pH - dependent" charge. An increase in CEC in the pH range 5 to 8 has been determined to be a characteristic of many Red-Yellow Podzolic and Reddish-Brown Lateritic soils (Coleman, Weed and McCracken, 1959); of tropical soils (Middleton and Westgarth, 1964); and of soils from Wisconsin (Helling et al., 1964). The pH-dependence of the non-organic portions of many of these soils was felt to be due, at least in part, to their content of allophane.

The nature and source of the surface charge on kaolinite has been the subject of many studies. Unlike the other clay minerals, small deviations from stoichiometry in kaolinites are impossible to detect by direct chemical analysis and consequently the presence or absence of isomorphic substitution has been difficult to determine.

Since CEC can be equated to the product of the surface charge density and the specific surface area, a direct correlation between particle size and CEC should exist. In most studies the effect of particle size is ignored since it is assumed that completely dispersed clays develop a specific range of surface area per unit weight of solid. However, some detailed studies have been carried out. For example, Ormsby et al. (1962) studied the relationship between particle size, surface area and CEC for kaolinite clays. A summary of the results is given in Table 13.4.

Soil organic matter can develop a negative surface charge by the disociation of H^+ from functional groups. The cation exchange capacity of the organic matter originates mainly from the exchangeable hydrogen present on carboxyl and phenolic groups especially at low pH (pH less than 7).

In terms of the uranium tailings environments, it is certain that cation exchange, reactions involving major cations, and trace metals, will be highly significant in the Saskatchewan in which moderate quantities of clay occur. A formula for CEC (meq/100 g) = (1% clay/2) + (% organic matter x 2), which predicts a CEC = 3.7 meq/100 g, agrees reasonably well with observations (2.2; 5.4 meq/100 g) for Key Lake tailings. This process will be less important in the Elliot Lake tailings that contain very little clay material.

The presence of abundant ferric hydroxides in both Elliot Lake and Saskatchewan tailings suggests that anion adsorption would occur in both environments.

Modelling Efforts in the Literature

The modelling of ion exchange processes during pore water flow through geologic media has met with mixed success. The most positive results have been obtained when

TABLE 13.4: SUMMARY OF CEC, PARTICLE SIZE AND SURFACE AREA DATA FROM ORMSBY ET AL. (1962)

Sample	Kaolinite Property	Particle - Size Fraction (um)					
		44-10	10-5	5-2	2-1	1.0-0.5	0.5-0.25
A	CEC	1.3	1.3	1.5	2.0	2.3	2.7
	S	5.0	5.9	6.7	8.6	8.8	8.8
H	CEC	1.5	1.5	1.6	2.2	2.4	4.4
	S	6.1	6.6	7.7	8.9	10.1	11.8
B	CEC	1.6	1.7	1.9	2.3	2.7	4.2
	S	6.3	6.8	8.5	9.8	10.5	14.0
E	CEC	1.6	1.6	1.6	2.6	2.9	3.9
	S	6.3	6.2	7.9	9.7	11.0	12.5

CEC - meq/100 g

S - surface area (m^2/g)

equilibrium speciation of the dissolved ions has been considered. The migration of major cations (Ca^{2+}, Mg^{2+}, Na^+, K^+) in groundwater through a sandy deposit was predicted (Dance and Reardon, 1983) by including exchange processes. Other modelling efforts involving field or laboratory (column) verification of exchange are reported by Lai and Jurinak (1972), Grove and Wood (1979), and Valocchi et al. (1981).

13.3 Application of Adsorption and CEC data to NUTP Modelling Work

It is recommended that the appropriate model for adsorption be used in developing research, component and source models. To interpret laboratory and field data, the site-binding type of model will be required in the future, although much current data will be in the form of a Langmuir, or Freundlich adsorption isotherm, or in the form of a linear distribution coefficient. For the source model, it is anticipated that the distribution coefficient will provide the most practical approach.

For CEC models, the literature reviewed indicates that CEC, as a function of solution conditions, is necessary for understanding particular observations. For example, adsorption capacity is often described as a "conditional adsorption capacity", conditional upon the solution pH. For purposes of a source model, it is anticipated that a particular CEC for one type of clay and a range of solution conditions will be adopted. Knowledge of the quantity of different types of clays in the tailings will allow one to build up a "composite" value for CEC for different tailings bodies.

Type of Data Available

The distribution coefficient, a selectivity coefficient, a Langmuir adsorption isotherm, a site binding model, and/or an equilibrium constant have been used by different investigators to describe "sorption" processes of the same metal in the same type of geologic material. Several compilations of data are available for CEC (Bruggenwert and Kamphorst, 1979) and other sorption processes. Adoption of any of this data will require detailed inspection of the original data (e.g., the type of surface used by Ames et al., 1983, etc.) to justify its use. In this section, sorption "data" for a few radionuclides and trace elements are discussed to demonstrate the complexity of the data available.

Several K_d values for radionuclides are given in Table 13.5 . For thorium for example, high values of K_d (Log $K_d = 7$) suggest that precipitation on the surface of the solid rather than "linear sorption" processes are occurring. The range of K_d for some radionuclides is also large, although some of the values are explainable by considering solution conditions and the concepts of the site binding model.

The individual and simultaneous variation of radium and barium adsorption on various geological materials was measured by Gillham et al. (1981). Their objective was to explore whether barium could be used as an analog for radium in adsorption experiments. They conclude that it could not be used as an analog because of naturally occurring barium in soils. They do, however, conclude that the distribution coefficient is a valid model for describing adsorption at low concentrations. Also, the adsorption of radium has been explored by Riese and Langmuir (1985). Their approach is a modified site binding model. They conclude that use of K_d is impractical to explain variations as a function of solution condition (competitive adsorption, pH, ionic strength, etc.).

Copper speciation in solution is summarized by Leckie and Davis (1979) while sorption behaviour is summarized by Pickering (1979). Pickering gives graphs for the pH dependence of sorption for various clays and gibbsites. He indiciates that sorption has been modelled by several different concepts (see Table 13.5, Part 3).

Lead adsorption increases with increase in pH but interpretation above pH 7 is complicated by the precipitation of lead oxyhydroxide (Rickard and Nriagu, 1978). CEC, Langmuir and Freundlich models have been used to model adsorption. In one investigation, the Langmuir and Freundlich models were statisfactory over a wide range of concentrations, with clays and organic matter being the dominant substrates contributing to adsorption.

Mercury adsorption is a function of its solution complexes (chloride versus hydroxo) and such variables as organic matter in the particulate phase. However, at the time of writing their paper (1979), Benes and Havlik (1979) conclude that laws governing mercury sorption processes are fragmentary.

Rickter and Theis (1980) present an excellent analysis of Ni sorption onto "laboratory surfaces" using the site binding model and REDEQL2. For modelling adsorption processes

TABLE 13.5: VALUES FOR SORPTION COEFFICIENTS FROM VARIOUS ENVIRONMENTS

---

1. Lakes and Oceans

Isotopes	Lakes		Ocean	
	log K_d	Ref.	log K_d	Ref.
Pb(II)	5.5 (±0.5)	(1)	5.5(±0.5)	(2,3)
Po(IV)	-	-	6 (±1)	(52,17)
Th(IV)	GT 6.5	(4)	7	(5)
U(VI)	approx. 4.0	(4)	2.2	(6)

References for above:

1 Santschi, unpublished data from Lake Zurich, Switerzerland
2 Santschi et al. (1980)
3 Cochran and Krishnaswami (1980)
4 Wahlgren et al. (1976)
5 Bacon and Anderson (1982)
6 Anderson (1981)

2. Geological Materials and Soils - Radionuclides

Radio-nuclide	Reference	K_d, mL/g	Prevailing Conditions	
Uranium	Rancon, 1973	37	river sediment (12% organic)	
		33	organic peat (60% moisture)	
		16	Oxidizing -	low organic sediment (1% organic)
		270	Conditions -	altered schist (clay, no organic)
		130	Pure illite	

TABLE 13.5: VALUES FOR SORPTION COEFFICIENTS FROM VARIOUS ENVIRONMENTS (cont'd)

Thorium	Rancon, 1973	1 to 10^5	Altered schist, pH increases from 1 to 5
		2 to 10^5	Illite, pH increases from 1 to 7
		10^6 to 50	River sediment (12% organic), pH increases from 7.6 to 14
		8x10 to 1.5 x 10	Organic peat, pH ranges from 6.7 to 7.4
		15 to 10	Clay, pH ranges from 7.0 to 7.4
	Nishiwaki, 1972	40 to 130	Silt-clay under seawater
Radium	Kirchmann,	1,500 to 3,000	Peat
	et al., 1966	150 to 300	Sand
	Serne, 1974	214 to 467	Rock solution (primarily quartz and feldspar)
	Gillham et al., 1981	50 to 100	Variety of geological materials

3. Geological Materials; Soils and Laboratory Surfaces - Trace Elements

Metal (Reference)	Sorbing Surface(s)	Model and Parameter Value
Copper (Pickering, 1979)	- Na-montmorillonite - Vermiculite - Bentonite - Na-illite - Attapulgite - Kaolinite - Illite - Na-Kaolinte - Gibbsite	- can be modelled as a distribution coefficient, a selectivity coefficient and a trace equilibrium constant e.g., distribution coefficient is 9 for Cu on clay in one investigation; e.g., selectivity coefficient equals 0.93 at pH 3.5 and 1.28 at pH 5.2 for Ca-montmoillonite - Cu exchange

TABLE 13.5: VALUES FOR SORPTION COEFFICIENTS FROM VARIOUS ENVIRONMENTS (cont'd)

Lead (Rickard and Nriagu, 1978)	- Utah Bentonite Clays pretreated by Ca - Manganite - Cryptomelane - Fresh ferro-manganese nodules	- Exchange Equilibrium Constant $K_{ex} = 1.4$ - EC = 8.3 mg/g - EC = 18.6 mg/g - EC = 8.2 mg/g (EC = exchange capacity)
Mercury (Benes and Havlik, 1979)	- Various	- see text
Nickel (Richter and Theis, 1980; Theis and Richter, 1979)	- Goethite - Amorphorus manganese oxide - Silica	- modification of site binding model (see discussion in text)
Zn (Pickering, 1980)	- Clays with some sands and certain experimental treatment	- Langmuir - Adsorption Capacity (T) = 43 - 147 meq/kg - Bonding Energy = 0.35 - 0.78 ppm
Zn (Dempsey and Singer, 1979)	- $Fe(OH)_3(am)$ - MnO_x	- Site Binding Model; for values, see reference
As (Ferguson and Graves, 1972)	- Aluminum hydroxide - Clays	- Not given
Ba (Gillham et al., 1981)	- Variety of geological materials	- Infer limits of K_d model - K_d varies from 60 to 3000 ml/g

in tailings, their results indicate the following. Ni does not begin to adsorb to goethite until the pH has increased to its zero point of charge. Ni adsorption onto silica becomes significant only at pH 8 and greater where formation of a $NiOH^+$ complex becomes important; this is also quite close to the pH (9) where nickel hydroxide precipitation becomes important (when pNi = 4.77).

For zinc sorption, the selectivity coefficient (CEC) and Langmuir isotherm have been used to examine zinc sorption onto clays and various soil mixtures containing clays (Pickering, 1980). Zinc adsorption as a function of pH, clay type and presence of silicic acid has also been examined. Zinc and calcium sorption onto amorphorus iron hydroxide and MnO_x has been interpreted (Dempsey and Singer, 1979) using the site binding model and 3 possible sites (SOH, SO^- and a bidentate structure using 2 of SOH, where S is the surface). Zinc sorption was independent of calcium sorption onto $Fe(OH)_3$(am).

For arsenic, Ferguson and Gavis (1972) note that arsenic is adsorbed by aluminum hydroxide and clays and hydrous iron oxides, but that it also coprecipitates with the hydrous iron oxides. At higher concentrations of arsenic, ferric arsenate is "quite insoluble".

13.4 Recommendations for Future Work on Adsorption Processes

It is recommended that:

1. A detailed analysis of literature data be made for K_d and CEC as a function of type of sorbing surface, solution conditions etc. From this, a set of values useful for a source model should be adopted.

2. A detailed study should be made of the site-binding model and literature, where it has been applied. The objective of this study would be to ascertain whether the K_d modelling methodology is sufficient for NUTP modelling purposes or whether a more detailed adsorption model is required. The work of Riese (1983) on Radium and Thorium sorption onto kaolinite and quartz using the site-binding model, would be a useful starting point. This detailed study should also consider Al and Fe sorption to quartz, etc.

From a time frame point of view, it would seem to make more sense that the second study (site-binding model) should proceed first before the critical compilation of K_d and CEC data. However, K_d data is available and it is so widely used that it is our judgement that these two studies should proceed in parallel, as separate studies, or as part of an overall study. Proceeding as one overall study is logical because evaluation of the site binding model will provide critical input into review of the K_d data.

14.0 THE DESCRIPTIVE ALGORITHM: PATHWAY DIAGRAMS FOR MODELLING MINERALS AND ELEMENTS OF CONCERN

An example of the development of a model for calcium has been given above in Section 2. The development uses a mass balance equation framed about a pathway diagram.

A pathway diagram describes the major physical, chemical and geochemical processes involving mobilization and transport of contaminants out of the tailings. Pathway diagrams for the major elements and minerals of concern to this project (Chapter 4) are now given. Definitions of arrows are given in Figure 14.1. These include equilibrium, coprecipitation equilibrium, kinetic and sorption control of solid-solution partitioning and fluid transport.

A summary of the major solids of each element considered in this report is given in Table 14.1.

14.1 Silica

Sources

Silica is the most abundant component of the uranium ore materials. It occurs in a number of forms such as quartz and a wide range of alumino-silicate minerals including clays.

Occurrence in Tailings

Many of the primary silicate minerals will be present in the tailings material. In addition, because dissolution of some silicates occurs more readily under low pH conditions, and because the solubility of amorphorus silica is rather constant and unaffected by pH, precipitation of the latter is likely both in the mill and in the tailings. A list of the most important primary and secondary sources of silica in uranium tailings is given in Table 14.1. Other minerals containing silica are given in Table 4.11.

TABLE 14.1: MAJOR SOLID PHASES COMPOSED OF THE ELEMENTS OF CONCERN IN URANIUM TAILINGS IN CANADA

	Solid Phase 1			Solid Phase 2			Solid Phase 3			Solid Phase 4		
	Name	Lit	Controls	Name	Lit	Controls	Name	Lit	Controls	Name	Lit	Controls
Major Elements (percentage range)												
Si (20-90)	Quartz	G	Kin (Surf)	Silica (amor)	F	Eq	Clays/Micas	F	Eq(?)/Kin	Feldspars	VG	Kin(Surf)
Al (3-10)	Feldspars (i.e., orthoclase)	VG	Kin (Surf)	Clays/Micas	F	Eq(?)/Kin	Hydroxides* (i.e., gibbsite)	G	Eq	Sulphates* (i.e., basaluminite)	F	Eq(?)
Ca (.3-2)	Carbonates	VG	Eq (pH)	Gypsum	G	Eq.	Apatite	P	Eq(?)	Clays (adsorbed)	G	Eq
K (1-3)	Feldspars	VG	Kin (Surf)	Micas	F	Kin	Clays (dissolution)	F	Eq(?)	Clays (adsorbed)	F	Eq(?)
Mg (0.5-5)	Chlorite	P	Kin(?)	Carbonates (i.e., dolomite)	F	Kin (?)	Pyroxenes	F	Kin (Surf)	Amphiboles	P	Kin (Surf)
Na (0.05-?)	Plagioclase (i.e., albite)	VG	Kin (Surf)	Tourmaline	P	Kin (?)	Clays (adsorbed)	F	Eq	Al-sulphates	F	Eq (?)
Fe (2-8) +II +III	Pyrite Hydroxide (am)*	G G	Kin (Transp) Eq	Chalcopyrite Oxide (i.e., goethite)	P G	Kin (Transp) Eq (dissolution)	Arsenopyrite Jarosite*	P F	Kin (Transp) Eq(?)	Siderite*	F	Eq
S (1-3)	Sulphides (i.e., pyrite)	G-P	Kin (Transp)	Gypsum	G	Eq	Jarosite*	F	Eq(?)			
C (.1-1)	Carbonates* (i.e., calcite)	VG-G	Eq	Graphite	P	Kin(?)	(Carbon dioxide)	G	Eq			
H	(Many minerals as hydroxides and water molecules)											
Minor Elements												
Ba	Barite*	F	Eq	Sulphides (replacement)	P	Kin						
Co	Carrollite	P	Kin(?)	Skutterudite	P	Kin(?)	Sulphides (replacement)	P	Kin(?)			
Cu	Sulphides	P	Kin(Transp)	Selenides (i.e., Berzelianite)	P	Kin(?)	Carbonates	P	Eq (?)	Hydroxides	P	Eq (?)
Mn	Oxides (i.e., manganite)	P	Eq(?)	Rhodochrosite*	P	Eq(?)						
Ni**	Arsenides (i.e., Nicollite)	P	Kin(?)	Sulphides (replacement)	P	Kin	Hydroxides* (i.e., $Ni(OH)_2$)	P	Eq(?)			

TABLE 14.1: MAJOR SOLID PHASES COMPOSED OF THE ELEMENTS OF CONCERN IN URANIUM TAILINGS IN CANADA

	Solid Phase 1			Solid Phase 2			Solid Phase 3			Solid Phase 4		
	Name	Lit	Controls	Name	Lit	Controls	Name	Lit	Controls	Name	Lit	Controls
Pb	Galena	P	Kin	Clausthalite	P	Kin(?)	Oxides	P	Eq(?)			
Ti	Ilmenite	P	Kin	Rutile	P	Kin	Brannerite	P	Kin			
Zn	Sphalerite	P	Kin	Sulphides (replacement)	P	Kin						
As**	Arsenides (i.e., Niccolite)	P	Kin(?)	Metal Salts*	P	Eq(?)	Metal Oxides (adsorbed)	F	Eq			
P	Apatite	P	Eq(?)	Monazite	P	Eq(?)	Metal Oxides (adsorbed)	F	Eq			
Se	Selenides (i.e., Clausthalite)	P	Kin(?)	Metal Salts* (i.e., ferric selenate)	P	Eq(?)						
Radionuclides												
U (238,234)	Brannerite	P	Kin(?)	Apatite (coprecipitate)	P	Eq(?)						
Th-230	Brannerite (secular eq)	P	Kin(?)	Hydroxides (i.e., $Th(OH)_4$)	P	Eq(?)						
Th-232	Monazite	P	Eq(?)	Thorite	P	Kin(?)						
Th-228	Monazite (secular eq)	P	Eq(?)	Thorite	P	Kin(?)						
Ra-226	(see U-238)			Sulphates (Ca, Ba, Sr)	F	Eq	Gypsum (coprecipitate) (see Ra-226)	G	Eq			
Ra-228	(see Th-232)											
Pb-210	(see U-238)			(see Pb)								
Po-210	(see U-238)			Sulphate	P	Eq(?)						

Note:
- Eq (pH) = Equilibrium (pH major influence)
- Eq(?) = Equilibrium (significant uncertainty)
- Kin (Surf) = Kinetic (surface control dominates)
- Kin (Transp) = Kinetic (transport control dominates)
- VG = Very Good
- G = Good
- F = Fair
- P = Poor
- * = Secondary phase (may be formed or added in mill and/or tailings)
- ** = May be major component in Saskatchewan tailings

Reaction Pathways

The pathway diagram for silica is given in Figure 14.1.

In general, the majority of silicate minerals will be far-from-equilibrium under the near-surface conditions of the tailings. The reactions of concern will, therefore, consist of kinetically controlled dissolution (see Section 11.4)

Exceptions to this behaviour would include amorphous silica (SiO_2) and perhaps some clays such as illite and chlorite.

14.2 Aluminum

Sources

The primary sources of aluminum in uranium tailings include the extensive array of alumino-silicate minerals and clays. Among these, the feldspar minerals are the most abundant and contain high percentages of Al. In general, the ores in Saskatchewan are comprised of larger quantities of aluminosilicates than those in the Elliot Lake region.

Occurrence in Tailings

Secondary minerals containing Al include hydroxides (i.e., amorphous or gibbsite) and possibly sulphate (i.e., basaluminite, jurbanite) or silicate phases (i.e., allophane). Residual aluminosilicate minerals will also be present in the tailings. A list of major primary and secondary sources of Al in uranium tailings is given in Table 14.1. Other aluminum minerals are given in Table 4.11.

Reaction Pathways

The pathway diagram for aluminum is given in Figure 14.2a.

- Aluminosilicates

Many of the minerals represented in this group will be unstable (i.e., far from thermodynamic equilibrium) under the near-surface conditions of the tailings. This group

FIGURE 14.1: PATHWAY DIAGRAM FOR SILICA

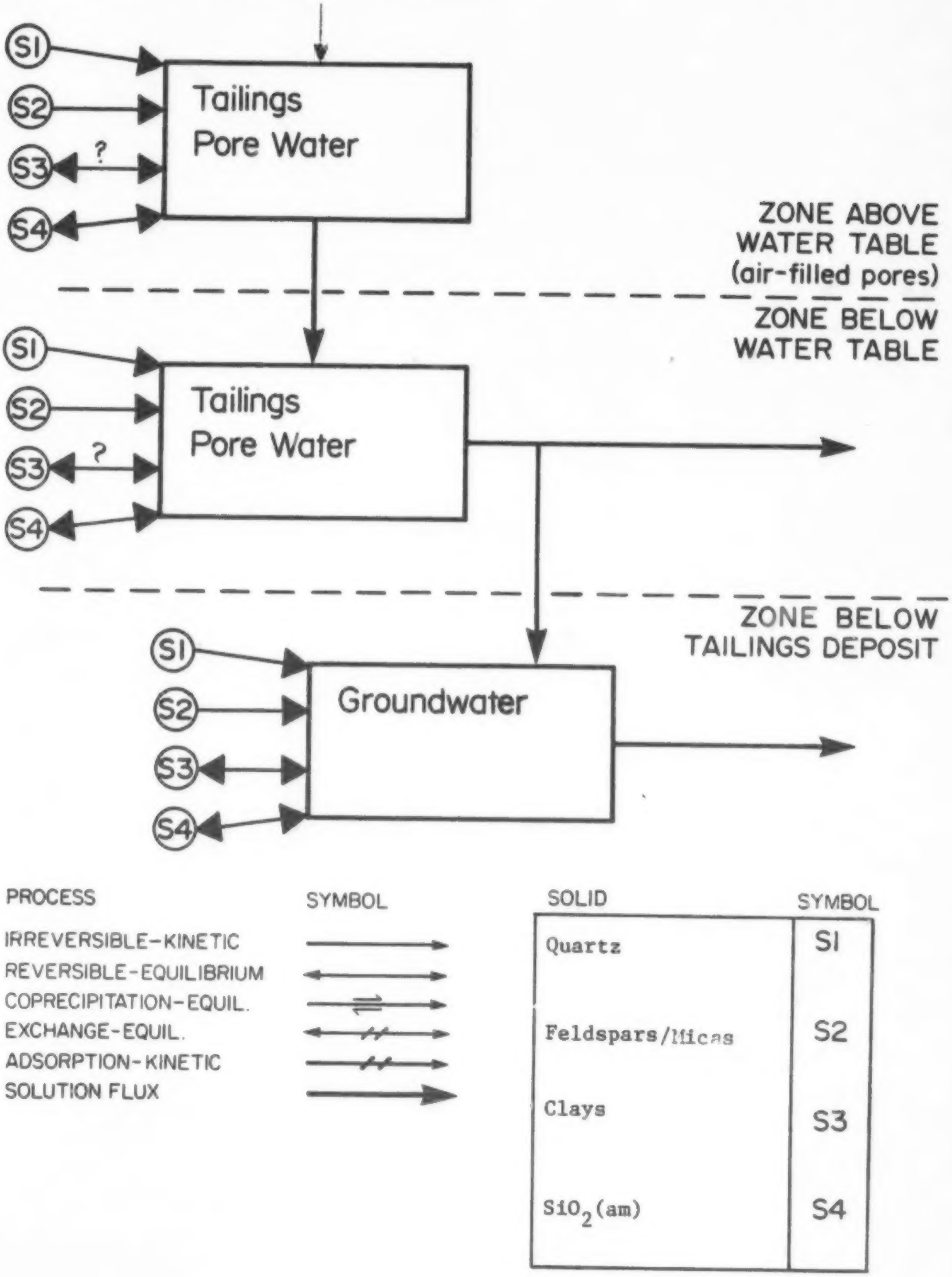
S1
S2
S3
S4
?
Tailings Pore Water
ZONE ABOVE WATER TABLE (air-filled pores)
ZONE BELOW WATER TABLE
Tailings Pore Water
ZONE BELOW TAILINGS DEPOSIT
Groundwater
PROCESS
SYMBOL
IRREVERSIBLE-KINETIC
REVERSIBLE-EQUILIBRIUM
COPRECIPITATION-EQUIL.
EXCHANGE-EQUIL.
ADSORPTION-KINETIC
SOLUTION FLUX
SOLID
SYMBOL
Quartz
S1
Feldspars/Micas
S2
Clays
S3
SiO2(am)
S4

FIGURE 14.2a: PATHWAY DIAGRAM FOR ALUMINUM

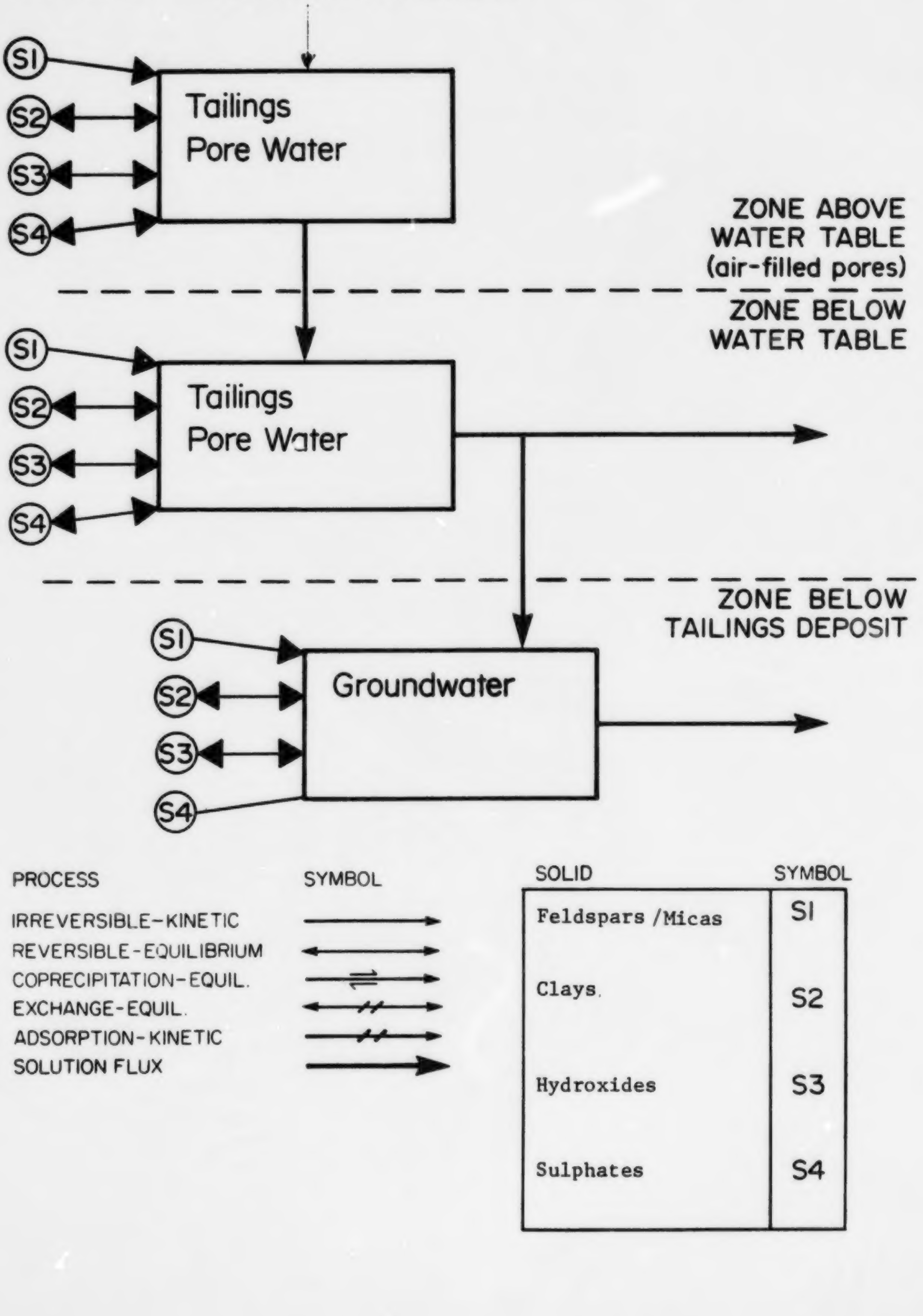

S1
S2
S3
S4
Tailings
Pore Water
ZONE ABOVE
WATER TABLE
(air-filled pores)
ZONE BELOW
WATER TABLE
Tailings
Pore Water
ZONE BELOW
TAILINGS DEPOSIT
Groundwater
PROCESS
SYMBOL
IRREVERSIBLE-KINETIC
REVERSIBLE-EQUILIBRIUM
COPRECIPITATION-EQUIL.
EXCHANGE-EQUIL.
ADSORPTION-KINETIC
SOLUTION FLUX

SOLID	SYMBOL
Feldspars /Micas	S1
Clays.	S2
Hydroxides	S3
Sulphates	S4

includes minerals such as the feldspars, amphiboles, pyroxenes and micas. Members of this group would move toward greater stability by dissolution. In general, dissolution rates associated with primary aluminosilicates are slow and hence kinetic controls are highly probable (see Chapter 11, Section 11.5).

Some aluminosilicate minerals, however, may exist at near equilibrium conditions at the earth's surface. Members of this group include the clay minerals (i.e., chlorite, illite) that are actually secondary minerals that formed within the ore deposit and associated rocks. In the tailings, these minerals may behave in a thermodynamic fashion; however, dissolution and formation rates of individual phases should be investigated to better define potential kinetic controls (see Chapter 11).

Some speculation has been made as to whether allophane controls Si and Al concentrations in some tailings-related pore waters. If this phase does exist, it would, by definition, be a reactive amorphous phase and hence equilibrium control is highly likely. Further investigation may be necessary to clarify the existence of such a solid phase.

- Hydroxides of Aluminum

The hydroxide phase of Al forms in the mill probably as an amorphous solid. At neutral to moderately acidic pH values, pore water in the tailings reflect equilibrium conditions with respect to an $Al(OH)_3$ phase that is intermediate in stability between an amorphous solid and gibbsite (Dubrovsky et al., 1985). These findings suggest that equilibrium controls can be used to model dissolution of such phases. Aluminum hydroxides form solids that are analogous to ferric hydroxides, in which the solubility product is not known exactly and can vary within the limits between the reactive amorphous phase and the more stable gibbsite phase.

- Sulphates of Aluminum

Aluminum sulphate solids are generally stable only at low pH and high sulphate activities (Nordstrom, 1982). There is evidence to suggest that alunite and basaluminite occur in natural acid-sulphate soils (van Breemen, 1973). In Elliot Lake tailings, that are characterized by low pH and high SO_4, solubility data suggest that the latter controls the Al concentrations (Dubrovsky et al., 1985). This suggests that equilibrium controls dominate for these minerals. The sulphur tracer data of de Hek et al. (1976) suggest that these solids will not form at more neutral pH (5-6) values.

Effect of Solution Complexation and Polymers on Solubility

The points concerning the effects of hydroxides of aluminum on its stability are illustrated in Figure 14.2b. The complexation constants for Al^{3+} and $Al(OH)^{2+}$ and their relationship to aluminum solubility are well defined, if one is sure of which phase is present. The complexation data for $Al(OH)_2^+$ is termed poor by Baes and Mesmer (1976). Also plotted on the diagram are sampling data from the saturated zone of Nordic (2-11 m below surface) obtained in July 1980 (Dubrovsky et al., 1985). Overall the data suggest that amphorus-$Al(OH)_3$ (Log K = -31.6) explains much of the observed aqueous concentrations of aluminum and that $Al(OH)_2^+$ is particularly important in explaining these data between pH 4.5 and 6. Alunite (aluminum sulphate) would not explain the data in this pH range because its influence occurs in the range of pH 3 and lower.

Figure 14.2b illustrates two other points concerning $Al(OH)_3^o$ and aluminum polymers. The $Al(OH)_3^o$ complex was hypothesized to occur by Baes and Mesmer (1976), but it has not, to our knowledge, been experimentally demonstrated to occur. Its existance would require that aluminum be more soluble than the data and detection limits suggest. In the pH range of 5.5 - 6.5 - the solubility line would be horizontal. The presence of the $Al(OH)_2^+$ complex seems to best explain the data.

With respect to aluminum polymers, large macromolecules such as $Al_{13}O_4(OH)_{24}{}^{7+}$ have been demonstrated to remain pseudo-stable in solution for a year or longer. They, particularly, have application in water treatment practice. The solubility line implied by their existance is given in Figure 14.2b. It is so far removed from field data that one can conclude that it doesn't occur in tailings systems.

14.3 Calcium

Sources

Primary sources of Ca in the ore are represented by minerals such as Ca-feldspar, clays and pyroxenes. In some ores that have been mined in Saskatchewan, Ca is present as

FIGURE 14.2b

Speciation Diagram for Aluminum (Amorphous $Al(OH)_3$ (s); Data from Baes & Mesmer, 1976)

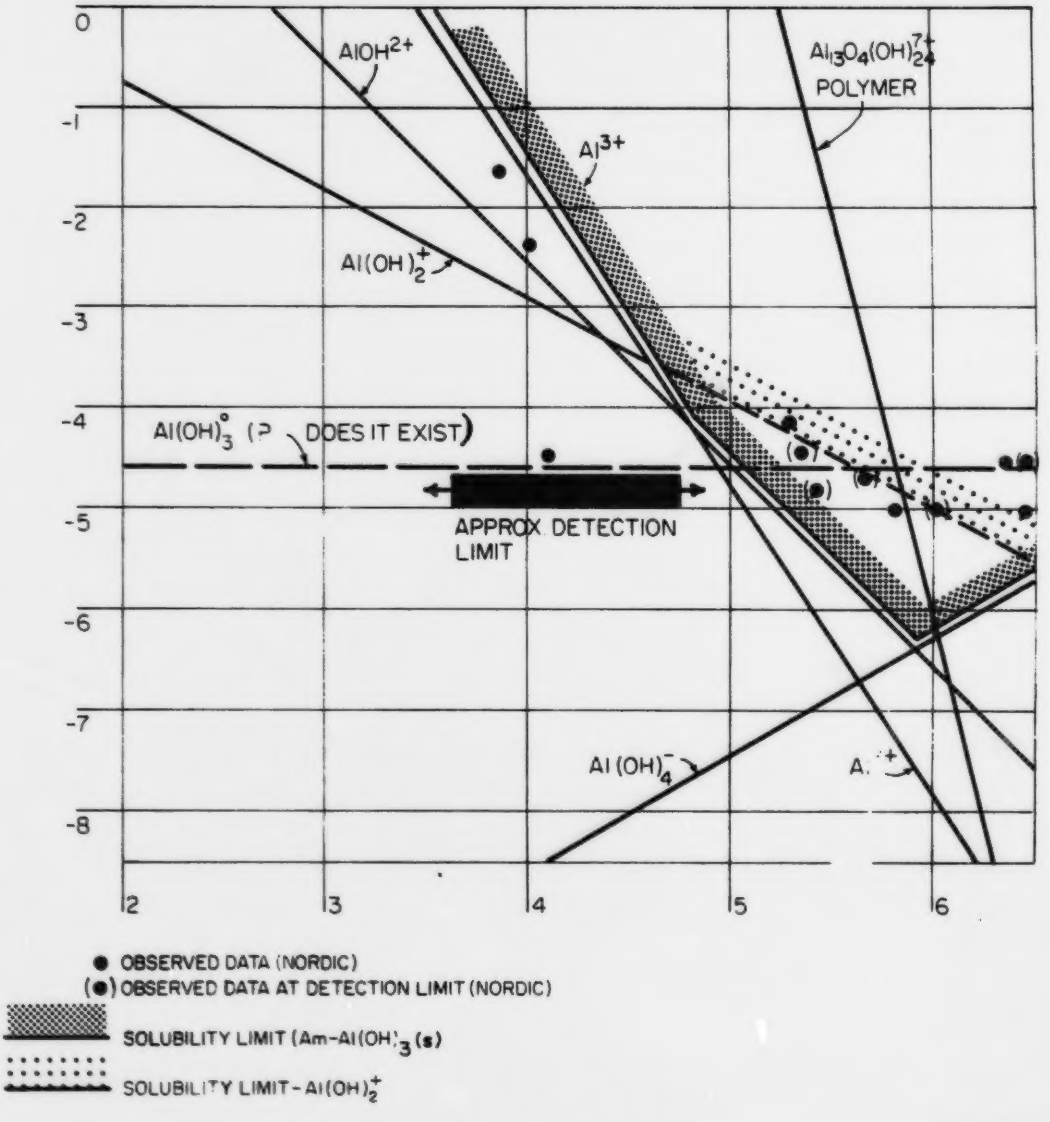

limestone ($CaCO_3$). Many ores that have been milled using the acid leach process have also been neutralized by the addition of lime and limestone. The major contribution of Ca to many tailings, therefore, is the slaked lime and limestone added in the mill circuit.

Occurrence in Tailings

Calcium will be present in the residual or undissolved fraction of the Ca-feldspars, clays and pyroxenes. The majority of Ca, however, will exist as gypsum that precipitate in the sulphuric acid solutions upon addition of lime and limestone. Ettringite has recently been observed in both Key Lake and Elliot Lake tailings (Knight and Piesold, 1985; Constable, 1983), but appears to constitute a minor portion of calcium sulphate minerals (for Key Lake, ettringite is 3.7% and gypsum 26% by weight of tailings). Some residual $CaCO_3$ has also been detected (usually less than 0.1% in Elliot Lake tailings, but 3% in Key lake tailings). The composition of carbonate was identified chemically in Key Lake tailings, but not mineralogically; this suggests to us that gypsum has formed a reaction coating on the exterior of residual carbonates similar to the observations of Rochelle (1981). Minor amounts of calcium may also be precipitated as calcium orthoarsenate in Key Lake tailings (2%). A list of the major primary and secondary sources of calcium in uranium tailings is given in Table 14.1. A list of other minerals containing calcium is given in Table 4.11.

Reaction Pathways

The pathway diagram for calcium is given in Figure 14.3.

o Gypsum

Gypsum is a moderately soluble mineral that dissolves and precipitates readily. Solubility data for Elliot Lake tailings pore-water suggests that gypsum is in equilibrium in almost all affected zones. The high production rates for SO_4 by pyrite oxidation also suggest that this phase may be actively precipitating in some areas. It is concluded that gypsum is controlled by equilibrium processes.

FIGURE 14.3: PATHWAY DIAGRAM FOR CALCIUM

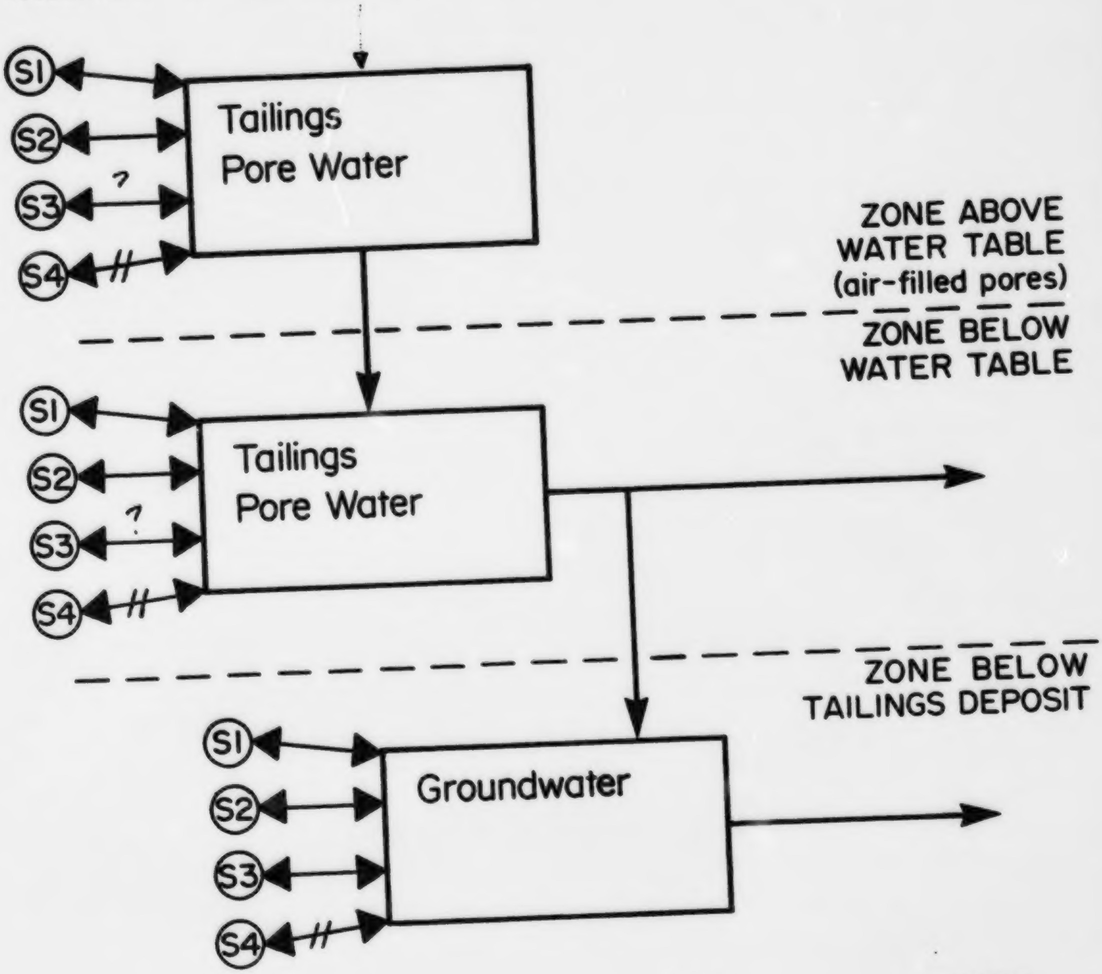
S1
S2
?
S3
S4
//
Tailings Pore Water
ZONE ABOVE WATER TABLE (air-filled pores)
ZONE BELOW WATER TABLE
S1
S2
?
S3
S4
//
Tailings Pore Water
ZONE BELOW TAILINGS DEPOSIT
S1
S2
S3
S4
//
Groundwater

PROCESS	SYMBOL
IRREVERSIBLE-KINETIC	→
REVERSIBLE-EQUILIBRIUM	↔
COPRECIPITATION-EQUIL.	⇌
EXCHANGE-EQUIL.	↔ //
ADSORPTION-KINETIC	→ //
SOLUTION FLUX	➞

SOLID	SYMBOL
Gypsum	S1
Carbonates	S2
Apatite	S3
Clays	S4

- Carbonate ($CaCO_3$)

Limestone has been used in mills for primary neutralization of acidic leaching solutions. This material is also present as a residual component of slaked lime that has been used for secondary neutralization.

Although only trace or small quantities have been detected, the $CaCO_3$ solid can have significant effects on pore water chemistry.

During rapid dissolution, such as occurs in the primary neutralization stage in the mill, the reaction appears to be kinetically controlled, either by precipitate coatings (e.g., gypsum, Figure 11.2) or by slower reaction rates at higher pH values (greater than about 3.5; see Chapter 11). At longer time scales, however, such as those occurring in natural soil or shallow geologic deposits, the evidence suggests that dissolution is essentially instantaneous (Reardon et al., 1980).

In terms of natural infiltration of rain and snowmelt through the tailings, it is highly likely that equilibrium controls dominate the dissolution of $CaCO_3$.

- Silicates

The dissolution of feldspars and pyroxenes will be kinetically controlled. As with most silicate minerals, conditions at the earth's surface usually represent a far-from-equilibrium state. For these particular minerals it is almost certain that kinetically controlled dissolution need only be considered.

Surface Adsorption

As a cation, Ca^{2+} will be subjected to cation exchange on clay surfaces. Generally, Ca^{2+} is preferentially held on exchange sites (compared to Na^+ and Mg^{2+}) so that the clay surfaces can represent a relatively large potential reservoir of this constituent. Such adsorption can be considered as an equilibrium process.

14.4 Iron

Sources

The primary sources of iron in uranium deposits depend on the nature of the ore itself. In the Elliot Lake type ores, pyrite is the major source of iron with other sulphides (i.e., pyrrhotite) and ferro-magnesiun minerals being minor constituents. In contrast, the Saskatchewan deposits contain significant amounts of primary ferric oxyhydroxides (i.e., hematite, geothite) generally with minor contributions by sulphides (i.e., chalcopyrite, pyrite, arsenopyrite, bornite, sphalerite).

During milling of the ore, some transformations of primary minerals occur. In general, the result of these reactions is to deplete the tailings in sulphide-minerals and increase the content of oxide and other non-sulphide phases before discharge. In addition, iron is added to the ore during milling in the form of steel grinding balls or rods.

Occurrence in Tailings

Minerals that form in the mill or shortly after discharge are referred to here as secondary minerals and hence as secondary sources. A list of the major primary and secondary sources of iron in uranium tailings is given in Table 14.1. Other iron minerals in tailings are given in Table 4.11. These solid phases represent potential controls on the solubility of iron. Actual controls are determined by the nature of the reactions and by the relative kinetic and thermodynamic properties of the individual solid phases.

Aqueous species will consist of the uncomplexed ferric and ferrous ion, together with their complexes with SO_4, Cl and OH among others. Major complexes of concern are given in Table 9.2.

Reaction Pathways

The pathway diagram for iron is given in Figure 14.4a.

FIGURE 14.4a: PATHWAY DIAGRAM FOR IRON

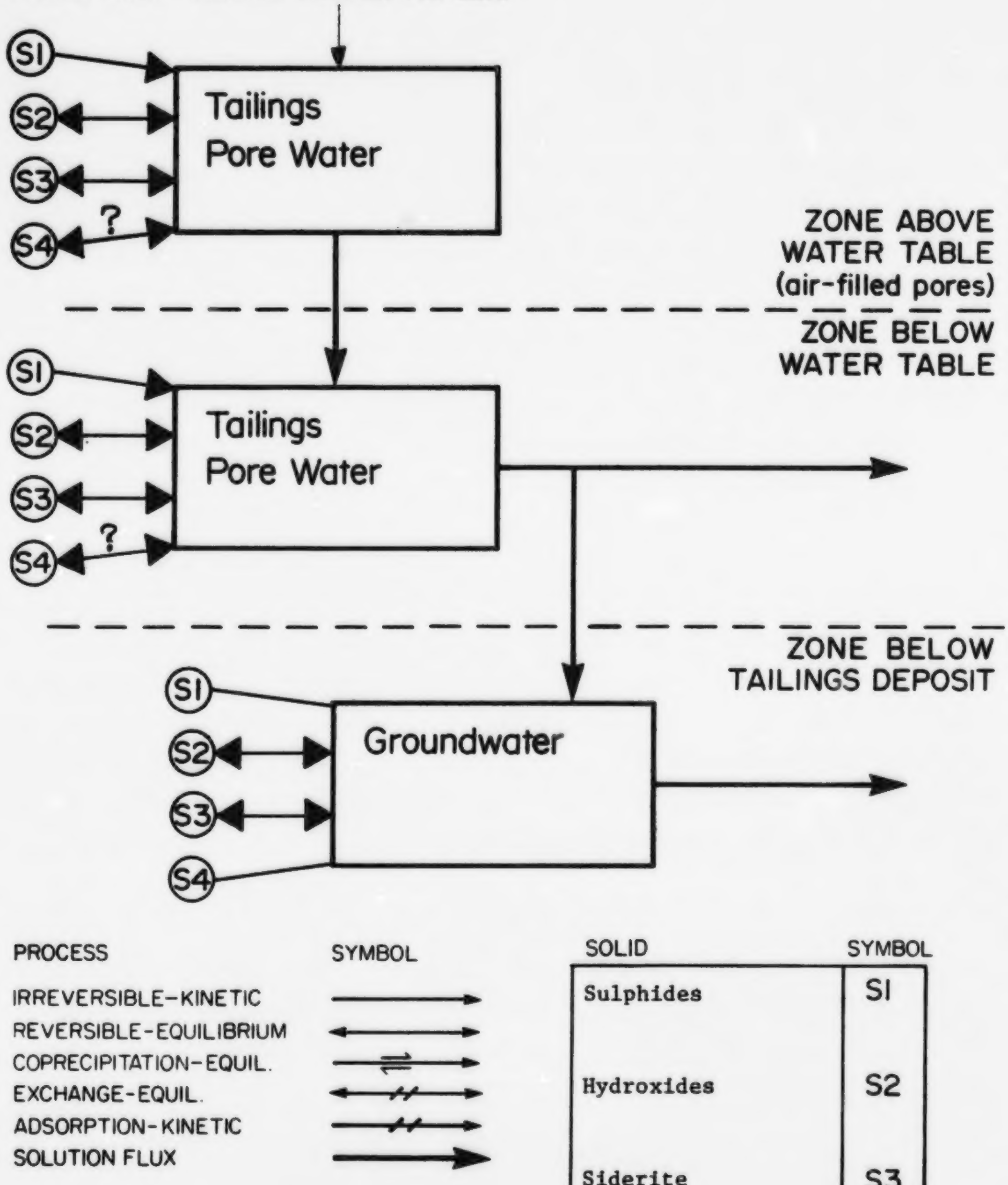
S1
S2
S3
S4
?
Tailings Pore Water
ZONE ABOVE WATER TABLE (air-filled pores)
ZONE BELOW WATER TABLE
S1
S2
S3
S4
?
Tailings Pore Water
ZONE BELOW TAILINGS DEPOSIT
S1
S2
S3
S4
Groundwater
PROCESS
SYMBOL
IRREVERSIBLE-KINETIC
REVERSIBLE-EQUILIBRIUM
COPRECIPITATION-EQUIL.
EXCHANGE-EQUIL.
ADSORPTION-KINETIC
SOLUTION FLUX

SOLID	SYMBOL
Sulphides	S1
Hydroxides	S2
Siderite	S3
Jarosite	S4

o Sulphide Minerals

It is well known that sulphide oxidation occurs at the earth's surface. These minerals are unstable in the atmosphere and many will readily oxidize when moisture and oxygen are present. The best studied example of such a reaction is that of pyrite oxidation which can be represented by,

$$FeS_2(s) + 15/2\,O_2 + 1/2H_2O \longrightarrow Fe^{2+} + 2SO_4 + H^+ \qquad (14.1)$$

Only under very special conditions will this reaction be reversible and even then, the reverse reaction is not likely to be kinetically favourable on the time scale of interest here. Therefore, this reaction is best represented by an irreversible process for which the kinetics are governed by physio-chemical and bio-chemical factors in a particular environment. Reviews of factors controlling the rate of pyrite oxidation are given by van Breeman (1972), Nordstrom (1982), Lowson (1982) and SENES (1984) among others. Other sulphides are expected to behave in a somewhat similar fashion with different values for their kinetic parameters. The need to represent dissolution (oxidation) in a kinetic framework, and potential approaches to predict actual rates are discussed in Chapter 11.

o Oxyhydroxides

Ferric iron forms a variety of solids as oxide phases. The stability of these solids generally depends on the conditions of formation, as well as the age of solid formed. Hematite is the common natural form, although goethite also occurs. In addition, amorphous oxyhydroxides can occur in environments in which ferrous iron is actively oxidizing and in which precipitation has been relatively recent.

Many environments display conditions which suggest that ferric iron concentrations are controlled by one of the oxide phases. In systems where ferric iron is actively precipitating, solubilities are relatively high. Those in which dissolution is occurring have concentrations of ferric iron that are lower, reflecting the greater stability of the residual oxide phases (Langmuir and Whittemore, 1971). A general formula and the resulting reaction in water can be represented by,

$$Fe(OH)_3 + 3H^+ = Fe^{3+} + 3H_2O \qquad (14.2)$$

Although there is some uncertainty as to the actual solubility constant controlling this reaction, the net effect is that ferric iron concentrations are controlled by thermodynamic equilibrium in most aqueous environments.

- Jarosite

Many acid sulphate soils in which pyrite oxidation occurs are characterized by the presence of jarosite (van Breemen, 1973). Some evidence also suggests that this phase occurs in uranium tailings in the Elliot Lake area (Kaiman, 1977; Dubrovsky et al., 1985).

Results from laboratory column studies suggest that jarosite forms in conjunction with pyrite oxidation and that equilibrium is established between that phase and amorphous ferric hydroxide (Miller, 1979). It is, therefore, likely that jarosite formation can be treated in a thermodynamic fashion during pathway calculations. Ferric hydroxides, jarosite and soluble complexes likely control the concentrations of dissolved Fe-III. Total Fe-III concentrations are shown as a function of pH in Figure 14.4b. Calculations for this diagram are based on the assumptions of goethite (alpha-FeOOH) solubility. Jarosite would tend to limit Fe(III) solubility significantly only in the range of pH=1 to 2.

- Siderite ($FeCO_{3(s)}$)

Ferrous carbonate occurs naturally in some environments. The kinetics of precipitation and dissolution are not well known. Some evidence suggests, however, that precipitation of siderite is occurring in the acidic plume below the Nordic site in the Elliot Lake region (Morin and Cherry, 1985). Siderite precipitation likely occurs when high-iron, acidic water contacts the naturally occurring calcium carbonate material in the underlying aquifer. Positive identification of the mineral has been hampered, however, by the natural tendency for oxidation to occur upon short exposure to air. Indirect evidence for siderite formation is found in contaminant plumes emanating from landfill-leachate which are observed to be at or slightly above saturation with respect to siderite (Nicholson et al., 1983; Buzska, 1981).

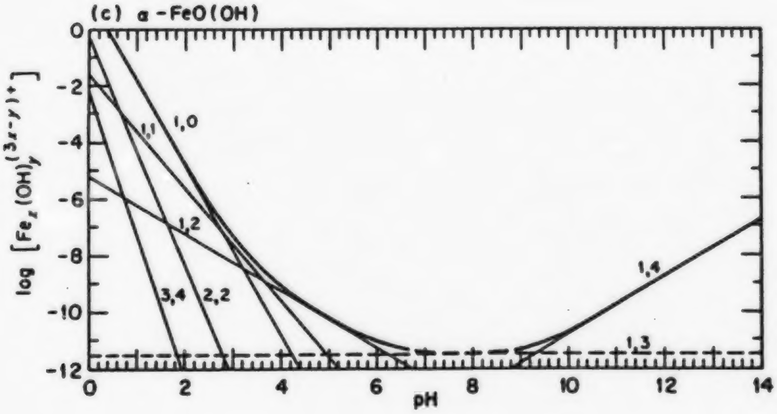

FIGURE 14.4b: DISTRIBUTION OF HYDROLYSIS PRODUCTS (x,y) at I=1 m and 25° in (a) 0.1 m Fe(III), (b) 10^{-5} m Fe(III), and (c) solutions saturated with ∞-FeO(OH); the heavy curve in (c) is the total concentration of Fe(III). (from Baes and Mesmer, 1976)

Dissolution of this mineral will likely occur quickly, particularly because this material would occur as a secondary precipitate. Siderite dissolution should, therefore, behave in a thermodynamically-controlled fashion.

The solubility of Fe-II, assuming hydrolysis complexes only, is given as a function of pH in Figure 14.4c. Sulphate complexes tend to increase solubility at lower pH, but siderite formation limits the solubility of Fe(II) at pH values above 5.

Surface Adsorption

As cations, both ferrous and ferric iron will be subject to cation exchange on clay surfaces. The quantity of iron on these surfaces depends on the available surfaces or clay content, as well as the concentration and types of competitive cations, including H^+.

Dissolved Species

The control of iron concentrations in solution is complex. It is generally accepted that ferric oxyhydroxide controls the levels of Fe(III) in solution whereas Fe(II) could be controlled by siderite solubility when carbonate is present or by hydroxide solids otherwise. Sulphate complexes play an important role in determining both Fe(II) and Fe(III) concentrations in solution. Chloride levels are also important in complex formation with Fe(III).

Redox Conditions

As with many elements that are characterized by different oxidation states in nature (Mn, N, S, C, As, Se, etc.), redox conditions affect solution composition and hence, ratios of Fe(II)/Fe(III). Because the different oxidation states of an element often behave in very different manners, the control on oxidation state can be of critical importance. Unfortunately, of almost all parameters in natural aqueous systems, redox conditions are probably the most ill-defined. Not only is the redox state difficult to measure but often the different redox-sensitive elements do not behave in an equilibrated fashion and kinetic constraints often result in poor comparisons among different species as to what the effective redox state of the solution is. This is one large uncertainty that will occur in any predictive model that is developed. This uncertainty will also be present for other

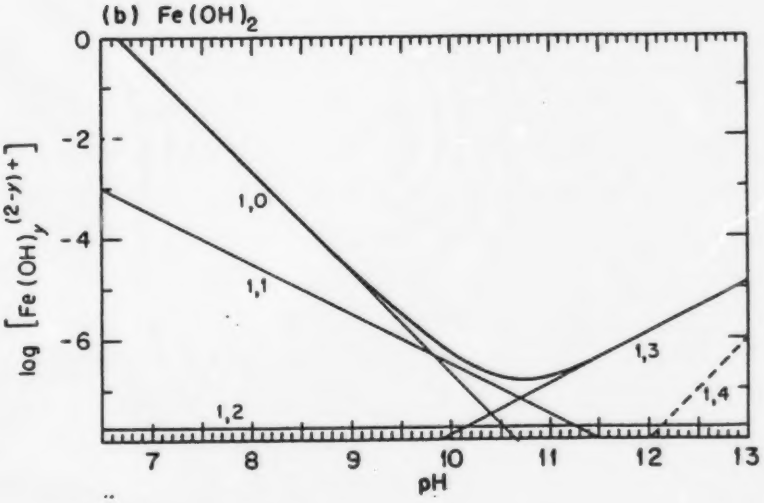

FIGURE 14.4c: DISTRIBUTION OF HYDROLYSIS PRODUCTS (x,y) at I=1 m and 25° in (a) 10^{-3} m Fe(II) and (b) solutions saturated with $Fe(OH)_2$. The dashed curves in (a) denote regions supersaturated with respect to $Fe(OH)_2$; the heavy curve in (b) is the total concentration of Fe(II). (from Baes and Mesmer, 1976)

redox-sensitive species. In the uranium tailings, this would have important consequences for Fe, S, C, As, Se and some trace metals.

At best, qualitative estimates of redox conditions can be made. For example, only Fe(II) would be expected to be present in significant concentrations in the presence of pyrite (Fe(III) is reduced) or sulphate may be reduced to sulphide in organic-rich zones, such as peat.

14.5 Sulphur

Sources

Sulphur occurs primarily and almost exclusively as metal sulphides in various ore types. In Elliot Lake ores, sulphur comprises about 3% by weight of the ore mostly as pyrite whereas in Saskatchewan ores, sulphur contents and minerals vary but are generally less important.

Occurrence in Tailngs

Gypsum that is produced during the neutralization of the sulphuric acid leach represents the largest reservoir of sulphate in the tailings. Sulphate solids containing aluminum (i.e., alunite, basaluminite, jurbanite) and iron (i.e., K-jarosite) are also likely to occur in the pyritic tailings but to a much lesser extent than gypsum. Ettringite ($Ca_6Al_2(SO_4)_3(OH)_{12}.26H_2O$) has recently been identified (Knight and Piesold, 1985; Constable and Snodgrass, 1982) and is probably formed during neutralization with calcium compounds. Ettringite is typically identified in concrete studies. Pyrite is the largest reservoir of sulphide in many tailings. Pyrite and other sulphides are a source of sulphate during pyrite oxidation in the unsaturated zone of the tailings deposit. A summary of major primary and secondary minerals containing sulphur is given in Table 14.1. Other minerals are summarized in Table 4.11.

Reaction Pathways

The pathway diagram for sulphur is given in Figure 14.5.

FIGURE 14.5: PATHWAY DIAGRAM FOR SULPHUR

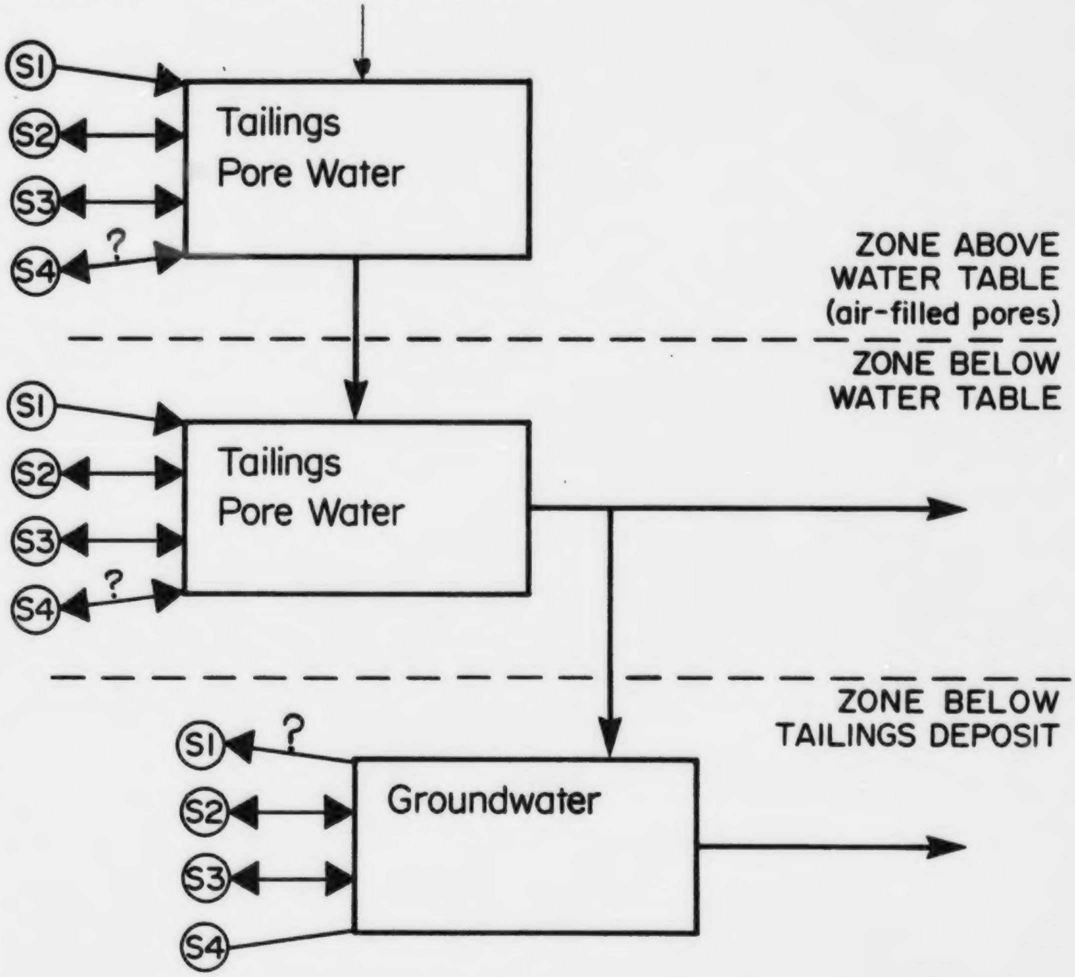
S1
S2
S3
S4
?
Tailings
Pore Water
ZONE ABOVE
WATER TABLE
(air-filled pores)
ZONE BELOW
WATER TABLE
S1
S2
S3
S4
?
Tailings
Pore Water
ZONE BELOW
TAILINGS DEPOSIT
S1
?
S2
S3
S4
Groundwater

PROCESS	SYMBOL
IRREVERSIBLE-KINETIC	→
REVERSIBLE-EQUILIBRIUM	↔
COPRECIPITATION-EQUIL.	⇌
EXCHANGE-EQUIL.	↔ //
ADSORPTION-KINETIC	→ //
SOLUTION FLUX	➔

SOLID	SYMBOL
Sulphides	S1
Gypsum	S2
Al-Sulphate	S3
Jarosite	S4

- Sulphides

Sulphide-mineral oxidation will occur as described above. Kinetic controls on dissolution and oxidation will dominate. In addition to releasing sulphate to tailings pore water, hydrogen ion production also occurs. Sulphide mineral oxidation is the cause of acidic pore water development in previously neutralized tailings.

- Gypsum

For reasons discussed above, equilibrium behaviour is expected to control dissolution and precipitation of gypsum.

- Al-and Fe-Sulphates

As stated above, equilibrium conditions are expected for basaluminite and alunite. Similar behaviour is expected for K-jarosite formation, provided bacteria are present, but kinetic control for jarosite dissolution is possible. The geochemical control on ettringite is not clear, but equilibrium control is plausible by analogy to concrete reactions.

14.6 Carbon

Sources

The sources of carbon are limited to trace organic carbon associated with U-mineralization in the ores and vegetative decay if vegetation is established. Trace-to-accessory quantities of carbonate in the form of calcite ($CaCO_3$) have also been found in ores located in Saskatchewan. In some tailings (i.e., Gunnar), organic matter may have been introduced concurrently with tailings deposition as sewage or other waste.

Occurrence in Tailings

Calcium carbonate has been added in many acid-leach mill circuits during primary neutralization and as a residual substance in slaked lime during secondary neutralization. In Elliot Lake tailings, this material may comprise up to a few tenths of

1%, by weight, of the tailings. In neutralized zones of the tailings that contain high ferrous iron concentrations, it is likely that siderite will have formed.

Graphite is present in Key Lake tailings at levels of 1 to 3%.

A summary of major primary and secondary minerals containing carbon is given in Table 14.1. Other minerals are summarized in Table 4.11.

Reaction Pathways

A pathway diagram for carbon is given in Figure 14.6.

- Calcite and Siderite

For reasons discussed previously, it is probable that calcite will behave in an equilibrium fashion. Similar behaviour is expected for siderite dissolution and precipitation. It should be noted, however, that the formation or presence of pure endmembers of these solids is unlikely, hence the thermodynamic data (i.e., solubility constants) will not necessarily correspond to reported values in the literature. An example of this is given by Morin et al. (1985) who conclude that highly supersaturated values for siderite in a number of contaminated geologic deposits represent discrepencies in the thermodynamic data used to calculate the degree of saturation present. This explanation is not definitive, however, and other explanations may be invoked, such as kinetic restrictions on precipitation.

- Carbon Dioxide

Dissolution of carbonate minerals by low pH solutions produces CO_2 gas. In zones above the water table in which interconected gas-filled pores are present, the CO_2 will degas to attain equilibrium with the solution phase. The resulting high concentrations of carbon dioxide in the pore spaces would induce mass transport, by diffusion and possibly advection, toward the tailings surface and the atmosphere. This is referred to as open-system dissolution of the carbonate minerals. The partial pressure of CO_2 gas, in this case, may remain relatively constant.

FIGURE 14.6: PATHWAY DIAGRAM FOR CARBON

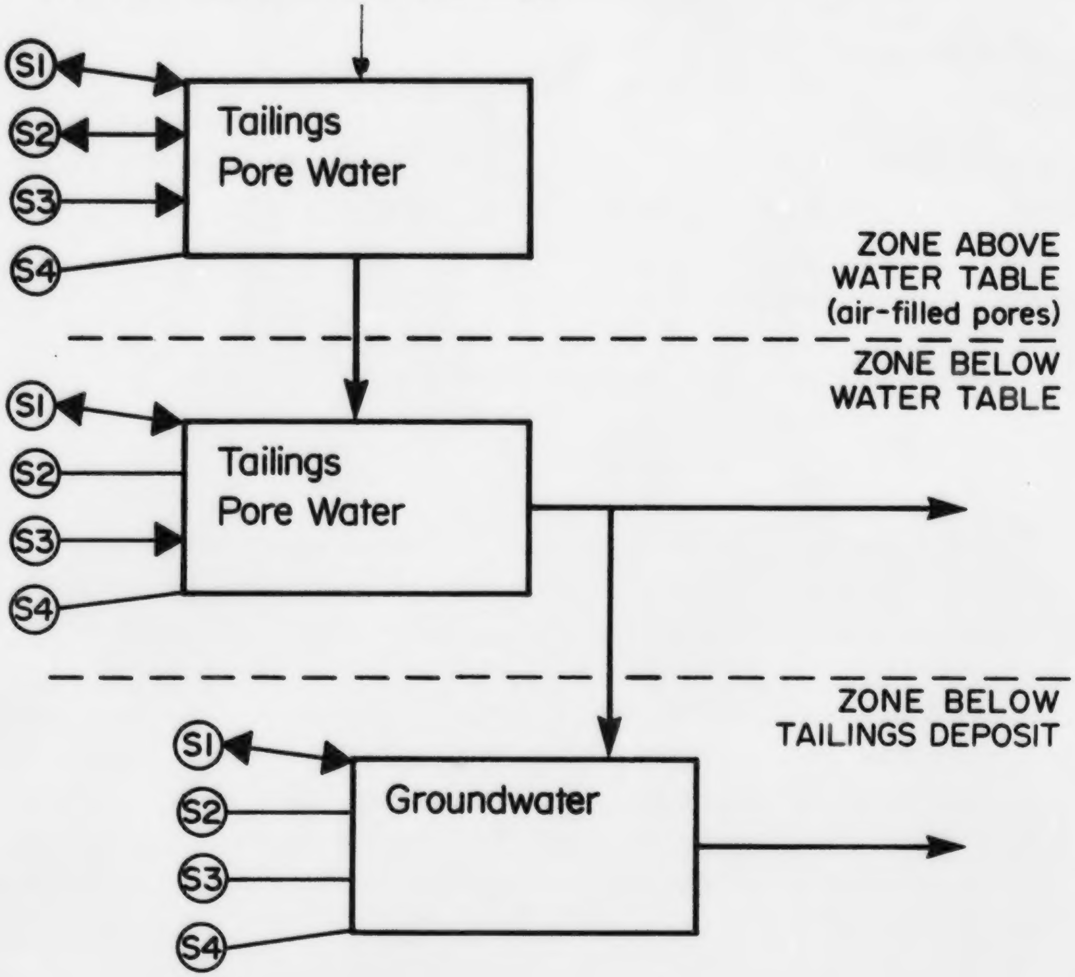
S1
S2
S3
S4
Tailings Pore Water
ZONE ABOVE WATER TABLE (air-filled pores)
ZONE BELOW WATER TABLE
S1
S2
S3
S4
Tailings Pore Water
ZONE BELOW TAILINGS DEPOSIT
S1
S2
S3
S4
Groundwater

PROCESS	SYMBOL
IRREVERSIBLE-KINETIC	→
REVERSIBLE-EQUILIBRIUM	↔
COPRECIPITATION-EQUIL.	—⇌→
EXCHANGE-EQUIL.	←//→
ADSORPTION-KINETIC	—//→
SOLUTION FLUX	➞

SOLID	SYMBOL
Carbonates	S1
CO_2 (gas)	S2
Graphite	S3
	S4

Similar dissolution below the water table occurs in a closed system in which the CO_2 remains as a dissolved component and is not lost to the gas phase. In the closed system, the partial pressure of CO_2 gas increases in response to dissolution and low pH conditions. During subsequent neutralization, if any occurs, the dissolved CO_2 provides a source of carbonate for further reactions such as siderite precipitation.

14.7 pH

The pH is defined as minus the log of the hydrogen activity. The hydrogen ion activity is equal to a chemical activity coefficient times the concentration of free hydrogen ion in solution. Hence,

$$pH = -\log (H^+) \tag{14.3}$$

Hydrogen ion originates from various complexes such as bicarbonate, dissociation of water molecules ($H_2O = H^+ + OH^-$), and dissolution reactions (e.g., oxidation of pyrite - see Equation 6.1; Table 6.1). Hence, its chemistry is quite complex.

pH as a Master Variable

Along with temperature, hydrological flow rate, Eh and other variables, pH may be viewed as a master variable in any geochemical system. In this context, pH regulates various mechanisms:

(i) the equilibrium concentration of various solids in solution (e.g., the solubility of Ca^{2+} in equilibrium with calcite changes as a function of pH; see Equation 6.12, Table 6.2);

(ii) the kinetic rate of dissolution of various solids is a function of solution pH (e.g., feldspars below pH 2.9; calcite between pH 2 and 7; see Chapter 10); and

(iii) the activity of some bacteria is strongly regulated by pH. For example, nitrifers substantially cease their activity below pH 5.5, whereas the optimum pH for T. ferrooxidans is in the range of 1-3.

But pH is, itself, regulated by complexation, precipitation and dissolution reactions. In most systems with pH greater than 3, the largest fraction of hydrogen ion in solution is complexed with inorganic anions such as CO_3^{2-} ($H_2CO_3^*$, HCO_3^-) or is regulated by its equilibrium relationship with hydroxyl ion (OH^-) according to

$$H^+ + OH^- = H_2O \qquad (14.4)$$
$$(H^+)(OH^-) = K_w$$

and complexation reactions of hydroxyl ions with various cations such as iron ($FeOH^{2+}$, $Fe(OH)_2^+$, $Fe(OH)_3^0$, $Fe(OH)_4^-$) and aluminum ($AlOH^{2+}$, $Al(OH)_2^+$, $Al(OH)_4^-$, $Al_2(OH)_4^{2+}$).

In addition to measureable pH, the porewater will also have a total acidity value. Total acidity is defined as the capacity of a solution to consume OH^- to attain a near-neutral pH. Many tailings pore waters may be characterized by near-neutral pH at depth but also have high acidity values. This can be shown for a solution with high Fe(II) concentrations at neutral pH.* When titrated with base and exposed to air the solution oxidizes rapidly and Fe(III) precipitates as the hydroxide phase, as in the reverse of Equation 6.2 (Table 6.1). In that case, the Fe(III) consumes the added base. This is a realistic way to view potential acidity because oxidation and precipitation of this type is expected if the tailings porewater eventually enters a stream or lake. In this way it can be shown that the total potential acidity of a solution may be far greater than is indicated by the pH or total TOT H alone.

Accordingly, in addition to pH being a master variable, it is regulated by other systems. This regulation is termed "a buffering system". The buffering system is composed of the soluble aqueous complexes. It may also be viewed as being composed of the solid system, although the solid system is a "secondary system" - solid-solution reactions control the total amount of inorganic cations and anions and TOT H in solution, but individual solution complexation reactions determine the actual pH.

Buffering Systems in Natural Waters

Three major types of buffering systems will influence pH in tailings pore water. They are:

(i) anions such as carbonate which complexes to form HCO_3^- and $H_2CO_3^*$. Other cations include SO_4^{2-} and S^{2-};

(ii) cations such as Fe^{3+}, Fe^{2+}, and Al^{3+}, and

(iii) cation exchange reactions with clays (e.g., the displacement of Ca^{2+} by 2 H^+).

In the groundwater literature, solids such as $Al(OH)_3(s)$, $Fe(OH)_3(s)$ and alumino silicates such as K-feldspar are sometimes also viewed as being H^+ buffering systems. As noted above, they are secondary systems, influencing the total concentration of Al^{3+}, Fe^{3+}, TOT H etc., in solution.

The roles of carbonate, sulphate and Fe^{3+} as buffering systems are given in Table 6.1 and 6.2 and used in the development of the example model in Chapter 6. The role of sulphide as a buffering system is given by the reactions:

$$HS^- = H^+ + S^{2-} \quad (14.5a)$$
$$H_2S = H^+ + HS^- \quad (14.5b)$$

The role of aluminum as a buffering system is determined through hydroxyl ion in the reactions:

$$Al^{3+} + OH^- = AlOH^{2+} \quad (14.6a)$$
$$AlOH^{2+} + OH = Al(OH)_2^+ \quad (14.6b)$$
$$Al(OH)_2^+ + 2OH^- = Al(OH)_4^- \quad (14.6c)$$

Modelling H^+ Exchange With Clays

Cation exchange is probably not itself a significant controller of the hydrogen activity, but rather of the amount of TOT H in the aqueous system. There are two types of reactions proposed for the interaction of protons with clays (Bouti, 1983) an exchange reaction with another cation, M^{+n} and at low pH's, a reaction involving Al^{+3}. Secondary products on the surfaces of soil particles such as $Al(OH)_3$, allophane, Fe_2O_3 and organics may act as reaction sites as well.

In intermediate pH ranges (5-8), exchange reactions can be described by

$$M^{+n}X + H^{+} \rightleftharpoons H^{+}X + 1/nM^{+n} \qquad (14.7)$$

Using the relationship from this equation that

$$\frac{(\text{ads M})}{(\text{ads H})} = \frac{\text{ads } K^{1} (M^{+})^{1/n}}{(H^{+})} \qquad (14.8)$$

and assuming that only M^{+n} and H^{+} react, one obtains a Langmuir type relationship (Bouti, 1983):

$$(\text{ads H}) = \frac{(\text{CEC})(H^{+})}{K^{1} + (H^{+})} \qquad (14.9)$$

where $K^{1} = \text{ads } K^{1} (M^{+n})^{1/n}$

Where a distinct break is observed in the titration curve between pH 4 and 5, the mechanism of H^{+} from solution exchanging for Al^{3+} in the crystal lattice has been invoked to explain this observation. In this case, a two-step Langmuir model has been used. It is:

$$(\text{ads } H^{+}) = \frac{\text{CEC}_{1}(H^{+})}{K_{1}^{1} + (K^{+})} + \frac{\text{CEC}_{2}(H^{+})}{K_{2}^{1} + (H^{+})} \qquad (14.10)$$

Adsorption at upper pH's and clay dissolution at low pH (pH less than 5) has been modelled by the equation:

$$(\text{ads } H^{+}) = \frac{\text{CEC}(H^{+})}{K^{1} + (H^{+})} + K_{D}^{1}(H)^{P} \qquad (14.11)$$

In the above equation, the symbols are:

(ads M) and (ads H) are adsorbed concentrations in eq/kg solid

(M^{+n}) and (H^+)	are porewater concentrations in eq/kg solution
ads K^l	is the conditional exchange constant (concentration $^{-n}$)
CEC	is the cation exchange capacity of the site
P	is a function of the dissolution reaction.

Determination of Major Buffering Systems

Buffering of solution-phase systems results from the distribution of protinated or hydrolysed species. This can be seen for the carbonate system in Figure 14.7a, which shows the species distribution ($H_2CO_3^o$, HCO_3^-, and CO_3^{2-}) with pH. At pH values where two species are equal in concentration, the buffer intensity is at a maximum (Figure 14.7a) and addition of acid or base results in less change in pH than at other pH values (Figure 14.7b). Higher concentrations of buffering species result in larger buffer capacities. Although dissolved species contribute to pH buffering, reactions with solids in hydrogeologic systems probably represent a more significant control on solution pH.

The close contact with solids and relatively long residence times for subsurface water generally result in significant acid-base reactions with the geologic materials. Because of the large potential reservoir of H^+ or OH^- in solid phases, the reactions with these materials may be many orders-of-magnitude greater than with initial solution species alone.

An example of the buffering capacity of solids representing fresh uranium tailings from Elliot Lake is given by Cherry et al (1983). In this case, the solids which have a relatively low buffer capacity due to small quantities of calcite, aluminum hydroxide and ferric hydroxide were titrated with sulphuric acid in a continuous flow-through column. In this way the number of pore volumes eluted from the column represent the quantity of acid added. The results show that major buffering occurs at 5 different pH values, shown as pH plateaus in Figure 14.7c. First, calcite is dissolved during which the minimum pH approaches 6.3. Further titration results in pH reduction to about 5.8 (Zone A), at which point siderite dissolution occurs (Zone B). Continued titration reduced the pH to about 4 where aluminum hydroxide dissolution results in the largest pH plateau (Zones C and D). A final pH buffer is evident at about pH=2.8 (Zone E) where ferric hydroxide dissolution occurs. These results have been compared to equilibrium simulations with good agreement between the laboratory and model results. They also compare reasonably well to the model simulation results for solids acidification in Chapter 10.

FIGURE 14.7: PATHWAY DIAGRAM FOR H

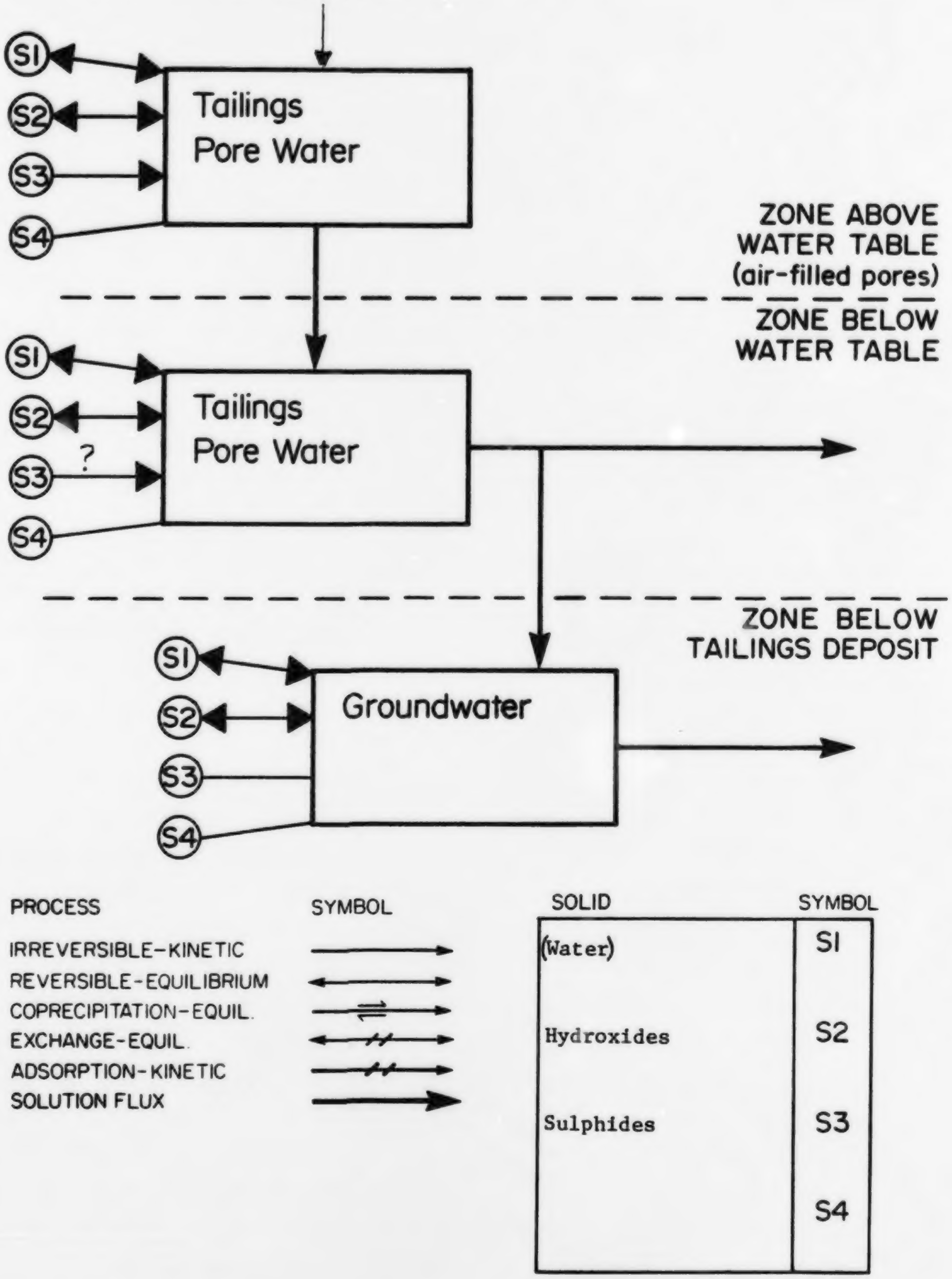
S1
S2
S3
S4
Tailings Pore Water
ZONE ABOVE WATER TABLE (air-filled pores)
ZONE BELOW WATER TABLE
S1
S2
?
S3
S4
Tailings Pore Water
ZONE BELOW TAILINGS DEPOSIT
S1
S2
S3
S4
Groundwater
PROCESS
SYMBOL
IRREVERSIBLE-KINETIC
REVERSIBLE-EQUILIBRIUM
COPRECIPITATION-EQUIL.
EXCHANGE-EQUIL.
ADSORPTION-KINETIC
SOLUTION FLUX
SOLID
SYMBOL
(Water)
S1
Hydroxides
S2
Sulphides
S3
S4

14 .7a

14 7b

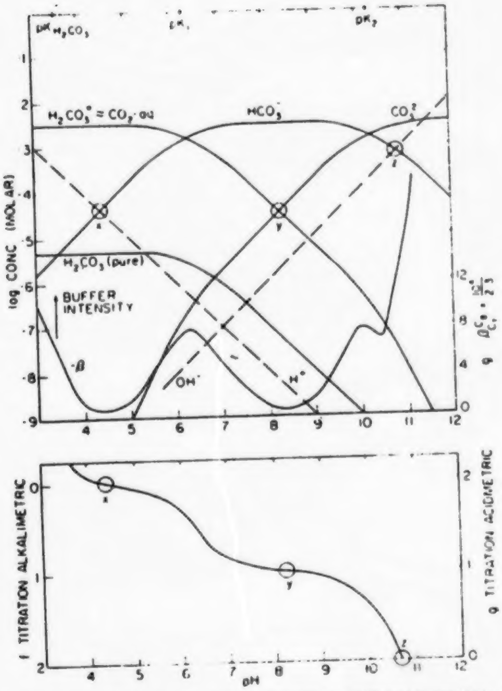

FIGURE 14 7 Distribution of solute species in aqueous carbonate system. This figure has been constructed under the assumption that C_T = constant = $10^{-2.5}$ M. The following equilibrium constants (typical for a fresh water of 25°C and corrected for an ionic strength of $I \approx 5 \times 10^{-3}$ to 10^{-2} M) have been used: $pK_{(hydration)} = -2.8$, $pK_1 = 6.3$, $pK_2 = 10.25$.

a: Ionization fractions as a function of pH.

b: Logarithmic equilibrium diagram. Because $[CO_2(aq)] \gg [H_2CO_3]$, $[CO_2aq] \approx [H_2CO_3^*]$. Note that H_2CO_3 is a much stronger acid than $CO_2(aq)$ or $H_2CO_3^*$. Pure H_2CO_3 has a pK value (where $[H_2CO_3] \doteq [HCO_3^-]$) of $pK_{H_2CO_3} = 3.5$. The equivalence points corresponding to pure solutions (C_T-molar) of $H_2CO_3^*$, $NaHCO_3$ and Na_2CO_3 are marked *x*, *y* and *z*, respectively. Buffer intensity is plotted as a function of pH.

c: Alkalimetric or acidmetric titration curve. Note that no pH jump occurs at the equivalence point *z*, because at this point the buffer intensity caused by high $[OH^-]$ is too large. (after Stumm & Morgan, 1981)

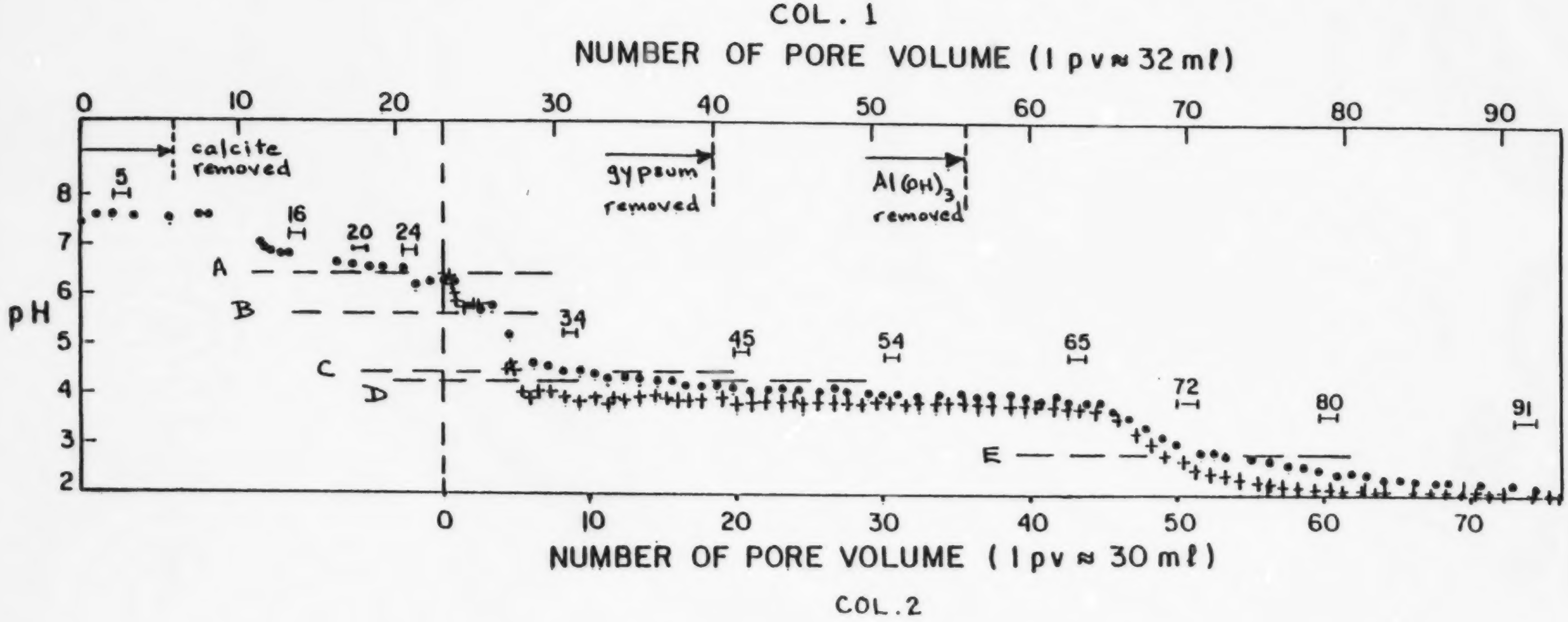

FIGURE 14.7c: **BUFFERING OF PERCOLATING WATER BY FRESH URANIUM MILL TAILINGS**

(Columns 1 and 2 of neutralized tailings were set up and sulphuric acid allowed to percolate through. The resultant pH profile is shown with model calculations. Data for Columns 1 and 2 overlain so that the points at which pH drops below approximately 3.9 coincide. The horizontal lines show equilibrium pH values predicted by the ADNEUT mixing cell model for the following sequence of solid phases: A) calcite-gypsum-$Al(OH)_3$-$Fe(OH)_3$; B) siderite-gypsum-$Al(OH)_3$-$Fe(OH)_3$; C) gypsum-$Al(OH)_3$-$Fe(OH)_3$; D) $Al(OH)_3$-$Fe(OH)_3$; E) $Fe(OH)_3$ (after Cherry et al., 1983).)

14.8 Nickel

Sources

The primary sources of nickel in uranium ore depend strongly on ore type and location. In general, nickel occurs as a substitution element or impurity in other metal sulphide minerals in Elliot Lake type ore-deposits. In contrast, significant quantities of nickel are present in a variety of sulphide and arsenide minerals that occur in many Saskatchewn ores. The important nickel-bearing minerals include niccolite, skutterudite, gersdorffite and pararammelsbergite.

Occurrence in Tailings

During the acid leach process, much of the nickel that it present in arsenide and sulphide minerals is dissolved. Nickel that occurs as an impurity in pyrite will not be significantly released, however, because of the relative stability of pyrite in the mill circuit.

The solubilized nickel precipitates as an oxide and/or hydroxide solids during neutralization prior to tailings discharge. Although precipitation of oxides, hydroxides, arsenates, carbonates and other solids is expected, a significant amount of coprecipitation with the abundant ferric hydroxide material should also occur when Ni concentrations are high in the mill. Primary and secondary forms of nickel solids are listed in Table 14.1. Other nickel minerals in tailings are given in Table 4.11.

Reaction Pathways

A pathway diagram for nickel is given in Figure 14.8.

o Sulphides and Arsenides

The residual primary sulphide and arsenide minerals containing nickel are expected to be unstable in the tailings deposit. Oxidation of these minerals will lead to dissolution of the nickel resulting in a potential for transport with the pore water and/or transformation to metastable solids of oxides, hydroxides and others. The dissolution of sulphide and arsenide minerals will be kinetically controlled, although the mechanisms

FIGURE 14.8: PATHWAY DIAGRAM FOR NICKEL

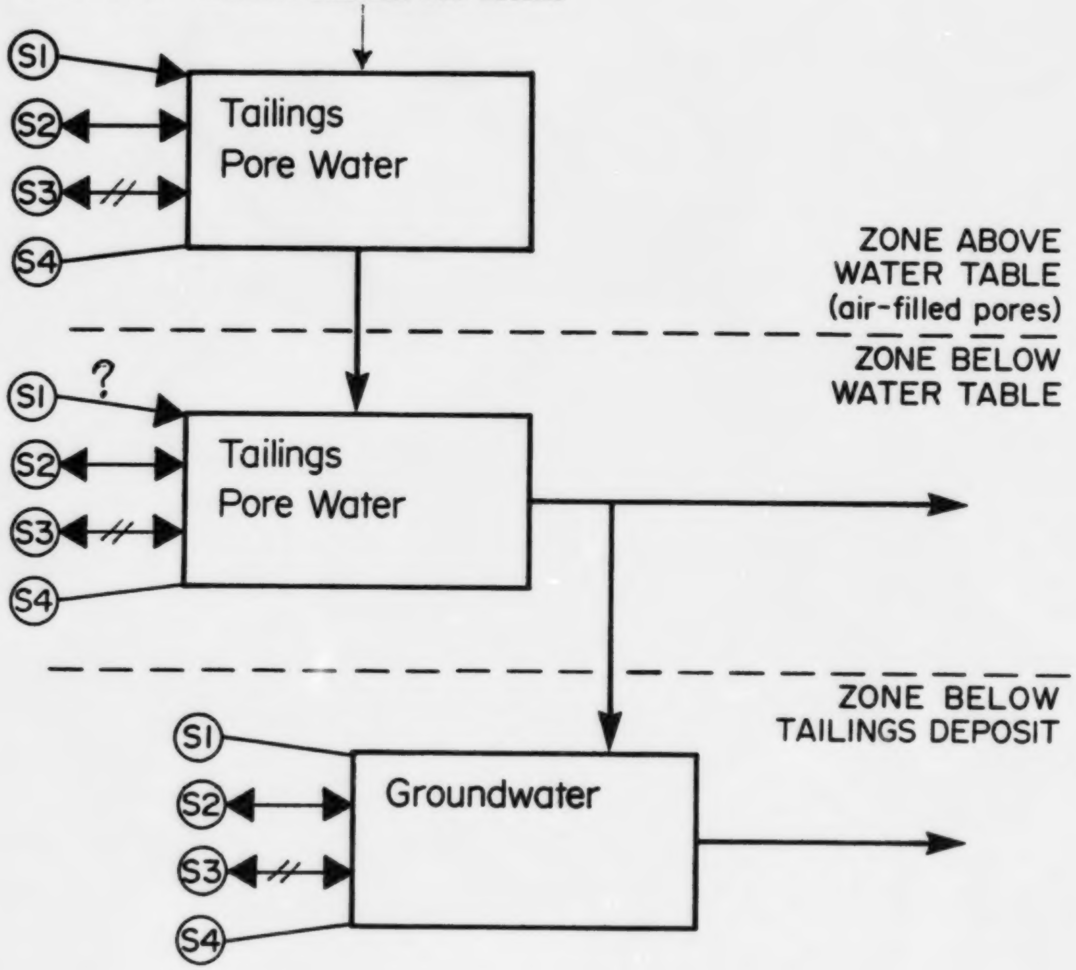
S1
S2
S3
S4
Tailings Pore Water
ZONE ABOVE WATER TABLE (air-filled pores)
ZONE BELOW WATER TABLE
S1
?
S2
S3
S4
Tailings Pore Water
ZONE BELOW TAILINGS DEPOSIT
S1
S2
S3
S4
Groundwater

PROCESS	SYMBOL
IRREVERSIBLE-KINETIC	→
REVERSIBLE-EQUILIBRIUM	↔
COPRECIPITATION-EQUIL.	–⇌→
EXCHANGE-EQUIL.	←//→
ADSORPTION-KINETIC	–//→
SOLUTION FLUX	➞

SOLID	SYMBOL
Arsenides Sulphides	S1
Oxides Sulphates	S2
Clays	S3
	S4

and controlling factors are not well understood. Oxidation of nickel sulphides would also generate hydrogen ions that could effectively lower pH values in the absence of sufficient buffer material and, therefore, increase the solubility of secondary nickel solids.

There is also an indication that nickel existing as an impurity in the pyrite in Elliot Lake tailings is mobilized in proportion to the amount of pyrite oxidized. The levels of nickel in this case are relatively low; hence formation of secondary solids would be limited.

Secondary Solids

The information on potential formation of secondary nickel solids in the environment is scarce. However, some speculation can be made, based on available thermodynamic data. These data suggest that solids such as $Ni(OH)_2$, $NiCO_3$, $Ni_3(PO_4)_2$ and possibly $Ni_3O_4 \cdot 2H_2O$ may occur. More study is needed to determine which of these solids would actually occur under favourable conditions and whether kinetic controls would hinder the formation of some.

Surface Adsorption

The cationic nature of Ni in solution would suggest that this element would be affected by ion exchange and adsorption processes. Some cation exchange constants are available (see Chapter 13), although nickel adsorption has been studied using other models. More study in this area is in order.

14.9 Arsenic

Sources

Primary minerals containing significant quantities of arsenic include niccolite, skutterudite and pararammelsbergite. These arsenic minerals are associated with the Saskatchewan ores, while they are not detectable in Elliot Lake type ores. The quantity of arsenic can be quite significant with concentrations of up to about 10% in some ore samples (Sherrit, 1980).

Occurrence in Tailings

Dissolution and oxidation of part of the primary arsenide minerals will occur within the mill circuit. It has been estimated that 60 to greater than 90% of the total available arsenic will be mobilized (Sherrit, 1980). Because the leach solution is oxidizing and because arsenic redox reactions are relatively rapid (Cherry et al., 1979), most of the dissolved arsenic would occur in the +V state. During neutralization of the tailings, formation of arsenate (V) and perhaps arsenite (III) salts is expected. Specifically, the precipitation of calcium orthoarsenate ($Ca_3(AsOH)_2.3H_2O$) has been hypothesized in Key Lake tailings (Knight and Piesold, 1985) as 2% by weight. In addition, adsorption of the anionic arsenic species onto ferric hydroxide precipitates will probably occur. In Key Lake tailings, the incongruent dissolution of calcium arsenate to haidingenite ($(CaO)_2.As_2O_5.3H_2O$) has been hypothesized to explain low levels of arsenic (LT 1 mg/L) observed below pH 10 (at such low levels, calcium arsenate solubility would allow 100 mg/L in pore water). A list of primary and possible secondary solids containing arsenic is given in Table 14.1. Other minerals are given in Table 4.11.

Reaction Pathways

A pathway diagram for arsenic is given in Figure 14.9.

o Arsenides

The dissolution and oxidation of the residual primary minerals in the tailings would be kinetically controlled. Mobilization and transformations to secondary solids would then be possible. Dissolution and/or oxidation rate data do not appear to be readily available.

Secondary Solids

The details of secondary arsenic minerals are not well known. It is probable that some arsenic solids form in the mill, with subsequent mobilization of dissolved arsenic in the tailings. Review of the solubility data suggests that only Ca, Ba and Fe(III) arsenates are stable enough to limit As (V) concentrations to those observed in the tailings effluent after neutralization. It is possible that arsenite (As III) salts would also be present initially, but those would tend to oxidize to arsenate in the oxidizing tailings environment.

FIGURE 14.9: PATHWAY DIAGRAM FOR ARSENIC

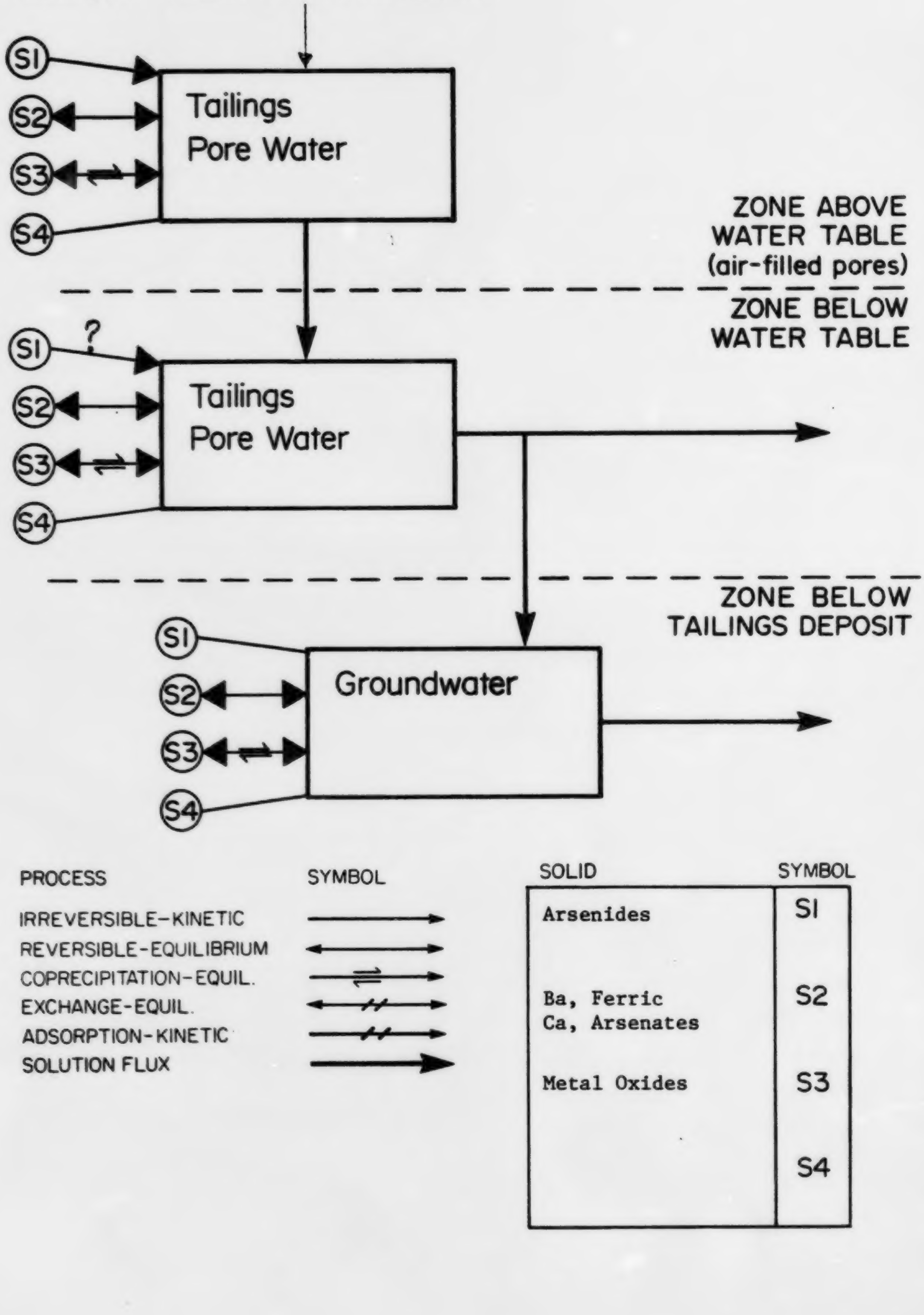
S1
S2
S3
S4
Tailings
Pore Water
ZONE ABOVE
WATER TABLE
(air-filled pores)
ZONE BELOW
WATER TABLE
?
Tailings
Pore Water
ZONE BELOW
TAILINGS DEPOSIT
Groundwater
PROCESS
SYMBOL
IRREVERSIBLE-KINETIC
REVERSIBLE-EQUILIBRIUM
COPRECIPITATION-EQUIL.
EXCHANGE-EQUIL.
ADSORPTION-KINETIC
SOLUTION FLUX
SOLID
SYMBOL
Arsenides
S1
Ba, Ferric
Ca, Arsenates
S2
Metal Oxides
S3
S4

Little is known about the potential secondary solids and therefore it is difficult to determine whether kinetic or thermodynamic controls would dominate. It is plausible that calcium orthoarsenate dissolution follows equilibrium relationships.

Surface Adsorption

Studies have shown that the anionic arsenic species that are dominant in neutral to alkaline solution are prone to adsorption on hydrous metal oxides (i.e., ferric hydroxide). Fresh precipitates of this material that would be relatively abundant have a greater affinity for adsorption.

14.10 Radionuclides in General

Sources

The main sources of radionuclides of concern to tailings management are U-238 and Th-232 decay series radionuclides. The major and minor daughters are given in Chapter 4.

The major sources of U-238 minerals in Elliot Lake ores are brannerite and uraninite; these ores generally contain 0.05 - 0.10% uranium. In Saskatchewan ores, the main mineral is pitchblende $(UO_2 \cdot UO_3)$ with some coffinite $((U(Si)_4)_{1-x}(OH)_{4x})$ and brannerite. Typical concentrations in Saskatchewan ores are 1 to 3%.

The major source of Th-232 minerals in Elliot Lake ores is monazite (Ce, La, Y, Th) (PO_4) with small amounts in other minerals. The extent of Th-232 minerals in Saskatchewan ores requires some synthesis. The data of Sherritt (1980) for Key Lake give Th-232 decay nuclide levels in laboratory studies on the effluent, but solid component concentrations are not given. Recent solids data for Key Lake (Knight and Piesold, 1985) indicate that Th is a trace constituent (0.001%). Th is also a trace constituent in Gunnar tailings. For the Mid-West deposit, the EIS report (Canada Wide Mines Ltd., 1981) indicates Th (.014 - .033%) and Phosphorus (.034 - .0036%) for "sandstone" and "massive ore".

Occurrence in Tailings

The radionuclides of U-238 are mainly redistributed into other chemical forms by milling because of 93-97% dissolution of U-238 in Elliot Lake ores and an extraction goal of 99% in Saskatchewan ores. The redistribution of Th-232 minerals is much less because acid is not as successful at attacking monazite. A rule of thumb is that 50% of Th-232 minerals are leached in Elliot Lake ores.

Pathway Diagrams

Two diagrams are given in Figures 14.10 and 14.11 for U-238 radionuclides and one diagram for Th-232 minerals in Figure 14.12. These diagrams are discussed below for each radionuclide.

The two diagrams for U-238 minerals represent two different levels of complexity. Level 1 considers one gypsum solid (S2), an aqueous form, a (Ca, Ba) SO_4 form (S3), an adsorbed form, a thorium hydroxide (S5) and a residual mineral (S6). Level 2 considers the same forms as Level 1, but adds a gypsum form (S1), a (Ca, Ba)SO_4 form for the other three radionuclides, a thorium hydroxide form for the U radionuclides and jarosite (S4).

Two gypsum forms are indicated in Figure 14.11 (Level 2) to indicate coprecipitation by gypsum formed in the partial neutralization and final neutralization tanks. This differentiation is probably not justifiable for long-term modelling purposes, meaning that S1 and S2 would be combined as one solid.

Various arrows between the compartments are explained in the definition of arrows on the page opposite the Figures. They allow one to differentiate between equilibrium, coprecipitation, and kinetic control on solid-solution behaviour. As well, arrows denoting outflow are given. For the unsaturated zone, the outflow arrow would be vertically downward. For the saturated zone, the outflow arrow would be to surface water or groundwater.

LEGEND

Symbol	Solid
S1	Gypsum (Partial Neutralization)
S2	Gypsum
S3	(Ca,Ba) SO_4
S4	jarosite
S5	thorium hydroxide
S6	residual minerals

Arrows

↓	decay
↱	outflow
→	dissolution
↔	equilibrium
⇄	coprecipitation

FIGURE 14.10 Radionuclide Pathway Model-
Level I
(Entitled Rad-1)

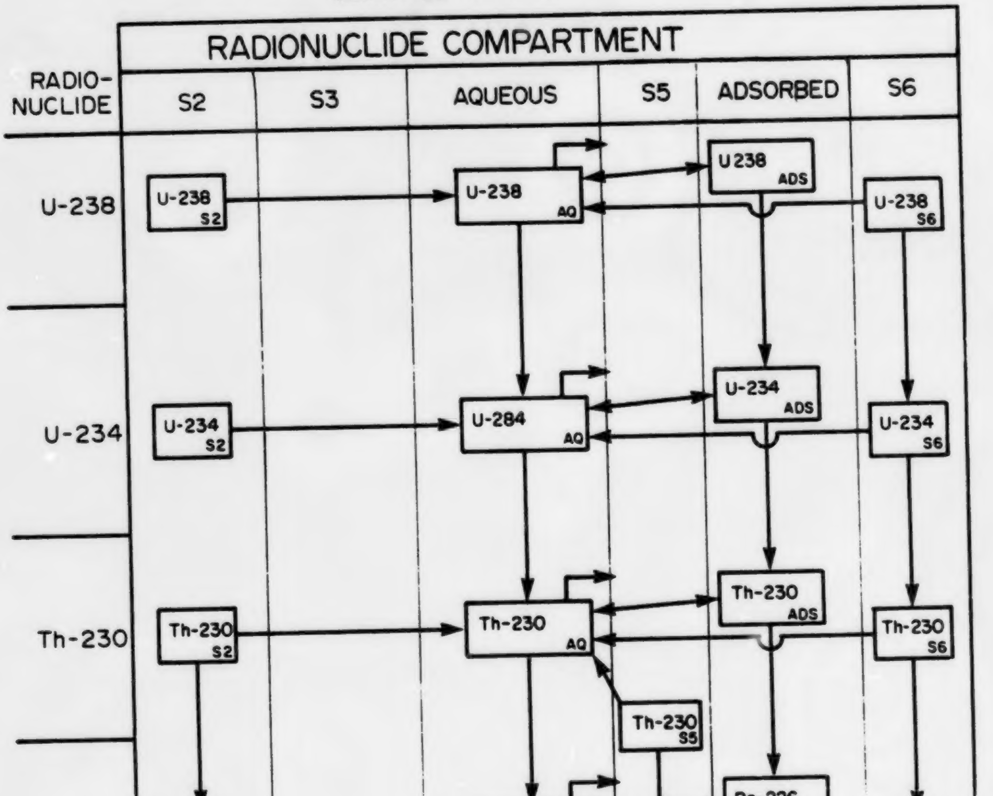
RADIONUCLIDE COMPARTMENT
RADIO-NUCLIDE
S2
S3
AQUEOUS
S5
ADSORBED
S6
U-238
U-238 S2
U-238 AQ
U238 ADS
U-238 S6
U-234
U-234 S2
U-284 AQ
U-234 ADS
U-234 S6
Th-230
Th-230 S2
Th-230 AQ
Th-230 ADS
Th-230 S6
Th-230 S5
Ra-226
Ra-226 S2
Ra-226 AQ
Ra-226 ADS
Ra-226 S6
Ra-226 S3
Ra-226 S5
Pb-210
Pb-210 S2
Pb-210 AQ
Pb-210 ADS
Pb-210 S6
Pb-210 S3
Pb-210 S5
Po-210
Po-210 S2
Po-210 AQ
Po-210 ADS
Po-210 S6
Po-210 S3
Po-210 S5
S2
S3
AQUEOUS
S5
ADSORBED
S6

LEGEND

Symbol	Solid
S1	Gypsum (Partial Neutralization)
S2	Gypsum
S3	(Ca,Ba) SO_4
S4	jarosite
S5	thorium hydroxide
S6	residual minerals

Arrows

↓	decay
↱	outflow
→	dissolution
↔	equilibrium
⇄	coprecipitation

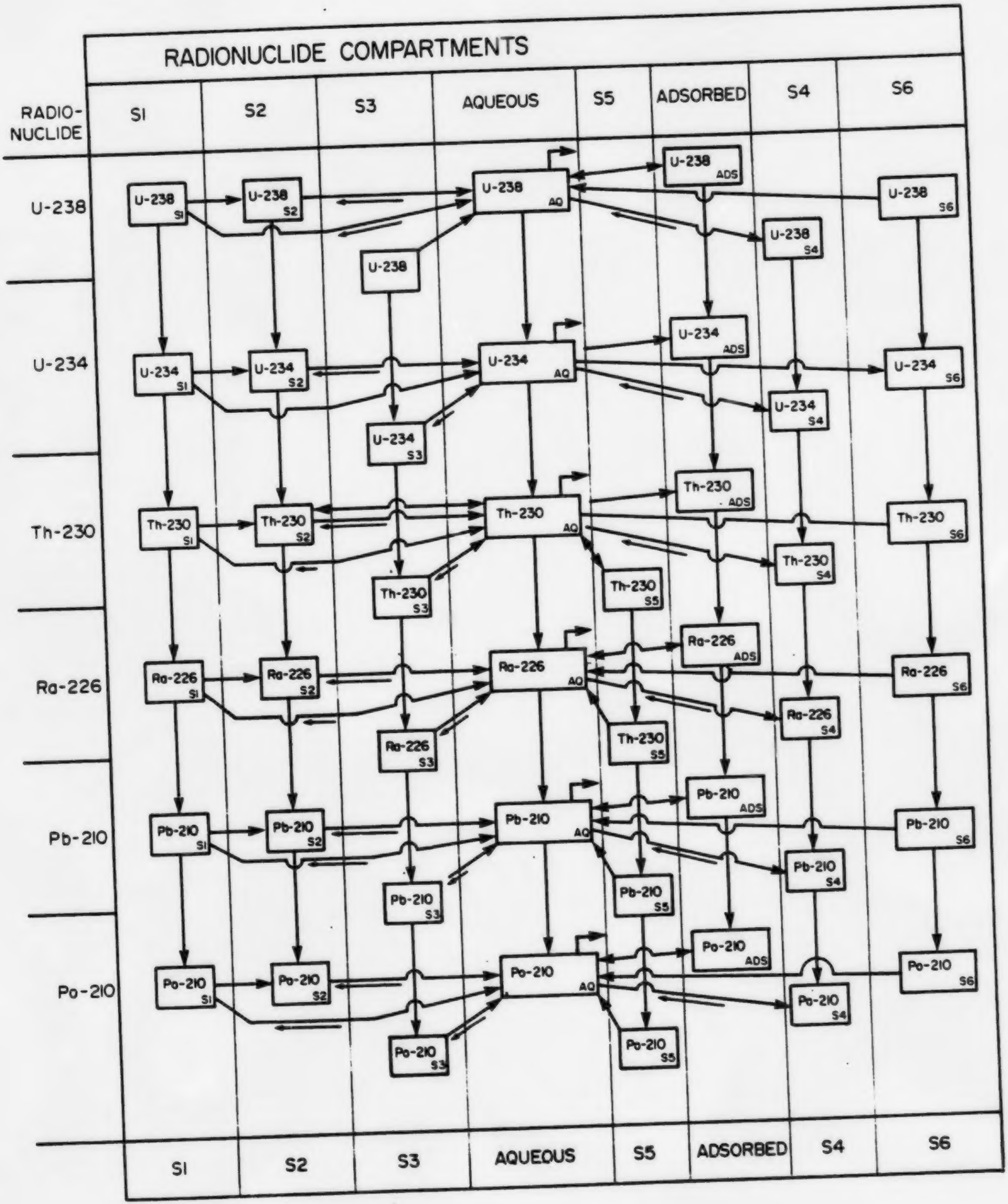
RADIONUCLIDE COMPARTMENTS
RADIO-NUCLIDE
SI
S2
S3
AQUEOUS
S5
ADSORBED
S4
S6
U-238
U-234
Th-230
Ra-226
Pb-210
Po-210
U-238 SI
U-238 S2
U-238
U-238 AQ
U-238 ADS
U-238 S4
U-238 S6
U-234 SI
U-234 S2
U-234 S3
U-234 AQ
U-234 ADS
U-234 S4
U-234 S6
Th-230 SI
Th-230 S2
Th-230 S3
Th-230 AQ
Th-230 S5
Th-230 ADS
Th-230 S4
Th-230 S6
Ra-226 SI
Ra-226 S2
Ra-226 S3
Ra-226 AQ
Th-230 S5
Ra-226 ADS
Ra-226 S4
Ra-226 S6
Pb-210 SI
Pb-210 S2
Pb-210 S3
Pb-210 AQ
Pb-210 S5
Pb-210 ADS
Pb-210 S4
Pb-210 S6
Po-210 SI
Po-210 S2
Po-210 S3
Po-210 AQ
Po-210 S5
Po-210 ADS
Po-210 S4
Po-210 S6
SI
S2
S3
AQUEOUS
S5
ADSORBED
S4
S6

FIGURE 14.II
Radionuclide Pathway Model-Level 2
(Entitled Rad-2)

LEGEND

Symbol	Solid
S1	Gypsum (Partial Neutralization)
S2	Gypsum
S3	(Ca,Ba) SO_4
S4	jarosite
S5	thorium hydroxide
S6	residual minerals

Arrows

↓	decay
↱	outflow
→	dissolution
↔	equilibrium
⇄	coprecipitation

FIGURE 14.12

Pathway Diagram for Th-232 Radionuclides

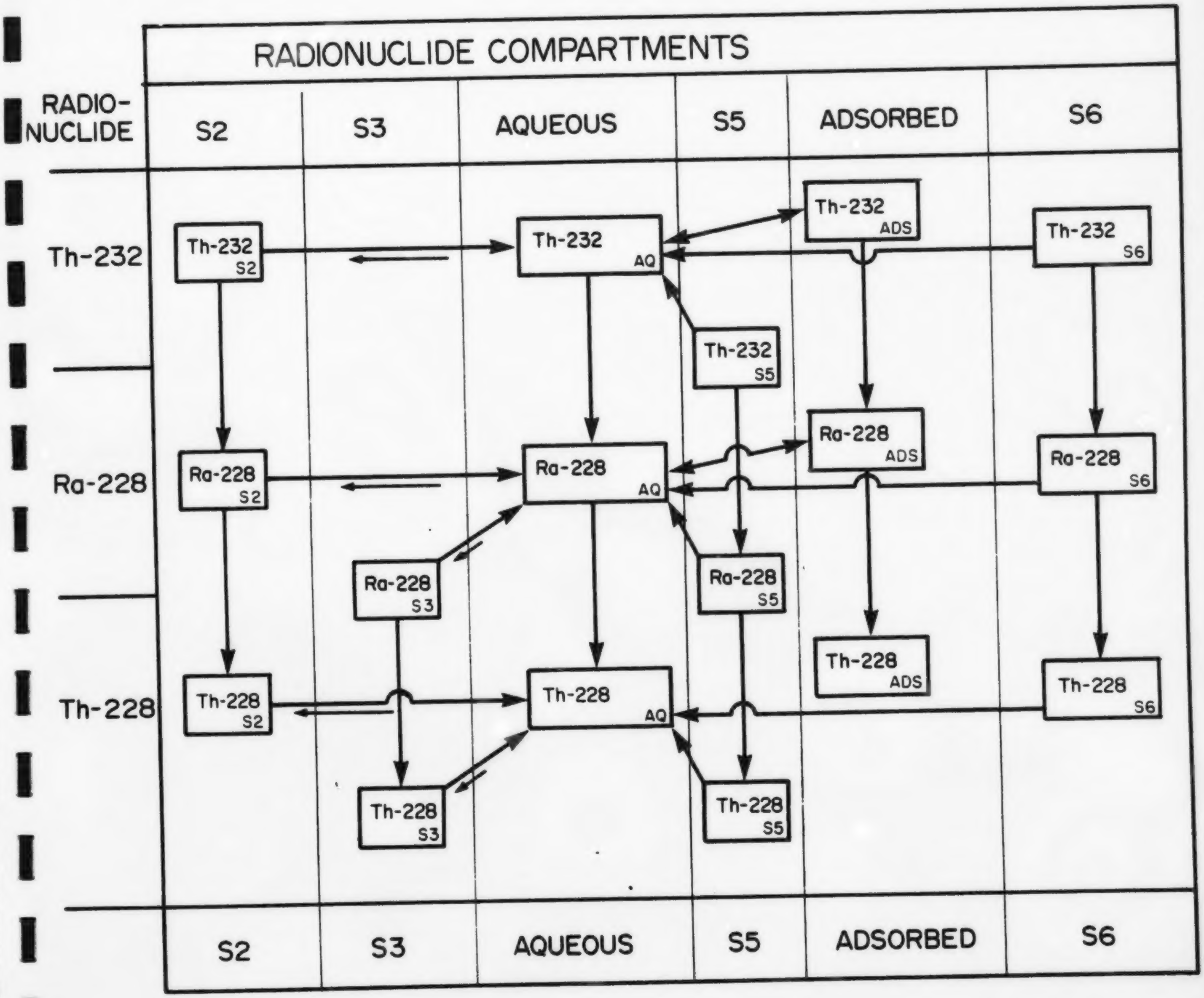
RADIONUCLIDE COMPARTMENTS
RADIO-NUCLIDE
S2
S3
AQUEOUS
S5
ADSORBED
S6
Th-232
Ra-228
Th-228
Th-232 S2
Th-232 AQ
Th-232 ADS
Th-232 S6
Th-232 S5
Ra-228 S2
Ra-228 AQ
Ra-228 ADS
Ra-228 S6
Ra-228 S3
Ra-228 S5
Th-228 S2
Th-228 AQ
Th-228 ADS
Th-228 S6
Th-228 S3
Th-228 S5
S2
S3
AQUEOUS
S5
ADSORBED
S6

LEGEND

Symbol	Solid
S1	Gypsum (Partial Neutralization)
S2	Gypsum
S3	(Ca,Ba) SO_4
S4	jarosite
S5	thorium hydroxide
S6	residual minerals

Arrows

↓	decay
↱	outflow
→	dissolution
↔	equilibrium
⇄	coprecipitation

14.11 U-238 and U-234

Pathway Diagram

The following points are made about the pathway diagram for U-238 and U-234:

1. The major mass of U-238/U-234 may be in the residual mineral (S6). It is assumed (without adequate evidence - see Chapter 11) that its dissolution is kinetically controlled.

2. The other major forms may be coprecipitated in gypsum (S1, S2); adsorbed; and aqueous. It is doubtful that significant quantities would be coprecipitated in (Ca, Ba)SO_4 or in $Th(OH)_4(s)$ as suggested in Figure 14.16 (Level 2).

3. U-238 is the main radionuclide which should be modelled, as the mass of U-234 is small relative to that of U-238. No major chemical isotope effect is expected for U-234 relative to U-238. It is plausible that in some environments, U-234/U-238 ratios will be out of secular equilibrium due to the ability of U-234 to be transported, compared to the relative inability of its parent Th-234 to move.

4. U in gypsum (S2) is assumed to be as a coprecipitate. Hence, gypsum dissolution behaviour will mainly influence S2.

14.12 Th-230, Th-232 and Th-228

Pathway Diagrams

The following points are made about the pathway diagrams for Th-230, Th-232 and Th-228.

1. The major forms of Th-232 and Th-228 are expected to be in the residual Th-232 mineral (S6) and mill-formed thorium hydroxide (S5) in Elliot Lake type ores. The major form of Th-230 is expected to be in thorium hydroxide (S5) because approximately 95% of it is leached in the leaching tanks. A residual amount would exist in the residual U-238 mineral (S6).

2. Because Th-232 is the largest mass fraction of the 3 thorium radionuclides, its behaviour needs to be modelled. The behaviour of the other radionuclides (Th-230, Th-228) can be predicted by the behaviour of Th-232. Accordingly, the dissolution of Th-230 and Th-228 from the hydroxide are represented by coprecipitation reactions in Figure 14.11-14.12.

3. The dissolution behaviour of Th-230 in the residual mineral (S6) will be controlled by that of the U-238 mineral.

4. Th-230 decay to Ra-226 (S5 and adsorbed forms) will be significant after 800-1000 years.

5. For certain time scales, the activity of Th-228 can be set equal to that of Ra-228 in solids S3, S5, and S6 because secular equilibrium will be attained.

6. The main form of thorium in solution between pH 1 and 4 will be sulphate, fluoride, etc., complexes. Above this pH range, the hydroxo-complexes are most important.

14.13 Ra-226 and Ra-228

1. The major form of Ra-226 in fresh tailings is expected in S3 (Ba, Ca, Pb, SO_4). Minor amounts will be in the residual U-mineral (S6). The major form of Ra-228 in fresh tailings is expected to be in residual Th-mineral (S6) and in (Ba, Ca, Pb) SO_4 (S3).

2. After 3 half-lives (ca two decades) the major form of Ra-228 will be in the Thorium hydroxide (S5, Figure 14.12 and residual Th-mineral (S6, Figure 14.12) forms, due to ingrowing.

3. After approximately 800 years, the thorium hydroxide form (S5) of Ra-226 will be significant due to ingrowing from Th-230.

4. The major unknown concerning Ra-226 in the first millenium, is the chemical form and geochemical control on the (Ca, Pb, Ba)SO_4 solid (S3) hypothesized to contain most of the Ra-226 and 50% of Ra-228 after milling. This is the subject of a separate NUTP research project. Over the long-term, the major question will be whether new quantities of this solid will precipitate, if thorium hydroxide containing Ra-226 (S5) dissolves.

5. Another major unknown, is the pH dependence of Ra-226 and Ra-228 adsorption behaviour in tailings for the range of 1-7. The recent thesis of Riese (1983) using the site binding adsorption model and NUTP research projects will furnish some information in this regard.

6. For certain time scales, the activity of Ra-228 can be set equal to that of Th-232 in solids S5 and S6, because secular equilibrium will be attained. This assumes that significant diffusion of Ra-228 from the thorium solid does not occur.

14.14 Pb-210

Pathway Diagrams

The following points are made about the pathway diagram for Pb-210.

1. The major form of Pb-210 after milling is assumed to be S2 (a coprecipitate of gypsum and $PbSO_4$ crystals). Minor amounts will be found in the aqueous form and in the residual U-mineral (S6).

2. The transport chemistry of Pb-210 will be controlled by that of stable Pb. It has not been adequately demonstrated, but it is assumed that most of the Pb and Pb-210, leached in the leaching pachucas is precipitated as $PbSO_4$ in the partial and final neutralization chambers.

3. After approximately one century, most of the Pb-210 will be in the (Ca, Ba) sulphate solid (S3), resulting from decay of Ra-226.

4. After approximately a millenium, most of the Pb-210 will be in the thorium-hydroxide solid (S5), provided that S5 remains stable over this time period. This results from the largest portion of Ra-226 activity being from Th-230 decay in S5 after a millenia.

5. Characterization of Pb complexes under different solution conditions is required, if substantial modelling of Pb-210 in solution is to be done.

6. For time scales of a millenium or longer, Pb-210 activity may be set equal to that of Ra-226 in S3, S5, and S6 due to the establishment of secular equilibrium, provided that these solids have not dissolved.

14.15 Po-210

Pathway Diagrams

The following points are made about the pathway diagrams for Po-210.

1. The major form of Po-210 in fresh tailings may be as a coprecipitate in gypsum (S2): this is unclear. The only definitive work that we found on the radiochemistry of Po-210 is that of Figgins (1961). The only major complex indicated there is a chloride complex. The major compounds indicated are $PoO_2(s)$, $PoO(OH)_2(s)$, $Po(SO_4)_2(s)$, $Po(NO_3)_4$ and possibly $Po(SeO_3)_2$. If Po is present in 1M H_2SO_4 as a sulphate complex, it can be expected to coprecipitate with gypsum, because of its affinity for sulphate. If not present as this complex, its chemistry and the assumption of the pathway diagram (dominant form of Po-210 in fresh tailings in S2) require refinement.

2. Within one year, Po-210 will have the same activity as Pb-210 in S2, S3, S5, and S6 due to secular equilibrium, provided that these solids do not dissolve and reprecipitate within this time frame.

3. Hence, the dominant origin of Po-210's activity in the tailings will be controlled by Pb-210 in S2 for 50 years or so, by Ra-226 in S3 for nearly a millenia and by Th-230 in S5 for the remainder of the time period (2,000 - 10,000 yr).

15.0 SUMMARY, CONCLUSIONS AND KEY RECOMMENDATIONS

15.1 General

This report has summarized the status of our ability to predict the chemical evolution of uranium mill tailings. The review of presently available data for identified chemical processes and transformations has indicated the areas which contain great uncertainties. In this chapter, the scope and principal findings of this report are reviewed. The general conclusions, key recommendations, and an approach to improving our understanding of key components of a source term model are also presented.

15.2 Synopsis of Principal Findings

In this section, the scope of this report is reviewed and a summary of findings in different chapters presented. For more detail, one should refer to the detailed summary for each chapter, given in a concluding section of each chapter.

Geochemical Problem to be Modelled

The objectives of a source-term model are to predict the evolution of minerals and the flux of contaminants from the tailings over time. This is, mathematically, an initial value problem which is strongly dependent upon the initial characteristics of the solid phase.

For modelling purposes it is conceptually useful to analyse the present geochemical state of the tailings (see Chapter 3 and 4) as being due to the following factors:

(i) the minerals initially present in the ore;
(ii) the effects of milling;
(iii) the effects of placement and the impoundment design; and
(iv) geochemical evolution from time of placement to the present.

The first two factors ('ore' and 'milling') are primarily chemical characteristics, while the third relates mainly to permeability and hydrologic pathways. The fourth is a combined geochemical-hydrological effect. It does not attempt to set priorities explicitly, although by leaving out certain suggestions given above (Chapters 2 to 14), it implicitly emphasizes the others.

This sequence is conceptually useful because contaminant discharge from tailings is dependent upon flow pathways and their geochemical state. The geochemical status of different elements in tailings at any point in time results from the following:

(a) the original mineralogical composition of the ore defines its initial characteristics;
(b) milling modifies the ore by dissolving minerals and by creating mill-formed precipitates; and
(c) the geochemical evolution of the pile from time of tailings placement to the present alters the initial assemblage.

Steps (a) and (b) define the general chemical and mineralogical characteristics of the tailings upon placement in the pile; the tailings design defines the major hydrological pathways through it, influencing the geochemical evolution. Knowledge of steps (a) and (b) are useful for understanding the characteristics of fresh tailings and essential for understanding those of old tailings.

With respect to our knowledge of factors affecting the geochemical evolution of tailings, much less is known about geochemical factors than flow pathways for purposes of probabilistic modelling. Hence, future priorities should be directed towards understanding geochemical controls on mineral-water interactions in the tailings pile.

For modelling, it is also useful to evaluate whether one or two geochemical processes dominate the biogeochemical evolution of the tailings. One process, pyrite oxidation, is particularly important in many Elliot Lake tailings; whether one or more processes dominate northern Saskatchewan tailings is not as clear, due mainly to a shortage of data.

In Elliot Lake tailings, the acidification of tailings due to pyrite oxidation and the resultant solution chemistry is the major short-term driving force. This process will continue in tailings having an unsaturated zone until all of the pyrite is consumed. Present rate data suggests that this would continue for ten to hundreds of years, depending upon the tailings characteristics (a decade in which kinetics control the overall oxidation rate in the top few cm; a century and greater in which gaseous oxygen transport controls the overall rate in a 2 m thick unsaturated zone - see Chapters 6 and 12). Because diffusion will increasingly retard the movement of oxygen to greater depths, oxidation rates should decrease with time. Oxidation introduces protons (H^+), iron (Fe^{2+}, Fe^{3+}) and sulphate into solution. These solution ions influence the dissolution kinetics of several minerals (e.g., K-feldspar; micas) and the solubility of others (gypsum, barium sulphate, iron minerals). It is hypothesized that these minerals control the solution concentrations of various radionuclides (e.g., thorium via pH, and Ra-226 through sulphate control on its coprecipitate).

Time Scales

The time scales of concern to this project are summarized in Figure 15.1. This figure is composed from Figure 7.5, the discussion on time scales in Chapter 7, the kinetic data of Chapter 11, and the results of the diffusion-reaction model in Chapter 12. The "mineral dissolution half-time" is the time for one-half of a 100 um particle to dissolve, ignoring the decrease in surface area over time.

Inspection of the figure allows one to determine the relative influence of radioactive decay and washout upon pore water concentrations. However one cannot make a similar determination for dissolution because, as solution saturation conditions are approached, recrystallization becomes important. For example, the half-time of feldspar dissolution (assuming no reprecipitation) at pH 2 is of the order of one hundred years. But the calculations given in Chapter 11 (Table 11.7) indicate that infiltrating pore water through the unsaturated zone will be saturated with respect to amorphorus silica. The net dissolution rate must then be evaluated by using a mass balance equation, with the appropriate kinetics of dissolution and precipitation.

The utility of the "mineral dissolution half-time" is that it provides a method for evaluating the life-time of the minerals. It also provides an order of magnitude method for evaluating whether minerals will be at equilibrium or not for different modelling time scales. For example, consider modelling time scales of 1 year and 500 years. For 1 year, calcite would generally be at equilibrium, while feldspar dissolution would be controlled by kinetics. For 500 years, calcite would be at equilibrium and possibly K-feldspar may be at equilibrium in the extreme case that the pH is 0.4. These examples point out why description of mineral dissolution as kinetically controlled must be referenced to the modelling time scale of concern.

Whether dissolution or equilibrium will dominate can be estimated roughly by comparing the steady-state concentration dictated by dissolution and advective flow to the equilibrium concentration. The equation:

$$C = rt_w\,(1 - \exp(-t/t_w)) \tag{15.1}$$

describes the pore water concentration (C) as a function of time if the initial pore water concentration is 0, t_w is the detention time of the pore water (e.g, years) and r is the dissolution rate (mol/m^3)/yr, for example). This expression ignores decay, recrystallization, and adsorption. The term, rt_w is the steady-state concentration. If the steady-state concentration is significantly less than the equilibrium concentration, then mineral dissolution will likely be kinetically controlled for the time frame of t_w.

To relate the time scales of Figure 15.1 to the computational time step, our analysis led us to suggest the use of a parameter, the chemical retention time in pore water, for relating these time scales to the computational time step. Consider a volume of pore water (V; m^3) influenced by dissolution (r_d; mol/m^3/yr), recrystallization (k; yr^{-1}) and hydrological outflow (Q; m^3/yr). The mass balance equation gives the pore water concentration (C) as:

$$\frac{VdC}{dt} = Vr_d - kCV - QC \tag{15.2}$$

These kinetics are analogous to those of Rimsted and Barnes (1980) for silica. Defining the chemical residence time (t_c) as the time to displace the mass of C present in V results in:

$$t_c = \frac{CV}{r_d} = \frac{1}{k + 1/t_w} \tag{15.3}$$

where t_w is the hydraulic detention time of the box (cell) under consideration ($t_w = V/Q$).

Equation 15.3 shows that the chemical residence time is a function of the hydraulic detention time of the groundwater and the recrystallization rate. Some care must be taken in using this expression because it is specific to the terms considered in the mass balance equation (15.2) and the kinetic expressions used. But it illustrates the point of concern. It shows that at short hydraulic detention times (e.g., 2 yrs), the chemical residence time (2.1 yr) is essentially determined by the hydrological character of the tailings when the recrystallization rate is 0.012 yr^{-1}. At long detention times ($t = 10{,}000$ yr; $t =$), the chemical retention time (85 yr) is essentially determined by the chemical processes and is independent of groundwater hydrology.

Aspects of Equilibrium and Adsorption Controls

Equilibrium and adsorption processes and models are evaluated in Chapters 8, 9 and 13. Several areas in equilibrium and adsorption models and data covered in this report require further work. They include:

(i) A comprehensive data base of equilibrium data for solubility products of various minerals and secondary precipitates and constants for solution complexes need to be developed and critically analysed to ascertain that the data is thermodynamically consistent;

(ii) The mineral assemblage present in certain tailings is still not well defined, particularly the minerals and secondary precipitates containing nickel and arsenic in Saskatchewan tailings and the coprecipitate controlling Ra-226. Fundamental work on their geochemistry is required before valid thermodynamic data can be clearly established;

(iii) A substantial amount of adsorption data is available for cation adsorption onto various model surfaces and geological materials. Unfortunately, the data are usually summarized using different models (e.g., cation exchange model; Langmuir model; site-binding model; linear distribution coefficient). These data need to be developed into a self-consistent modelling framework to be of use to the NUTP modelling program; and

(iv) The linear distribution coefficient is the most probable adsorption model for a source-term model. Yet it depends strongly on solution conditions (Riese, 1983) and is incorrect at concentration levels where the available adsorption sites are nearly saturated. It is suggested that results from the literature, and other models be analysed with the site-binding model to develop self-consistent data and then synthesized into K_d or Langmuir-type models with the limitations and appropriate statistical distributions specified as a function of particular solution concentrations. Use of distribution functions for K_d's for particular solution characteristics is the approach being used in the probabilistic assessment of the high level waste program for clays, granite, and soil.

Aspects of Kinetic Controls

Factors influencing the kinetics of dissolution of minerals are evaluated in Chapters 7 and 11. Several areas of kinetic controls require further evaluation at a fundamental or laboratory level. These relate primarily to a lack of data on dissolution rates of potentially critical minerals. They also include the need to examine mineral interactions subject to kinetic controls. Specific areas requiring further work include the following:

(i) Dissolution kinetics of the following critical minerals are uncertain:

- **Nickel arsenide and chalcopyrite minerals:** Assessing the significance of these minerals awaits further mineralogical and mill data. If they are all dissolved in the leaching tanks, then they are not critical minerals requiring assessment. Assuming that 20-40% of the minerals are not leached, then the chemical kinetics and the role of bacteria in catalysing their kinetics need assessment.

- **Monazite:** Approximately 50% or more of Th-232 remains unleached in Elliot Lake ores. Since Th-232 in solution will control the solid-solution behaviour of dissolved Th-230, Th-232, and Th-228, the dissolution kinetics of this mineral are critical. Also some consideration should be given to $Th(OH)_4$ to ascertain whether equilibrium or kinetics controls its dissolution.

- **Metal Sulphates:** the kinetics of dissolution of strontium sulphate, barium sulphate and lead sulphate require further analyses in the role that these play in controlling the solid solution behaviour of radionuclides, such as Ra-226, Pb-210, Po-210 and Ra-228.

- **Residual Uranium Minerals:** Much of uranium in tailings may be in residual or refractory minerals. Their kinetics have not been adequately addressed in this report.

(ii) Dissolution kinetics of the following minerals appears to be adequate, but should be updated as more information becomes available:

- Silica
- Feldspars, Micas
- Pyrite

(iii) The dissolution rate of pyrite under the combined influence of transport and reaction has been modelled in Chapter 10. This report hypothesizes that oxygen transport (gaseous diffusion) may limit pyrite oxidation. A modelling analysis shows that knowledge of the diffusivity coefficient is much more important than the potential rate of oxidation. Field and laboratory analyses are required to validate these calculations.

Evolution of Minerals in Tailings

The evolution of minerals can be evaluated by assuming equilibrium conditions, using kinetic concepts or a combination of these. In this report, equilibrium reactions among an assemblage of minerals (gypsum, pyrite, goethite, gibbsite, calcite) and subsets were simulated under oxidizing conditions in a closed system. The results are given in Chapter 10 and Appendix B. This assemblage was chosen as a significant subset of all possible equilibrium-dominated minerals present in a tailings pile. Far-from-equilibrium micas and other aluminosilicates were not evaluated because thermodynamic treatment of these minerals was not appropriate. However, the minerals chosen predict pertinent geochemical features expected in a tailings pile.

The simulation predicts that pyrite oxidation controls the expected geochemical evolution of the tailings. The calculated pH is buffered by the pyrite-goethite system for several cases. Only in one case does aluminum hydroxide significantly buffer the system. When present, calcite is the dominant buffering system.

As the system is titrated by an oxidant, the simulation calculates that goethite, mellanerite ($FeSO_4.7H_2O$), siderite ($FeCO_3$), jarosite ($KFe_3(SO_4)_2(OH)_6.6H_2O$) and solution species replace the initial mineral assemblage. Gypsum is generally stable along the reaction pathways.

Comparison of the calculations with field observations suggests that the buffering by calcite and gibbsite is observed in the field, but that the buffering by pyrite-goethite is not observed. The lack of buffering by pyrite-goethite may result from non-equilibrium conditions in the field between pyrite and (Fe^{2+}) or from the presence of a pseudo-stable phase of iron hydroxide ($Fe(OH)_3(s)$). The predicted formation of siderite and jarosite have also been inferred from pore-water data.

Simulations of equilibrium assemblages have limitations for non-equilibrium controlled dissolution. But they have several advantages. Firstly, they predict the energetically most favoured sequence. Secondly, they provide a conceptual and organizational focus for determining the most probable sequence when many different sequences of solution-mineral reactions are possible. Finally, as summarized in the descriptive algorithm in Chapter 14, we hypothesize that many of the minerals of concern to tailings management are at equilibrium with pore water. They represent one fundamental building block for developing a source-term model.

Further work with reaction code pathway simulations should be carried out using all possible minerals and subsets. Some efforts to simulate the effects of kinetics can be made by removing kinetically controlled minerals from the suite and using their dissolution rates as the reaction pathways. To do this simulation, a comprehensive, internally consistent, set of thermodynamic constants for equilibria between solids and solution and complexation should be developed. This is done in this report for several minerals and secondary precipitates.

Further work should also involve evaluation of the evolution of minerals by combining reaction pathway codes with transport codes (which has already been done to a limited extent) and by developing kinetic transport models to evaluate mineral evolution at a research model level.

To incorporate these efforts into a source-term model suitable for probabilistic assessment, it would be useful to run a kinetic-transport-equilibrium model for subsets of minerals in a Monte Carlo simulation mode. This should aid aggregation of the results from detailed component models into the formulation of a source-term model.

Descriptive Algortithm

Descriptive algortihms have been developed for all the chemical elements and radionuclides of Table 1.1 and are given in Chapter 14 and Appendix A. They take the form of a transformation diagram. A typical descriptive algorithm for calcium (Figure 14.3) is reviewed here (Figure 15.2).

The transformation diagram describes the significant chemical states for a two-box model format (the unsaturated zone and saturated zone) and what transformations occur between these states. The type of transformation for each process is given in the legend. By writing a mass balance about each box, one obtains a mathematical model to describe its transformation. The resultant equations are not presented in this report; rather the diagrams would be used as the basis for writing the equations.

The descriptive algorithm for calcium emphasizes the following:

(i) equilibrium conditions are maintained with calcite (limestone) and gypsum;
(ii) equilibrium or kinetic conditions may affect apatite relationships with pore water;
(iii) calcium reversibly adsorbs to clays;
(iv) infiltrating rainwater mixes with tailings pore water in the unsaturated zone, moves to the saturated zone and then moves either to surface water or to deeper groundwater.

The algorithm assumes that the depth of the unsaturated zone is constant on an annual time scale and that the problem is mainly a source-term problem (i.e., that rainfall itself contributes only a small portion to the total export of contaminants and major elements from the tailings).

For a particular application, only a few of the solid phases given in Figure 15.2 might be considered in a source-term model. For example, it is doubtful that clays or apatite are present in appreciable quantities, in Elliot Lake tailings, although calcium adsorption may be significant on other surfaces.

5.3 Conclusions

The following are the conclusions of this report.

1. Chemical evolution of tailings and pore water is driven by thermodynamics (i.e., chemical stability).

2. Equilibrium calculations should be conducted where appropriate to simplify calculations.

3. Kinetic data, where available, should be evaluated in terms of expected or effective residence times of pore water to determine whether kinetic or equilibrium processes dominate in the system.

4. Preliminary component models show that:

   - certain assemblages of minerals behave thermodynamically so that field observations and calculations are in good agreement;
   - some minerals (i.e., pyrite) do not exhibit equilibrium behaviour either during dissolution or in reactions with other minerals, and hence kinetic terms are needed; and
   - a pyrite oxidation-transport model shows that diffusion controls the effective reaction rate over the long-term even when a wide range of reaction rates are used. The rate of oxidation and hence acidification should decrease with time.

5. A source-term model should include:

- equilibrium calculations for certain components;
- kinetic dissolution (speciation)/precipitation of certain components;
- residence time; and
- mass balance on individual components.

15.4 Key Recommendations

This section presents a summary of needs to better evaluate or predict the chemical behaviour of tailings systems over extended periods of time. The recommendations also include tasks that may help to simplify the rather complex problem to one that is more readily manageable.

15.4.1 Future Modelling Needs

The following modelling work is diagnostic in nature:

- Reaction code pathway models should be used to determine the potential outcomes of various mineral assemblages that apply to the different ore and tailings types. This would help to identify the major controlling factors.

- Kinetic factors should be included in such a model to determine the sensitivity of the results to the incorporation of the various kinetically-controlled mineral phases.

- Simplification of these more complex models could be performed and a probabilistic analysis of the source-term model made.

- A general sensitivity analysis to identify key reactions, parameters and mineral assemblages should be made.

The following will validate some of the concepts used in a source-term model.

- The reaction pathway codes should be used to simulate the observed behaviour of tailings systems that have been investigated both in the field and in the laboratory (lysimeter studies).

15.4.2 Fundamental Information

For a more precise understanding of chemical behaviour in a mineral-water system, specific details are needed, as follows:

- review and updating, where necessary, of the thermodynamic data base; this includes solubility products for minerals expected to attain equilibrium, complexation constants for inorganic complex species and enthalpies of formation for these;
- extension of the thermodynamic data base to include important radionuclides (i.e., U, Ra, Th, Pb, Po);
- consideration of the errors and uncertainties associated with the data and their effects on predicted behaviour;
- determination of the tailings mineralogy in detail, especially for tailings in Saskatchewan, with quantitative information to determine the relative importance of the identified minerals;
- because of their potential importance in Saskatchewan tailings, kinetic studies are needed to evaluate controls and expected behaviour of Ni-arsenide oxidation;
- because of their potential importance in restricting specific radionuclide concentrations, specific studies of trace mineral formation are needed; examples include $(Ba, Ra)SO_4$ and jarosite in which Ra may be significantly incorporated; and
- evaluation of the redox controlling processes is needed for more precise prediction of pathways for redox-sensitive species; these species include major components and others of concern such as Fe, S, As, Se and U.

15.4.3 Possible Approach to Improved Understanding

A possible time sequence is presented for conducting experiments and developing data and models for the source submodel of the probabilistic assessment. It is referenced to Figure 2.2 and develops possible activities in terms of

(i) mill, field and laboratory data,
(ii) component and research models, and
(iii) source model.

It does not attempt to set priorities explicitly, although by leaving out certain suggestions given above (Chapter 2 to 14), it implicitly emphasizes the others.

The description of the research and modelling needed, reflects our key philosophy, expounded upon in this report, that the future geochemical state is a function of the original composition of the ore, the effects of milling, and geochemical processes in the tailings.

STUDY AREA 1: MILL, FIELD AND LABORATORY DATA

I. Elemental and Mineralogical Characteristics of the Ore

Elements:

- Generally speaking, useful values of the percentage composition of elements in the ores are available for Elliot Lake from Rio Algom. Information available to us from Denison is more sketchy. Useful information for Saskatchewan ores is available, but the Saskatchewan ores tend to be more variable in their composition.

- For probabilistic modelling purposes, it would be useful to demonstrate the modelling for Elliot Lake and Saskatchewan-type ores.

Minerals:

- o Generally, useful information for defining mineralogy of Elliot Lake ores is available. Information for defining Saskatchewan ores is also available, but more recent. The Saskatchewan mineralogy is also more variable. For particular minerals, such as the nickel arsenide - pyrite groupings, the definition of mineralogy is inadequate, partially because of the several oxidation states that arsenic, iron and sulphur can have in the unit cell of these minerals.

- o Future work should involve a second look at the mineralogy of Saskatchewan ores and possibly involve some additional NUTP funded work for specific groupings of ores.

Modelling:

- o Quantitative calculation of the quantity of minerals should be made to give a statistical distribution for modelling purposes.

Selection of Elements:

- o A list of key elements of concern should be prepared. A list for consideration is given in Table 4.10 and 14.1.

II. Milling Modifications of Ores

- o The objective here is to provide good estimates of the types and quantities of mill-formed precipitates that will be produced in the mill.

- o The calculation should attempt to give a statistical distribution of the mass of each precipitate formed per kg of ore.

Data Available:

- o Data are available for the chemistry of solutions in the leaching pachucas (LP), partial neutralization (PN) and final neutralization (FN) chambers for Rio

Algom (Elliot Lake). Some data are available for Saskatchewan mills in the form of laboratory leaching tests, but data for full-scale operation are not as readily available.

Problems with Mill Data:

- The current data from Rio Algom for the leaching pachucas is comprehensive in scope. More data for the PN and FN would be useful.

- We conclude, in the Ra-226 project, that the chemical concentration of elements in the LP underestimates the actual amounts of precipitates formed. Hence, special laboratory studies are needed to evaluate exactly how much secondary precipitates form in the mill. These studies should be compared to dissolution studies on actual tailings material.

Thermodynamic Calculations of Mill Solutions

- We have analysed the supersaturation ratios for some Rio Algom data. More work is required. Due to gypsum precipitation, some care is required in their interpretation, particularly for elements involved in coprecipitation reactions.

Suggested Studies

1. Carefully sample 60°C LP liquors, dilute to prevent gypsum precipitation, and analyse for radionuclides, cations and anions.

2. Conduct comparative leaching studies with perchloric acid, nitric acid and sulphuric acid to judge which elements are leached and reprecipitated by sulphuric acid in the leaching pachucas. Some care is required with perchloric and nitric acid because of their "perceived oxidizing" capability. However, their "oxidizing" capability is said to be negligible in the 1 Molar range, the concentration of Rio's leaching pachucas. This may need to be confirmed.

3. Conduct experiments allowing the 60°C leach water to cool and to precipitate solids. Analyse the solids.

4. Conduct experiments involving addition of limestone and lime to the leaching solutions (in the absence of solids) and determine which precipitates form. Use this knowledge to "calibrate" mineralogical analyses (SEM-XRE etc.) of fresh tailings. In particular this should be done for Saskatchewan ores.

5. Conduct thermodynamic (equilibrium: solubility, complexation) calculations of mill water (LP, PN, FN) solutions and those of the laboratory solutions. Use these calculations to infer the sequential formation of mill-formed precipitates, through the mill.

III. Initial Composition of Tailings

1. Calculate (quantitatively) the composition of minerals and secondary precipitates in the fresh tailings.

2. Estimate statistical distributions (uncertainty) for these compositions.

3. Check these compositions using equilibrium calculations and groundwater data from field sites.

IV: Effect of New Mill Technologies and Mill Management Options

- We have not extensively analyzed or made any recommendations for this area in this report, other than to acknowledge its importance in Figure 2.2, and to acknowledge the importance of milling upon defining the initial state of tailings.

STUDY AREA 2: RESEARCH AND COMPONENTS MODELS

I: Stability Assessment

Conduct a qualitative assessment of the stability of different minerals and mill-formed precipitates as a conceptual tool to determine whether subsequent modelling predictions make sense.

- The background to this is discussed in Chapter 3.
- Relevant ideas are referenced to:
  - change in redox condition (low redox condition in ore, changed to higher redox conditions in the unsaturated zone)
  - change in topographical position and nearness to significant hydrological pathways
  - temperature (e.g., aluminosilicates formed at high temperatures, are now in a low temperature environment).

II: Selection of Time and Space Scales

- Time and spatial scales of models need to be selected (see Chapter 7). This is partly a modelling decision and partly an NUTP program management decision. A quantitative approach to development of time scales is outlined in Chapter 7 (Sections 7.6 and 7.7).

III: Calibration and Validation Procedures

- Tests (qualitative, quantitative) for calibration and validation of research and component models need to be developed before the models are used (see Chapter 7).

IV: Qualitative Assessment of Kinetic vs Equilibrium Controls on Different Minerals

- This is a key area for source-term model development. It appears that calcite dissolution can be treated as an equilbrium controlled process while pyrite (biochemical) and quartz and feldspar (chemical) behaviour must be treated as kinetically controlled processes.

- An overview of equilibrium or kinetic controls should be developed for all minerals of concern in a qualitative fashion.

o Where knowledge is lacking, guesses can be made using analogies to the stability constant (see Chapter 11.1, referenced to Table 11.1).

o The overview should also be referenced to the location in the tailings (pyrite is unstable in unsaturated zone; $CaSO_4$ may be unstable in a more reducing, saturated zone)

o The assessment should be made with reference to the time scale of of each box (saturated, unsaturated zone).

o The assessment should mention the spatial scale of available data. For example:

- 10 um films for dissolution kinetics
- 2 m thick unsaturated zone for "source-term model"
- 100 ha surface area for source-term model

V: Reaction Code Pathway Calculations

o The objective of these calculations is to determine the dominant mineralogical controls upon pH, radionuclides and chemical elements of toxicological concern to allow simplification to a format useful for a "source-term" model.

o A set of model systems of increasing complexity should be defined and the evolution of minerals at equilibrium determined.

o A check of these calculations should be made with field data. This will provide some "validation" of which minerals may be at equilibrium for various time scales.

o A set of model systems should be developed (where possible), which emulate kinetic controls in dissolution of particular minerals.

o If possible, these results should be used to estimate parameter values and statistical distributions.

Note: Some of these calculations have been done in this project. They provide a focus for the consideration of more complete systems. Sets of additional calculations could include:

(a) alumino-silicate minerals, and
(b) nickel arseno-pyrite minerals.

(Comment: these two areas will take some time)

VI: Thermodynamic Data Base Development

- A comprehensive, well-justified thermodynamic data base should be developed. This could proceed, or could be done in parallel with reaction code pathway calculation. Because such data is compiled in standard programs (e.g., REDEQL2, GEOCHEM, PHREEQE, EQ3/EQ6, WATEQF, CHEMP) pathway calculations are quite feasible, immediately. The problem with many of these programs is that they do not have all minerals of concern to uranium tailings management in their data base. Thus, while many of them can provide initial calculations, none can provide comprehensive assessments.

- We have developed (with AECL) a start on this well justified data base (see Chapter 10).

VII: Kinetic Calculations

- Minerals, for which kinetics control, should be assessed. We have developed data for a few. Key ones for future work include residual thorium minerals and residual nickel arseno-pyrite minerals. Laboratory studies on these would be useful. In particular the nickel arseno-pyrite minerals should include an assessment of the potential effects of biologically-induced oxidation.

- Data from lysimeters should be developed into estimates of leaching rates of residual uranium and thorium minerals.

- Kinetic calculations should be added into appropriate computer codes. A new generation of reaction pathway codes with this capability is currently being developed.

- Simple kinetic models for key minerals should be formulated and reaction pathways calculated. This will aid interpretation of reaction pathway code calculations and those of the next section.

VIII: Quantitative Evaluation of Thermodynamics vs Kinetic Controls in Mineral Dissolution

Available laboratory and field data should be continually assessed to determine whether equilibrium or kinetics controls dissolution of minerals. These assessments should be as quantitative as possible.

IX: Probabilistic Model of Tailings Processes

- A combined equilibrium - kinetic, mass balance model of key minerals should be developed. Its calculations would be used to conduct calibration-verification studies of available field data and that gathered from Gunnar and Lacnor.

- The model should be cast into a probabilistic framework (e.g., Monte Carlo simulation) and predicted fluxes and distributions of elements and radionuclides of concern made.

- These results will aid simplification of the source model to a scale compatible with the overall probabilistic assessment.

X: Studies of Hydrological Models

- A study using existing watershed hydrology models and field data from Gunnar and Lacnor should be made to identify key processes. Aggregation of the results of the study would allow one to check hydrological assumptions of the source model, or to incorporate new hydrological aspects into the source model.

- A study of results from existing finite element (or finite difference) models on other tailings sites should be made and the results aggregated up to the simple scale of the 1, 2, or 3 box model chosen for the source model. Given the relative unknowns in geochemistry versus hydrological pathways, it is doubtful that running a finite element difference/hydrology model on Lacnor or Gunnar is justified, other than in very limited scope.

XI: Special Studies

1. Pyrite oxidation
   - much work has been done. These ideas should be applied to the Nickel arseno-pyrite minerals of Saskatchewan ores

2. Geochemical controller on Ra-226 and Pb-210 in tailings. Recommendations for this study are developed in a separate project.

AREA 3: DEVELOPMENT OF SOURCE-TERM MODEL

This would proceed in parallel with the above studies.

16.0 ACKNOWLEDGEMENTS

This work was funded by a research contract from the National Uranium Tailings Program, Department of Energy, Mines and Resources, Government of Canada to Beak Consultants Limited and via a subcontract to Atomic Energy of Canada Ltd. The interaction with the scientific authority (Mr. Walter Harrison) and his colleagues (R. John, G. Feaseby, H. Steger, R. Holmes) at the National Uranium Tailings Program (CANMET) on this contract, and with fellow workers at BEAK (D.L. Lush, M.F. Holloran, P. Groeneweg), at AECL (N. Garisto, R. Lemire, F. Garisto) and other institutions (J. Cherry, N. Dubrovsky at the University of Waterloo; O.E. Hileman at McMaster University) are gratefully acknowledged.

The aid of Rio Algom (A. Vivyurka, E. Barnes) in supplying past data on the leaching pachucas, other NUTP projects (BEAK, 1985; Knight-Piezold, 1985) for sampling data of the LP of Rio Algom, and a geochemical analysis of Key Lake data, respectively, are acknowledged.

17.0 REFERENCES

Aagaard, P., and H.C. Helgeson (1982). "Thermodynamic and kinetic constraints on reaction rates among minerals and aqueous solutions. I, Theoretical considerations." Am. J. Sci., 282, 237-285.

Aller, R.C. (1984). "The importance of relief burrow structures and burrow irrigation in controlling sedimentary solute distributions." Geochim. Cosmochim. Acta, 48, 1929-1934.

Ames, L.L., J.E. McGarrah, B.A. Walker and P.F. Salter (1983). "Uranium and Radium Sorption on Amorphous Ferric Oxyhydroxide." Chem. Geol. 40, 135.

Anderson, M.A., J.F. Ferguson, and J. Gavis. (1976). "Arsenate Adsorption on Amorphous Aluminum Hydroxide". J. Colloid Inter. Sci., 54(3). p. 391-399.

Anderson, R.R. (1981). "The Marine Geochemistry for Thorium and Protactinium." Ph.D. Thesis, Woods Hole Oceanogr Inst., p. 287.

Atkinson, B. and H.W. Fowler (1974). "The significance of microbial film in fermenters." Advances in Biochemical Engineering, 3, Chapter 6, Springer-Verlag, New York.

Bacon, M.P. and R.F. Anderson (1982). J. Geophys. Res., 87, 2045-2056.

Baes and Mesmer (1976). The Hydrolysis of Cations, Wiley. p. 112-122.

BEAK. (1982). "An approach to the calculation of dose-commitment arising from different methods for the long-term management of uranium mill tailings through aquatic pathways". Atomic Energy Control Board of Canada Report. INFO-0097.

BEAK. (1985). "On the Geochemical Mechanism Controlling Ra-226 Dissolution in Uranium Mill Wastes (Tailings)". Report for the National Uranium Tailings Program.

Benes, P. (1982). "Physico-Chemical Forms and Migration in Continental Waters of Radium from Uranium Mining and Milling" in Environmental Migration of Long-lived Radionuclides. AEA Publication No. 1AEA-SM-257/84. pp. 3-23.

Benes, P. and B. Havlik (1979). "Speciation of mercury in natural waters." In: The Biogeochemistry of Mercury in the Environment. (J.O. Nriagu, ed.) Elsevier, pp. 175-210.

Berner, R.A. (1978). "Sulphate Reduction and the Rate of Deposition of Marine Sediments". Earth Planet Sci. Letters, 37, 492-498.

Berner, R.A. (1978) "Rate Control of Mineral Dissolution under Earth Surface Conditions." Am. J. Sci., 278, 1235-1252.

Berner, R.A. (1979). " A New Look at Biogenous Material in Deep Sea Sediments." Am. Bio. Special Report, 6, 6-10.

Berner, R.A. (1981). "Kinetics of Weathering and Diagenesis." IN: Kinetics of Geochemical Processes (A.C. Lasaga and R.J. Kirkpatrick, Ed.) Mineral. Soc. Am., pp. 111-134.

Berner, R.A. (1984). "Sedimentary pyrite formation: An update." Geochim. Cosmochim. Acta, 48, 605-615.

Berner, R.A. and G.R. Holdren (1979). "Mechanism of Feldspar Weathering, II, Observations of Feldspars from Soils." Geochim. Cosmochim. Acta, 43, 1173-1186.

Berner, R.A. and J.W. Morse (1974). "Dissolution Kinetics of Calcium Carbonate in Sea Water, IV, Theory of Calcite Dissolution." Am. J. Sci., 274, 108-134.

Berner, R.A., E.L. Sjoberg and J. Schott (1980a). "Mechanisms of Pyroxene and Amphibole Weathering, I Experimental Studies." IN: Third International Symposium on Water-Rock Interaction: Proceedings, pp 44-45. Alberta Research Council, Edmonton.

Berner, R.A., E.L. Sjoberg, M.A. Velbel, and M.D. Krom (1980b). "Dissolution of Pyroxenes and Amphiboles during Weathering." Science, 207, 1205-1206.

Bjerle, I., G. Rochelle, and H. Sverdrup (1982). "Limestone Dissolution in Acid Lakes." Vatten, 38(2), 156-163.

Blair, R.D., J.A. Cherry, T.P. Lim and A.J. Vivyurka (1980). "Groundwater monitoring and contaminant occurrence at an abandoned tailings area, Elliot Lake, Ontario." In Brawner, C. (ed.) Proc. First Intern. Conf. on Uranium Mine Waste Disposal, Soc. Mining Engineers of AIME.

Bolt, G.H. and M.G.M. Bruggenwert (1978). "Soil Chemistry, A. - Basic Elements". Amsterdam: Elservier Scientific Publ. Co.

Boulden, D.R. (1968). "Models for describing the diffusion of oxygen and other mobile constituents across the mud-water interface." J. Ecol., 56, 77-87.

Bouti, W. (1983). "Water Acidification Model". Ph.D. Thesis McMaster University.

Brown, J.B. (1971). "Jarosite - Goethite Stabilities at 25°C". Mineral Deposita, (Berl), 6. p. 245-252.

Bruggenwert, M.G.M. and A. Kamphorst (1979). Survey of experimental information on cation exchange in soil systems. IN: G.H. Bolt (ed.) Soil Chemistry B. Physico-Chemical Models. Elsevier Sci. Publ. Co., Amsterdam, 141-203.

Busenberg, E. and C.V. Clemency (1976). "The Dissolution Kinetics of Feldspars at 25°C and 1 atm CO_2 Partial Pressure." Geochim. Cosmochim. Acta, 40, 41-50.

Buszka, P. (1981). "Hydrogeochemistry of Contaminated Groundwater in Sand Aquifers at a Landfill Near North Bay, Ontario." M.Sc. Thesis, University of Waterloo, Dept. of Earth Sciences.

Cabrera, F. and O. Talibudeen (1978). "The release of Aluminum from Alumino-Silicate Minerals: II Kinetics". Clays and Clay Minerals, 26(6): 434-440.

Cabrera, F. and O. Talibudeen (1979). "The Release of Aluminum from Alumino-Silicate Minerals: II Acid Base Potentiometric Titrations." Clays and Clay Minerals 27: 113-118.

Cassford, G.E., W.A. House and A.D. Pethybridge (1983). "Crystallisation Kinetics of Calcite from Calcium Bicarbonate solutions between 278.15 and 303.15 K." J. Chem. Soc. Faraday Trans. I, 79, 1617-1632.

Chan, P.K. and G.T. Rochelle (1982). "Limestone Dissolution: Effects of pH, CO_2 and Buffers Modelled by Mass Transfer." ACS Symp. Ser., pp. 75-97.

Chan, P.K. and G.T. Rochelle (in press). "Limestone Dissolution: Effects of pH, CO_2 and buffers modelled by mass transfer." ACS Symp. Ser. 1982.

Chang, C.S., J.H. Dempsey, R.H. Borgwardt, A.J. Toprac and G.T. Rochelle (1982). "Effect of Limestone Type and Grind SO_2 Scrubber Performance." Environ. Prog., 1(1), 59-65.

Cherry, J.A., A.U. Shaikh, D.E. Tallman and R.V. Nicholson (1979). "Arsenic species as an indicator of redox conditions in groundwater". J. Hydro., 43:373-392.

Cherry, J.A. and R.V. Nicholson (May 1980). "As(III)-As(V) speciation in leachate contaminated groundwater flow". Ann. Meeting Geol. Assoc. Can. Halifax.

Cherry, J.A., R.W. Gillham, E.J. Reardon, N.M. Dubrovsky and R.V. Nicholson (1983). "Continuation Study on Hydrochemical Processes in Abandoned Uranium Tailings from the Elliot Lake District, Ontario". Waterloo Research Institute Rept. 204-02.

Cherry, J.A., R.W. Gillham, N.M. Dubrovsky, R.V. Nicholson and D.J.A. Smyth (1982). "Field and Laboratory Investigations of Acidic Pre Water in Pyritic Uranium Tailings at Elliot Lake, Ontario". Waterloo Research Institute Rept.

Cherry, J.A., A.V. Shaikh, D.E. Tallman and R.V. Nicholson (1979). Arsenic speciation as an indicator of redox conditions in groundwater. J. Hydrol., 43: 373-392.

Cherry, J.A., R.W. Gillham and R.V. Nicholson (1984). The study of kinetic controls on pyrite oxidation with application to abandonment of pyritic uranium tailings. Research Report for National Uranium Tailings Program, Waterloo Research Institute Report, 310-07, 67 p.

Choppin, G.R. and K.L. Nash (1981). "Dissociation kinetics of Thorium and Humic Acid" J. Inorg. Nucl. Chem., 43. p. 357-359.

Christoffersen, J. and M.R. Christoffersen (1976). "The Kinetics of Calcium Sulphate Dihydrate in Water". J. Crystal Growth, 35, pp 79-88.

Christoffersen, M.R., J. Christoffersen, M.P.C. Weijnen and G.M. van Rosmalen (1982). "Crystal Growth of Calcium Sulphate Dihydrate at Low Super Saturation". J. Crystal Growth, 58, pp 585-595.

Clarke, P.J. et al. (1980). Key Lake Project. Process Development, Key Lake Mining Corporation, Sherrit Gordon Mines Ltd., 116 p.

Cochran, J.K. and S. Krishnaswami (1980). Amer. J. Sci., 280, 849-889.

Cody, R.D. (1981). "Lenticular Gypsum." Geology, 9, 1016-1028.

Cody, R.D. and A.B. Hull (1980). "Experimental growth of primary anhydrite at low temperatures and water salinities." Geology, 8, 505-509.

Coleman, N.T. and D. Craig (1961). "The Spontaneous Alteration of Hydrogen Clay". Soil Sci. 91: 14-18

Coleman, N.T., S.B. Weed and R.J. McCracken (1959). "Cation-exchange Capacity and Exchangeable Cations in Piedmont Soils of North Carolina". Proc. Soil Sci. Soc. Am. 23, pp. 146-149.

Constable, T. and W.J. Snodgrass (1984). "Leachates of Radioactive Constituents from Uranium Mine Tailings - Final Report" Second Draft. To appear as an Environment Canada Report.

Cotton, F.A. and G. Wilkinson (1980). Advanced Inorganic Chemistry, Fourth Edition, Wiley.

Crank, J. (1979). "The Mathematics of Diffusion." Clarendon Press, Oxford.

Davis, J.A., R.O. James and J.O. Leckie (1978). Surface ionization and complexation at the oxide/water interface, I. Computation of electrical double layer properties in simple electrolytes. J. Colloid Interface Sci., 63(3): 480-499.

Davis, J.A. and J.O. Leckie. (1978). Surface ionization and complexation at the oxide/water interface, II. Surface properties of amorphous iron oxyhydroxides and adsorption of metal ions. J. Colloid Interface Sci., 67(1): 90-107.

Davis, J.A. and J.O. Leckie (1980). "Surface Ionization and Complexation at the Oxide-Water Interface. III. Adsorption of Anions." J. Colloid Interface Sci., 74, 32.

Dean, W.E., G.R., Davies, and R.Y. Anderson (1975). "Sedimentological significance of nodular and laminated anhydrite." Geology, 3, 367-372.

Dempsey, B.A., and P.C. Singer (1980). "The Effects of Calcium on the Adsorption of Zinc by MnOx(s) and $Fe(OH)_3$(am)." In: Contaminants and Sediment: Part 2: Analyses, Chemistry, Biology. (R.A. Baker, ed.) Ann Arbor Science, pp. 333-354.

Dreybrodt, W. (1980). "The Deposition of Calcite from Thin Films of Natural Calcareous Solutions and the Growth of Speleotherms." Chem. Geol., 29, 89-105.

Dreybrodt, W. (1981a). "The kinetics of Calcite Precipitation from thin films of Calcareous Solutions." Chemical Geology, 32, 237-245.

Dreybrodt, W. (1981b). "The Kinetics of the Dissolution of Calcite and its Applications to Karstification." Chem. Geol., 31, 245-269.

Dreybrodt, W. (1981c). "Mixing Corrosion in $CaCO_3$ - CO_2 - H_2O Systems and Its role in the Karstification of Limestone Areas." Chem. Geol., 32, 221-236.

Driscoll, C.T., J.P. Baker, J.J. Bisogni and C.L. Schofield (1982). "Aluminum Speciation and Equilbria in Dilute Acidic Surface Waters of the Adirondack Region of New York State". Paper presented to the Division of Environmental Chemistry, American Chemical Society, Las Vegas, Nevada, March 28 - April 2, 1982.

Dubrovsky, N.M., J.A. Cherry, E.J. Reardon and A.J. Vivyurka (1985). Geochemical evolution of inactive pyritic tailings in the Elliot Lake uranium district: 1, the groundwater zone, Can. Geotech. J., 22:110-128.

Ferguson, J.F. and J. Gavis (1972). "A review of the arsenic cycle in natural waters". Water Res., 6. 1259-1274.

Figgins, P.F. (1961). "The radiochemistry of Polonium." NAS-NRC Nation Sciences Council Nuclear Sciences Series. NAS-NS-3037. pp 1-68.

Fleer, V.N. (1982). "The Dissolution Kinetics of Anorthite ($CaAl_2Si_2O_8$) and Synthetic Strontium Feldspar ($SrAl_2Si_2O_8$) in Aqueous Solutions at Temperatures Below 100°C: With Applications to the Geological Disposal of Radioactive Nuclear Wastes." Ph.D. Thesis, Pa. State Univ. University Park.

Freeze, A. and J. Cherry. (1979). Groundwater McGraw Hill.

Frost, R.R. and R.A. Griffin (1977). Effect of pH on adsorption of arsenic and selenium from landfill leachate by clay minerals. Soil Sci. Soc. Amer. Proc., 41:53-57.

Garrels, R.M. and M.W. Thompson (1960). Amer. J. Sci, 258, A57.

Garvin, G. and A. Freeze (1984a). Theoretical Analyses of U. "Role of Groundwater Flow in the Genesis of Stratabound Ore Deposits: Part 1: Mathematical and Numerical Model" Am. J. Sci., 284:1085-1124.

Garvin, G. and A. Freeze (1984b). Theoretical Analyses of U. "Role of Groundwater Flow in the Genesis of Stratabound Ore Deposits: Part 2: Quantitative Results" Am. J. Sci., 284:1125-1174.

Gill, J.S. and G.H. Nancollas (1980). "Kinetics of Growth of Calcium Sulphate Crystals at Heated Metal Surfaces." J. Crystal Growth, 48, 34-40.

Gillham, R.W., H.D. Sharma, M.R. Reddy, E.L. Cooper and J.A. Cherry (1981). Barium and Radium Migration in Unconsolidated Canadian Geological Materials. Atomic Energy Control Noard of Canada Research Report, INFO-0048.

Godbee, H.W., E.L. Compere, D.S. Joy, A.H. Kibbey, J.G. Moore, C.W. Weston, O.U. Anders and R.M. Neilson (1980). "Application of Mass Transfer to the Leaching of Radionuclides from Waste Solids." Nuclear and Waste Management, 1, 29-35.

Goldhaber, M.B. (1982). "Experimental study of metastable sulfur oxy-anion formation during pyrite oxidation at pH 6-9 and 30°C." Am. J. Sci. 283: 193-217.

Goldich, S.S. (1938). "A study of rock weathering." J. Geol., 46: 17-58.

Golders (1985). "Lac Nor Monitor Study." NUTP Report (In prep.).

Grandstaff, D.E. (1980). "The Dissolution rate of Forsterite Olivine from Hawaiian Beach Sand." IN: Third International Symposium on Water-Rock Interaction; Proceedings, pp. 72-74, Alberta Research Council, Edmonton.

Grauer, R. and W. Stumm (1982). DieKoordinationschemic.....Losungen. Colloid and Polymer Sci., 260:959-970.

Grove, D. and W. Wood (1979). Prediction and field verification of subsurface water quality changes during artificial recharge, Lubbock, Texas. Ground Water, 17(3): 250-257.

Hahn, H.H. (1969). Ph.D. Thesis, Harvard University.

Hahn, H.H. and W. Stumm (1970). "Coagulation by Al (III). The Role of Adsorption of Hydrolyzed Aluminum in the Kinetics of Coagulation" in (Weber Ed) Adsorption from Aqueous Systems.

Harremoes, P. (1976). Half-order reactions in biofilm and filter kinetics. Dept. Sanit. Eng., Techn. Univ. Denmark.

Harremoes, P. and M. Riemer (1975). Report on pilot-scale experiments on down-flow filter denitrification. Report 75-1, Dept. Sanit. Eng., Techn. Univ. Denmark.

Harris, G.P. (1980). "Temporal and Spatial Scales in Phytoplankton Ecology." IN: Mechanisms, Methods, Models and Management. Can. J. Fish. Aquat. Sci., 37, 877-900.

Helgeson, H.C., W.M. Murphy, and P. Aagaard (1984). "Thermodynamic and Kinetic Constraints on Reaction Rates among Minerals and Aqueous Solutions, II, Rate Constants, Effective Surface Area, and the Hydrolysis of Feldspar." Geochim. Cosmochim. Acta, 48,(12), 2405-2432.

Helling, C.S., G. Chesters and R.B. Corey (1964). "Contribution of Organic Matter and Clay to Soil Cation Exchange Capacity as Affected by the pH of the Saturating Solution". Soil Sci. Soc. Proc., pp. 517-520.

Hoffman, F.O., D.L. Shaeffer, C.W. Miller, and C.T. Gartner (1978). "The Evaluation of Models Used for the Environmental Assessment of Radionuclide Releases". Oak Ridge National Laboratory. CONF - 770901.

Holdren, G.R., Jr., and R.A. Berner (1979). "Mechanism of Feldspar Weathering, I, Experimental Studies." Geochim. Cosmochim. Acta, 43, 1161-1171.

House, W.A. (1981a). "Kinetics of crystallisation of calcite from calcium bicarbonate solutions." J. Chem. Soc. Faraday Trans., 77, 341-359.

House, W.A. (1981b). "An Experimental Investigation of Carbon Dioxide Adsorption during Calcite Precipitation." Colloids and Surfaces, 2, 119-131.

House, W.A. and J.A. Tutton (1982). "An Investigation of Heterogeneous Nucleation of Calcite." J. Crystal Growth, 56, 699-710.

IEC BEAK (1983). "Hydrogeochemical Studies on WTC Uranium Tailings Lysimeters". Report for CANMET Mineral Scenarios Laboratories. Ottawa, Ontario.

IUPAC (1982). Stability Constants of Metal-Ion Complexes Part A Inorganic Ligands. Eric Hogfeldt (ed.) IUPAC Chem. Data Series No. 21, Pergamon Press (New York).

Ivarson, K.C. (1973). "Microbial Formation of Basic Ferric Sulphates." Can. J. Soil. Sci., 53, 315-323.

Ivarson, K.C., R.O. Hallbery and T. Wadsten (1976). "The pyritization of basic ferric sulphates in acid sulphate soils. A microbiological interpretation". Can. J. Soil. Sci., 65. p. 393-406.

Ivarson, K.C., G.J. Ross and N.M. Miles (1978). "Alterations of micas and feldspars during microbial formation of basic ferric sulphates in the laboratory". Soil Sci. Soc. Am. Proc., 42. p. 518-524.

Ivarson, K.C., G.J. Ross, and N.M. Miles (1979). "The Microbiological Formation of Basic Ferric Sulphates II Crystallization in Presence of Potassium-, Ammonia-, and Sodium-Salts." Soil Sci. Soc. Am. J., 43. p. 908-912.

Ivarson, K.C. G.J. Ross and N.M. Miles (1980). "Microbial Formation of Basic Ferric Sulphates 3. Influence of Clay Minerals on Crystallization". Can. J. Soil., 60(1). p. 137-140.

Ivarson, K.C., G.J. Ross and N.M. Miles (1980). "The Microbial formation of Basic Ferric Sulphates and Influence of Clay Minerals on Crystallization." Can. J. Soil Sci., 60, 177-140.

Ivarson, K.C., G.J. Ross and N.M. Miles (1981). "Formation of Radium Jarosite during the Microbial Oxidation of Ferrous Iron at Room Temperature." Canad. Mineral., 19, 429-434.

Ivarson, K.C., G.J. Ross and N.M. Miles (1982). "Microbial Transformation of Iron and Sulphur and Their Applications to Acid Sulphate Soils and Tidal Marshes." IN: Acid Sulphate Weathering., Soil Sci. Society of America, pp. 57-76.

Kagawa, M., M.E. Sheehan and G.H. Nancollas (1981). "The Crystal Growth of Gypsum in An Ammoniacal Environment." J. Inorg. Nucl. Chem., 43, 917-920.

Kaiman, S. (1977). Mineralogical Examination of Old Tailings from the Nordic Lake Mine, Elliot Lake, Ontario. CANMET, Energy, Mines and Resources Canada. Report MRP-MSL, 78-85 (IR).

Kaul, L.W. and P.N. Froelich (1984). "Modelling estuarine nutrient geochemistry in a simple system." Geochim. Cosmochim. Acta, 48, 1417-1433.

Kazmierczak, T., E. Schuttringer, B. Tomazic and G.H. Nancollas (1981). "Controlled Composition Studies of Calcium Carbonate and Sulphate Crystal Growth." Croatia. Chemica. Acta, 54(4), 277-287.

Kazmierczak, T.F., M.B. Tomsen and G.H. Nancollas (1982). "Crystal Growth of Calcium Carbonate. A Controlled Composition Kinetic Study" J. Phys. Chem., 86, 103-107.

Keller, D.M., R.E. Massey, and O.E. Hileman (1978a). "Studies on nucleation phenomena occurring in aqueous solutions supersaturated with calcium sulphate". Can J. Chem., 56(6). p. 831-838.

Keller, D.M., R.E. Massey, and O.E Hileman (1978b). "Studies on nucleation phenomena occurring in aqueous solutions supersaturated with calcium sulphate: Part II: The induction time". Can. J. Chem., 56(24). p. 3096-3103.

Keller, D.M., R.E. Massey, and O.E. Hileman (1980). "Studies on nucleation phenomena occurring in aqueous solutions supersaturated with calcium sulphate III The cation: anion ration". Can. J. Chem., 58(20). 2127-2131.

Kester, D.R., R.H. Byrne and Y.J. Lians. "Marine Chemistry in the Coastal Environment". T.M. Church, Ed. Am. Chem. Societ; Symposium Sries, No. 18, Washington D.C., 1975, pp 56.

Kilborn (1979). An Assessment of the Long-Term Suitability of Present and Proposed Methods for the Management of Uranium Mill Tailings. Report for Atomic Energy Control Board.

Kirshmann, R., R. Boulenger, A. Lafontaine (1966). Absorption of Ra-226 Cultivated Plants. Proc. First Internat. Congress of Radiation Protection, Rome, Part 2, pp. 1045.

Klapwijk, A. and W.J. Snodgrass (1983). "Concepts for, and Calculation of the Rate of Stabilization of Sediments", Proceedings WPCF Session on Sediment Oxygen Demand. Hactcher, K.J., Ed.

Knight and Piesold. (1985). "Monitoring of Layered Uranium Tailings - Phase 1". Report for NUTP, Energy, Mines and Resources, Ottawa, Canada.

LaMotta, E. (1974). "Evaluation of diffusion resistances in substrate utilization by biological films." Ph.D. Thesis, University of North Carolina, Chapel Hill, NC, 27514.

Lai, S.H. and J.J. Jurinak (1972). The transport of cations in soil columns at different pore water velocities. Soil Sci. Soc. Am. Proc., 36:730-733.

Langmuir, D. and A.C. Reise (1985). Thermodynamic Properties of Radium. Draft.

Langmuir, D. and D.O. Whitmore (1971). Variations in the stability of precipitated ferric oxyhydroxides. IN: Nonequilibrium Systems in Natural Water Chemistry, Advances in Chemistry Series, 106:209-234.

Langmuir, D. and J.S. Herman. (1980). "The Mobility of Thorium in Natural Waters at Low Temperatures". Geochim. Cosmochim. Acta, v. 44, p. 1753-1766.

Lasaga, A.C. (1981). "Rate Laws of Chemical Reactions." IN: Kinetics of Geochemical Processes, Rev. Mineral., Vol. 8, Edited by A.C. Lasaga and R.J. Kirkpatrick, pp. 1-67. Mineralogical Society of Americal, Washington, D.C.

Lasaga, A.C. (1981). "Rate Laws of Chemical Reactions." IN: Kinetics of Geochemical Processes, (A.C. Lasaga and R.J. Kirkpatrick, Ed.). Mineral Soc. Am. pp 1-68.

Lasaga, A.C. (1984). "Chemical Kinetics of Rock-Water Interactions." J. Geophys. Res., 89(B6) (June 10) 4009-4025.

Leckie, J.O. and J.A. Davis (1979). "Aqueous Environmental Chemistry of Copper." In: Copper in the Environment: Part 1: Ecological Cycling (J.O. Nriagu, ed.) Wiley, pp. 217-254.

Lerman, A. (1977). Lakes Chemistry, Physics, Geology, Sprnger-Verlag.

Lerman, A. (1971). "Time to Chemical Steady-States in Lakes and Oceans." IN: Nonequilibrium Systems in Natural Water Chemistry, Advances in Chemistry Series 106, American Chemical Society, Washington, D.C., USA.

Levenspiel, O. (1972). Chemical Reaction Engineering. Wiley and Sons, New York, 2nd Edition.

Li, Y.H. and S. Gregory (1979). "Diffusion of ions in sea water and in deep-sea sediments." Geochimica et Cosmochimica Acta, 38, 703-714.

Lin, F. and C.V. Clemency (1981). The Kinetics of Dissolution of Muscovites at 25°C and 1 atm CO_2 Partial Pressure." Geochim. Cosmochim. Acta, 45, 571-576.

Lowson, R.T. (1982). "Aqueous oxidation of pyrite by molecular oxygen." Chem. Rev., 82(5): 461-497.

Lundgren, D.G. and M. Silver (1980). "Ore leaching by bacteria." Ann. Rev. Microbiol., 34: 263-83.

MacLaren (1977). "Environmental Assessment of Elliot Lake Expansion."

Marquardt, D.W. (1963). "An algorithm for least squares estimation of nonlinear parameters." J. Soc. Indust. Appl. Math., 11, 431-445.

Massey, R.E. and O.E. Hileman (1977). "Toward an understanding of rates of crystal nucleation from solution with a variable driving force". Can. J. Chem., 55(8). p. 1285-1293.

Meserole, Glover, Stewart (1981). "Studies of the Major Factors Affecting Magnesium Limestone Dissolution." ACS Symposium 29/3-3/4 1981, Atlanta, Georgia.

Metcalfe and Eddy (1979). Wastewater Engineering, McGraw-Hill.

Middleton, K.R. and D.R. Westgrath (1964). "A Rapid Method for Estimating Exchangeable H and Exchange Capacity in Soils of the Moist Tropics". Soil Sci. 97(4): 222-228.

Miller, R.J. (1965). "Mechanisms for Hydrogen to Aluminum Transformations in Clays". Soil Sci. Soc. Am. Proc. 29(1): 36-39.

Miller, R.J. (1968). "Electron Micrographs of Acid-edge Attack of Kaolinite". Soil Sci. *105*: 166-177.

Miller, S.D. (1979). *Chemistry of pyrite strip-mine spoil*. Ph.D. Dissertation, Yale University, New Haven, 189 p.

Miller, S.D. (1980). "Sulphur and Hydrogen in Buffering in Pyrite Strip - Mine Spoil." In: *Biogeochemistry of Ancient and Modern Environments*. (Trudinger and Walter, Eds.) Springer Verlag. p. 537-543.

Morel, F. and J.J. Morgan (1972). "A Numerical Method for Computing Equilibria in Aqueous Chemical Systems". *Environ. Sci. Technol.*, *6*. p. 58-67.

Morin, K.A. and J.A. Cherry (1984). An occurrence of trace amounts of siderite near a uranium-tailings impoundment, Elliot Lake, Ontario, and its implication in controlling contaminant migration. Submitted to Chemical Geology.

Morin, K.A., J.A. Cherry, T.P. Lim and A.J. Vivyurka (1982). Contaminant migration in a sand aquifer near an inactive tailings impoundment, Elliot Lake, Ontario. *Can. Geotech. J.*, *19*:49-62.

Morin, K.A. (1985). 1984 Geochemical study of the acidic contaminant plume near Nordic Main uranium tailings impoundment, Elliot Lake, Ontario. Research Report Prepared for the National Uranium Tailings Program, Energy, Mines and Resources Canada.

Nancollas, G.H. (1979). "The Growth of Crystals in Solution" *Adv. Coll. Interf. Sci.*, *16*, 215-252.

Nancollas, G.H. (1983). "The Mechanism of Precipitation of Biological Minerals. The Phosphate, Oxalates and Carbonates of Calcium." *Croatica. Chemica. Acta*, *56*(4), 741-752.

Nancollas, G.H. and M.M. Reddy (1974). "The Kinetics of Scale Forming Minerals." *Soc. Petrol. Engr. J.*, *SPE 4360*, 117-125.

Nancollas, G.H. and M.M. Reddy (1974). "Crystal Growth Kinetics of Minerals Encountered in Water Treatment Processes" in *Aqueous Environmental Chemistry of Metals*. (A.J. Rubin, Ed.) Ann Arbor Science, Ann Arbor MI. p. 219-253.

Nancollas, G.H. and K. Sawada (1982). "Formation of Scales of Calcium Carbonate Polymorphs: The Influence of Magnesium Ion and Inhibitors." *J. Petrol. Tech.*, *Paper 03-8992*, 645-652.

Nancollas, G.H, T.F. Kazmierczak and E. Schuttringer (1981). "A Controlled Compsotion Study of Calcium Carbonate Crystal Growth: The difference of Scale Inhibitors." *Corrosion - NACE*, *37*(2), 76-81.

Nancollas, G.H., K. Sawada and E. Schattringer (1983). "Mineralization Reactions Involving Calcium Carbonate and Phosphates." IN: *Biomineralization and Biological Metal Accumulation* (P. Westbroek and E.W. de Jong, Ed.). Reidel Publishing Company, 155-169.

Nash, K.L. and G.R. Choppin (1980). "Interaction of Humic and fulvic acids with Th(IV)". J. Inorg. Nucl. Chem., 42. p. 1045-1050.

Nathwani, J.S. and C.R. Philips (1978). "Rates of Leaching from Contaminated Soils." Water, Air and Soil Pollution, 9, 453-465.

Nathwani, J.S. and C.R. Phillips (1979). "Rate Controlling Processes in the Release of Ra-226 from Uranium Mill Tailings." Water Air and Soil Pollution, 11, 309-317.

Nesbitt, H.W., and G.M. Young (1984). "Prediction of Some Weathering Trends of Plutonic and Volcanic Rocks Based on Thermodynamic and Kinetic Considerations." Geochim. Cosmochim. Acta, 48, 1523-1534.

Nicholson, R.V. (1984). "Pyrite Oxidation in Carbonate-Buffered Systems: Experimental Kinetics and Control by Oxygen Diffusion in a Porous Medium." Ph.D. Thesis, University of Waterloo, 176 pp.

Nicholson, R.V. and R.W. Gillham. (1985). Pyrite oxidation in carbonate-buffered solution: The effect of oxide coatings on oxidation rates. (in preparation)

Nicholson, R.V., J.A. Cherry and E.J. Reardon (1983). "Migration of contaminants in groundwater at a landfill: A case study." 6 Hydrogeochemistry. J. Hydrol., 63: 131-176.

Nielsen, A. (1964). Kinetics of Precipitation, MacMillan, 149 p.

Nielson, A. (1981). Theory of Electrolyte Crystal Growth. The Parabolic Rate Law. Pure & Appl. Chem., 53:2025-2039.

Nishiwaki, Y., Y. Honda, Y. Kimura, H. Morishima, T. Koga, Y. Miyaguchi, H. Kawai (1972). Behaviour and distribution of radioactive substances in coastal and estuarine waters, in radioactive contamination of the marine environment. Internat. Atomic Energy Agency Report, IAEA-SM-185/11.

Nordstrom, D.K. (1982). "Aqueous pyrite oxidation and the consequent formation of secondary iron minerals." In: Acid Sulphate Weathering, Soil Sci., Soc. Amer., Spec. Publ. No. 10, pp. 37-56.

Nordstrom, D.K. (1982). "The effect of sulfate on aluminum concentrations in natural waters: some stability relations in the system Al_2O_3 - SO_3 - H_2O at 298K." Geochim. Cosmochim. Acta., 46: 681-692.

Nriagu, J.O. (Ed.) (1976). Environmental Biogeochemistry. Ann Arbor Science. Ann Arbor, 2 volumes.

Nriagu, J.O. (Ed.) (1978a). The Biogeochemistry of Lead in the Environment. Wiley, 2 volumes.

Nriagu, J.O. (Ed.) (1978b). Sulphur in the Environment. Wiley.

Nriagu, J.O. (Ed.) (1979a). The Biogeochemistry of Mercury in the Environment. Elsevier. 696 pp.

Nriagu, J.O. (Ed.) (1979b). Copper in the Environment. Wiley, 2 volumes.

Nriagu, J.O. (Ed.) (1980a). Calcium in the Environment. Wiley, 2 volumes.

Nriagu, J.O. (Ed.) (1980b). Nickel in the Environment. Wiley, 2 volumes.

Nriagu, J.O. (Ed.) (1980c). Zinc in the Environment. Wiley. 453 pp.

Nriagu, J.O. (1983). "Arsenic enrichment in lakes near the smelters at Sudbury, Ontario". Geoch. et Coscomch Acta, 47. p. 1623-1526.

O'Connor, D.J. and J.P. Connelly (1980). Water Research, 14: 1517-1523.

Osthaus, B. (1955). "Kinetic Studies on Montmorillonites and Nontronite by the Acid-dissolution Technique". Clay and Caly Minerals, 4: 301-321.

Ostrovskii, S.V., S.A. Amirova, and M.K. Kalugina (1969). "Solubility of calcium sulphate in concentrated sulphuric acid." Zh. Neorg. Khim., V14, N9 (in Russion; chem. Abs. 71129378).

Paces, T. (1983). "Rate constants of dissolution derived from the measurements of mass balance in hydrological catchments." Geochim. Cosmochim. Acta., 47:1855-1863.

Parkhurst, D.L., D.C. Thorstenson, and L.N. Plummer (1982). "PHREEQE - A Computer Program for Geochemical Calculation". U.S.G.S. 80-96. Government of United States.

Pickering, W.F. (1980). "Zinc Interaction with Soil and Sediment Components." In: Zinc in the Environment: Part 1: Ecological Cycling. (J.O. Nriagu, ed.) Wiley, pp. 113-160.

Pickering, W.F., (1979). "Copper Retention by Soil/Sediment Components." In: Copper in the Environment: Part 1: Ecological Cycling. (J.O. Nriagu, ed.) Wiley, pp. 89-122.

Plotnikov, V.I. (1964). "Coprecipitation of small amounts of selenium and zinc with metal hydroxides." Russian J. Inorg. Chem., 9(2): 245-247.

Plummer, L.N. and F.T. Mackenzie (1974). "Predicting Mineral Solubility from Rate Data: Application to the Dissolution of Magnesian Calcites." Am. J. Sci., 274, 61-83.

Plummer, L.N. and E. Busenberg (1982). "The Solubilities of Calcite, Aragonite and Vaterite in CO_2 - H_2O solutions between 0 and 90^{o}C and an evaluation of the aqueous model for the system $CaCO_3$ - CO_2 - H_2O." Geochim. Chosmochim. Acta, 46, 1011-1040.

Plummer, L.N. and E.T. Sundquest (1982). "Total Individual Ion Activity Coefficients of Calcium and Carbonate in Seawater at 25^{o}C and 35% Salinity, and Implications to the Agreement Between Aparent and Thermodynamic Constants of Calcite and Aragonite." Geochim. Cosmochim. Acta, 46, 247-258.

Plummer, L.N., B.F. Jones and A.H. Truesdell (1976). "WATEQF - A FORTRAN IV version of WATEQ, a computer program for calculatig chemical equilibrium of natural waters." Water Resources Invest., 76-13, U.S. Geological Survey, 63 pp.

Plummer, L.N., T.M.L. Wigley, and D.L. Parkhurst (1978). "The kinetics of Calcite dissolution in CO_2- Water Systems at 5°C to 60°C and 0.0 to 1.0 Atm CO_2", Am. J. Science, 278, p. 179-216.

Plummer, L.N., T.M.L. Wigley, and D.L. Parkhurst (1979). "Critical Review of the Kinetics of Calcite Dissolution and Precipitation" in Chemical Modelling in Aqueous Systems. (E.A. Jeanne, Ed.) ACS Series 93, p. 537-573.

Rancon, D., (1973). "The Behaviour in Underground Environments of Uranium and Thorium Discharged by the Nuclear Industry." In: Environment Behaviour of Radionuclides Released in the Nuclear Industry, Intern. Atomic Energy Agency Report, IAEA-SM-172/55.

Reardon, E.J., A.A. Mozeto and P. Fritz (1980). "Recharge in northern clime calcareous sandy soils: soil water chemistry and carbon-14 evolution." Geochim. Cosmochim. Acta., 44: 1723-1735.

Reckhow, K.H. (1979). "Empirical Lake Models for Phosphorus Development, Applications, Limitation and Uncertainty." IN: Perspectives in Lake Ecosystem Modelling, Ann Arbor Science, Ann Arbor, MI, pp. 193-222.

Reddy, M.M. and G.H. Nancollas (1976). "The Crystallization of Calcium Carbonate IV: The Effect of Magnesium, Strontium, and Sulphate Ions." J. Crystal Growth, 35, 33-38.

Reddy, M.M., and K.K. Wang (1980). "Crystallization of Calcium Carbonate in the Presence of Metal Ions." J. Cryst. Growth, 50, 470-480.

Reddy, M.M. and W.D.Gaillard (1981). "Kinetics of Calcium Carbonate (Calcite) - Seeded Crystallization: Influence of Solid Solution Ratio on the Reaction Rate Constant." J. Collard. Interf. Sci., 80(1), 171-178.

Reddy, M.M., L.N.P. Summer and E. Busenberg (1981). "Crystal Growth of Calcite from Calcium Bicarbonate Solutions at Constant PCO_2 and 25°C: A Test of a Calcite Dissolution Model." Geochim. Cosmochim. Acta, 45(8), 1281-1289.

Reimers, C.A., S. Kalhorn, S.R. Emerson and K.H. Nealson (1984). "Oxygen consumption rates in pelagic sediments from the Central Pacific." Geochim. Cosmochim. Acta, 48, 903-910.

Remington, R.D. and M.A. Schork (1970). Statistics with Applications to the Biological Sciences and Health Sciences, Prentice-Hall, 418 pp.

Reynolds, M.E.R., H.E. Burkhart, and R.F. Daniels (1981). "Procedures for Statistical Validation of Stochastic Simulation Models." Forest Science, 27(2), 349-364.

Richter, R.O. and T.L. Theis (1980). "Nickel Speciation in a Soil/Water System." In: Nickel in the Environment. (J.O. Nriagu, ed.) Wiley, pp. 189-202.

Rickard, D.T. and J.O. Nriagu (1978). "Aqueous Environmental Chemistry of Lead." In: the Biogeochemistry of Lead in the Environment. (J.O. Nriagu, ed.) Elsevier, pp. 219-284.

Riese, A.C. (1983). "Adsorption of Radium and Thorium onto Quartz and Kaolinite: A Comparison of Solution/Surface Equilibria Models." Ph.D. Thesis, Colorado School of Mines.

Rimsaite, J. (1978). "Application of mineralogy to the study of multi-stage uranium mineralization in remobilized uranium deposits, Saskatchewn." p. 403-430.

Rimstidt, J.D. and H.L. Barnes. (1980). "The Kinetics of Silica on Water Reactions". Geochimica Cosmochimica Acta, 44, 1683-1699.

Ringbom, A. (1963). Complexation in Analytical Chemistry, Wiley-Interscience, New York.

Robertson, J.A. (1978). Uranium deposits in Ontario. IN: M.M. Kimberly (ed.) Min. Assoc. Can., Short course in Uranium deposits: Their mineralogy and origin, 229-280.

Rochelle, G. (1981). "Dissolution of Calcite in Aqueous Solution." ACS National Meeting, Atlanta, Georgia, March 29-30, 1981.

Ross, C.J., K.C. Ivarson and N.M. Miles (1982). "Microbial formation of Basic Ferric Sulphates in Laboratory Systems and in Soils." IN: Acid Sulphate Weathering, Soil Sci. Society of America, pp. 77-94.

Ross, G.J. and K.C. Ivarson (1980). "The occurence of basic ferric sulphates in some Canadian Soils." Can. J. Soc. Sci., 61, 99-107.

Sung, W. and J.J. Morgan. (1980). Environ. Sci. & Tech , 14, 561.

Santschi, P.H., D. Adler, M. Amdurer, Y.H. Li and J. Bell (1980). Earth Planet Sci. Lett., 47, 327-335.

Santschi, P.H., Y.H. Li, D.M. Adler, M. Amdurer, J. Bell and U.P. Nyfleler (1983). The Relative Mobility of Natural (Th, Pb, Po) and Fallout (Pa, Am, Cs) Radionuclides in the Marine Environment: Results in Model Ecosystems and Narragansett Bay. Geochimica et Cosmochimica Act,47:201-210.

Satterfield, C.M. 1970. "Mass transfer in heterogeneous catalysis." M.I.T. Press, Cambridge, MA.

Schaefer, W. and E. Hunger (1969). "Solubility of calcium sulphate in salt-containing, diluted sulphuric acid." Z. Chem, 9, N12 (Chem. Abs. 7205977)

Schofield, R.K. (1949). "Effect of pH on Electric Charges Carried by Clay Particles". J. Soil Sci., 2: 1-8.

Schott, J., R.A. Berner, and E.L. Sjoberg (1981). "Mechanism of Pyroxene and Amphibole Weathering, I, Experimental Studies of Iron-Free Minerals." *Geochim. Cosmochim. Acta*, *45*, 2123-2135.

Senes (1981). "Quirke Lake Tailings Study, Stage 1, Background Information". Submitted to Rio Algom and Denison Mines Ltd.

Senes, (1984). Assessment of the mechanism of bacterially assisted oxidation of pyritic uranium tailings. Report to the National Uranium Tailings Program, July 1984.

Serne, R.J., D. Rai, M.J. Mason and M.A. Maleche (1977). Batch Kol Measurements of Nuclides to Estimate Migration Potential at the Proposed Waste Isolation Pilot Plant in New Mexico. Battelle Pacific Northwest Laboratories Report, PNL-2448.

Sherritt Gordon Mines Ltd. and Key lake Mining Corporation (1980). Key Lake Project, Process Development. Papers Presented at the 19th Annual Conference of Metallurgists of CIM, Halifax, N.S., August, 116 pp.

Sherwood, T.K., R.L. Pigford and C.R. Wilke (1975). *Mass Transfer.* McGraw Hill.

Sigg, L., and W. Stumm (1980). "The Interaction of Anions of Weak Acids with the Hydrous Geothite (-FeOOH) Surface *Colloids and Surfaces*" *2*, pp. 101-117.

Sillen, L.G. and A.E. Martell (1964). *Stability Constants*, Special Publication *17*, The Chemical Society (London).

Sillen, L.G. and A.E. Martell (1971). *Stability Constants - Supplement No. 1*, Special Publication 25, The Chemical Society (London).

Silverman, M.P. and D.G. Landgren (1959). *J. Bacteriol.*, *77*, pp. 642.

Singer, P.A. and W. Stumm (1970). "Acid mine drainage: the rate determining step". *Science*, *167*. p. 1121-1123.

Sjoberg, E.L. (1979). "Kinetics and Mechanism of Calcite Dissolution in Aqueous Solutions at Low Temperatures." Diss. Geologiska Institutioen, Stockholm.

Smyth, D.J.A. (1981). Hydrogeological and geochemical studies above the water table in an inactive uranium tailings impoundment near Elliot Lake, Ontario. Unpublished M.Sc. Project, University of Waterloo, Waterloo, Ontario.

Snodgrass, W.J. (1979). "Predictive Water Quality Models for the Great Lakes: Some Capabilities and Limits." IN: *Perspectives in Lake Ecosystem Modelling*, Ann Arbor Science, Ann Arbor, MI, 171-192.

Snodgrass, W.J. (1983). "Comparsion of the Kinetic Formulation for Three SOD Models", Proceedings, WPCF Session on Sediment Oxygen Demand. Hatcher, K.J., Ed.

Snodgrass, W.J. (1983). "Temporal Scale Estimation for Water Bodies Using Mass Balance Concepts." IN: *Environmental Systems* (Elfalfon Ed.) Enclyclopedia of Systems and Control. Pergamon Press. (In press).

Snodgrass, W.J., D.L. Lush and J. Capabianco (1983). "Implications of Alternative Geochemical Controls on the temporal behaviour of Elliot Tailings." In: Management of Wastes from Uranium Mining and Milling. International Atomic Energy Agency, Vienna Publ. IAEA-SM-26219. p. 285-310.

Snodgrass, W.J., D.L. Lush, P.M. McKee and R.R. Walker (1983). "An Approach to the Calculation of Dose Commitment Arising from Different Methods for the Long-term Management of Uranium Mill Tailings Through Aquatic Pathways". Atomic Energy Control Board Report. INFO-0097.

Stephenson, J.P. (1978). "Biological fluidized bed denitrification of wastewater." Master's Thesis, Dept. of Chemical engineering McMaster University, Hamilton, Ontario.

Stroes, S. (1983). "Studies on S-MnO_2 for Copper Speciation Measurements". Ph.D. Thesis, McMaster University.

Stumm, W. (1982). "Surface Chemical Theory as an aid to Predict the Distribution and the Fate of Trace Constiutents and Pollutants in the Aquatic Environment." Wat. Sci. Tech. 14, pp. 481-491.

Stumm, W. and J.J. Morgan (1981). Aquatic Chemistry. McGraw-Hill.

Stumm, W., R. Kummert and L. Sigg (1980). "A Ligand Exchange Model for the Adsorption of Inorganic and Organic Ligands at the Hydrous Oxide Interface." Croatica Chemcial Act, 53(2), pp. 291-312.

Stumm, W. and G.F. Lee (1961). Ind. Eng. Chem., 53, 143.

Sverdrup, H., H. Eklund and I. Bjerle (1981). "Kalkning av rinnande vatten erfarenheter fran enfluidiserad kalkbrunn - MOVER." Vatten, 37(4), 388-393.

Sverdrup, H. and I. Bjerle (1982). "Dissolution of Calcite and Other Related Minerals in Acidic Aqueous Solution in a pH - stat." Vatten, 38(1), 59-73.

Sverdrup, H. and I. Bjerle (1983). "The Calcite Utilization Efficiency and the Long-Term Effect on Alkalinity in Several Swedish Lake Timing Projects." Vatten, 39(1), 41-54.

Temple, K.L. and E.W. Delchamps (1953). Appl. Microbiol, 1, 255.

Theis, T.L. and R.O. Richter (1979). "Chemical Speciation of Heavy Metals in Power Plant Ash Pond Leachate." Environ. Sci. Technol., 13:219-224.

Thomann, R.V. (1972). Systems Analysis and Water Quality Management. McGraw Hill.

Thomann, R.V. (1982). "Verification of Water Quality Models." J. Environ. Engr. Div., ASCE, 108, #EE5, 923-940.

Thomann, R.V. (1972). Systems Analysis and Water Quality Management. McGraw Hill.

Tomson, M.B., and G.H. Nancollas (1978). "Mineralization Kinetics: A Constant Composition Approach." Science, 200, 1059-1060.

Toprac, A.J. and G.T. Rochelle (1982). "Limestone Dissolution in Stack Gas Denitrification. Environ. Prog. 1, 52-58.

Trudinger, P.A. and M.R. Walter (Ed.) (1980). Biogeochemistry of Ancient and Modern Environments. 723 pp.

UNSCLEAR (United Nations Scientific Committee on the Effects of Atomic Radiation). (1982). "Ionizing Radiation: Sources and Biological Effects". United Nations Report with Annexes.

Valocchi, A.J., R.L. Street and P.V. Roberts (1981). Transport of ion-exchanging solutes in groundwater: Chromatographic theory and field simulation. Water Resour. Res., 17(5):1517-1527.

van Breeman, N. (1972). Soil forming processes in acid sulfate soils. p. 66-130. IN: H. Dost, (ed.) Acid Sulfate Soils. Publ. 18(1), Internat. Inst. for Land Recl. and Improv., Wageningen, the Netherlands.

van Breeman, N. (1973). dissolved Aluminum in Acid Sulfate Soils and in Acid Mine Waters. Soil Sci. Soc. Amer. Proc. 37: 694-697.

van Olphen, H. (1963). "An Introduction to Clay Colloid Chemistry". Interscience Publishers, New York, 302 pp.

Wagner, D.P., D.S. Fanning, J.E. Foss, M.S. Patterson and P.A. Snow (1982). "Morphological and Mineralogical; Features Related to Sulphate Oxidation and Natural Disturbed Land Surfaces in Maryland." IN: Acid Sulphate Weathering, Soc. Sci. American, 109-146.

Wahlgren, M.A. and K.A. Orlandini (1982). "Comparison of the Geochemical Behaviour of Plutonium, Throium and Uranium in Selected North American Lakes. Symposium Proceedings, Migration in the Terrestrial Environment". International Atomic Energy Agency. Public. IAEA-SM-257/89, pp 757-774.

Wahlgren, M.A., J.J. Alberts, D.M. Nelson, K.A. Orlandini (1976). IN: Transuranium Nuclides in the Environment, IAEA-SM-199/44, Vienna, p. 9-23.

Walker, R.R. and W.J. Snodgrass (1983). "Modelling Sediment Oxygen Demand in Hamilton Harbor", Proceedings WPCF Session on Sediment Oxygen Demand. Hatcher, K.J., Ed.

Williamson, K. and P.L. McCarty (1976a). "A Model of Substrate Utilization by Bacterial Films." Wat. Poll. Cont. Fed., 48, 9-24.

Williamson, K. and P.L. McCarty (1976b). "Verification studies of the biofilm model for bacterial substrate utilization." Wat. Poll. Contr. Fed., 48, 281-296.

Wolery, T.J. (1983). "EQ3NR. A Computer Program for Geochemical Aqueous Speciation - Solubility Calculations - User's Guide and Documentation". Lawrence Livermore National Laboratory. UCRL - 53414.

Wolfe, P.J. (1965). "Non-linear least squares (GAUSHAUS)." University of Wisconsin Computing Center, ID Code C0017-00/SOO17-00, 34 pp.

Wood, W.W. (1978). Use of laboratory data to predict sulfate sorption during artificial groundwater recharge. Groundwater, 16(1): 22-31.

Wuhrmann, (1964). "Microbial aspects of water pollution." Adv. Applied Microbiology, 6, 109-151.

Zobell, C.E. and D.A. Andersen (1936). "Observations on the multiplication of bacteria in different volumes of stored ice water and the influence of oxygen tension and solid surfaces." Biol. Bull., 71, 324-342.

Zollinger, E. and W. Stumm (1972). "The bacterial oxidation of pyrite". Arch. Microbiol, 83. p. 110-119.

APPENDIX A

PATHWAY DIAGRAMS FOR OTHER ELEMENTS AND RADIONUCLIDES

Appendix A.1 Sodium, Potassium and Magnesium

Sources

The major sources of these cations are represented by silicate minerals. Feldspars and amphiboles contain Na. Feldspars also contain K. Pyroxenes, amphiboles and clays such as chorite can contribute Mg during dissolution.

Occurrrence in Tailings

Some transformations have likely occurred in the milling process. The formation of jarosite in the tailings would likely result in the uptake of potassium into that solid. The formation of secondary magnesium solids (e.g., magnesium hydroxide) during neutralization is also likely. In addition, these elements would have been contributed to tailings pore water during fertilization of old-tailings areas to induce the growth of grasses. This is likely to be a minor contribution, that has occurred on a limited basis, in only certain tailings deposits. A summary of the major primary and secondary minerals containing these elements is given in Table 14.1. Other minerals are summarized in Table 4.11.

Reaction Pathways

Reaction pathways for Na, K and Mg are given in Figures A.1a, A.1b and A.1c respectively.

- Silicates

As with most silicates, kinetically controlled dissolution will dominate in the subsurface tailings environment.

- Jarosite (Potassium)

This mineral phase is stable at low pH and high-sulphate activities. As discussed previously, jarosite reactions are probably controlled by equilibrium processes for its formation and possibly by kinetic or equilibrium processes for its dissolution.

FIGURE A.1a: PATHWAY DIAGRAM FOR SODIUM

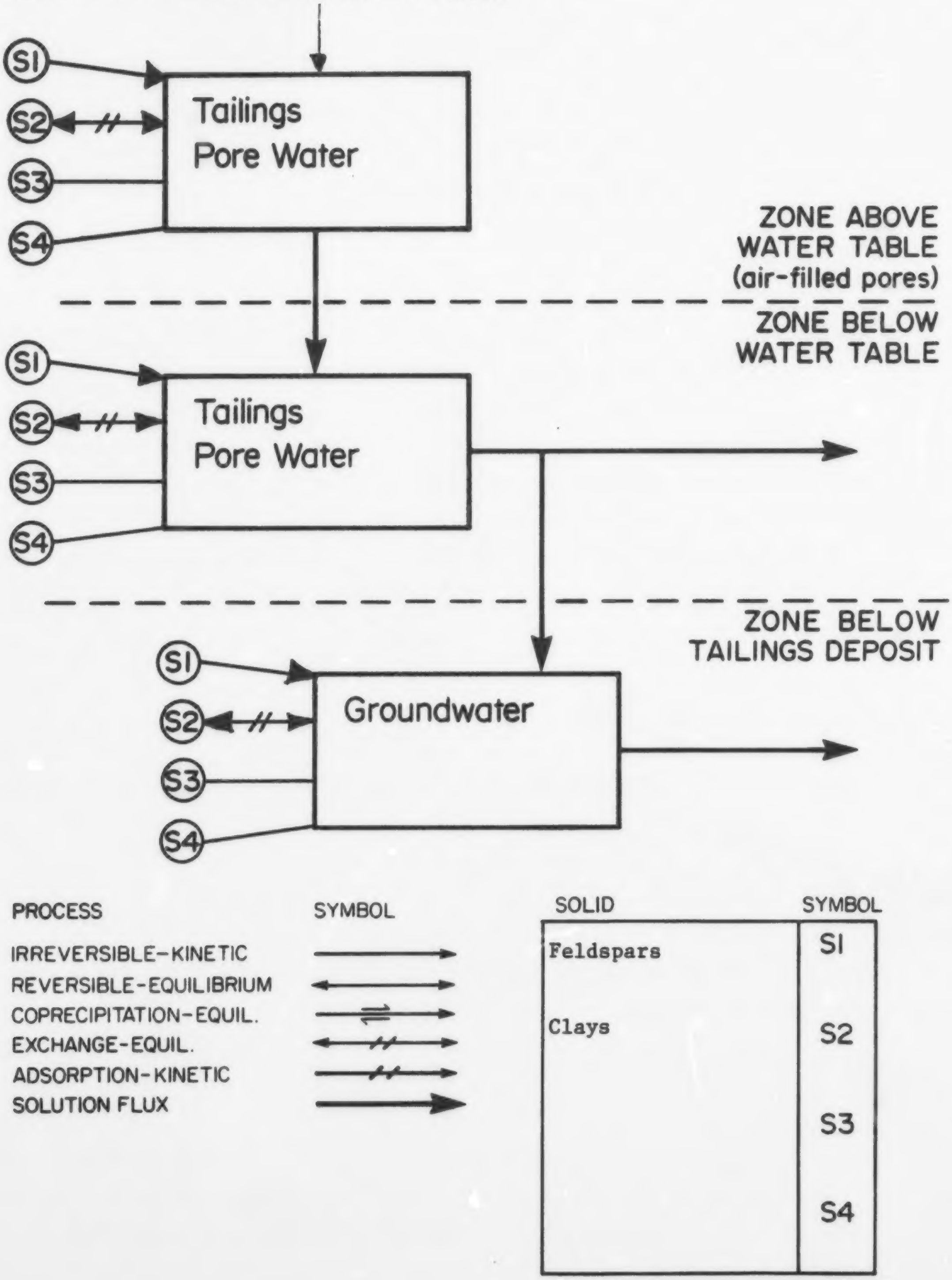
S1
S2
S3
S4
Tailings Pore Water
ZONE ABOVE WATER TABLE (air-filled pores)
ZONE BELOW WATER TABLE
S1
S2
S3
S4
Tailings Pore Water
ZONE BELOW TAILINGS DEPOSIT
S1
S2
S3
S4
Groundwater
PROCESS
SYMBOL
IRREVERSIBLE-KINETIC
REVERSIBLE-EQUILIBRIUM
COPRECIPITATION-EQUIL.
EXCHANGE-EQUIL.
ADSORPTION-KINETIC
SOLUTION FLUX

SOLID	SYMBOL
Feldspars	S1
Clays	S2
	S3
	S4

FIGURE A.1b: PATHWAY DIAGRAM FOR POTASSIUM

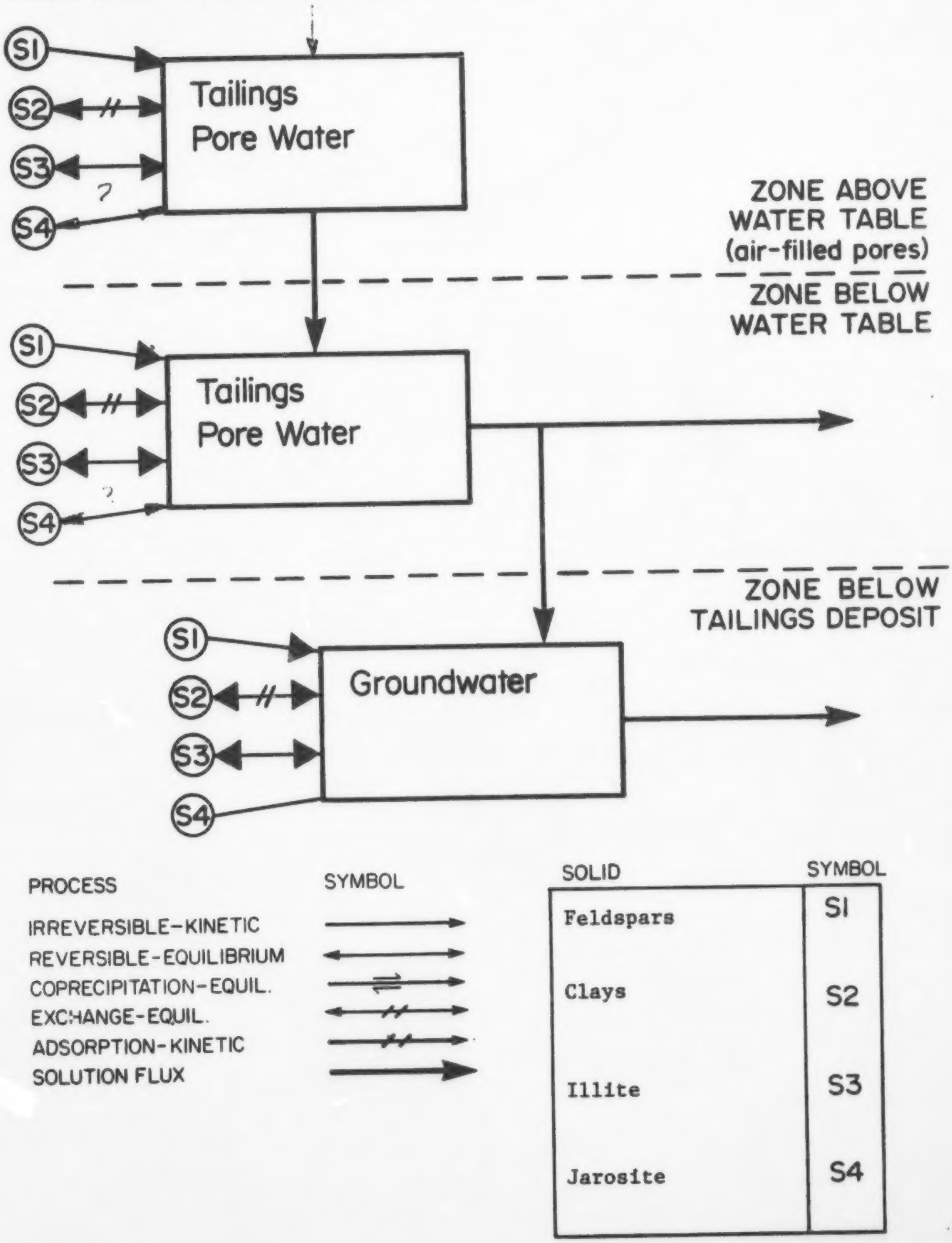
S1
S2
S3
S4
Tailings
Pore Water
?
ZONE ABOVE
WATER TABLE
(air-filled pores)
ZONE BELOW
WATER TABLE
S1
S2
S3
S4
Tailings
Pore Water
?
ZONE BELOW
TAILINGS DEPOSIT
S1
S2
S3
S4
Groundwater
PROCESS
SYMBOL
IRREVERSIBLE-KINETIC
REVERSIBLE-EQUILIBRIUM
COPRECIPITATION-EQUIL.
EXCHANGE-EQUIL.
ADSORPTION-KINETIC
SOLUTION FLUX
SOLID
SYMBOL
Feldspars
S1
Clays
S2
Illite
S3
Jarosite
S4

FIGURE A.1c: PATHWAY DIAGRAM FOR MAGNESIUM

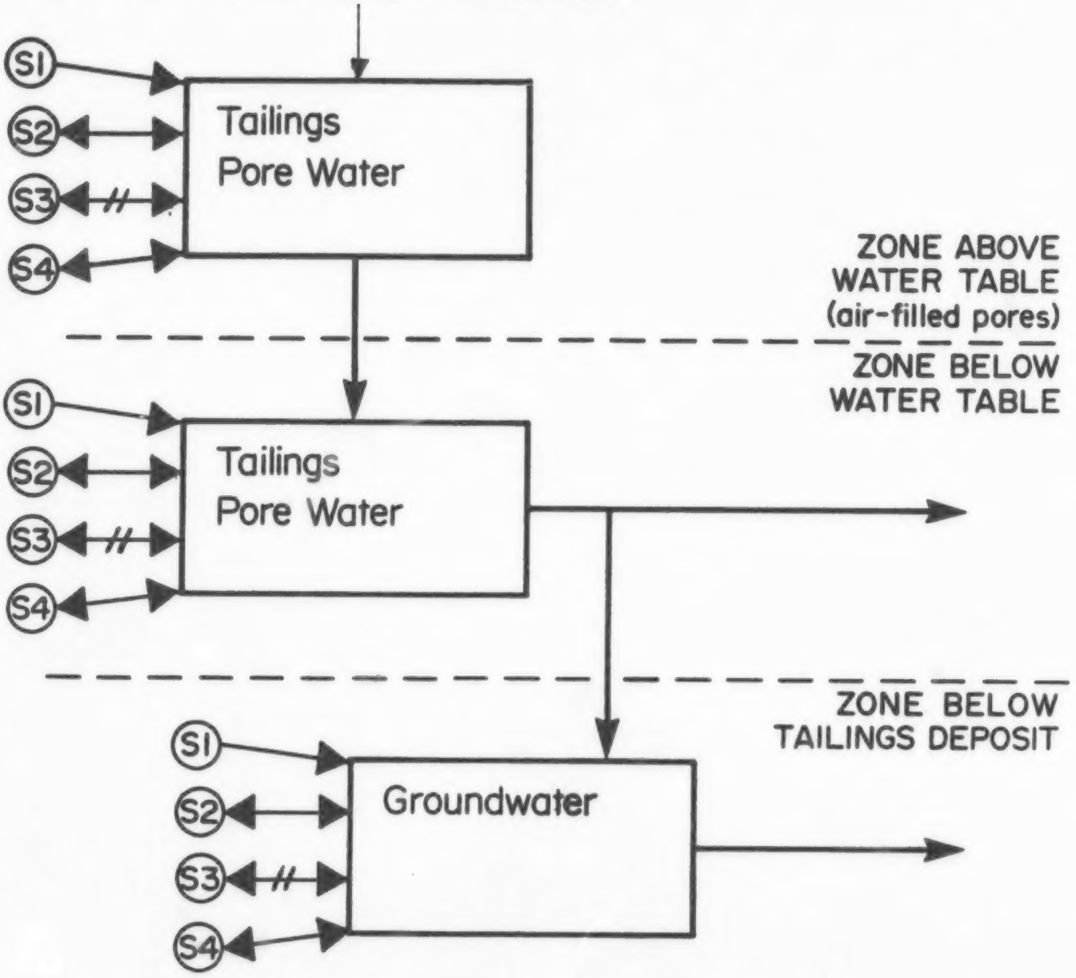
S1
S2
S3
S4
Tailings Pore Water
ZONE ABOVE WATER TABLE (air-filled pores)
ZONE BELOW WATER TABLE
S1
S2
S3
S4
Tailings Pore Water
ZONE BELOW TAILINGS DEPOSIT
S1
S2
S3
S4
Groundwater

PROCESS	SYMBOL
IRREVERSIBLE-KINETIC	⟶
REVERSIBLE-EQUILIBRIUM	⟷
COPRECIPITATION-EQUIL.	⟶ ⇌ ⟶
EXCHANGE-EQUIL.	⟵ // ⟶
ADSORPTION-KINETIC	⟶ // ⟶
SOLUTION FLUX	⟹

SOLID	SYMBOL
Amphiboles Pyroxenes	S1
Carbonates	S2
Clays	S3
Chlorite	S4

Surface Adsorption

All of these species behave as cations in solution and all will be subject to cation exchange. Of the four major cations (Ca^{2+}, Mg^{2+}, Na^+, K^+), potassium has the greatest affinity for exchange sites on clay surfaces and therefore generally exhibits the largest relative retardation during transport through a porous medium.

Appendix A.2 Chloride

Sources

Chloride ion is a rather minor component in the tailings environment. The major sources occur as impurities within various minerals with no particularly dominant mineral phase occurring in the ore deposits. Chlorapatite, if it occurs, would be the only specific mineral phase to release Cl.

Occurrence in Tailings

During milling, chlorate has sometimes been added to the leach to promote oxidation and enhance mobilization of the uranium in the +VI oxidation state. Chlorate is readily reduced to Cl^- after which it is transported in the mill leach solution to the tailings deposit. Addition of fertilizer to the tailings has contributed Cl^- to the tailings pore water; but as stated previously, this would be limited in extent.

Reaction Pathways

A pathway diagram for chloride is given in Figure A.2.

Of all chemical constituents considered here, Cl^- is the least reactive in the taiings and surrounding natural environment. Many studies have shown that Cl^- is generally conservative and therefore moves with the pore water unaffected by chemical processes.

FIGURE A.2: PATHWAY DIAGRAM FOR CHLORIDE

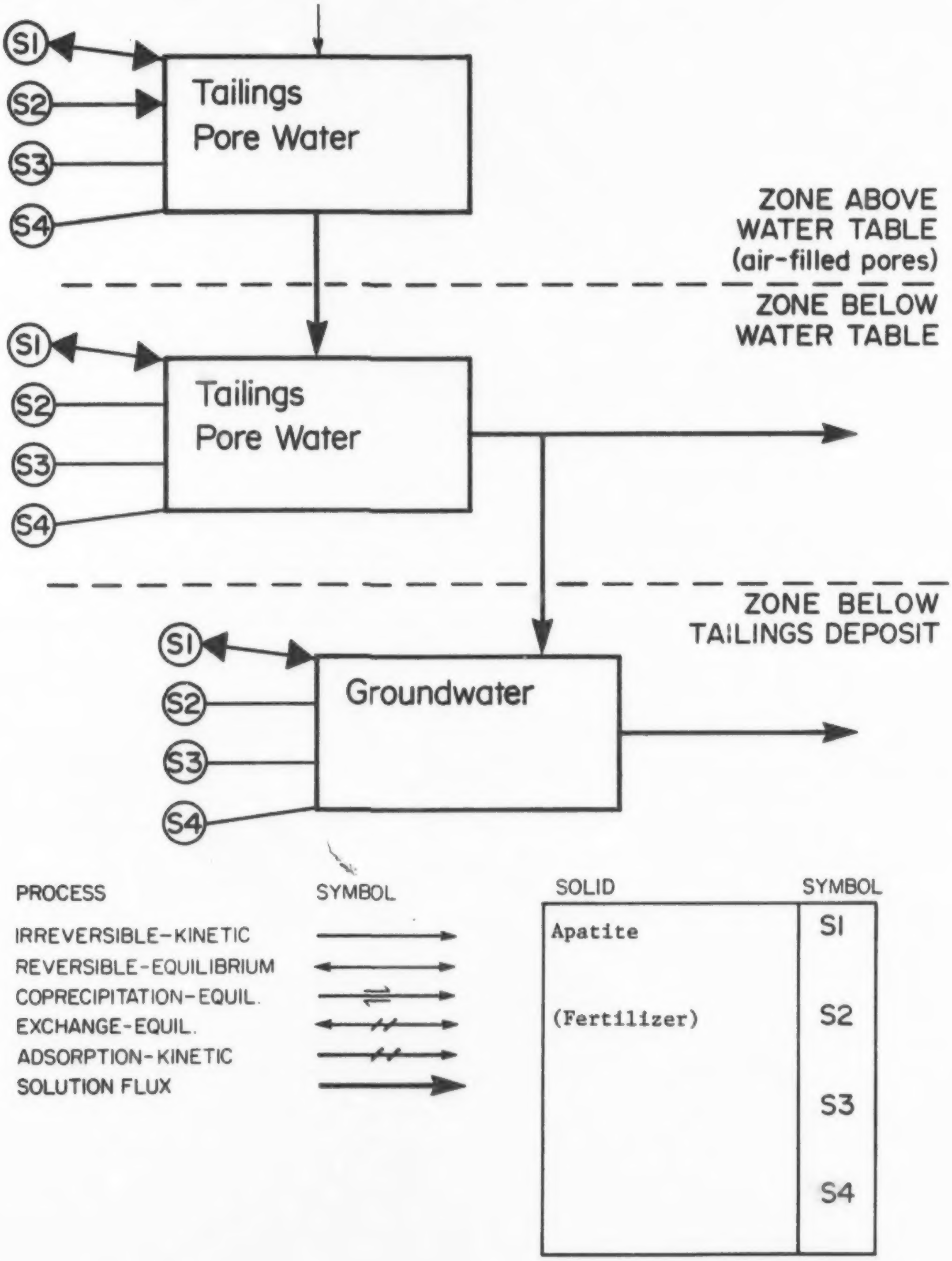
S1
S2
S3
S4
Tailings Pore Water
ZONE ABOVE WATER TABLE (air-filled pores)
ZONE BELOW WATER TABLE
Tailings Pore Water
ZONE BELOW TAILINGS DEPOSIT
Groundwater
PROCESS
SYMBOL
IRREVERSIBLE-KINETIC
REVERSIBLE-EQUILIBRIUM
COPRECIPITATION-EQUIL.
EXCHANGE-EQUIL.
ADSORPTION-KINETIC
SOLUTION FLUX

SOLID	SYMBOL
Apatite	S1
(Fertilizer)	S2
	S3
	S4

Appendix A.3 Cobalt

Sources

Cobalt occurs as a primary arsenide and sulphide (e.g., linnaeite Co_3S_4) in Saskatchewan ores and as a replacement element or impurity in the pyrite and associated sulphides in the Elliot Lake ores. Skutterudite is the dominant cobalt mineral in the former category although carrollite and linnaeite may also occur to a lesser extent.

Occurrence in Tailings

Dissolution of much of the primary cobalt arsenide material will likely occur in the acid leach process. This suggests that secondary solids would likely form during neutralization of the tailings prior to discharge. The major sinks for cobalt are expected to be hydroxides and coprecipitation with, and adsorption on, ferric hydroxides. A list of potential primary and secondary solids containing cobalt is given in Table 14.1. Other minerals containing cobalt are given in Table 4.11.

Reaction Pathways

A pathway diagram for cobalt is given in Figure A.3.

- Arsenides

Dissolution and oxidation of residual primary cobalt arsenides will be kinetically controlled. Because nickel also occurs in the same mineral phases as does cobalt, their dissolution rates will probably be similar.

Secondary Solids

Very little information was found on the existence and properites of secondary cobalt solids. It might be expected that the hydroxides $Co(OH)_2$ and $Co(OH)_3$ would form at high pH values. It seems unlikely that the mixed valence Co_3O_4 would form in the mill or tailings environments. It is not known whether thermodynamic or kinetic processes control solid-solution interaction.

FIGURE A.3: PATHWAY DIAGRAM FOR COBALT

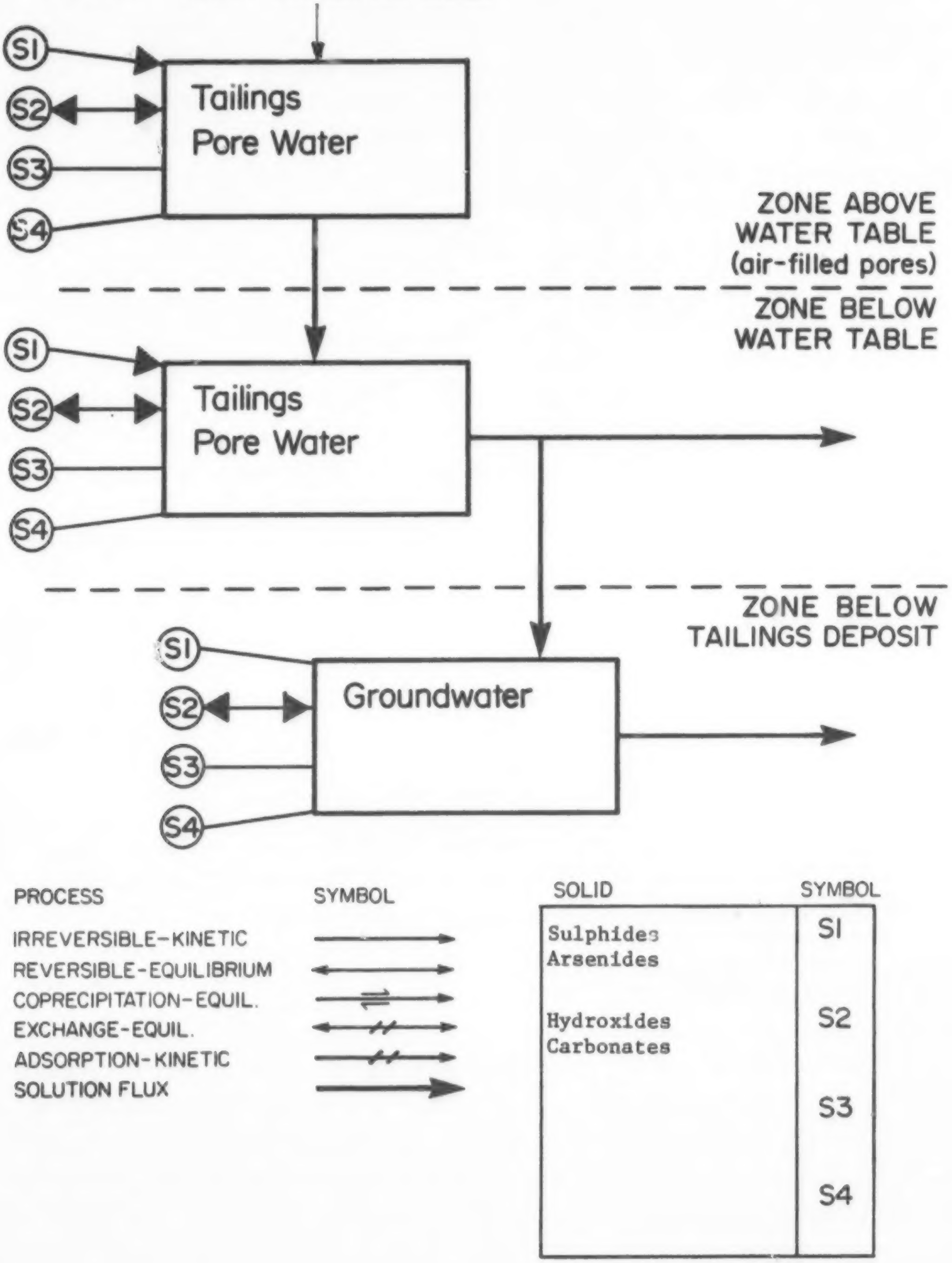
S1
S2
S3
S4
Tailings
Pore Water
ZONE ABOVE
WATER TABLE
(air-filled pores)
ZONE BELOW
WATER TABLE
Tailings
Pore Water
ZONE BELOW
TAILINGS DEPOSIT
Groundwater
PROCESS
SYMBOL
IRREVERSIBLE-KINETIC
REVERSIBLE-EQUILIBRIUM
COPRECIPITATION-EQUIL.
EXCHANGE-EQUIL.
ADSORPTION-KINETIC
SOLUTION FLUX
SOLID
SYMBOL
Sulphides
Arsenides
S1
Hydroxides
Carbonates
S2
S3
S4

Surface Adsorption

The cationic nature of the dissolved species suggests that cobalt would be influenced by exchange on clays. Although little is known about exchange constants, analogous behaviour to Ni and to some extent Fe is expected. Adsorption isotherms for Co on various surfaces have been derived in laboratory studies.

Appendix A.4 Manganese

Sources

Manganese constitutes a minor-to-trace component in the various uranium ore types. There are no obvious primary minerals of significance other than probable oxides. The manganese may also occur as a replacement or as an impurity in iron minerals.

Occurrence in Tailings

The oxidizing environment in the acid leach circuit suggests that any solubilized Mn would occur as Mn(+IV). This could result in solubility control by the MnO_2 solid. The formation of $MnCO_3$ solid during neutralization may also be possible if Mn occurs in the (+II) state. A list of major primary and secondary sources of manganese is given in Table 14.1. Other minerals are given in Table 4.11.

Reaction Pathways

A pathway diagram for manganese is given in Figure A.4.

o Oxides

The oxidation of manganese from (+II) to (+IV) has been observed to be kinetically controlled. Oxides of both forms are known but the dissolution rates are not known precisely.

Another significant unknown is represented by the redox condition in the pore water. Because of the potentially numerous oxidation states of Mn, different redox potentials will represent metastable conditions for different solid phases.

FIGURE A.4: PATHWAY DIAGRAM FOR MANGANESE

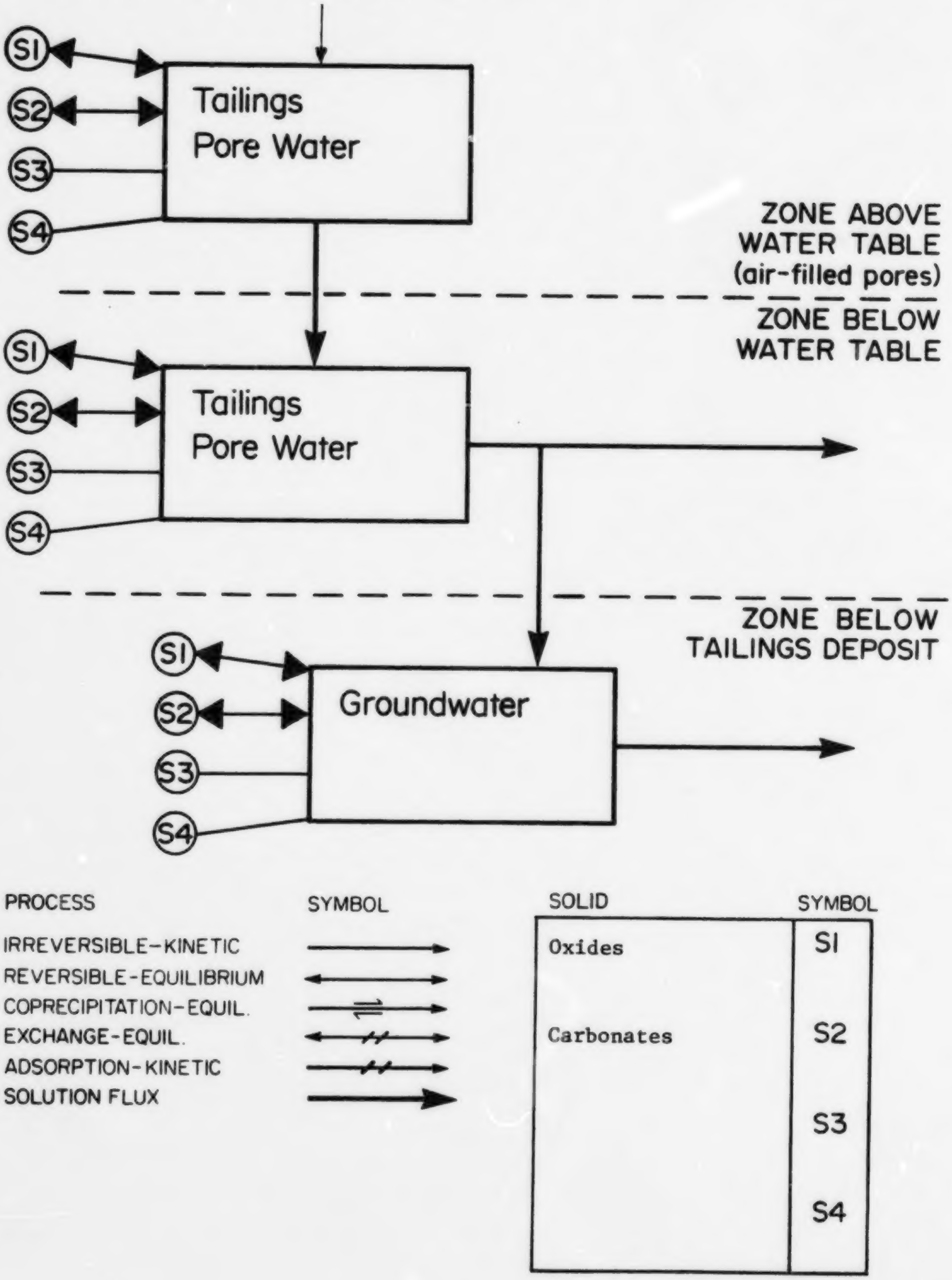
S1
S2
S3
S4
Tailings Pore Water
ZONE ABOVE WATER TABLE (air-filled pores)
ZONE BELOW WATER TABLE
Tailings Pore Water
ZONE BELOW TAILINGS DEPOSIT
Groundwater
PROCESS
SYMBOL
IRREVERSIBLE-KINETIC
REVERSIBLE-EQUILIBRIUM
COPRECIPITATION-EQUIL.
EXCHANGE-EQUIL.
ADSORPTION-KINETIC
SOLUTION FLUX
SOLID
SYMBOL
Oxides
S1
Carbonates
S2
S3
S4

Appendix A.5 Lead

Sources

The primary sources for lead are represented by minerals such as galena and clausthalite in the Saskatchewn ore. It is found in significant quantities in U-238 and Th-232 containing minerals in Elliot Lake ores being the stable end member of the two decay chains (respectively, Pb-206 and Pb-208). It is probably present as an impurity in the other sulphide minerals associated with Elliot Lake ores.

Occurrence in Tailings

The milling process is expected to result in oxidation and dissolution of the primary lead minerals present as sulphides and in dissolution of Pb present in uranium minerals. A secondary mineral phase would then form under the leach circuit conditions. In the high sulphate, low pH leach solution, the formation of anglesite ($PbSO_4$) is most probable. Small quantities could coprecipitate with gypsum. After neutralization, other phases such as cerrusite ($PbCO_3$) and $Pb_3(PO_4)_2$ could represent the concentration-limiting solids. A list of major primary and secondary sources of lead is given in Table 14.1. Other minerals are given in Table 4.11.

Reaction Pathways

A pathway diagram for lead is given in Figure A.5.

- Sulphides and Selenides

The residual sulphide and selenide minerals containing lead in the tailings would oxidize under kinetically-controlled conditions. Rates in the mill would be relatively high and those in the tailings would be considerably lower. The Pb(II) oxidation state would be most stable in solution.

Secondary Solids

The dissolution of primary lead minerals could result in the reprecipitation of other solids. Because of the high sulphate concentrations, $PbSO_4$ could be stable above pH

FIGURE A.5: PATHWAY DIAGRAM FOR LEAD

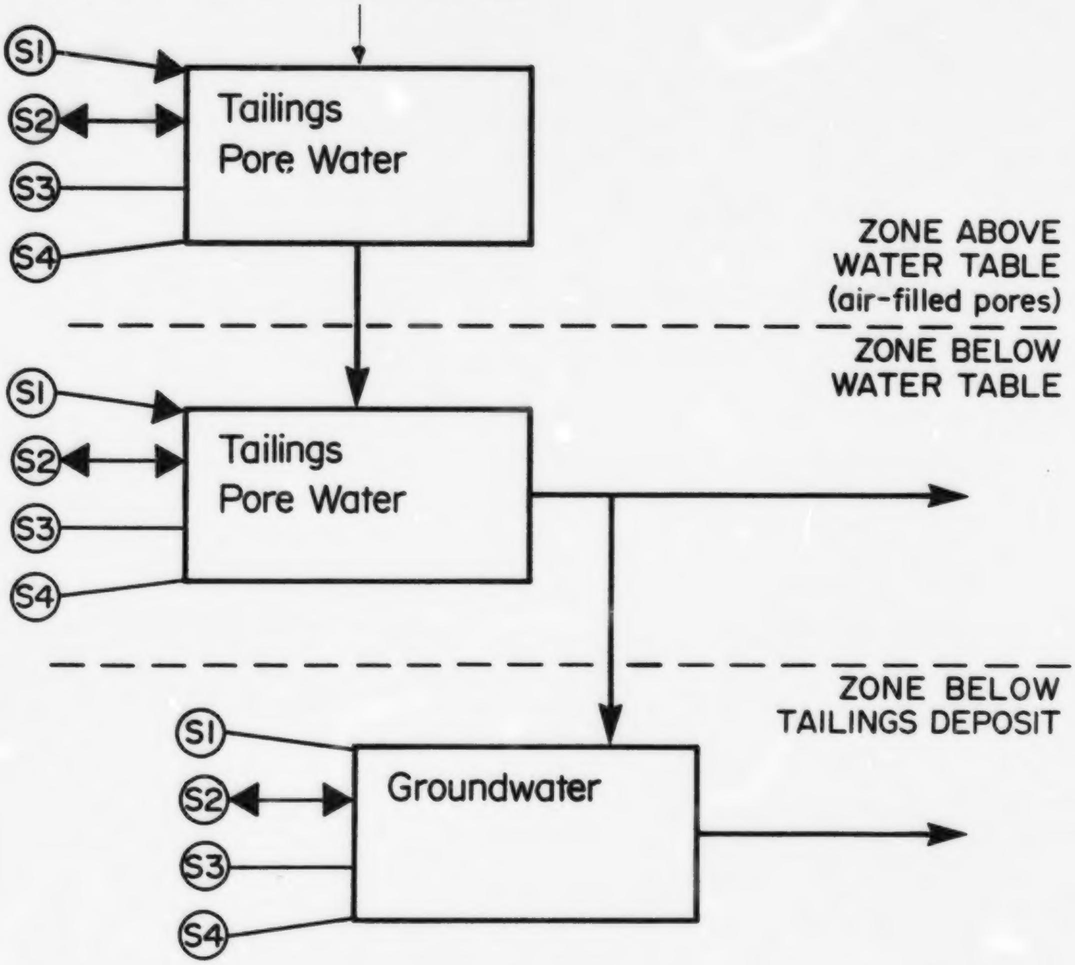
S1
S2
S3
S4
Tailings
Pore Water
ZONE ABOVE
WATER TABLE
(air-filled pores)
ZONE BELOW
WATER TABLE
S1
S2
S3
S4
Tailings
Pore Water
ZONE BELOW
TAILINGS DEPOSIT
S1
S2
S3
S4
Groundwater

PROCESS	SYMBOL
IRREVERSIBLE-KINETIC	⟶
REVERSIBLE-EQUILIBRIUM	⟷
COPRECIPITATION-EQUIL.	—⇌→
EXCHANGE-EQUIL.	←//→
ADSORPTION-KINETIC	—//→
SOLUTION FLUX	➞

SOLID	SYMBOL
Sulphides Selenides	S1
Oxides Sulphates Carbonates	S2
	S3
	S4

values of about 2. At higher pH levels, the carbonate ($PbCO_3$) and phosphate phases ($Pb_3(PO_4)_2$) could control the solubility of Pb, particularly in carbonate aquifers.

There has been little documented evidence to show the occurrence of these solids. If they do form, however, it is probable that equilibrium processes would dominate the precipitation and redissolution processes. In the tailings, these secondary minerals could redissolve during flushing by dilute rain water and snowmelt.

Surface Adsorption

The cationic nature of lead in solution (Pb^{2+}) suggests that it would be involved in cation exchange reactions. Exchange constants are not known. Adsorption isotherms on some solids have been determined.

Appendix A.6 Copper

Source

Copper is a trace constituent in the Elliot Lake ores but is more abundant in the high grade ores of Saskatchewan. Chalcopyrite is common to both types of deposits but the latter also contains bornite, covellite, chalcocite and copper selenides.

Occurrence in Tailings

Transformations through dissolution and oxidation are likely to occur in the mill leaching tank. The final products containing Cu in the tailings would then consist of oxides and possible carbonates. A list of major primary and secondary sources of copper is given in Table 14.1. Other minerals are given in Table 4.11.

Reaction Pathways

A pathway diagram for copper is given in Figure A.6.

FIGURE A.6: PATHWAY DIAGRAM FOR COPPER

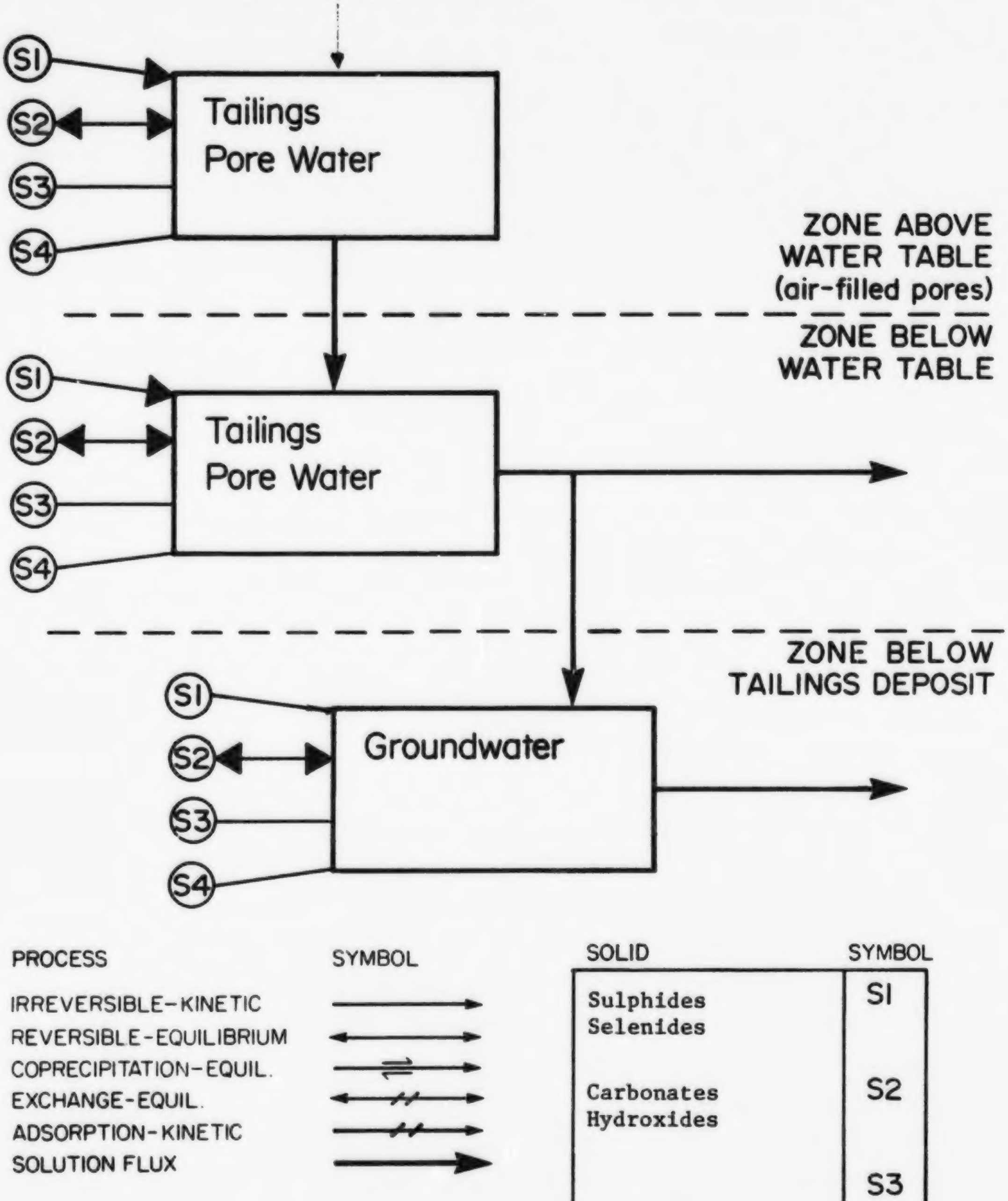
S1
S2
S3
S4
Tailings Pore Water
ZONE ABOVE WATER TABLE (air-filled pores)
ZONE BELOW WATER TABLE
S1
S2
S3
S4
Tailings Pore Water
ZONE BELOW TAILINGS DEPOSIT
S1
S2
S3
S4
Groundwater
PROCESS
SYMBOL
IRREVERSIBLE-KINETIC
REVERSIBLE-EQUILIBRIUM
COPRECIPITATION-EQUIL.
EXCHANGE-EQUIL.
ADSORPTION-KINETIC
SOLUTION FLUX

SOLID	SYMBOL
Sulphides Selenides	S1
Carbonates Hydroxides	S2
	S3
	S4

o Sulphides and Selenides

Significant oxidation of the copper sulphides will occur in the mill. Any residual primary sulphides will then be subject to oxidation and dissolution with the tailings. The copper would then be available for further transformation, such as precipitation as solid oxides or for mobilization in the tailings pore water. Kinetic reaction controls would dominate.

Secondary Solids

Oxides and possibly carbonates could be responsible for limiting copper concentrations in the tailings pore water. The dissolution and precipitation reactions would probably approach equilibrium conditions. Further study may be needed to determine whether such minerals occur in the tailings.

Surface Adsorption

As a divalent cation, Cu^{2+} in solution would be subject to cation exchange processes. Extensive work is available describing Cu adsorption onto various surfaces but such adsorption is not described as a cation exchange process.

Appendix A.7 Titanium

Sources

Primary minerals of concern in the uranium ores include ilmenite and brannerite. The first is an oxide containing iron, the second is an oxide containing uranium. Both are refractory (highly resistant to weathering) minerals that alter very little with time. The simple oxide, rutile is also refractory and may be present as well.

Occurrence in Tailings

Although not much is known with regard to transformations in Ti minerals, it is highly probable that the primary minerals remain essentially unaltered during the milling process. A list of primary and secondary sources of Ti is given in Table 14.1. Other minerals are given in Table 4.11.

Reaction Pathways

A pathway diagram for titanium is given in Figure A.7.

- Oxides

The dissolution of oxide solids appears to be controlled by kinetic factors. Titanium usually occurs in sub-milligram per litre concentrations in water and would presumably be transported through the tailings without considerable transformation.

Surface Adsorption

Cation exchange and adsorption processes may occur.

Appendix A.8 Barium

Sources

Primary sources of Ba in uranium ores consist of barite and as a substitution or impurity in calcium-rich and other minerals.

Occurrence in Tailings

Dissolution of barium that may occur in the mill leaching tanks results in precipitation of a significant portion of the Ba as a sulphate ($BaSO_4$). This solid and minerals containing residual Ba as an impurity represent the forms of this element in the tailings. A list of major primary and secondary minerals is given in Table 14.1. Other minerals are given in Table 4.11.

Reaction Pathways

A pathway diagram for barium is given in Figure A.8.

FIGURE A.7: PATHWAY DIAGRAM FOR TITANIUM

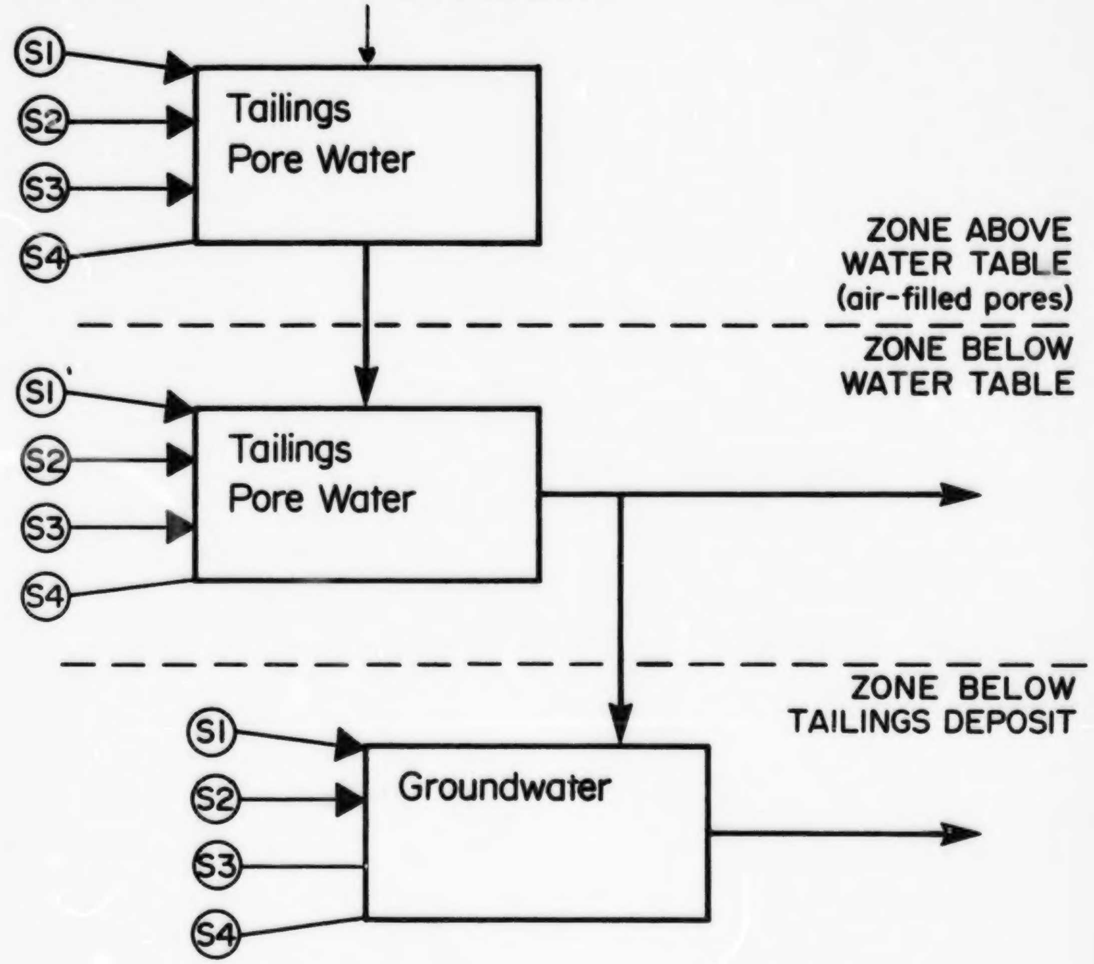
S1
S2
S3
S4
Tailings Pore Water
ZONE ABOVE WATER TABLE (air-filled pores)
ZONE BELOW WATER TABLE
S1
S2
S3
S4
Tailings Pore Water
ZONE BELOW TAILINGS DEPOSIT
S1
S2
S3
S4
Groundwater

PROCESS	SYMBOL
IRREVERSIBLE-KINETIC	$\longrightarrow$
REVERSIBLE-EQUILIBRIUM	$\longleftrightarrow$
COPRECIPITATION-EQUIL.	$\xrightarrow{\rightleftharpoons}$
EXCHANGE-EQUIL.	$\longleftrightarrow$ //
ADSORPTION-KINETIC	$\longrightarrow$ //
SOLUTION FLUX	➞

SOLID	SYMBOL
Ilmenite	S1
Rutile	S2
Branerite	S3
	S4

FIGURE A.8: PATHWAY DIAGRAM FOR BARIUM

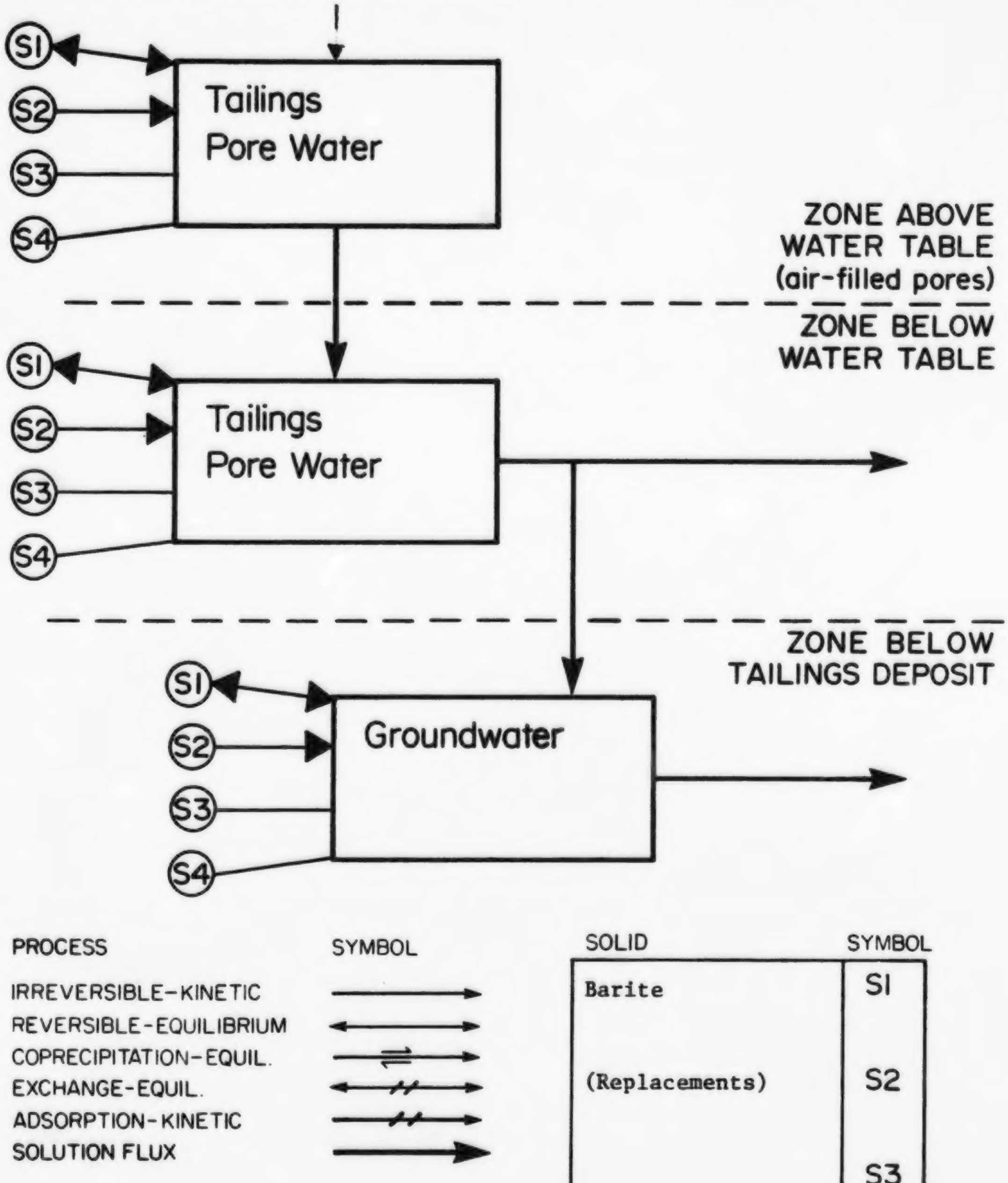
S1
S2
S3
S4
Tailings Pore Water
ZONE ABOVE WATER TABLE (air-filled pores)
ZONE BELOW WATER TABLE
Tailings Pore Water
ZONE BELOW TAILINGS DEPOSIT
Groundwater
PROCESS
SYMBOL
IRREVERSIBLE-KINETIC
REVERSIBLE-EQUILIBRIUM
COPRECIPITATION-EQUIL.
EXCHANGE-EQUIL.
ADSORPTION-KINETIC
SOLUTION FLUX

SOLID	SYMBOL
Barite	S1
(Replacements)	S2
	S3
	S4

- Sulphates

Dissolution of the barite would likely be controlled by equilibrium conditions. In this way, only small concentrations of Ba would be available in the pore water for transport through the tailings.

Although Ba constitutes a minor-to-trace component in the tailings, it may be important in coprecipitation of the dissolved Ra that occurs in much lower but potentially harmful concentrations.

Surface Adsorption

Ba occurs as a divalent cation and as such would be subject to cation exchange reactions. It's adsorbing characteristics have been extensively studied.

Appendix A.9 Selenium

Sources

Selenium is associated with the high-grade uranium deposits of Saskatchewan. Both lead and copper selenides have been identified in the ores.

Occurrence in Tailings

Presumably, the selenides react in a manner analogous to the sulphides and arsenides. It seems probable then that the primary minerals oxidize and dissolve to a significant degree in the mill leach circuit. There do not appear to be many candidates for secondary solid formation. If analogies to arsenic are made, ferric iron and barium may play a role in limiting selenium concentrations. The exact nature of such solids has not been documented. A list of major primary and secondary minerals is given in Table 14.1. Other minerals are given in Table 4.11.

Reaction Pathways

A pathway diagram for selenium is given in Figure A.9.

FIGURE A.9: PATHWAY DIAGRAM FOR SELENIUM

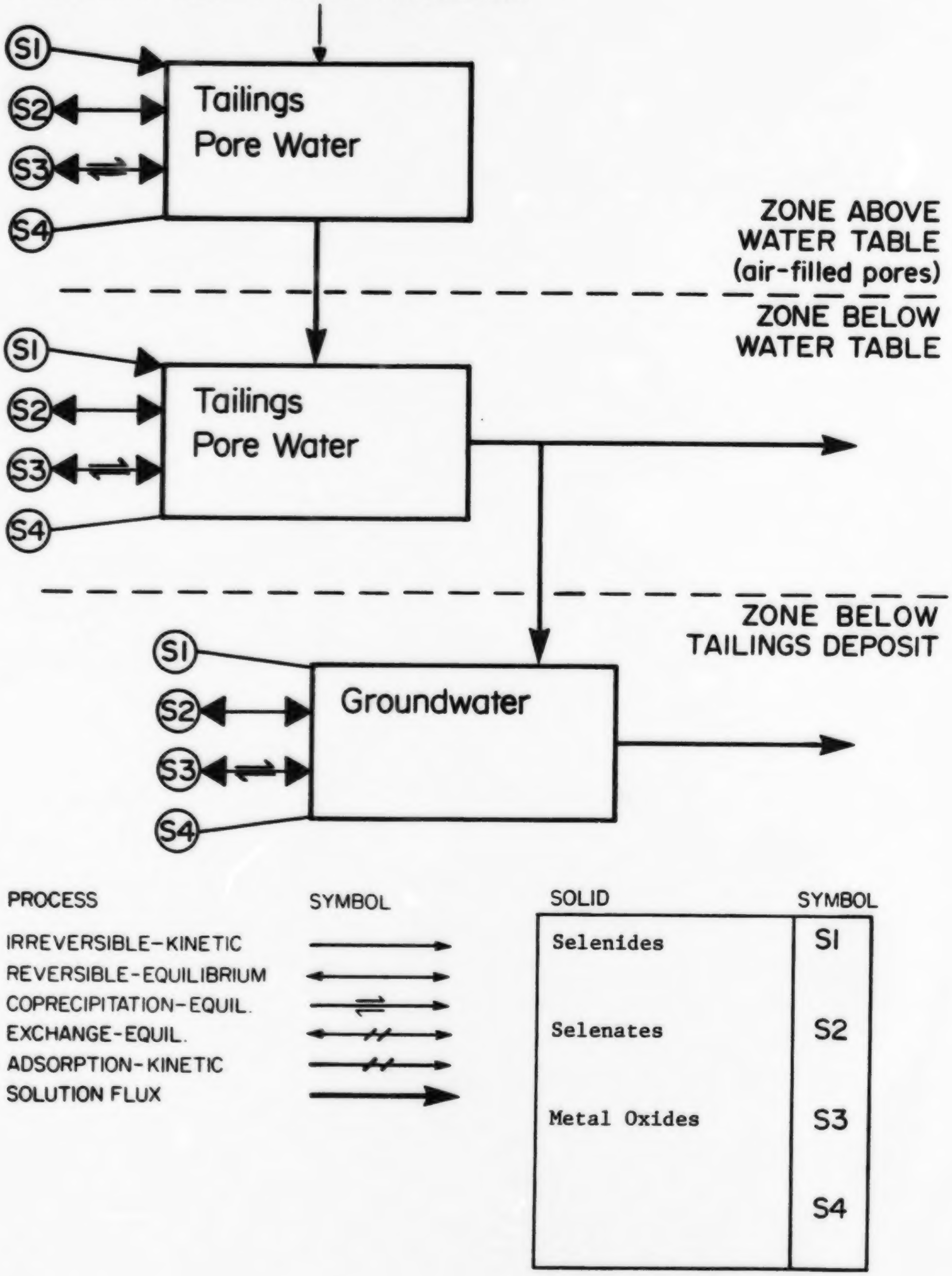
S1
S2
S3
S4
Tailings Pore Water
ZONE ABOVE WATER TABLE (air-filled pores)
ZONE BELOW WATER TABLE
S1
S2
S3
S4
Tailings Pore Water
ZONE BELOW TAILINGS DEPOSIT
S1
S2
S3
S4
Groundwater
PROCESS
SYMBOL
IRREVERSIBLE-KINETIC
REVERSIBLE-EQUILIBRIUM
COPRECIPITATION-EQUIL.
EXCHANGE-EQUIL.
ADSORPTION-KINETIC
SOLUTION FLUX
SOLID
SYMBOL
Selenides
S1
Selenates
S2
Metal Oxides
S3
S4

o Selenides

The residual selenides of lead and copper will be subjected to oxidation in the tailings deposits. Oxidation would result in mobilization of the Se in tailings pore water, either in the +IV or +VI oxidations states.

Secondary Solids

Depending on the pH and redox conditions, the formation of some metal salts may be favoured. Unfortunately, little information is available to know what solids would be involved.

Surface Adsorption

Selenium can occur as a neutral species or more often as an anion in solution. It is known that adsorption occurs on both hydrous metal oxides (Plotnikiv, 1964) and clays (Frost and Griffin, 1977) with the former being more significant. Because of the potential to form species representing two oxidation states as well as the pH dependence, prediction of adsorption behaviour would be difficult.

APPENDIX B

CHEMICAL MODELLING IN THE URANIUM TAILINGS SYSTEM: PYRITE DISSOLUTION

C-8206.195.4

CHEMICAL MODELLING IN THE URANIUM TAILINGS SYSTEM. PYRITE DISSOLUTION

Nava C. Garisto, Robert J. Lemire and Frank Garisto
Atomic Energy of Canada Limited
Research Company
Whiteshell Nuclear Research Establishment
Pinawa, Manitoba
ROE 1LO

1985 March

CONTENTS

		Page
INTRODUCTION		1
SECTION I:	REACTION PATH CALCULATIONS FOR PYRITIC TAILINGS	2
SECTION II:	THE THERMODYNAMIC DATABASE	4
SECTION III:	RESULTS AND DISCUSSION	8
SECTION IV:	SUMMARY	17
REFERENCES		18
FIGURES		21
APPENDIX A		

INTRODUCTION

This report presents the results of a chemical modelling project done for IEC Beak Consultants Limited during the period 1985 February to March. The objective of the study was to carry out modelling work in support of laboratory and field data collected by IEC Beak Consultants Limited for the development of a compartmental model of pyritic tailings associated with uranium mill tailings. The present work is an extension of the preliminary study presented in reference [1].

Section I in the present report explains the application of reaction path calculations to the study of pyritic tailings.

Section II describes the thermodynamic data on which the calculations are based.

Section III describes and discusses the results of a series of reaction path calculations, taking into account increasingly complex components of the pyritic tailings system.

Section IV contains a summary of this work.

SECTION I: REACTION PATH CALCULATIONS FOR PYRITIC TAILINGS

When FeS_2 (pyrite) is initially put in contact with an oxidizing solution, the FeS_2-solution system is not in equilibrium and FeS_2 undergoes irreversible oxidative dissolution. As more and more oxidant is added to the solution, FeS_2 is progressively destroyed and other solids may form. The reaction path calculations attempt to simulate this process using thermodynamics.

In a reaction path simulation, FeS_2 is placed in contact with the solution at time t=0. Other solids present in the system (e.g. $CaSO_4 \cdot 2H_2O$, $Fe(OH)_3$, $Al(OH)_3$) may be added at this time as well. Products of the dissolution process are then studied as a function of the reaction coordinate ξ ($\xi=0$ at t=0) defined as the number of moles of oxidant consumed per kilogram of water [2-6]. That is, at each value of ξ, an equilibrium calculation is performed for the solids of interest in 1 kilogram of water and ξ moles of oxidant. All the chemical species of interest are included in these equilibrium calculations and the chemical speciation is determined for both aqueous and solid phases. Effectively, the reaction path calculation can be regarded as a titration of the FeS_2-solution system with an oxidant. The oxidants used in the calculations described below are dissolved oxygen $O_2(aq)$, and an oxidizing solution made up of $\Sigma Fe + 2SO_4^{2-} + H^+$, where ΣFe denotes total iron with $[Fe^{3+}]/[Fe^{2+}] = 10^4$ (see Section III for details).

It should be emphasized that the reaction path calculations presented below simulate reactions in a closed system, in the sense that solids that precipitate are available for dissolution as the reaction progresses (ξ increases). However, the system is open to an external source of oxidant.

The calculations have been carried out with the CHEMical reaction Path program CHEMP [6]. CHEMP can be used for reaction path calculations in two modes:

(i) a predetermined constant pH mode and

(ii) a floating pH mode, where the pH is controlled by the reactions in the system.

The calculations presented in this report were all done using the floating pH mode.

SECTION II: THE THERMODYNAMIC DATABASE

Except for the species discussed below, all Gibbs energies were taken as identical to those reported previously [1]. For the convenience of the reader, the database assessment from reference [1] is given in Appendix A.

The selected value of $\Delta_f G^o$ ($Al(OH)_3(s)$, gibbsite) = -1154.9 kJ·mol^{-1} was taken from Hemmingway et al. [7]. The values for the Gibbs energies of formation of aqueous aluminum species were then based on this gibbsite value. Hemmingway and Robie [8] and Sadiq and Lindsay [9] used similar gibbsite solubility data determined independently by Kittrick [10] and Singh [11] to determine $\Delta_f\bar{G}^o(Al^{3+}) = -489.4$ kJ·mol^{-1}, respectively. However, more recent work by Bloom and Weaver [12], May et al. [13] and Couturier et al. [14] have given data indicating a more positive value for the Gibbs energy of this aqueous species can be justified.

May et al. [13] determined the solubility of gibbsite as a function of pH. Their data below pH 6.7 is in good agreement with earlier studies [10,11]. Near pH 6.7 there is a distinct break in the solubility curve, and the reported solubilities above pH 6.7 are lower than would be expected by extrapolation of the low pH data. May et al. [13] attributed this to conversion of the gibbsite to a more stable solid, perhaps boemite. Bloom and Weaver [12] and Couturier et al. [14] correctly pointed out that it is more likely the results in basic solution reflect the true solubility of gibbsite, while the high results below pH 6.7 reflect the higher solubility of less crystalline material. Bloom and Weaver [12] showed that solubility measurements using commercially prepared gibbsite, pretreated with an acid solution, gave a value of $K_{so} = 7.55$ for the reaction

$$Al(OH)_3 + 3H^+ = Al^{3+} + 3H_2O \quad . \qquad \text{(II-1)}$$

Combining this with the CODATA [15] value of $\Delta_f G^o(H_2O)$, and the value $\Delta_f G^o$ (gibbsite) selected above, gave $\Delta_f\bar{G}^o(Al^{3+}) = -486.4$ kJ·mol^{-1}.

May et al. [13] reported an average value of 2.38×10^{-15} for the equilibrium constant for the reaction of the stable solid in basic solutions (assumed by us to be gibbsite) to form $Al(OH)_4^-$

$$Al(OH)_3 + H_2O = Al(OH)_4^- + H^+ \quad . \tag{II-2}$$

From this a value of $\Delta_f\bar{G}^o(Al(OH)_4^-) = -1308.6$ kJ·mol^{-1} was calculated. The difference, $\Delta_f\bar{G}^o(Al(OH)_4^-) - \Delta_f\bar{G}^o(Al^{3+}) = -822.2$ kJ·mol^{-1}, compares well with a value of -822.0 kJ·mol^{-1} calculated from the data of Couturier et al. [14] using $\log_{10} K = -22.20$ for the reaction

$$Al^{3+} + 4H_2O = Al(OH)_4^- + 4H^+ \quad . \tag{II-3}$$

A value of $\Delta_f\bar{G}^o(AlOH^{2+}) = -695.1$ kJ·mol^{-1} was calculated from $\log_{10} K = -5.00$ [14] for

$$Al^{3+} + H_2O = AlOH^{2+} + H^+ \tag{II-4}$$

and our value for $\Delta_f\bar{G}^o(Al^{3+})$.

Because it was based on solubility measurements using the same solid, the ratio of the equilibrium constants for reactions (II-5) and (II-6)

$$Al(OH)_3(s) + H^+ = Al(OH)_2^+ + H_2O \tag{II-5}$$

$$Al(OH)_3(s) + 2H^+ = AlOH^{2+} + 2H_2O \tag{II-6}$$

in the work of May et al. [13] was assumed to be correct. Therefore, using our value for $\Delta_f\bar{G}^o(AlOH^{2+})$, the value $\Delta_f\bar{G}^o(Al(OH)_2^+) = -902.9$ kJ·mol^{-1} was calculated. Both May et al. [13] and Couturier et al. [14] considered the neutral aqueous species $Al(OH)_3$ to be unimportant, and it has been omitted in the present database. Polymeric aluminum hydrolysis species [16] have also been neglected as they are unlikely to be important under geological conditions.

Literature data for bayerite are sparse. Both Hemmingway and Robie [8] and Sadiq and Lindsay [17] relied on the work of Russell et al. [18] who reported $\log_{10} K = -13.84$, -13.95 and -14.82 for

$$\text{bayerite} + H_2O = Al(OH)_4^- + H^+ \quad . \qquad \text{(II-7)}$$

With our value for $Al(OH)_4^-$ these gave $\Delta_f G^o(Al(OH)_3, \text{bayerite}) =$ -1150, -1151 and -1156 $kJ \cdot mol^{-1}$ respectively. We have selected $\Delta_f G^o(Al(OH)_3, \text{bayerite}) = -1155.$ $kJ \cdot mol^{-1}$ (i.e., equal to the value for gibbsite within the error limits of the experiments).

The solubility product of amorphous $Al(OH)_3$ has been reported by many groups [16]. The values obtained, of course, vary with the particular sample used. The value chosen by Sadiq and Lindsay [17], supposedly based on work by Kittrick [19], is traceable to early enthalpy of solution measurements [20] and an estimated value for the entropy [21]. We have followed Naumov et al. [22] in using $pK = 22.28$ for

$$Al(OH)_3 \text{ (amorphous)} = Al(OH)^{2+} + 2OH^- \qquad \text{(II-8)}$$

from Goto [23]. This gave $\Delta_f G^o(Al(OH)_3, \text{amorphous}) = -1137$ $kJ \cdot mol^{-1}$.

The values of the association constants of Al^{3+} with SO_4^{2-}, $\log_{10} K_1 = 3.01$ and $\log_{10} K_2 = 1.89$, were taken from Izatt et al. [24]. Calculations using our value for $\Delta_f \bar{G}^o(Al^{3+})$ gave $\Delta_f \bar{G}^o(AlSO_4^+) = -1248.1$ $kJ \cdot mol^{-1}$ and $\Delta_f \bar{G}^o(Al(SO_4)_2^-) = -2003.4$ $kJ \cdot mol^{-1}$.

An estimate of $\Delta_f G^o$ (jarosite) $= -3297$ $kJ \cdot mol^{-1}$ was made by reanalysis of the data of Kashkay et al. [25] using consistent values for the relevant iron equilibria [1] and the CODATA value for $\Delta_f \bar{G}^o(K^+, aq)$. It should be noted that the value for jarosite differs by several $kJ \cdot mol^{-1}$ from the value originally calculated [25], and the overall uncertainty in the value for this mineral is quite large.

The additions to the database are summarized in Table I. For all other species we used the Gibbs energies documented in Appendix A.

TABLE I: SPECIES ADDED TO THE DATABASE*

Species	$\Delta_f G^o/(kJ \cdot mol^{-1})$
$Al(OH)_3$ (gibbsite)	-1154.9
$Al(OH)_3$ (amorphous)	-1137.
Al^{3+}	-486.4
$AlOH^{2+}$	-695.1
$Al(OH)_2^+$	-902.9
$Al(OH)_4^-$	-1308.6
$AlSO_4^+$	-1248.1
$Al(SO_4)_2^-$	-2003.4
$Al(OH)_3$ (bayerite)	-1155.
K^+	-282.47
$KFe_3(SO_4)_2(OH)_6$ (jarosite)	-3297.

* Data for other species used are given in Appendix A.

SECTION III: RESULTS AND DISCUSSION

The initial conditions for the different cases studied using reaction path calculations are summarized in Table II. These conditions (cases 1A.1, 1B.1, etc.) were chosen to correspond with those requested by IEC Beak [26] (cases 1A, 1B, etc.). For each case, the initial amounts of solids in the system (i.e., FeS_2 (pyrite), $Fe(OH)_3$ (amorphous), $CaSO_4 \cdot 2H_2O$ (gypsum), $Al(OH)_3$ (gibbsite) and $CaCO_3$ (calcite)) are listed in moles*.

Gibbsite was used in the calculations to represent $Al(OH)_3(s)$. The Gibbs energy of formation of bayerite has an uncertainty of several $kJ \cdot mol^{-1}$, and is equal to the value for gibbsite within the uncertainty of the individual $\Delta_f G^o$ values. Elemental sulfur and mixed aluminum-sulfate solids (e.g. $Al_4SO_4(OH)_{10} \cdot 5H_2O$) were not included in the calculations.

Activity corrections were neglected in the present calculations. All the aqueous concentrations are reported in $mol \cdot kg^{-1}$ and all the solid abundances are in moles. The calculations were done using a floating pH mode, for 298.15 K and an initial potassium ion concentration equal to 1.50×10^{-3} $mol \cdot kg^{-1}$. For reaction (III-1), the conversion of hydronium jarosite to jarosite,

$$K^+ + (H_3O)Fe_3(SO_4)_2(OH)_6 = H^+ + H_2O + KFe_3(SO_4)_2(OH)_6, \qquad \text{(III-1)}$$

$\Delta_R G = -23.7$ $kJ \cdot mol^{-1}$. For solutions with a potassium ion concentration equal to that selected for these calculations, hydronium jarosite can only be formed if the hydrogen ion activity (molal scale) is unrealistically high (> 20). Hence, hydronium jarosite was not found as an equilibrium solid for any of the cases described here.

---

* The liquid to solid ratio in the system is approximately 0.25.

TABLE II: THE REACTION PATH RUNS*

Case number	FeS_2 (pyrite)	$Fe(OH)_3$ (amorphous)	$CaSO_4 \cdot 2H_2O$ (gypsum)	$Al(OH)_3$ (gibbsite)	$CaCO_3(s)$ (calcite)	Titrant
1A.1	1.668	1.22	2.22	-	-	$O_2(aq)$
1A.2	1.668	-	2.22	-	-	$O_2(aq)$
1B.1	1.668	1.22	2.22	-	-	$\Sigma Fe+2SO_4^{2-}+H^+$
1B.2	-	1.22	2.22	-	-	$\Sigma Fe+2SO_4^{2-}+H^+$
1C.1	0.1192	1.22	2.22	-	-	$\Sigma Fe+2SO_4^{2-}+H^+$
2A.1	1.668	1.22	2.22	0.816	-	$O_2(aq)$
2A.2	1.668	-	2.22	0.816	-	$O_2(aq)$
3A.1	1.668	1.22	2.22	-	0.08	$O_2(aq)$
4A.1	1.668	1.22	2.22	0.816	0.08	$O_2(aq)$
4B.1	-	1.22	2.22	0.816	0.08	$\Sigma Fe+2SO_4^{2-}+H^+$
4C.1	0.1192	1.22	2.22	0.816	0.08	$\Sigma Fe+2SO_4^{2-}+H^+$

* In addition to the listed solids (amounts given in moles) the systems also contain 1 kilogram of water and 1.50×10^{-3} $mol \cdot kg^{-1}$ K^+.

The results of the calculations are presented in Figures 1-33. These figures show the changes in H^+ concentration, solid abundances and Fe^{2+}, Fe^{3+} concentrations along the reaction path for the various cases.

Cases 1A.1 and 1A.2

Case 1A.1 is our Reference Case. In this case, the system initially contains pyrite, amorphous $Fe(OH)_3$ and gypsum (see Table II). The reaction of this system with $O_2(aq)$ is described in Figures 1-3, which show the H^+ concentration, the abundances of solids in the system and changes in the concentrations of Fe^{3+} and Fe^{2+}, respectively, as a function of the reaction coordinate (i.e., the number of moles $O_2(aq)$ consumed in the reaction).

The amorphous $Fe(OH)_3$ converts to goethite according to equation III-2:

$$Fe(OH)_3 = FeOOH + H_2O \qquad \Delta_R G = -27.3\ kJ \cdot mol^{-1} \qquad \text{(III-2)}$$

The Gibbs energy of this reaction, $\Delta_R G$ (III-2), is always negative and, hence, goethite (and not $Fe(OH)_3$) is observed along the reaction path for all cases treated in this report.

The pH decreases from pH = 5 to pH = 1 following pyrite dissolution (Figures 1,2). The pyrite dissolution is accompanied by goethite dissolution and by precipitation of $FeSO_4 \cdot 7H_2O$ in a limited region of the reaction path.

It is possible to rationalize the results of the reaction path calculations (which were carried out using the complete set of reactions representing the system FeS_2-$CaSO_4.2H_2O$-$Fe(OH)_3$-$KFe_3(SO_4)_2(OH)_6$-H_2O) using several key reactions. In particular, the oxidative dissolution of pyrite and the pH buffering by goethite are easily explained.

The oxidative dissolution of pyrite can be explained in terms of two reactions: (i) reaction of pyrite with $O_2(aq)$:

$$FeS_2 + 7/2\ O_2(aq) + H_2O = Fe^{2+} + 2\ SO_4^{2-} + 2\ H^+ \qquad \text{(III-3)}$$

where each mole of $O_2(aq)$ consumes only 2/7 moles of pyrite and produces 4/7 moles of H^+; and (ii) reaction of pyrite with goethite:

$$FeS_2 + 14\ FeOOH + 26\ H^+ = 15\ Fe^{2+} + 2\ SO_4^{2-} + 20\ H_2O \qquad \text{(III-4)}$$

$$\Delta_R G\ (\text{III-4}) = -562.57\ \text{kJ}\cdot\text{mol}^{-1}.$$

Since $\Delta_R G$ (III-4) is very large and negative, each mole of H^+ produced by the pyrite oxidation (equation III-3), will be consumed in the reaction of pyrite with goethite (equation III-4). Each mole of H^+ (produced in reaction III-3) consumes 1/26 moles of pyrite and 14/26 moles of goethite. Therefore, the overall effect of one mole of $O_2(aq)$ is as follows:

$$[(2/7) + (4/7)(1/26)] = 4/13 \text{ moles pyrite consumed, and}$$

$$(4/7)(14/26) = 4/13 \text{ moles goethite consumed.}$$

In order to consume all the goethite (1.22 moles), we need to add approximately 3.965 moles of $O_2(aq)$. Once all the goethite is consumed, each additional mole of $O_2(aq)$ consumes only 2/7 moles of pyrite (see equation III-3) and not 4/13 moles of pyrite.

After dissolution of the goethite, the H^+ concentration increases dramatically (see Figures 1 and 2) since the H^+ produced in pyrite dissolution is no longer removed from the system, except for its reaction with sulfate: $H^+ + SO_4^{2-} = HSO_4^-$. After consumption of goethite is complete, the sum of the amounts of HSO_4^- and H^+ in solution are approximately equal to the number of moles of H^+ formed by reaction III-3.

The effect of goethite on the pH of the system is shown by comparison of cases 1A.1 and 1A.2. In case 1A.2 $Fe(OH)_3$ (amorphous) was not included as one of the initial solids present (see Figures 4-6) and the pH along the path is indeed much lower than that observed in case 1A.1.

Continuation of the reaction path calculation beyond the point where all the pyrite is consumed (see Figure 2) shows that the added $O_2(aq)$ oxidizes $FeSO_4 \cdot 7H_2O$ to form goethite (which reappears in the system at high reaction coordinates) and jarosite, and the concentrations of oxidized iron species in solution increases significantly (see for example Figure 3). The increase in the $[Fe^{3+}]/[Fe^{2+}]$ ratio indicates an increase in the redox potential E (volts) where:

$$E = -0.05916 \log_{10} \left[9.28 \times 10^{-14} \frac{[Fe^{2+}]}{[Fe^{3+}]} \right] \quad . \qquad \text{(III-5)}$$

The formation of jarosite can be explained in terms of the following reactions:

(i) in the presence of goethite:

$$K^+ + 3\ FeOOH + 2\ SO_4^{2-} + 3\ H^+ = KFe_3(SO_4)_2(OH)_6 \qquad \text{(III-6)}$$

(ii) in the absence of goethite:

$$K^+ + 3\ Fe^{3+} + 2\ SO_4^{2-} + 6\ H_2O = KFe_3(SO_4)_2(OH)_6 + 6\ H^+ \quad . \qquad \text{(III-7)}$$

From reaction III-6

$$\Delta_R G\ \text{(III-6)}\ [kJ \cdot mol^{-1}] = -51.6 + 17.124\ pH - 11.416 \log_{10}[SO_4^{2-}] - 5.708 \log_{10}[K^+]. \qquad \text{(III-8)}$$

The condition for jarosite formation via reaction III-6 is $\Delta_R G$ (III-6) < 0. For $[K^+] = 1.50 \times 10^{-3}\ \mathrm{mol \cdot kg^{-1}}$ this condition is:

$$\log_{10}[SO_4^{2-}] > 1.5\ pH - 3.1_0 \qquad \text{(III-9)}$$

i.e., low pH values and sufficiently high sulfate concentrations favour the formation of jarosite.

From reaction III-7

$$\begin{aligned} \Delta_R G\ (\text{III-7})\ [\mathrm{kJ \cdot mol^{-1}}] &= -51.9 - 34.248\ pH \qquad \text{(III-10)} \\ &\quad - 17.124 \log_{10}[Fe^{3+}] \\ &\quad - 11.416 \log_{10}[SO_4^{2-}] \\ &\quad - 5.708 \log_{10}[K^+] \quad . \end{aligned}$$

For $[K^+] = 1.50 \times 10^{-3}\ \mathrm{mol \cdot kg^{-1}}$ the condition $\Delta_R G$ (III-7) < 0 implies:

$$\log_{10}[SO_4^{2-}] > -1.5 \log_{10}[Fe^{3+}] - 3pH - 3.1_4 \qquad \text{(III-11)}$$

For example,

(i) if $[SO_4^{2-}] = 10^{-5}\ \mathrm{mol \cdot kg^{-1}}$, then $\Delta_R G$ (III-7) < 0 implies:

$$\log_{10}[Fe^{3+}] > 1.24 - 2\ pH \qquad \text{(III-12)}$$

(ii) if $[SO_4^{2-}] = 10^{-3}\ \mathrm{mol \cdot kg^{-1}}$, then $\Delta_R G$ (III-7) < 0 implies:

$$\log_{10}[Fe^{3+}] > -0.09 - 2\ pH \qquad \text{(III-13)}$$

(iii) if $[SO_4^{2-}] = 10^{-1}\ \mathrm{mol \cdot kg^{-1}}$, then $\Delta_R G$ (III-7) < 0 implies:

$$\log_{10} [Fe^{3+}] > -1.423 - 2\ pH. \qquad \text{(III-14)}$$

At a given total iron concentration, the formation of jarosite is favoured by a high concentration of Fe^{3+} and hence by a high redox potential (see equation III-5).

Cases 1B.1 and 1C.1

In cases 1B.1 and 1C.1 (see Table II) the system is titrated with $\Sigma Fe + 2\ SO_4^{2-} + H^+$ and the oxidizing agent is the ferric ion. The ratios of species in this oxidizing mixture are:

$$[Fe^{3+}] : [Fe^{2+}] : [SO_4^{2-}] : [H^+] = 1.0 : 1.0 \times 10^{-4} : 2.0 : 1.0\ .$$

In case 1C.1, the amount of FeS_2 is 1/14 of that used in case 1A.1 [26].

In case 1B.1 (see Figures 7-9) and 1C.1 (see Figures 13-15) the pyrite and goethite are gradually dissolved and $FeSO_4 \cdot 7H_2O$ is formed. The $FeSO_4 \cdot 7H_2O$ does not dissolve towards the end of the reaction path (unlike its behavior in the Reference Case 1A.1) since it cannot be oxidized by the oxidant, Fe^{3+}.

The dissolution of FeS_2 and FeOOH with the titrant $\Sigma Fe + 2\ SO_4^2 + H^+$ can be described in terms of the two reactions:

$$FeS_2 + 8\ H_2O + 14\ Fe^{3+} = 15\ Fe^{2+} + 2\ SO_4^{2-} + 16\ H^+ \qquad \text{(III-15)}$$

and

$$FeS_2 + 14\ FeOOH + 26\ H^+ = 15\ Fe^{2+} + 2\ SO_4^{2-} + 20\ H_2O \qquad \text{(III-4)}$$

The direct reaction of FeS_2 with the oxidant Fe^{3+} (reaction III-15), should be compared to reaction III-3

$$FeS_2 + 7/2\ O_2(aq) + H_2O = Fe^{2+} + 2\ SO_4^{2-} + 2\ H^+ \quad . \qquad \text{(III-3)}$$

The stoichiometry of these two reactions shows that, in the absence of goethite, the effect of 4 moles (i.e., 14 x 2/7 moles) of Fe^{3+} would be equivalent to the effect of 1 mole of $O_2(aq)$. However, this is not true in the presence of goethite since the oxidation of FeS_2 also occurs via reaction III-3, which proceeds until the H^+ produced in reactions III-3 or III-15 is consumed. An explicit calculation shows that, in the presence of goethite, 1 mole of Fe^{3+} would consume 3/26 moles of pyrite and 16/26 moles of goethite. (This should be compared with the effect of $O_2(aq)$: 1 mole of $O_2(aq)$ consumes 4/13 moles of pyrite and 4/13 moles of goethite). Note that the titrant ($\Sigma Fe + 2\ SO_4^{2-} + H^+$) contains H^+ in addition to Fe^{3+}. This H^+ will also contribute to the dissolution of pyrite and of goethite and must therefore be considered in explaining the reaction path calculation: 1 mole of Fe^{3+} plus 1 mole of H^+ (in the titrant) consume 3/26 + 1/26 i.e., 4/26 moles of pyrite and 16/26 + 14/26, i.e., 30/26 moles of goethite as long as goethite is present in the system.

Case 1B.2

Pyrite is not present in case 1B.2 (see Table II, Figures 10-12). In this case goethite gradually dissolves because the titrant is acidic. The major iron species forming in solution are $FeSO_4^+$ and $Fe(SO_4)_2^-$.

Cases 2A.1 and 2A.2

Cases 2A.1 and 2A.2 (Figures 16-21) show the effect of gibbsite on the system.

The results of case 2A.1 are similar to those of the Reference Case 1A.1. In case 2A.1 (as well as in case 2A.2) some jarosite forms but its maximum abundance is only 0.95 x 10^{-3} moles, and it, therefore, does not appear in the figures. The abundance of jarosite is lower here than in case 1A.1 because aluminum complexes sulfate to form $Al(SO_4)_2^-$ and $AlSO_4^+$ so that less SO_4^{2-} is available for jarosite formation (see equations III-8 - III-14).

In case 2A.2, $Fe(OH)_3$ (amorphous) is not included in the calculation and the calculated pH in the beginning of the reaction path is lower than that in case 2A.1 (which contains both $Fe(OH)_3$ and gibbsite) but higher than that in case 1A.2 (which contains neither $Fe(OH)_3$ nor gibbsite). The difference in the pH behavior between cases 1A.2 and 2A.2 can be attributed to the contribution of the buffering capacity of gibbsite.

Case 3A.1

In this case (see Figures 22-24) the initial pH is higher than that calculated in the Reference Case 1A.1 due to the presence of calcite. The calcite is converted to siderite as pyrite and goethite dissolve. Siderite is present in the system as long as goethite is also present. Once the goethite is completely dissolved, the pH drops and siderite is dissolved.

Cases 4A.1 - 4C.1

These cases show the combined effect of calcite and gibbsite on the system (see Figures 25-33). In cases 4A.1 and 4C.1 the major effects are the formation of siderite and the higher pH values observed when calcite is one of the added solids as compared to cases calculated in the absence of calcite (e.g., as seen in the comparison of cases 4A.1 and 2A.1).

Case 4B.1 can be explained in terms of a simple titration with H^+ rather than in terms of a redox reaction. The initial components of the system are already oxidized and the H^+ in the titrant ($\Sigma Fe + 2\ SO_4^{2-} + H^+$) dissolves the calcite, gibbsite and goethite.

SECTION IV: SUMMARY

A preliminary thermodynamic database for the system FeS_2-$CaCO_3$-$CaSO_4$-$Al(OH)_3$-H_2O at 298.15 K was compiled, evaluated and documented. This database was used in thermodynamic reaction path calculations simulating the oxidative dissolution of pyrite by dissolved oxygen or by ferric ions, in the presence of gypsum and ferric hydroxide. The effect of gibbsite and calcite presence on the reaction was studied and the effectiveness of dissolved oxygen and of ferric ions is carrying out the oxidative dissolution of pyrite was compared.

REFERENCES

[1] Garisto, N.C., Lemire, R.J., Fleer, V.N. and Garisto, F., "Chemical modelling of mineral dissolution in the uranium tailings system." Unpublished report (to IEC Beak Consultants Limited) C-8206.195.3, October 1984.

[2] Helgeson, H.C., Garrels, R.M. and MacKenzie, F.T. "Evaluation of irreversible reactions in geochemical processes involving minerals and aqueous solutions-II. Applications." Geochim. Cosmochim. Acta 33, 455 (1969).

[3] Wolery, T.J. "Calculations of chemical equilibrium between aqueous solution and minerals: The EQ3/6 software package." National Technical Information Service UCRL-52658 (1979).

[4] Reed, M.H. "Calculation of multicomponent chemical equilibria and reaction processes in systems involving minerals, gases and an aqueous phase." Geochim. Cosmochim. Acta 46, 513 (1982).

[5] Plummer, L.N., Parkhurst, D.L. and Thorstenson D.C. "Development of reaction models for ground-water systems." Geochim. Cosmochim. Acta 47, 665, (1983).

[6] Garisto, N.C. and Garisto, F. "Reaction path calculations of mineral alteration products: application to nuclear fuel waste management." Nucl. Chem. Waste Management 5, 17 (1984).

[7] Hemmingway, B.S., Robie, R.A., and Kittrick, J.A. "Revised values for the Gibbs free energy of formation of [$Al(OH)_4^-(aq)$], diaspore, boemite and bayerite at 298.15 K and 1 bar, the thermodynamic properties of kaolinite to 800 K and 1 bar, and the heats of solution of several gibbsite samples." Geochim. Cosmochim. Acta. 42, 1533 (1978).

[8] Hemmingway, B.S. and Robie, R.A. "The entropy and Gibbs free energy of formation of the aluminum ion." Geochim. Cosmochim. Acta. 41, 1402 (1977).

[9] Sadiq, M. and Lindsay, W.L. "Standard free energy of formation of some chemical species: discrepancies and selections." Arab. J. Sci. Eng. 6, 95 (1981).

[10] Kittrick, J.A. "The free energies of formation of gibbsite and $Al(OH)_4^-$ from solubility measurements." Soil Sci. Soc. Am. Proc. 30, 595 (1966).

[11] Singh, S.S. "The solubility product of gibbsite at 15°, 25° and 35°C." Soil Sci. Soc. Am. Proc. 38, 415 (1974).

[12] Bloom, P.R. and Weaver, R.M. "Effect on removal of reactive surface material on the solubility of synthetic gibbsite." Clays and Clay Min. 30, 281 (1982).

[13] May, H.M., Helmke, P.A. and Jackson, M.L. "Gibbsite solubility and thermodynamic properties of hydroxy-aluminum ions in aqueous solution at 25°C." Geochim. Cosmochim. Acta. 43, 861 (1979).

[14] Couturier, Y., Michard, G. and Sarazin, G. "Constantes de formation des complexes hydroxydés de l'aluminium en solution aqueuse de 20 a 70°C." Geochim. Cosmochim. Acta. 48, 649 (1984).

[15] CODATA Task Group. "CODATA recommended key values for thermodynamics, 1977." J. Chem. Thermodynam. 10, 903 (1978).

[16] Baes, Jr., C.F. and Mesmer, R.E. "The hydrolysis of cations." John Wiley & Sons, New York, 1976. Chapter 6.

[17] Sadiq, M. and Lindsay, W.L. "Selection of standard free energies of formation for use in soil chemistry." Colorado State University Experiment Station Technical Bulletin 134 (1979).

[18] Russell, A.S., Edward, J.D. and Taylor, C.S. "Solubility and density of hydrated aluminas in NaOH solutions." Trans. Am. Inst. Min. Met. Eng. 203, 1123 (1955).

[19] Kittrick, J.A. "Soil minerals in Al_2O_3-SiO_2-H_2O system and theory of their formation." Clay Mineral. 17, 157 (1969).

[20] Rossini, F.D., Wagman, D.D., Evans, W.H., Levine, S. and Jaffe, I. "Selected values of chemical thermodynamic properties, Parts I and II." U.S. National Bureau of Standards Circular 500, Washington, 1952.

[21] Latimer, W.M., "Oxidation potentials." 2nd edn., Prentice-Hall Inc., Englewood Cliffs, NJ, 1952.

[22] Naumov, G.B., Ryzhenko, B.N. and Khodakovsky, I.L., "Handbook of thermodynamic data." Atomizdat, Moscow, 1971, English translation by G.J. Soleimani NTIS PB-226 722 (1974).

[23] Goto, K., "Solubility of aluminum hydroxide." J. Chem. Soc. Japan 81, 1268 (1960).

[24] Izatt, R.M. Eatough, D., Christensen, J.J. and Bartholomew, C.H. "Calorimetrically determined log K, ΔH^o, and ΔS^o values for the interaction of sulphate ion with several bi- and tri-valent metal ions." J. Chem. Soc. (A) 47, (1969).

[25] Kashkay, Ch. M., Borovskaya, Yu. B. and Babazade, M.A. "Determination of $\Delta G_{f\ 298}$ of synthetic jarosite and its sulphate analogues." Geochem. Int. (Eng. Transl.) (5) 115 (1975).

[26] Snodgrass, W.J. (IEC Beak Consultants Limited). Letter to N. Garisto, January 29, 1985.

Figure 1: H^+ concentration as a function of the reaction coordinate, for case 1A.1.

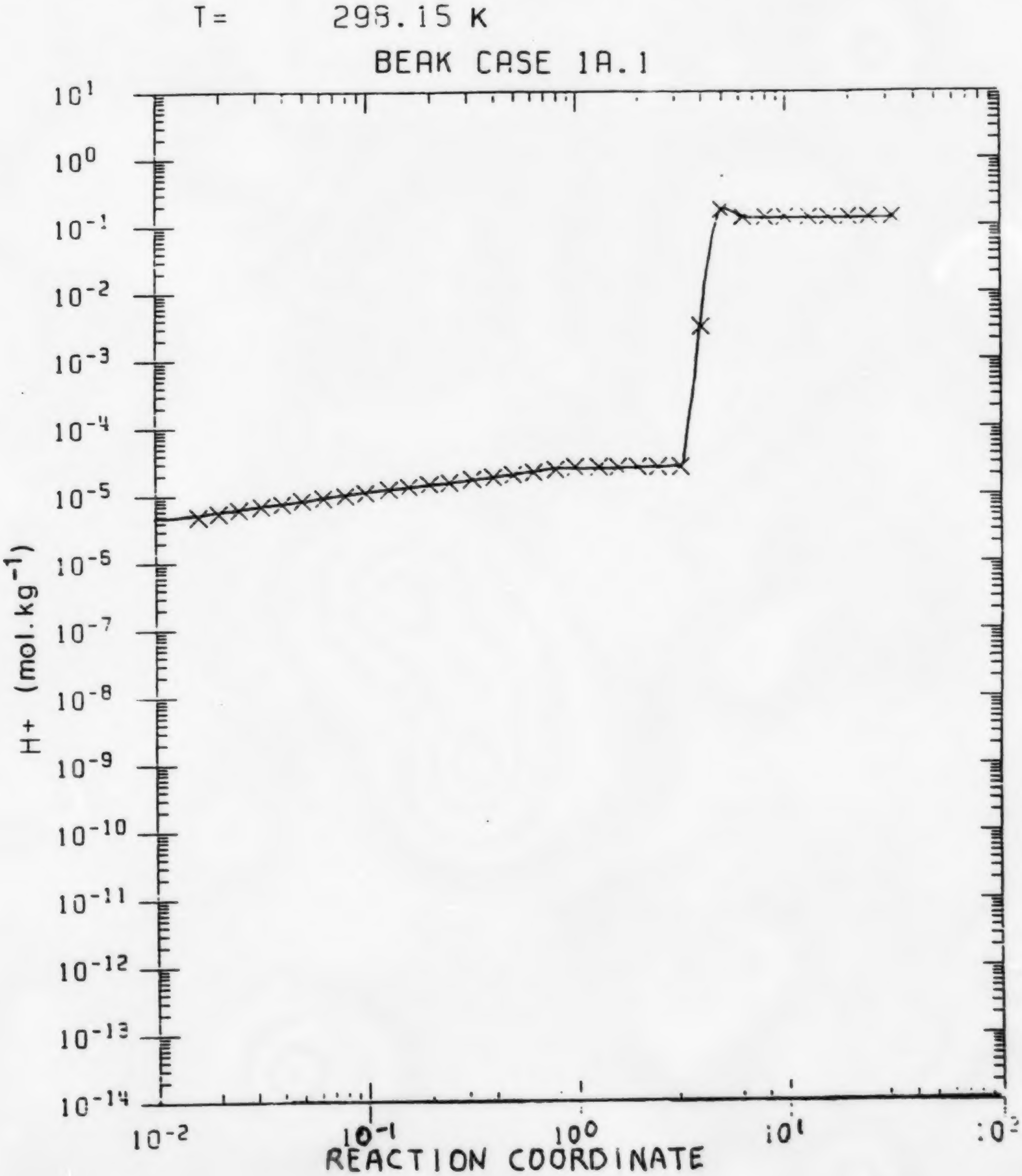

Figure 2: The abundances of solids as a function of the reaction coordinate, for case 1A.1.

○ — $CaSO_4 \cdot 2H_2O$, ◇ — FeS_2 (pyrite),
△ — FeOOH(α), ⋈ — $FeSO_4 \cdot 7H_2O$,
* — jarosite.

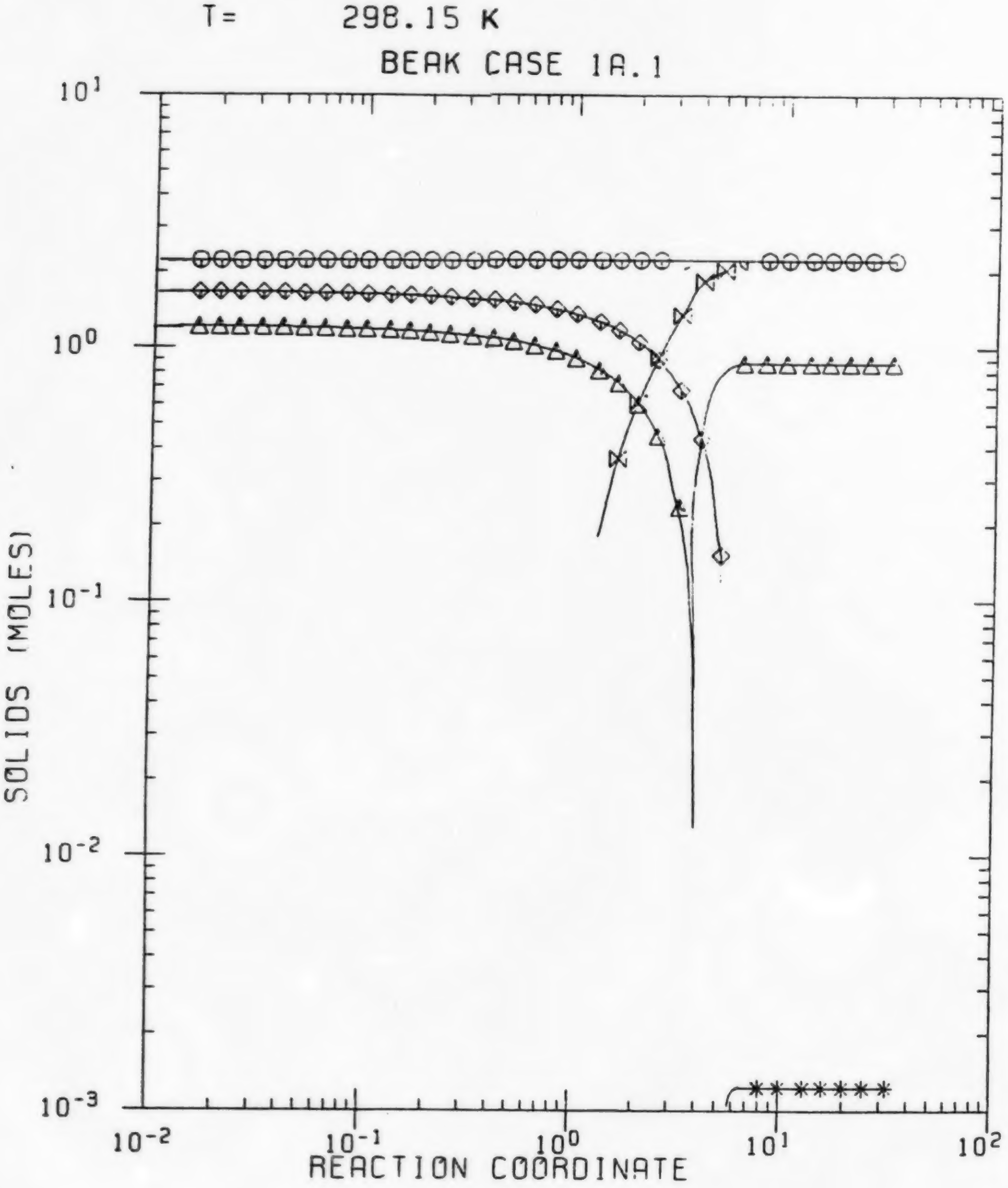

Figure 3: The concentration of Fe^{2+} (—o—) and Fe^{3+} (—◇—) as a function of the reaction coordinate, for case 1A.1.

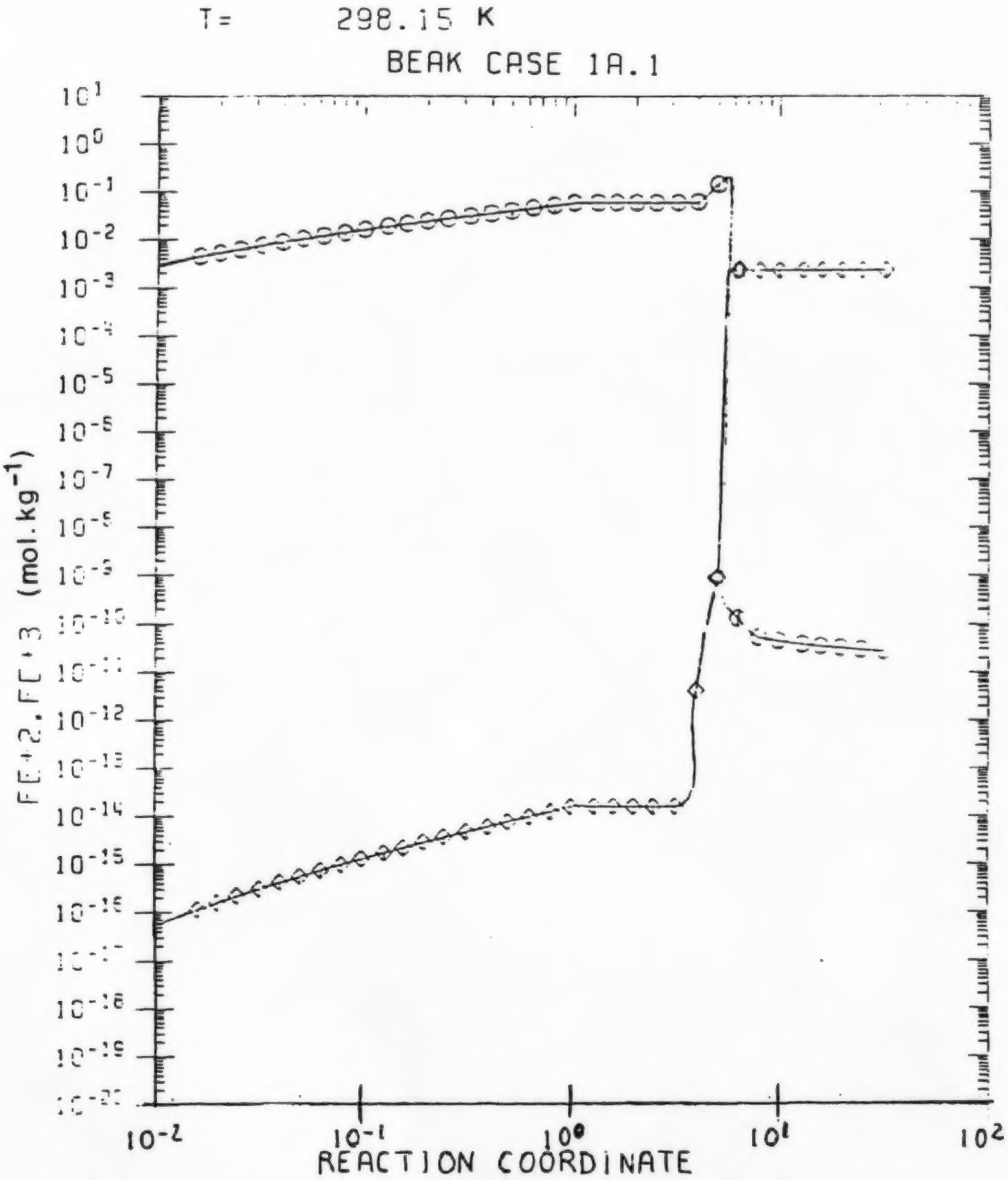

Figure 4: H^+ concentration as a function of the reaction coordinate, for case 1A.2.

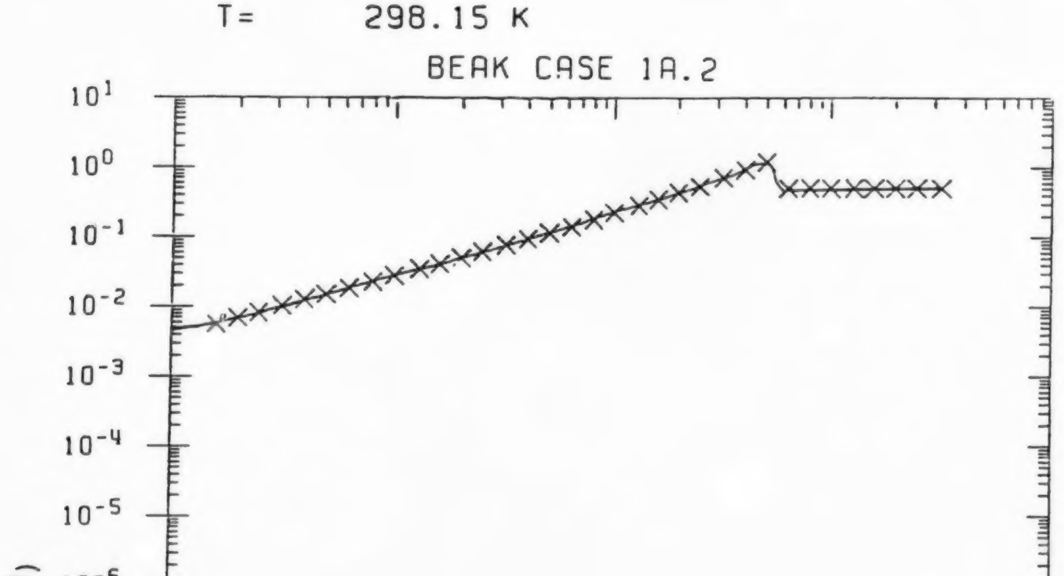

Figure 5: The abundances of solids as a function of the reaction coordinate, for case 1A.2.
○ — $CaSO_4 \cdot 2H_2O$, ◇ — FeS_2(pyrite),
△ — $FeSO_4 \cdot 7H_2O$.

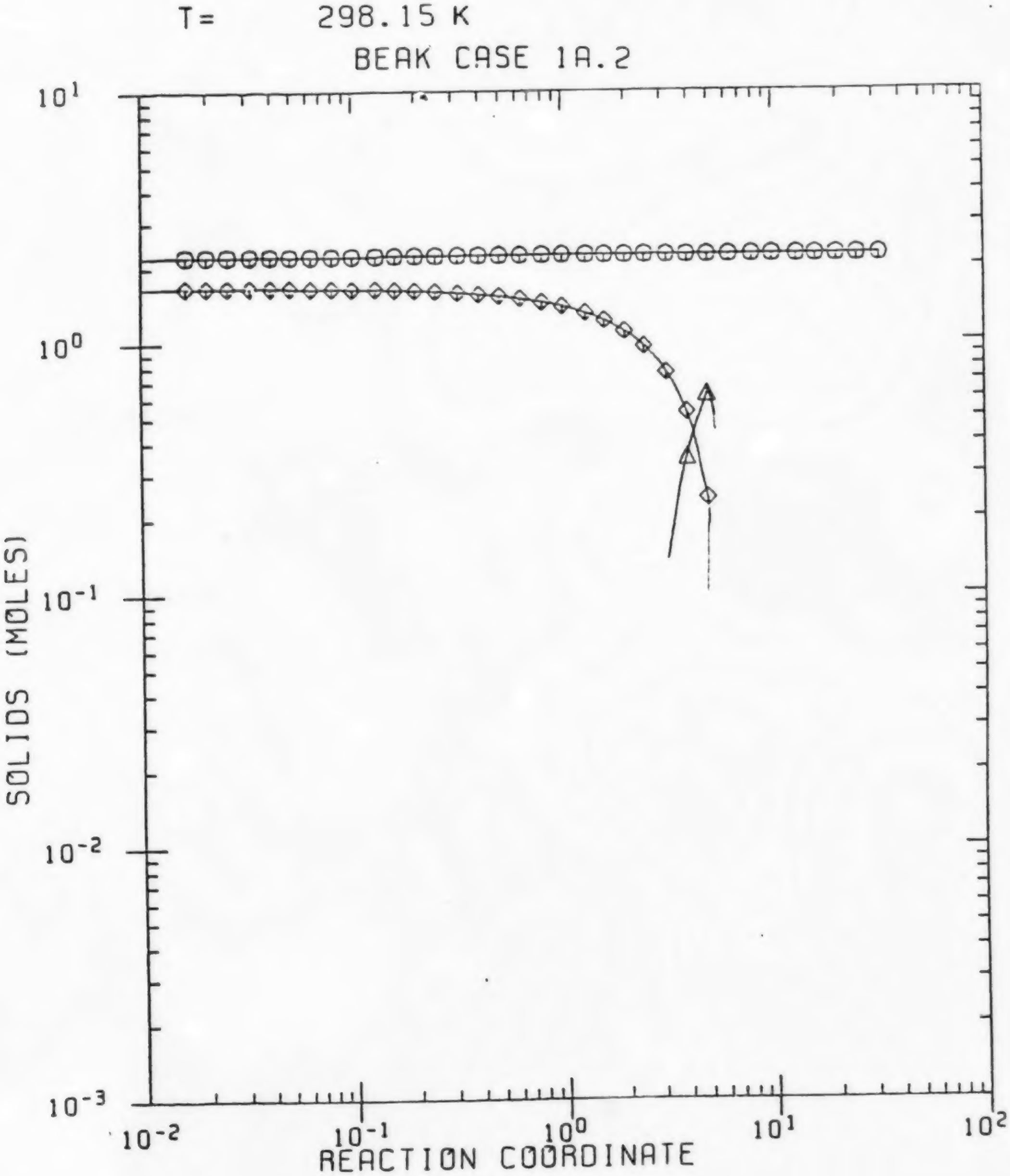

Figure 6: The concentrations of Fe^{2+}(—○—) and of Fe^{3+}(—◇—) as a function of the reaction coordinate, for case 1A.2.

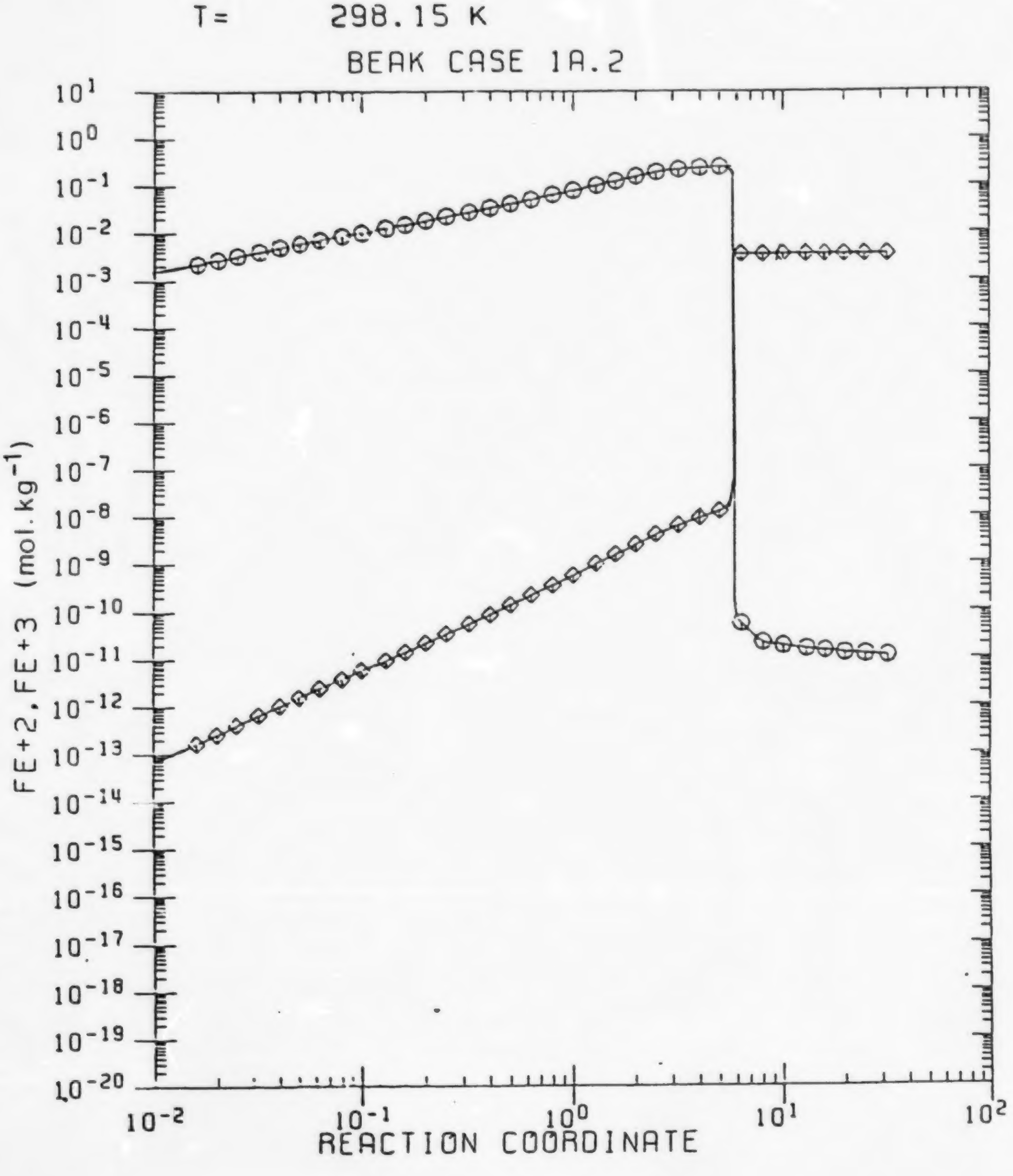

Figure 7: H^+ concentration as a function of the reaction coordinate, for case 1B.1.

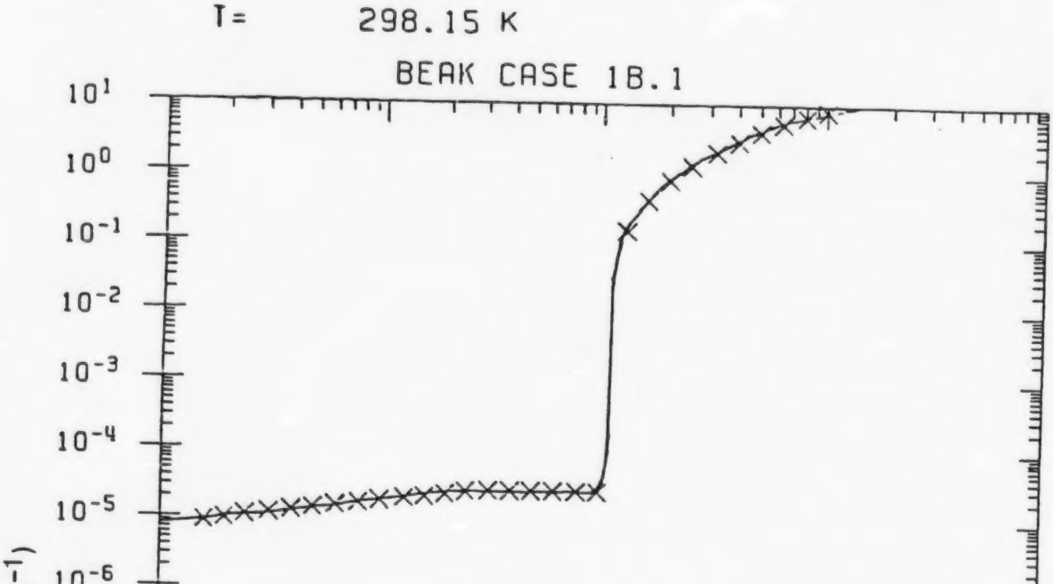

Figure 8: The abundances of solids as a function of the reaction coordinate, for case 1B.1.
○ — $CaSO_4 \cdot 2H_2O$, ◇ — FeS_2(pyrite),
△ — FeOOH(α), * — $FeSO_4 \cdot 7H_2O$.

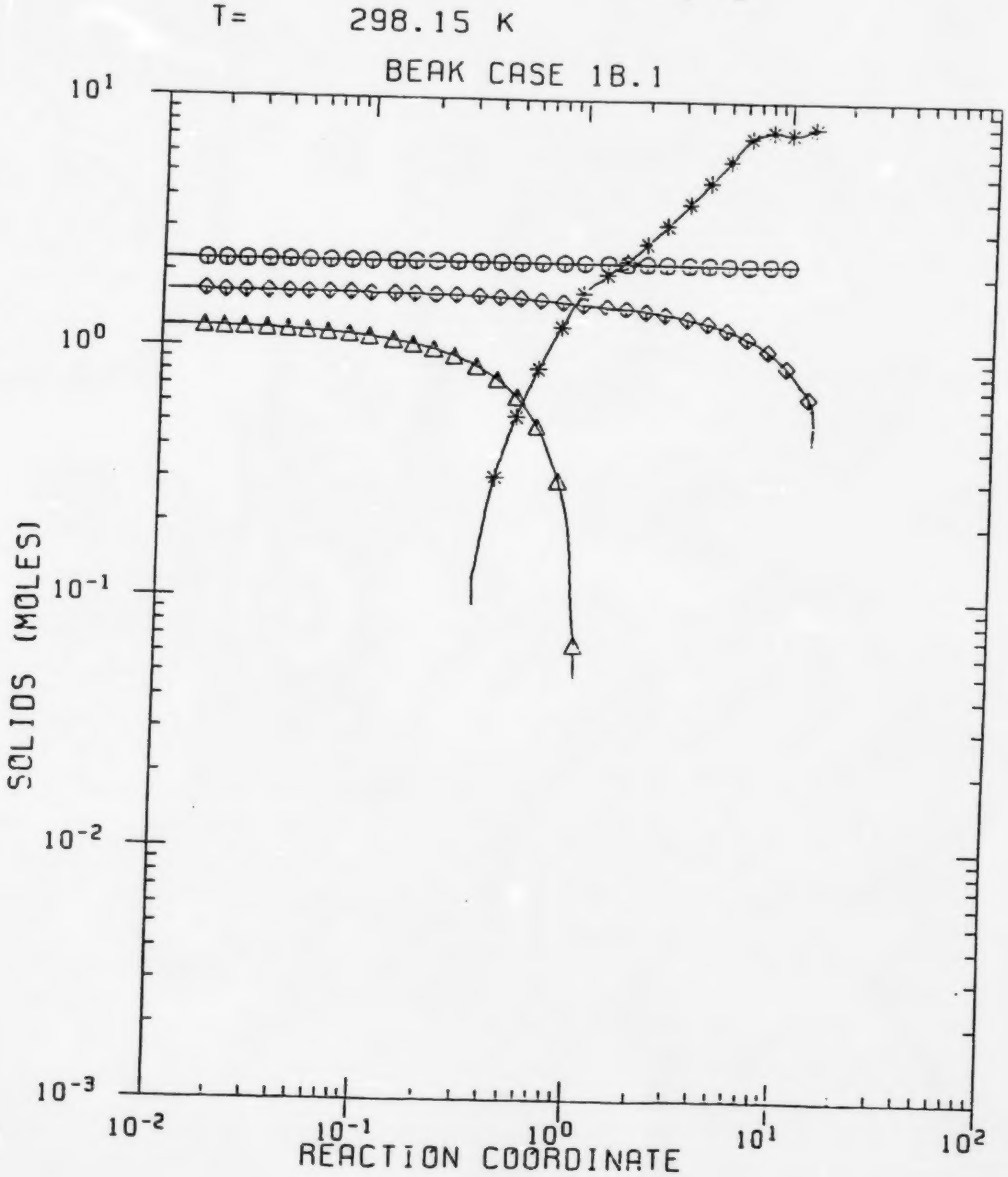

Figure 9: The concentrations of Fe^{2+}(○—) and Fe^{3+}(◇—) as a function of the reaction coordinate, for case 1B.1.

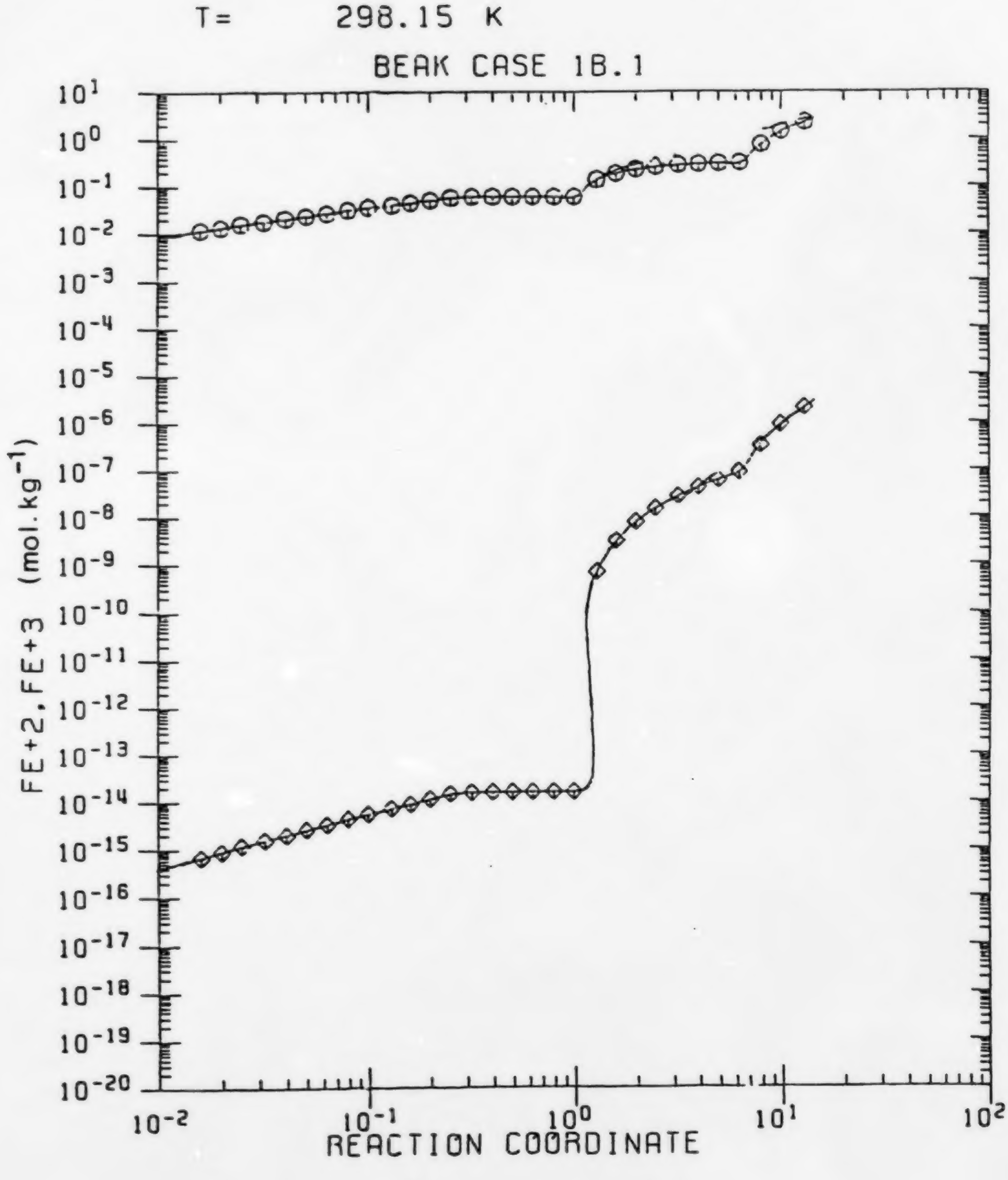

Figure 10: H^+ concentration as a function of the reaction coordinate, for case 1B.2.

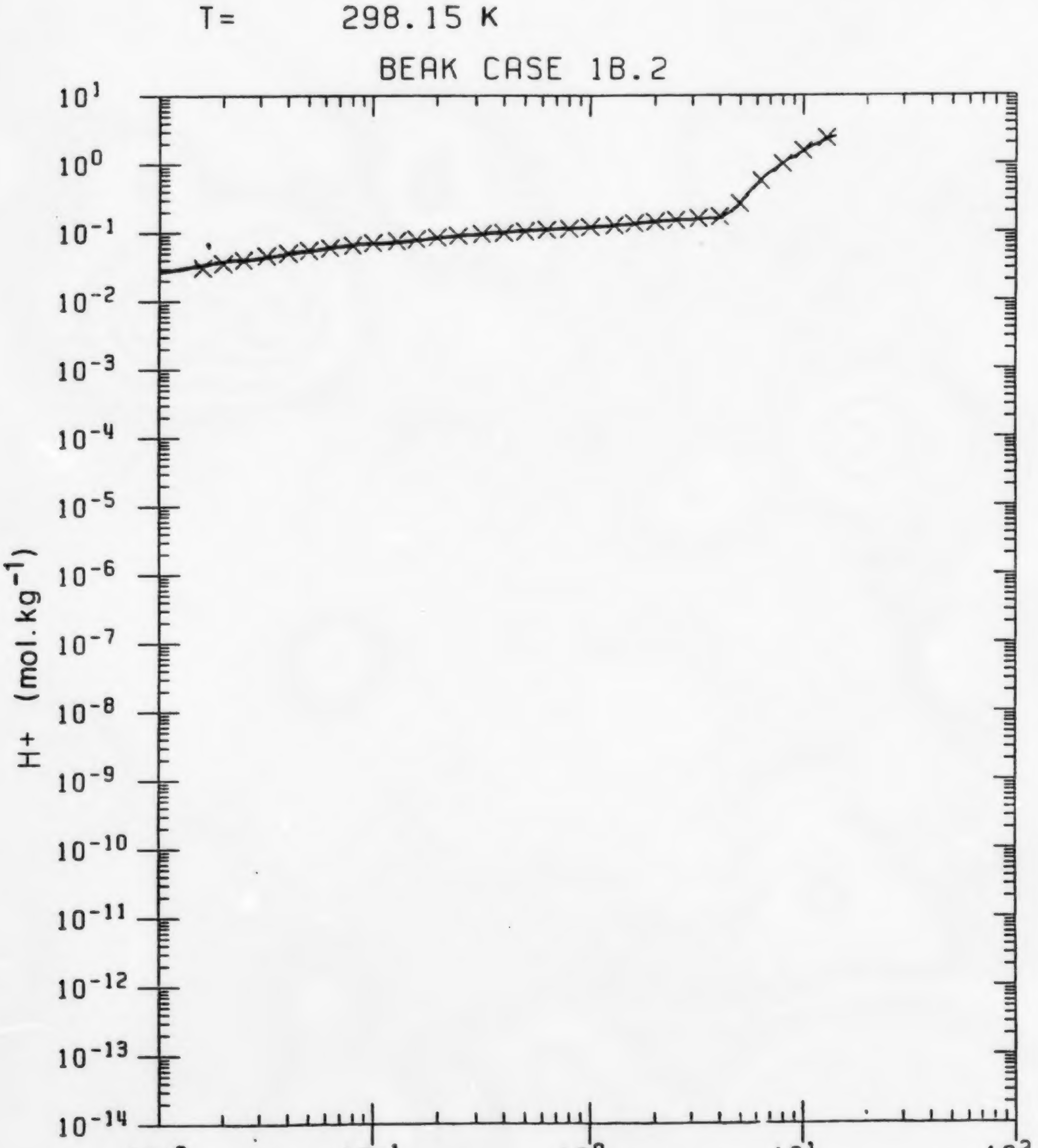

Figure 11: The abundances of solids as a function of the reaction coordinate, for case 1B.2.
O – $CaSO_4 \cdot 2H_2O$, ◇ – FeOOH(α),
Δ ___ jarosite.

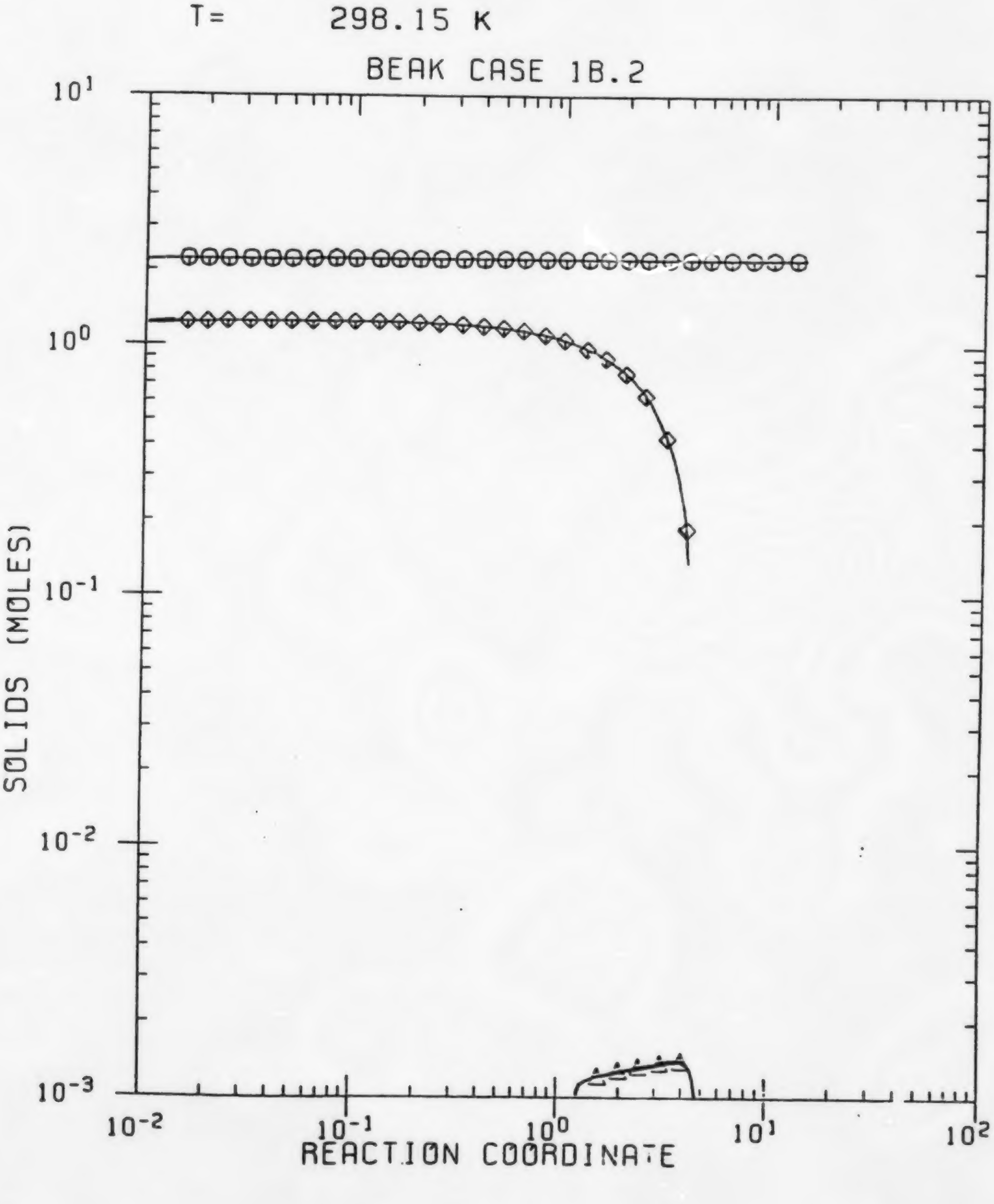

Figure 12: The concentrations of Fe^{2+} (○–) and Fe^{3+} (◇–) as a function of the reaction coordinate, for case 1B.2.

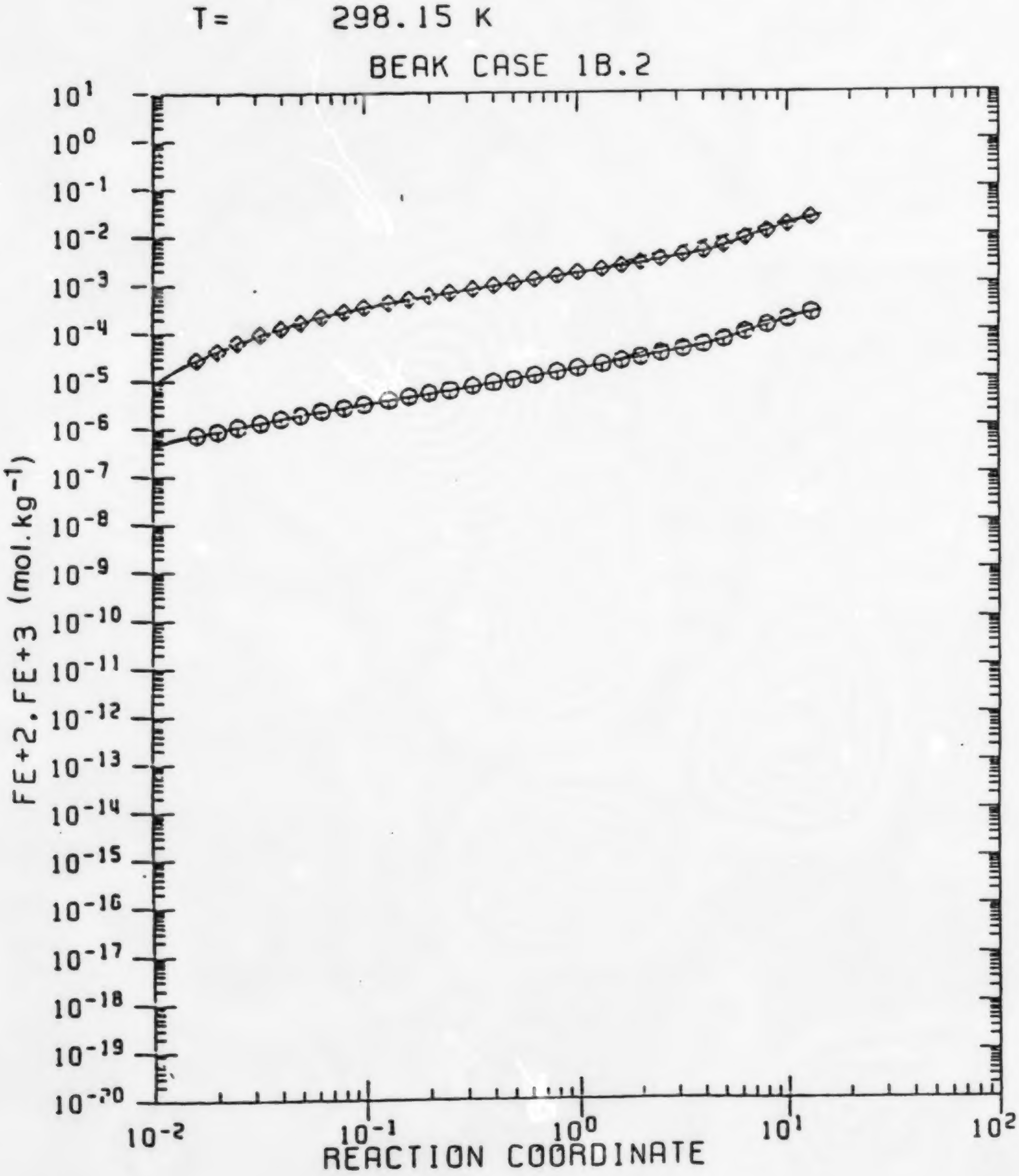

Figure 13: H^+ concentration as a function of the reaction coordinate, for case 1C.1.

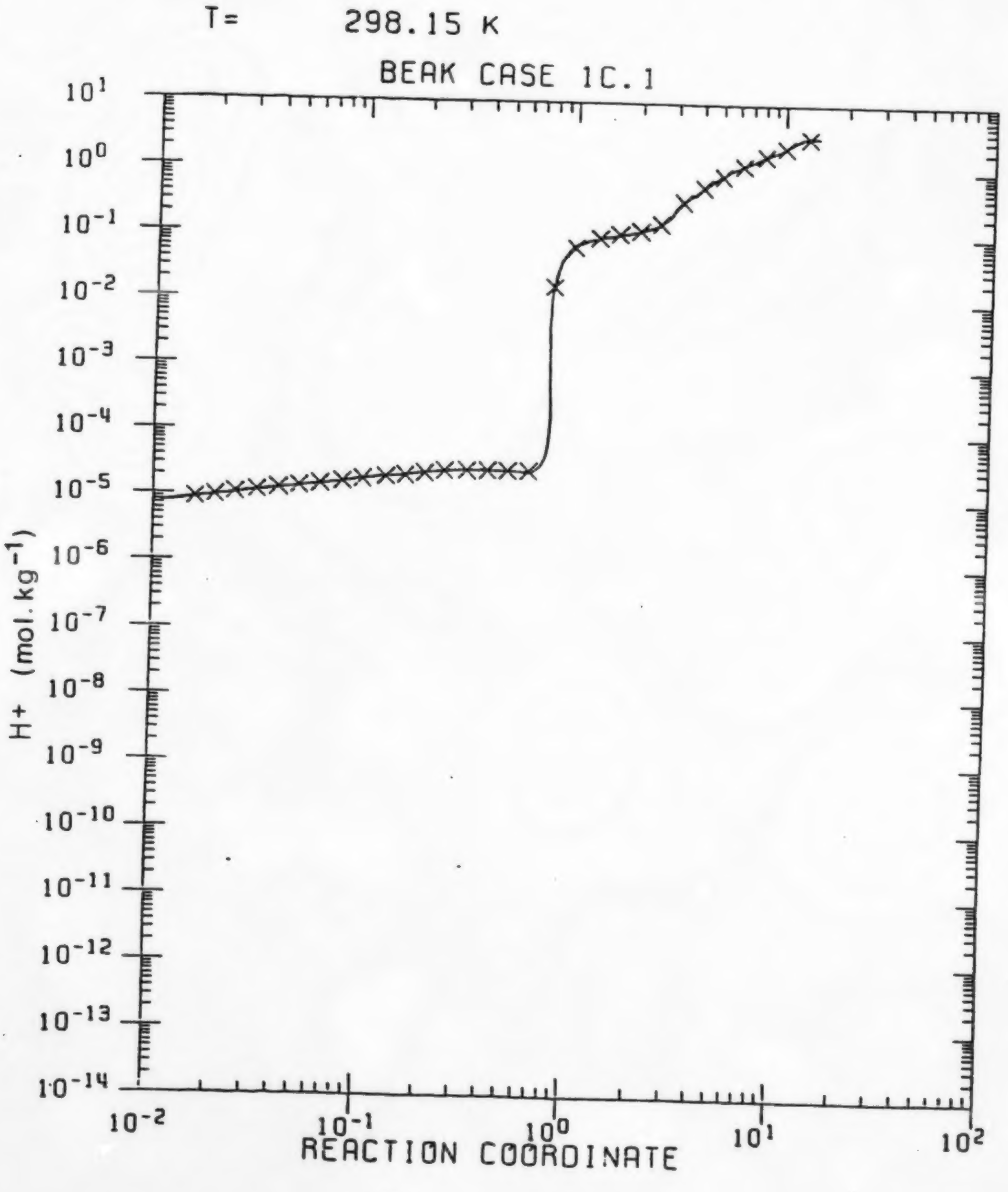

Figure 14: The abundances of solids as a function of the reaction coordinate, for case 1C.1.
○ — $CaSO_4 \cdot 2H_2O$, ◇ — $FeOOH(\alpha)$,
Δ — FeS_2 (pyrite), * — $FeSO_4 \cdot 7H_2O$.

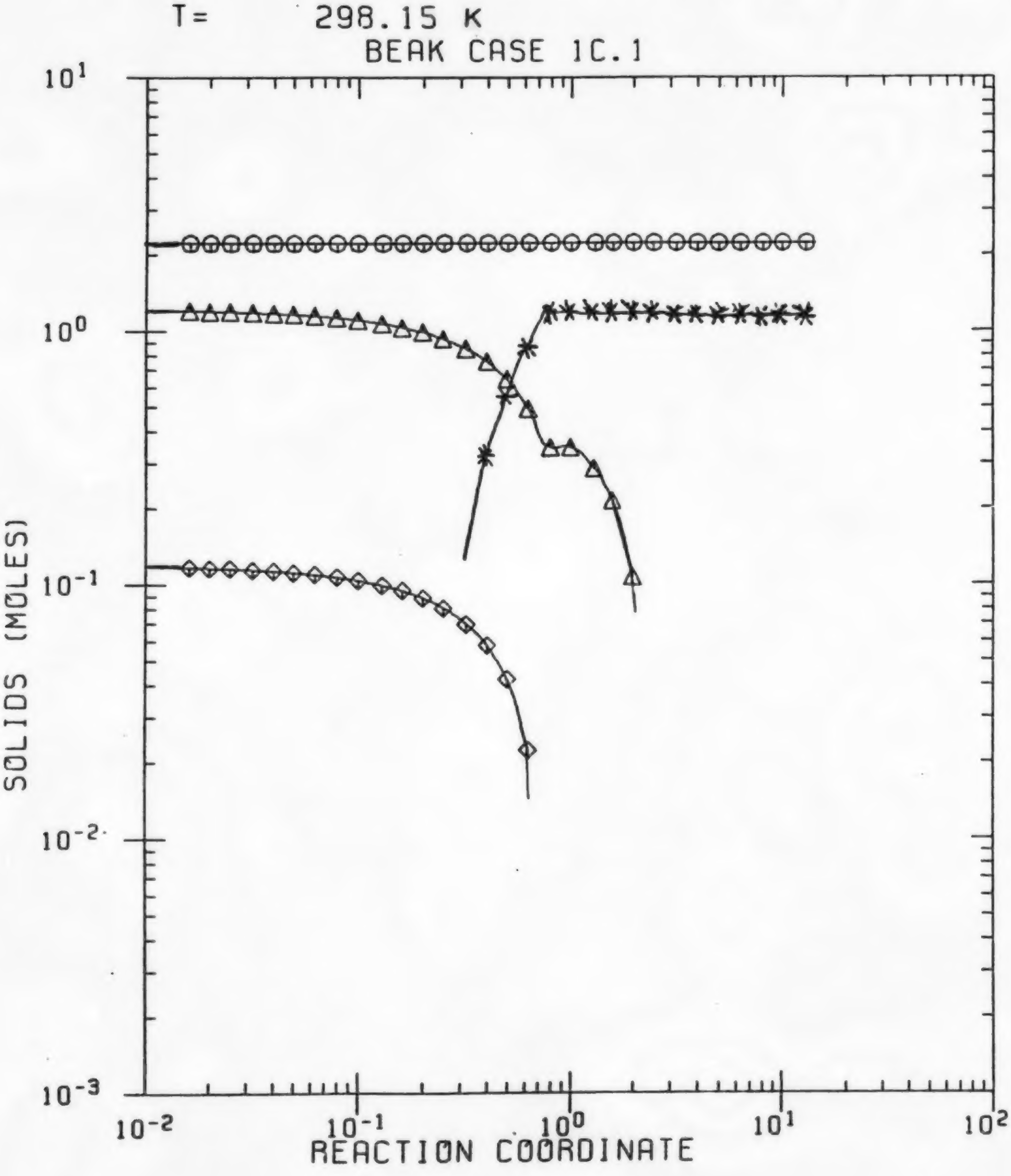

Figure 15: The concentrations of Fe^{2+} (○ –) and Fe^{3+} (◇ –) as a function of the reaction coordinate, for case 1C.1.

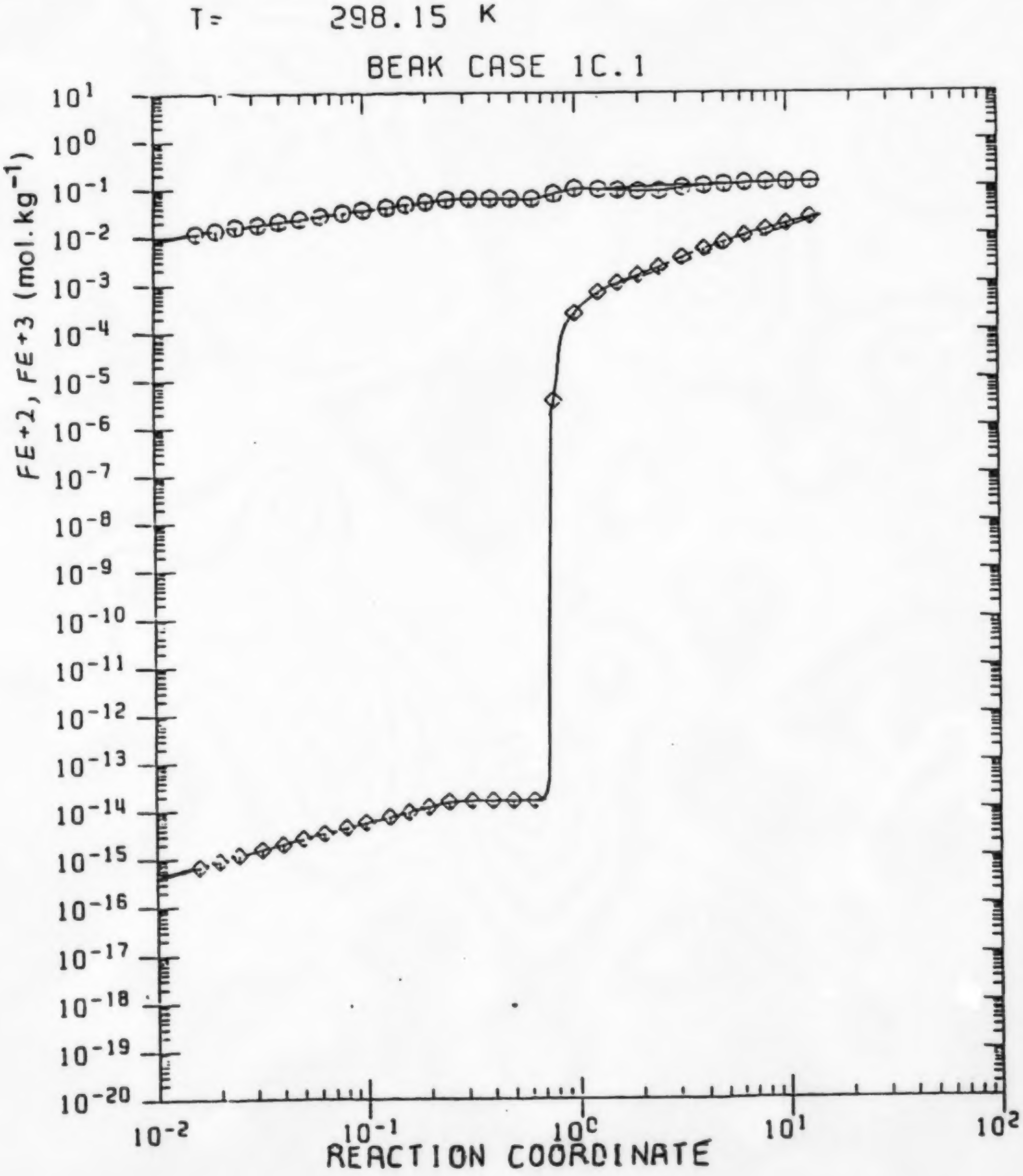

Figure 16: H^+ concentration as a function of the reaction coordinate, for case 2A.1.

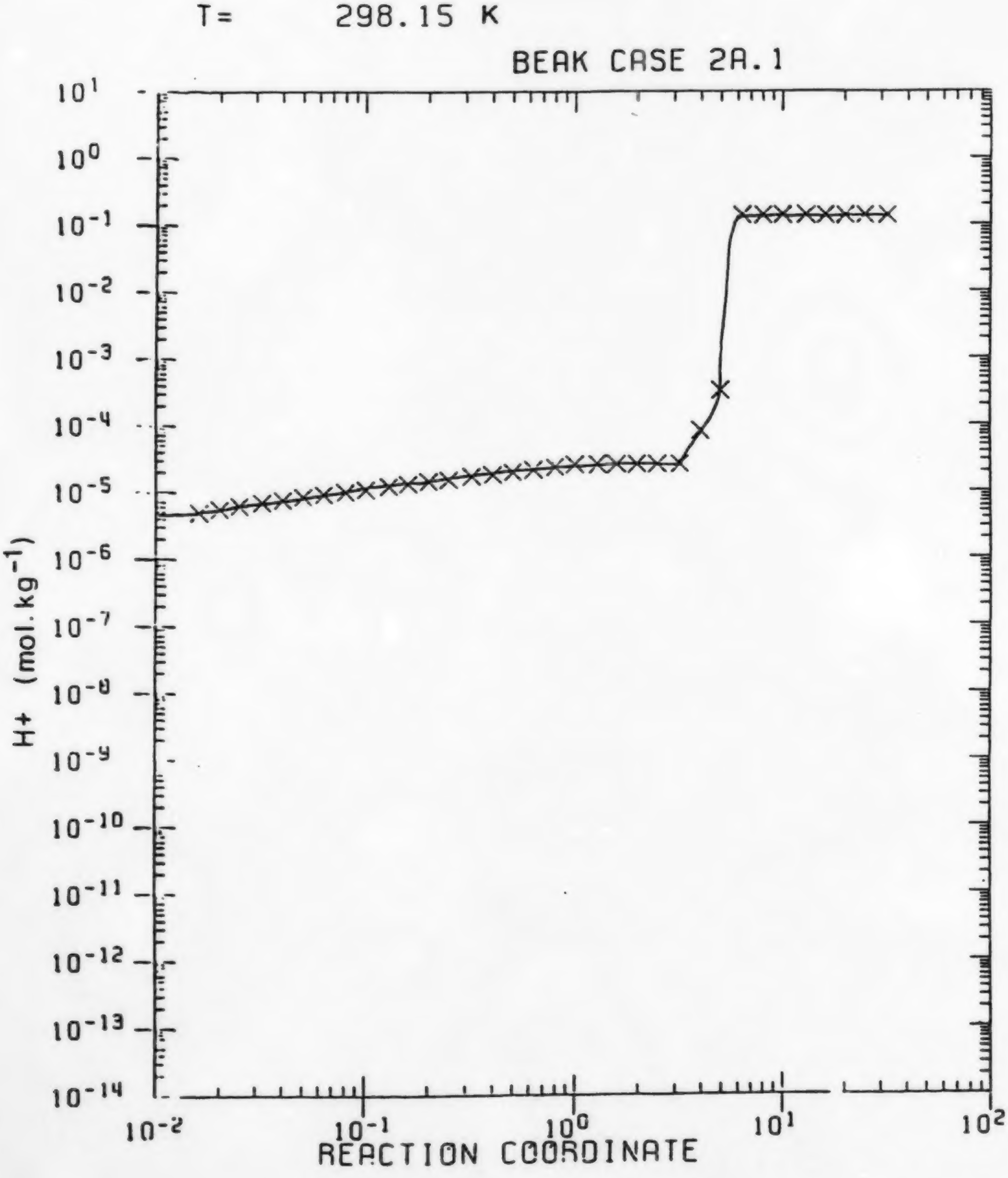

Figure 17: The abundances of solids as a function of the reaction coordinate, for case 2A.1.
○ — $CaSO_4 \cdot 2H_2O$, ◇ — FeS_2 (pyrite),
Δ — FeOOH(α), ⋈ — $Al(OH)_3$ (gibbsite),
* — $FeSO_4 \cdot 7H_2O$.

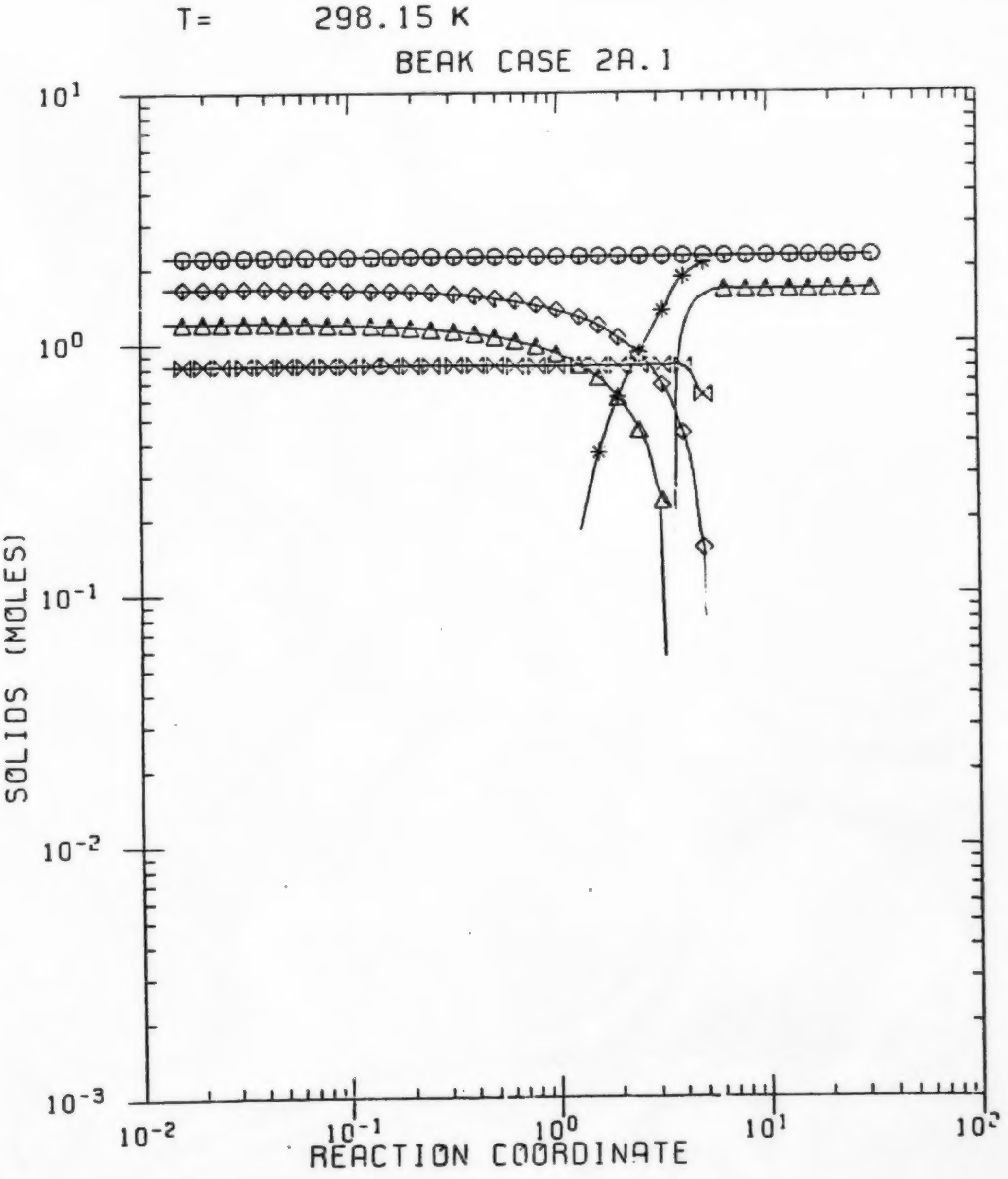

Figure 18: The concentrations of Fe^{2+} (⊗ –) and Fe^{3+} (x –) as a function of the reaction coordinate, for case 2A.1.

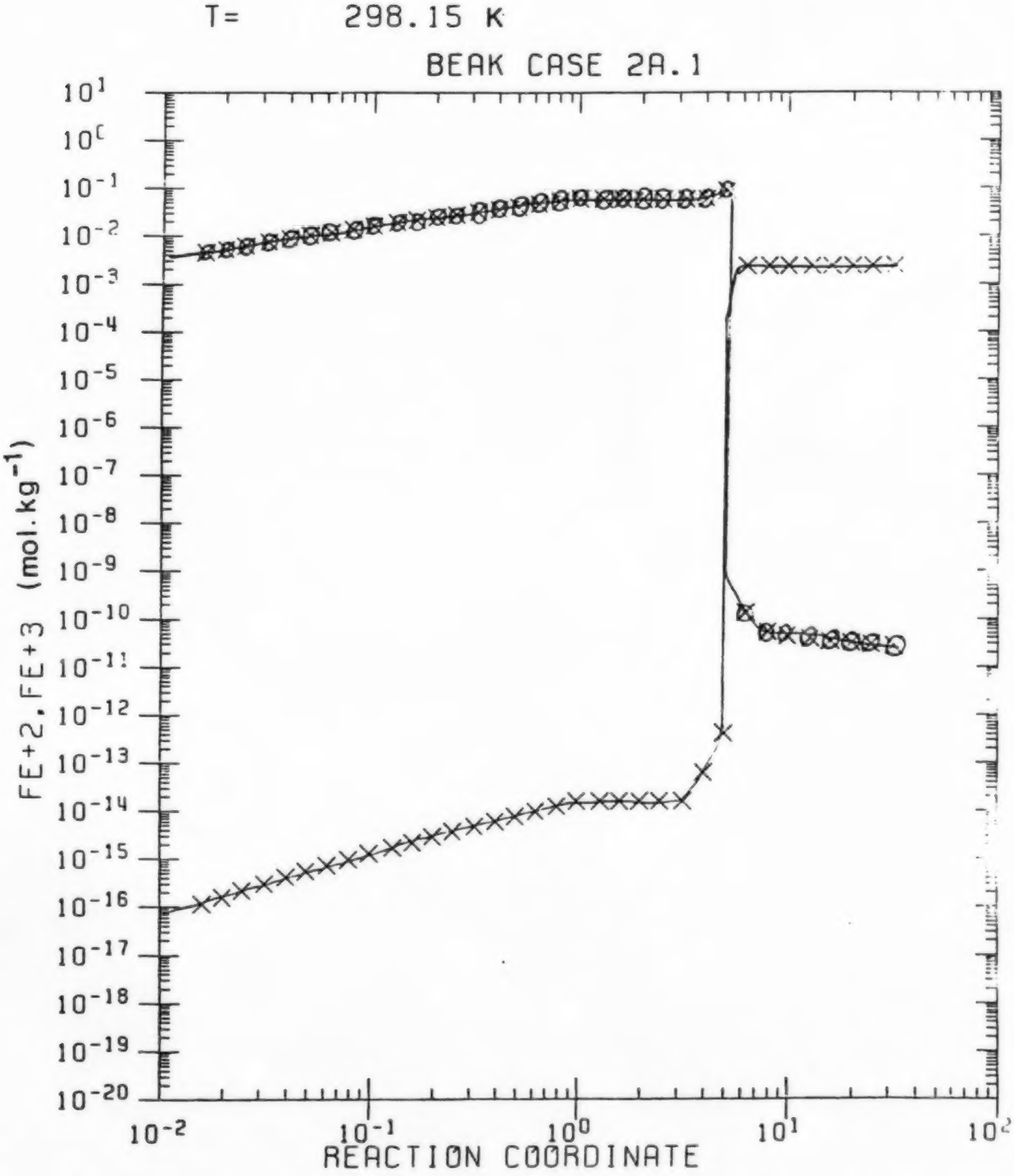

Figure 19: H^+ concentration as a function of the reaction coordinate, for case 2A.2.

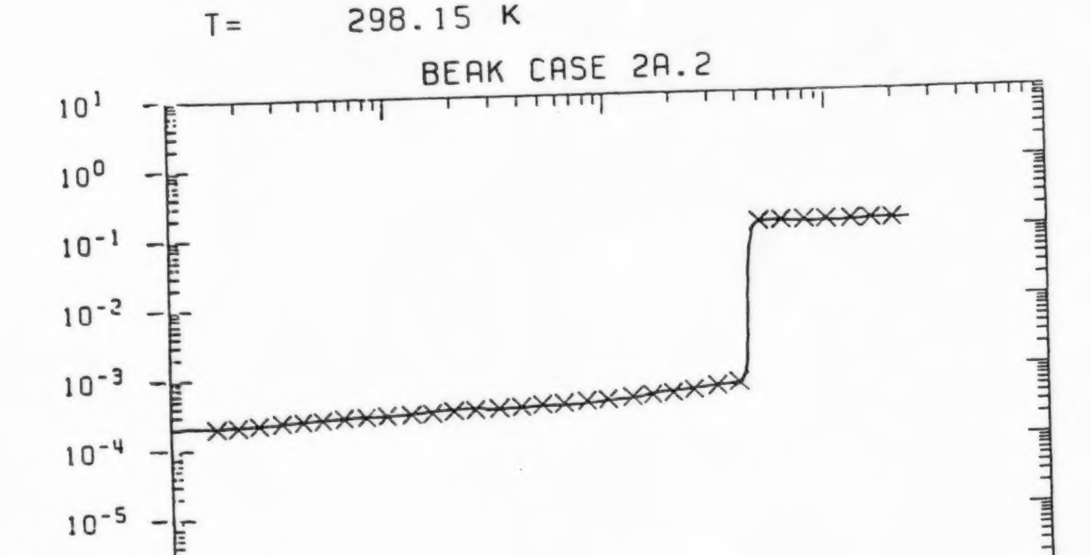

Figure 20: The abundances of solids as a function of the reaction coordinate, for case 2A.2.
○ — $CaSO_4 \cdot 2H_2O$, ◇ — FeS_2 (pyrite),
* — $FeSO_4 \cdot 7H_2O$, Δ — FeOOH(α),
⋈ — $Al(OH)_3$ (gibbsite) .

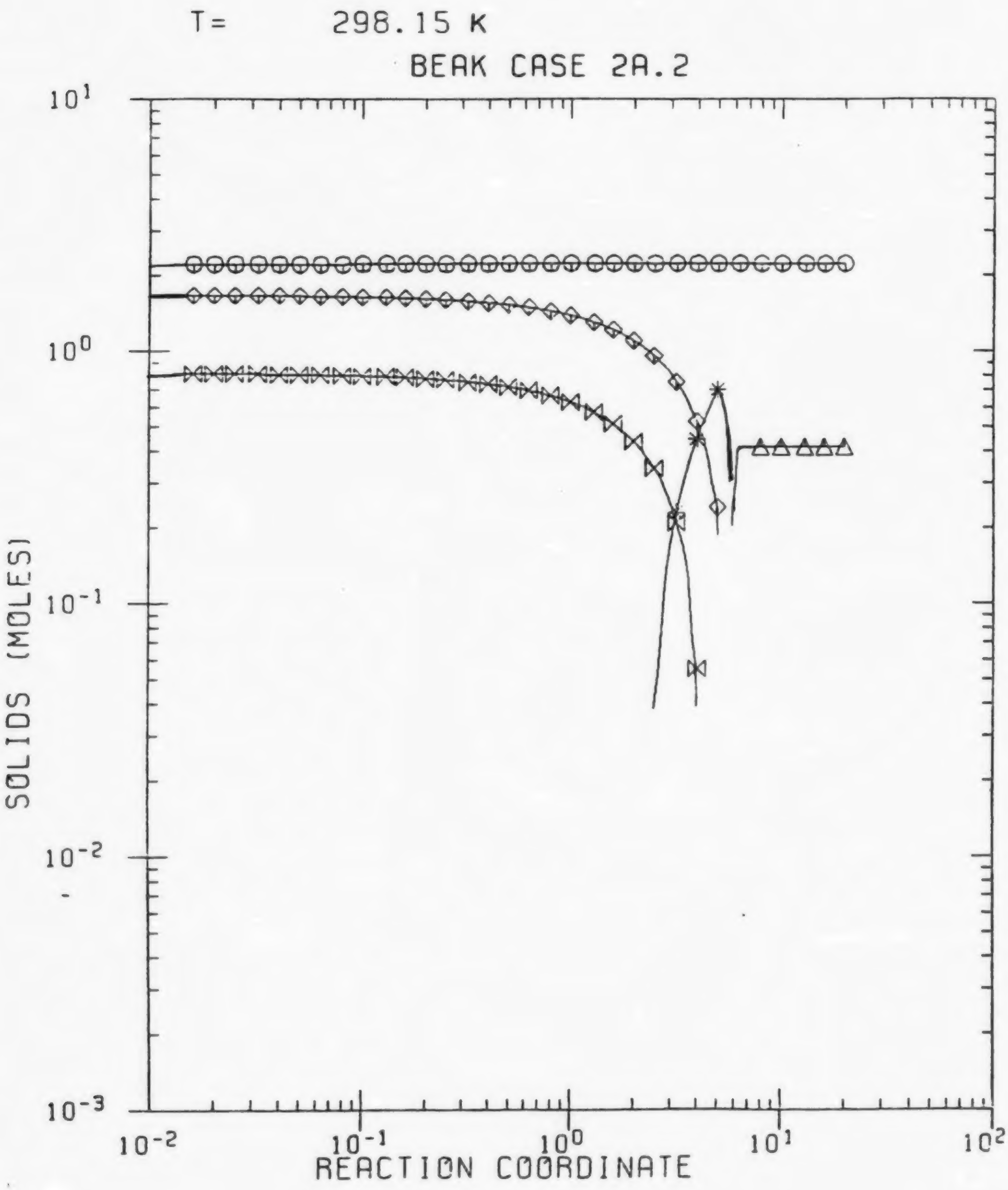

Figure 21: The concentrations of Fe^{2+} (O—) and Fe^{3+} (◇—) as a function of the reaction coordinate, for case 2A.2.

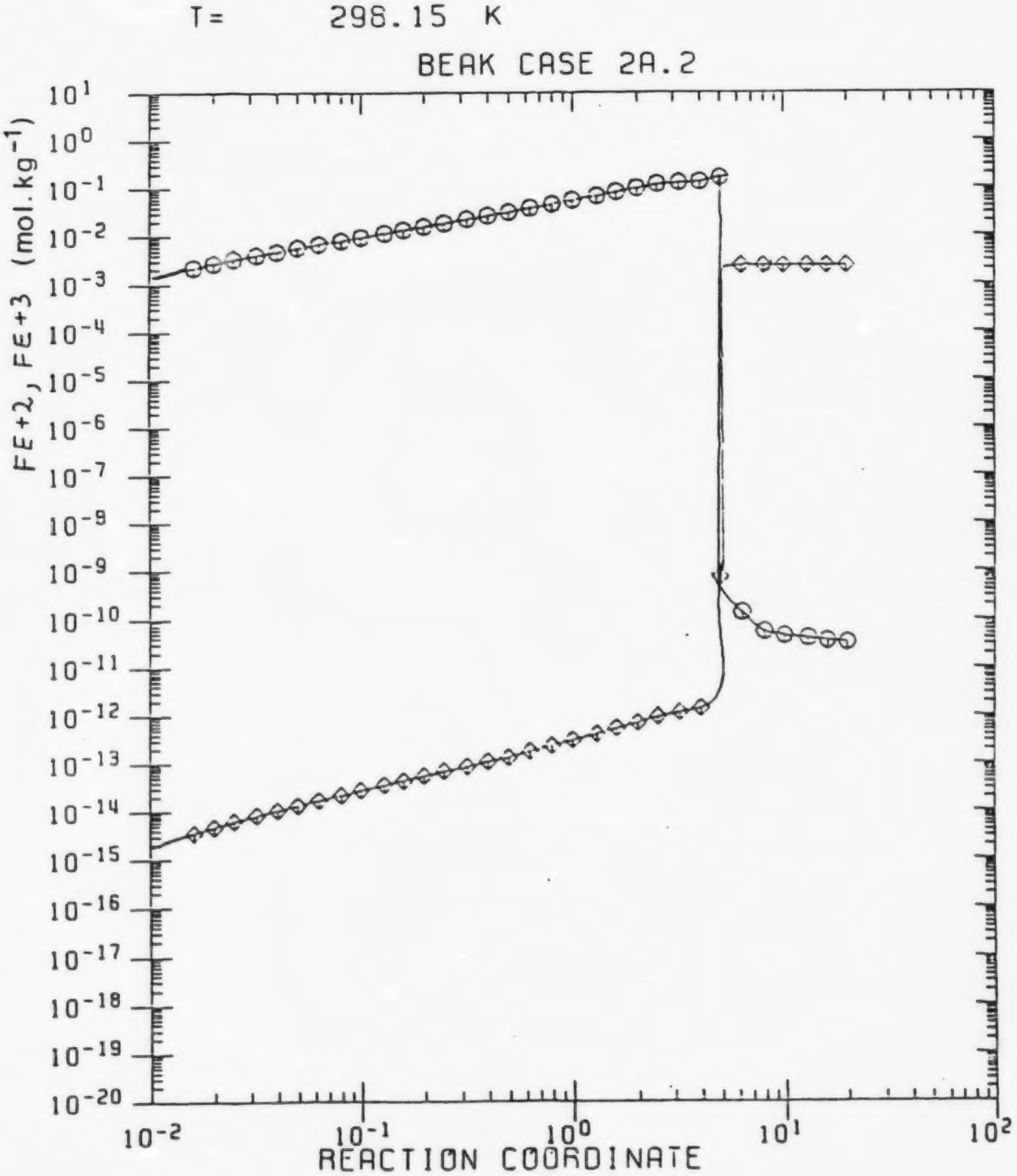

Figure 22: H^+ concentration as a function of the reaction coordinate, for case 3A.1.

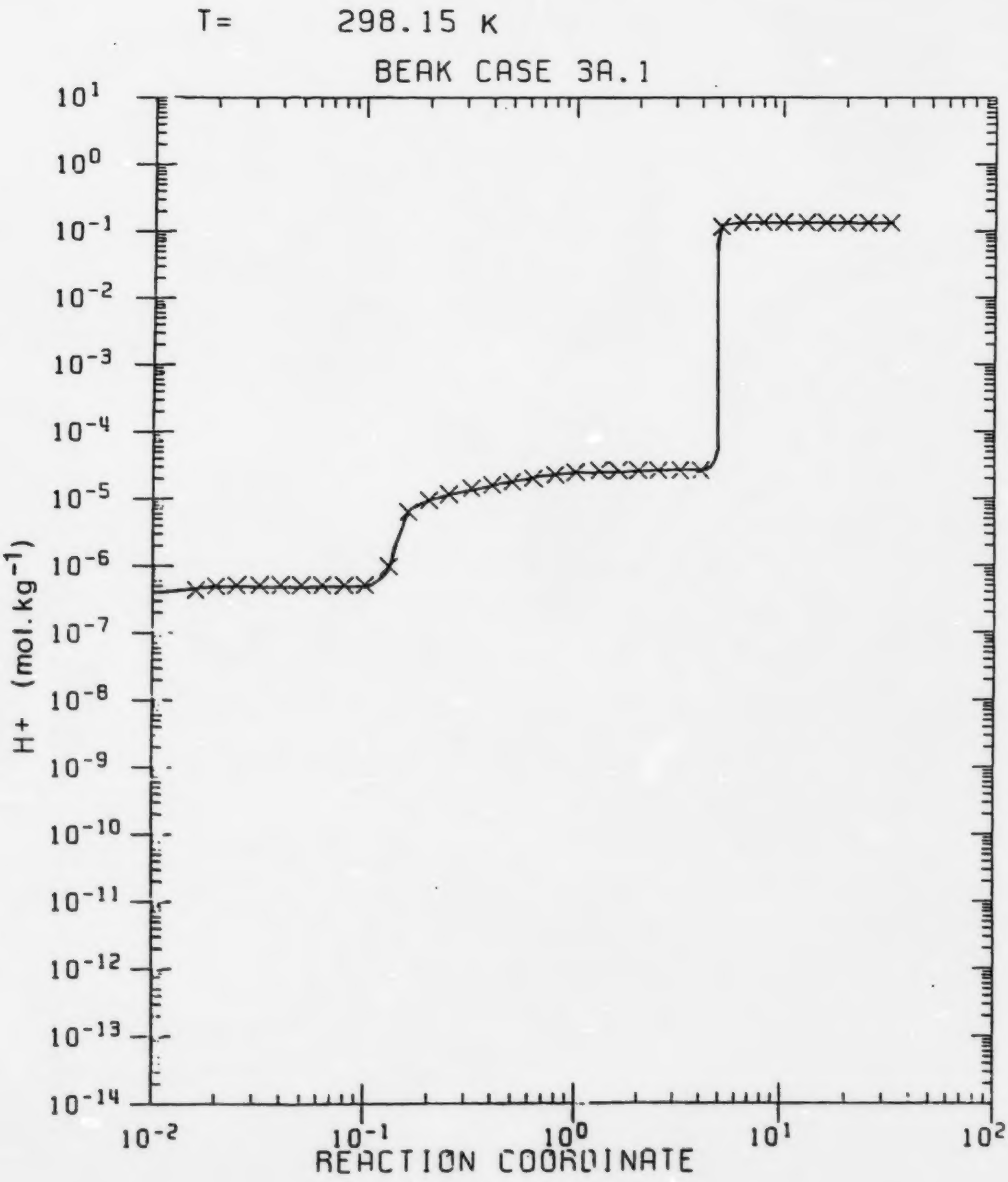

Figure 23: The abundances of solids as a function of the reaction coordinate, for case 3A.1.

○ — $CaSO_4 \cdot 2H_2O$, ◇ — FeS_2 (pyrite),

Δ — FeOOH(α), ⋈ — $FeSO_4 \cdot 7H_2O$,

* —— jarosite, ⧖ — $CaCO_3$ (s),

● — $FeCO_3$ (s).

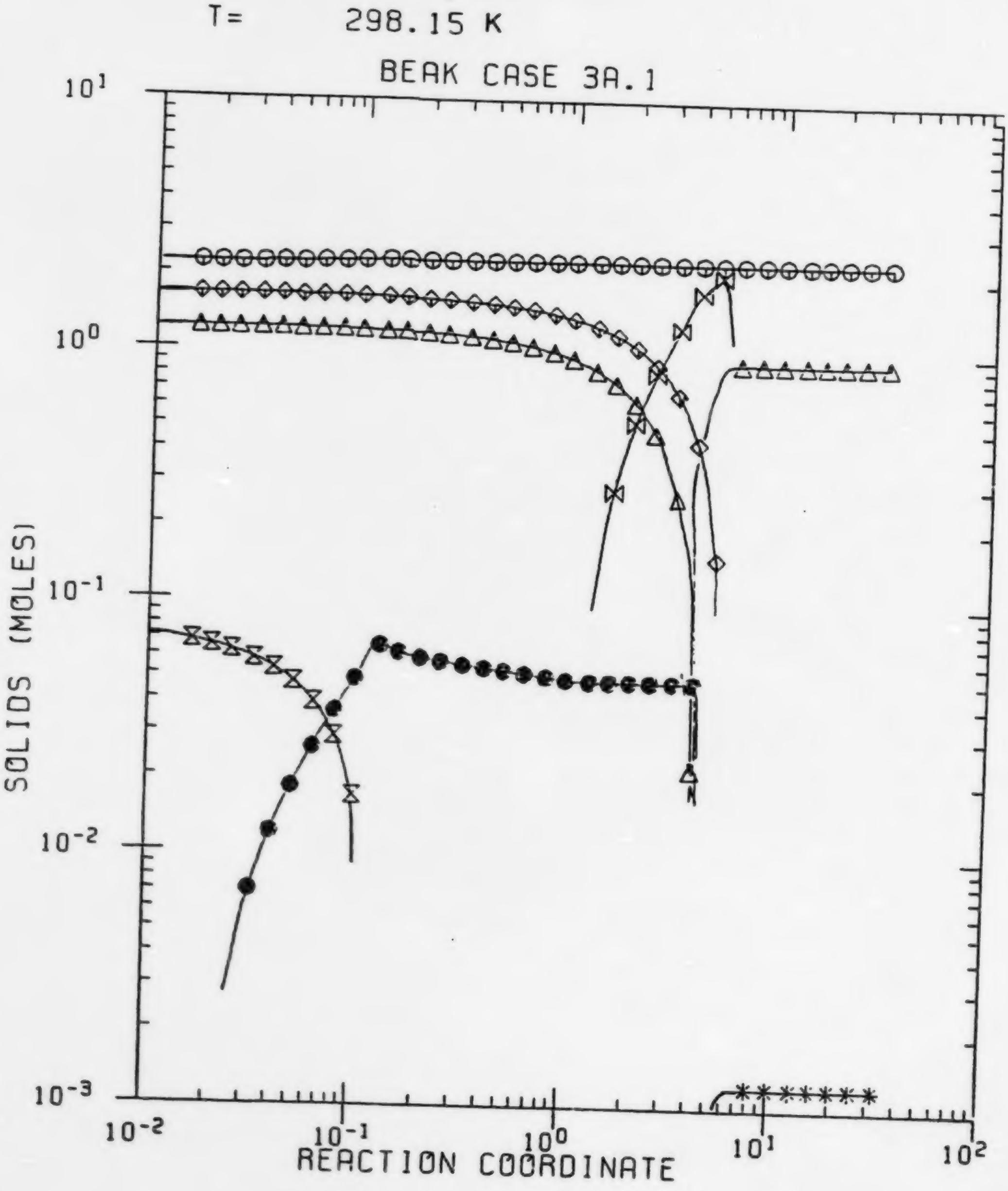

Figure 24: The concentrations of Fe^{2+} (○ –) and Fe^{3+} (◇ –) as a function of the reaction coordinate, for case 3A.1.

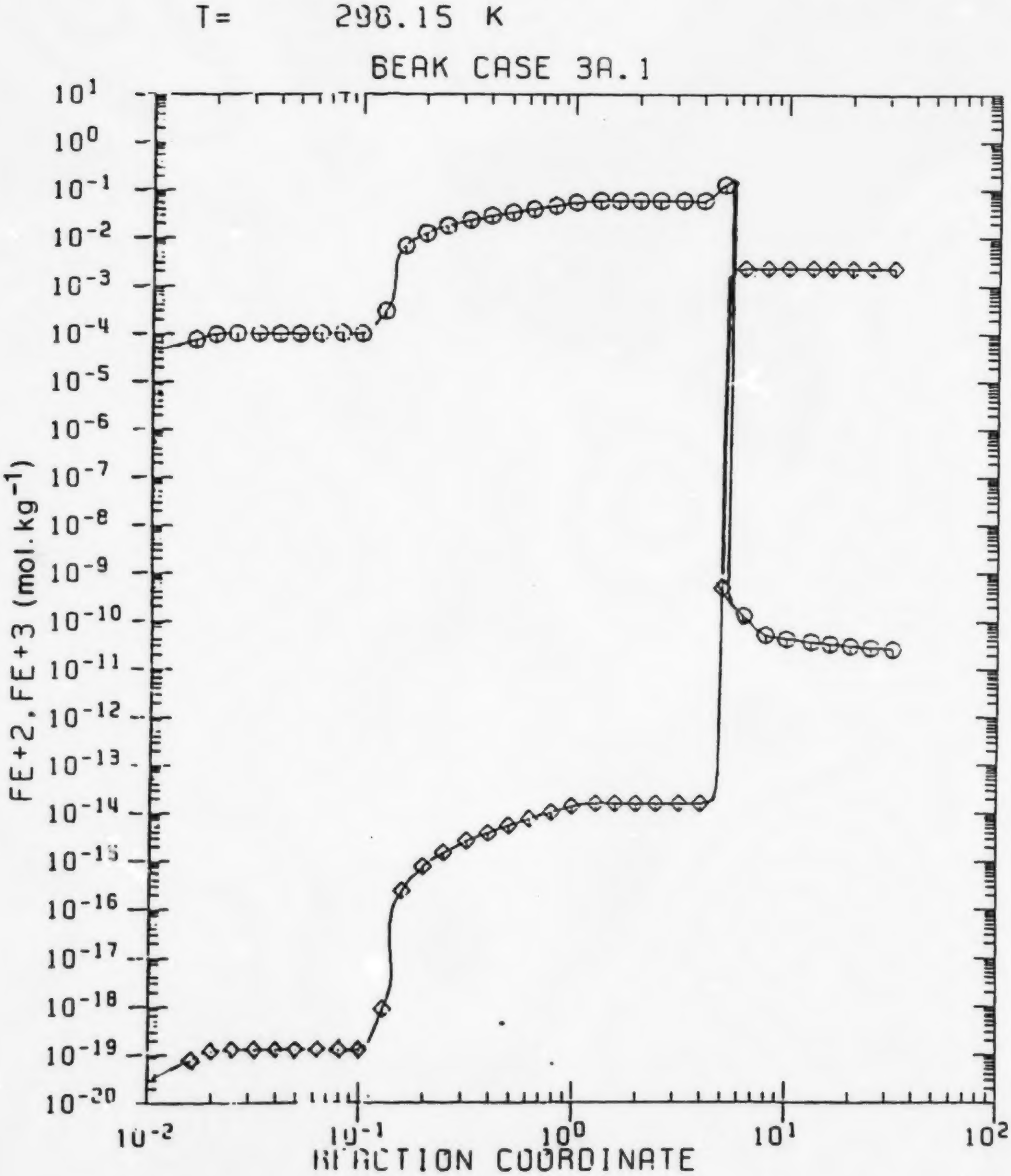

Figure 28: H^+ concentration as a function of the reaction coordinate, for case 4B.1.

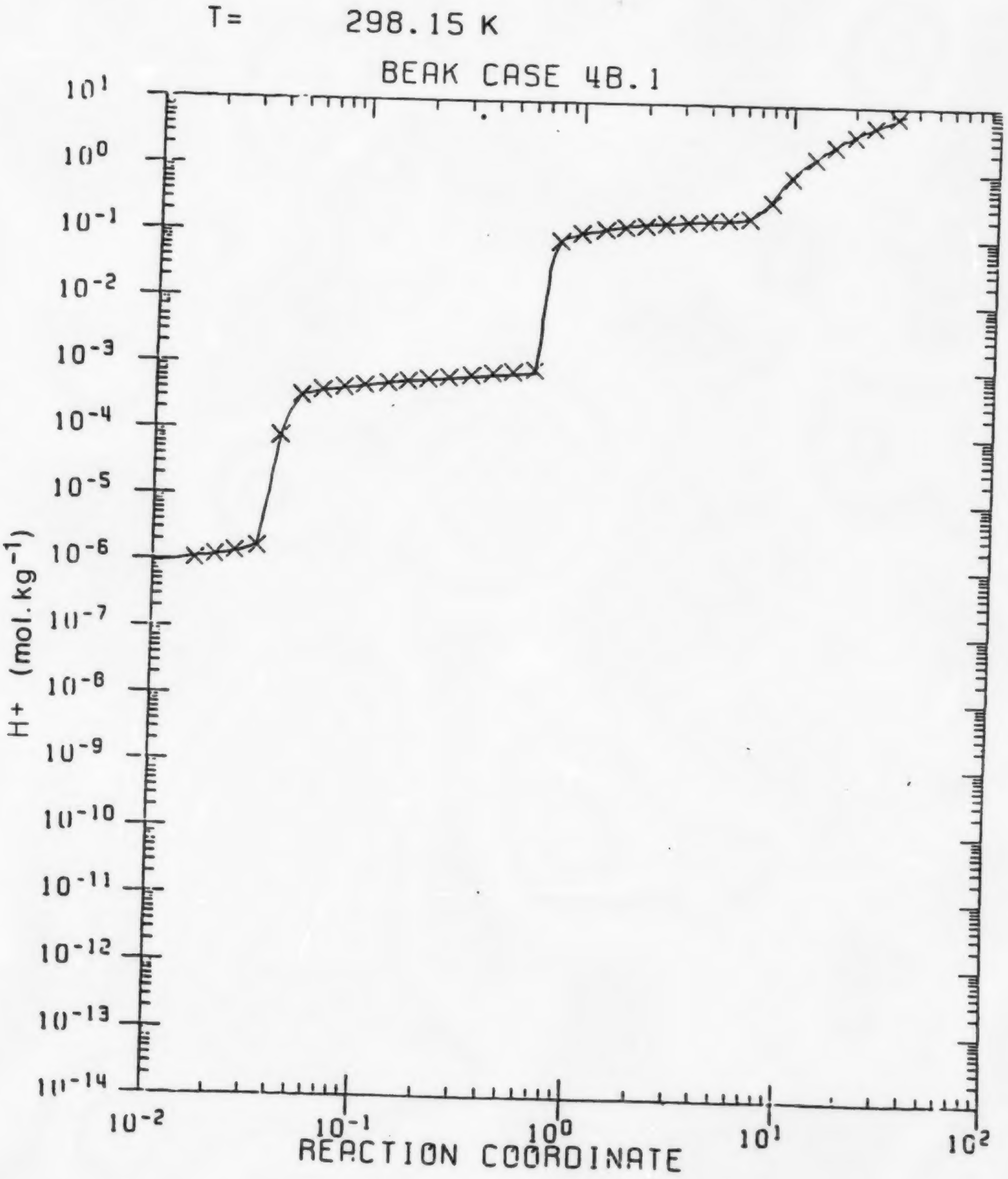

Figure 29: The abundances of solids as a function of the reaction coordinate, for case 4B.1.
O – $CaSO_4 \cdot 2H_2O$, ◇ – FeOOH(α), * – $CaCO_3$ (s)
Δ —— jarosite, ⋈ – $Al(OH)_3$ (gibbsite)

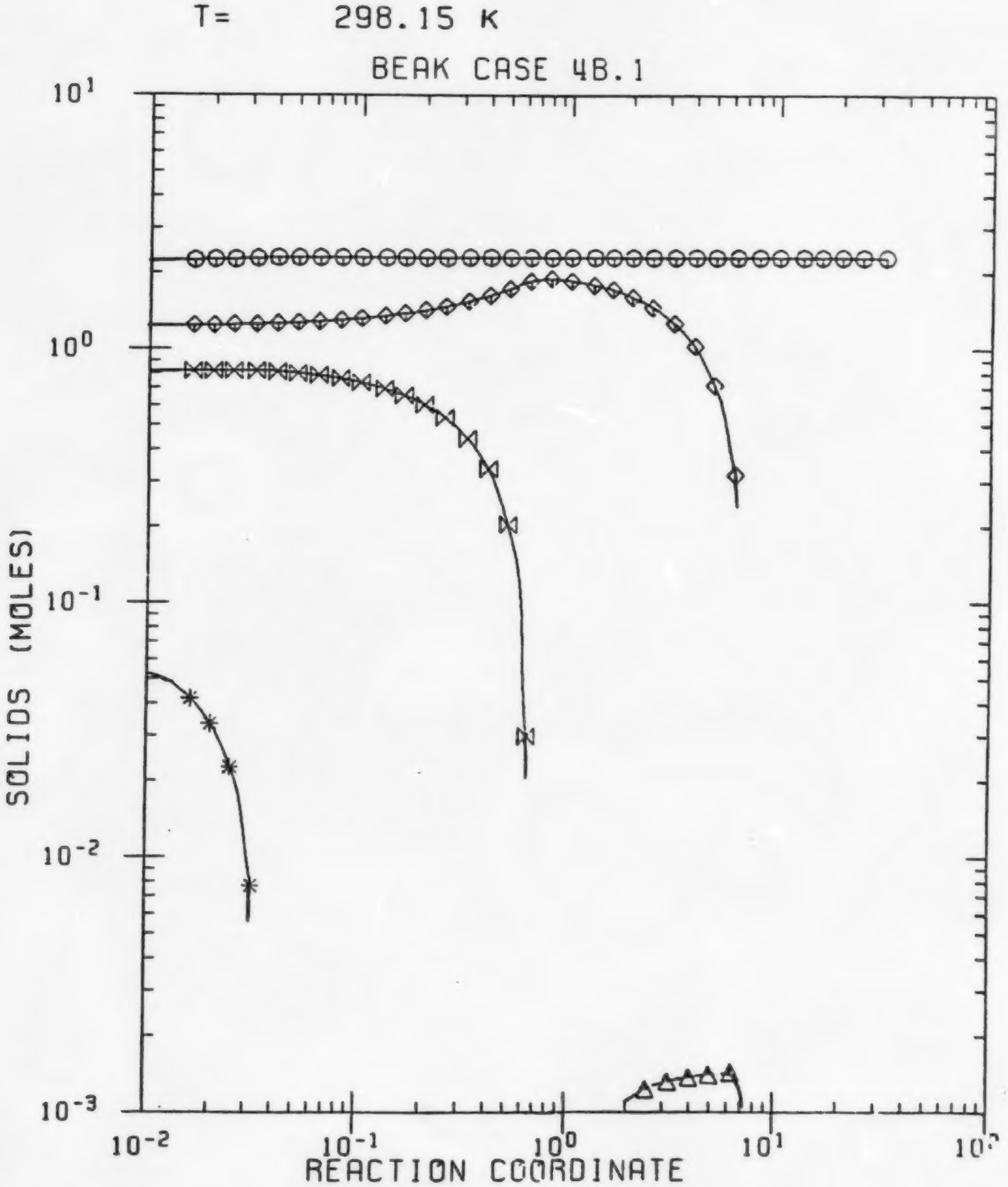

Figure 30: The concentrations of Fe^{2+} (o –) and Fe^{3+} (◇ –) as a function of the reaction coordinate, for case 4B.1.

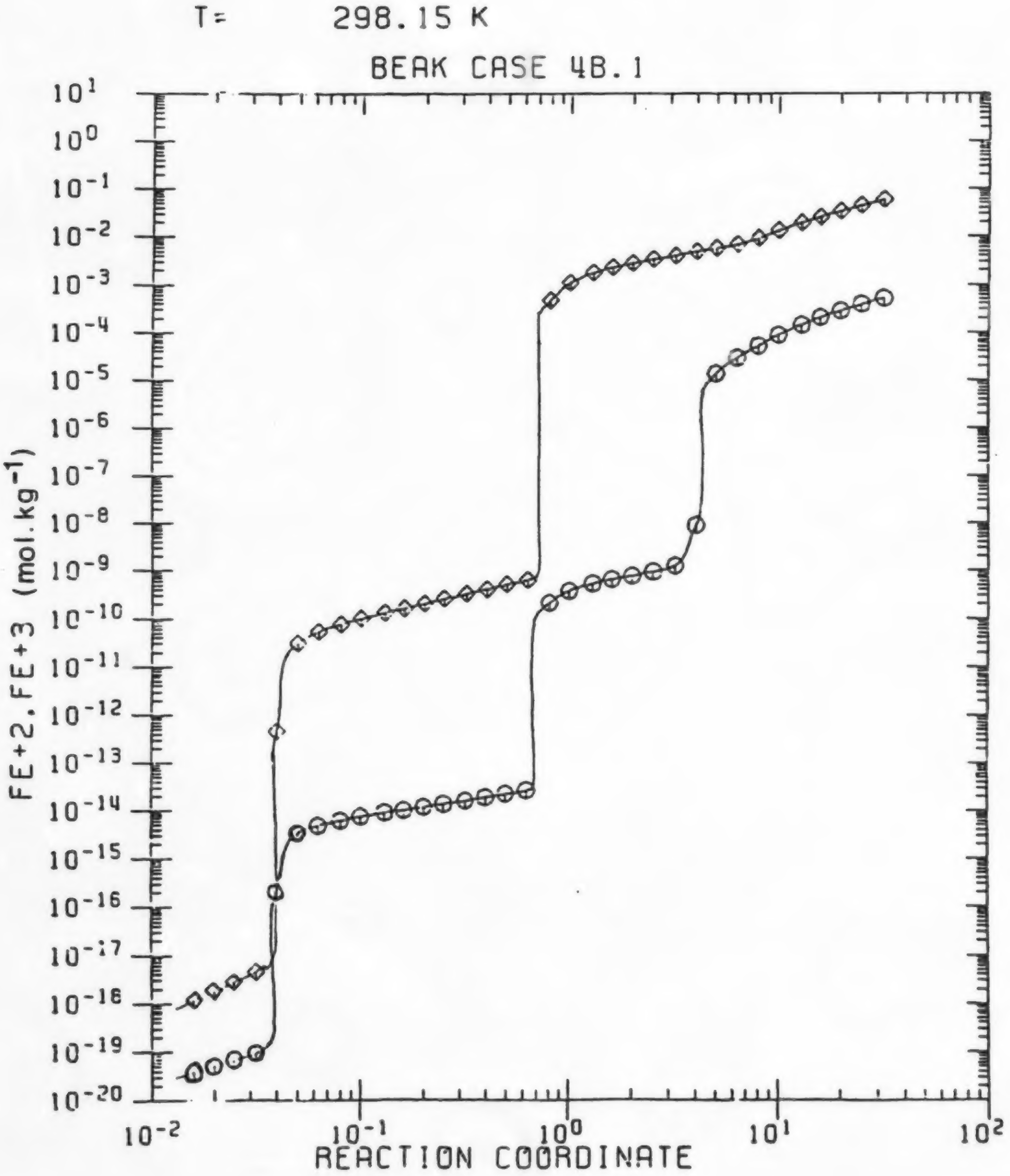

Figure 31: H^+ concentration as a function of the reaction coordinate, for case 4C.1.

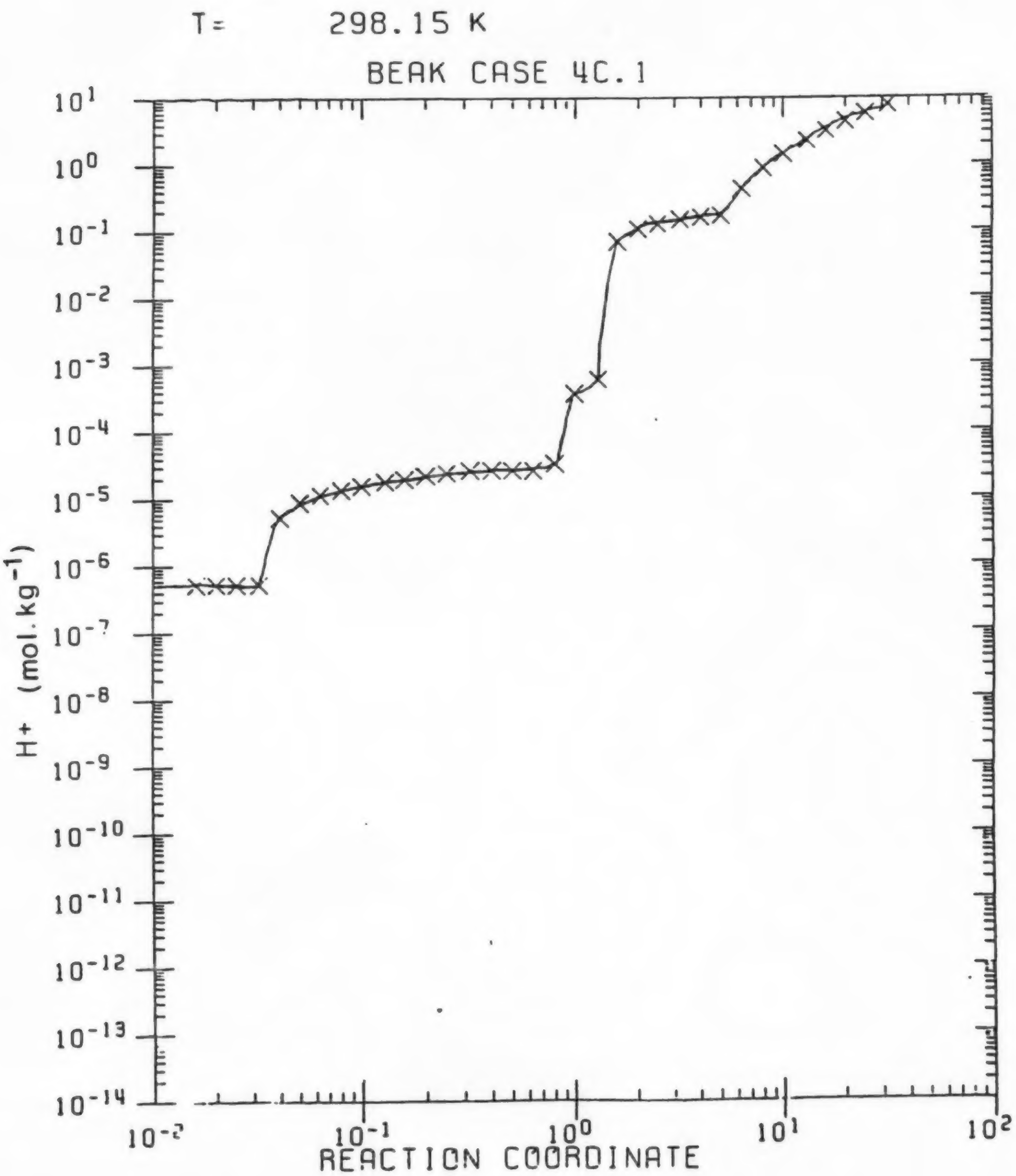

Figure 32: The abundances of solids as a function of the reaction coordinate, for case 4C.1.

○ — $CaSO_4 \cdot 2H_2O$, Δ — FeOOH(α)

◇ — FeS_2 (pyrite), ⋈ — $FeSO_4 \cdot 7H_2O$,

* —— jarosite, ● — $Al(OH)_3$ (gibbsite),

⧖ — $CaCO_3$ (s), ◆ — $FeCO_3$ (s).

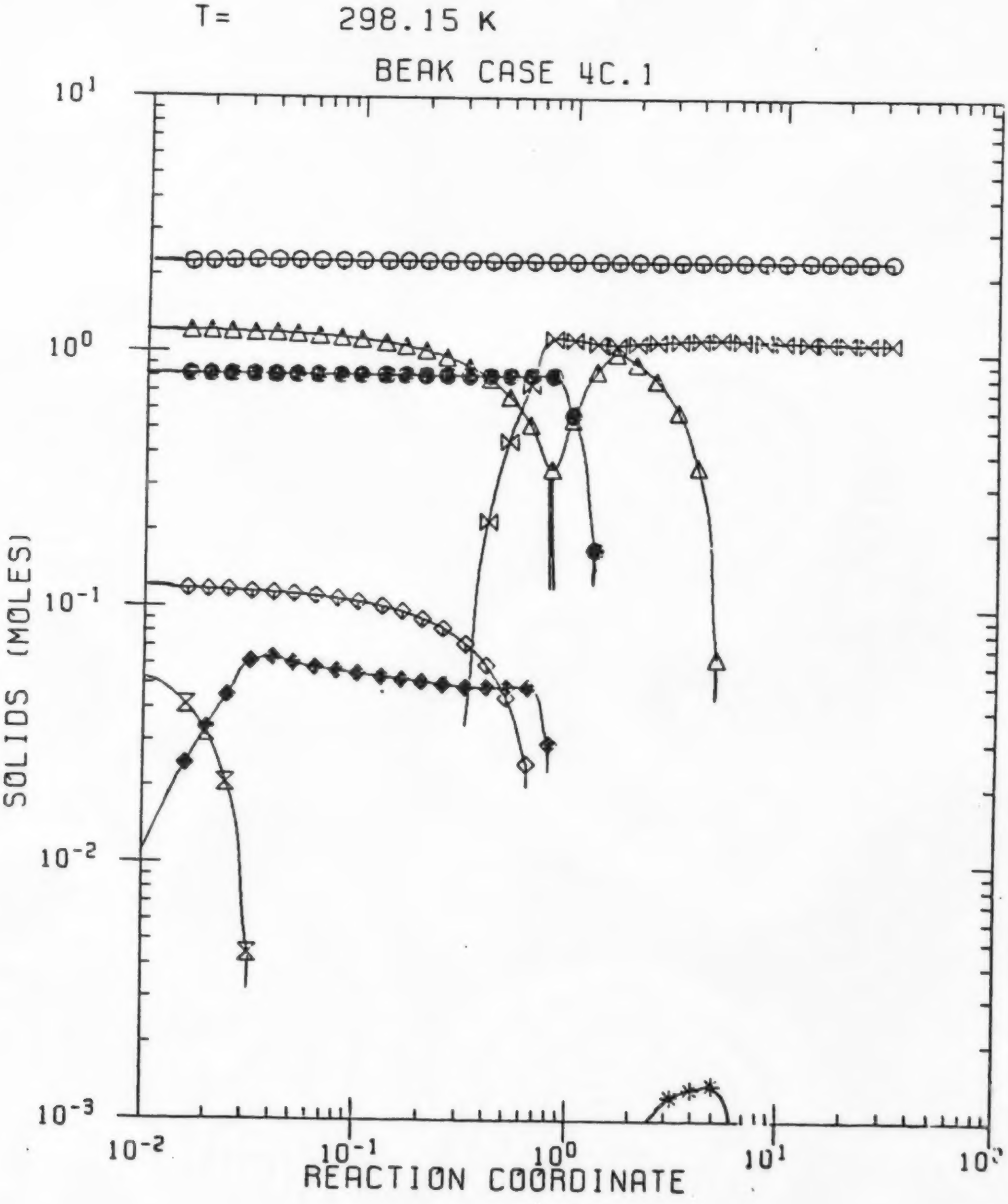

Figure 33: The concentrations of Fe^{2+} (○ –) and Fe^{3+} (◇ –) as a function of the reaction coordinate, for case 4C.1.

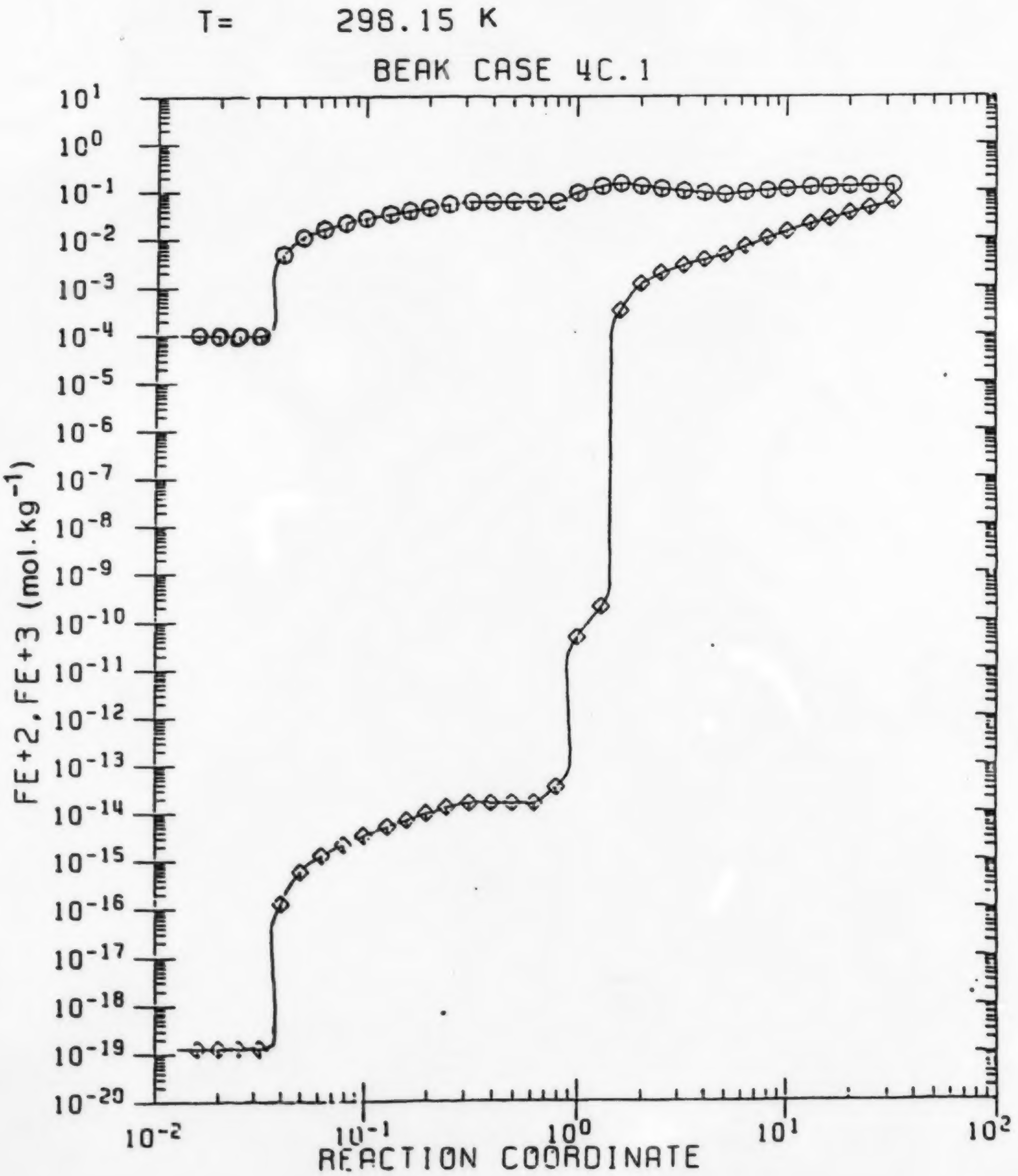

APPENDIX A

Values of Gibbs energies of formation at 25°C for approximately fifty species in the Fe-Ca-S-carbonate-H_2O system were selected for the database. Whenever possible, given the time available, an attempt was made to keep the data internally consistent and also consistent with the CODATA compilation [A.1].

For Fe^{2+} and Fe^{3+} the values of $\Delta_f\bar{G}^\circ$ are those chosen by Sadiq and Lindsay (1979) [A.2]. (The more recent re-evaluation by Sadiq and Lindsay (1981) [A.3] gives similar values). These values were used with the hydrolysis constants selected by Baes and Mesmer [A.4] to derive $\Delta_f\bar{G}^\circ$ for the aqueous hydrolysis species of iron ($FeOH^{2+}$, $Fe(OH)_2^+$, $Fe(OH)_3(aq)$, $Fe(OH)_4^-$, $Fe_2(OH)_2^{4+}$, $Fe_3(OH)_4^{5+}$, $Fe(OH)^+$, $Fe(OH)_2(aq)$, $Fe(OH)_3$, $Fe(OH)_4^{2-}$). The values of Δ_fG° for the iron (II) hydrolysis species are somewhat more positive than those given in most compilations, but are still more negative than values calculated from the recent work of Tremaine and LeBlanc [A.5].

Values for Δ_fG° of Fe_3O_4, α-Fe_2O_3, α-FeO(OH) and γ-FeO(OH) were taken from Sadiq and Lindsay [A.2]. Their method of determining Δ_fG° (γ-FeO(OH)) =-483.3 kJ•mol^{-1} was considered better than that used by Baes and Mesmer [A.4]. The equilibrium data for amorphous α-FeO(OH) from Lengweiller et al. [A.6] as reported by Sadiq and Lindsay [A.2] was then used to calculate Δ_fG° (FeO(OH)(am)) =-482.9 kJ•mol^{-1}.

In a document supplied by IEC Beak [A.7] a "pK_{sp}" of 39.96 was suggested for a "soluble", "amorphous" phase of ferric hydroxide. The value given here for FeO(OH)(am) is for a slightly more stable form (pK_{sp}=40.4). Freshly precipitated $Fe(OH)_3$ has a much lower pK_{sp} (Langmuir (1969) [A.8] suggests 37.2) and we have used this to obtain Δ_fG° ($Fe(OH)_3$(am)). The value supplied by IEC Beak is greater than any pK_{sp} values tabulated for $Fe(OH)_3$(am) by Sadiq and Lindsay, and could refer to a hydrolyzed iron (III) solid intermediate between freshly precipiated $Fe(OH)_3$ and amorphous FeO(OH). The IEC Beak value has not been used.

Δ_fG° values for $H_2S(g)$, $H_2S(aq)$,HS^- and S^{2-} were taken from Sadiq and Lindsay [A.2]. The JANAF [A.9] value for $H_2S(g)$ is slightly (0.19kJmol^{-1}) more positive than the Sadiq and Lindsay value, but this difference is well within the estimated errors (0.4kJ mol^{-1} [A.2]).

JANAF has recently re-evaluated the Gibbs energies of formation of the solid ion sulphides. Their value for pyrite is based on more recent data than those considered by Sadiq and Lindsay [A.2]. The markasite value from JANAF has also been chosen as it depends directly on the pyrite value. The same methodology was used to derive $\Delta_f G°$ (markasite) by both JANAF and Sadiq and Lindsay. However, for troilite, FeS, the JANAF compilers differ from Sadiq and Lindsay in the method used to calculate $\Delta_f G°$. The JANAF value was preferred because the calculation procedure seemed better, and also to maintain consistency with the pyrite value. However, the JANAF value was modified to make it consistent with the Sadiq and Lindsay value for $\Delta_f G°(H_2S(g))$.

JANAF gives a value of $\Delta_f G°$ (pyrrhotite)=-106.86 $kJ \cdot mol^{-1}$ for a composition $Fe_{0.877}S$. Comparison with the value for troilite suggests that $\Delta_f G°(Fe_7S_8) = 8(\Delta_f G°(Fe_{0.877}S))$ within an estimated error of <1 $kJ.mol^{-1}$ (i.e., less than the error in the pyrrhotite Gibbs energy of formation value). Fe_7S_8 is used because it is a much more tractable formula for most computer programs.

$\Delta_f G°$ values for the iron sulphate solids and complexes are from Sadiq and Lindsay [2].

The CODATA values for Ca^{2+} and CaO[A.1] were chosen. The analysis used to obtain Gibbs energies of formation for the other calcium solids and aqueous species follows that of Sadiq and Lindsay, but values have been adjusted to be consistent with the CODATA values for Ca^{2+} and CaO. The value used here for $\Delta_f \bar{G}°(CO_3^{2-})$ [see Ref [A.10]] also differs from Sadiq and Lindsay's value. Thus the Gibbs energies of formation of $FeCO_3(s)$ and of the calcium carbonate species reflect this choice for CO_3^{2-}, although the analysis of Sadiq and Lindsay has been followed.

Values for $\Delta_f G°(CaFe_2O_4)$ and $\Delta_f G°(CaS)$ are from Sadiq and Lindsay. The latter value has large error limits and no attempt has been made to adjust the value to consistency with the other data.

The value for pK_{sp} for hydronium jarosite (HJ) was initially taken as 82.1 as suggested in a letter from IEC Beak [A.7] - presumably calculated by Nordstrom from Kashkay et al (1975) [A.11]. The solubility product was presumed to refer to the reaction:

$$3Fe^{3+} + 5OH^{-} + 2SO_4^{2-} + 2H_2O \rightleftarrows H_3O(Fe(OH)_2)_3(SO_4)_2$$

thus,

$$pK_{sp} = \log_{10} \left[a^3(Fe^{3+}) \cdot a^2(SO_4^{2-}) \cdot a^5(OH^{-}) \right].$$

The value of pK_{sp} combined with our values for the Gibbs energies of formation of Fe^{3+}, SO_4^{2-}, OH^{-} and H_2O gave $\Delta_f G°(HJ) = -3269$ kJ.mol^{-1}, and this value was used for some of our calculations (Section II).

Later, on obtaining a copy of the original reference by Kashkay et al [11], it became obvious that the supplied value of pK_{sp} was inconsistent with the solubility data in the original reference or with the definition of pK_{sp} given above. Recalculation gave $pK_{sp} = 75.4$ using the same auxiliary data [A.12] used by Kashkay et al. Full recalculation of the solubility data from reference [A.11] (for hydronium-jarosites and the other jarosites listed) in a method completely consistent with the database presented here would be a minor project in itself. A rough recalculation for HJ using a subset of equilibrium constants consistent with our database gives $pK_{sp} = 74.9$ and $\Delta_f G°(HJ) = -3228$ kJ.mol^{-1} (i.e., only about 4 kJ.mol^{-1} different from the value reported originally in reference [A.11]).

Two further points should be made concerning the table of jarosite data supplied by IEC Beak [A.7]. First, the difference in the $\Delta_f G°$ values for natrojarosite and hydronium-jarosite are not consistent with the differences in the supplied values of pK_{sp}. Second, the value given for jarosite is based on an estimate from a mixed K^+/Na^+ solid.

The value for $\Delta_f G°(O_2(aq))$ was taken from NBS-270-3 [A.13]. (The value for $O_2(aq)$ was needed by the program for the oxidative dissolution calculations, but was not used directly to calculate values of the redox potentials).

No literature data were found for Fe/HS^{-} aqueous solution complexes.

The database is given in Table A.1. The name HYDRON which appears in this table refers to hydronium-jarosite (HJ).

TABLE A.1: THE DATABASE

SPECIES	$\Delta_f G^\circ$ (25°) $\mathrm{kJ \cdot mol^{-1}}$
H+	0.
H2O	-237.18
OH-	-157.34
CA+2	-552.8
FE+2	-91.21
FE+3	-16.82
CO3-2	-527.99
HCO3-	-586.95
H2CO3	-623.20
SO4-2	-744.54
HSO4-	-755.88
S-2	85.81
HS-	12.18
H2S(AQ)	-27.91
S2-2	82.63
FEOH+	-274.1
FE(OH)2(AQ	-447.9
FE(OH)3-	-625.6
FE(OH)4-2	-777.2
FEOH+2	-241.4
FE(OH)2+	-458.7
FE(OH)3(AQ	-660.
FE(OH)4-	-842.
FE2(OH)2+4	-491.1
FE3(OH)4+5	-963.0
FE(OH)2(S)	-492.9
FEOOH(ALFA	-491.3
FE(OH)3AMF	-701.18
FE2O3ALFA	-744.12
FE3O4(S)	-1018.7
FECO3(S)	-677.65
FESO4(S)	-820.6
FESO4.7H2O	-2510.
FE2SO43(S)	-2251.
FESO4(AQ)	-848.3
FESO4+	-785.0
FE(SO4)2-	-1536.6
FES2(PYRIT	-160.06
FES	-102.14
FE7S8(S)	-854.9
CAO	-603.48
CAOH+	-717.6
CA(OH)2(S)	-898.68
CACO3(AQ)	-1098.8
CAHCO3+	-1146.2
CACO3(S)	-1128.9
CASO4(AQ)	-1310.5
CASO4(S)	-1322.5
CASO42H2O	-1798.2
CAS	-473.
CAFE2O4	-1414.6
O2(AQ)	16.318
HYDRON	-3228.

REFERENCES

[A.1] CODATA Task Group. "CODATA Recommended Key Values for Thermodynamics, 1977", J. Chem. Thermodynam. 10, 903 (1978).

[A.2] Sadiq, M. and Lindsay, W.L. "Selection of Standard Free Energies of Formation for Use in Soil Chemistry", Colorado State University Experiment Station Technical Bulletin 134 (1979).

[A.3] Sadiq, M. and Lindsay, W.L. "Standard Free Energy of Formation of Some Chemical Species: Discrepancies and Selections", Arabian J. Sci. Eng. 6, 95 (1981).

[A.4] Baes, Jr., C.F. and Mesmer, R.E. "The Hydrolysis of Cations", John Wiley & Sons, New York, 1976.

[A.5] Tremaine, P.R. and LeBlanc, J.C. "The Solubility of Magnetite and the Hydrolysis and Oxidation of Fe^{2+} in Water to 300°C", J. Solution Chem. 9, 415 (1980).

[A.6] Lengweiler, H., Buser, W. and Feitknecht, W. "Die Ermittlung der Löslichkeit von Eisen (III) - hydroxid in Wässeriger Lösung", Helv. Chim. Acta 44, 805 (1961).

[A.7] Nicholson, R. (IEC Beak). Letter to N. Garisto (Ref. 2250.1), Table 2, August 16, 1984.

[A.8] Langmuir, D. "The Gibbs Free Energies of Substances in the System $Fe-O_2-H_2O-CO_2$ at 25°C". U.S. Geol. Sur. Prof. Paper 650-B (1969) (as quoted in reference [2]).

[A.9] JANAF, "JANAF Thermochemical Tables, 1982 Supplement", J. Phys. Chem. Ref. Data, 11, 834-39, 855 (1982).

[A.10] Lemire, R.J. and Tremaine, P.R. "Uranium and Plutonium Equilibria in Aqueous Solutions to 200°C". J. Chem. Eng. Data 25, 361 (1980).

[A.11] Kashkay, Ch. M., Borovskaya, Yu.B. and Babazade, M.A. "Determination of $\Delta G^\circ_{f\ 298}$ of Synthetic Jarosite and its Sulphate Analogues", Geochem. Int. (Eng. Transl.) (5) 115 (1975).

[A.12] Naumov, G.B., Ryzhenko, B.N. and Kodakovsky, I.L. Handbook of Thermodynamic Data (1971). (Eng. Transl. by G.J. Soleimani).

[A.13] Wagman, D.D., Evans, W.H., Parker, V.B., Halow, I., Bailey, S.M. and Schumm, R.H. "Selected Values of Chemical Thermodynamic Properties", U.S. National Bureau of Standards Technical Note 270-3 (1968).